

THE UNIVERSITY of ADELAIDE

Modern Structural Analysis of Subsurface Provinces: A Case Study on the Cooper and Eromanga Basins, Australia

David Kulikowski

The Australian School of Petroleum
The University of Adelaide

This thesis is submitted in fulfilment of the requirements for the degree of

Doctor of Philosophy

from the Australian School of Petroleum, Faculty of Engineering, Computer and Mathematical Sciences, the University of Adelaide

December 2017

TABLE OF CONTENTS

THESIS ABSTRACT iii
DECLARATION iv
STATEMENT OF AUTHORS' CONTRIBUTIONS v
ACKNOWLEDGEMENTS vi
PUBLICATION LIST 9

1. CONTEXTUAL STATEMENT 11

2. LITERATURE REVIEW OF THE STUDY AREA 14
2.1. INTRODUCTION 14
2.2. THE WARBURTON BASIN (BASEMENT) 14
2.2.1. Introduction 14
2.2.2. Tectonostratigraphic Evolution 16
2.2.3. Basement Structural Features 18
2.3. THE COOPER BASIN 22
2.3.1. Introduction 22
2.3.2. Structural Evolution 26
2.3.3. Stratigraphic Evolution 29
2.4. THE EROMANGA BASIN 31
2.4.1. Introduction 31
2.4.2. Tectonostratigraphic Evolution 32
2.5. PRESENT-DAY STRESS 33
2.6. PETROLEUM SYSTEM 35
2.6.1. Source Rocks 35
2.6.2. Sealing Rocks 35
2.6.3. Hydrocarbon Migration 36
2.7. NATURAL FRACTURES 37

3. METHODOLOGIES 38
3.1. INTRODUCTION 38
3.2. CALCITE TWIN STRESS INVERSION TECHNIQUE (CSIT) 38
3.2.1. Fundamentals of Calcite Twinning 38
3.2.2. Sample Collection and Processing 43
3.2.3. Quantification of Paleo-stress Tensors 49
3.3. NATURAL FRACTURE ANALYSIS 54
3.3.1. Introduction 54
3.3.2. Data Processing 55
3.3.3. Stress Inversion 56
3.4. SEISMIC DATA ANALYSIS 58
3.4.1. Introduction 58
3.4.2. Seismic Time-to-Depth Conversion 60
3.4.3. Analysis Techniques 63
3.5. GEOMECHANICAL MODELLING 68
3.5.1. Introduction 68
3.5.2. Quantifications 69

4. BIBLIOGRAPHY 71

5. THESIS BODY 89
5.1. MANUSCRIPT 1: Seismic depth conversion uncertainty 90
5.2. MANUSCRIPT 2: Tectonic history of the Cooper-Eromanga Basin 99
5.3. MANUSCRIPT 3: Basement structural architecture 128
5.4. MANUSCRIPT 4: Stratigraphic architecture and fault activity 161
5.5. MANUSCRIPT 5: Fault reactivation with in situ stress 203
5.6. MANUSCRIPT 6: Fault reactivation with paleo-stress 225
5.7. MANUSCRIPT 7: Fracture networks in 3D seismic data 267
5.8. MANUSCRIPT 8: Temperature, pressure and fracture distribution 289
5.9. MANUSCRIPT 9: Review of the Cooper and Eromanga Basins 309

6. THESIS CONCLUSIONS 367

7. APPENDIX 369
7.1. CO-AUTHOR MANUSCRIPT A: Optimising hydraulic fracturing 370
7.2. CO-AUTHOR MANUSCRIPT B: 3D Hydraulic Fracturing with a DFN 386
7.3. POSTER PRESENTATION A: The APPEA Conference 412
7.4. POSTER PRESENTATION B: The ASP Annual Board Meeting 414
7.5. SPOKEN PRESENTATION A: GeoFrac Consortium Board Meeting 416
7.6. SPOKEN PRESENTATION B: The AAPG International Conference 417
7.7. SPOKEN PRESENTATION C: GeoFrac Consortium Board Meeting 418
7.8. SPOKEN PRESENTATION D: The APPEA Conference 419
7.9. SPOKEN PRESENTATION E: The ASEG-PESA-AIG Conference 420
7.10. SPOKEN PRESENTATION F: The ASP research seminar 421
7.11. SPOKEN PRESENTATION G: The ASP research seminar 422
7.12. RESEARCH SCHOLARSHIP A: AAPG Grants-in-Aid 423
7.13. RESEARCH HONOUR A: Selected as IMNIS Student 425
7.14. RESEARCH HONOUR B: Featured in PETROSYS Map Book v6 426

THESIS ABSTRACT

The Cooper-Eromanga Basin is Australia's largest onshore hydrocarbon province with significant unconventional hydrocarbon potential; however, due to the lack of outcrop, geological data is not easily measured. To mitigate this issue, an approach that can be used to provide a modern structural analysis of subsurface provinces with limited outcrop is presented in this thesis. A holistic approach integrating many datasets, techniques, methodologies, and software has provided better constraints on the structural geology, geophysics and tectonic evolution of the province. Hydrocarbon exploration in the basin has transitioned to technically challenging plays (pinch-out traps, low relief structures, basin centred gas, etc.), but these programs have been somewhat hampered by a poor understanding of the structural geology, geophysics and tectonic evolution of the basin, with previous work using low resolution and sparse 2D seismic data that remained in the time-domain.

Apart from this approach, the key deliverable of this project was constraining the orientation and magnitude of six tectonic events (N-S Alice Springs, SE-NW Mid-Permian, NE-SW Daralingie, E-W Hunter-Bowen, E-W Late Cretaceous, and N-S Paleogene Events) that have controlled the evolution of the Cooper-Eromanga Basin. The integration of geophysical data, calcite twin stress inversion analysis and rock mechanics presented a new combination of data to constrain the tectonic evolution of subsurface provinces. These complete paleo-stress tensors were integrated with six geomechanical models to constrain hydrocarbon migration pathways through time, finding that since the critical moment (90 Ma), NE-SW striking high angle (60°) faults were likely facilitating hydrocarbon migration. Under contemporary stresses, the regional SE-NW strike-slip faults are most likely to reactivate and complicate hydraulic fracture stimulation treatments.

Considering that a detailed structural architecture map was not available in literature, all available 2D seismic lines and 12 3D seismic surveys were interpreted to generate a modern basement fault map and detailed fault models for each seismic survey. Four of these surveys cover major basin ridges and were used to constrain the tectonostratigraphic evolution of the basin. Extensive on-lapping features were created along major structures during the structural events, particularly within Permian stratigraphy. The timing of structural movement is important; however, for economic production of hydrocarbons, a detailed understanding of the natural fracture network in tight sand reservoirs is fundamental. This led to a study that would map the distribution of >6000 temperature samples, >8000 pressure samples, and natural fracture data from 11 borehole image logs across the basin. Following this, the spatial and temporal distribution of subsurface permeable natural fracture networks was presented for five 3D seismic surveys using seismic curvature analysis and a geomechanical model. This model found that E-W striking natural fractures are optimally oriented to form structural sweet-spots and are commonly associated with E-W elongate structures.

To better understand the seismic time-to-depth conversion accuracy within the basin, an automated cross-validation method was developed to generate a significant statistical database from 13 D seismic surveys, 73 interpreted horizons, and 657 wells. The results showed that a single method should not be used for the entire basin, as the most accurate method and expected error changes depending on the unique dataset. To conclude this research, a thorough literature review was carried out to synthesis the new research and integrate it with previous literature. The approach used in this thesis has significant value to all subsurface provinces with limited outcrop that has prevented detailed structural and geomechanical analysis, leaving significant research gaps.

DECLARATION

I, **David Kulikowski**, certify that this work contains no material which has been accepted for the award of any other degree or diploma in my name, in any university or other tertiary institution and, to the best of my knowledge and belief, contains no material previously published or written by another person, except where due reference has been made in the text. In addition, I certify that no part of this work will, in the future, be used in a submission in my name, for any other degree or diploma in any university or other tertiary institution without the prior approval of the University of Adelaide and where applicable, any partner institution responsible for the joint award of this degree.

I give consent to this copy of my thesis when deposited in the University Library, being made available for loan and photocopying, subject to the provisions of the Copyright Act 1968. I acknowledge that copyright of published works contained within this thesis resides with the copyright holders of those works.

I also give permission for the digital version of my thesis to be made available on the web, via the University's digital research repository, the Library Search and also through web search engines, unless permission has been granted by the University to restrict access for a period of time.

I acknowledge the support I have received for my research through the provision of an Australian Government Research Training Program Scholarship.

12nd of December 2017

David Kulikowski **Date**

STATEMENT OF AUTHORS' CONTRIBUTIONS

The research summarised in the papers that constitute this thesis was undertaken at the Australian School of Petroleum (ASP), the University of Adelaide. The research was partly sponsored by the Geofrac Consortium, which includes the sponsoring companies Santos, Beach Energy, BG Group (QGC), Halliburton and Chevron, and included several PhD candidates, Honours/Masters students, and researchers. As such, some research required collaboration with peers, other than my supervisory team, to maintain a high level of research quality. The contribution of peers towards this thesis is evidenced in the author sequence and percentage contribution found within the statement of authorship documents, and in the acknowledgement section of each paper/manuscript.

ACKNOWLEDGEMENTS

The work produced within this thesis could not have been completed without the support, financial contribution and encouragement provided by the following people:

My Supervisory Team: Khalid Amrouch and Dennis Cooke.

I would like to thank you both for your encouragement, feedback and patience through this very long and memorable period of my life. Completing this degree will always be one of the biggest highlights of my life, so thank you both for helping me make this possible. I would particularly like to thank Khalid for his efforts to go above and beyond what is normally expected of supervisors. I thoroughly enjoyed spending hours discussing new research ideas and the impact that they would have on the industry and within the academic realm. I appreciate all of the honest feedback that you gave me. Even if my appreciation wasn't always obvious at the times, I would not have been able to complete this degree to the standard that I have if it wasn't for your help. So thank you for moulding me into a scientist and for helping me put together a piece of work that I am very proud of.

The Geofrac Consortium.

I would like to acknowledge the financial contribution made by the GeoFrac Consortium, which includes the sponsoring companies: Santos Ltd, Beach Energy, Chevron, Halliburton and GB Group (QGC). Without your generous financial contribution, this research would not have been possible.

The Australian School of Petroleum.

Thank you to everyone at the ASP who provided support, encouragement, and motivation. I would particularly like to thank everyone involved in the ASP Research Seminar group for allowing me to frequently present my research and seek peer review.

Additional Thanks.

I wish to thank Santos Ltd for allowing me to work as a technical assistant (1 day per week) in the production and optimisation engineering team for the first two years of my PhD, and for providing data towards my research. Thank you again to Santos Ltd and also to Woodside Energy for accepting me into their structured three-month long research programs (2015/16 and 2016/17, respectively), which helped to refine and broaden my research skills. Thank you to everyone else who was a part of my life during the eight to nine years while I was at university. Special thanks to fellow PhD Candidates Alexander Robson, Michael E. Gray, and Sunny Mishra for their helpful feedback and support during the course of this degree.

PUBLICATION LIST

Conference Extended Abstract

Kulikowski, D., Hochwald, C., Cooke, D., Amrouch, K. (2016). *A statistical approach to assessing depth conversion uncertainty on a regional dataset: Cooper-Eromanga Basin*. Extended abstract #200 at the ASEG-PESA-AIG 25th International Geophysical Conference and Exhibition, Adelaide, Australia, doi:10.1071/aseg2016ab200.

Borazjani, S., **Kulikowski, D.**, Amrouch, K., McCabe, P., Bedrikovetsky, P. (2017). *Composition changes of hydrocarbons during secondary petroleum migration*. The APPEA Journal, extended abstract, accepted.

First Authored Peer Reviewed Journals

Kulikowski, D., Hochwald, C., Amrouch, K. (2017). *An automated cross-validation method to assess seismic time-to-depth conversion accuracy: A case study on the Cooper and Eromanga basins, Australia.* Geophysical Prospecting, under review. Not in thesis - incomplete approval process at Santos at time of thesis submission.

Kulikowski, D., Amrouch, K. (2017). *Combining geophysical data and calcite twin stress inversion to refine the tectonic history of subsurface and offshore provinces: A case study on the Cooper-Eromanga Basin, Australia*. Tectonics, 36(3), 515-541, doi:10.1002/2016TC004366.

Kulikowski, D., Amrouch, K., Cooke, D., Gray, M.E. (2017). *Basement structural architecture and hydrocarbon conduit potential of polygonal faults in the Cooper-Eromanga Basin, Australia*. Geophysical Prospecting, doi:10.1111/1365-2478.12531.

Kulikowski, D., Amrouch, K. (2017). *3D seismic analysis investigating the relationship between stratigraphic architecture and structural activity in the intra-cratonic Cooper and Eromanga basins, Australia*. Marine and Petroleum Geology, under review.

Kulikowski, D., Amrouch, K., Cooke, D. (2016). *Geomechanical modelling of fault reactivation in the Cooper Basin, Australia*. Australian Journal of Earth Sciences, 63(3), 295-314, doi:10.1080/08120099.2016.1212925.

Kulikowski, D., Amrouch, K. (2017). *4D modelling of fault reactivation using complete paleo-stress tensors from the Cooper-Eromanga Basin, Australia*. Australian Journal of Earth Sciences, under review.

Kulikowski, D., Amrouch, K., Burgin, H.B. (2017). *Mapping permeable subsurface fracture networks: A case study on the Cooper Basin, Australia*. Journal of Structural Geology, under review.

Kulikowski, D., Cooke, D., Amrouch, K. (2016). *Constraining the distribution and relationship between overpressure, natural fracture density and temperature in the Cooper Basin, Australia*. The APPEA Journal, 56, 11-28, doi:10.1071/AJ15002.

Kulikowski, D., Amrouch, K., Pokalai, K., Gray, M.E. (2017). *A comprehensive review of the Cooper and Eromanga Basins, Australia*. Unsubmitted.

Co-Authored Peer Reviewed Journals

Pokalai, K., **Kulikowski, D.**, Johnson, Jr., R.L., Haghighi, M., Cooke, D. (2016). *Development of a new approach for hydraulic fracturing in tight sand with pre-existing natural fractures*. The APPEA Journal, 56, 225-238, doi:10.1071/AJ15017.

Pokalai, K., **Kulikowski, D.**, Amrouch, K., Haghighi, M., Johnson, Jr., R. (2017). *Integrated 3D modelling of hydraulic fracturing in tight reservoirs with pre-exisitng natural fractures and complex stress conditions: Case study in the Cooper Basin, Australia*. Journal of Petroleum Science and Engineering, under review.

Pokalai, K., **Kulikowski, D.**, Haghighi, M., Amrouch, K. (2018). *Mathematical concepts behind hydraulic fracturing models*. Unsubmitted.

Burgin, H.B., **Kulikowski, D.**, Amrouch, K. (2018). *Neotectonic fault reactivation in the deep-water Otway Basin, Australia*. Unsubmitted.

Borazjani, S., **Kulikowski, D.**, Amrouch, K., McCabe, P., Bedrikovetsky, P. (2017). *Deep bed filtration of hydrocarbons during secondary petroleum migration*. Unsubmitted.

Burgin, H.B., Amrouch, K., **Kulikowski, D.** (2018). *4D fault reactivation modelling using 3D seismic surveys and complete paleo-stress tensors from the passive southern margin of Australia*. Unsubmitted.

Gray, M.E., Daniel, R., Kaldi, J., **Kulikowski, D.** (2018). *Determining the accuracy of pseudo-capillary pressure curves generated from nuclear magnetic resonance (NMR) data: A case study from the Cooper Basin, Australia*. Unsubmitted.

Burgin, H.B., Amrouch, K., Rajabi, M., **Kulikowski, D.**, Holford, S.P. (2018). *Determining structural environments through natural fracture and calcite twin analysis: A case study in the Otway Basin*. The APPEA Journal, accepted.

Robson, A.G., Holford, S.P., King, R.C., **Kulikowski, D.** (2018). *Structural evolution of horst and half-graben structures proximal to a transtensional fault system determined using 3D seismic data from the Shipwreck Trough, offshore Otway Basin, Australia*. Marine & Petroleum Geology, 89(3), 615-634, doi:10.1016/j.marpetgeo.2017.10.028.

1. CONTEXTUAL STATEMENT

The objective of this thesis is to provide an approach that can be used to better understand the structural geology and tectonic evolution of subsurface provinces with the goal of improving the efficiency of oil and gas exploration and development, using the Cooper-Eromanga Basin (Australia) as a case study. Previous research in this subsurface basin was limited to poor resolution, sparse and old 2D seismic data that remained in the time domain, which has led to uncertain conclusions on the timing, orientation and regime of tectonic events. Seismic data resolution also significantly decreases below thick Permian coal measures making it difficult to interpret and analyse fault growth. The lack of quality seismic data, coupled with no Cooper Basin outcrop at surface within the study area, has prevented detailed research into the structural geology of the basin. To enhance the technical understanding of the Cooper-Eromanga Basin we firstly develop an automated cross-validation method to determine the accuracy of common seismic time-to-depth conversion methods, followed by several structural analysis methods that are applied to micro-, meso-, and macro-scale structural data from the South Australian portion of the basin.

The importance of accurate seismic time-to-depth conversion was realised when using 3D seismic data, where fault geometries can change and the presence of oil-rich, low relief structural traps are questionable depending on the method used. The most accurate time-to-depth conversion method for the basin was previously explored; however, these studies had a local focus, with a small number of well controls, and limited to selected horizons. To assess the accuracy of four common time-to-depth conversion methods, an automated cross-validation method was created to analyse a regional dataset consisting of 13 3D seismic surveys, 73 two-way-time (TWT) grids, and 657 wells (Manuscript 1). Results found that although the average velocity method was the most accurate on a high-level, the most accurate time-to-depth conversion method and expected error changed by tens of feet depending on the unique dataset and the combination of significant variables. This constrained the uncertainty of seismic time-to depth conversion methods that will be used for seismic data analysis.

Stress inversion of natural fracture, fault, and calcite twin data constrained the timing, orientation and stress-regime of successive tectonic events (Manuscript 2). The inversion of calcite twin data following Etchecopar's technique provided more accurate constraints on the paleo-stress orientations, maximum differential stress magnitudes and stress regimes of the six tectonic events affecting the Cooper-Eromanga Basin. Calcite twin stress inversion was performed on six core samples. The method uses known calcite twin and cleavage plane geometries and the notion that twinning will occur when a resolved shear stress of at least 10 MPa is applied to a calcite crystal. The results found six stress tensors that are represented by natural fractures and faults. Natural fractures

were collated into six regionally pervasive conjugate fracture sets. The fundamental rock failure principals were used to infer a stress tensor for their development, which aligned with faults and calcite twin inversion results.

Faults were measured from selected 3D seismic surveys in Manuscript 2; however, the distribution of these fault sets and the regional basement fault architecture had not been defined. Considering that a detailed basement fault map of the basin was not available in literature, we used all publicly available 2D seismic lines together with 12 3D seismic volumes to interpret the major basement faults across the study area (Manuscript 3). Detailed fault models were created for each 3D seismic survey. The extent of the Cretaceous polygonal fault system and the distribution of individual polygonal faults that extend into oil-rich Lower Cretaceous reservoirs were mapped. The likelihood that these penetrative faults are acting as hydrocarbon conduits from Lower Cretaceous reservoirs into shallow Cretaceous sediments was assessed through geomechanical modelling. Results found that faults striking between 060°N and 140°N with high to near vertical dip angles are optimally oriented to be associated with the tertiary migration of hydrocarbons into shallow sediments.

As the structural architecture of the basin was now well defined (Manuscript 3), we investigated the tectonostratigraphic evolution of the basin using seven 3D seismic surveys (Manuscript 4). Each seismic survey was depth converted, structurally interpreted, and divided into isopach maps for key stratal-units to identify periods of fault movement and structural trap development. The true fault geometries and the timing of fault activity, as evidenced from erosional and on-lapping features from seismic data, were analysed from each seismic survey with the help of attribute analysis and the interpretation of key cross-sections. This study identified the timing of fault movement and linked major fault set development and/or reactivation with tectonic events.

To complete the stress profile of the basin, the present-day stress was used to geomechanically model the risk of fault reactivation (Manuscript 5). Geomechanical modelling was performed on the Swan Lake and Dullingari three-dimensional (3D) seismic surveys. These seismic surveys were converted from the time-domain to the depth-domain and structurally interpreted. The Dilation Tendency, Slip Tendency and Fracture Stability of faults was modelled and calculated, showing that SE-NW striking strike-slip faults are most likely to reactivate and act as hydrocarbon conduits. A system of Cretaceous aged polygonal faults was identified in both seismic surveys, suggesting that the fault system is much more widespread than previously thought (Waterson et al., 2000).

To provide a better understanding of fault reactivation through time, we incorporate geomechanical modelling with paleo-stress data obtained from calcite twin stress inversion results to calculate the

Slip Tendency and Dilation Tendency of faults at six key stages of basin development (Manuscript 6). In doing so, we also complete the paleo-stress tensors by incorporating rock mechanics data and an understanding of rock failure through time to constrain the absolute magnitude of paleo-principal stresses. The results of this study provide information on the fault geometries that were most likely to act as hydrocarbon conduits and most likely to shear reactivate through time. This has direct implications for hydrocarbon migration pathway and structural evolution models within the basin, as well as providing a new approach for investigating fault movement through time.

While investigating methods of mapping subsurface natural fractures and faults, the curvature attribute consistently showed a close similarity to measured data. This led to a study investigating the subsurface distribution of permeable natural fracture networks along the low permeability Patchawarra Formation (Manuscript 7). This gas-rich formation relies heavily on pre-existing natural fracture networks that can enhance hydrocarbon production. A geomechanical model of in situ stress was integrated with curvature analysis of five 3D seismic surveys and natural fractures interpretation from 11 borehole image logs to identify structural “sweet-spots” in known petroleum fields. The distribution of highly permeable SE-NW and E-W striking high angle (>50^{o} dip) fractures was found to be concentrated along E-W elongate anticlines.

As the low permeability Permian aged reservoirs commonly require hydraulic fracturing and an understanding of the subsurface natural fracture geometries to improve the economics, an analysis into the regional natural fracture geometry, density, and potential relationship with increased pore pressure resulting from a recent increase in temperature was investigated (Manuscript 8). The spatial distribution of natural fracture density was integrated with pore pressure and temperature data from 1095 petroleum wells to find a relationship between shallow volcanics, high geothermal gradients, and overpressure. Finally, a hydraulic fracture simulation modelled the interaction with induced and natural fractures to improve drilling and hydraulic fracturing processes (Co-Author Publication A). This led to quantifying the effectiveness of hydraulic fracturing in an alternating stress regime with pre-existing natural fractures (Co-Author Publication B).

To summarise this extensive research and to integrate the findings with existing literature, a modern review of the Cooper-Eromanga Basin was written (Manuscript 9). This forms the discussion aspect of the thesis and provides a broad scale overview of the basin that can be disseminated within exploration companies or read by researchers. The review combines the methodologies presented within this thesis and discusses all aspects of geology, geophysics, production and optimisation engineering, and presenting the key research gaps for the Cooper-Eromanga Basin, Australia.

2. LITERATURE REVIEW OF THE STUDY AREA

2.1. INTRODUCTION

Many entirely subsurface provinces were considered as case studies; however, the Cooper and Eromanga (Cooper-Eromanga) basins were chosen based on the significant seismic coverage and well control that was publicly available. This case study was also chosen because of the value that this research would have on constraining the tectonic evolution and structural geology of this poorly understood province. The region is composed of four individual sedimentary basins each with a unique spatial architecture that represent specific periods of time and isolated by regional unconformities. The Cambrian to Silurian Warburton Basin, Permian to Triassic Cooper Basin, Jurassic to Cretaceous Eromanga Basin, and Paleogene to Quaternary Lake Eyre Basin also have unique petroleum potential and therefore varying amounts of well data.

This study focuses on Australia's largest onshore hydrocarbon province, the low permeability Cooper-Eromanga Basin. This stratigraphic interval overlies the Warburton Basin, which is considered as basement, and is overlain by the Lake Eyre Basin, which represents the most recent sediment deposition (overburden). Deep structures have been shown to control the architecture of the overlying basins so although this study focuses on the stratigraphy within the Cooper-Eromanga Basin, it is important to understand the distribution and characteristics of faults within the Warburton Basin and the extent to which they penetrate and effect overlying stratigraphy. The natural fracture distribution and the present-day stress conditions are important aspects for this low permeability province that requires hydraulic fracturing for effective hydrocarbon production.

2.2. THE WARBURTON BASIN (BASEMENT)

2.2.1. Introduction

The Early Palaeozoic pericratonic Warburton Basin resides below the Cooper Basin and extends into the Northern Territory (Gatehouse, 1986). The basin is constrained by the Arunta Block to the north, Musgrave Block and Amadeus Basin to the west, and the Gawler Block and Arrowie Basin to the south (**Fig. 1**) (Gatehouse, 1986). Seismic data and core form the basin identified Cambrian to Devonian aged folded and faulted carbonates, igneous rocks and reservoir quality sands (Gatehouse, 1986). The early hydrocarbon exploration targeting the Warburton basin was focused on the Innamincka Dome in 1957 with little success (Gatehouse, 1986). However, petroleum potential may exist where Warburton Basin reservoir quality sandstones are found to juxtapose against the overlying Permian source rocks, which can occur through the inversion of normal faults.

The dominant structural grain is NE-SW and SE-NW trending and is linked to the Adelaidean extensional event (Razaee and Sun, 2007). Episodic reactivation of Warburton Basin fault systems has influenced structuring and depositional patterns of overlying Cooper and Eromanga basins, which is why understanding the structural evolution of the Warburton Basin is vital for understanding the structural and stress evolution of the Cooper Basin (Sun, 1997). Researchers have also inferred that basement structures may have influenced hydrocarbon migration from Permian source rocks into Cooper and Eromanga basin reservoir rocks (Kantsler et al., 1984; Lowe-Young et al., 1997; Grant-Wooley et al., 2015).

The Late Cambrian Kalladeina Formation (transgressive systems tract), Middle Cambrian Coongie Limestone Member (high-stand systems tract), and Diamond Bog Dolomite (high-stand systems tract) are carbonate rich sequences. Carbonate rich units in the Warburton Basin have been subject to thermal degradation by Carboniferous igneous intrusions and acidic conditions, encouraging calcite mobility and subsequent precipitation in overlying Permian formations, and may be related to the high carbon dioxide concentration in produced gas (Kantsler et al., 1984; Lemon et al., 2012). A fracture analysis on Warburton Basin core was conduct by Sun (1997), who concluded that many natural fractures contain calcite fill ideal for calcite twin stress inversion analysis (Sun, 1999).

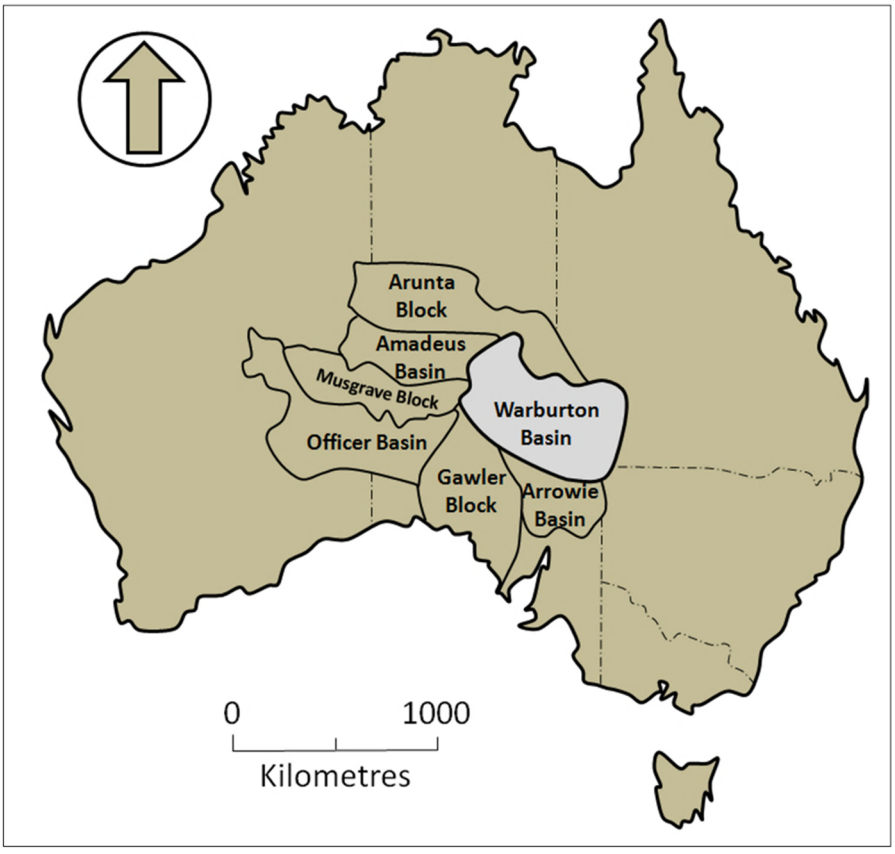


Fig. 1 Location of the Warburton Basin and adjacent basins and blocks (modified after Sun, 1997).

2.2.2. Tectonostratigraphic Evolution

Adelaidean (650-575 Ma) rifting in a SE-NW direction developed NE-SW striking normal faults and SE-NW striking strike-slip faults, which have a large control on the structural and depositional activity of the overlying basins (Apak et al., 1997; Razaee and Sun, 2007). The major deformational event occurred during the Carboniferous Alice Springs Orogeny (ASO). This event reactivated pre-existing faults and caused major exhumation of sediments that were eroded, creating a regional unconformity within the Silurian Innamincka Formation (Sun, 1997; Razaee and Sun, 2007). This unconformity marks the boundary between the Warburton and Cooper basins (Sun, 1997). **Fig. 2** summarises the tectonism, lithology, possible erosional boundaries and stratigraphic sequences of the Warburton Basin (Razaee and Sun, 2007).

The N-S Delamerian Orogeny (550 Ma) is known to have had an influence on central Australia (Gatehouse, 1986; Boger and Miller, 2003), but there is little evidence of its effect in the Cooper-Eromanga Basin region, albeit Williams (1975) suggests that it may have extended to the Northern Territory border. Timing of normal fault development in the Warburton Basin stratigraphy is concurrent with N-S Delamerian Orogeny, inferring that this event potentially had no effect on the Warburton Basin region (Gatehouse, 1986). The Benambran Orogeny (440 Ma) was an oblique compression between eastern Gondwana and the intra-oceanic Macquarie Arc (Glen et al., 2007). North directed oblique strike-slip movement and E-W thrusting was concentrated along the north trending subducting arc and may have affected the Warburton Basin (Glen et al., 2007).

N-S compression during the ASO enhanced the lateral displacement of pre-existing strike-slip faults (Apak et al., 1997). These strike-slip faults significantly reduce reservoir properties and compartmentalise hydrocarbon fields in the overlying Cooper Basin (Grant-Wooley et al., 2015). This event exhumed the uranium-rich Carboniferous Big Lake Granite Suit that increased local geothermal gradients and promoted the mobility of carbonates that are now evident as cements within natural fractures (Rezaee and Sun, 2007; Glikson et al., 2013). Carbonates are present in a significant portion of the Warburton Basin stratigraphy (**Fig. 2**) and coupled with becoming mobile and precipitating within natural fractures, is one of the contributors to the significant carbon dioxide concentration within produced gas. This episode of exhumation is evident in the stratigraphy as a regional unconformity and separates the Cooper and Warburton basins (Sun, 1997). Basement faults were periodically reactivated and influenced fault development and sediment deposition in the overlying basins (Apak et al., 1997).

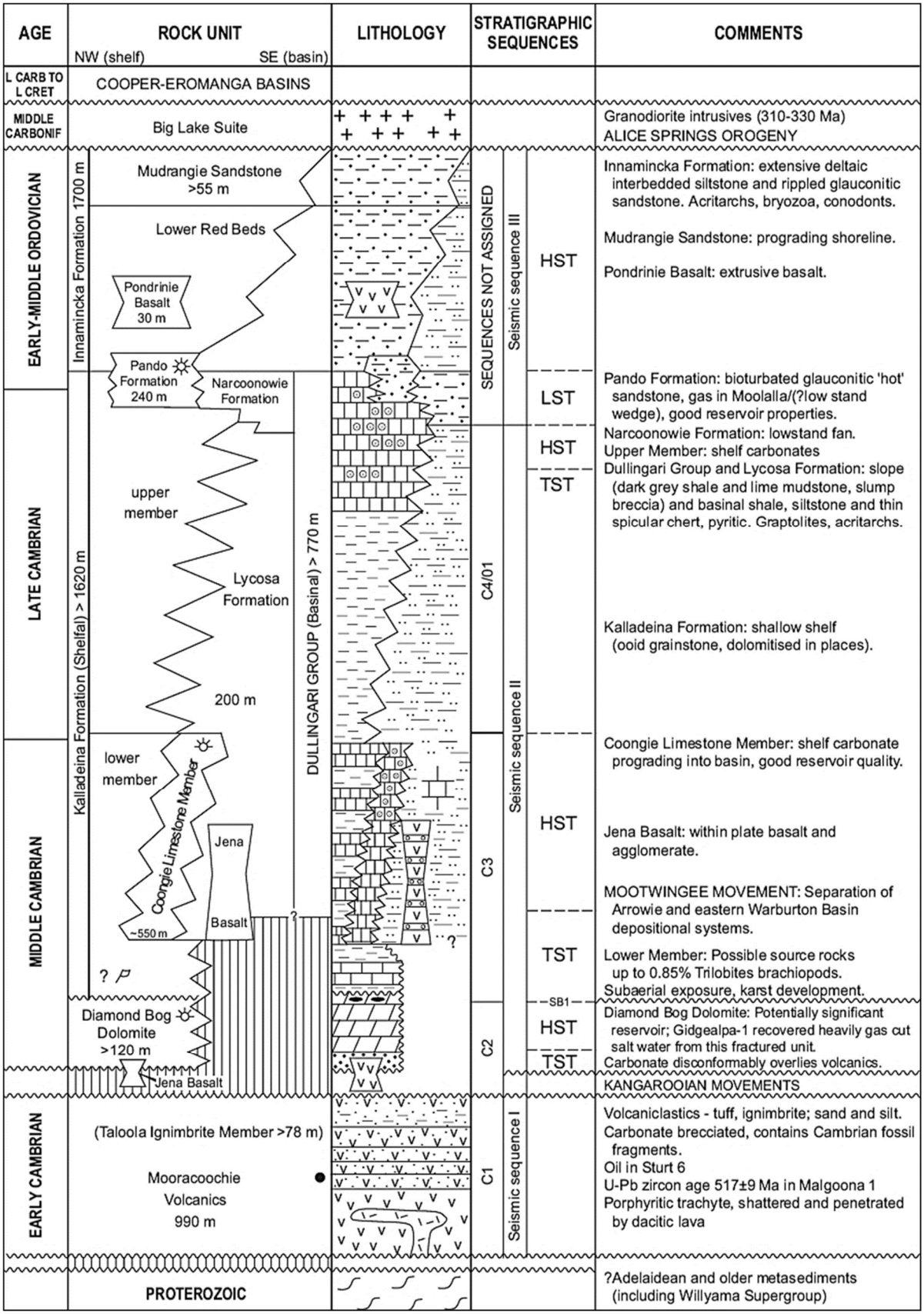


Fig. 2 Stratigraphic column of the Warburton Basin (Razaee and Sun, 2007).

2.2.3. Basement Structural Features

The Cooper Basin is an intra-cratonic basin that has experienced at least five individual events. The basin is elongate in an NE-SW direction with three major troughs isolated by high angle NE-SW striking inverse normal faults (GMI and MN ridges) that extend from the underlying Warburton basin. Near vertical SE-NW strike-slip faults are abundant throughout the Warburton and Cooper basins and likely developed during the early stages of Cooper Basin formation and reactivated by subsequent events. Wrench faulting, positive flower structures, thrust faults, pull-apart basins, and imbricate thrust sheets are suggested to exist within the Warburton Basin and significantly control the stratigraphy and structural architecture of the Cooper Basin.

2.2.3.1. Wrench Faulting (Patchawarra Trough)

Wrench faults form in strike-slip stress regimes with extensional stresses that form opposite movement of two adjacent crustal blocks along a dividing plane (Wilcox et al., 1973). This movement generates predictable fold (en echelon) and fracture (riedel) patterns (Wilcox et al., 1973). The most valuable of these structures are en echelon folds, which form early during plastic deformation and may exist as petroleum traps (Wilcox et al., 1973). Continued wrenching promotes two vertical and intersecting fracture sets to develop (Wilcox et al., 1973). Riedel shears develop first at 10-30^{o} (R_1), followed by conjugate riedel shears at 70-90^{o} (R_2) to the wrench fault strike (Wilcox et al., 1973). These sets of antithetic (R_1) and synthetic (R_2) shear fractures have opposing sense of shear (**Fig. 3**) (Dresen, 1990). With progressive stress, tensional gashes (T) and shear fractures (X and P) develop (Wilcox et al., 1973). The sense of shear forces minor rotation, where sinistral shear will rotate crustal blocks anti-clockwise, and dextral shear creates clockwise rotation (Wilcox et al., 1973). Down warping of the Cooper Basin in the Triassic (NNW tilting) and again in the Late Triassic (NNE tilting) is likely influenced by this type of wrenching (Wilcox et al., 1973; Apak et al., 1997).

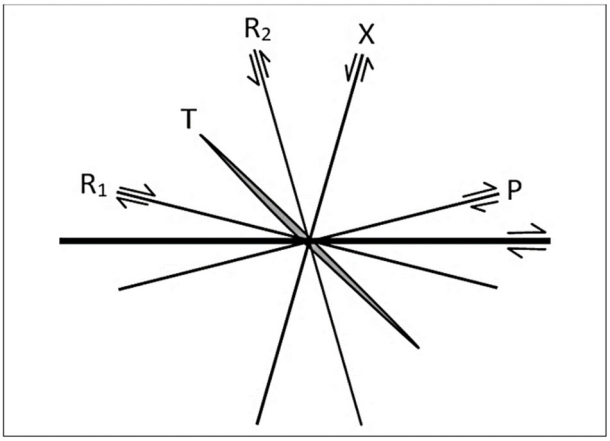


Fig. 3 Shear fractures and faults in a wrench fault system. $\boldsymbol{R_1}$ (synthetic) and $\boldsymbol{R_2}$ (antithetic): Riedel shears; $\boldsymbol{T}$: tension gash; and $\boldsymbol{X}$ and $\boldsymbol{P}$: shear fractures (Dresen, 1990).

2.2.3.2. Positive Flower (pop-up) Structures

Positive flower structures form in strike-slip regimes within the contractional jog between two strike-slip faults (**Fig. 4**) (Woodcock and Fischer, 1986). An initial basement fault is generated, upon which back-thrusts and wedges develop into a transpressional positive flower structure with thrust faults defining the framework (Woodcock and Rickards, 2003). These structures are best seen in seismic cross section perpendicular to the strike of major faults within the basement. Considering that the basin has an abundance of basement strike-slip faults, the presence of pop-up structures is highly likely and may form important structures. Some previous works (Apak et al., 1997) have suggested that hydrocarbon fields located within the Patchawarra Trough have characteristics of pop-up features that may also follow a linear path through the trough. The presence of strike-slip faults is a known occurrence within the basin (Apak et al., 1997; Grant-Wooley et al., 2015) so the presence of these features is highly likely.

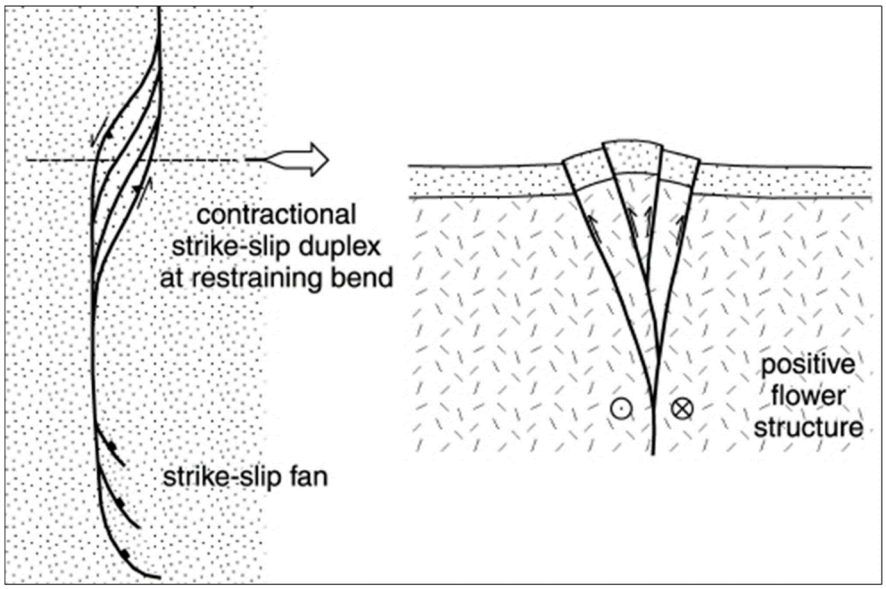


Fig. 4 The framework of a positive flower structure (Woodcock and Rickards, 2003).

2.2.3.2.1. Inverted Normal Faults

Eisenstadt and Paor (1987) proposed that thrust faults, which are typically low angled, develop along ramps and connect along flat faults, before propagating towards the surface and towards the basement (**Fig. 5**). These structures develop within convergent and strike-slip stress regimes where compressive forces displace a crustal block along an inclined plane (**Fig. 6**). The high angle nature of inverted faults within the study area implies that they likely originated as normal faults during the Adelaidean extensional event (Kuang et al., 1985; Apak et al., 1997; Abul Khair et al., 2015). Subsequent tectonic events likely reactivated these faults creating their present-day inverted fault nature (Apak et al., 1997; Abul Khair et al., 2015).

The difficulty in constraining the timing of fault development and fault activity in the Warburton Basin is in the poor seismic quality below thick Permian coal measures, which prevents detailed fault growth analysis. A technique for defining the evolution of fault activity in poor seismic resolution data can be particularly useful for constraining migration pathways and tectonic evolution models for the Cooper-Eromanga Basin. The spatial distribution of basement faults is presently not available in literature and would be most beneficial as a basement fault map and presented as stereographic projections to allow fault dip angle and strike to be presented.

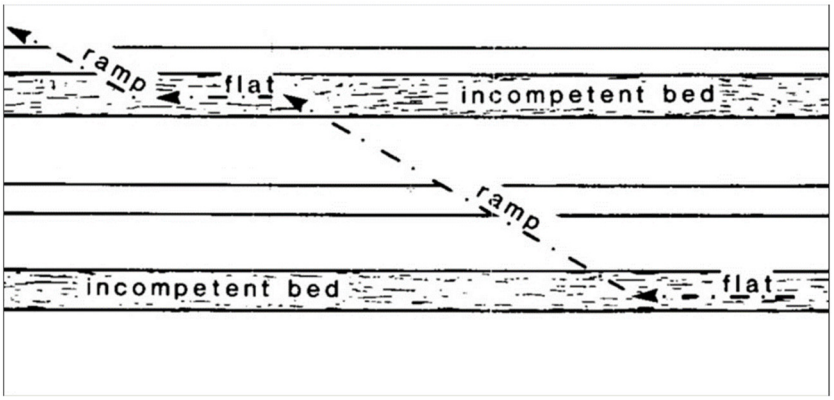


Fig. 5 Development of thrust faults (Eisenstadt and Paor, 1987).

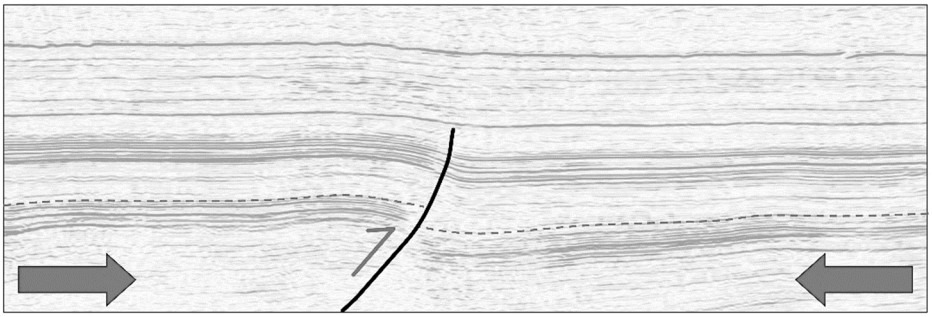


Fig. 6 A seismic cross-section showing a typical high angle reverse fault possibly formed through the reactivation of a pre-existing normal fault.

2.2.3.3. Pull-apart Basins

Pull-apart basins develop within sidesteps (jogs) of major strike-slip faults (Dooley and McClay, 1997). Extension between the two major offset faults produces rhombohedra shaped sag that is constrained by two parallel oblique-slip extensional faults steeply dipping to the centre of the pull-apart basin (**Fig. 7**) (Dooley and McClay, 1997). These structures may have formed during strike-slip stress regime conditions and subsequently reactivated to form local pockets of high angle reverse faults, strike-slip faults and dormant normal faults (Sun, 1997). The high intensity of strike-slip faults known to exist within the study area may have formed local, or reginal, depocenters that are presently poorly understood.

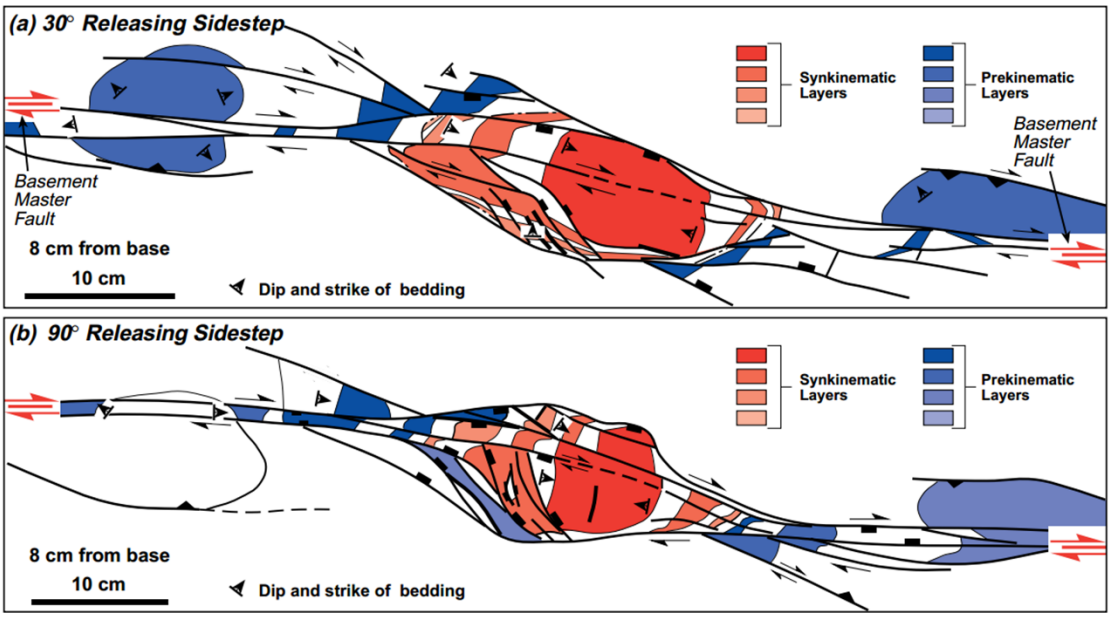


Fig. 7 The typical structural response to pull-apart basins at two different releasing angles (30° and 90°) (Dooley and McClay, 1997).

2.2.3.4. Imbricate Fan System (GMI Ridge)

Imbricate fan systems develop in compressional regimes where thrusts duplicate the shape and size of adjacent faults (Boyer and Elliott, 1982). In this case, thrust faults overlap and converge to a single, through going fault (Boyer and Elliott, 1982). Imbricate fans are separated into two types, leading and trailing (**Fig. 8**). These are distinguished by determining whether the majority of slip is at the back or the front of the system (Boyer and Elliott, 1982). A leading imbricate fan will have maximum slip on the front of the system. A trailing imbricate fan will have the largest slip at the back of the system. The GMI Ridge shows characteristics of a leading imbricate fan system (Sun, 1997). The quality of seismic data below the Permian coal measures prevents researchers from accurately interpreting the deep basement structures; however, as better resolution seismic data becomes available, it is likely that the structural history of the basin becomes better constrained.

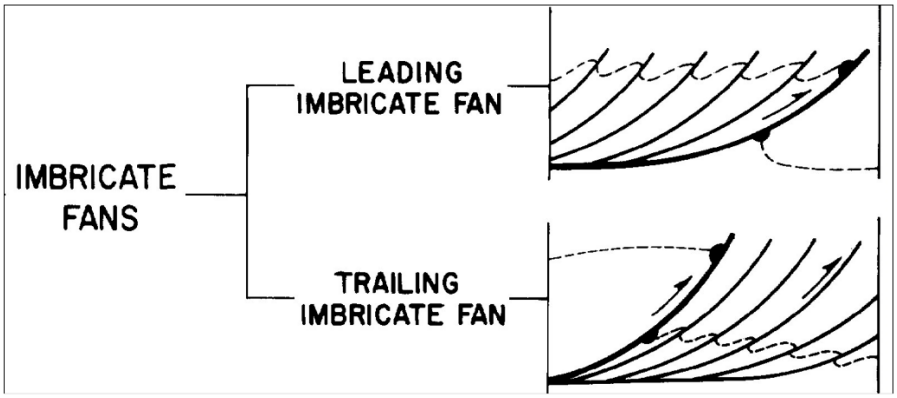


Fig. 8 Structure of leading and trailing imbricate fan systems (Boyer and Elliott, 1982).

2.3. THE COOPER BASIN

2.3.1. Introduction

The Late Carboniferous to Middle Triassic intra-cratonic Cooper Basin extends $130{,}00\ km^2$ across central and eastern Australia with unconformable boundaries separating it from the underlying Cambrian-Carboniferous Warburton Basin, and overlying Jurassic-Cretaceous Eromanga Basin (**Fig. 9a** & **Fig. 10**) (Kantsler et al., 1984; Bradshaw, 1993; Apak, 1997; Gravestock and Jensen-Schmidt, 1998; Mavromatidis, 2006; Reynolds et al., 2006). The South Australian portion of the Cooper Basin contains the greatest thickness of hydrocarbon bearing formations and therefore the majority of well data (Reynolds et al., 2006). This basin contains a highly complex stratigraphic architecture that is a result of several successive structural reorganisations (Kuang, 1985; Apak et al., 1997). As such, the structural and stratigraphic evolution is discussed in individual chapters. Within this low permeability hydrocarbon-rich basin there are 121 gas and 25 oil fields that have been developed since the first gas discovery at Gidgealpa 2 in 1963 (**Fig. 11**) (Gravestock et al., 2011). Gas is mostly reservoired within the Toolachee and Patchawarra Formations, with an estimated 80% of oil reservoired within the Early Permian Tirrawarra sandstone (Gravestock et al., 2011).

The NE-SW elongate Patchawarra, Nappamerri and Tenappera troughs are separated by the NE-SW striking Gidgealpa-Merrimelia-Innamincka (GMI) and Murteree-Nappacoongee (MN) ridges (Apak et al., 1997). Large inverted normal faults and strike-slip fault systems trend NE-SW and SE-NW, respectively (Apak et al., 1997). The Cooper Basin structural and depositional features are largely controlled by reactivation of pre-existing Warburton Basin normal faults that developed during the SE-NW Adelaidean extensional event; however, due to limited high-resolution 3D seismic data and a decrease in seismic resolution below Permian coals, fault growth models and accurate constraints on paleo-stress orientations have been difficult (Apak et al., 1997). The highly complex structural history of the basin has been simplified by combining tectonic events into three major compressional phases, post initial extension (Kuang, 1985 Sun, 1985; Apak et al., 1997): (1) Carboniferous N-S to SE-NW compression; (2) Permian compression/strike-slip (4 phases); (3) Jurassic-present-day E-W compression, with a N-S compressional pulse during the Paleogene.

Although the general timing of events has been somewhat constrained from 2D seismic interpretation, the paleo-stress orientations and magnitudes are yet to be accurately constrained. The use of hard data, such as natural fractures, faults, and calcite twins can be useful for defining the complex tectonic evolution of the basin (e.g. Amrouch, 2010; Arboit et al., 2015, 2017).

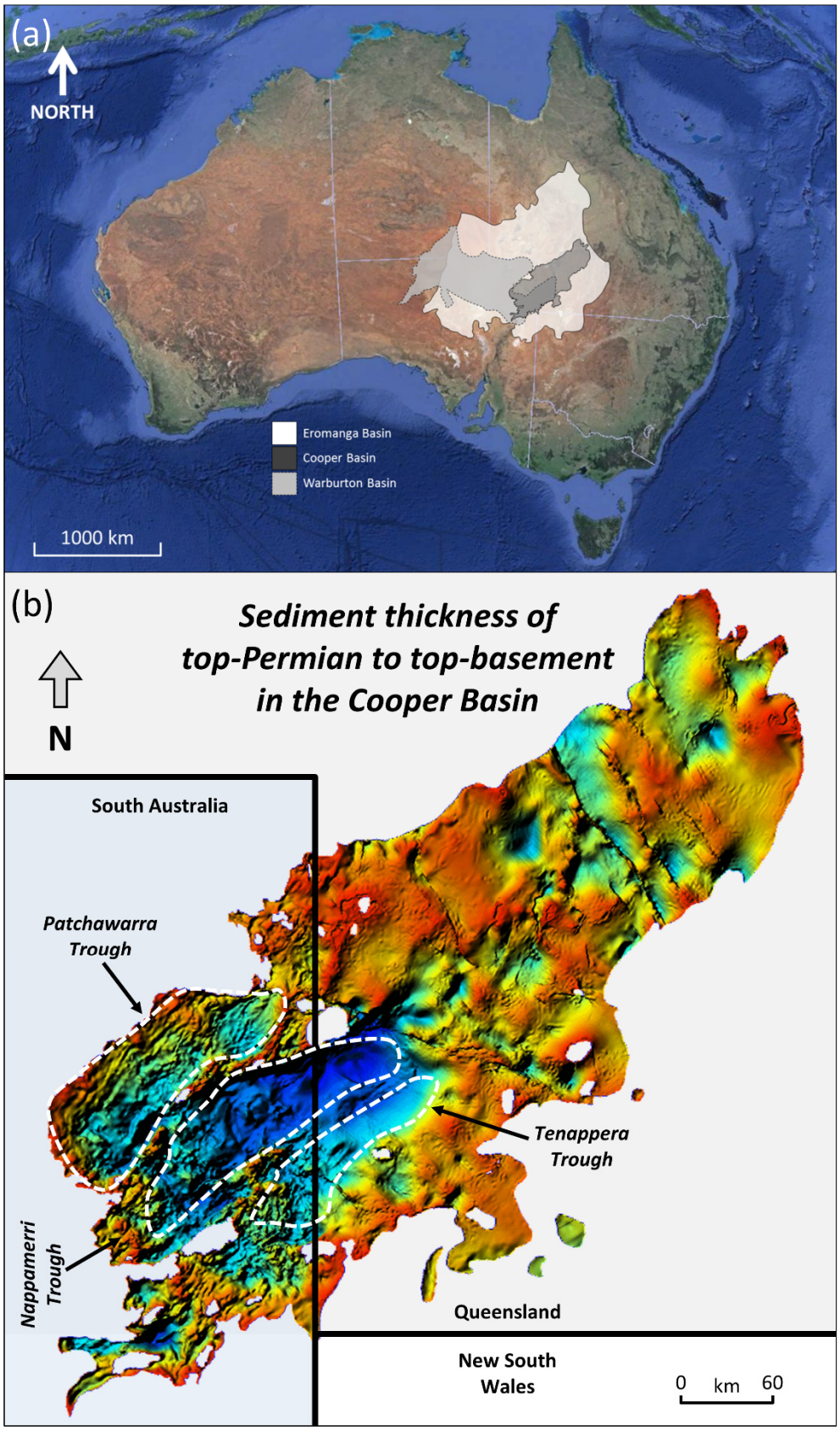


Fig. 9 (a) Location of Warburton, Cooper and Eromanga basins (Map: Google Earth); (b) Permian sediment thickness (blue: thick; red: thin; white: not present) within the Cooper Basin. NE-SW trending Patchawarra, Nappamerri, and Tenappera troughs are isolated by the Gidgealpa-Merrimelia-Innamincka and Murteree-Nappacoongee ridges, respectively. (SARIG, 2015).

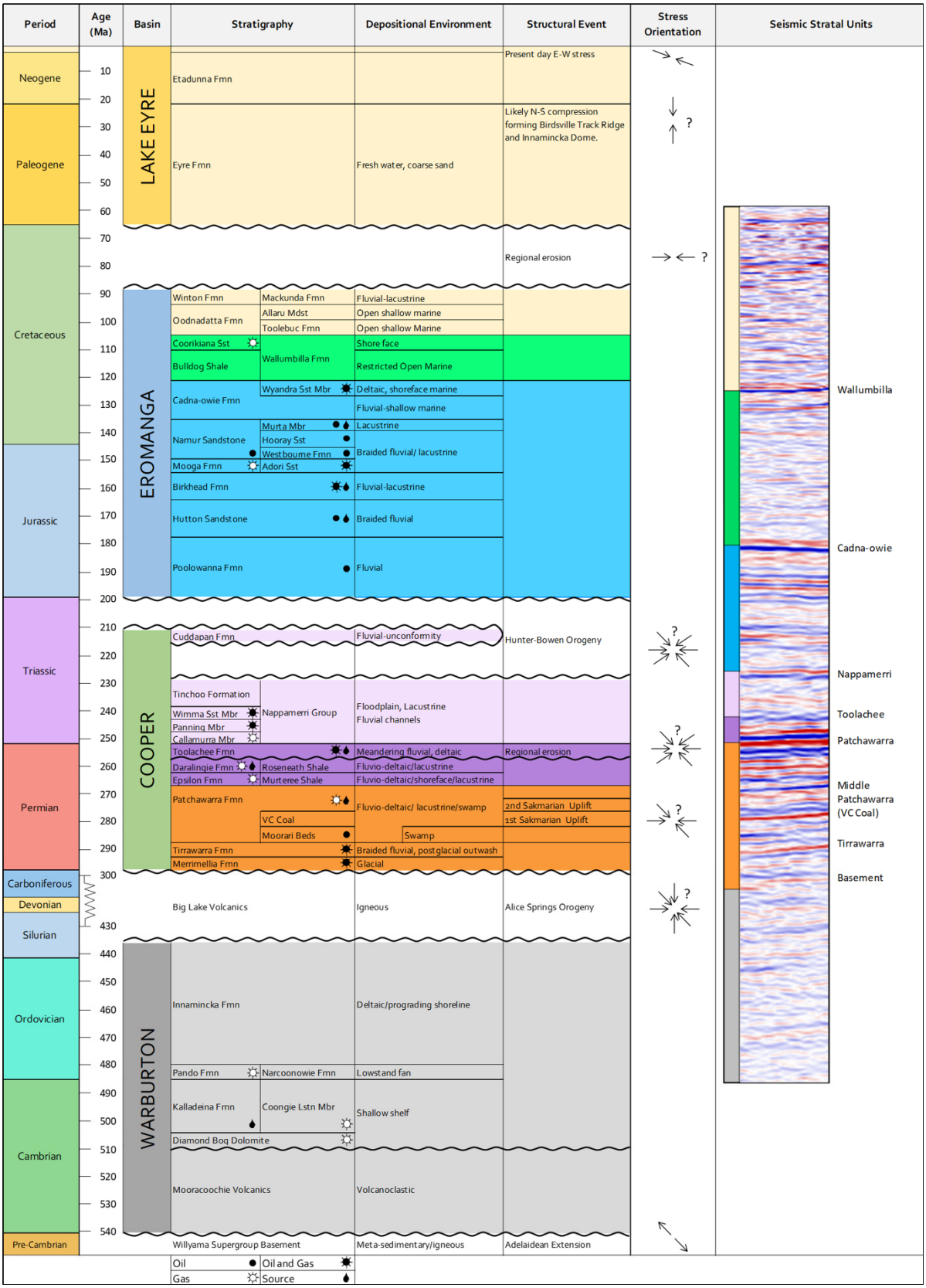


Fig. 10 Stratigraphy of the Warburton, Cooper and Eromanga basins and uncertainty associated with paleo-stress orientations.

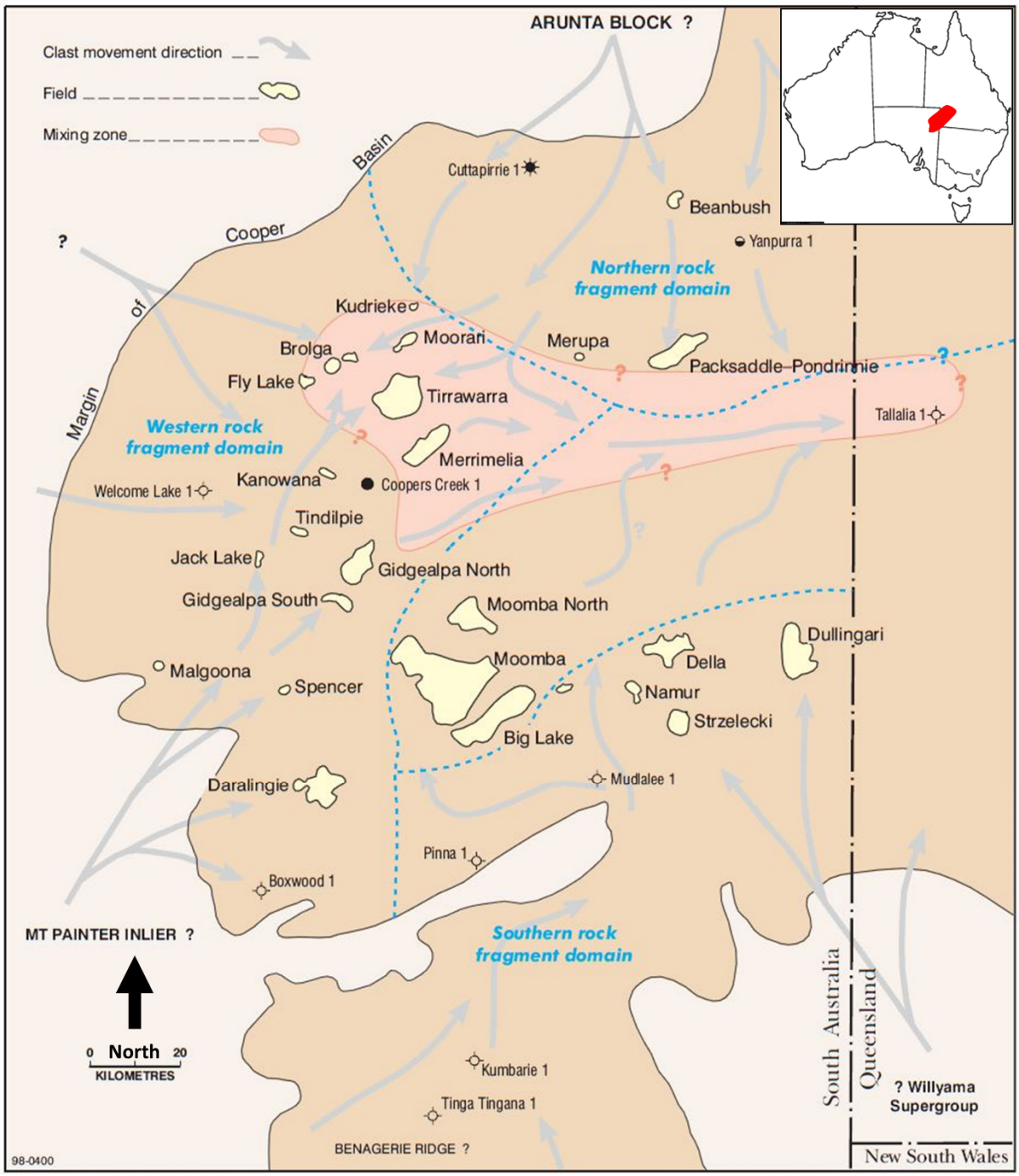


Fig. 11 Sediment transport and major petroleum fields of the Cooper Basin. Transport direction varies through time and controlled by structural highs (Alexander et al., 2011).

2.3.2. Structural Evolution

Kuang (1985) simplified the highly complex structural history of the Cooper Basin by combining structural events into the three major phases after the initial Pre-Cambrian extensional event (650 Ma), as mentioned earlier. Apak et al. (1997) concluded, "at least four events deformed the Permian to Triassic aged Cooper Basin strata". A summary of the structural history from five of the most influential and recent publications is given in **Table 1**. This summary highlights the uncertainty associated with the structural and stress history of the Cooper Basin. Considering that the Cooper Basin is entirely subsurface in the South Australian portion of the basin, the events have historically been identified through the integration of sparse 2D seismic data interpretation, with previous works, and continent scale tectonic events. This technique can lead to large uncertainties, as the far field tectonic source of stress may not necessarily be recorded in intracratonic basins (Tavani et al., 2015), and also the sparse 2D seismic data can show apparent rather than true fault geometries.

We integrated the works of many authors spanning nearly 50 years to summarise all potential structural events that may have affected the Cooper Basin. These include: (1) SE-NW Neo-Proterozoic extension (650 Ma); (2) Benambran Orogeny (440 Ma); (3) Late Silurian Orogeny (425-420 Ma); (4) N-S or SE-NW Alice Spring Orogeny (ASO) (400-300 Ma); (5) E-W or SE-NW Kanimblan Orogeny (340-300 Ma); (6) E-W or SE-NW First Sakmarian event (273 Ma); (7) E-W or SE-NW Second Sakmarian event (270 Ma); (8) NE-SW or E-W or SE-NW shortening creating the Daralingie unconformity (258 Ma); (9) E-W or SE-NW or NE-SW Hunter-Bowen Orogeny (245-190 Ma); (10) possible, but uncertain, N-S shortening (100-95 Ma); (11) E-W Late Cretaceous event (95-55 Ma); (12) E-W to SE-NW event (55-23 Ma); (13) N-S event (33-23 Ma); (14) SE-NW event (23-11 Ma); (15) NE-SW event (11-6 Ma); and (16) present-day ESE-WNW strike-slip to compressional stress (e.g. Gregory et al., 1967; Senior et al., 1968; Powell, 1984; Kuang, 1985; Shaw, 1991; Veevers et al., 1991; Apak et al., 1997; Gravestock and Jensen-Schmidt, 1998; Muller et al., 2012).

Although we present 16 possible stages of basin development, recent authors suggest that four to five major events, together with an initial period of extension, can explain the present-day structural architecture. Below, we present the most simplistic structural evolution model that agrees with the present-day architecture of the basin.

Initial accommodation space and NE-SW and NW-SE structural lineaments were developed in the Warburton Basin during SE-NW Neo-Proterozoic extension (650 Ma) focused along the NE-SW oriented Tasman Line (Apak et al., 1997; Haines et al., 2001; Muller et al., 2012). Following initial extension, compression during the N-S to SE-NW Silurian to Carboniferous ASO (350 Ma) rejuvenated pre-existing NE-SW striking lineaments to form the Gidgealpa-Merrimelia-Innamincka

Table 1 Structural history of the Cooper Basin summarised by various authors (Kuang, 1985; Apak et al., 1997; Gravestock and Jensen-Schmidt, 1998; Muller et al., 2012; Abul Khair et al., 2013).

EVENTS	Kuang (1985)	Apak et al. (1997)	Gravestock & Jensen-Schmidt (1998)	Muller et al. (2012)	Abul Khair et al. (2013)
Present-day	-	-	-	ESE-WNW stress	-
Neogene Event	-	-	-	SE-NW shortening generating broad-wave-length folding and faulting (23-11 Ma) switching to NE-SW stress (11-6 Ma)	-
Late Cretaceous to Paleocene Event	E-W compression most severe of the 3 events	-	Early Tertiary (E-W) compression enhanced closure on pre-existing structures and created other structures independently	N-S stress from ridge push along north Australian plate (100 Ma) changing to E-W stress caused by development of mid-ocean ridge east of Australia (95-55 Ma)	-
Hunter-Bowen Orogeny	Triassic NE-SW wrench induced compressional stress	E-W shortening during the late Middle Triassic (245 Ma)	Large-scale collision on the eastern plate margin creating the Nappamerri Group unconformity (212-190 Ma)	-	E-W compression
Daralingie Event	Reactivation of SW-NE faults & dominated by thrusting and wrenching	Low intensity limited to basin highs/ basin margins (258 Ma)	Significant hiatus recorded on crests and mid-flank areas of major ridges	-	E-W or SE-NW compression
Sakmarian Event		Two periods of uplift: 273 and 270 Ma	Two periods of uplift	-	E-W or SE-NW compression
Alice Springs Orogeny		-	Warburton Basin strata deformed by post-Ordovician NW compression correlating to the stress vector between E-W Kanimblan Orogeny and N-S Alice Springs Orogeny	-	SE-NW compression
Kanimblan Orogeny		E-W event (340-320 Ma)		-	SE-NW compression
Late Silurian Orogeny	-	Deformation and shortening	-	-	-
Benambran Orogeny	-	Deformation and shortening	-	-	-
Adelaidean Extension	-	SE-NW extension (650-575 Ma)	-	-	-

(GMI) and Murteree-Nappacoongee (MN) Ridges (Apak et al., 1997). These ridges now isolate the Patchawarra, Nappamerri and Tenappera Troughs (**Fig. 9b**) (Mavromatidis, 2006; Reynolds et al., 2006). The ASO also exhumed Carboniferous granite intrusion (Big Lake Granite Suit) that increased local hydrothermal activity and promoted carbonate precipitation within existing natural fractures (Rezaee and Sun, 2007; Glikson et al., 2013). This episode of exhumation is marked by a regional unconformity that separates the Cooper and Warburton Basins (Kuang, 1985; Apak et al., 1997; Sun, 1997; Mavromatidis, 2006).

A period of SE-NW to E-W shortening is inferred from erosional unconformities during the Sakmarian (270 Ma) (Apak et al., 1997). Regional erosion of the Middle to Late Triassic Daralingie Formation was suggested by Kuang (1985) to have resulted from a wrench induced NE-SW shortening event (258 Ma); however, it is possible that this was the result of E-W or SE-NW compression (Apak et al., 1997; Mavromatidis, 2006). The maximum burial depth of Cooper Basin strata was reached in the Late Triassic, prior to the E-W (or SE-NW or NE-SW) Hunter-Bowen Orogeny (220 Ma), which exhumed 2700 m of sediments and tilted the basin towards the NNE (Apak et al., 1997; Mavromatidis, 2006). Apak et al. (1997) highlighted the uncertainty of predicting stress directions based on seismic interpretation of present-day faults and folds by suggesting that the Hunter Bowen Orogeny was either E-W or SE-NW oriented. Collins (1991) researched the effect of the Hunter-Bowen Orogeny on the Sydney Basin, concluding that the maximum horizontal stress varied from E-W to NE-SW through time.

Exhumation eased during the Lower Jurassic (200 Ma) during an extended period of ‘sag’ that deposited fluvial, lacustrine, and marine sediments, reaching maximum burial depths in the Upper Cretaceous (Mavromatidis, 2006). This prolonged period of deposition ended with the onset of the E-W Upper Cretaceous event, which is considered to be the most severe event affecting the Permian-Triassic Cooper Basin (Kuang, 1985; Apak et al., 1997; Gravestock and Jensen-Schmidt, 1998; Mavromatidis, 2006). Existing folds and faults were enhanced and independent structures created (Gravestock and Jensen-Schmidt, 1998; Muller et al., 2012). Post the critical moment (90 Ma) in the hydrocarbon system, three events jeopardised hydrocarbon preservation. These include: (1) E-W or SE-NW event (95-23 Ma) that inverted pre-existing N-S striking normal faults and created NE-SW oriented folds (Gregory et al., 1967; Senior et al., 1968); (2) N-S or SE-NW event (23-11 Ma); and (3) a present-day ESE-WNW compression to strike-slip stress regime (Lowe-Young et al., 1997; Reynolds et al, 2004; Muller et al, 2012).

2.3.3. Stratigraphic Evolution

Collision between Gondwana and Laurasia during the Middle Carboniferous initiated uplift in central Australia during a major continental glaciation (Apak et al., 1997; Alexander et al., 2011). Ice sheets retreated during the Asselian to Sakmarian, leaving localised ice blocks on structural highs (Alexander et al., 2011). The regional unconformity that exists between the Warburton and Cooper Basins marks a structural event (ASO) that caused widespread deformation of basement units and formed erosional scours for the glacial early Permian Merrimelia Formation to be deposited (Apak et al., 1997; Alexander et al., 2011).

The Merrimelia Formation marks the base of the Permian Cooper Basin, together with Early Paleozoic volcanic and Carboniferous granitic intrusions (Kantsler et al., 1984). Deposition of the Merrimelia Formation is absent from the Moomba, Toolachee and Murteree area, inferring that these regions were topographic highs during the Late Carboniferous to Early Permian age (Kantsler et al., 1984; Apak et al., 1997). The Tirrawarra Formation transitioned from glacial to fluvial dominated and thickens in the Patchawarra and Nappamerri troughs during a period of structural quiescence (Apak et al., 1997). Thick Merrimelia and Tirrawarra formation sandstones exist along the GMI ridge, inferring that this was not a pronounced feature during the early deposition of Cooper Basin sediments (Apak et al., 1997). Australia transitioned into a peat swamp and floodplain environment during the Early Permian to Early Triassic (Alexander et al., 2011).

Lacustrine delta sediments alternate in organic rich shales, coals and sands and form the Permian Patchawarra Formation, which holds the largest hydrocarbon volume in the Cooper Basin (Boreham and Hill, 2011). Initial deposition was wide spread, with sediments increasing in thickness towards continually sinking depocenters, particularly within the Pinna area (**Fig. 11**) (Apak et al., 1997). Lower Patchawarra Formation units began to onlap across the GMI and NM ridges, marking the first Sakmarian uplift event (Apak et al., 1997). Wrench induced down warping increased during the middle Patchawarra Formation deposition, with sands thickening to the north and south of the basin (Apak et al., 1997). Sands continued to thin across pre-existing highs in the Della, Daralingie, Gidgealpa and Toolachee areas (Apak et al., 1997). The middle Patchawarra Formation thick interbedded organic rich shale and coal packages that source and seal hydrocarbons to adjacent sandstones (Bradshaw, 1993; Gravestock and Jensen-Schmidt, 1998; Boreham and Hill, 2011).

The second Sakmarian compression is most evident along the GMI and NM ridges and the northern flank of the Patchawarra Trough, where middle Patchawarra Formation units markedly pinch out (Kantsler et al., 1984; Apak et al., 1997). Compression and down warping continued until the upper Patchawarra Formation blanketed most structural highs (Apak et al., 1997). Sedimentation reached a

maximum rate of 80m/million years at this time (Kantsler et al., 1984). The depositional environment transitioned to mostly shoreline and deltaic deposits, controlled primarily by syn-depositional faulting and pre-existing structural features (Apak et al., 1997). The upper-most Patchawarra Formation channels become heavily influenced by local faulting during the transgressive transition into the overlying lacustrine Murteree Shale (Apak et al., 1997). The transgression was from the east to north, maintaining shoreline and distributary mouth bar deposition across the southern and western portion of the basin before succumbing to a regional sea level rise (Bradshaw, 1993; Apak et al., 1997; Gravestock and Jensen-Schmidt, 1998).

Easterly regression returned the western and southern regions of the basin to shoreline, distributary and deltaic conditions and deposited the Epsilon Formation reservoirs (Apak et al., 1997). A similar transgression to the Murteree Shale followed, depositing the Roseneath Shale (Apak et al., 1997). Regression brought back conditions similar to the Epsilon Formation deposition, depositing cycles of regressive sandstones, shales and coals that form the Daralingie Formation (Apak et al., 1997). Compression during the late Permian reactivated major faults and eroded much of the Daralingie Formation across all structural highs until the Cooper Basin was peneplaned (Apak et al., 1997).

Late Permian sedimentation of the fluvial Toolachee Formation marks the transition to structural quiescence and pronounced sag (Apak et al., 1997). Cyclic sand, shale and coal were deposited in a dominantly meandering river environment and show thickening in the Nappamerri Trough and Toolachee area (Kantsler et al., 1984). Thinning of the Toolachee Formation is observed along many anticlines, inferring structural growth, with the upper Toolachee Formation transitioning to lacustrine dominated shales and coals (Kantsler et al., 1984; Apak et al., 1997). Nappamerri Group sediments (Triassic) consist of sand, variously coloured shales and a distinct lack of coals, indicating an oxidising, warm and humid environment in the Early to Middle Triassic (Kantsler et al., 1984; Apak et al., 1997). Maximum sedimentation rate of the Nappamerri Group reached 30 m/million years (Kantsler et al., 1984). The Nappamerri Group is regionally deposited and thickens to the north, inferring that the drainage system shifted to the rapidly sinking northern Cooper Basin during this time (Apak et al., 1997). Maximum burial depth was reached in the Triassic (~235 Ma), prior to Late Triassic compression (**Fig. 12**) (Mavromatidis, 2006).

This compression reactivated major pre-existing faults and eroding up to 500 m of sediments in the southern basin (Kantsler et al., 1984; Apak et al., 1997). This E-W compression induced major down-warping of the east Cooper Basin, marking an unconformable boundary between the Cooper and Eromanga Basins (Kantsler et al., 1984; Apak et al., 1997; Alexander et al., 2011).

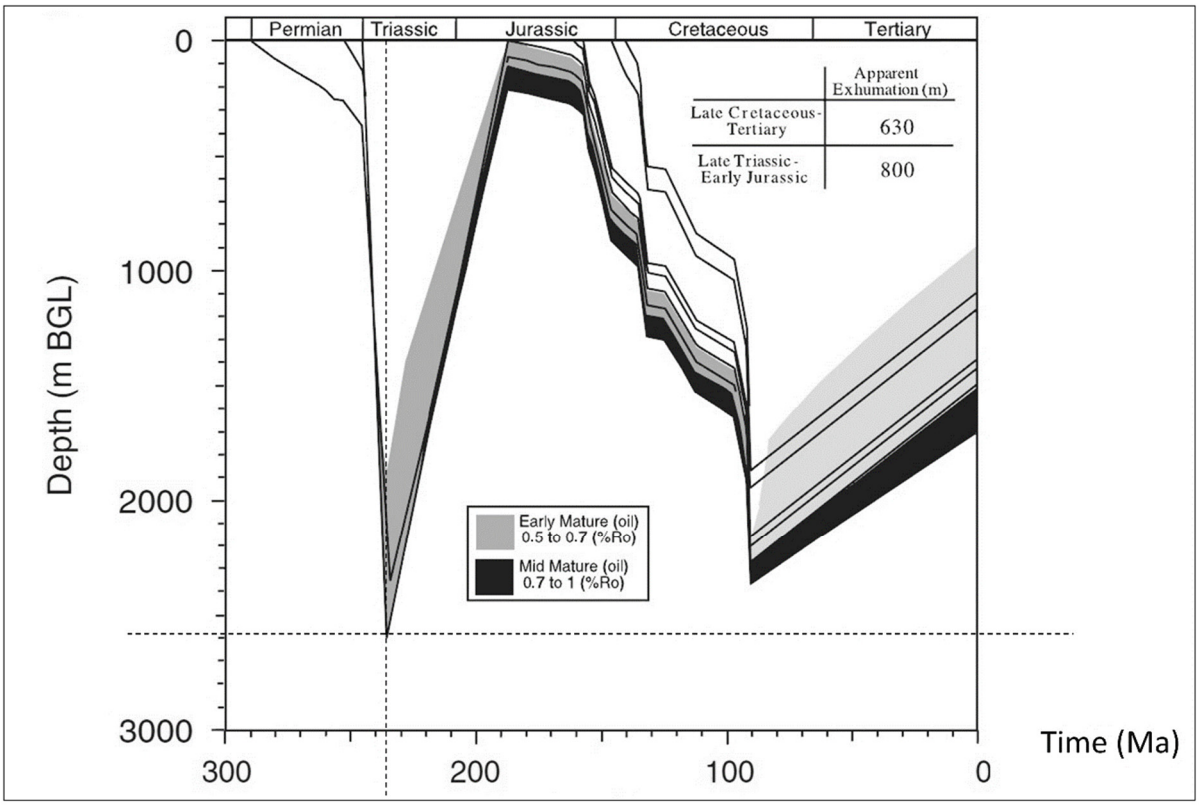


Fig. 12 The burial history of the Cooper and Eromanga Basins (after Mavromatidis, 2006).

2.4. THE EROMANGA BASIN

2.4.1. Introduction

The Eromanga Basin overlies the Cooper and Warburton basins and spans an area of $1{,}000{,}000\ km^2$ across central Australia (**Fig. 9a**) (Lowe-Young et al., 1997). Deposition was uninterrupted and coincides with a prolonged period of tectonic quiescence between the Jurassic and Cretaceous periods. The lower portion of the basin is host to the multi-aquifer system that comprises the Great Artesian Basin as well as several hydrocarbon-hosting reservoirs, particularly within the Cooper Basin region where most exploration activity has been focused (Alexander and Hibburt, 1996; Lowe-Young et al., 1997). Hydrocarbon exploration commenced in the 1950's with over 1000 wells being drilled; however, it was not until 1976 that the first commercial hydrocarbon was produced from the Namur 1 well (Alexander and Hibburt, 1996). The basin is now known for its extensive oil potential particularly within the high permeability (up to 2500 mD) braided fluvial Hutton and Namur sandstones (**Fig. 10**) (Green et al., 1989; Alexander and Hibburt, 1996). Significant reserves have also been discovered within the Poolowanna, Birkhead and Murta formations, and the McKinlay Member (Green et al., 1989). These are typically structurally enclosed by low amplitude four-way-dip anticlines or drapes over pre-existing structural highs (Lowe-Young et al., 1997).

2.4.2. Tectonostratigraphic Evolution

As the Late Triassic Hunter-Bowen Event subsided, accommodation space developed through basin-wide sag, depositing of the fluvial Poolowanna Formation onto the regional unconformity that separates the Cooper and Eromanga basins (Green et al. 1989; Hoffman, 1989; Lowe-Young et al. 1997). Accommodation space continued to grow during a prolonged period of tectonic quiescence that saw the depositional environment transition to a braided fluvial, fluvial-lacustrine, and braided fluvial-lacustrine, depositing the Hutton Sandstone, Birkhead Formation, and the Mooga Formation and Adori Sandstone, respectively (Green et al. 1989; Hoffman, 1989; Lowe-Young et al. 1997). Braided fluvial-lacustrine conditions continued during the Lower Cretaceous, depositing the Namur Sandstone, Westbourne Formation, Hooray Sandstone, and the oil-rich Murta Member (Lowe-Young et al., 1997). The Murta Member is an organic-rich source rock that may be sourcing overlying reservoir quality sandstones through potentially permeable fault conduits (Watterson et al., 2000).

Overlying the Murta Member is the fluvial-shallow marine Cadna-Owie Formation, which has a strong reflectance in seismic data (Green et al., 1989; Lowe-Young et al., 1997). The depositional environment continued to change, transitioning to deltaic and shoreface marine conditions that deposited the Wyandra Sandstone Member, which contains some oil and gas potential (Lowe-Young et al., 1997). Following this, restricted open marine conditions deposited the fine-grained Bulldog Shale and Wallumbilla Formation, which then transitioned to shoreface conditions, deposited the overlying Middle Cretaceous Coorikiana Sandstone (Green et al., 1989; Lowe-Young et al., 1997). Shallow open marine conditions then deposited the Oodnadatta Formation, Toolebuc Formation, and Allaru Mudstone (Lowe-Young et al., 1997). An intense system of polygonal faults is present within the Middle Cretaceous interval that likely developed through a density inversion that resulted in dewatering (Watterson et al., 2000). The system is largely layer bound but can extend into the underlying Cadna-Owie Formation and into the oil-rich Murta Member (Watterson et al., 2000).

Finally, the fluvial-lacustrine Late Cretaceous Winton Formation was deposited onto the Mackunda Formation before being exhumed and partially eroded by a Late Cretaceous E-W oriented event, which forms the boundary between the Eromanga and Lake Eyre basins (Lowe-Young et al., 1997). Prior to exhumation, the Winton Formation was deposited at a rate of 200 m/million years (Kantsler et al., 1984). NE-SW trending anticlines and fault-bounded anticlines were developed across the region and form present-day low amplitude hydrocarbon traps (Lowe-Young et al., 1997). After the critical moment in the hydrocarbon system (90 Ma), a N-S oriented Paleogene event enhanced structures (Innamincka Dome and Birdsville Track Ridge) and potentially reactivated pre-existing faults that may have jeopardised hydrocarbon preservation (Alexander and Hibburt, 1996).

2.5. PRESENT-DAY STRESS

Present-day stress propagation through the Indo-Australian plate originates from mid-ocean ridge push and resisting continent-continent collision forces along the New Zealand convergent plate boundary (**Fig. 13a**) (Reynolds et al., 2002; Reynolds et al., 2006; Hillis et al., 2008). The Cooper Basin is subject to a present-day strike-slip to reverse stress regime oriented approximately E-W (**Fig. 13b**) (Reynolds et al., 2006; Muller et al., 2012). The strike of the New Zealand collisional boundary is approximately normal to the maximum horizontal stress direction (σ_H), inferring that it may have a primary control on intraplate stresses (Hillis et al., 2008). This σ_H rotates to an N-S orientation on the eastern and western margins of the basin (**Fig. 14**) (Reynolds et al., 2005).

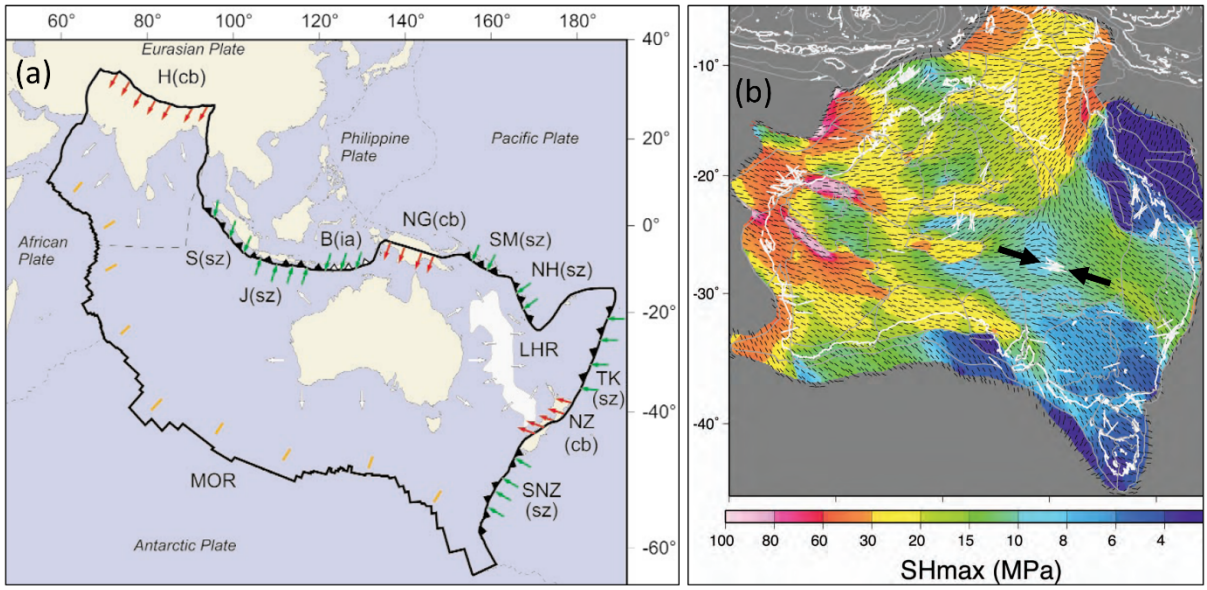


Fig. 13 (a) Orientation of reginal stresses originating from tectonic plate boundaries (Reynolds et al., 2003); and (b) Present-day stress map of Australia showing an ESE-WNW maximum horizontal stress direction (Muller et al., 2012).

Several authors have quantified the present-day stress magnitudes in the Cooper Basin (Van Ruth et al., 2003; Flottmann et al., 2004; Reynolds et al., 2004; Reynolds et al., 2006; Nelson et al., 2007; Backe et al., 2010; King et al., 2011; Abul Khair et al., 2013). The vertical stress (σ_v) is commonly worked using a function between depth, density and pore pressure (Zoback et al., 2003). The minimum horizontal stress (σ_h) is typically calculated from petroleum well data such as leak-off tests (LOT's), hydraulic fracture information and pressures while drilling (PWD) (Zoback et al., 2003). The σ_h is particularly useful during hydraulic fracture treatments as it provides an approximate wellbore pressure required to initiate fractures into the formation (Zoback et al., 2003). The σ_h ranges from 0.55-1.2 psi/ft in the Cooper Basin and is suggested to be approximately equal to σ_v, giving an

alternating stress regime between strike-slip and compression (Flottmann et al., 2004; Nelson et al., 2007; Reynolds et al., 2006). However, well test data may be misleading, as the pressures may represent closure of pre-existing natural fractures, rather than initiation of induced fractures (Nelson et al., 2007). Estimates of the σ_v, σ_h and pore pressure are used to approximate the σ_H by following the frictional limit theory (Sibson, 1974). Drilling induced tensile fractures and borehole breakout patterns from image logs can also be used to calculate the σ_H (Nelson et al., 2007).

The differential stress ($\sigma_H - \sigma_h$) in the upper crust is approximately 50 MPa at 2.8 km and thus capable of transferring high stress from convergent Indo-Australian plate boundaries to the plate centre (Reynolds et al., 2006). Late Cretaceous tectonic loading increased the mean stress (~50 MPa at 2.8 km) and potentially contributed to over pressure in the Cooper Basin (van Ruth, 2003). Local variations in stress orientation may be linked to stress perturbation by faults, local rock heterogeneities or structural anomalies, which may be the result of contradicting stress orientations observed within the Patchawarra Trough (NW-SE), GMI Ridge (WNW-ESE) and Nappamerri Trough (E-W) (Reynolds et al., 2005).

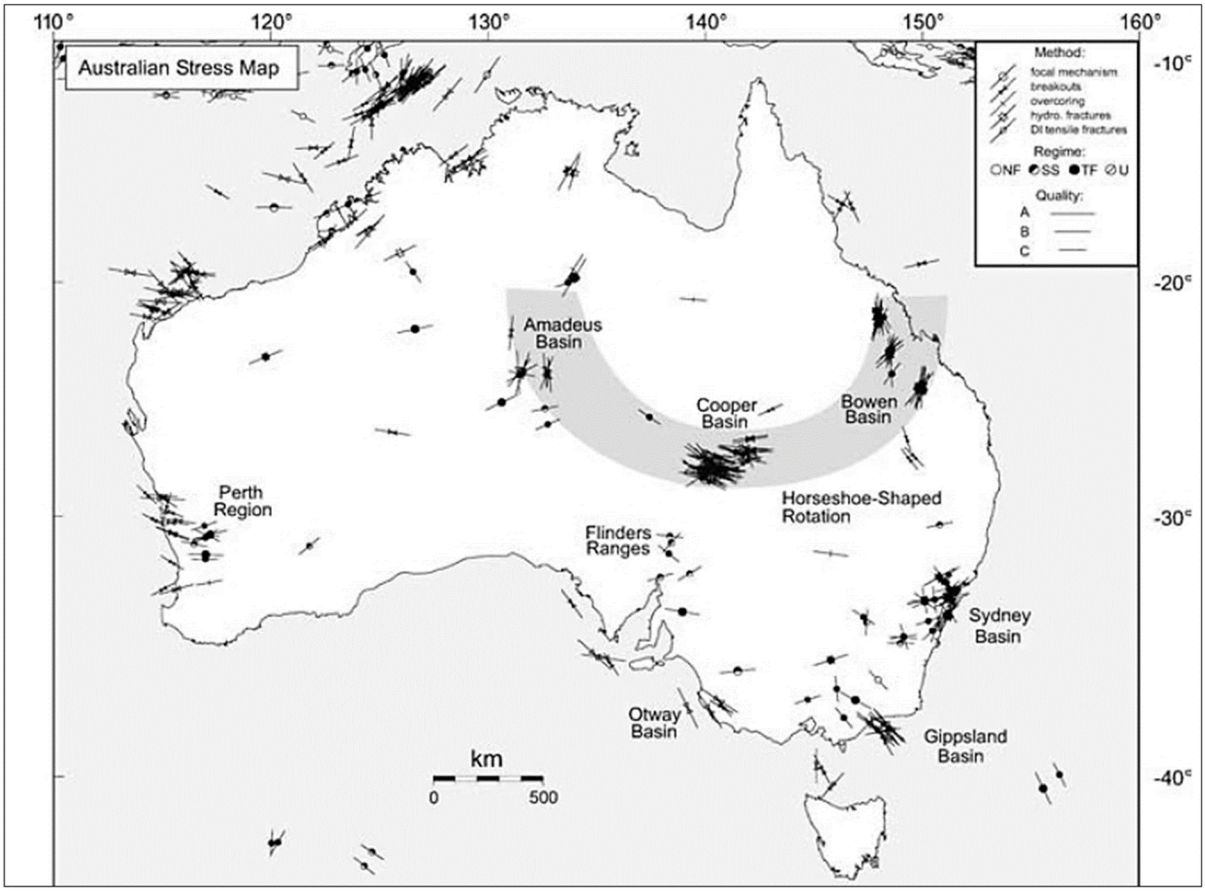


Fig. 14 Maximum horizontal stress orientation in Australia (Reynolds et al., 2005).

2.6. PETROLEUM SYSTEM

2.6.1. Source Rocks

Hydrocarbon in the Cooper Basin is principally sourced from intra-formational coals and carbonaceous shales containing type III kerogens (Boreham and Hill, 2011). A large volume of gas is present with relatively small volumes of liquids that are only found in localised areas (Kantsler et al., 1984). Isotopic composition of intra-formational coals and carboniferous shales indicates fresh water origin and dominated by high order plants (Kantsler et al., 1984; Boreham and Hill, 2011). The Toolachee, Daralingie, Epsilon and Patchawarra formations contain an average total organic content (TOC) of 3.9% and 6.9 kg/tonne of hydrocarbon calculated from S2 pyrolysis (Boreham and Hill, 2011). The Nappamerri Trough is over mature and contributes only dry gas (Boreham and Hill, 2011). The most organic rich source rock is found within the Toolachee Formation, averaging 214 kg/tonne (Hydrogen index) across the Cooper Basin (Boreham and Hill, 2011). Liquid hydrocarbon yields remain low in Permian reservoirs due to high vitrinite and inertinite (Type III kerogens) composition in all shale and coal measures (Kantsler et al., 1984).

The hydrocarbon source for the overlying Eromanga Basin is questionable; however, it is likely that the hydrocarbon is either sourced from non-marine Jurassic aged rocks, has migrated (tertiary migration) from Permian shales and coals through fault conduits and across unconformities, or a combination of both (Kantsler et al., 1984). Jurassic aged units contain oil and gas; however, only gas has been discovered in Cretaceous aged formations in the Strzelecki, Packsaddle and Nappacoongee regions (Kantsler et al., 1984). Permian aged source rocks are currently within the gas window, with Upper Jurassic to Lower Cretaceous source rocks currently at peak oil generation (Kantsler et al., 1984). Fracture stimulation of source rocks is currently being trialled as an unconventional target.

2.6.2. Sealing Rocks

Intra-formational fluvial-lacustrine to lacustrine shales and coal measures form cyclically deposited low permeable seals, as well as acting as source rocks to the overlying reservoirs (Bradshaw, 1993; Gravestock and Jensen-Schmidt, 1998). Vertically stacked intra-formational shales and coals have the highest influence on sealing hydrocarbons in the Cooper Basin (Gravestock et al., 2011). The Murteree and Roseneath shales are highly efficient seals to the Patchawarra and Epsilon formations respectively; however, intra-formational shales hold back hydrocarbon to individual and compartmentalised intra-formational sandstone reservoirs (Gravestock et al., 2011). The Jurassic Arrabury Formation and Cretaceous Bulldog Shale form regional seals to Eromanga Basin reservoirs and the Toolachee Formation respectively (Gravestock et al., 2011).

2.6.3. Hydrocarbon Migration

Permian and Triassic aged source rocks reached the hydrocarbon generation window as early as the Middle Triassic during maximum burial (**Fig. 12**) (Mavromatidis, 2006). Hydrocarbon generation levels increased upon a secondary sag period in the Middle Cretaceous (Deighton and Hill, 2011). Relatively minor hydrocarbon generation and migration begun in the Middle Triassic, peaked in the Late Cretaceous, and continues today (Lowe-Young et al., 1997; Mavromatidis, 2006).

Structural traps developed prior to the Late Cretaceous aged critical moment, with hydrocarbon accumulations withstanding three subsequent structural events (**Fig. 15**) (Lowe-Young et al., 1997). A better understanding of paleo-structures prior to the Tertiary aged compression is necessary to better constrain migration pathways, locating accumulations and assessing the preservation potential of hydrocarbon accumulations (Lowe-Young et al., 1997). Reactivation of faults after the critical moment is believed to have developed migration pathways for hydrocarbons into Eromanga Basin reservoirs; however, very little research has been conducted on the reactivation potential of faults and the timing of fault movement (Boreham and Hill, 2011).

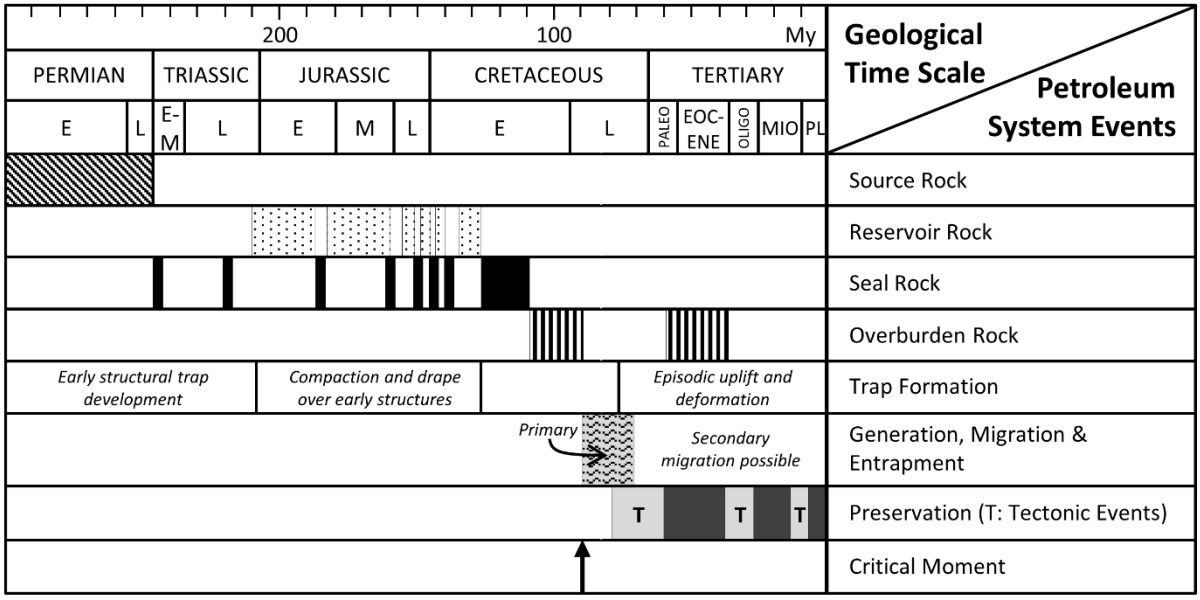


Fig. 15 Cooper-Eromanga petroleum system events (modified after Lowe-Young et al., 1997).

2.7. NATURAL FRACTURES

A confidential report was compiled on the natural fractures within the Cooper Basin by Hillis et al., (1997). Little regional work has been done on fracture distribution in the Cooper Basin (Flottmann et al., 2004; Nelson et al., 2007; Backe et al., 2010; King et al., 2011; Abul Khair et al., 2012; Abul Khair et al., 2013), although Sun (1999) analysed many wells in the underlying Warburton Basin. Two sets of high angle orthogonal fractures were found to exist in the Warburton Basin, with set 1 striking NNE-SSW and ESE-WNW, and set 2 striking NE-SW and NW-SE (Sun, 1999). A key finding from this work was the confirmed presence of calcite cement within natural fractures (Sun, 1999). Backe et al. (2010) analysed image logs from Big Lake 54 and Moomba 74 and integrated the results with 3D seismic data attribute analysis. Natural fracture orientations in the Moomba-Big Lake area were found to strike N160^{o}, N20^{o}, N100^{o} and a set striking N80^{o} and N140^{o} (Backe et al., 2010). The timing of natural fracture development and the complete natural fracture geometry (strike and dip angle relative to bedding plane) was overlooked. King et al. (2011) analysed the strike of natural fractures within the Moomba/Big Lake Field using image log interpretation and seismic attribute analysis, finding that NE-SW and SW-NE striking fractures are abundant and pervasive through the local area.

Abul Khair et al. (2012) followed on from the work of King et al. (2011) by integrating most positive and most negative curvature with borehole image log interpretation to constrain natural fracture geometries along seismic time-slices within the Moomba/Big Lake Field. This study also investigated the accuracy and appropriateness of using seismic attributes to infer the presence of natural fractures. Their findings showed a close correlation between seismic attributes, particularly most positive curvature, and the natural fracture strike interpreted from borehole image logs within the Moomba/Big Lake Field. This positive result presents an opportunity to map the spatial and temporal distribution of natural fractures across most of the basin (where 3D seismic data is available). Abul Khair et al. (2015) performed stress inversion of natural fractures in the Moomba/Big Lake Field to conclude that four major events are responsible for present-day fracture and fault geometries. NNE-SSW and ESE-WNW striking fractures were found with dip angles typically below 60° (Abul Khair et al., 2015).

Fracture sets from 3D seismic data are defined based only on strike geometry, which leads to assumptions that may present erroneous results. To consider low and high dipping fractures as belonging to the same set, given that they have similar strike orientations, is an obvious error. A regional natural fracture study using hard data (borehole image logs and core) will provide better constraints on the regional natural fracture sets present in the low permeability basin.

3. METHODOLOGIES

3.1. INTRODUCTION

The following chapter integrates a series of methods that were used to reach the aim of this thesis, which was to provide a modern approach for understanding the structural geology and tectonic evolution of entirely subsurface provinces where direct measurement from outcrop is not possible. The methodology is strongly geophysical based but also includes data taken from well core. Most of the manuscripts presented in this thesis provide novel approaches that use existing software and methods to combat the limitation of data accessibility. Other than the lack of outcrop, the seismic data quality is significantly reduced by thick Permian coal measures that prevent detailed analyses (i.e. fault growth). Therefore, to generate new finding required considerable abstract thinking and pushing the limits of scientific research. The methodology can be broken down into three areas; (1) application of the calcite twin stress inversion technique to measurements obtained from core samples to constrain the paleo-stress tensors; (2) a series of geophysical analysis techniques applied to 2D/3D seismic data; and (3) integration of geophysical methods with geomechanical models and complete paleo-stress tensors to define structural happenings through time and present-day. The scale of inspection between these methodologies are large and require care when upscaling from local (calcite twin data) to regional (seismic fault data) scales. Upscaling results is difficult; however, uncertainty can be reduced by obtaining/analysing a large dataset that spans the entire area. Three data scales (calcite twin, fracture and fault) are independently analysed before being integrated.

3.2. CALCITE TWIN STRESS INVERSION TECHNIQUE (CSIT)

3.2.1. Fundamentals of Calcite Twinning

3.2.1.1. CHARACTERISTICS AND DEVELOPMENT OF TWINNING

Calcite twinning is a plastic deformation mechanism responding to dislocation gliding that typically occurs at temperatures between 25 and 400^{o}C, in low-confining pressures, and with low (10 ±4 MPa) critical resolved shear stresses (RSS) (Turner, 1953; Turner et al., 1954; Lacombe and Laurent, 1996; Laurent et al., 2000; Amrouch, 2010; Lacombe, 2010). An observed twin is the manifestation of a dislocation wedge that migrates along the sliding plane (e twin) (**Fig. 16**); however, multiple twins are often present in a calcite crystal. The twin plane is a large atomic density plane that separates the twin domain from the host crystal, or the non-twin domain, and if the crystal is composed of only two twin components (twinned by reflection), the twin is said to be simple. If the crystal contains repeated twin components, the crystal contains multiple twins. If a twin is a small simple shear domain, the twin plane (atomic plane common to both parts) is the geometrical equivalent of the shear plane. The orientation of twin development follows well defined geometric laws (**Fig. 17**).

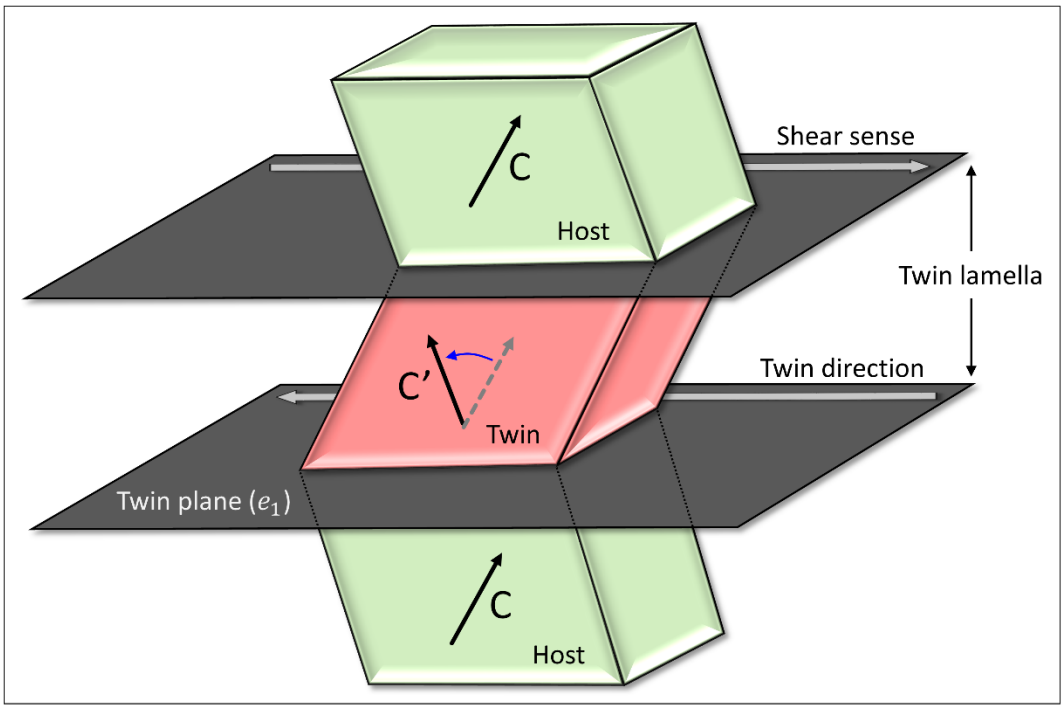


Fig. 16 Change in optical axis (C) between host and twin (C') portions of the crystal. The shear sense is towards the optical axis in the host crystal (modified after Lacombe et al., 1990; Amrouch, 2010).

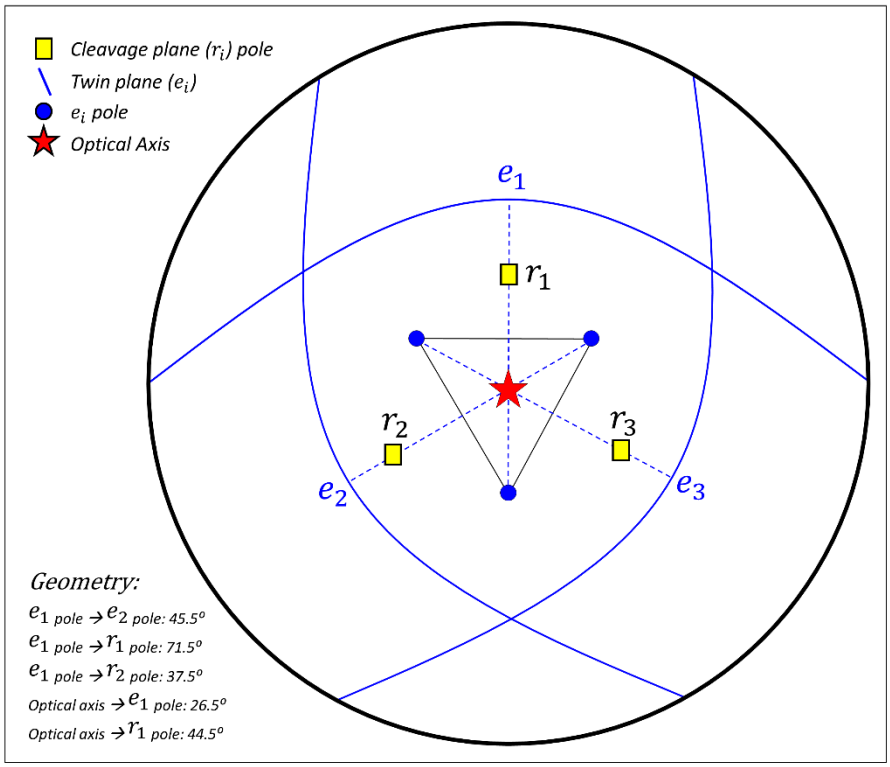


Fig. 17 Structural configuration of a calcite crystal (modified *after Turner and Orozco, 1976*).

The direction of twinning is defined as the straight line that binds the position of a given atom before twining and after slippage, and therefore corresponds to the sliding, or shear, direction (**Fig. 16**). This direction is represented by the twin plane that has a distorted optical axis relative to the host crystal (**Fig. 16**). It also coincides with the intersection of the twin plane e_1 and the cleavage planes r_2 or r_3. Each crystal has three potential twin planes $[01\bar{1}2]$ which are arranged symmetrically with respect to the optical axis (axis of ternary symmetry) (**Fig. 17**) (Amrouch, 2010). Twinning can only develop along these planes because of its atomic structure, and can be likened to a pre-existing fault that experiences subsequent reactivation that creates slickensides, which can be analysed to determine the shear direction. Where the optical axis of a calcite crystal is vertical, the relative displacement of atoms above the twin plane move towards the moving optical axis as in an 'inverse fault' (from bottom to top) (Turner et al., 1954). A twin lamella is geometrically similar to a micro-shear corridor, where the twinned crystal portion is situated between two twinned planes in which the atoms have been realigned to not reflect the alignment within the host crystal (non-twinned portion) (**Fig. 16**). Twinning will occur if the shear stress applied in the direction of twining reaches a critical value. The critical resolved shear stress (CRSS), or twinning threshold (τ_s), represents the stress that must be applied in the direction of twinning for a twin to develop. The CRSS value is obtained through **Eq. 1**:

$$\boldsymbol{\tau_a = \sigma * S} \qquad (Eq.1)$$

Where σ is the stress applied to the critical point and S the Schmid factor (Amrouch, 2010) (**Eq. 2**):

$$\boldsymbol{S = \cos(\alpha) * \cos(\beta)} \qquad (Eq.2)$$

Here, α is the angle between the direction of compression and the direction normal to the twin plane, and β is the angle between the compression direction and the twin displacement vector. Rowe and Rutter (1990) found that high S values relate to high twinning volumes. The twinning threshold value is largely independent of temperature, fluid pressure and isostatic pressure, but is dependent on the grain size and distribution (Newman, 1994), and on the internal deformation that causes the grain to harden (Laurent et al., 2000). A value of 10 MPa is typically used for grains with an average size is between 300-400 µm (Turner et al., 1954, Laurent, 1984, Lacombe and Laurent, 1996). The common threshold values used in inversions are typically between ~5-10 MPa, but must be adapted to the grain size and the percentage of deformation for each unique dataset (Lacombe, 2001; 2010). Laurent et al. (2000) demonstrated that the twinning threshold strongly depends on the internal strain (strain hardening) and fluctuates between 5-7 MPa for weakly deformed areas (~1% deformation) and 13-15 MPa in the moderately deformed zones (towards 4% deformation).

3.2.1.2. INFLUENCE OF VARIABLES ON RESULTS

3.2.1.2.1. Effect of Temperature

Temperature has an important role on the appearance of twins, but not on the development, as it is not a thermo-activated mechanism. However, the twinning density can be affected by the temperature as it is easier to create new twins than to widen existing twins at temperatures below 170-200^{o}C (Amrouch, 2010). The simple shear deformation is then absorbed by many very fine twins, so the twinning density increases. Conversely, at temperatures above 200^{o}C, it is easier to thicken the twins than to create new ones. High temperature conditions would therefore be captured in calcite as thick individual twins but a low twin density. The twin width and density can be used to infer temperature conditions (Ferrill, 1998; Ferrill et al., 2004; Janssen et al., 2007).

The average thickness of the calcite twins is directly correlated with the deformation temperature so that the fine twins are dominant at a temperature below 170^{o}C and that the thick twins dominate at temperatures above 200^{o}C. Beyond 250^{o}C, dynamic recrystallization becomes an important mechanism. The twinning density (n twin planes/mm) correlates inversely with temperature, and the combination of twinning intensity data with the thickness of twins can give information on both the intensity and temperature of deformation. This relationship can therefore provide an indication of paleotemperature conditions that rocks were exposed to (Amrouch, 2010).

3.2.1.2.2. Effect of Grain Size

Several experimental studies (Schmid & Paterson, 1977; Casey et al., 1978; Spiers, 1982; Spiers & Rutter, 1984; Rowe and Rutter, 1990) have shown that the twinning incidence and volume fraction increase with increasing grain size. Under the same differential stress conditions, the larger calcite crystals are therefore expected to contain a larger number of twins than small crystals. This is due to the relationship between grain boundary and grain volume, which is related to twinning. Therefore, as the grain size increases, the twinning threshold value would decrease, reiterating the importance of understanding grain size variations within samples when applying inversion methods. This is difficult in samples that exhibit a high grain size variation as the specified value is constant.

3.2.1.2.3. Effect of Internal Deformation

Several experimental studies have shown that it is easier to twin undeformed crystals than to develop new twins in heavily deformed or twisted crystals (strain hardening phenomenon) (Amrouch, 2010). It is therefore expected that the more distorted the crystals, the more difficult it is to develop new twins. Importantly, at higher temperatures or significant deformation, other mechanisms take over (sliding on the cleavage, r, planes) that may result in a curved shape of certain twins. Assuming that calcite crystals of different sizes have recorded the same differential

stress for a given tectonic event and considering the influence of grain size on the twinning threshold, the value that should be chosen for the latter will depend heavily on the grain size (Rowe and Rutter, 1990; Rocher et al., 2004). Amrouch (2010) compared the evolution of the twinning threshold value as a function of crystal size finding that the smaller the grain size the higher the twinning threshold. The findings also showed that the smaller the crystal size the lower the deformation rate for the same sample and for the same tectonic event.

In cases of polyphase tectonic events, where calcite crystals have recorded more than one event, it is necessary to consider the effect of crystal hardening by the first twining event, which will increase the threshold value for new twins to develop. These cases are only applicable for quantifying the complete stress tensors (paleo-principal stress magnitudes) and not in defining the orientation. Determining the threshold value that is required for defining the complete paleo-stress tensors therefore requires an understanding of the internal deformation exhibited within the calcite crystal. This can be done by considering the average thickness of the twins, the number of twins, and the thickness of the twins with respect to the diameter of the grain (Amrouch, 2010). The twinning incidence, the twin volume fraction and the twin density are independent of the deformation rate (Friedman and Heard, 1974; Tullis, 1980; Rowe and Rutter, 1990).

3.2.1.2.4. Effect of Differential Stress

Experimental data has shown that for any given grain size, temperature, or confining pressure, the differential stress ($\sigma_1 - \sigma_3$) is one of the factors that can significantly influence the number of twins per millimetre in a calcite crystal (twin density), the percentage of twin volume fraction, and the percentage of twinned incidence crystals (Rowe and Rutter,1990; Amrouch, 2010). Given that the grain size remains constant, an increase in differential stress will correspond to a higher twin density, higher volume of twinning, and higher twinning incidence. It should be noted that the formation of a mechanical twin is a discontinuous process at all scales. The initiation of a twinned micro-element requires higher stresses than the subsequent development and propagation of the twin from this micro-element. It is also important to note that the differential constraint threshold corresponds to the constraint necessary for the propagation of the twin after its initial development. The mechanical twins initiate in zones of concentrated stress, such as the mechanical discontinuities (grain boundaries, triple points, etc.) typical to all grains.

3.2.1.2.5. Effect of Isotropic Pressure and Fluid Pressure

Turner et al. (1954) showed that the normal stress on twin planes increases the critical shear stress necessary to twin by <1% of the value of this normal stress. Friedman and Heard (1974) confirm that the twins do not appear if the sample is subjected only to isotropic pressure (Amrouch, 2010).

3.2.2. Sample Collection and Processing

As the Cooper Basin does not outcrop at surface in our study area, calcite samples are obtained solely from oriented core (**Fig. 18**). Core samples are selected based on the availability of core, the presence of an image log or dip meter log for re-orientation, and the likelihood of a given formation to contain calcite filled fractures or matrix. Samples that are obtained from outcrop are easily orientable, but a requirement for subsurface province is that the core being sampled is oriented. In cases where the core is not oriented, the oriented borehole image logs and dip metre logs within the cored well can be used. This would require comparison of fracture and bedding planes in both the sampled core and the geophysical data. Once the samples are oriented to true north they are processed and converted into thin sections (**Fig. 19**) and the calcite crystals are measured using the universal stage microscope (**Fig. 20**), they form a significant dataset that is oriented to an arbitrary north dictated by the placement of the individual slides on the microscope. To re-orient the dataset back to the true north in which they were originally collected, a series of rotations were required and are unique for each thin section (**Fig. 21**).

Ideally the collected samples would cover a wide range of stratal units and be from different locations in the basin; however, data collection will always be subject to the availability of core, ability of the sample to be re-oriented, and the presence of calcite within fractures or matrix. If sample collection is not affected by these factors, they should ideally be situated within 3D seismic data coverage and within well that contain borehole image logs. This simply improves the reliability of upscaling the micro-scale calcite twin stress inversion results to the meso-scale natural fracture analysis, and finally to the macro-scale fault data obtained from seismic data. The integration of stress tensor results with the 3D geomechanical models, that are developed using 3D seismic data, also becomes more representative of the region. The dataset used in this study was chosen mostly based on the availability of borehole image logs, core and high quality seismic data, but nonetheless remained in close spatial proximity to one another (**Fig. 18**).

The Kalladeina Formation is limestone rich and grades from shale, siltstone and sandstone within the Warburton Basin (basement). The presence of calcite filled fractures within this formation is relatively more likely, and was therefore the primary target for sampling. Once core samples were selected (**Fig. 19a**), the core is re-oriented to true north and marked on the core sample (x, y, and z direction) for reference during thin section preparation. The core sample is marked with a rectangle approximately 6x3 cm across the calcite vein, or matrix, in three orthogonal planes; XY, XZ, and YZ planes. A diamond blade saw is used to cut the sample into three 6x4x1 cm rectangular prisms (**Fig. 19b**). These XY, XZ and YZ samples are marked to remain oriented. Additional notches are cut into

each orthogonal sample; 1 notch in the corner where the two directions converge, and either 1 notch (for the XY plane), 2 notches (XZ plane), or 3 notches (YZ plane) on the opposite side to the corner notch (**Fig. 19b**). The notches can then be transferred to thin sections (**Fig. 19c**). **Fig. 19d** illustrates the orthogonal geometry of the thin sections along the three (XY; XZ; YZ) planes.

A universal stage microscope was used for all calcite twin measurements (**Fig. 20**). This is a specialist microscope capable of measuring crystal optical properties and planar features, such as twin planes, principal optical angels and cleavage planes, using up to five-axes. Thin sections are firstly cleaned then placed on a layer of glycerine and held in place by an overlying glass hemisphere coated with glycerine, allowing light to pass without deviation. The orientation that the thin section is placed on the microscope must be noted as the measurements will be based on this arbitrary microscope north position. Before measuring twin data, the microscope should be centred correctly so that when rotating through the z-axis the view is rotated through the centre of the image and not oblique. Calcite twin (and un-twinned) planes, principal optical axes, cleavage planes (where possible), and crystal size are all measured from thin sections in preparation for Etchecopar's calcite twin stress inversion technique (**Fig. 19e**).

The calcite twins are typically linear features transecting the entire crystal and have a measurable dip and dip direction. The twinning can be more recognisable in cross-polarised light when the untwinned host calcite crystal is placed into extinction. The host crystal will appear dark (near black) with the twins present as bright colours. This is due to the realignment of atoms (and therefore optical axis) within the twin lamella relative to the host crystal (**Fig. 16**). Once twin planes are identified, the strike is easily measured by rotating the microscope platform through the z-axis to align the twin in a N-S direction and reading the rotated value. The dip angle is more difficult; while the twin is in the N-S direction, the microscope platform is rotated through the y-axis until the twin reaches the smallest observed thickness. The dip angle can be towards the microscope east or west.

Fig. 23 depicts the process involved in measuring each calcite crystal (minimum 30 per slide) within each thin section (3 thin sections per sample) per sample. While measuring the visible twin planes for a given calcite crystals, the optical axis for the crystal (**Fig. 17**) is also defined and is used to determine the geometry of the untwinned (did not reach conditions required for twinning to occur) planes. This provides an additional constraint to stress inversion not possible with inversion of other structural data such as slickensides on a fault plane. The optical axis describes the optical symmetry of the calcite crystal where the passing light is normal to the curvature of the crystal and therefore suffers no birefringence (double refraction). This axis is observed under cross-polarised light and is observed when the crystal becomes extinct (loss of light).

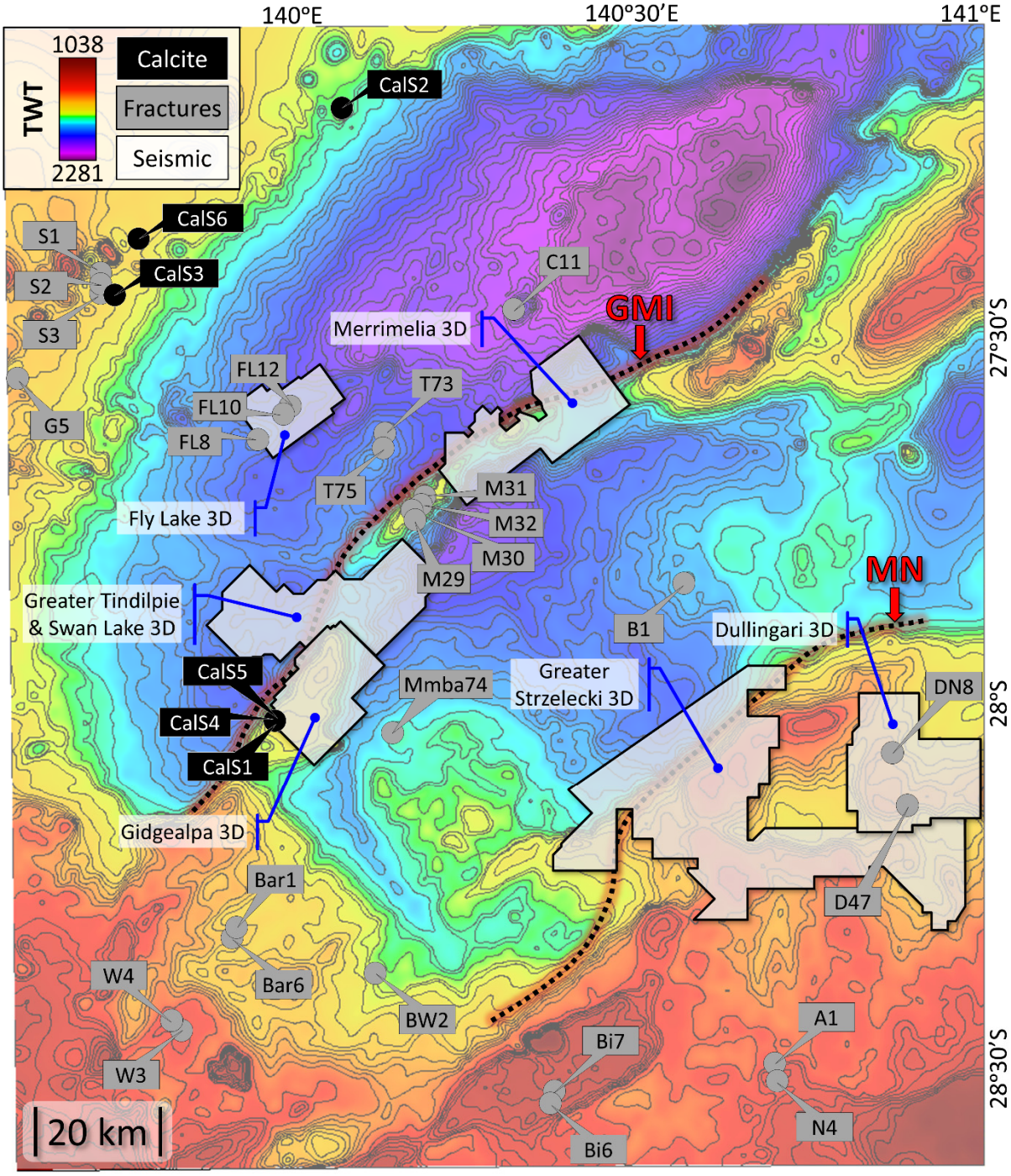


Fig. 18 The location of calcite samples and image logs (fractures) used for this research.

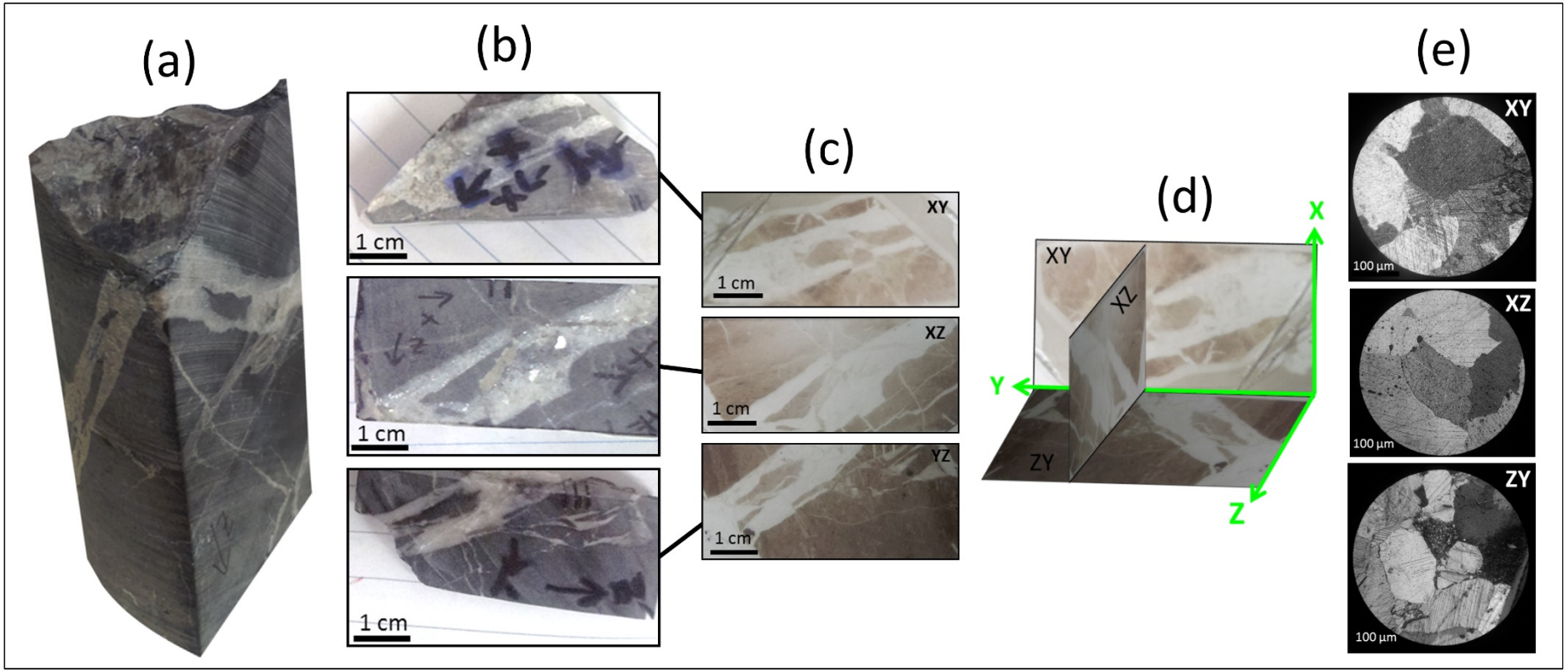


Fig. 19 The process to convert core samples into oriented and measurable thin sections. (a) Core sample with calcite filled fracture; (b) Cut sore samples into approximately 6x4x1 cm rectangular prism. Note notches on the samples; 1 notch in the corner where the two directions converge, and either 1 notch (for the XY plane), 2 notches (XZ plane), or 3 notches (YZ plane) on the opposite side to the corner notch; (c) Thin sections created from rectangular prisms retaining the notches; (d) The geometry of the thin sections along the three planes (XY, XZ, YZ planes); and (e) Calcite crystals viewed under a universal stage microscope with twinning planes visible.

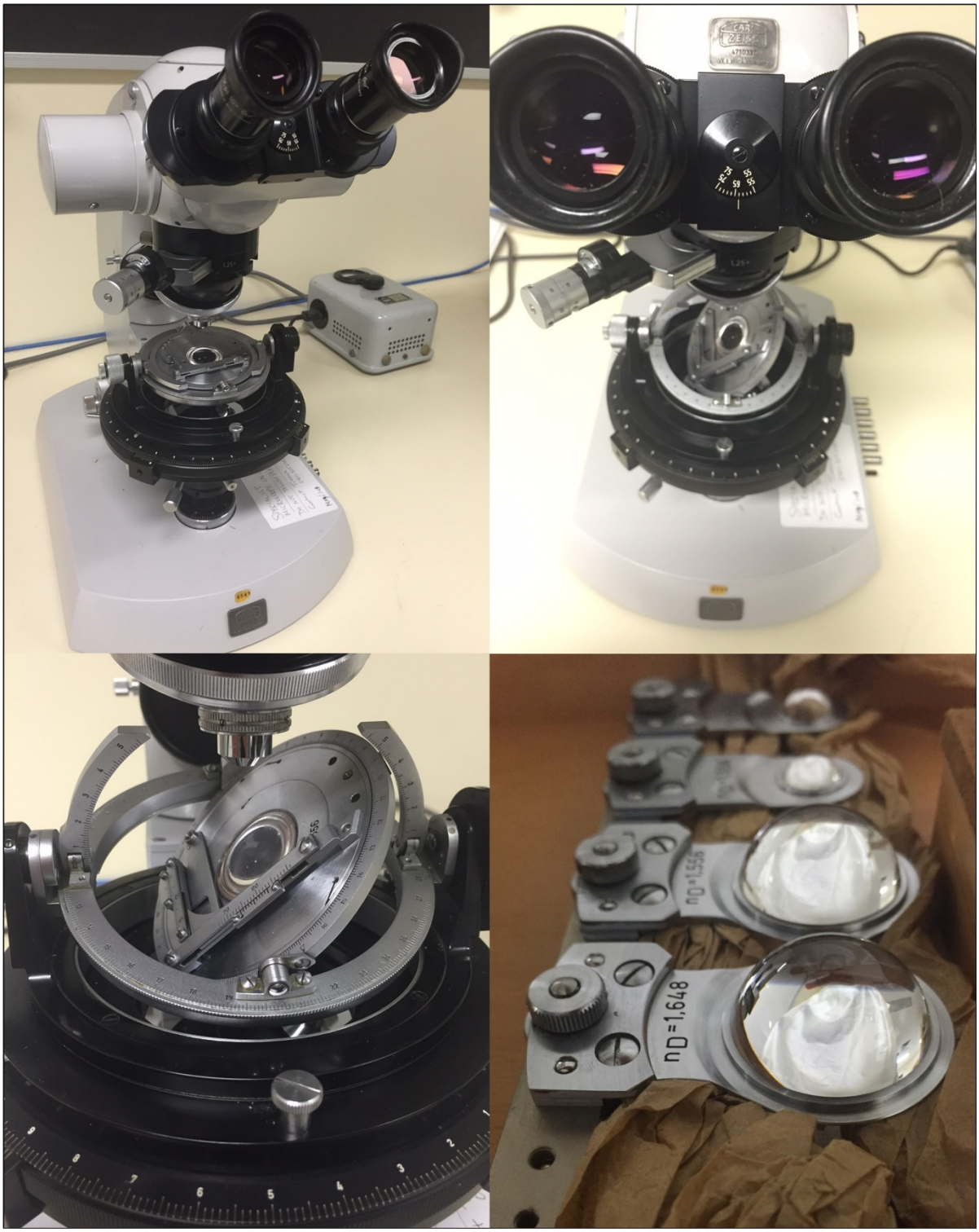


Fig. 20 The Universal Stage Microscope used to measure twinning planes, cleavage planes and principal optical angles of calcite crystals within the 21 thin sections. Thin sections are placed on a layer of glycerine and held in place by an overlying glass hemisphere coated with glycerine, allowing light to pass without deviation.

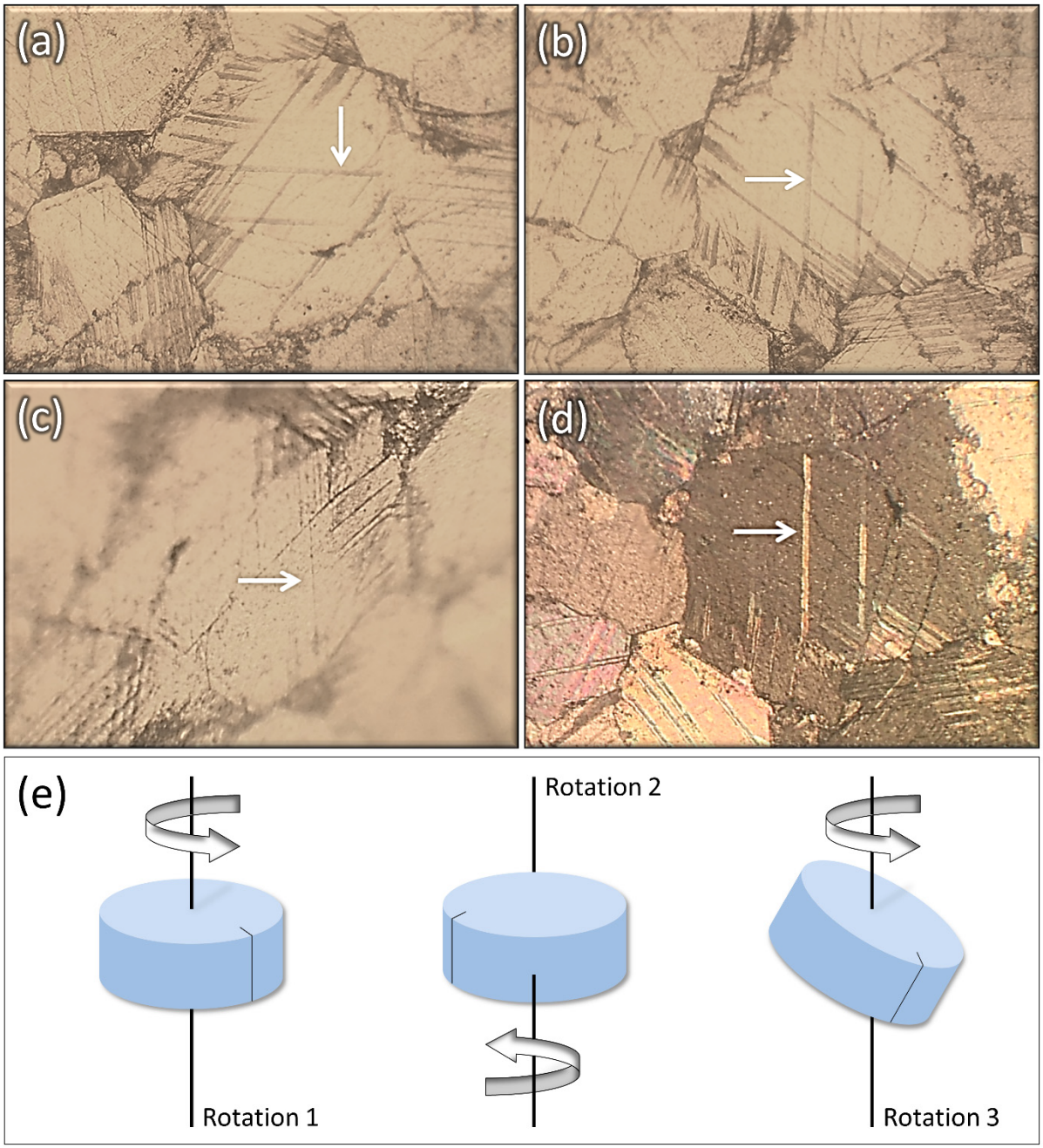


Fig. 21 A high level view of the steps involved in measuring and processing individual calcite twins. (a) Select a calcite crystal with visible twinning; (b) Orient the given twinning plane to align in an arbitrary N-S orientation when viewed. The strike of the twin plane is measured from the microscope stage and written down. Take note of the relatively thick twin plane, which is due to observing the apparent thickness of the plane; (c) Change the dip of the microscope stage until the true thickness of the twin plane is observed (thin twin plane). Write this number down, as together with the strike these describes the geometry of the twin plane relative to the microscope orientation; and (d) Measure the principal optical angle of the calcite crystal such that the crystal is in extinction. The measurements are then rotated to true north, not microscope north, and can be used for calcite twin inversion analysis. (e) the three rotations required to orient the measured twin data back to the true north direction.

3.2.3. Quantification of Paleo-stress Tensors

3.2.3.1. INTRODUCTION

Turner (1953) first suggested the use of calcite twinning to infer paleo-principal stresses. Twinning in calcite is a deformation mechanism responding to simple shear that is applied to part of the host crystal (Lacombe and Laurent, 1996). The twinned lamella is oriented parallel to the direction of shear, and can be likened to slickensides on a fault plane (**Fig. 16**) (Lacombe and Laurent, 1996). Any stress acting on a plane is resolved into three components (X, Y and Z). Temperature and normal stress have negligible effect on calcite twinning and are typically ignored in calculations (Lacombe and Laurent, 1996).

The resolved shear stress defines the applied stress acting on a plane in the twinning direction (T_s). The critical value (T_a) defines the minimum stress required for twinning to occur. Therefore, theoretically for twinning to develop, T_s must exceed T_a (Lacombe and Laurent, 1996). Through numerous experimental results, a critical resolved shear stress of 10 MPa has been proposed for samples containing homogenous grain size between 200 and 400 μm and with less than 3% deformation strain (Lacombe and Laurent, 1996). Grain size must be considered, as fine-grained rocks prevent the spreading and widening of shear mode cracks due to larger boundary forces preventing crystal expansion (Rowe and Rutter, 1990). Strain is assumed to be heterogeneously distributed between grains (Rowe and Rutter, 1990).

The volume (%) of twinning within calcite and the twinning incidence (I_t) (number of calcite crystals with visible twinning) increase with increasing differential stress ($\sigma_1 - \sigma_3$) (Rowe and Rutter, 1990). Calcite twinning can occur at low temperatures (25^{o}C), low confining pressures and at low differential stresses in poorly deformed sedimentary rocks (Lacombe and Laurent, 1996). Therefore, even shallowly buried calcite crystals can be twinned. As the crystal structure of calcite is known (**Fig. 17**), the orientation of non-visible twinned planes, which did not reach the conditions required for twinning to occur, can be determined through basic crystal rotations that incorporates the unique principal optical angle of each crystal and the visible twinned planes.

Methods for constraining a stress tensor from calcite crystals were developed by Carey and Brunier (1974), Carey (1979), Angelier and Goguel (1979), Etchecopar (1981), and Lacombe and Laurent (1996). Etchecopar (1981) developed an inversion technique that can be used to constrain a stress tensor for polyphase tectonic events. The process involves applying a stress tensor that best represents all twinned (reached conditions required for twinning) and un-twinned (did not reach conditions required for twinning) planes. Etchecopar's method is used for the analysis of our data.

3.2.3.2. ETCHECOPAR'S METHOD (1981)

Assumptions:

- State of stress is homogenous.
- The tangential forces applied to a medium cause parallel displacement.
- Stress tensor is symmetric, i.e. no torque.

The displacement is characterised by the stress tensor T, which can be redefined into an isotropic pressure part P and deviatoric part D. Deviation from the principal axes is measured by the Euler's angles (ψ, θ and Φ). These quantities (σ_1, σ_2, σ_3, ψ, θ and Φ) must be found to define the tensor T. The force acting on a plane, with unit normal n**,** has a tangential component f_t defined by **Eq. 3**:

$$\boldsymbol{f_t = T.n - (n.T.n)n} \qquad (Eq.3)$$

Eq. 3 is used to then define the unit vector given by **Eq. 4**.

$$\boldsymbol{t = \frac{f_t}{||f_t||}} \qquad (Eq.4)$$

This is summarised in **Fig. 22.**

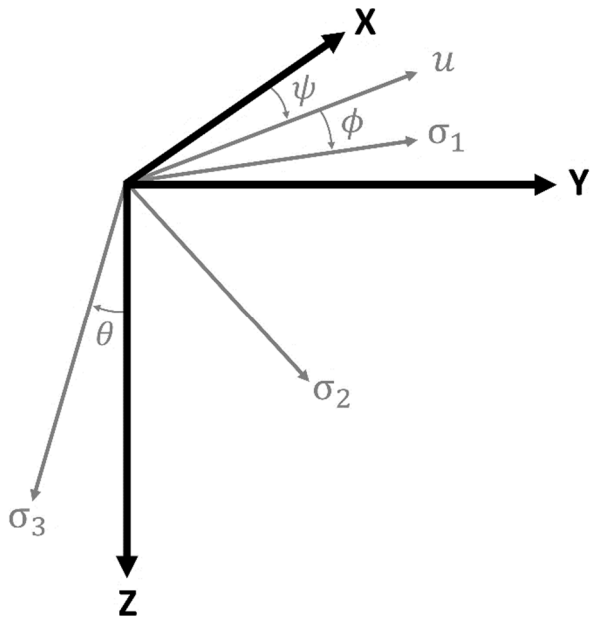


Fig. 22 Stress resolved into three components ($\boldsymbol{X}$, $\boldsymbol{Y}$ and $\boldsymbol{Z}$) using Euler's angles ($\boldsymbol{\psi}$, $\boldsymbol{\theta}$ and $\boldsymbol{\Phi}$) that specify the principal stress directions ($\boldsymbol{\sigma_1}$, $\boldsymbol{\sigma_1}$ and $\boldsymbol{\sigma_3}$) (Etchecopar, 1981; Lacombe and Laurent, 1996).

The pressure tensor P cannot contribute to the tangential force since it only applies a force normal to the plane. The deviatoric tensor D therefore plays the crucial role. The orientation and direction of unit vector t remains constant when the T component is multiplied by a positive constant. The unit vector t, in the tangential force direction, depends on the principal stress direction (ψ, θ and Φ) and the shape ration (R; where 0 ≤ R ≤ 1) given in **Eq. 5**.

$$\boldsymbol{R = \frac{\sigma_2 - \sigma_3}{\sigma_1 - \sigma_3}} \qquad (Eq. 5)$$

Euler's angles and the shape ration define a reduced stress tensor T', where the complete stress tensor, T, is defined by **Eq. 6**. Where I is the unit matrix, k and l are scalars that are > 0 ($k = \sigma_1 - \sigma_3 > 0; l = \sigma_3$) (Lacombe, 2007).

$$\boldsymbol{T = kT' + lI} \qquad (Eq. 6)$$

The maximum differential stress is therefore defined and reduced to $(\sigma_1 - \sigma_3) = 1$ (Etchecopar, 1984). The RSS acting along a given e-plane would then lie between -0.5, or $(-(\sigma_1 - \sigma_3)/2)$, and +0.5, or $(-(\sigma_1 - \sigma_3)/2)$ (Jamison and Spang, 1976; Etchecopar, 1984). Inversion of the data would then begin by applying randomly chosen parameters (ψ, θ, Φ, R) to more than 100 tensors to generate a theoretical striation direction for each of the N planes. Optimising the trial tensors to incorporate the largest number of compatible data is done by calculating the penalisation function, f, which is ideally reduced to 0, but increases when incompatible data is incorporated (**Fig. 23**).

$$\boldsymbol{f = \sum_{j=1}^{N} (\tau_{sj} - \tau'_a)} \qquad (Eq. 7)$$

Where τ'_a is the minimum RSS applied to the twinned planes that are compatible with a given trial, and τ_{sj} is the RSS of the j^{th} un-twinned plane whose RSS is greater than the τ'_a. The number of j^{th} untwinned plane greater than the RSS, or N, depends on the trial stress tensor (Etchecopar, 1984; Amrouch, 2010). The optimal reduced stress tensor can therefore be defined by incorporating the maximum number of twinned planes while reducing **Eq. 7**. The differential stress magnitude is then defined by using a constant RSS value (typically 10 ±4 MPa) and using the following relationships: $(\sigma_1 - \sigma_3) = \tau_a/\tau_a$, and $(\sigma_2 - \sigma_3) = \phi(\sigma_1 - \sigma_3)$.

The proportion of twinned and un-twinned planes incorporated into a given tensor solution can be adjusted to incorporate a larger number of twinned planes while also introducing some un-twinned planes (**Fig. 23b**), which is reflected in the f value (**Eq. 7**). After constraining a stress tensor that best represents the given data set, all twinned planes used in that simulation are removed (**Fig. 23a**). If sufficient twinned data remains (30% of original dataset), the process can be repeated using all un-twinned plans and the remaining twinned planes to define a new stress tensor. This process can be applied to mono-phase data to quantify the confidence of results. This is particularly important in areas that have a complex structural history, such as the Cooper Basin, as it is necessary to identify and group twinned planes formed by individual events to then constrain unique stress tensors for each phase. This procedure is a continuation from Etchecopar's method and is applicable to the Cooper Basin, which has been affected by at least five major individual and successive events throughout its structural history.

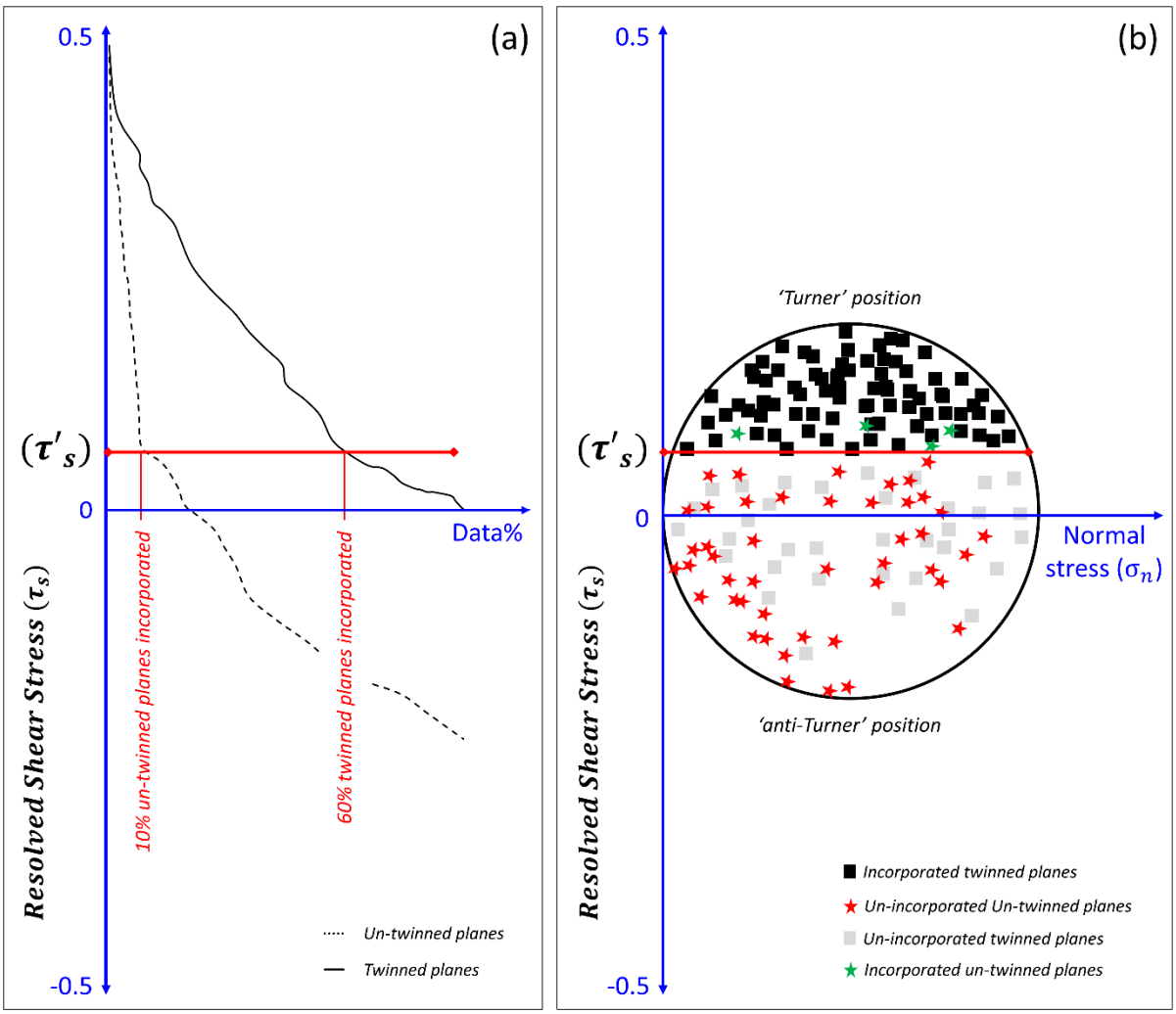


Fig. 23 Schematic representation of the normalised shear stress in terms of the twinned and un-twinned planes. (b) Pseudo-Mohr circle illustrating the compatible and incompatible data for a given stress tensors (after Lacombe and Laurent, 1995; Amrouch, 2010).

3.2.3.3. QUANTIFYING PRINCIPAL STRESS MAGNITUDES

To complete the stress tensor results, the principal stress magnitudes must be constrained by incorporating rock mechanics data. The results thus far provide information on the deviatoric component of the tensor (Lacombe and Laurent, 1992), giving access to the maximum ($\sigma_1 - \sigma_3$) and minimum ($\sigma_2 - \sigma_3$) differential stress magnitudes. These values provide two diameters for constructing the paleo-Mohr's circle. To place this paleo-Mohr's circle in the correct location, one of the three effective principal stress magnitudes needs to be known (Lacombe, 2010). By assuming that one principal stress is vertical, the paleo-vertical stress magnitude can be calculated through simple density and stratigraphic thickness relationships, while considering paleo-pore pressures. This value calculated here can be used to place the paleo-Mohr's circle in the correct location (Amrouch, 2010; Lacombe, 2010). Alternatively, the failure and reactivation envelopes can be used as a guide to place the Mohr's circle at the maximum effective stress conditions prior to rock failure or reactivation occurring (Lacombe and Laurent, 1992; Lacombe, 2001; Amrouch, 2010; Lacombe, 2010). This location would correspond to the intersection between the maximum differential stress circle and the failure envelope. The use of the failure and reactivation envelopes would therefore require an understanding of fracture and fault development and/or reactivation at specific periods of time (Lacombe and Laurent, 1992; Lacombe, 2001; Amrouch, 2010).

3.2.3.4. CALIBRATION TO THE BEDDING PLANE AND SAMPLED VEIN GEOMETRIES

The principal stresses obtained from the optimal stress tensor must be compared to the bedding plane geometry from which they were sampled, as it may provide insights into the timing of events relative to the bedding tilting event. This is most effective where the bedding plane is significantly inclined and where two principal stresses lie within the bedding plane, or where the stresses are horizontal with inclined bedding. In the first example, it would be wise to un-tilt the bedding plane and accompanying principal stresses as it was present prior to the bedding plane tilting event. The second example would suggest that a tilting event occurred prior to the stress tensor solution event. Care should be taken when following this approach, however, as local stress perturbations can be caused by local folding or faulting that may incidentally incline the stress tensor solution. This form of stress perturbation is commonly attributed to the development of fractures and faults that do not align with the regional stress field (Tavani et al., 2015) and may also influence the development of calcite twins within a given sample. Stress perturbation may also be present on a more local scale with rotation of stress direction associated with pre-existing faults.

Comparing the principal stresses to the geometry of the sampled fracture (or vein) can also provide insights into the timing of events, if the timing of natural fracture development and cementation is well understood or better yet if the calcite precipitation can be dated. Comparing the stress tensors to the geometry of the sampled vein can be done to determine which stress tensor is optimally oriented to induce tensile reactivation (dilation) and subsequent calcite cementation. For example, if the principal stress orientations are optimally oriented to have dilated/developed a given natural fracture (where σ_3 is normal to the plane), it is expected that this stress tensor is recording the opening, and subsequent calcite cementation, of the fracture, with the remaining stress tensors occurring subsequent to this. The comparison of the tensor solution with the bedding plane and sampled vein geometries can provide significant relative chronologies.

3.3. NATURAL FRACTURE ANALYSIS

3.3.1. Introduction

As direct fracture measurements are not available from outcrop, borehole image logs (27 wells) and core are used for this study. Borehole image logs measure the electrical resistivity or acoustic reflection of the borehole at centimetre scale. A typical electro-imaging tool contains six pads, each with 150 microelectrodes, which press against the borehole wall to measure the change in resistivity (Nie et al., 2013). Digital data is converted into an oriented resistivity image log using Paradigm's *GEOLOG* software to enable manual natural fracture interpretation. Depending on the type of image log (resistive or acoustic), appropriate filters and processes from the software's *Geomage* application are used to generate the best visual representation of the borehole as possible (**Fig. 24**). Conductive, or open, fractures are filled with electrically conductive drilling fluids. Resistive, or closed, fractures appear as light sinusoids due to electrically resistive cements preventing conductive drilling fluids from entering the fracture. Natural fractures, particularly within tight sands and shales, can improve the recovery of hydrocarbons and, when targeted by optimised wellbore trajectory, can improve the economic significance of reservoirs. It is therefore vital to constrain the natural fracture geometries within the Cooper Basin tight reservoirs, and to determine which natural fracture set is open to fluid flow given the present-day stress tensor.

Fracture data are grouped into formations to easily correlate time and compare fracture geometry between wells. Fracture orientation, dip angle, depth, vertical intensity, geometry relative to bedding, and where possible, the chronology between successive fractures and mode of fracture (mode 1, 2, or 3) are measured either from the borehole image log or directly from core samples.

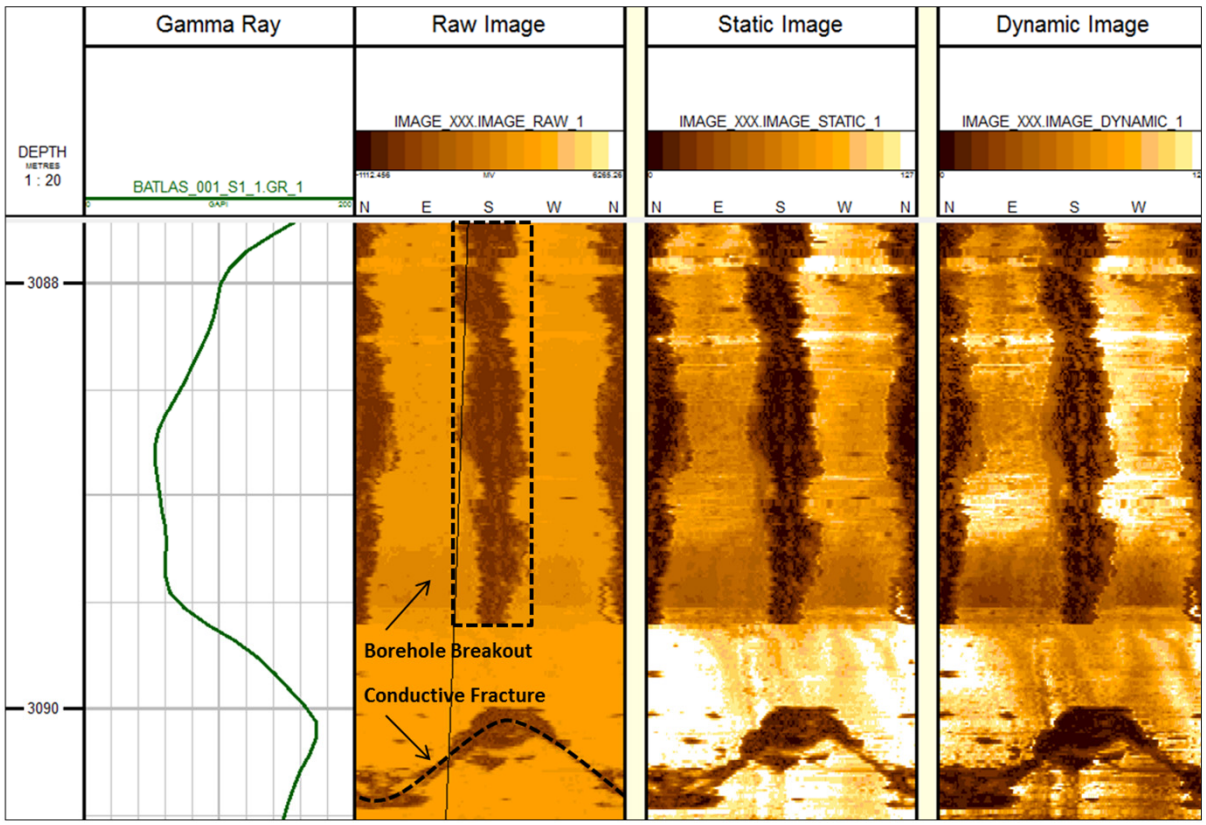


Fig. 24 Conductive (open) natural fracture and borehole breakout interpretation form a borehole image log run in the Cooper Basin.

3.3.2. Data Processing

Regional fracture sets can be identified based on common ranges of strike and dip angle relative to the bedding plane. With fracture data isolated to time and space bins, it is possible to reveal natural fracture trends that were not easily identified in a single stereonet dump of all fracture data or with fracture geometry vs depth graphs. Bedding dip angle may need to be rotated to horizontal by stereographic rotation to align fracture planes with a given fracture set geometry. Fractures that met the geometric criteria (orientation and dip angle range) of a given pervasive fracture set after stereographic rotation, to bring the bedding angle to horizontal, is a commonly used technique to provide comprehensive evidence for a pre-fold origin (Hancock, 1985; Bellahsen et al., 2006). The mode of fracturing is also considered for defining natural fracture sets. After natural fracture sets are identified, they are analysed in natural fracture stress inversion software (Win-tensor) that simulates paleo-stress tensors that are most-likely to have developed a given natural fracture set based on their geometry to the bedding plane.

3.3.3. Stress Inversion

Natural fracture development requires a differential stress to be equal to, or greater than, the rock strength and typically results from structural activity (Zoback et al., 1989; Dresen, 1990; Sibson, 2003; Zoback et al., 2003). Rock failure can also be induced by increases in pore pressure that reduce the effective principal stress magnitudes and effectively shift the Mohr's circle to left (**Fig. 25**). If the pore pressure increase is sufficiently high, the Mohr's circle can intersect the reactivation and failure envelopes. The stress tensor responsible for rock failure controls the fracture geometries that are developed, which are heavily dependent on the orientation of principal stresses (σ_1, σ_2 and σ_3) and the stress regime (**Fig. 25**) (Anderson, 1951). An understanding of the complete natural fracture geometry, while considering the bedding plane, allows us to predict the most likely stress orientation and regime that was responsible for their development (Anderson, 1951). A change in orientation, dip angle and density with depth commonly can also infer a change in structural activity (Seeburger and Zoback, 1982). Therefore, the chronology, geometry and deformation associated with natural fractures and faults can be used to provide insights into the structural evolution and stress regime during their formation (e.g. Ramsay, 1968; Price and Cosgrove et al., 1990; Silliphant et al., 2002; Bergbauer and Pollard, 2004; Rogers et al., 2004; Bellahsen et al., 2006; Amrouch, 2010; Amrouch et al., 2010a; Aubourg et al., 2010; Beaudoin et al., 2012; Beaudoin et al., 2014; Arboit et al., 2015). Fundamental rock failure principals are used to infer the stress regime and orientation responsible for the development of a given conjugate fracture set.

The mode of fracturing is a crucial aspect of stress inversion, as each mode is handled differently and can provide incorrect stress orientations is mishandled. Shear (mode 2) fractures develop with strike directions approximately 30^{o} on either side of the σ_1 direction (θ), with σ_3 bisecting the other 120^{o} angle (180-2θ) formed (**Fig. 25a, 25b & 25c**). Extensional, or tensile, fractures develop with the plane normal to the σ_3 direction, and striking parallel to the σ_1 direction (**Fig. 25d**) (Anderson, 1951). From these examples, it is obvious that analysis of shear and tensile fractures requires different criteria. To perform an inversion study using natural fracture data, it is important to have a significant dataset that is representative of the entire province, and to constrain the mode of fracturing present. Stress perturbations caused by the presence of faults or folds is a known phenomenon that can develop natural fractures that are not aligned with the far-field tectonic stresses (Tavani et al., 2015). It is therefore also important to determine whether measured data is representative of the local or far-field stresses. Once regional natural fracture sets are defined, the stress inversion can begin. The distribution of fracture sets with depth can also provide information on the timing of events, where if a fracture set is present in lower stratigraphy ant not present in overlying sections, it is likely that the event responsible for the fracture set development occurred at approximately this boundary.

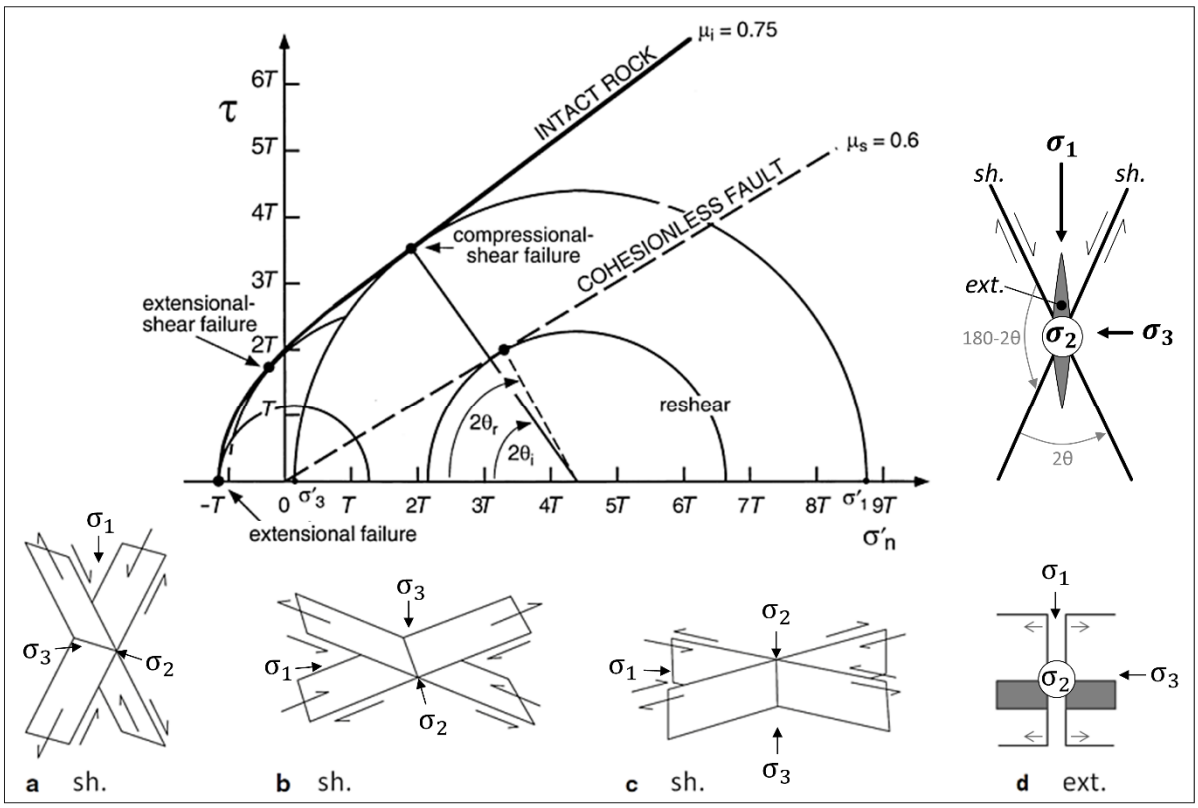


Fig. 25 Mohr's circle with failure (intact) and reactivation (cohesionless) envelopes showing the conditions necessary for brittle failure and reactivation. The geometry of newly formed fractures relative to the maximum (σ_1), intermediate (σ_2), and minimum (σ_3) principal stresses. (a), (b) and (c) show conjugate shear (sh.) fracture development, and (d) shows the development of extensional (ext.) fractures (modified after Sibson, 2003; Singhal and Gupta, 2010).

This methodology allows us to investigate the complex tectonic evolution of provinces by relating the development of conjugate natural fracture sets with the timing of basin evolution. Similar studies have been performed on the Bighorn Basin in Wyoming (Bellahsen et al., 2006; Amrouch et al., 2010a; Beaudoin et al., 2012; Beaudoin et al., 2014), revealing a polyphase stress evolution identified from fracture and fault analysis, and later confirmed through the investigation of rock physical properties (Amrouch et al., 2010b). Silliphant et al. (2002) constrained joint development pre, during and post folding in the Split Mountain anticline in Utah using fundamental rock failure principals. These principals, together with fold-fracture relationships, are used to analyse the regional natural fracture data to constrain the timing of their development. Understanding the mode of fracturing is the most important aspect of the study, as paleo-stress interpretation is different for different modes of fracturing. Care must therefore be taken to constrain the mode of fracturing by matching the borehole image log to core.

3.4. SEISMIC DATA ANALYSIS

3.4.1. Introduction

In entirely subsurface provinces, understanding the structural geology is only possible through drilling wells or acquiring geophysical data. For this reason, a significant portion of this thesis is dedicated to 2D and 3D seismic data analysis. Basic seismic analysis techniques such as fault and horizon picking in cross-section and depth-slice, and isopach mapping form the foundation for more advanced techniques that include mapping fracture networks by incorporating the seismic curvature attribute, identifying large scale faults by developing incoherency seismic volumes, and basic reflectivity mapping to identify changes in seismic reflector amplitude. These seismic attributes provide important high density structural data that would otherwise not be available. However, as seismic data is acquired in the time-domain, seismic time-to-depth conversions must be as accurate as possible, as calculation errors may lead to incorrect depths, generation of pseudo-structures, and flattening of real structures. This is a key uncertainty in the Eromanga Basin, as the presence of oil-rich low amplitude structural traps can depend on the time-to-depth conversion method used.

This study utilises 12 publicly available 3D seismic surveys from the South Australian portion of the Cooper Basin. These include, Moomba 3D (1997), Spencer-Kiana-Muteroo 3D (2007), Greater Strzelecki 3D (2001), Dullingari 3D (1997), Gidgealpa 3D (2002), Greater Tindilpie & Swan Lake 3D (2000), Fly Lake 3D (2000), Coonatie 3D (2000), Merrimelia (extension) 3D (1998), Pondrinie 3D (1997), Sprigg (extension) 3D (2005), and Cuttapirrie 3D (1981) (**Fig. 26a**). These were chosen based on their high density of wells that contained adequate well control (well check-shot and formation top data), and their relative locations to major structural features, such as the GMI and MN ridges. All publicly available 2D seismic lines were also incorporated for regional analyses (**Fig. 26b**).

Most recent works (Grant-Woolley et al., 2014) have shown evidence of strike-slip faults that likely developed during the early structural development of the Cooper Basin, and an example of dextral strike-slip faults is presented for the Gidgealpa Field (**Fig. 27**). Misinterpretation of strike-slip faults can effect reservoir development due to cataclasis and stress rotation within reservoirs (Ramsay; 1967; Grant-Wooley et al., 2014). These works have formed a good basis for further, more regional, structural analysis with the use of 3D seismic data and cutting edge seismic processing software to better understand the stress regime and orientation associated with early structural events that have controlled much of the structural development of the Cooper Basin. A key uncertainty within the basin is the distribution and geometry of regional basement faults and the timing of their development and reactivation.

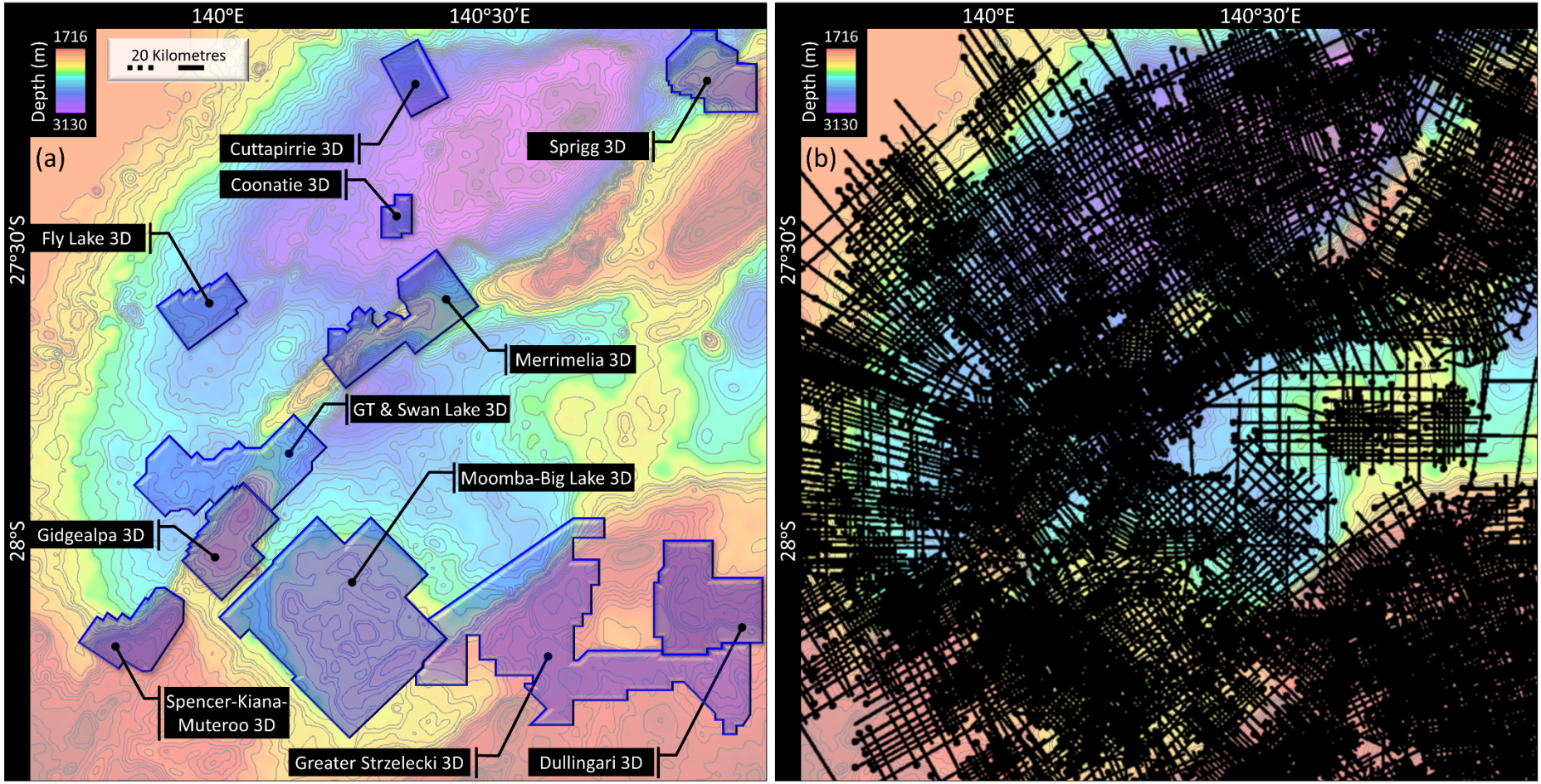


Fig. 26 Location of (a) 3D seismic data and (b) 2D seismic lines used during this research.

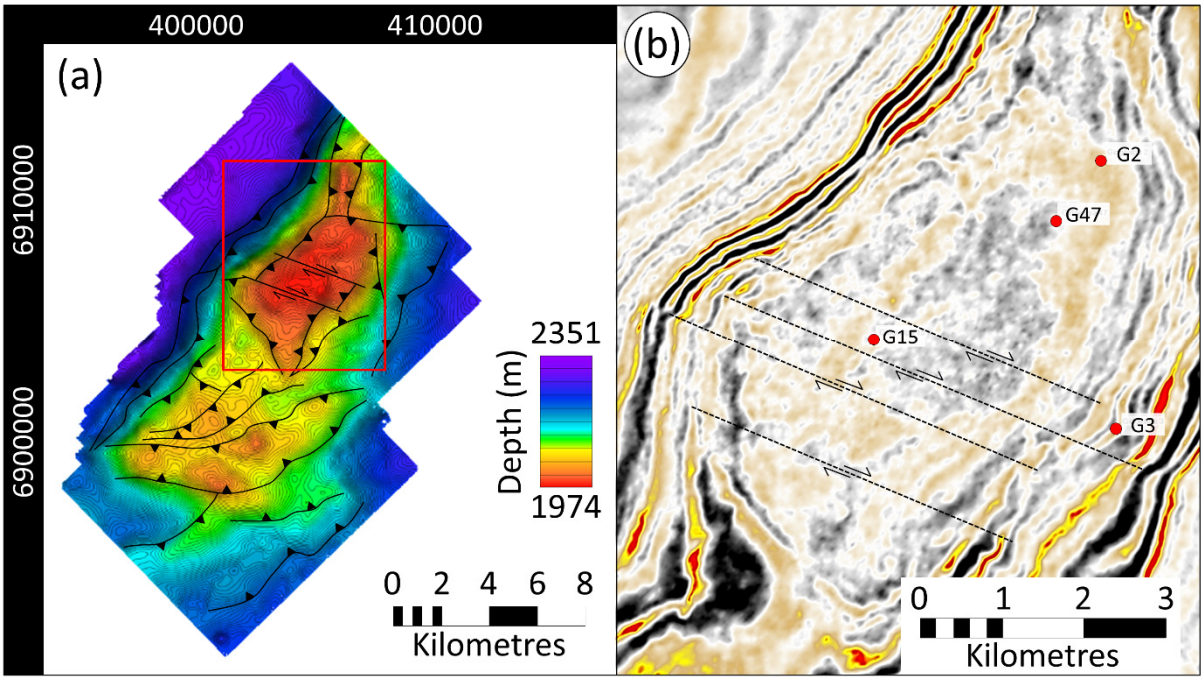


Fig. 27 Evidence of dextral strike-slip faults within the Gidgealpa 3D basement units.

3.4.2. Seismic Time-to-Depth Conversion

3.4.2.1. INTRODUCTION

Depth conversion and ensuring a 1:1 vertical to horizontal scale is vital for accurate structural interpretation and for fault measurements, as fault angles will be different in TWT when compared to true depth (**Fig. 28**). Errors are introduced into isopach maps, true fault geometry measurements and curvature analysis during the depth conversion process as there are many methods that can be used; average velocity, interval velocity, stacking velocity and kriging with external drift (using TWT or stacking velocities). Inaccurate time-to-depth conversion can also lead to errors when geomechanical modelling of fault reactivation is assessed, as the dip angle of faults is a crucial element to all calculations. The accuracy of seismic time-to-depth conversion methods have been investigated in the past; however, this was performed on a limited dataset that tested two methods, and one of which is not commonly used in the basin (Hillis et al., 1995). A regional study on the time-to-depth conversion uncertainty would provide better constraints on choosing the most accurate method to use for a particular dataset. The cross-validation method is a way of testing the accuracy of depth conversions, where n well controls are used to depth convert seismic data, with the $n^{th} + 1$ well used to calculate the error by comparing the predicted depth with the true well depth. This method can be automated using the surface modelling module in PETROSYS software and can incorporate different time-to-depth conversion methods for several seismic reflection surfaces. The software also allows statistics (number of wells, distance to well control, etc.) to be captured.

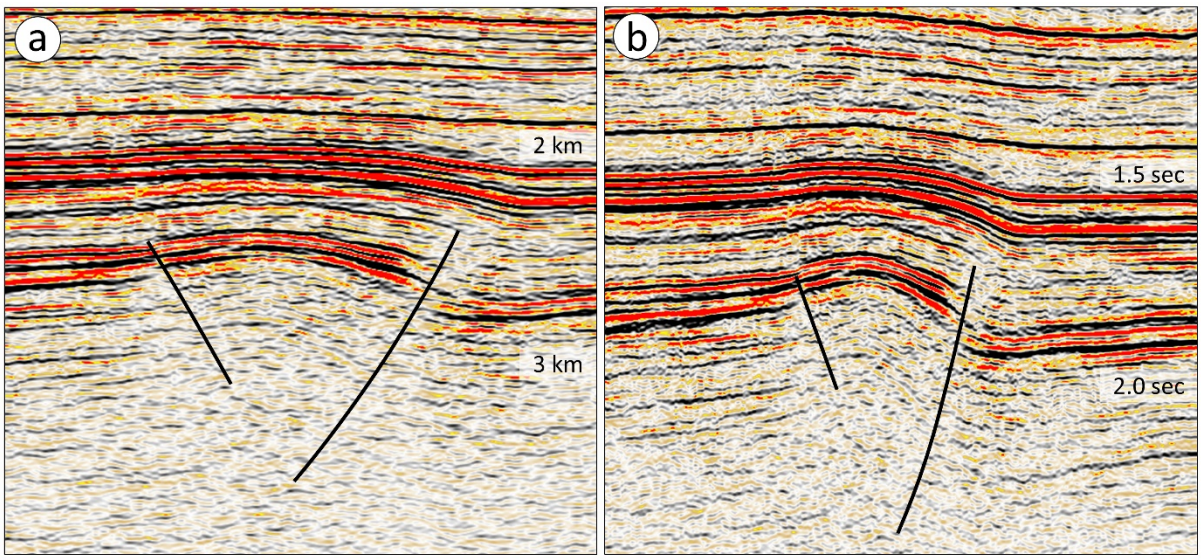


Fig. 28 Structural interpretation of faults within the Dullingari Field with the vertical axis shown in true depth (a) and time (b). It is clear that the fault geometries are very different. Interpretation of faults in time may mislead the interpreter into believing that the faults are strike-slip due to the high angle, when in fact they are dipping approximately 60 degrees.

3.4.2.2. TIME-TO-DEPTH CONVERSION METHODS

3.4.2.2.1. Average Velocity Method

The average velocity (V_a) method is the simplest and most commonly used seismic time-to-depth conversion method. This simple approach does not explicitly consider velocity anomalies but provides a final velocity to tie the well depth precisely. This velocity is obtained for as many well locations that penetrate a given seismic reflector, where the true depth (Δz: depth in feet) is obtained from well data and the interpreted time (Δt: one-way-time in seconds) is obtained from seismic data. This requires that the seismic reflector characteristics are known and easily identified in a seismic cross-section. The ratio of the two measured values provides the required V_a to tie the well and seismic data, such that;

$$\boldsymbol{V_a} = \frac{\sum_{k=1}^{n} \boldsymbol{z_k}}{\sum_{k=1}^{n} \boldsymbol{t_k}} = \frac{\boldsymbol{\Delta Z\ (ft)}}{\boldsymbol{\Delta t\ (s)}} \qquad (Eq.8)$$

Where k represents the k^{th} reflector that is measured from n well locations. The time-to-depth conversion process would then involve multiplying the resultant V_a (generated from the maximum number of wells) with the seismic data (one-way-time: OWT in seconds), to give the true depth;

$$\boldsymbol{True\ Depth = V_a * OWT} \qquad (Eq.9)$$

3.4.2.2.2. Time-depth Trend Method

The time-depth (T-D) trend method utilises the relationship between the TWT from seismic data and true depth from wells for a given seismic reflector. This method is closely related to the average velocity method; however, the T-D pairs at a given well location for a given seismic reflector are plotted on a two-way graph. The relationship is then defined by a linear ($y = mx + c$), or occasionally exponential ($y = ax^2 + bx + c$), trend, where y is depth, x is time, m is slope, and a, b, and c are constants. The T-D trend equation can then be used to convert the seismic data to depth.

3.4.2.2.3. Interval Velocity Method

The interval velocity (V_i) method is applied to provinces that have an abrupt change in velocity across significant stratigraphic packages, or if velocity anomalies, such as cementation, overpressure or heavily faulted/fractured rock, need to be accurately considered. A look at continuous velocity logs and synthetic seismograms shows that velocities are not always constant with depth and can abruptly increase or decrease depending on the rock composition (Al Chalabi, 1974). The most basic V_i model would divide the subsurface into key stratigraphic packages that have unique velocities and can range to highly complex models that contain localised intervals within these stratigraphic packages. For the simplistic V_i models the depth can be calculated by;

$$\boldsymbol{Depth} = \sum_{\boldsymbol{j=1}}^{\boldsymbol{n}} \boldsymbol{V_i}(\boldsymbol{t_{j+1}} - \boldsymbol{t_j}) \qquad (Eq. 10)$$

Where n is the number of intervals (layers) used to define the subsurface that are bound by the j^{th} reflectors, which are measured in the time-domain, t (one-way-time), at a given well location.

3.4.2.2.4. Grid-based Method

To perform seismic time-to-depth conversion on the complete volume is often time consuming and not necessary for generating simple reflector maps. To fast-track the conversion process time-to-depth conversion is often performed using gridding software, or horizon maths tools built into seismic processing and interpretation software. For the purpose of generating depth maps, only the interpreted two-way-time (TWT) seismic reflector grid, rather than the seismic volume, is converted. In this case the interpreted TWT grid is multiplied by a constant velocity to generate a depth grid. The chosen velocity can be obtained relatively simply from the average velocity or time-depth trend methods, or from a previous model. To take into account the spatial velocity variation the velocities at particular well locations can also be gridded and subsequently multiplied by the interpreted TWT grid. Furthermore, the velocities or depths at the well location can be gridded using the kriging with external drift (KED) method using the interpreted TWT grid as an external drift to guide the

interpolation between the primary (well) dataset. The interpolated points follow the trend of the secondary dataset using values derived from the wells. The KED method requires variogram modelling between the primary and secondary (drift) dataset to define the change between data with increasing distance between a pair of wells, similar to a weighting system where well controls that are closer to the interpolation point have a stronger influence than well controls farther away.

3.4.3. Analysis Techniques

3.4.3.1. Introduction

The 3D surveys were individually processed using cutting-edge software (DUG Insight) to allow seismic filters, attributes, and time-to-depth conversion methods to be applied. Interpretation utilised standard techniques (Mitchum et al., 1977; Vail et al., 1977) that incorporated seismic reflector tracing, calculating chronostratigraphic thickness (isopach maps), and attribute mapping. For this study, the incoherency and curvature attributes were found to be the most valuable as these visually enhance the presence of faults and fractures for a given seismic reflector that may otherwise have been overlooked in the original volume (Neves et al., 2004; Mai et al., 2009; Basir et al., 2013).

3.4.3.2. Fault Interpretation

Fault interpretation was guided by the structural evolution of the Cooper-Eromanga Basin, in that extensional, compressional and strike-slip fault may all be present. Faults were interpreted at a line spacing of 10-20 (200-400 m) depending on their length, but also dependent on the complexity, which was highlighted using incoherency (**Fig. 28**), where more structurally complex the fault plane was the closer the line spacing needed to be. Strike-slip faults typically appear vague in cross-section, but can have large lateral offset when viewed in depth-slice. Faults are recognised in cross-section by observing reflector offset, linear seismic features associated with incoherent reflectors, or the presence of fault shadow that appears as incoherent seismic data along a fault plane.

Precise fault interpretation becomes difficult with depth as seismic resolution often decreases making it difficult to capture the fault plane roughness or texture, which can be valuable during geomechanical modelling. Put simply, although a fault plane is optimally oriented to reactivate, there may be subtle sections within the fault plane that are not consistent with the broader trend and this should be captured during interpretation. The decreased vertical seismic resolution in this province prevents the fault plane roughness (texture) being interpreted, and also prevents quantitative fault growth analysis, which can constrain the timing of fault growth. Incorporating this analysis into our study was not possible; however, this should be considered for other subsurface provinces with high resolution seismic data, such as those acquired offshore.

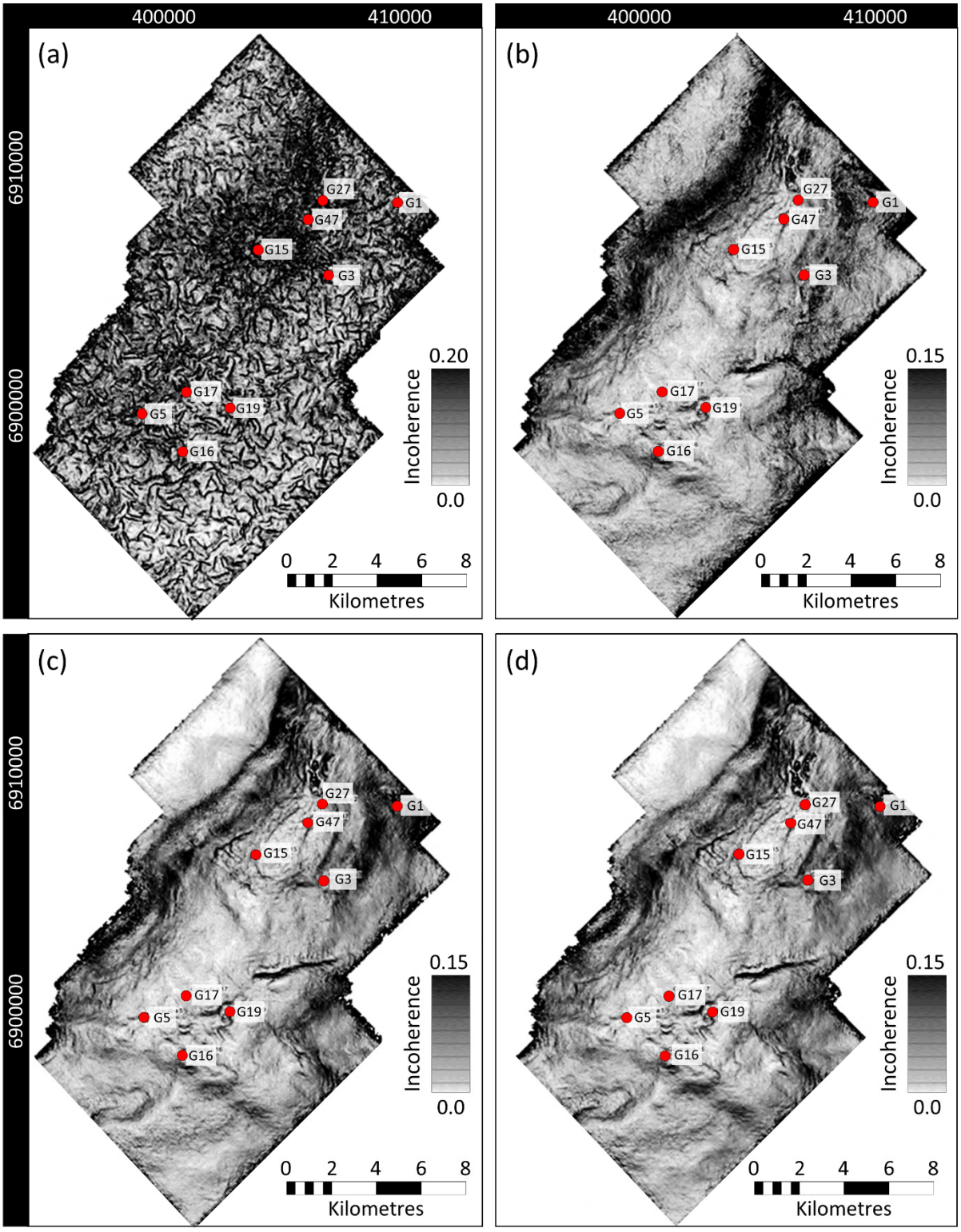


Fig. 29 Incoherency maps in the Gidgealpa 3D along horizons in order of (a) shallow to (d) deep showing faults in black. A system of polygonal faults is identified in (a), with major basement faults highlighted particularly will in (c) and (d).

3.4.3.3. Reflector Interpretation

Interpretation of a given reflector was initially picked from well formation tops to identify the reflector corresponding to the horizon of interest. The reflector was then traced along arbitrary lines that tied together all the well controls to create an initial framework. Interpretation was assisted with a standard amplitude snapping function that places the pick in the centre of the reflector (where amplitude is strongest). The reflector was picked along in-lines and cross-lines and finally propagated (interpolated) using the seismic volume as a guide. A framework of six reflectors was used that correspond to the Wallumbilla Formation, Cadna-owie Formation, Nappamerri Group, Toolachee Formation, Patchawarra Formation, and VC Coal. Attributes were extracted along these reflectors to provide stratigraphy-specific structural data. These reflector surfaces were also used to divide the seismic data into five key stratal units that would be used for isopach mapping.

3.4.3.4. Isopach Mapping

Isopach maps are calculated by subtracting a shallow horizon surface from a deeper surface to generate a stratigraphic thickness. This is used to define thickening trends of individual packages across a study area where thickening may infer an increase in the accommodation space, and a thinning may infer erosion post deposition, or restricted accommodation space. Reactivation along pre-existing faults can be interpreted in areas which show reduced stratal unit thickness across paleo-highs with known inverted faults, or thickening of packages towards a fault to infer normal reactivation (Mitchum et al., 1977; Stanmore & Johnstone, 1988; Apak et al., 1997). Isopach maps were created between five key reflector surfaces and integrated with regional and seismic scale fault interpretation to constrain periods of structural activity and describe the depositional trends trough time. Gidgealpa 3D shows significant structural control on deposition during the Permian (**Fig. 30d**).

3.4.3.5. Incoherency Analysis

A useful seismic attribute for identifying faults is incoherency (also referred to as coherency or similarity), which was introduced by Bahorich and Farmer (1995) and developed by Gersztenkorn and Marfurt (1999). The seismic amplitude volume is re-processed using DUG Insight software and can be extracted along the interpreted seismic reflectors or visualised in depth-slice. The value of this attribute is that it visually enhances the discrepancies along a seismic horizon (**Fig. 29**) or depth-slice to highlight discontinuities that may have otherwise been overlooked (Neves et al., 2004; Mai et al., 2009; Basir et al., 2013). For a given reflector, if amplitude abruptly changes, say from positive to negative reflectance, this would be highlighted and infer reflector displacement caused by faulting. Incoherency analysis was used as a first-pass look to identify the expected fault distribution and geometries before fault interpretation.

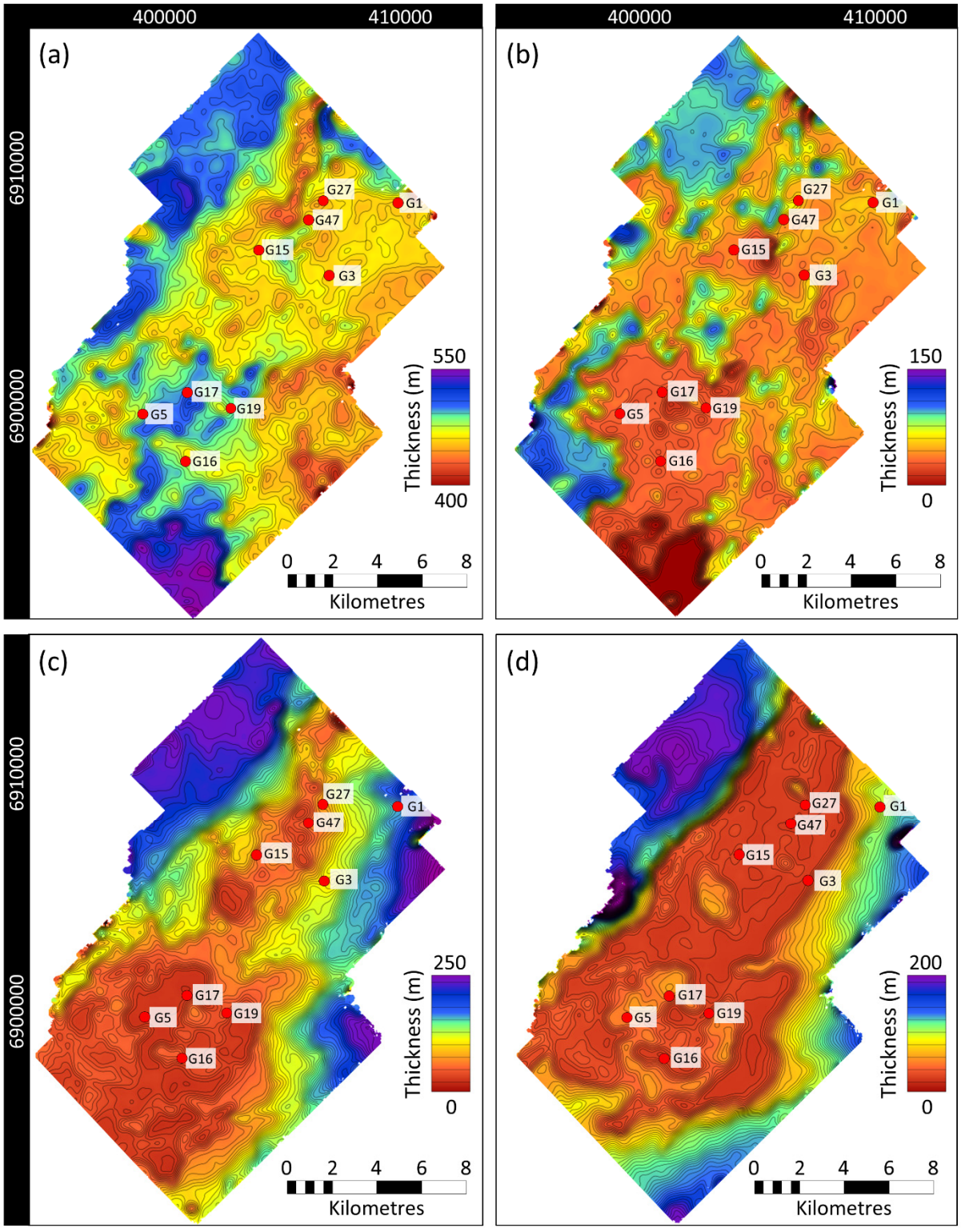


Fig. 30 Thickness isopach maps between various horizons in order of youngest (a) to oldest (d) showing areas of thinning through time. This example shows a high level stratigraphic evolution of the Gidgealpa 3D with distinct structural control on deposition in (c) and (d).

3.4.3.6. Curvature Analysis

The relationship between seismic curvature and natural fractures is in the stress re-distribution when a stratal-unit (or bed) is folded or bent. Anticlinal folding alters the bed lengths and exerts compressional and extensional stresses towards the base and crest of the anticline, respectively, creating fractures with known geometries (Ferrill and Groshong, 1993; Roberts, 2001). However, reflectors can curve through other mechanisms, such as erosion or the depositional environments (dunes, on-lapping, clinoforms, etc.), so the tectonostratigraphic history must be well understood. Prior to calculating curvature, a 3D subsurface dip field volume is created from the depth converted volume to provide the dip angle of reflectors. The value for curvature is the rate of change of the direction of a curve, such that for any point (P) the curvature (K) is defined as the rate of change of the dip angle ($d\omega$) in terms of the arc length (dS) (Roberts, 2001). dS is taken from the osculating circle with a common tangent to P and with the greatest possible contact with the curve (Roberts, 2001). The radius of the osculating circle is the radius of curvature (R). In 2D, K is defined as;

$$\boldsymbol{K = \frac{d\omega}{dS} = \frac{2\pi}{2\pi R} = \frac{1}{R}} \qquad (Eq. 11)$$

As we are using 3D seismic data, K can have an infinite number of directions all with unique values, but, for any P there is a single intersecting plane normal to the surface that has the largest curvature value, or maximum curvature (K_{max}) (Roberts, 2001). Perpendicular to this plane is the minimum curvature (K_{min}) (Roberts, 2001). The K_{max} and K_{min} are the principal curvatures and can be used to derive curvature for planes that are normal to the surface (Roberts, 2001). The angle (δ) between a normal curvature plane (K_i) and the K_{max} is used to calculate K_i (**Eq. 12**). This process is performed using DUG Insight software and the results can be extracted for any reflector surface.

$$\boldsymbol{K_i = (K_{max})cos^2\delta + (K_{min})sin^2\delta} \qquad (Eq. 12)$$

From this calculation, there can be maximum (positive) and minimum (negative) values, which define contrasting areas of a structure. Given that anticlines with four-way-dip closure commonly trap hydrocarbons in this province, most wells are drilled on crests. This positive bending of the stratigraphy is calculated using the most positive curvature (K_+), and defines the natural fractures present along these crests (**Eq. 13**). Where a, b and c are derived from a local quadratic surface with a 3x3 grid cell approach (Roberts, 2001).

$$\boldsymbol{K_+ = (a+b) + \sqrt{(a-b)^2 + c^2}} \qquad (Eq. 13)$$

3.5. GEOMECHANICAL MODELLING

3.5.1. Introduction

Geomechanical modelling of fault reactivation potential defines the risk of fault slip, fault opening (or dilation), and fault reactivation, which provide insights into the potential escape of hydrocarbons through recently active faults, or the sealing potential of faults. The relative risk of fault reactivation can be assessed given that the complete present-day stress tensor, fault geometry, pore pressure, and the rock failure envelope are well constrained. This form of modelling has been conducted in many basins around the world (Morris et al., 1996; Wiprut and Zoback, 2000; Wiprut and Zoback, 2002; Worum et al., 2004; van Ruth et al, 2006; Moech et al., 2009; Macdonald et al., 2012; Swierczek et al., 2013), however, never in the Cooper Basin. These models often ignore important factors such as cementation, plane roughness, and local pressure variation, in favour of simplicity. Nonetheless, the reactivation potential of inverted and strike-slip faults are analysed in this highly complex stress field that can alternate between a compressive and strike-slip stress regime. To create the model, structural interpretation of 3D seismic surveys is required and must be performed in the depth-domain. A thorough understanding of the present-day stress tensor is also required. Input data was collated from authors who have comprehensively constrained the present-day stress tensor (**Table 2**) (Reynolds et al., 2006; Nelson et al., 2007). We model each of the study areas (Dullingari and Swan Lake) (**Fig. 26a**), under compressive and strike-slip stress regimes and collate pore pressure data from various well tests. This methodology of assessing the likelihood of fault reactivation is also integrated with paleo-stress tensors to define the evolution of fault reactivation, presenting a novel approach for constraining fault activity in areas with poor seismic data quality.

Table 2 Present-day stress data used for geomechanical modelling of faults in the Cooper Basin at 3 km depth (Reynolds et al., 2006; Nelson et al., 2007). σ_H: maximum horizontal stress; σ_h: minimum horizontal stress; σ_v: vertical stress; P_p: pore pressure.

Stress Regime	σ_H (MPa)	σ_H azimuth	σ_h (MPa)	σ_v (MPa)	P_p (MPa)	Fault Rock Scenario	Cohesion (MPa)
Strike-Slip	114.0	101°N	51.9	57.0	30.0	New/Healed	10.0
						Cohesionless	0.0
Compressional	114.0	101°N	57.0	51.9	30.0	New/Healed	10.0
						Cohesionless	0.0

3.5.2. Quantifications

3.5.2.1. SLIP TENDENCY

The slip tendency (T_s) generates an assessment of the relative risk of fault slip under the present-day stress. This is calculated using the effective normal (σ'_n) and shear stress (τ) magnitudes, with the sense of motion dictated by the maximum resolved shear stress direction relative to the fault plane (Morris et al., 1996). Shear reactivation occurs when the resolved shear stress acting on a fault plane is equal to or exceeds the frictional resistance to sliding (Ferrill et al., 1999). As fictional resistance to sliding is dependent on σ'_n (Jaeger et al., 2007), the T_s is the ratio between τ and σ'_n. **Eq. 14** describes the likelihood that a fault will slip, with **Fig. 31a** illustrating how the equation is derived. This value is a relative measure based on the dataset and ranges from high ($T_s = 1$) to low ($T_s = 0$) likelihood of slip. The application of slip tendency is most useful for identifying which fault or fracture geometry is optimally oriented, given the stress conditions, to preferentially reactivate. For a quantitative measure, the fracture stability measurement calculates the pore pressure increase required to induce failure.

$$\boldsymbol{T_s = \frac{\tau}{\sigma'_n}} \qquad (Eq.14)$$

3.5.2.2. DILATION TENDENCY

The ability of a fault plane to act as a fluid conduit under the present-day stress, or undergo tensile reactivation (dilate), is modelled using the dilation tendency (T_d) attribute. The T_d is again a relative measure that is governed by the σ'_n acting on the fault plane when normalised to the differential stress, which directly influences the fault aperture (Ferrill et al., 1999; Mildren et al., 2005). It is important to note that although a fault or fracture plane may shear reactivate, it may not necessarily be optimally oriented to remain dilated and may subsequently closed. Faults that seal hydrocarbon reservoirs or that extend from source to overlying reservoirs may act as hydrocarbon conduits for primary, secondary, or tertiary migration that can be predicted using the T_d. The equation used to measure T_d is shown below (**Eq. 15**), and ranges from high ($T_d = 1$) to low ($T_d = 0$) likelihood of tensile reactivation. A visual representation of how this equation is derived with respect to the maximum (σ'_1) and minimum (σ'_3) effective normal stresses is shown in **Fig. 31b**.

$$\boldsymbol{T_d = \frac{\sigma'_1 - \sigma'_n}{\sigma'_1 - \sigma'_3}} \qquad (Eq.15)$$

3.5.2.3. FRACTURE STABILITY

Fracture stability analysis is used to illustrate the relative increase in pore pressure (ΔP) required to initiate fault reactivation on a given fault plane. The ΔP is closely related σ_1 (**Eq. 16**; where α is Biot's coefficient that describes the difference between the total and effective stresses, and v is the Poisson ratio) and when increased can effectively shifts the Mohr circle to the left (reducing the effective principal stress magnitudes) until the projected fault plane intersects the composite failure or reactivation envelope (**Fig. 31c & 31d**). This attribute is calculated using the complete present-day stress tensor, pore pressure, fault geometry, composite failure envelope, and fault surface cohesion (Ferrill et al., 2004; Mildren et al., 2005). Two cases were considered for each stress regime when calculating the fracture stability; (1) fault planes with a cohesion of 10 MPa to model healed faults or new fault development (**Fig. 31c**); and (2) cohesionless fault planes to simulate no frictional resistance to reactivate and emphasise regions along a fault surface most likely to reactivate (**Fig. 31d**). The fracture stability analysis is most applicable to basins implementing fracture stimulation, such as the Cooper Basin, as associated increases in reservoir pressure can lead to fault reactivation.

$$\boldsymbol{\Delta\sigma_1 = \alpha\left(\frac{1-2v}{1-v}\right)\Delta P_p} \qquad (Eq.16)$$

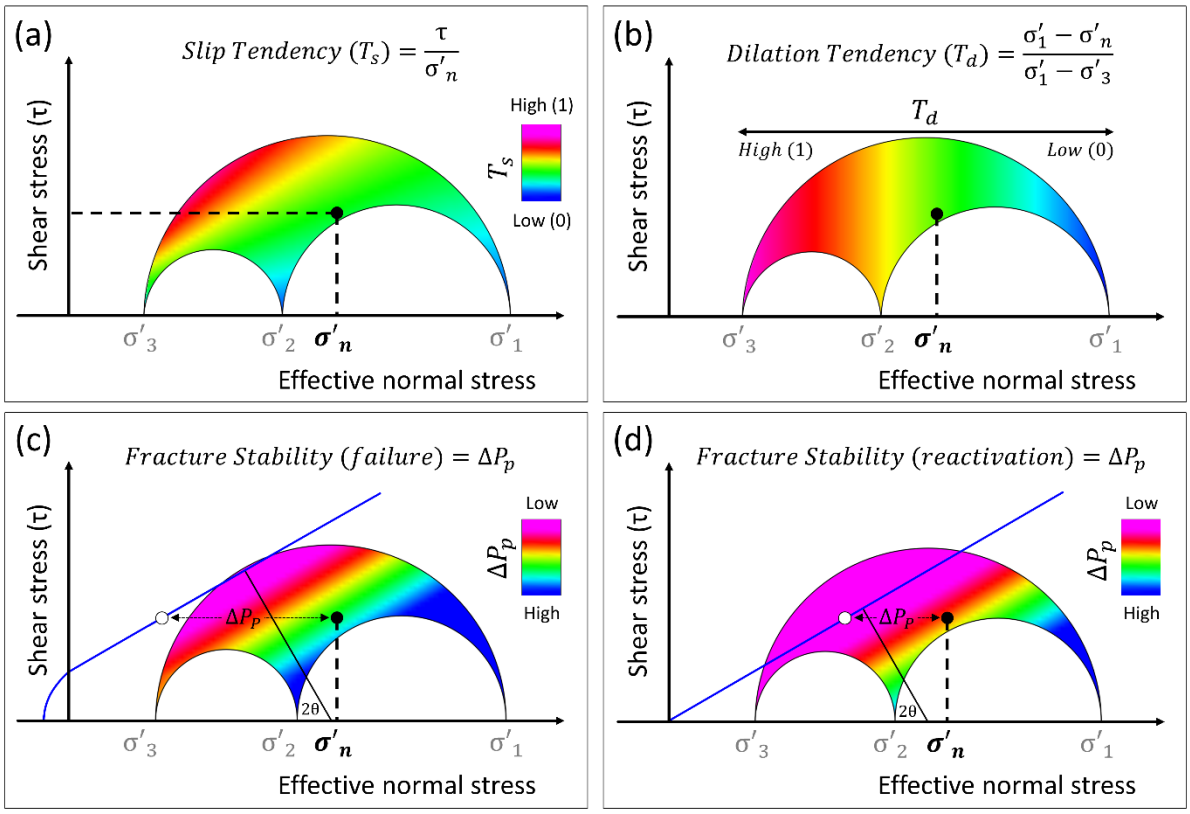


Fig. 31 The definition of: (a) slip tendency; (b) dilation tendency; (c) fracture stability for shear failure; and (d) fracture stability for shear reactivation (*modified after Mildren et al., 2005*).

4. BIBLIOGRAPHY

Aadnoy, B. S. (1990). Inversion technique to determine the in-situ stress field from fracturing data. Journal of Petroleum Science and Engineering, 4(2). 127-141.

Abul Khair H., Cooke D. & Hand M. (2013). The effect of present day in situ stresses and paleo-stresses on locating sweet spots in unconventional reservoirs, a case study from Moomba-Big Lake fields, Cooper Basin, South Australia. Journal of Petroleum Exploration and Production Technology 3, (4), 207-221.

Abul Khair H., Cooke D. & Hand M. (2015). Seismic mapping and geomechanical analyses of faults within deep hot granites, a workflow for enhanced geothermal system projects. Geothermics 53, 46-56.

Abul Khair, H.A., Cooke, D., King, R., Hand, M., & Tingay, M. (2012). Preliminary workflow for subsurface fracture mapping using 3D seismic surveys: A case study from the Cooper Basin, South Australia. In: Geothermal Research Council Conference, Reno, Nevada 36, 339-350.

Ainsworth, R. B. (2010). Prediction of stratigraphic compartmentalization in marginal marine reservoirs. Geological Society, London, Special Publications, 347(1). 199-218.

Al-Chalbi, M. (1974). An analysis of stacking, RMS, average, and interval velocities over a horizontally layered ground. Geophysical Prospecting, 22(3), 458-475.

Al-Dossary, S., & Marfurt, K.J. (2006). 3D volumetric multispectral estimates of reflector curvature and rotation. Geophysics 71(5), 41-51.

Alexander, E. M., & Hibburt, J. (Eds.). (1996). Petroleum Geology of South Australia: Eromanga Basin. Petroleum Division, SA Department of Mines and Energy.

Alexander, E.M., Gravestock, D.I., Cubitt, C., & Chaney, A. (1998). Lithostratigraphy and environments of deposition. In: Gravestock, D.I., Hibburt, J.E., Drexel, J.F., (Eds.), The Petroleum Geology of South Australia. Vol. 4: Cooper Basin, South Australia. Department of Primary Industries and Resources. Report Book, 98/9, 69-116.

Allmendinger, R.W., Cardozo, N.C., & Fisher, D. (2012). Structural Geology Algorithms: Vectors & Tensors: Cambridge, England, Cambridge University Press, p. 1-289.

Amrouch, K. (2010). Apport de l'analyse microstructurale à la compréhension des mécanismes de plissement. Exemples de structures plissées aux USA (Wyoming) et en Iran (Zagros), Thèse, Université Pierre et Marie Curie – Paris 6, 2010-03, 477 p.

Amrouch, K., Beaudoin, N., Lacombe, O., Bellahsen, N., & Daniel, J. M. (2011). Paleostress magnitudes in folded sedimentary rocks, Geophys. Res. Lett., 38, L17301, doi:10.1029/2011GL048649.

Amrouch, K., Lacombe, O., Bellahsen, N., Daniel, J. M., & Callot, J. P. (2010a). Stress and strain patterns, kinematics and deformation mechanisms in a basement-cored anticline: Sheep Mountain Anticline, Wyoming. Tectonics, 29(1).

Amrouch, K., Lacombe, O., Mouthereau, F., & Dissez, L. (2005). Quantification of orientations and magnitudes of the late Cenozoic paleostresses in the Zagros folded belt from calcite twin analysis. In Thrust Belts and Foreland Basins, International Meeting, Rueil-Malmaison, 31-35.

Amrouch, K., Robion, P., Callot, J. P., Lacombe, O., Daniel, J. M., Bellahsen, N., & Faure, J. L. (2010b). Constraints on deformation mechanisms during folding provided by rock physical properties: A case study at Sheep Mountain anticline (Wyoming, USA), Geophysical Journal International, 182(3), 1105-1123.

Anderson, E. M. (1951), The Dynamics of Faulting and Dyke Formation with Applications to Britain, Oliver and Boyd, Edinburgh.

Angelier, J., & Goguel, J. (1979). Sur une méthode simple de détermination des axes principaux des contraintes pour une population de failles. CR Acad. Sci. Paris, 288, 307-310.

Angelier, J. (1989). From orientation to magnitudes in paleostress determinations using fault slip data. Journal of Structural Geology, 11(1), 37–50.

Angelier, J., & Mechler, P. (1977). Sur une method graphique de recherche des contraintes principals egalement utilisable en tectonique et en seismologie: la method des diedres droits, Bull. Soc. Geol., XIX, N°6, 1309–1318.

Apak, S. N., Stuart ,W. J., Lemon, N. M., & Wood, G. (1997). Structural evolution of the Permian-Triassic Cooper Basin, Australia: Relation to hydrocarbon trap styles. American Association of Petroleum Geologists Bulletin 81, 533-555.

Arboit, F., Amrouch, K., Collins, A. S., King, R., & Morley, C. (2015). Determination of the tectonic evolution from fractures, faults, and calcite twins on the southwestern margin of the Indochina Block, Tectonics, 34(8), 1576-1599, doi:10.1002/2015TC003876.

Arboit, F., Amrouch, K., Morley, C., Collins, A. S., & King, R. (2017). Palaeostress magnitudes in the Khao Khwang fold-thrust belt, new insights into the tectonic evolution of the Indosinian orogeny in central Thailand, Tectonophysics, doi: 10.1016/j.tecto.2017.01.008.

Backé, G., Abul Khair, H., King, R., & Holford, S. (2011). Fracture mapping and modelling in shale-gas target in the Cooper basin, South Australia. The Australian Petroleum Production and Exploration Association Journal 51, 397-410.

Bahorich, M., & Farmer, S. (1995). 3-D seismic discontinuity for faults and stratigraphic features: The coherence cube. The Leading Edge 14, (10), 1053-1058.

Baisch, S., Vörös, R., Weidler, R., & Wyborn, D. (2009). Investigation of fault mechanisms during geothermal reservoir stimulation experiments in the Cooper Basin, Australia. Bulletin of the Seismological Society of America, 99(1). 148-158.

Balch, A. H., Lee, M. W., Miller, J. J., & Ryder, R. T. (1982). The use of vertical seismic profiles in seismic investigations of the earth. Geophysics, 47(6), 906-918.

Balch, A.H., & Lee, M.W. (1984). Vertical Seismic Profiling: Techniques, Applications, and Case Histories. International Human Resources Development Corporation, Boston, 488 p.

Barber, D. J., & Wenk, H. R. (1979). Deformation twinning in calcite, dolomite, and other rhombohedral carbonates. Physics and Chemistry of Minerals, 5(2). 141-165.

Barton C. A., Moos D., Peska, P., & Zoback M. D. (1997). Utilizing wellbore image data to determine the complete stress tensor: application to permeability anisotropy and wellbore stability. The Log Analyst, 38, (06), 21-33.

Barton, C. A., Zoback, M. D., & Moos, D. (1995). Fluid flow along potentially active faults in crystalline rock. Geology, 23, 683-686.

Basir, H. M., Javaherian, A., & Yaraki, M. T. (2013). Multi-attribute ant-tracking and neural network for fault detection: A case study of an Iranian oilfield. Journal of Geophysics and Engineering, 10, 015009.

Baudon, C., & Cartwright, J. (2008). The kinematics of reactivation of normal faults using high resolution throw mapping. Journal of Structural Geology, 30(8), 1072–1084.

Beardsmore, G.R. & Cull, J.P. (2001). Crustal heat flow; a guide to measurement and modelling, Cambridge University Press, Cambridge.

Beaudoin, N., Koehn, D., Lacombe, O., Lecouty, A., Billi, A., Aharonov, E., & Parlangeau, C. (2016). Fingerprinting stress: stylolite and calcite twinning paleopiezometry reveal the complexity of progressive stress patterns during folding – the case of the Monte Nero anticline in the Apennines, Italy. Tectonics, 35(7), 1687-1712.

Beaudoin, N., Leprêtre, R., Bellahsen, N., Lacombe, O., Amrouch, K., Callot, J. P., Emmanuel, L., & Daniel, J. M. (2012). Structural and microstructural evolution of the Rattlesnake Mountain Anticline (Wyoming, USA): new insights into the Sevier and Laramide orogenic stress build-up in the Bighorn Basin. Tectonophysics, 576, 20-45.

Bell, J. S. (1996a). In situ stresses in sedimentary rocks (part 2): applications of stress measurements: Geoscience Canada, 23, 135-153.

Bell, J. S. (1996b). In situ stresses in sedimentary rocks (part 1): measurement techniques: Geoscience Canada, v. 23, p. 85-100.

Bellahsen, N., Fiore, P., & Pollard, D. D., (2006). The role of fractures in the structural interpretation of Sheep Mountain Anticline, Wyoming. Journal of Structural Geology, 28(5), 850-867.

Bennion, D. B., Thomas, F. B., & Bietz, R. F. (1996). Low permeability gas reservoirs: problems, opportunities and solutions for drilling, completion, stimulation and production. In SPE Gas Technology Symposium.

Bergbauer, S., & Pollard, D. D., (2004). A new conceptual fold-fracture model including prefolding joints, based on the Emigrant Gap anticline, Wyoming. Geological Society of America Bulletin, 116(3-4), 294-307.

Bergerat, F. (1985). Déformations cassantes et champs de contrainte tertiaires dans la plate-forme européenne (Doctoral dissertation, Université Pierre et Marie Curie-Paris VI).

Berry, F.A. (1973). High fluid potentials in California Coast Ranges and their tectonic significance. AAPG Bulletin, 57(7), 1219-1249.

Bethke, C.M., & Marshak, S. (1990). Brine migrations across North America-the plate tectonics of groundwater. Annual Review of Earth and Planetary Sciences, 18, 287.

Bilotti, F., & Shaw, J.H. (2005). Deep-water Niger Delta fold and thrust belt modelled as a critical-taper wedge: The influence of elevated basal fluid pressure on structural styles. AAPG Bulletin, 89(11), 1475-1491.

Boger, S. D., & Miller, J. M. (2004). Terminal suturing of Gondwana and the onset of the Ross–Delamerian Orogeny: the cause and effect of an Early Cambrian reconfiguration of plate motions. Earth and Planetary Science Letters, 219(1). 35-48.

Boreham, C. J., & Hill, A. J. (1998). Source rock distribution and hydrocarbon geochemistry. In: Gravestock, D. I., Hibburt, J. E., & Drexel, J. F. (Eds). (1998). The petroleum geology of South Australia. Vol. 4: Cooper Basin. South Australia. Department of Primary Industries and Resources. Report Book, 98/9.

Boucher, R. K. (2001). Cooper Basin ridges: are they structural? MESA Journal 21, 30-32.

Bowers, G.L. (1995). Pore pressure estimation from velocity data: accounting for overpressure mechanisms besides undercompaction, SPE Drilling and Completions, 10(2), 89-95.

Boyer, S. E., & Elliott, D. (1982). Thrust systems. AAPG Bulletin, 66(9). 1196-1230.

Bradshaw, M. T. (1993). Australian petroleum systems. Petroleum Exploration Society of Australia Journal 21, 43-53.

Breckels, I. M., & Van Eekelen, H. A. M. (1983). Relationship between horizontal stress and depth in sedimentary basins: J Pet Technol, V34, N9, Sept 1982, P2191–2199. In International Journal of Rock Mechanics and Mining Sciences & Geomechanics Abstracts (Vol. 20, No. 1, p. A2). Pergamon.

Bredehoeft, J. D., Djevanshir, R. D., & Belitz, K. R. (1988). Lateral fluid flow in a compacting sand-shale sequence, south Caspian Sea. AAPG Bulletin, 72, 416–424.

Burkhard, M. (1993). Calcite twins, their geometry, appearance and significance as stress-strain markers and indicators of tectonic regime: a review. Journal of Structural Geology, 15(3). 351-368.

Burrus, J. (1998). Overpressure models for clastic rocks, their relation to hydrocarbon expulsion: a critical re-evaluation. Memoirs-American Association of Petroleum Geologists, 35-64.

Cardozo, N., & Allmendinger, R.W. (2013). Spherical projections with OSXStereonet. Computers & Geosciences, v. 51, p. 193-205, doi: 10.1016/j.cageo.2012.07.021.

Carey, E., & Brunier, B. (1974). Analyse théorique et numérique d'un modèle mécanique élémentaire appliquéà l'étude d'une population de failles, C.R. Acad. Sci., Paris, Ser. D, 279, 891-894.

Carey, E. (1979). Recherche des directions principales des contraintes associées au jeu d‘une population de failles. Rev. Géol. Dyn. Géogr. Phys. 21, 57-66.

Cartwright, J. & Lonergan, L. (1997). Seismic expression of layer-bound fault systems of the Eromanga and North Sea Basins. Exploration Geophysics, v. 28(3), p. 323-331.

Casey, M., Rutter, E., Schmid, S., Siddans, A., & Whalley, J. (1978). Texture development in experimentally deformed calcite rocks. Texture of Materiels 2: 231-240.

Childs, C., Nicol, A., Walsh, J. J., & Watterson, J. (1996). Growth of vertically segmented normal faults. Journal of Structural Geology, 18(12), 1389–1397.

Chopra, S., & Marfurt, K. (2007). Curvature attribute applications to 3D surface seismic data. The Leading Edge 26(4), 404-414.

Christie-Blick, N. (1985). Deformation and basin formation along strike-slip faults.

Clevis, Q., Tucker, G. E., Lock, G., Lancaster, S. T., Gasparini, N., Desitter, A., & Bras, R. L. (2006). Geoarchaeological simulation of meandering river deposits and settlement distributions: A three-dimensional approach. Geoarchaeology, 21(8). 843-874.

Collins, A. S., & Pisarevsky, S. A. (2005). Amalgamating eastern Gondwana: the evolution of the Circum-Indian Orogens. Earth-Science Reviews, 71(3), 229-270.

Constantin, J., Laurent, P., Vergély, P., & Cabrera, J. (2007). Paleo-deviatoric stress magnitudes from calcite twins and related structural permeability evolution in minor faults: Example from the toarcian shale of the French Causses Basin, Aveyron, France. Tectonophysics, 429(1), 79-97.

Cooke, D., Tyiasning, S., & Abul Khair, H. A. (2016). Unexpected behaviors of stimulated fractures in the high-stress Cooper Basin. The Leading Edge, 35(1), 78-84.

Craddock, J. P., & Van Der Pluijm, B. A. (1999). Sevier-Laramide deformation of the continental interior from calcite twinning analysis, west-central North America. Tectonophysics, 305, 275-286.

Davies, R. J., Ireland, M. T., & Cartwright, J. A. (2009). Differential compaction due to the irregular topology of a diagenetic reaction boundary: a new mechanism for the formation of polygonal faults. Basin Research, 21(3), 354-359.

Deighton, I., & Hill, A. J. (1998). Thermal and Burial History. In: Gravestock, D. I., Hibburt, J. E., & Drexel, J. F. (Eds). (1998). The petroleum geology of South Australia. Vol. 4: Cooper Basin. South Australia. Department of Primary Industries and Resources. Report Book, 98/9.

Direen, N. G., & Crawford, A. J. (2003). The Tasman Line: where is it, what is it, and is it Australia's Rodinian breakup boundary? Australian Journal of Earth Sciences, 50(4). 491-502.

Dooley, T., & McClay, K. (1997). Analog modeling of pull-apart basins. AAPG bulletin, 81(11). 1804-1826.

Dove, P. M., & Hochella, Jr, M. F. (1993). Calcite precipitation mechanisms and inhibition by orthophosphate: In situ observations by Scanning Force Microscopy. Geochimica et Cosmochimica Acta, 57(3). 705-714.

Dresen, G. (1991). Stress distribution and the orientation of Riedel shears. Tectonophysics, 188(3), 239-247.

Durant, R., Woodroof, R., Stephens, T., Thom, W., McGowen, J., & Scott, M. P. (2013). Investigating Hydraulic Fracturing in Tight Gas Sand and Shale Gas Reservoirs in the Cooper Basin. In SPE Unconventional Resources Conference and Exhibition-Asia Pacific. Society of Petroleum Engineers.

Eisenstadt, G., & De Paor, D. G. (1987). Alternative model of thrust-fault propagation. Geology, 15(7). 630-633.

Elliott, L. G. (1993). Post-Carboniferous tectonic evolution of eastern Australia. APEA Journal, 33, 215-215.

Etchecopar, A., Vasseur, G., & Daignieres, M. (1981). An inverse problem in microtectonics for the determination of stress tensors from fault striation analysis. Journal of Structural Geology, 3(1). 51-65.

Etchecopar, A. (1984). Etude des e tats de contraintes en tectonique cassante et simulation de de formation plastique (approche mathe matique), the se doctorates-sciences, 270 pp. Univ. Sci. et Tech. du Langue-doc, Montpellier, France.

Evans, P. R. (1988). The formation of petroleum and geological history of Australia. In: Petroleum in Australia: the first century. APEA Journal, Special Publication, 26-47.

Faber, E., & Stahl, W. (1984). Geochemical surface exploration for hydrocarbons in North Sea. AAPG Bulletin 68, (3), 363–386.

Fang, H., Yongchuan, S., Sitian, L., & Qiming, Z. (1995). Overpressure retardation of organic-matter maturation and petroleum generation: a case study from the Yinggehai and Qiongdongnan Basins, South China Sea. AAPG Bulletin, 79(4), 551-562.

Faulkner, D. R., Jackson, C. A. L., Lunn, R. J., Schlische, R. W., Shipton, Z. K., Wibberley, C. A. J., & Withjack, M. O. (2010). A review of recent developments concerning the structure, mechanics and fluid flow properties of fault zones. Journal of Structural Geology, 32(11), 1557-1575.

Ferrill, D. A. (1991). Calcite twin widths and intensities as metamorphic indicators in natural low-temperature deformation of limestone. Journal of Structural Geology, 13(6). 667-675.

Ferrill, D.A., & Groshong, R.H. (1993). Kinematic model for the curvature of the northern Subalpine Chain, France. Journal of Structural Geology 15(3-5), 523-541.

Ferrill, D. A. (1998). Critical re-evaluation of differential stress estimates from calcite twins in coarse-grained limestone. Tectonophysics, 285(1), 77–86.

Ferrill, D. A., Winterle, J., Wittmeyer, G., Sims, D., Colton, S., Armstrong, A., & Morris, A. P. (1999). Stressed rock strains groundwater at Yucca Mountain, Nevada. GSA Today, 9(5), 1-8.

Ferrill, D. A., & Morris, A. P. (2003). Dilational normal faults. Journal of Structural Geology, 25, 183-196.

Ferrill, D. A., Morris, A. P., Evans, M. A., Burkhard, M., Groshong Jr, R. H., & Onasch, C. M. (2004). Calcite twin morphology: a low-temperature deformation geothermometer. Journal of Structural Geology, 26(8). 1521-1529.

Finkbeiner, T., Zoback, M., Stump, B.B., & Flemings, P.H. (2001). Stress, pore pressure, and dynamically constrained hydrocarbon columns in the south Eugene Island field, Gulf of Mexico. AAPG Bulletin, 85, 1007-1031.

Finlayson, D. M., Leven, J. H., & Etheridge, M. A. (1988). Structural styles and basin evolution in Eromanga region, eastern Australia. AAPG Bulletin, 72(1). 33-48.

Flottmann, T., Campagna, D. J., Hillis, R., & Warner, D. (2004). Horizontal microfractures and core discing in sandstone reservoirs, Cooper Basin, Australia. In: Eastern Australasian basins symposium II: Petroleum Exploration Society of Australia Special Publication (pp. 689-694).

Friedman, M., & Stearns, D. W. (1971). Relations between stresses inferred from calcite twin lamellae and macrofractures, Teton Anticline, Montana. Geological Society of America Bulletin, 82(11), 3151-3162.

Friedman M., & Heard H.C. (1974). Principal stress ratios in cretaceous limestones from Texas Gulf coast. AAPG Bulletin, 58(1), 71-78.

Friedman, M., Teufel, L. W., & Morse, J. D. (1976). Strain and stress analyses from calcite twin lamellae in experimental buckles and faulted drape-folds. Philosophical Transactions of the Royal Society of London A: Mathematical, Physical and Engineering Sciences, 283(1312), 87-107.

Gajewski, D., & Pšenčik, I. (1990). Vertical seismic profile synthetics by dynamic ray tracing in laterally varying layered anisotropic structures. Journal of Geophysical Research: Solid Earth, 95(B7), 11301-11315.

Ganley, D. C., & Kanasewich, E. R. (1980). Measurement of absorption and dispersion from check shot surveys. Journal of Geophysical Research: Solid Earth, 85(B10), 5219-5226.

Gatehouse, C. G. (1986). The geology of the Warburton Basin in South Australia. Australian Journal of Earth Sciences, 33, 161-180.

Gay, A., Lopez, M., Cochonnat, P., Levaché, D., Sermondadaz, G., & Seranne, M. (2006). Evidences of early to late fluid migration from an upper Miocene turbiditic channel revealed by 3D seismic coupled to geochemical sampling within seafloor pockmarks, Lower Congo Basin. Marine and Petroleum Geology, 23, 387–399.

Ge, S., & Garven, G. (1989). Tectonically induced transient groundwater flow in foreland basin. Origin and evolution of sedimentary basins and their energy and mineral resources, 145-157.

Geotrack (1997). Apatite fission track analysis from several Cooper and Eromanga wells, South Australia. Geotrack report 668 prepared for Mines and Energy South Australia: South Australia. Department of Primary Industries and Resources, South Australia. Open file Envelope, 8426.

Gephart, J. W. (1990). Stress and the direction of slip on fault planes. Tectonics, 9(4), 845-858.

Gersztenkorn, A., & Marfurt, K. J. (1999). Eigenstructure-based coherence computations as an aid to 3D structural and stratigraphic mapping. Geophysics, 64(5), 1468-1479.

Glen, R. A. (1992). Thrust, extensional and strike-slip tectonics in an evolving Palaeozoic orogen—a structural synthesis of the Lachlan Orogen of southeastern Australia. Tectonophysics, 214(1), 341-380.

Glen, R. A., Meffre, S., & Scott, R. J. (2007). Benambran Orogeny in the Eastern Lachlan Orogen, Australia. Australian Journal of Earth Sciences, 54(2-3), 385-415.

Glikson, A. Y., Uysal, I. T., Fitz Gerald, J. D., & Saygin, E. (2013). Geophysical anomalies and quartz microstructures, Eastern Warburton Basin, North-east South Australia: Tectonic or impact shock metamorphic origin? Tectonophysics, 589, 57-76.

González-Casado, J. M., & García-Cuevas, C. (2002). Strain analysis from calcite e-twins in the Cameros basin, NW Iberian Chain, Spain. Journal of Structural Geology, 24(11), 1777-1788.

Goodman, R. E. (1980). Introduction to Rock Mechanics. John Wiley & Sons, New York, 2, 576.

Grant-Woolley, L., Kong, A., Schoemaker, B., Nasreddin, H., & Montague, E. T. (2014). Identification of Strike-Slip faults provides insights into the further development of mature Cooper Basin fields. SPE Asia Pacific Oil and Gas Conference and Exhibition, Adelaide, SPE 171492-MS.

Grauls, D. J., & Baleix, J. M. (1994). Role of overpressures and in situ stresses in fault-controlled hydrocarbon migration: A case study. Marine and Petroleum Geology, 11, 734–742.

Gravestock, D. I., & Jensen-Schmidt, B. (1998). Structural setting. In: The petroleum geology of South Australia. Vol. 4: Cooper Basin (eds. D.I. Gravestock, J.E. Hibburt and J.F. Drexel), pp 69-115. South Australia. Department of Primary Industries and Resources. Report Book, 98/9.

Gray, D. R., & Foster, D. A. (2004). Tectonic evolution of the Lachlan Orogen, southeast Australia: historical review, data synthesis and modern perspectives. Australian Journal of Earth Sciences, 51(6), 773-817.

Green, P. M., Brain, T. J., & John, B. H. (1989). Possible stratigraphic controls on hydrocarbon distribution within the Jurassic-Early Cretaceous rocks, Eromanga Basin, southern Queensland. In: The Cooper and Eromanga Basins, Australia (ed. B.J. O'Neil), pp. 251-264. Petroleum Exploration Society of Australia, Society of Petroleum Engineers, Australian Society of Exploration Geophysicists (S.A. Branches), Adelaide (Proceedings of Cooper and Eromanga Basins Conference).

Gregory, C. M., Senior, B. R., & Galloway M. C. (1967). The geology of the Connemara, Jundah, Canterbury, Windorah and Adavale 1:250,000 shet areas, Queensland. Bureau of Mineral Resources.

Grohmann, C. H, & Campanha, G. A. C. (2010). OpenStereo: Open source, cross-platform software for structural geology analysis, paper presented at 2010 AGU Fall Meeting, San Francisco, California.

Groshong, R. H. (1972). Strain calculated from twinning in calcite. Geological Society of America Bulletin, 83(7), 2025–2038.

Groshong, R. H. (1974). Experimental Test of Least-Squares Strain Gage Calculation Using Twinned Calcite. Geological Society of America Bulletin, 85(12), 1855-1864.

Groshong, R. H., Teufel, L. W., & Gasteiger, C. (1984). Precision and accuracy of the calcite strain-gage technique. Geological Society of America Bulletin, 95(3). 357-363.

Haines, P. W., Hand, M., & Sandiford, M. (2001). Palaeozoic synorogenic sedimentation in central and northern Australia: A review of distribution and timing with implications for the evolution of intracontinental orogens. Australian Journal of Earth Sciences, 48, 911-928.

Hancock, P. L. (1985). Brittle microtectonics: Principles and practice. Journal of Structural Geology, 7, 437–457.

Hardage, B. A. (1985). Vertical seismic profiling. The Leading Edge, 4(11), 59-59.

Harding, T. P. (1974). Petroleum traps associated with wrench faults. AAPG bulletin, 58(7). 1290-1304.

Harding, T. P. (1985). Seismic characteristics and identification of negative flower structures, positive flower structures, and positive structural inversion. AAPG Bulletin, 69(4). 582-600.

Hauge, P. S. (1981). Measurements of attenuation from vertical seismic profiles. Geophysics, 46(11), 1548-1558.

Healy, D., Jones, R. R., Holdsworth, R. E. (2006). Three-dimensional brittle shear fracturing by tensile crack interaction. Nature, 439, 64-67.

Healy, J.H., Rubey, W.W., Griggs, D.T., & Raleigh, C.B. (1968). The Denver earthquakes: Disposal of waste fluids by injection into a deep well has triggered earthquakes near Denver, Colorado. Science, 161, 1301-1310.

Heath, R., McIntyre, S., & Gibbins, N. (1989). A Permian origin for Jurassic reservoired oil in the Eromanga Basin. In: The Cooper and Eromanga Basins, Australia (ed. B.J. O'Neil), pp. 405-416. Petroleum Exploration Society of Australia, Society of Petroleum Engineers, Australian Society of Exploration Geophysicists (S.A. Branches), Adelaide (Proceedings of Cooper and Eromanga Basins Conference).

Heidbach, O., Tingay, M., Barth, A., Reinecker, J., Kurfeß, D., & Müller, B. (2010). Global crustal stress pattern based on the World Stress Map database release 2008. Tectonophysics, 482(1). 3-15.

Hempton, M. R., & Neher, K. (1986). Experimental fracture, strain and subsidence patterns over en echelon strike-slip faults: implications for the structural evolution of pull-apart basins. Journal of structural geology, 8(6). 597-605.

Hillis, R. R., Morton, J. G. G., Warner, D. S., & Penney, R. K. (2001). Deep basin gas: A new exploration paradigm in the Nappamerri Trough, Cooper Basin, South Australia. The Australian Petroleum Production and Exploration Association Journal, 41(1), 185-200.

Hillis, R. R. (1998). The influence of fracture stiffness and the in situ stress field on the closure of natural fractures. Petroleum Geoscience, 4(1). 57-65.

Hillis, R. R., & Reynolds, S. D. (2000). The Australian stress map. Journal of the Geological Society, 157(5). 915-921.

Hillis, R. R., & Reynolds, S. D. (2003). In situ stress field of Australia. Geological Society of America Special Papers, 372, 49-58.

Hillis, R. R., Enever, J. R., & Reynolds, S. D. (1999). In situ stress field of eastern Australia. Australian Journal of Earth Sciences, 46(5). 813-825.

Hillis, R. R., Sandiford, M., Reynolds, S. D., & Quigley, M. C. (2008). Present-day stresses, seismicity and Neogene-to-Recent tectonics of Australia's 'passive' margins: intraplate deformation controlled by plate boundary forces. Geological Society, London, Special Publications, 306(1), 71-90.

Hillis, R. R., Macklin, T. A., & Siffleet, P. (1995). Regional depth-conversion of mapped seismic two-way-times in the Cooper-Eromanga Basins. Exploration Geophysics, 26(2/3), 412-418.

Hoffman, K. L. (1989). The influence of pre-Jurassic tectonic regimes on the structural development of the southern Eromanga Basin, Queensland. In B. J., O'Neil (Ed.) The Cooper and Eromanga Basins, Australia (pp. 315–328). Adelaide SA: Proceedings of Petroleum Exploration Society of Australia, Society of Petroleum Engineers, Australian Society of Exploration Geophysicists (SA Branches).

Holgate, F. (2005). Exploration and Evaluation of the Australian Geothermal Resource (Ph.D. thesis). Australian National University.

Horvitz, E. P., & Ma, S. (1988). Hydrocarbons in near-surface sand, a geochemical survey of the dolphin field in North Dakota. Association of Petroleum Geochemical Explorationists Bulletin 4, (1), 30–46.

Hovadik, J. M., & Larue, D. K. (2007). Static characterizations of reservoirs: refining the concepts of connectivity and continuity. Petroleum Geoscience, 13(3), 195-211.

Igboekwe, M. U., & Ohaegbuchu, H. E. (2011). Investigation into the weathering layer using up-hole method of seismic refraction. Journal of Geology and Mining Research, 3(3), 73-86.

Jadoon, Q. K., Roberts, E., Blenkinsop, T., Raphael, A. J., & Shah, S. A. (2016). Mineralogical modelling and petrophysical parameters in Permian gas shales from the Roseneath and Murteree formations, Cooper Basin, Australia. Petroleum Exploration and Development, 43(2), 277-284.

Jaeger, J. C., Cook, N. G., & Zimmerman, R. (2007). Fundamentals of rock mechanics. 4th ed., Blackwell Publishing, Oxford, United Kingdom.

Jamison, W. R., & Spang, J. H. (1976). Use of calcite twin lamellae to infer differential stress. Geological Society of America Bulletin, 87(6), 868–872.

Janssen, C., Rybacki, E., & Dresen, G. (2007). Critical Re-Evaluation of Calcite Twins as a Low-Temperature Deformation Geothermometer. Geophysical Research Abstracts, 9, 1607-7962/gra/EGU2007-A-02228.

Johnson, R. L. Jr., Abul Khair, H., Jeffrey, R. G., Meyer, J. J., Stark, C., & Tauchintz, J. (2015). Improving fracture initiation and potential impact on fracture coverage by implementing optimal well planning and drilling methods for typical stress conditions in the Cooper Basin, Central Australia. The APPEA Journal and Conference Proceedings, 55, extended abstract.

Jolie, E., Moeck, I., & Faulds, J. E. (2015). Quantitative structural geological exploration of fault-controlled geothermal systems—A case study from the Basin-and-Range Province, Nevada (USA). Geothermics 54, 54-67.

Kantsler, A. J., Prudence, T. J. C., Cook, A. C., & Zwigulis, M. (1984). Hydrocarbon habitat of the Cooper/Eromanga basin, Australia. In: Petroleum geochemistry and basin evolution (eds. G. Demaison and R. J. Murris), pp 373-390. American Association of Petroleum Geologists Memoir 35.

Katz, Y., Weinberger, R., & Aydin, A. (2004). Geometry and kinematic evolution of Riedel shear structures, Capitol Reef National Park, Utah. Journal of Structural Geology, 26(3). 491-501.

King, R. C., Hillis, R. R., & Reynolds, S. D. (2008). In situ stresses and natural fractures in the Northern Perth Basin, Australia. Australian Journal of Earth Sciences, 55(5). 685-701.

King, R., Abul Khair, H., Bailey, A., Backé, G., Holford, S., & Hand, M. (2011). Integration of In-Situ Stress Analysis and Three-Dimensional Seismic Mapping to Understand Fracture Networks in Australian Basins. Australian Geothermal Energy Conference 2011, 129-134.

Kuang, K. S. (1985). History and style of Cooper-Eromanga Basin structures. Exploration Geophysics, 16, 245-248.

Lacombe, O., Angelier, J., Laurent, P., Bergerat, F., & Tourneret, C. (1990). Joint analyses of calcite twins and fault slips as a key for deciphering polyphase tectonics: Burgundy as a case study. Tectonophysics, 182(3), 279–300.

Lacombe, O. (1992). Maclage, fracturation et paléocontraintes intraplaques : application à la plateforme carbonatée ouest-européenne. Ph.D. Thesis, VI, Université de Paris, 316.

Lacombe, O., Angelier, J., & Laurent, P. (1992). Determining paleostress orientations from faults and calcite twins: A case study near the Sainte-Victoire Range (southern France). Tectonophysics, 201(1), 141–156.

Lacombe, O., & Laurent, P. (1992). Determination of principal stress magnitudes using calcite twins and rock mechanics data. Tectonophysics, 202(1), 83-93.

Lacombe, O., Laurent, P., & Angelier, J. (1994). Calcite twins as a key to paleostresses in sedimentary basins: Preliminary results from drill cores of the Paris basin. In F. Roure (Ed.), Peri-Tethyan Platforms, Revue Institut Français du Pétrole, Technip, Paris, 197-210.

Lacombe, O., & Laurent, P. (1996). Determination of deviatoric stress tensors based on inversion of calcite twin data from experimentally deformed monophase samples: Preliminary results. Tectonophysics, 255(3), 189–202.

Lacombe, O. (2001). Paleostress magnitudes associated with development of mountain belts: Insights from tectonic analyses of calcite twins in the Taiwan Foothills. Tectonics, 20(6), 834–849, doi:10.1029/2001TC900019.

Lacombe, O., Mouthereau, F., Kargar, S., & Meyer, B. (2006). Late Cenozoic and modern stress fields in the western Fars (Iran): Implications for the tectonic and kinematic evolution of central Zagros. Tectonics, 25, TC1003, doi:10.1029/2005TC001831.

Lacombe, O. (2007). Comparison of paleostress magnitudes from calcite twins with contemporary stress magnitudes and frictional sliding criteria in the continental crust: Mechanical implications. Journal of Structural Geology, 29(1), 86–99.

Lacombe, O., Amrouch, K., Mouthereau, F., & Dissez, L. (2007). Calcite twinning constraints on late Neogene stress patterns and deformation mechanisms in the active Zagros collision belt. Geology, 35(3), 263–266.

Lacombe, O., Malandain, J., Vilasi, N., Amrouch, K., & Roure, F. (2009). From paleostresses to paleoburial in fold–thrust belts: Preliminary results from calcite twin analysis in the Outer Albanides. Tectonophysics, 475(1), 128-141.

Lacombe, O. (2010). Calcite twins, a tool for tectonic studies in thrust belts and stable orogenic forelands. Oil & Gas Science Technology–Revue IFP Energies Nouvelles, 65(6), 809–838.

Lacombe, O. (2012). Do fault slip data inversions actually yield “paleostresses” that can be compared with contemporary stresses? A critical discussion. Comptes Rendus Geoscience, 344(3), 159-173.

Laurent, P. (1984). Les macles de la calcite en tectonique: Nouvelles me thodes dynamiques et premieres applications, these doctorat-es-sciences, 324 pp., Univ. Sci. et Tech. du Languedoc, Montpellier, France.

Laurent, P., Kern, H., & Lacombe, O. (2000). Determination of deviatoric stress tensors based on inversion of calcite twin data from experimentally deformed monophase samples. Part II. Axial and triaxial stress experiments. Tectonophysics, 327(1), 131–148.

Lemon, D., O'Neill, B., & Ngothai, Y. (2012). A mineralogical study of the wellbore scale from Santos-operated cooper basin wells. Chemeca 2012: Quality of life through chemical engineering: 23-26 September 2012, Wellington, New Zealand, 1414.

Li, Z. X., Bogdanova, S. V., Collins, A. S., Davidson, A., De Waele, B., Ernst, R. E., Fitzsimons, I. C. W., Fuck, R. A., Gladkochub, D. P., Jacobs, J., Karlstrom, K. E., Lu, S., Natapov, L. M., Pease, V., Pisarevsky, S. A., Thrane, K., & Vernikovsky, V. (2008). Assembly, configuration, and break-up history of Rodinia: a synthesis. Precambrian research, 160(1), 179-210.

Lin, A., & Yamashita, K. (2013). Spatial variations in damage zone width along strike-slip faults: An example from active faults in southwest Japan. Journal of Structural Geology, 57, 1-15.

Lisle, R.J. (1994). Detection of zones of abnormal strains in structures using Gaussian curvature analysis. AAPG Bulletin 78(12), 1811-1819.

Lowe-Young, B. S., Mackie, S. I., & Heath, R. S. (1997). The Cooper-Eromanga petroleum system, Australia: Investigation of essential elements and processes. Indonesian Petroleum Association. Proceedings of the Petroleum Systems of SE Asia and Australasia Conference, Jakarta, 199-211.

Luo, M., Wood, J. R., & Cathles, L. M. (1994). Prediction of thermal conductivity in reservoir rocks using fabric theory. Journal of applied geophysics, 32(4). 321-334.

Macdonald, J., Backé, G, King, R., Holford, S., & Hillis, R. (2012). Geomechanical modelling of fault reactivation in the Ceduna Sub-basin, Bight Basin, Australia. Geological Society, London, Special Publications 367, (1), 71-89.

Mackie, S. (2015). History of Petroleum Exploration and Development in the Cooper and Eromanga Basins. AAPG/SEG International Conference and Exhibition, Melbourne, Australia, Search and Discovery Article #10814.

Maerten, L., Maerten, F., Lejri, M., & Gillespie, P. (2016). Geomechanical paleostress inversion using fracture data. Journal of Structural Geology, 89, 197-213.

Mai, H. T., Marfurt, K. J., & Chávez-Pérez, S. (2009). Coherence and volumetric curvatures and their spatial relationship to faults and folds, an example from Chicontepec basin. Proceedings of the Society of Exploration Geophysicists International Exposition and Annual Meeting, Houston, 1063-1067.

Mann, D.M., & Mackenzie, A.S. (1990). Prediction of pore fluid pressures in sedimentary basins. Marine and Petroleum Geology, 7, 55–65.

Mavromatidis, A. (2006). Burial/exhumation histories for the Cooper-Eromanga Basins and implications for hydrocarbon exploration, Eastern Australia. Basin Research 18, 351-373.

Mavromatidis, A. (2008). Two layer model of lithospheric compression and uplift/exhumation in an intracratonic setting: an example from the Cooper–Eromanga Basins, Australia. International Journal of Earth Sciences, 97(3). 623-634.

McClay, K., & Bonora, M. (2001). Analog models of restraining stepovers in strike-slip fault systems. AAPG Bulletin, 85(2). 233-260.

Mcgowen, J.M., Gilbert, J.V. & Samari, E. (2007). Hydraulic Fracturing Down Under. Hydraulic Fracturing Technology Conference, College station, Texas, 29–31 January, SPE-106051-MS.

Meissner, F.F., (1978). Petroleum geology of the Bakken Formation. Williston Basin Symposium, Montana Geological Society 24th Annual Conference, 207-227.

Meixner, T. J., Gunn, P. J., Boucher, R. K., Yeates, T. N., Richardson, L. M., & Frears, R. A. (2000). The nature of the basement to the Cooper Basin region, South Australia. Exploration Geophysics, 31. 24-32.

Metcalfe, I. (2013), Gondwana dispersion and Asian accretion: tectonic and palaeogeographic evolution of eastern Tethys. Journal of Asian Earth Sciences, 66, 1-33.

Michael, A. J. (1984). Determination of stress from slip data: faults and folds. Journal of Geophysical Research: Solid Earth, 89(B13), 11517-11526.

Mildren, S. D., Hillis, R. R., Lyon, P. J., Meyer, J. J., Dewhurst, D. N., & Boult, P. J. (2005). FAST: A new technique for geomechanical assessment of the risk of reactivation-related breach of fault seals. In

Evaluating fault and cap rock seals. AAPG Hedberg Series: AAPG Hedberg Series, no. 2 (eds. P. Boult and J. Kaldi), pp. 73-85. AAPG.

Mitchum, R. M., Vail, P. R., & Sangree, J. B. (1977). Stratigraphic interpretation of seismic reflection patterns in depositional sequences. Part 6, in Seismic Stratigraphy-Application to Hydrocarbon Exploration, AAPG, Tulsa, Okla, 8, 117-133.

Moeck, I., Kwiatek, G., & Zimmermann, G. (2009). Slip tendency analysis, fault reactivation potential and induced seismicity in a deep geothermal reservoir. Journal of Structural Geology 31(10), 1174-1182.

Moore, P. S. (1986). An exploration overview of the Eromanga Basin. Contributions to the geology and hydrocarbon potential of the Eromanga Basin. Geological Society of Australia Special Publication, 12, 1-8.

Morris, A., Ferrill, D. A., & Henderson, D. B. (1996), Slip-tendency analysis and fault reactivation. Geology, 24(3), 275-278.

Mount, T. J. (1981). Dullingari North 1--an oil discovery in the Murta Member of the Eromanga Basin. Australian Petroleum Exploration Association Journal, 21(1), 71-77.

Müller, R. D., Dyksterhuis, S., & Rey, P. (2012). Australian paleo-stress fields and tectonic reactivation over the past 100 Ma. Australian Journal of Earth Sciences, 59, 13-28.

Müller, R. D., & Dyksterhuis, S. (2005). Current and palaeo-stress models for central Australian basins. In Proceedings of the Central Australian Basins Symposium, Alice Springs, 1-9.

Müller, R. D., Flament, N., Matthews, K. J., Williams, S. E., & Gurnis, M. (2016). Formation of Australian continental margin highlands driven by plate–mantle interaction. Earth and Planetary Science Letters, 441, 60-70.

Murray, G. H. (1968). Quantitative fracture study-Spanish Pool, McKenzie County, North Dakota. AAPG Bulletin, 52(1), 57-65.

Myers, J. S., Shaw, R. D., & Tyler, I. M. (1996). Tectonic evolution of Proterozoic Australia. Tectonics, 15(6), 1431-1446.

Nelson, E. J., Meyer, J. J., Hillis, R. R., & Mildren, S. D. (2005). Transverse drilling-induced tensile fractures in the West Tuna area, Gippsland Basin, Australia: implications for the in situ stress regime. International Journal of Rock Mechanics and Mining Sciences, 42(3), 361-371.

Nelson, E. J., Chipperfield, S. T., Hillis, R. R., Gilbert, J., & McGowen, J. (2007). Using geological information to optimize fracture stimulation practices in the Cooper Basin, Australia. Petroleum Geoscience, 13(1), 3-16.

Nelson, E. J., Chipperfield, S. T., Hillis, R. R., Gilbert, J.,McGowen, J., & Mildren, S. D. (2007). The relationship between closure pressures from fluid injection tests and the minimum principal stress in strong rocks. International Journal of Rock Mechanics and Mining Sciences, 44, 787-801.

Nelson, E., Hillis, R., Sandiford, M., Reynolds, S., & Mildren, S. (2006). Present-day state-of-stress of southeast Australia. APPEA journal, 46(1), 283-305.

Nemcok, M., & Lisle, R. J. (1995). A stress inversion procedure for polyphase fault/slip data sets. Journal of Structural Geology, 17(10), 1445-1453.

Neves, F. A., Zahrani, M. S., & Bremkamp, S. W. (2004). Detection of potential fractures and small faults using seismic attributes. The Leading Edge, 23, (9), 903-906.

Newman, J. (1994). Influence of grain size and grain size distribution on methods for estimating paleostresses from twinning in carbonates. Journal of Structural Geology, 16(12), 1589-1601.

Nie, X., Zou, C., Pan, L., Huang, Z., & Liu, D. (2013). Fracture analysis and determination of in-situ stress direction from resistivity and acoustic image logs and core data in the Wenchuan Earthquake Fault Scientific Drilling Borehole-2 (50–1370m). Tectonophysics, 593, 161-171.

Oldham, A. C., & Gibbins, N. M., (1995). Lake Hope 3D-A case study. Exploration Geophysics, 26, 383-394.

Osborne, M. J. & Swarbrick, R. E. (1997). Mechanisms for generating overpressure in sedimentary basins: a re-evaluation. AAPG Bulletin, 81(6), 1023-1041.

Othman, A. A., Fathy, M., & Maher, A. (2016). Use of spectral decomposition technique for delineation of channels at Solar gas discovery, offshore West Nile Delta, Egypt. Egyptian Journal of Petroleum, 25(1), 45-51.

Partyka, G., Gridley, J., & Lopez, J. (1999). Interpretational applications of spectral decomposition in reservoir characterization. The Leading Edge, 18(3), 353-360.

Pokalai, K., Fei, Y., Ahmad, M., Haghighi, M., & Gonzalez, M. (2015a). Design and optimisation of multi-stage hydraulic fracturing in a horizontal well in a shale gas reservoir in the Cooper Basin, South Australia. The APPEA Journal 55, 1–14.

Pokalai, K., Haghighi, M., Sarkar, S., Tyiasning, S., & Cooke, D. (2015b). Investigation of the Effects of Near-Wellbore Pressure Loss and Pressure Dependent Leakoff on Flowback during Hydraulic Fracturing with Pre-Existing Natural Fractures. SPE/IATMI Asia Pacific Oil and Gas Conference and Exhibition, Nusa Dua, Bali, SPE-176440.

Pollard, D. D., & Aydin, A. (1988). Progress in understanding jointing over the past century. Geological Society of America Bulletin, 100(8), 1181–1204.

Price, N.J., & Cosgrove, J.W. (1990). Analysis of geological structures. Cambridge University Press, Cambridge.

Radke, B. (2009). Hydrocarbon and Geothermal Prospectivity of Sedimentary Basins in Central Australia; Warburton, Cooper, Pedirka, Galilee, Simpson and Eromanga Basins. Geoscience Australia Record 2009/25.

Raleigh, C.B., Healy, J.H. & Bredehoeft, J.D. (1976). An experiment in earthquake control at Rangeley, Colorado. Science, 191, 1230-1237.

Ramsay, J. G. (1962). The geometry of conjugate fold systems. Geol. Mag., 99(06), 516–526.

Reches, Z. E., Baer, G., & Hatzor, Y. (1992). Constraints on the strength of the upper crust from stress inversion of fault slip data. Journal of Geophysical Research: Solid Earth, 97(B9), 12481-12493.

Rees, P. M., Ziegler, A. M., Gibbs, M. T., Kutzbach, J. E., Behling, P. J., & Rowley, D. B. (2002). Permian phytogeographic patterns and climate data/model comparisons. The Journal of Geology, 110(1), 1-31.

Reeves, C., & De Wit, M. (2000). Making ends meet in Gondwana: retracing the transforms of the Indian Ocean and reconnecting continental shear zones. Terra Nova, 12(6), 272-280.

Reynolds, S. D., Mildren, S. D., Hillis, R. R., & Meyer, J. J. (2006). Constraining stress magnitudes using petroleum exploration data in the Cooper-Eromanga Basins, Australia. Tectonophysics, 415, 123-140.

Reynolds, S. D., Coblentz, D. D., & Hillis, R. R. (2002). Tectonic forces controlling the regional intraplate stress field in continental Australia: Results from new finite element modelling. Journal of Geophysical Research, 107(B7). 2131.

Reynolds, S. D., Coblentz, D. D., & Hillis, R. R. (2003). Influences of plate-boundary forces on the regional intraplate stress field of continental Australia. Geological Society of America Special Papers, 372, 59-70.

Reynolds, S. D., Mildren, S. D., Hillis, R. R., & Meyer, J. J. (2004). The in situ stress field of the Cooper Basin and its implications for hot dry rock geothermal energy development. In PESA Eastern Australasian Basins Symposium II (2004: Adelaide, South Australia).

Reynolds, S. D., Mildren, S. D., Hillis, R. R., Meyer, J. J., & Flottmann, T. (2005). Maximum horizontal stress orientations in the Cooper Basin, Australia. implications for plate-scale tectonics and local stress sources. Geophysical Journal International, 160, 331-343.

Rezaee, M. R., & Sun, X. (2007). Fracture-Filling Cements in the Palaeozoic Warburton Basin, South Australia. Journal of Petroleum Geology, 30(1), 79-90.

Roberts, A. (2001). Curvature attributes and their application to 3D interpreted horizons. First Break, 19(2), 85-100.

Roberts, G. A., Chipperfield, S. T., & Miller, W. K. (2000). The evolution of a high near-wellbore pressure loss treatment strategy for the Australian Cooper Basin. In SPE Annual Technical Conference and Exhibition. Society of Petroleum Engineers.

Robson, A. G., King, R. C., & Holford, S. P. (2016a). 3D seismic analysis of gravity-driven and basement influenced normal fault growth in the deepwater Otway Basin, Australia. Journal of Structural Geology, 89, 74-87.

Robson, A. G., King, R. C., & Holford, S. P. (2016b). Structural evolution of a gravitationally detached normal fault array: analysis of 3D seismic data from the Ceduna Sub-Basin, Great Australian Bight. Basin Research, 1-20, doi:10.1111/bre.12191.

Rocher, M., Cushing, M., Lemeille, F., Lozac'h, Y., & Angelier, J. (2004). Intraplate paleostresses reconstructed with calcite twinning and faulting: improved method and application to the eastern Paris Basin (Lorraine, France). Tectonophysics, 387(1), 1-21.

Rocher, M., Lacombe, O., Angelier, J., & Chen, H. W. (1996). Mechanical twin sets in calcite as markers of recent collisional events in a fold-and-thrust belt: Evidence from the reefal limestones of southwestern Taiwan. Tectonics, 15(5), 984-996.

Rocher, M., Lacombe, O., Angelier, J., Deffontaines, B., & Verdier, F. (2000). Cenozoic folding and faulting in the south Aquitaine Basin (France): insights from combined structural and paleostress analyses. Journal of Structural Geology, 22(5), 627-645.

Rocher M., Cushinga M., Lemeille F., Lozac'h Y, & Angelier J. (2004). Intraplate paleostresses reconstructed with calcite twinning and faulting: improved method and application to the eastern Paris Basin (Lorraine, France). Tectonophysics, 387, 1–21

Rowe, K. J., & Rutter, E. H. (1990). Palaeostress estimation using calcite twinning: experimental calibration and application to nature. Journal of Structural Geology, 12(1). 1-17.

Rutqvist, J., Rinaldi, A. P., Cappa, F., & Moridis, G. J. (2013). Modeling of fault reactivation and induced seismicity during hydraulic fracturing of shale-gas reservoirs. Journal of Petroleum Science and Engineering, 107, 31-44.

Sandiford, M., Wallace, M., & Coblentz, D. (2004). Origin of the in situ stress field in south-eastern Australia. Basin Research, 16(3), 325-338.

Schmid, S.M., & Paterson, M.S. (1977). Strain analysis in an experimentally deformed oolitic limestone. In: Saxena, K., Battacharji, S. (Eds.), Energetics of Geological Processes. Springer-Verlag, New York, 67-93.

Seeburger, D. A., & Zoback, M. D. (1982). The distribution of natural fractures and joints at depth in crystalline rock. Journal of Geophysical Research: Solid Earth, (1978–2012), 87(B7), 5517-5534.

Senior, B. R., Galloway, M. C., Ingram, J. A., & Senior, D. (1968). The geology of the Barrolka, Eromanga, Durham Downs, Thargomindah, Tickalara and Bulloo 1:250,000 Sheet areas, Queensland. Bureau of Mineral Resources.

Shaw, R. D., Etheridge, M. A., & Lambeck, K. (1991). Development of the Late Proterozoic to Mid-Paleozoic, intracratonic Amadeus Basin in central Australia: A key to understanding tectonic forces in plate interiors. Tectonics, 10(4), 688-721.

Sibson, R. H. (1985). A note on fault reactivation. Journal of Structural Geology, 7(6), 751-754.

Sibson, R. H. (1990). Conditions for fault-valve behaviour. Geological Society, London, Special Publications, 54(1), 15-28.

Sibson, R. H. (1996). Structural permeability of fluid-driven fault-fracture meshes. Journal of Structural Geology, 18, 1031-1042.

Sibson, R. H. (2003). Brittle-failure controls on maximum sustainable overpressure in different tectonic regimes. AAPG Bulletin, 87(6), 901-908.

Silliphant, L. J., Engelder, T., & Gross, M. R. (2002). The state of stress in the limb of the Split Mountain anticline, Utah: constraints placed by transected joints. Journal of Structural Geology, 24(1), 155-172.

Spang, J. H. (1972). Numerical method for dynamic analysis of calcite twin lamellae. Geological Society of American Bulletin, 83(2). 467-472.

Spencer, C. W. (1987). Hydrocarbon generation as a mechanism for overpressuring in Rocky Mountain region. AAPG Bulletin, 71(4), 368-388.

Sperner, B., & Ratschbacher, L. (1994). A turbo program package for graphical presentation and stress analysis of calcite deformation. Z. Dtsch. Geol. Ges., 145, 414-423.

Spiers, C.J. (1982). The development of deformation textures in calcite rocks. PhD Thesis. University of London, England, UK.

Spiers, C. J., & Rutter, E. H. (1984). A calcite twinning paleo-piezometer. Progress in Experimental Petrology, D25, 241-245.

Stainsby, S. D., & Worthington, M. H. (1985). Q estimation from vertical seismic profile data and anomalous variations in the central North Sea. Geophysics, 50(4), 615-626.

Stanmore, P. J. (1989). Case studies of stratigraphic and fault traps in the Cooper Basin, Australia. In The Cooper and Eromanga Basins, Australia. Proceedings of the Cooper and Eromanga Basins Conference, Adelaide (pp. 361-369).

Stanmore, P. J., & Johnstone, E. M. (1988). The search for stratigraphic traps in the southern Patchawarra trough, South Australia. The APPEA Journal, 8(1), 156-166.

Stuart, W. J. (1976). The genesis of Permian and lower Triassic reservoir sandstones during phases of southern Cooper Basin development. The APEA Journal, 16(1), 27-48.

Sun, Q., Wu, S., Lü, F., & Yuan, S. (2010). Polygonal faults and their implications for hydrocarbon reservoirs in the southern Qiongdongnan Basin, South China Sea. Journal of Asian Earth Sciences 39, (5), 470-479.

Sun, X. (1997). Structural style of the Warburton Basin and control in the Cooper and Eromanga Basins, South Australia. Exploration Geophysics, 28, (3), 333-339.

Sun, X. (1999). Fracture analysis of the Eastern Warburton Basin (Early Paleozoic). South Australia. National Centre for Petroleum Geology and Geophysics. Report Book, 99, 00014.

Swierczek, E., Zhen-dong, C., Holford, S., Backé, G., King, R., & Mitchell, A. (2013). Quantifying fault reactivation risk in the western Gippsland basin using geomechanical modelling. The APPEA Journal, 53, 255-272.

Tavani, S., Storti, F., Lacombe, O., Corradetti, A., Muñoz, J. A., & Mazzoli, S. (2015). A review of deformation pattern templates in foreland basin systems and fold-and-thrust belts: Implications for the state of stress in the frontal regions of thrust wedges. Earth-Science Reviews, 141, 82-104.

Tingay, M., Hillis, R., Swarbrick, R., Morley, C. & Damit, A. (2007). 'Vertically transferred'' overpressures in Brunei: Evidence for a new mechanism for the formation of high magnitude overpressures. Geology, 35, 1023–1026.

Tingay, M.R., Hillis, R.R., Swarbrick, R.E., Morley, C.K., & Damit, A.R. (2009). Origin of overpressure and pore-pressure prediction in the Baram province, Brunei. AAPG Bulletin, 93(1), 51-74.

Tourneret, C., & Laurent, P. (1990). Paleo-stress orientations from calcite twins in the North Pyrenean foreland, determined by the Etchecopar inverse method. Tectonophysics, 180(2). 287-302.

Tripathy, V., & Saha, D. (2015). Inversion of calcite twin data, paleostress reconstruction and multiphase weak deformation in cratonic interior–Evidence from the Proterozoic Cuddapah basin, India. Journal of Structural Geology, 77, 62-81.

Tullis, T.E. (1980). The use of mechanical twinning in minerals as a measure of shear stress magnitudes. Journal of Geophysical Research, 85, 6263-6268.

Turner, F. J. (1953), Nature and dynamic interpretation of deformation lamellae in calcite of three marbles. American Journal of Science, 251(4), 276-298.

Turner, F. J., Griggs, D. T., & Heard, H. (1954). Experimental deformation of calcite crystals. Geological Society of America Bulletin, 65(9), 883–934.

Turner, F. J., & Orozco, M. (1976). Crystal bending in metamorphic calcite, and its relations to associated twinning. Contributions to Mineralogy and Petrology, 57(1). 83-97.

Tyiasning, S., & Cooke, D. (2015). A comparison of competing amplitude variation with offset techniques applied to tight gas sand exploration in the Cooper Basin of Australia. Interpretation, 3(3), SZ15-SZ26.

Tyiasning, S., & Cooke, D. (2016). Anisotropy signatures in the Cooper Basin of Australia: Stress versus fractures. Interpretation, 4(2), SE51-SE61.

Vail, P. R., Mitchum, R. M., & Thompson, S. (1977). Seismic stratigraphy and global changes of sea-level. Part 3: Relative changes of sea level from coastal onlap, in Seismic Stratigraphy-Applications to Hydrocarbon Exploration. AAPG Memoirs, AAPG, Tulsa, Okla, 26, 63-81,

Van der Meer, D. G., Torsvik, T. H., Spakman, W., Van Hinsbergen, D. J. J., & Amaru, M. L. (2012). Intra-Panthalassa Ocean subduction zones revealed by fossil arcs and mantle structure. Nature Geoscience, 5(3), 215-219.

van Ruth, P. J., Nelson, E. J., & Hill R. R. 2006. Fault reactivation potential during CO2 injection in the Gippsland Basin, Australia. Exploration Geophysics, 37(1), 50-59.

Van Ruth, P. & Hillis, R. (2000). Estimating pore pressure in the Cooper Basin, South Australia: sonic log method in an uplifted basin. Exploration Geophysics, 31(1/2), 441-447.

Van Ruth, P., Hillis, R., Tingate, P., & Swarbrick, R. (2003). The origin of overpressure in 'old' sedimentary basins: an example from the Cooper Basin, Australia. Geofluids, 3(2), 125-131.

Veevers, J. J., & Powell, C. M. (1984). Uluru and Adelaidean regimes. In J. J. Veevers (ed.), Phanerozoic earth history of Australia: Oxford, Clarendon Press, 329–339.

Veevers, J. J., Powell, C. M., & Roots, S. R. (1991). Review of seafloor spreading around Australia. I. Synthesis of the patterns of spreading. Australian Journal of Earth Sciences, 38(4), 373-389.

Veevers, J. J., Jones, J. G., & Powell, C. M. (1982). Tectonic framework of Australia's sedimentary basins. APEA Journal, 22(1), 283-300.

Wangen, M. (2001). A quantitative comparison of some mechanisms generating overpressure in sedimentary basins. Tectonophysics, 334, 211-234.

Watterson, J., Walsh, J., Nicol, A., Nell, P. A. R., & Bretan, P. G. (2000). Geometry and origin of a polygonal fault system. Journal of the Geological Society, 157(1), 151-162.

Weathers, M. S., Bird, J. M., Cooper, R.F., & Kohlstedt, D. L. (1979). Differential stress determined from deformation-induced microstructures of the Moine Thrust Zone. Journal of Geophysical Research: Solid Earth, 84(B13), 7495-7509.

Weng, X., Kresse, O., Cohen, C., Wu, R., & Gu, H. (2011). Modeling of hydraulic-fracture-network propagation in a naturally fractured formation. SPE Production and Operations, 26(4), 368-380.

White, A. J., Traugott, M. O., & Swarbrick, R. E. (2002). The use of leak-off tests as means of predicting minimum in-situ stress. Petroleum Geoscience, 8(2). 189-193.

Wilcox, R. E., Harding, T. T., & Seely, D. R. (1973). Basic wrench tectonics. AAPG Bulletin, 57(1), 74-96.

Williams, G. D., Powell, C. M., & Cooper, M. A. (1989). Geometry and kinematics of inversion tectonics. Geological Society, London, Special Publications, 44(1), 3-15.

Willis, I. L., Brown, R. E., Stroud, W. J., & Stevens, B. P. J. (1983). The early Proterozoic Willyama supergroup: Stratigraphic subdivision and interpretation of high to low-grade metamorphic rocks in the Broken Hill Block, New South Wales. Journal of the Geological Society of Australia, 30(1/2), 195-224.

Wiprut, D., & Zoback, M. D. (2000). Fault reactivation and fluid flow along a previously dormant normal fault in the northern North Sea. Geology, 28(7), 595-598.

Wiprut, D., & Zoback, M. D. (2002). Fault reactivation, leakage potential, and hydrocarbon column heights in the northern North Sea. Norwegian Petroleum Society Special Publications, 11, 203-219.

Woodcock, N. H., & Fischer, M. (1986). Strike-slip duplexes. Journal of structural geology, 8(7), 725-735.

Woodcock, N. H., & Rickards, B. (2003). Transpressive duplex and flower structure: Dent Fault System, NW England. Journal of Structural Geology, 25(12), 1981-1992.

Wopfner, H. (1988). Oil and gas in Australia. GeoJournal, 16(4), 371-386.

Worum, G., van Wees, J. D., Bada, G., van Balen, R. T., Cloetingh, S., & Pagnier, H. (2004). Slip tendency analysis as a tool to constrain fault reactivation: A numerical approach applied to three-dimensional fault models in the Roer Valley rift system (southeast Netherlands). Journal of Geophysical Research: Solid Earth, 109(B2), 1-16.

Yan, D. P., Zhang, B., Zhou, M. F., Wei, G. Q., Song, H. L., & Liu, S. F. (2009). Constraints on the depth, geometry and kinematics of blind detachment faults provided by fault propagation folds: An example

from the Mesozoic fold belt of South China. Journal of Structural Geology, 31, 150–162, doi: 10.1016/j.jsg.2008.11.005.

Yang, Z., Crosby, D. G., Akgun, F., Khurana, A. K., & Rahman, S. S. (1997). Investigation of the factors influencing hydraulic fracture initiation in highly stressed formations. In Asia Pacific oil & gas conference & exhibition, 247-258.

Yassir, N. A., & Bell, J.S. (1996). Abnormally high fluid pressures and associated porosities and stress regimes in sedimentary basins. SPE Formation evaluation, 11(1), 5-10.

Zoback, M. D., & Harjes, H. P. (1997). Injection-induced earthquakes and crustal stress at 9 km depth at the KTB deep drilling site, Germany. Journal of Geophysical Research, 102(B8), 18477-18491.

Zoback, M. D., Barton, C. A., Brudy, M., Castillo, D. A., Finkbeiner, T., Grollimund, B. R., & Wiprut, D. J. (2003). Determination of stress orientation and magnitude in deep wells. International Journal of Rock Mechanics and Mining Sciences, 40(7). 1049-1076."

Zoback, M. L., Zoback, M. D., Adams, J., Assumpcao, M., Bell, S., Bergman, E. A., Blumling, P., Brereton, N. R., Denham, D., Ding, J., Fuchs, K., Gay, N., Gregersen, S., Gupta, H. K., Gvishiani, A., Jacob, K., Klein, K., Knoll, P., Magee, M., Mercier, J. L., Muller, B. C., Paquin, C., Rajendran, K., Stephansson, O., Suarez, G., Suter, M., Udias, A., Xu, Z. H., & Zhizhin, M. (1989). Global patterns of tectonic stress. Nature, 341(6240), 291-298.

Zoback, M. D., & Harjes, H. P. (1997), Injection-induced earthquakes and crustal stress at 9 km depth at the KTB deep drilling site, Germany. Journal of Geophysical Research, 102(18), 18,477-18,491.

5. THESIS BODY

The body of this thesis contains research chapters in the form of publications or un-published manuscripts. Each chapter begins with a statement outlining the purpose, methods, and key results of the manuscript followed by an author contribution document outlining the contributions made by each author. For chapters that have been published, the final journal edition is included. Unpublished manuscripts are included and may be formatted differently to the thesis based on the requirements given by the journal that they have been/will be submitted to.

5.1. MANUSCRIPT 1: Seismic depth conversion uncertainty

A Statistical Approach to Assessing Depth Conversion Uncertainty on a Regional Dataset: Cooper-Eromanga Basin, Australia

This work was presented at the 2016 ASEG-PESA-AIG Conference in Adelaide and forms the framework of the full-length paper "An automated cross-validation method to assess seismic time-to-depth conversion accuracy: A case study on the Cooper-Eromanga Basin, Australia", which could not be included in the thesis due to the extended approval process at Santos Ltd.

Accurate seismic time-to-depth conversion has been shown to have significant implications on the success of exploration wells targeting low amplitude Jurassic to Cretaceous structural traps. The presence of these traps can depend on the conversion method being used and has resulted in many dry wells targeting 'pseudo-structures'. This study used 13 three-dimensional seismic surveys, 73 interpreted two-way-time reflector grids, and 657 wells to calculate approximately 10000 error values and their associated variables (number of wells used, closest well distance, average well distance, inside or outside well data envelope, crest or flank well, and the formation being depth converted). The results found that although the average velocity method was the most accurate on a regional level (±25 ft error), the most accurate method can change and the expected error can deviate by 10's of feet depending on the combination and value of the most significant variables. Using cluster analysis, the most significant variables were found to be the closest well distance, the spatial location (field), the formation being depth converted, and the location of the well that is predicted relative to the existing well data envelope (inside or outside envelope).

CITATION:

Kulikowski, D., Hochwald, C., Cooke, D., & Amrouch, K. (2016). A Statistical Approach to Assessing Depth Conversion Uncertainty on a Regional Dataset: Cooper-Eromanga Basin. ASEG-PESA-AIG 25th International Geophysical Conference and Exhibition, Adelaide, Australia, 488-494, extended abstract #200, doi:10.1071/ASEG2016ab085.

Statement of Authorship

Title of Paper:	A Statistical Approach to Assessing Depth Conversion Uncertainty on a Regional Dataset: Cooper-Eromanga Basin, Australia
Publication Status:	**Manuscript Published**
Publication Details:	Kulikowski, D., Hochwald, C., Cooke, D., & Amrouch, K. (2016). A Statistical Approach to Assessing Depth Conversion Uncertainty on a Regional Dataset: Cooper-Eromanga Basin, Australia. ASEG-PESA-AIG 2016 Conference, Adelaide. Extended abstract #200, 484-490, doi:10.1071/aseg2016ab200.

Principal Author

Principal Author (Candidate):	David Kulikowski		
Contribution to the Paper:	Completing and running looping script, data collection, analysis, interpretation, and writing.		
Overall percentage (%):	45%		
Certification:	This paper reports on original research I conducted during the period of my Higher Degree by Research candidature and is not subject to any obligations or contractual agreements with a third party that would constrain its inclusion in this thesis. I am the primary author of this paper.		
Signature:		Date:	12 September 2017

Co-Author Contribution

By signing the Statement of Authorship, each author certifies that:

i. the candidate's stated contribution to the publication is accurate (as detailed above);

ii. permission is granted for the candidate to include the publication in the thesis; and

iii. the sum of all co-author contributions is equal to 100% less the candidate's stated contribution.

Name of Co-Author:	Catherine Hochwald (45%)		
Contribution to the Paper:	Research setup, script framework, analysis of results and complete a review of paper.		
Signature:		Date:	22 September 2017

Name of Co-Author:	Dennis Cooke (5%)		
Contribution to the Paper:	Feedback on manuscript structure and a complete review of paper.		
Signature:		Date:	12 September 2017

Name of Co-Author:	Khalid Amrouch (5%)		
Contribution to the Paper:	Feedback on manuscript structure and a complete review of paper.		
Signature:		Date:	12 September 2017

ASEG-PESA-AIG 2016
25TH GEOPHYSICAL
CONFERENCE & EXHIBITION
Interpreting the Past, Discovering the Future

A Statistical Approach to Assessing Depth Conversion Uncertainty on a Regional Dataset: Cooper-Eromanga Basin, Australia.

David Kulikowski*
University of Adelaide
North Tce, Adelaide, 5005
david.kulikowski@adelaide.edu.au

Catherine Hochwald
Santos Ltd
60 Flinders St, Adelaide, 5000
cathy.hochwald@santos.com

Dennis Cooke
University of Adelaide
North Tce, Adelaide, 5005
dennis.cooke@adelaide.edu.au

Khalid Amrouch
University of Adelaide
North Tce, Adelaide, 5005
khalid.amrouch@adelaide.edu.au

SUMMARY

Deciding on the most accurate grid based depth conversion method can often be an arbitrary choice made by geophysicists, particularly if previous research is limited. The importance of accurate depth conversion is particularly crucial in the Cooper-Eromanga Basin, where the presence of oil rich, low relief structural traps are questionable depending on the method used. Previous depth conversion studies are limited to local scales, limited well control and a focus on select horizons. To investigate the depth conversion uncertainty on a regional scale, this research performs a comprehensive and regionally extensive depth conversion analysis utilising 13 3D seismic surveys with 73 interpreted TWT grids and 657 wells. Depth conversions were performed using the 4 most commonly used methods; average (pseudo) velocity, time-depth trend, kriging with external drift using TWT, and kriging with external drift to tie stacking velocities to average well velocities.

To manage the large volume of data, a looping script was written to automate the depth conversion process and utilise the cross-validation, or blind-well method (use n wells to predict the $n^{th}+1$ well). Statistics on several variables were captured after each loop, with cluster analysis performed on the final data set to test variable significance on depth conversion accuracy. A database of approximately 10000 error calculations found that although the average velocity method is the most accurate at a high level (average absolute error ~24.9 feet), the best method and the expected error changes significantly (tens of feet) depending on the combination and value of the most significant variables. The variables which impacted uncertainty the most were; location (3d survey), formation, distance to the nearest well, and the spatial location of the predicted well relative to the existing well data envelope.

Key words: Cooper Basin; Eromanga Basin; 3D seismic data; depth conversion; velocity modelling.

INTRODUCTION

The introduction of three-dimensional (3D) seismic data has become almost essential for successful hydrocarbon exploration and development; the probability of a successful exploration well within 3D seismic data is >50%, in contrast to ~18% without (Aylor, 1998; Méndez-Hernández, 2003). 3D seismic data can provide an accurate image of the subsurface enabling petroleum companies to interpret and model subsurface structures, stratigraphy, reserves estimates and fluid dynamics. However, since seismic data is acquired in the time domain, an accurate time to depth conversion is essential, particularly in petroleum provinces, such as the Cooper-Eromanga Basin (Figure 1a), where the presence of oil-rich low relief structural traps changes on a local scale and can depend on the depth conversion method being used (Lowe-Young et al., 1997).

The Permian aged Cooper Basin is Australia's largest onshore hydrocarbon province, with the overlying Jurassic to Cretaceous aged Eromanga Basin consisting of low relief structural traps that contain the majority of the oil currently being explored for (Kulikowski et al., 2016a; Lowe-Young et al., 1997; Pokalai et al., 2016). To predict whether low relief structural traps exist within the province, geophysicists must select a depth conversion method that provides minimum error. However, as a detailed study had not been performed, many researchers adopt the most basic methods (Kulikowski et al., 2015; Kulikowski et al., 2016b), or choose to retain seismic data in the time domain (Kuang 1985; Apak et al., 1997; Hillis et al., 2001).

A seismic depth conversion analysis was performed by Hillis et al. (1995) comparing the accuracy of the interval velocity and velocity anomaly (Vo-K) methods; however, their research was restricted to a local study area and performed on two horizons, the Cadna-owie Formation and the Toolachee Formation. They showed that the velocity anomaly method is superior to the interval velocity method; however, these methods are not commonly used in the Cooper-Eromanga Basin. Subsequent research by Rady et al. (2006) and Joraandstad et al. (1999) investigated the depth conversation uncertainty on a local scale using average velocity, interval velocity and stacking velocity methods. These studies both focused on one 3D seismic survey consisting of 15 wells each and with a focus on Jurassic to Cretaceous aged horizons. Their results had contradicting conclusions albeit their research was performed using similar data sets.

To address the limitations in previous studies, this regional, grid-based study uses statistical analysis to examine the four most commonly used depth conversion methods in the Cooper-Eromanga Basin, while also investigating the impact of the most significant variables on depth conversion accuracy.

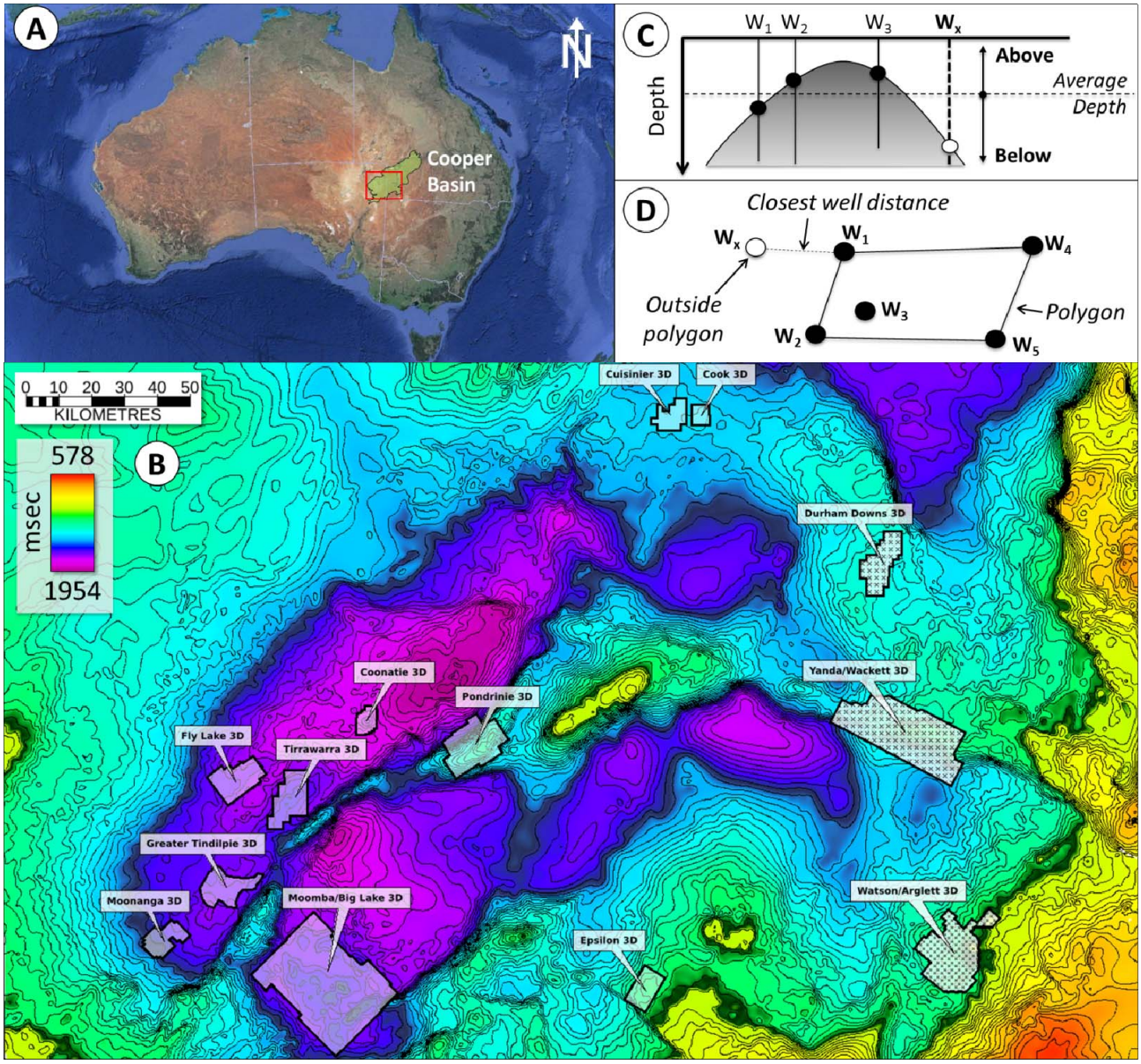


Figure 1: (a) Location map of the Cooper Basin, Australia, with the study area in red. (b) Location map of the 3D seismic surveys used. Surveys with dotted fill lack usable stacking velocities. (c) Schematic of how the *above or below* variable statistic is calculated. This is used as a proxy for crestal or flank well (d) Outer perimeter wells defining the well envelope used to determine the inside or outside polygon variable. Closest and average well distances are also calculated. These variable statistics are used to determine their individual significance on depth conversion accuracy.

DATA SET

Selecting the data for this study required a set of seismic surveys with a good spatial distribution across the study area and a diverse cross section of geological settings. This process used 13 3D seismic surveys, which include Coonatie 3D, Tirrawarra 3D, Fly Lake 3D, Greater Tindilpie 3D, Moonanga 3D, Moomba/Big Lake 3D, Epsilon 3D, Watson/Arglett 3D, Yanda/Wackett 3D, Durham Downs 3D, Cook 3D, and Cuisinier 3D (Figure 1b). These seismic surveys have good Eromanga and Cooper basin reflectors that can be consistently found across the surveys. Of the 73 TWT seismic grids, the majority of interpreted grids come from the Cretaceous aged Cadna-owie Formation, Late Permian aged Toolache Formation, and Middle Permian aged Patchawarra Formation. Other horizons used in this study come from the Namur Sandstone, Murta Member, Birkhead Formation, Hutton Sandstone, top Nappamerri Group, Callamurra Member, Epsilon Formation, Murteree Shale, Tirrawarra Formation and top Basement. Stacking velocity files were available for all 3D seismic surveys, excluding Durham Downs 3D, Yanda/Wackett 3D, and Watson/Arglett 3D (Figure 1b). As such, the KED using stacking and average velocities method could not be performed on these 3 fields. A total of 657 wells were used, ranging in distribution from 6 wells in the Moonanga 3D to 338 wells in the Moomba/Big Lake 3D.

Variogram modelling was also essential for depth conversion methods using kriging with external drift. It should be noted that variograms were defined using all available well data within a given seismic survey, ignoring the fact that the variogram would

change and become more defined with increasing well control. To counter this limitation, only fields with greater than 15 wells would be recommended to use kriging based methods. To generate realistic depth conversion scenarios, the inclusion of wells into the looping script is ordered by the drill date.

METHOD

In order to decrease the computational time of performing 4 depth conversion methods (Figure 2) a script was created within *Petrosys* that looped over the 4 methods with an increasing amount of well control per loop. This method is commonly known as the cross-validation method; 3 wells are used in the depth conversion to predict the 4th well, then 4 wells to predict the 5th well and so forth (*n* wells to predict the $n^{th}+1$ well). The error for each loop is calculated by comparing the predicted depth at the location of the $n^{th}+1$ well, with the known depth of the $n^{th}+1$ well. A total of approximately 2500 predicted vs true depth data points, together with an equal volume of variable statistics, were collected for each of the 4 depth conversion methods.

The statistics captured during each loop included; average depth of the wells used in the depth conversion, whether the well to be predicted is up-dip or down-dip from the existing wells, whether the well to be predicted is spatially inside or outside the existing well control envelope, distance between the predicted well and the closest well, and the average distance from the predicted well to the existing wells (Figure 1c & 1d).

To compare the relative significance of the variables on depth conversion error, cluster analysis was performed on the complete data set. Cluster analysis groups data such that within clusters the variability is minimised, and between clusters the variability is maximised (Kaufman & Rousseeuw, 2009). The distance between clusters is calculated using the Euclidean distance equation (Equation 1; where *a* and *b* are two points with dimensions *k*), which has a value of zero when clusters are identical, and a high value when clusters show little similarity. This statistical approach is used to compare the significance of variables and the impact they can have on the time to depth conversion error value, but mostly to assess their individual hierarchal importance (greater Euclidean distance infers more important). These results will provide geophysicists with a better understanding as to which variables have a greater impact on their time to depth conversion accuracy, and which have a relatively negligible effect.

$$Euclidean\ Distance = \sqrt{\sum_{j=1}^{k}\left(a_j - b_j\right)^2} \quad (1)$$

The four depth conversion methods used are described below.

Average (pseudo) Velocity (V_{avg}) Method

The average (pseudo) velocity method is the most commonly used method in the region and has been proven to be an effective method for modelling the earth's velocity (Baerg, 1991). At any given well location, the true depth (Δd feet) taken from the well and the interpreted time (Δt sec) taken from seismic data are known (Figure 2a). This enables a V_{avg} to be calculated by dividing Δd by Δt. This simple arithmetic is re-calculated after each loop. The newly created V_{avg} grid is then multiplied by the interpreted TWT seismic grid to generate a depth grid. To calculate the depth conversion error, the true depth of the well that is being predicted ($n^{th}+1$ well, where n is the number of wells being used for depth conversion) is compared to the depth from the depth grid at the given coordinates.

Time-Depth Trend Method

The time-depth trend method uses a similar relationship to the average (pseudo) velocity method, where depth and time values are obtained from wells and seismic data respectively. However, rather than computing V_{avg}, the points are plotted to find a linear relationship between time and depth (Figure 2b) which is then used to directly convert the TWT grid to depth. This method then requires the resultant depth grid to be tied to the well control by means of a gridded error correction factor. A unique time-depth trend relationship is defined for each loop within the script as well control increases.

KED using a TWT grid as the External Drift Method

Kriging with external drift (KED) is an interpolation method commonly used in gridding, where the primary data set is completely honoured, and a secondary data set is used as a background, or external guide (Figure 2c). This method utilises well depths as the primary data set with the interpreted TWT grid as the external drift. The interpolation technique can be viewed as a weighting system, where the closest wells have a stronger influence on the interpolated value than data from more distant wells. Weightings for KED are calculated through variogram modelling, which is based on the dissimilarity in pairs of data with changing distance (Hudson & Wackernagel, 1994). Generally, as the spacing of data increases the dissimilarity between data increases. This trend continues until at some distance (range) the dissimilarity between points reaches a maximum value (sill) and begins following a near horizontal path. Theoretical variogram modelling was performed using a spherical method.

KED using Stacking and Average Velocities Method

Similar to KED using TWT as the external drift, KED using stacking and average velocities is an interpolation technique with weightings defined through variogram modelling. A velocity value is obtained at each common mid-point in the seismic volume for a

given reflector by correcting for the natural move-out effect. Using the densely spaced stacking velocity data for each reflector, a velocity grid is created to guide kriging. This method utilises pseudo average velocity from wells as the primary data set with stacking velocity used in the background to calculate a velocity grid (Figure 2d). The output velocity grid is multiplied by the TWT grid to determine depth. It is important to note that lateral velocity anomalies can have a large impact on the velocity model generated through this method, and geophysicists must have a good understanding of the subsurface geology before solely relying on this method for time to depth conversion.

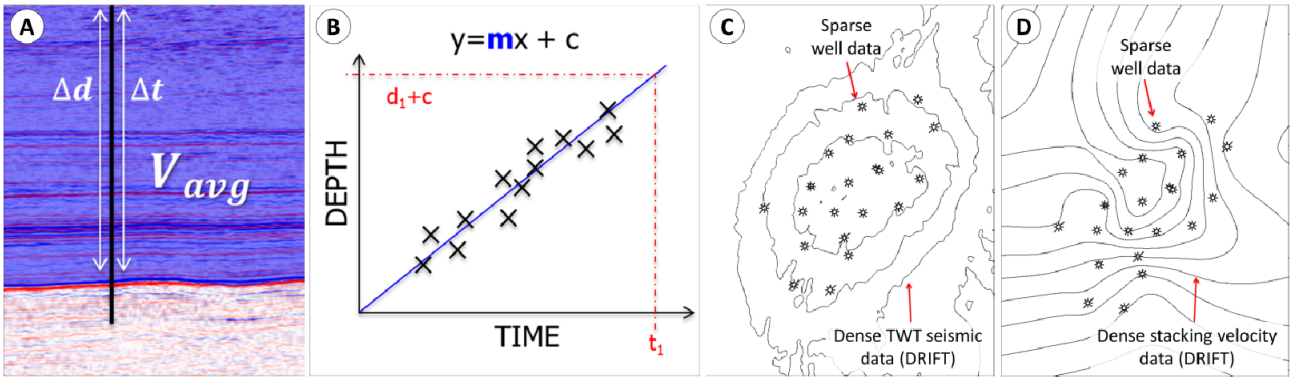


Figure 2: (a) The average (pseudo) velocity (V_{avg}) method uses a uniform velocity from datum to the target horizon. Velocities are obtained dividing measured depth from wells (Δd feet) by the one-way-time from seismic data (Δt sec). (b) Time-depth trend method fits a linear trend through time data plotted against depth. (c) Kriging with external drift using a TWT grid as the external drift honours the well data (depth) completely and interpolates depth using the TWT grid as a structural guide with values based on a variogram model. (d) Similar to (2c), this method uses the average velocity from wells and the stacking velocity grid as a guide with the output velocity grid multiplied by the TWT grid to calculate depth.

RESULTS

To calculate a representative average expected error, the authors use the absolute error value (negative values are multiplied by -1 to give only positive values). Figure 3a shows the absolute average error value for the 4 methods and is split by seismic survey. The average (pseudo) velocity method shows the lowest absolute error value (24.9 feet) and lowest standard deviation (57.3 feet) of the methods. Although the KED using stacking and average velocities method was found to have the largest absolute error value (29.5 feet), the difference between this and the average velocity method is only 4.6 feet. This difference may be significant in very low relief structural traps; however, a more significant error range can be fashioned with a 1 msec error in seismic interpretation or the variance of significant variables.

Testing the importance of variables utilised the cluster analysis technique. Data was split into Cooper and Eromanga basin formations and found a distance between clusters of approximately 9 feet (Figure 3b), inferring that this variable may be more significant than deciding upon the depth conversion method, which has a range of only 4.6 feet. Isolating data into being inside or outside the existing well envelope (Figure 1d) unearthed a significant distance between clusters of approximately 16 feet (Figure 3c). This highlights the importance of the well location relative to the existing well envelope, which is almost twice as significant as isolating data into the Cooper and Eromanga basin formations. Wells being predicted on a crest or flank (above or below) surprisingly had an almost negligible distance between clusters of less than 3 feet (Figure 3d).

The data also formed well shaped clusters based on the seismic survey being depth converted (cluster 1: *Cook 3D, Tirrawarra 3D, Cuisinier 3D, Fly Lake 3D, Coonatie 3D*; cluster 2: *Moomba/Big Lake 3D, Greater Tindilpie 3D, Epsilon 3D*; cluster 3: *Moonanga 3D*; cluster 4: *Watson 3D, Durham Downs 3D*; cluster 5: *Yanda/Wackett 3D*; cluster 6: *Pondrinie 3D*), where the distance between clusters was calculated to be approximately 23 feet. Clustering the data into the 2 main regional groups found a spatial trend, in that all seismic surveys located within the Patchawarra and Nappamerri troughs, as well as the Epsilon, Cook and Cuisinier 3D seismic surveys could be grouped into 1 cluster. Further research into the significance of this cluster should investigate the structural, sedimentological, mineralogical and cementation similarities between the areas covered by these surveys and the potential influence of surface conditions (statics) on depth conversion accuracy.

Reflectors with similar depths were expected to form clusters; however the data did not cluster coherently in this way. The clusters that did form did not appear to be based on depth, since reflectors from the Patchawarra Formation formed clusters with Eromanga Basin reflectors. The distance between these clusters was calculated to be approximately 43 feet and appear to be one of the more significant variables, together with the seismic survey and the well location relative to existing well envelope.

A variable often viewed as being one of the major contributors to depth conversion accuracy is the number of wells present. It would seem intuitive that increasing well control would provide a more accurate depth conversion; however, this relationship is surprisingly not present within the data set (Figure 3e). The number of wells present during depth conversion is plotted against the average absolute error to find a near horizontal trend. Another variable that is considered to be influential is the distance to a known well control, where a smaller distance to a well control would provide more accurate results. This relationship was tested (Figure 3f) and found a strong correlation between depth conversion accuracy and the proximity to well control.

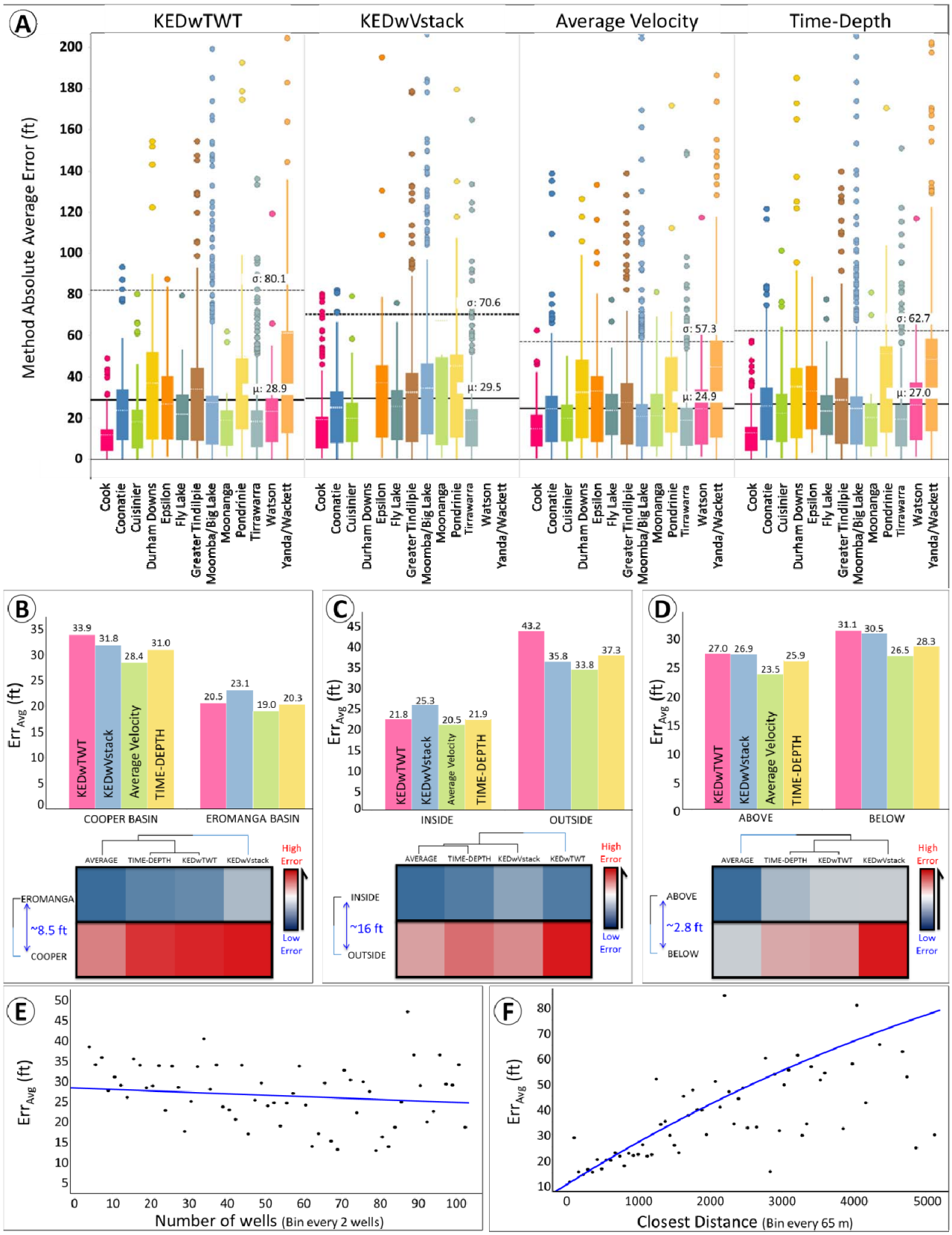


Figure 3: (a) Data split by method and seismic survey showing the absolute average error and standard deviation of each method (expected (+/-) error). (b) Data split by Cooper and Eromanga basin formations with a distance between clusters of 8.5 feet. (c) Data slit by inside or outside the well data envelope (polygon) (Figure 1d) with a distance between clusters of 16 feet. (d) Data split by above or below the average well depth with a distance between clusters of 2.8 feet. (e) Testing the relationship between the number of wells present during depth conversion and the average absolute error. (f) Constraining the relationship between the closest distance to a well control and the average absolute depth conversion error.

CONCLUSIONS

While the average (pseudo) velocity method has the smallest average absolute error on a high level (24.9 feet), the significance of variables such as location, formation, well location relative to the existing well data envelope and closest distance have shown to significantly impact the expected error, as well as the most accurate method. Future depth conversions should therefore use a data specific method rather than taking a blanket approach to depth conversion. Taking a single, 'standard' method approach can result in errors in the range of tens of feet which are large enough to destroy valid structures, or create pseudo ones. Surprisingly, the number of well control points appears to have an insignificant impact on depth uncertainty. It is important to reiterate that accurate seismic interpretation is the most crucial aspect of predicting the true subsurface geology.

This research promotes the creative and innovative use of existing software to investigate problems that have long existed, but that have never been explored due to time requirements for manual handling. This looping script was used to develop a depth conversion decision tree that now allows geophysicists to select the best (lowest prediction error) method for their given data set. This can be replicated and applied to any region around the world with 3D seismic data and well control. Future application would be most beneficial to regions where the most accurate depth conversion method and significant variables have not yet been identified, and also to regions with an uncertain presence of hydrocarbon-rich low relief structural traps.

ACKNOWLEDGMENTS

Thank you to Ben Moretti who provided valuable comments, feedback and software training. Thank you also to the Santos Cooper Basin geophysicists who provided interpreted seismic data and feedback during the early stages of the project. The authors appreciate the feedback provided by Alasdair Hamilton, Malcolm Horton, Michael Giles, Steve Mackie, and also the Santos Cooper West Development Team. Petrosys software was used to create the time to depth conversion looping script, with TIBCO Spotfire the software of choice for statistical analysis. Thank you to the GeoFrac Consortium for financial contribution, which includes the sponsoring companies Santos, Beach Energy, Chevron, Halliburton and BG Group (QGC).

REFERENCES

Apak, S.N., Stuart, W.J., Lemon, N.M., and Wood, G., 1997, Structural evolution of the Permian-Triassic Cooper Basin, Australia: relation to hydrocarbon trap styles: American Association of Petroleum Geologists Bulletin, 81(4), 533-555.

Aylor Jr, W.K., 1998, The role of 3-D seismic in a world-class turnaround: The Leading Edge, 17(12), 1678-1678.

Baerg, J.R., 1991, Traveltime in media with linear velocity-depth functions: Consortium for Research in Elastic Wave Exploration Seismology Research Report, 27, 461-466.

Hillis, R.R., Macklin, T.A., and Siffleet, P., 1995, Regional depth-conversion of mapped seismic two-way-times in the Cooper-Eromanga Basins: Exploration Geophysics, 26(2/3), 412-418.

Hillis, R.R., Morton, J.G.G., Warner, D.S., and Penney, R.K., 2001, Deep basin gas: A new exploration paradigm in the Nappamerri Trough, Cooper Basin, South Australia: The Australian Petroleum Production and Exploration Association Journal, 41(1), 185-200.

Hudson, G., and Wackernagel, H., 1994, Mapping temperature using kriging with external drift: theory and an example from Scotland: International Journal of Climatology, 14(1), 77-91.

Joraandstad, S., 1999, Use of stacking velocity for depth prediction and lithological indication in the Challum Field of the Cooper/Eromanga Basin, Queensland: Honours Thesis, National Centre of Petroleum Geology and Geophysics, the University of Adelaide.

Kaufman, L., and Rousseeuw, P.J., 2009, Finding groups in data: an introduction to cluster analysis: John Wiley & Sons, 344.

Kuang, K.S., 1985, History and style of Cooper–Eromanga Basin structures: Exploration Geophysics, 16(2/3), 245-248.

Kulikowski, D., Amrouch, K., Al Barwani, K.H., Liu, W., and Cooke, D., 2015, Insights into the tectonic stress history and regional 4D natural fracture distribution in the Australian Cooper Basin using Etchecopar's calcite twin stress inversion technique, 2D/3D seismic interpretation and natural fracture data from image logs and core: American Association of Petroleum Geologists International Conference and Exhibition, Melbourne, Victoria, 13–16 September, extended abstract number #2224164.

Kulikowski, D., Cooke, D., and Amrouch, K., 2016a, Constraining the distribution and relationship between overpressure, natural fracture density and temperature in the Cooper Basin: The Australian Petroleum Production and Exploration Association Journal, 56, 1-18, in press.

Kulikowski, D., Amrouch, K., and Cooke, D., 2016b, Geomechanical Modelling of Fault Reactivation in the Cooper Basin, Australia: Australian Journal of Earth Sciences, accepted.

Lowe-Young, B.S., Mackie, S.I., and Heath, R.S., 1997, The Cooper-Eromanga Petroleum System, Australia: Investigation of Essential Elements and Processes: Indonesian Petroleum Association, Proceedings of the Petroleum Systems of SE Asia and Australasia Conference, 199-211.

Méndez-Hernández, E., 2003, A brief history and recent advances in seismic technology for the petroleum industry in Mexico: The Leading Edge, 22(11), 1116-1119.

Pokalai, K., Kulikowski, D., Johnson, Jr., R.L., Haghighi, M., and Cooke, D., 2016, Development of a new approach for hydraulic fracturing in tight sand with pre-existing natural fractures: The Australian Petroleum Production and Exploration Association Journal, 56, in press.

Rady, T.A., 2006, Depth-conversion of seismic reflection data in the Eromanga Basin, South Australia: Honours Thesis, Australian School of Petroleum, the University of Adelaide.

View publication stats

5.2. MANUSCRIPT 2: Tectonic history of the Cooper-Eromanga Basin

Combining geophysical data and calcite twin stress inversion to refine the tectonic history of subsurface and offshore provinces: A case study on the Cooper-Eromanga Basin, Australia

This new approach is applicable to other provinces that do not have easily accessible outcrop by integrating geophysics (seismic and well data) with calcite twin stress inversion analysis to constrain paleo-stress tensors, using the subsurface Cooper-Eromanga Basin, Australia, as a case study. Six tectonic events have been constrained and the likely origin of far-field tectonic stresses through time has been discussed. This work forms a framework for geomechanical models simulating the tectonic evolution of the basin and provides constraints on the paleo-stress orientations and regimes, which were previously uncertain or unknown. Future work will analyse an adjacent region to provide more constraints on Australia's tectonic evolution.

CITATION:

Kulikowski, D., & Amrouch, K. (2017). Combining Geophysical Data and Calcite Twin Stress Inversion to Refine the Tectonic History of Subsurface and Offshore Provinces: A Case Study on the Cooper-Eromanga Basin, Australia. Tectonics, 36(3), 515-541, doi:10.1002/2016TC004366.

Statement of Authorship

Title of Paper:	**Combining Geophysical Data and Calcite Twin Stress Inversion to Refine the Tectonic History of Subsurface and Offshore Provinces: A Case Study on the Cooper-Eromanga Basin, Australia**
Publication Status:	**Manuscript Published**
Publication Details:	Kulikowski, D., & Amrouch, K. (2017). Combining Geophysical Data and Calcite Twin Stress Inversion to Refine the Tectonic History of Subsurface and Offshore Provinces: A Case Study on the Cooper-Eromanga Basin, Australia. *Tectonics*, 36(3), 515-541, doi:10.1002/2016TC004366.

Principal Author

Principal Author (Candidate):	David Kulikowski		
Contribution to the Paper:	Data collection, interpretation, measurement, analysis, and writing.		
Overall percentage (%):	80%		
Certification:	This paper reports on original research I conducted during the period of my Higher Degree by Research candidature and is not subject to any obligations or contractual agreements with a third party that would constrain its inclusion in this thesis. I am the primary author of this paper.		
Signature:		Date:	28 March 2017

Co-Author Contribution

By signing the Statement of Authorship, each author certifies that:

i. the candidate's stated contribution to the publication is accurate (as detailed above);

ii. permission is granted for the candidate to include the publication in the thesis; and

iii. the sum of all co-author contributions is equal to 100% less the candidate's stated contribution.

Name of Co-Author:	Khalid Amrouch (20%)		
Contribution to the Paper:	Supported analysis of calcite, natural fracture/fault data and a complete review of paper.		
Signature:		Date:	28 March 2017

AGU PUBLICATIONS

Tectonics

RESEARCH ARTICLE
10.1002/2016TC004366

Key Points:
- New approach for constraining the paleostress of subsurface and offshore provinces
- First study to reconstruct the tectonic stress history of the Cooper-Eromanga Basin
- Integrating geophysical and structural data to constrain tectonic events

Combining geophysical data and calcite twin stress inversion to refine the tectonic history of subsurface and offshore provinces: A case study on the Cooper-Eromanga Basin, Australia

David Kulikowski[1] **and Khalid Amrouch**[1,2]

[1]Australian School of Petroleum, University of Adelaide, Adelaide, South Australia, Australia, [2]Centre for Tectonics Resources and Exploration (TRaX), Department of Physical Sciences, University of Adelaide, Adelaide, South Australia, Australia

Correspondence to:
D. Kulikowski,
david.kulikowski@adelaide.edu.au

Citation:
Kulikowski, D., and K. Amrouch (2017), Combining geophysical data and calcite twin stress inversion to refine the tectonic history of subsurface and offshore provinces: A case study on the Cooper-Eromanga Basin, Australia, *Tectonics*, *36*, 515–541, doi:10.1002/2016TC004366.

Received 21 OCT 2016
Accepted 27 FEB 2017
Accepted article online 6 MAR 2017
Published online 21 MAR 2017

©2017. American Geophysical Union. All Rights Reserved.

Abstract The use of core samples, borehole image logs, and seismic data is common practice for obtaining valuable structural data; however, these data are often obtained in isolation from other methods and not usually used for paleostress inversion processes. Therefore, for the first time, we present a new approach for constraining paleoprincipal stress orientations and regimes by integrating geophysical data (seismic and well data) with calcite twin principal stress orientation inversion analysis to refine the evolution of entirely subsurface or offshore basins; a case study on the subsurface Cooper-Eromanga Basin, Australia. Calcite samples were collected from oriented core, natural fracture data collected from borehole image logs, and fault data interpreted from three-dimensional seismic surveys. The analysis of microscale, mesoscale and macroscale data constrained the paleoprincipal stress orientations and regimes of six successive tectonic events: (1) NNW-SSE oriented strike-slip Carboniferous Alice Springs event; (2) SE-NW oriented compressional Mid-Permian event; (3) NE-SW oriented strike-slip Late Permian Daralingie event; (4) E-W compressional Late Triassic Hunter-Bowen event; (5) E-W compressional Late Cretaceous event; and (6) N-S compressional Paleogene event. This study shows the applicability of integrating geophysics with calcite twin stress inversion to decipher the tectonic evolution of entirely subsurface and offshore provinces.

1. Introduction

Investigating paleostresses from present-day large-scale geological structures calls for a cautious approach, particularly in regions affected by successive tectonic events, where faults are repeatedly reactivated and poor two-dimensional (2-D) and three-dimensional (3-D) seismic data quality prevents detailed fault growth analysis. In such regions, it is vital to integrate stress inversion techniques that are proven to generate meaningful results. The chronology, geometry, and deformation associated with calcite twinning [*Tourneret and Laurent*, 1990; *Lacombe and Laurent*, 1996; *Lacombe*, 2001; *Lacombe et al*., 2007], natural fractures [*Silliphant et al*., 2002; *Bergbauer and Pollard*, 2004; *Bellahsen et al*., 2006], and faults [*Michael*, 1984; *Gephart*, 1990; *Nemcok and Lisle*, 1995; *Tavani et al*., 2015], as well as any combination of the three [*Friedman and Stearns*, 1971; *Amrouch et al*., 2010a, 2010b, 2011; *Beaudoin et al*., 2012, 2016; *Arboit et al*., 2015, 2017], have provided valuable insights into the development of paleostress inversion techniques and in constraining the tectonic evolution of complex provinces. However, these data are typically obtained from sampled outcrop with only a small number of researchers attempting to use core [*Lacombe et al*., 1994; *Rocher et al*., 2000], which has prevented paleostress analysis in regions entirely overlain by loose sediment or provinces located offshore. Although the previous use of borehole image logs, seismic data, and core data has individually been used to measure valuable fracture, fault, and calcite twin data, respectively, the combination of these sources for the purpose of paleoprincipal stress analysis has not previously been explored.

As such, we present an approach that incorporates principal paleostress orientation inversion of calcite twin data (measured from thin section) integrated with inferred paleostress orientations and regimes from natural fracture and fault sets. Throughout the manuscript, the mode 2 mesoscale discontinuities measured from borehole image logs are referred to as natural fractures, and macroscale discontinuities measured from 3-D seismic data are referred to as faults. Many subsurface and offshore provinces with little, to no, accessible outcrop would benefit from such an approach to diminish the uncertainty of paleostress orientations; thus,

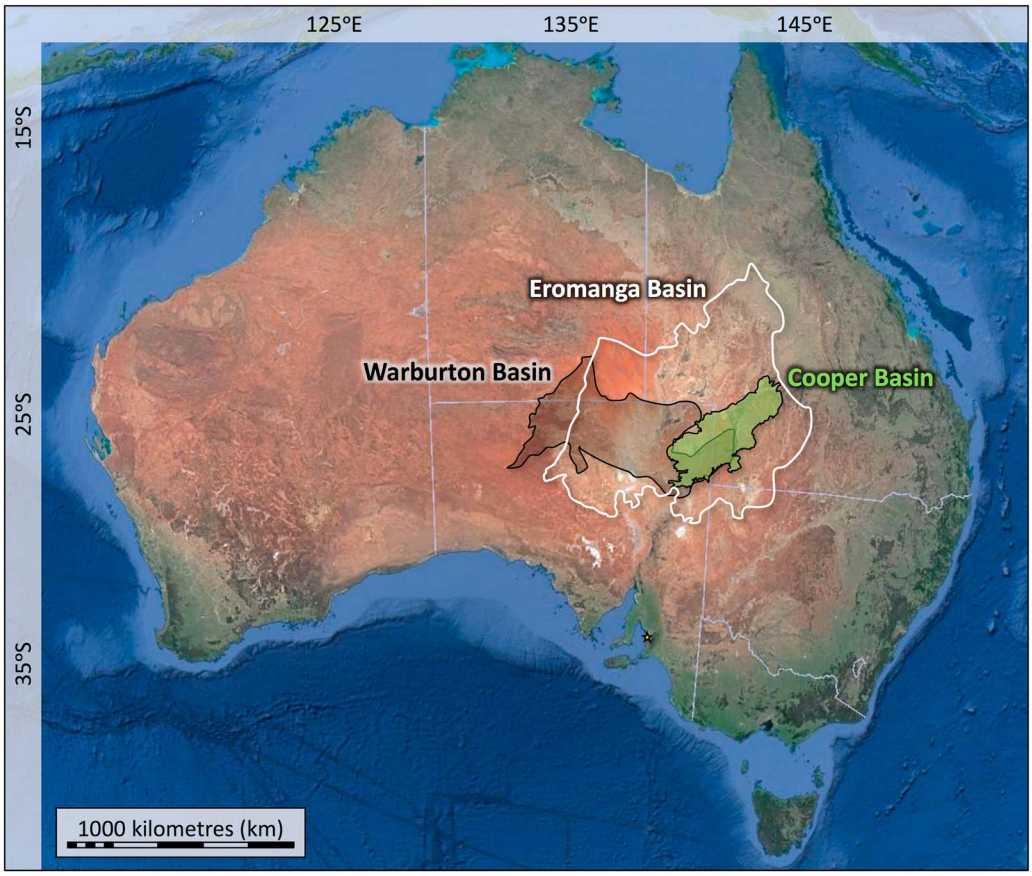


Figure 1. Location of the Warburton, Cooper, and Eromanga Basins, Australia [after *Kulikowski et al*., 2016a].

for the first time, we integrate microscale calcite twins (obtained from six well cores), mesoscale natural fractures (measured from 27 borehole image logs) and macroscale faults (measured from six 3-D seismic surveys) from the Cooper-Eromanga Basin, Australia (Figure 1). This basin represents Australia's largest onshore hydrocarbon province with tremendous value in unconventional tight sand oil and gas [*Pokalai et al*., 2016] and is currently being developed for its basin-centered gas potential [*Hillis et al*., 2001]. The current basin evolution model, particularly the paleostress orientations, remains uncertain, as much of the structural analysis is based on poor resolution and sparse 2-D seismic data [*Kuang*, 1985; *Apak et al*., 1997]. Recent work by *Khair et al*. [2015] has constrained the development of natural fractures and faults through stress inversion modeling within the Moomba/Big Lake 3-D seismic survey. This relatively smaller-scale study focused on a portion of the Nappamerri Trough and is not representative of the basin scale. Besides this study, there has not been any stress inversion analyses focused on the Cooper-Eromanga Basin due to the lack of exposed rock at surface.

The use of calcite twins to determine paleostress [*Etchecopar*, 1984] and strain [*Groshong*, 1972, 1974; *Friedman et al*., 1976] has been successfully performed in areas such as the Zagros belt (Iran) [*Lacombe et al*., 2007], Rocky Mountains (Wyoming) [*Craddock and Van Der Pluijm*, 1999; *Amrouch et al*., 2010a, 2010b, 2011; *Beaudoin et al*., 2012], Causses Basin (France) [*Constantin et al*., 2007], Iberian Chain (Spain) [*González-Casado and García-Cuevas*, 2002], Cuddapah Basin (India) [*Tripathy and Saha*, 2015], Indochina Block (Thailand) [*Arboit et al*., 2015, 2017], Pyrenees-Provence Domain [*Lacombe et al*., 1992; *Rocher et al*., 2000], Taiwan [*Rocher et al*., 1996; *Lacombe*, 2001], Albanides [*Lacombe et al*., 2009], and the Apennine Mountains (Italy) [*Beaudoin et al*., 2016]. The purpose of the following research is to provide better constraints on the principal stress orientation and stress regime of tectonic events through the analysis of microscale calcite twins, mesoscale natural fractures, and macroscale faults.

Conjugate fracture sets were regionally identified and analyzed in isolation to calcite twin results. The paleostress analysis of conjugate fractures followed the fundamental rock failure principles [*Anderson*, 1951] to provide insights into the evolution of stress regimes and orientations and the timing of fracture development. The integration of natural fracture and fault results with calcite twin principal stress orientation inversion results has shown a strong correlation between the microscale, mesoscale, and macroscale analyses, which has allowed us to define the stress orientation of the six major tectonic events that have affected the evolution of the Cooper-Eromanga Basin.

2. Geological Setting

The intracratonic Permian to Triassic Cooper Basin extends across 130,000 km^2 of South Australia and Queensland and is unconformably isolated from the overlying Jurassic to Middle Cretaceous Eromanga Basin and underlying Cambrian to Middle Silurian Warburton Basin (Figure 3) [*Kantsler et al*., 1984; *Kuang*, 1985; *Bradshaw*, 1993; *Apak et al*., 1997; *Gravestock and Jensen-Schmidt*, 1998; *Mavromatidis*, 2006]. These regional unconformities mark successive periods of exhumation and reactivation along preexisting Cambrian basement-involved faults [*Apak et al*., 1997; *Sun*, 1997; *Mavromatidis*, 2006]. The structural architecture of the basin is dominated by NE-SW striking faults, which include the major faults bounding the Gidgealpa-Merrimelia-Innamincka (GMI) and Murteree-Nappacoongee (MN) ridges (Figure 2) that form prolific hydrocarbon fields within the basin [*Kuang*, 1985; *Apak et al*., 1997]. These major ridges isolate the NE-SW elongate Patchawarra (PT), Nappamerri (NT), and Tenappera (TT) troughs (Figure 2). Much of the original research explored the evolution of the basin using sparse poor-resolution 2-D seismic data, with only very recent works utilizing new 3-D seismic data [*Grant-Woolley et al*., 2014; *Kulikowski et al*., 2016a, 2016b, 2017]. There does remain some uncertainty regarding the maximum principal stress orientation of paleotectonic events, which can be attributed to limited high resolution 3-D seismic data at depths and poor exposure at surface. As newly acquired 3-D seismic data become available, and the resolution of seismic data with depth improves, it is likely that the evolution and architecture of the basin become more tightly constrained.

The present-day understanding of the evolution of the Cooper-Eromanga Basin shows that NE-SW striking normal faults and SE-NW striking vertical faults likely developed during Adelaidean (650–575 Ma) rifting, which was oriented normal to the NE-SW striking Tasman Line that separated eastern Australia from the rest of the continent [*Apak et al*., 1997; *Haines et al*., 2001; *Müller et al*., 2012]. Subsequent structuring took place during five major events: (1) Carboniferous Alice Springs event (ASE), (2) Mid-Permian event, (3) Late Permian Daralingie event, (4) Late Triassic Hunter-Bowen event, and (5) Late Cretaceous event [e.g., *Kuang*, 1985; *Apak et al*., 1997; *Gravestock and Jensen-Schmidt*, 1998; *Reynolds et al*., 2006; *Khair et al*., 2013]. These events likely reactivated preexisting NE-SW and SE-NW striking basement-involved faults and generated new compressive and strike-slip features throughout the basin [*Kantsler et al*., 1984; *Grant-Woolley et al*., 2014; *Kulikowski et al*., 2016a]. These events were likely followed by a compressive N-S Late Paleogene event and a present-day ESE-WNW oriented strike-slip stress regime event [*Reynolds et al*., 2002, 2005, 2006].

The regional unconformity isolating the Warburton and Cooper basins was generated through the exhumation of Warburton Basin sedimentary rocks during the Carboniferous ASE (Figure 3) [*Apak et al*., 1997; *Rezaee and Sun*, 2007; *Glikson et al*., 2013]. This event is thought to have also caused the following: (1) the exhumation of the Carboniferous Big Lake Granodiorite and (2) the dextral and sinistral reactivation of SE-NW and NE-SW striking faults, respectively [*Apak et al*., 1997; *Rezaee and Sun*, 2007; *Glikson et al*., 2013]. Glacial sediments (Merrimelia Formation) were deposited onto this regional unconformity, with fluvially deposited sediments (Tirrawarra Formation) soon following [*Kantsler et al*., 1984; *Apak et al*., 1997]. The Late Carboniferous to Early Permian Merrimelia and Tirrawarra formations locally onlap onto structural highs developed by the ASE, inferring that these were prominent features and had an influence on the depositional architecture at this time. The deposition of these sediments marks the initial period of flexural relaxation that generated accommodation space for Cooper Basin deposition [*Apak et al*., 1997]. The overlying Patchawarra Formation was deposited under fluvial, peat swamp, and flood plain conditions, reflected by the repeatedly stacked sands, shales, and coals [*Alexander et al*., 1998; *Boreham and Hill*, 1998; *Pokalai et al*., 2016]. The middle Patchawarra Formation shows evidence to suggest two periods of uplift during the Mid-Permian [*Kantsler et al*., 1984; *Apak et al*., 1997].

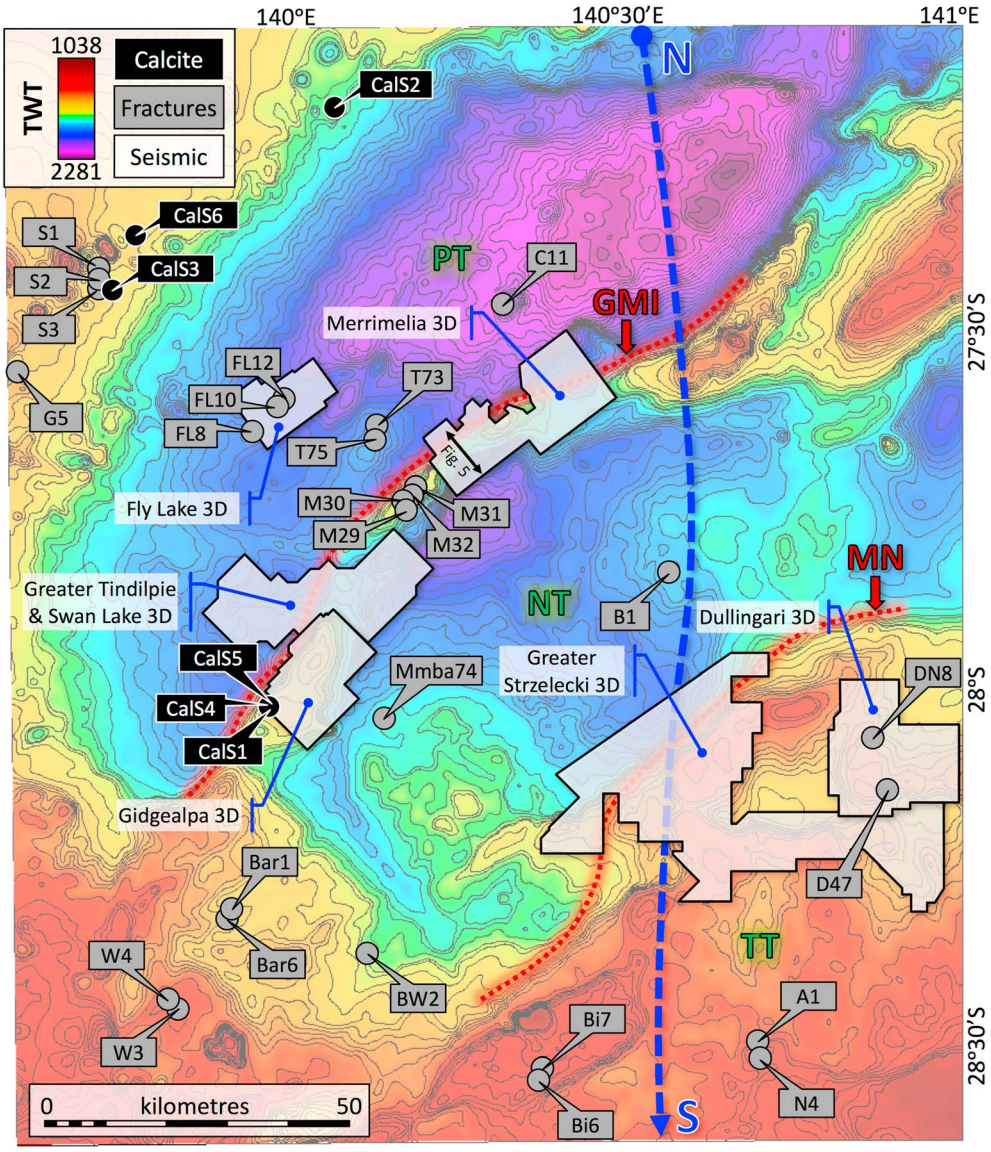


Figure 2. Study area showing the two-way time (TWT) to the top Permian overlaid by the location of wells and seismic data. Location of the Gidgealpa-Merrimelia-Innamincka (GMI) and Murteree-Nappacoongee (MN) ridges, and the Patchawarra (PT), Nappamerri (NT), and Tenappera (TT) troughs are shown. Location of the regional N-S cross section (Figure 10a) (blue dashed line) and cross section through Merrimelia 3-D (Figure 5) are shown.

Interpretation of 2-D seismic lines shows the lower to middle Patchawarra Formation onlapping onto paleostructural highs at approximately 270 Ma and again at 273 Ma, suggesting two periods of uplift (compressional or strike-slip) that were oriented between E-W and SE-NW and corresponding to the Mid-Permian event [*Kantsler et al.*, 1984; *Apak et al.*, 1997; *Khair et al.*, 2013]. This event continued during the upper Patchawarra Formation deposition causing an east to west transgression, which deposited the Murteree Shale, Epsilon Formation, Roseneath Shale, and Daralingie Formation in fluvio-deltaic, shoreface, and lacustrine environments [*Bradshaw*, 1993; *Apak et al.*, 1997; *Gravestock and Jensen-Schmidt*, 1998]. Following the deposition of the Daralingie Formation, a period of low-intensity uplift (compressional or strike-slip) is recorded on paleostructural highs as a regional unconformity corresponding to the Late Permian Daralingie event [*Kuang*, 1985; *Apak et al.*, 1997; *Mavromatidis*, 2006]. Meandering fluvial to deltaic conditions soon followed during a period of postcompressional flexural relaxation, depositing the Toolachee Formation coals, sands, and shales [*Kantsler et al.*, 1984; *Apak et al.*, 1997]. Flexural relaxation continued during the

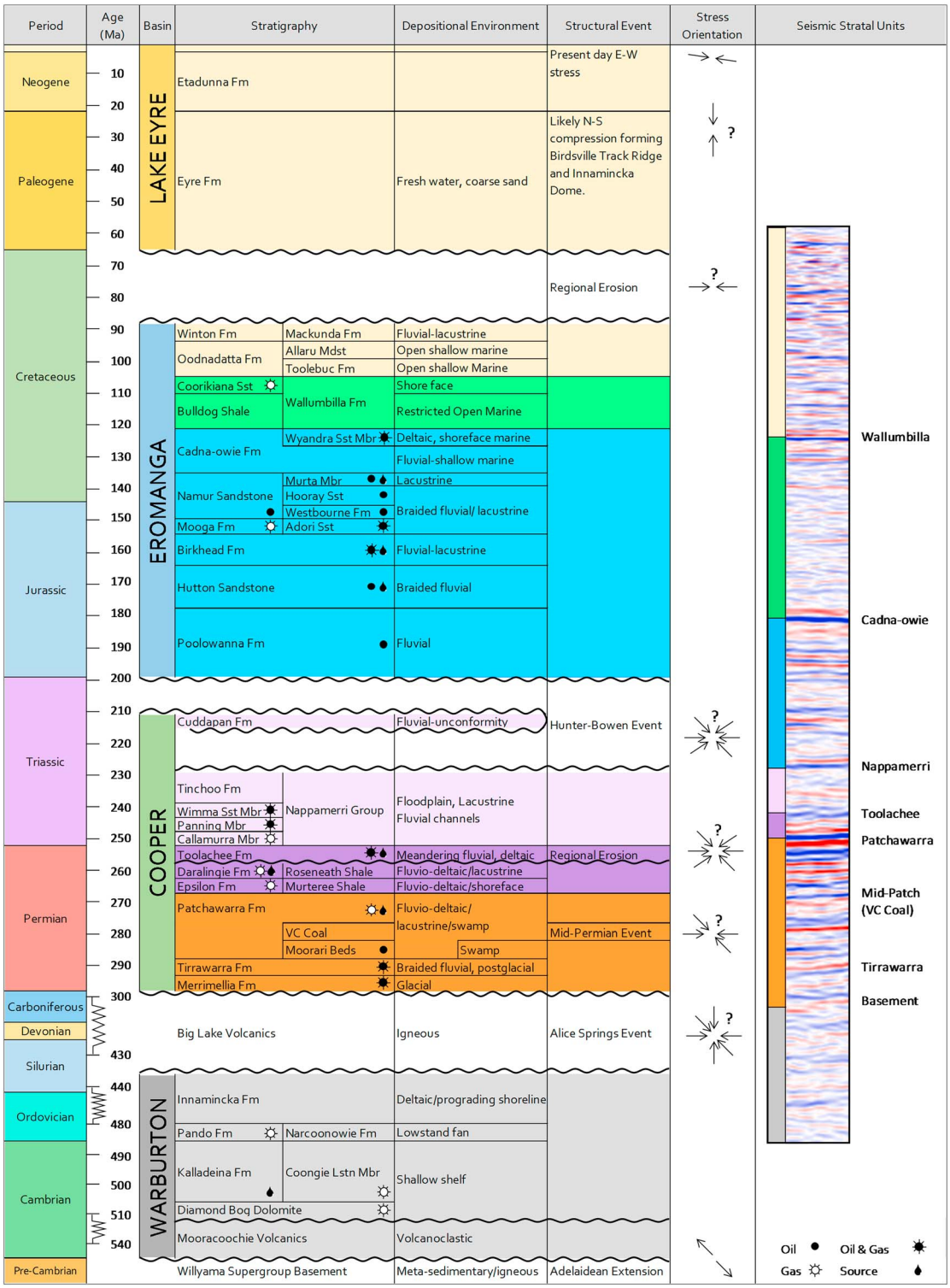


Figure 3. A tectonostratigraphic summary of the Warburton, Cooper, Eromanga, and Lake Eyre Basins alongside a typical seismic reflection profile.

floodplain, lacustrine, and fluvial channel deposition of the Nappamerri Group sediments prior to the compressional Triassic Hunter-Bowen event, which uplifted and peneplaned Cooper Basin sediments to generate the unconformable boundary isolating it from the overlying Eromanga Basin (Figure 3) [*Kantsler et al.*, 1984; *Apak et al.*, 1997; *Alexander et al.*, 1998; *Mavromatidis*, 2006].

Postcompressional flexural relaxation generated accommodation space for the fluvial deposition of Jurassic to Lower Cretaceous Eromanga Basin sediments that grade into lacustrine and open shallow marine sediments in the Upper Cretaceous [*Green et al*., 1989; *Hoffman*, 1989; *Lowe-Young et al*., 1997]. The critical point in the Cooper Basin hydrocarbon system, where hydrocarbon generation, migration, and accumulation had all commenced, is believed to have occurred at approximately 90 Ma and immediately followed by the E-W oriented compressional Late Cretaceous event. This event regionally eroded the upper Eromanga Basin sediments (Winton Formation), marked by the regional unconformity between the Eromanga and Lake Eyre basins [*Kuang*, 1985; *Green et al*., 1989; *Hoffman*, 1989; *Apak et al*., 1997; *Lowe-Young et al*., 1997; *Gravestock and Jensen-Schmidt*, 1998; *Mavromatidis*, 2006]. A possible N-S compressional event during the Late Paleogene may have reactivated faults and influenced the preservation of existing hydrocarbon accumulations [*Müller et al*., 2012]. Present-day stress has been constrained by multiple authors, showing a mean maximum horizontal stress orientation of 101°N under a strike-slip to compressional stress regime [*Reynolds et al*., 2002; *Sandiford et al*., 2004; *Reynolds et al*., 2006; *Hillis et al*., 2008; *Müller et al*., 2012].

3. Methodology

3.1. Overview

To better constrain the stress orientation and regime through time, calcite twins (from oriented core samples), natural fractures (from borehole image log interpretation and core analysis), and seismic scale faults (from 3-D seismic data) are measured and analyzed. Analysis of paleostress tensors measured from, or the combination of, fault slip, fracture, and calcite deformation data has been applied to many regions of the world [e.g., *Ramsay*, 1962; *Angelier and Mechler*, 1977; *Etchecopar et al*., 1981; *Etchecopar*, 1984; *Tourneret and Laurent*, 1990; *Lacombe*, 2001; *Amrouch et al*., 2010a; *Arboit et al*., 2015, 2017]. However, the combination of geophysical data (faults and fractures) and calcite twin data is presented here for the first time. The application of this approach for paleostress analysis will be most beneficial to subsurface and offshore provinces, where outcrop is limited and where paleostress constraints have historically relied solely on high-resolution seismic data for fault growth analysis [*Williams et al*., 1989; *Childs et al*., 1996; *Baudon and Cartwright*, 2008; *Robson et al*., 2016a, 2016b]. The use of seismic data in this way cannot provide nearly as many stress parameters as calcite twin stress inversion analysis.

3.2. Stress Inversion of Calcite Twins

Calcite twinning is a plastic deformation mechanism responding to dislocation gliding that typically occurs at temperatures between 25 and 400°C, in low-confining pressures, and with low (10 ± 4 MPa) critical resolved shear stresses (RSS) [*Turner*, 1953; *Turner et al*., 1954; *Lacombe and Laurent*, 1996; *Laurent et al*., 2000; *Amrouch*, 2010; *Amrouch et al*., 2010a, 2011; *Lacombe*, 2010]. The high sensitivity to twinning of calcite makes it the most likely mineral to provide useful tectonic information [*Lacombe*, 2007]. The RSS threshold depends on the grain size and the internal deformation [*Rowe and Rutter*, 1990; *Laurent et al*., 2000; *Amrouch*, 2010; *Lacombe*, 2010]. Where temperatures exceed 400°C, the "twinning regime" transitions to the "intracrystalline slip regime," where deformation is accommodated along *r* planes [*Burkhard*, 1993; *Sperner and Ratschbacher*, 1994]. Analysis of twin data has been proven to efficiently and accurately constrain five of the six parameters required to define the complete stress tensor of individual paleotectonic events [*Lacombe*, 2007, 2010; *Amrouch et al*., 2010a; *Amrouch*, 2010]. This inversion technique is also capable of obtaining polyphase paleostress orientations and stress magnitudes [*Lacombe et al*., 1992; *Rocher et al*., 2004; *Amrouch et al*., 2010a; *Arboit et al*., 2015, 2017]. Analysis of measured *e* planes assumes that their development was under a homogenous stress field and that they were not rotated after formation [*Lacombe*, 2007].

Inversion of measured calcite twin data is similar to that used to analyze slip on a slickenside lineation along a fault plane [*Etchecopar*, 1984; *Lacombe*, 2007]. The inversion of twin data is more complete as it incorporates not only twinned planes but also untwinned (did not reach conditions for twinning to occur) planes to find a unique stress tensor, which explains the maximum number of twinned planes and all of the untwinned planes [*Tourneret and Laurent*, 1990]. The stress tensor that best fits the distribution of twinned and untwinned planes must meet the major requirement that all consistent twin planes have sustained a RSS larger than that exerted on all of the untwinned planes [*Lacombe*, 2007]. This inversion process is repeated if more than 30% of the measured twinned planes from a given sample are not explained by this unique stress tensor. This second stage of inversion incorporates the remaining twinned planes and the entire set

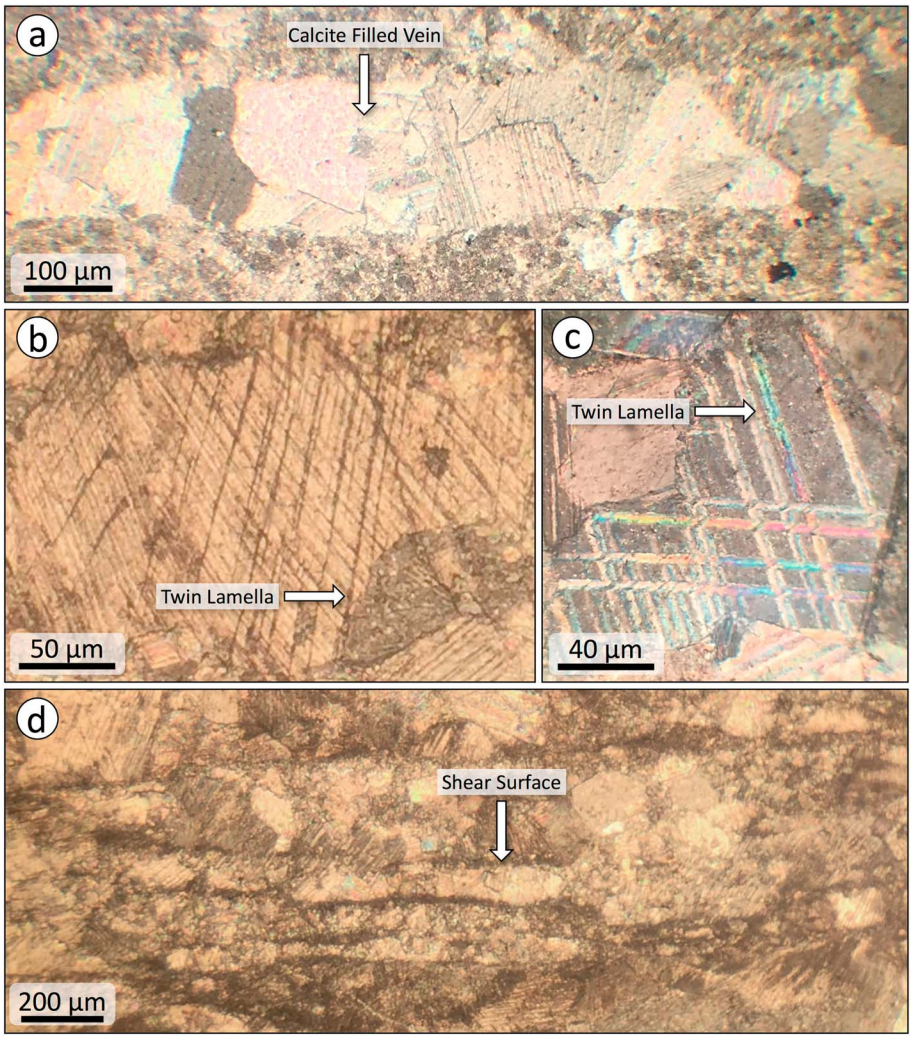


Figure 4. Examples of microscope images obtained from Gidgealpa 5 showing (a) calcite-filled natural fracture under cross-polarized light; (b) thin twins; (c) thick twins under cross-polarized light; and (d) shear surfaces.

of untwinned planes to efficiently separate superimposed twinning events while calculating a secondary stress tensor [*Tourneret and Laurent*, 1990].

The calcite twin stress inversion technique (CSIT) computes four (maximum principal stress orientation: σ_1; intermediate principal stress orientation: σ_2; minimum principal stress orientation, σ_3, and differential stress ratio, $R = (\sigma_2 - \sigma_3)/(\sigma_1 - \sigma_3)$) of the six stress parameters. The four parameters define a reduced stress tensor, $\mathbf{T}'$, such that the complete stress tensor, $\mathbf{T}$, is defined as $\mathbf{T} = k\mathbf{T}' + l\mathbf{I}$, where k and l are scalars ($k = \sigma_1 - \sigma_3 > 0$; $l = \sigma_3$) and $\mathbf{I}$ is the unit matrix [*Lacombe*, 2007]. The maximum differential stress is then reduced to $(\sigma_1 - \sigma_3) = 1$ [*Etchecopar*, 1984]. Hence, the RSS acting along an *e* plane lies between −0.5 and +0.5 or between $-(\sigma_1 - \sigma_3)/2$ and $+(\sigma_1 - \sigma_3)/2$ [*Jamison and Spang*, 1976; *Etchecopar*, 1984]. The inversion process begins by applying several trial stress tensors to the data set. For each of these tensors, the stress components are calculated; however, as untwinned planes will be incorrectly incorporated into some of these tensors, the penalization function, *f*, must be reduced, ideally to 0, and defined as

$$f = \sum_{j=1}^{N} (\tau_{sj} - \tau_{a'})$$

where $\tau_{a'}$ is the minimum RSS applied to the twinned planes compatible with the trial stress tensor, and τ_{sj} is the RSS of the *j*th untwinned plane whose RSS is greater than $\tau_{a'}$, where the number of such untwinned

Table 1. Results of CSIT[a]

Sample Name	Formation	Age Period	Sampled Vein (fracture set)	[b]Mean Bedding	Mean Calcite Size (μm)	Principal Stress Axes			Differential Stress Ratio (R)	Max. Differential Stress (MPa)	Total Data (T/UT)	T/UT Agreeing with Tensor	Penalization Function (f)
						σ_1	σ_2	σ_3					
CalS5b	Kalladeina	Cambrian	61/343 (fracture set 6)	15/190	422	03/172	70/075	20/263	0.70	43 ± 9	145/62	39/55	0.49
CalS1	Merrimelia	E. Permian	57/032 (fracture set 5)	15/060	474	13/318	69/190	16/052	0.80	52 ± 10	201/60	56/51	0.49
CalS2	Kalladeina	Cambrian	71/210 (fracture set 5)	10/270	431	22/301	45/056	36/194	0.40	55 ± 11	196/71	61/61	0.93
CalS3	Kalladeina	Cambrian	Matrix	15/180	420	00/306	40/216	50/036	0.50	50 ± 10	194/67	69/55	0.45
CalS2b	Kalladeina	Cambrian	71/210 (fracture set 5)	10/270	441	21/219	60/086	20/317	0.40	53 ± 11	140/71	50/61	0.99
CalS1b	Merrimelia	E. Permian	57/032 (fracture set 5)	15/060	474	32/065	48/291	25/171	0.60	57 ± 11	163/60	58/48	0.93
CalS4	Merrimelia	E. Permian	64/121 (fracture set 6)	15/060	475	06/238	80/004	08/147	0.40	53 ± 11	215/58	74/48	0.79
CalS5	Kalladeina	Cambrian	61/343 (fracture set 6)	15/190	422	17/260	29/160	55/016	0.50	52 ± 10	208/62	63/54	0.58
CalS6b	Kalladeina	Cambrian	72/266 (fracture set 1)	10/130	1421	08/272	47/173	42/009	0.50	67 ± 13	105/55	40/51	0.47
CalS4b	Merrimelia	E. Permian	64/121 (fracture set 6)	15/060	475	05/078	71/333	18/170	0.30	45 ± 9	141/58	68/51	0.49
CalS3b	Kalladeina	Cambrian	Matrix	15/180	420	07/170	74/284	15/078	0.40	63 ± 13	125/67	69/58	0.62
CalS6	Kalladeina	Cambrian	72/266 (fracture set 1)	10/130	1421	03/178	82/068	08/268	0.40	46 ± 9	167/55	62/47	0.53

[a]For sample locations refer to Figure 2. T/UT refers to the number of twinned/untwinned planes. Sampled Vein, Mean Bedding, and Principal Stress Axes are quoted as dip angle/dip direction.
[b]Mean Bedding was measured across a 1 m interval. Mean calcite size was measured along the longest axis.

planes, N, depends on the trial tensor (see *Etchecopar* [1984] and *Amrouch* [2010], for more detail). After the optimal reduced stress tensor is found by incorporating the maximum number of twinned planes while reducing the penalization function, f, the principal stress orientations and the differential stress ratio are calculated. To calculate the fifth stress parameter, the differential stress magnitude, one uses a constant RSS (10 ± 4 MPa) required for twinning and uses $(\sigma_1 - \sigma_3) = \tau_a/\tau_{a'}$ and $(\sigma_2 - \sigma_3) = \phi(\sigma_1 - \sigma_3)$. Where $\tau_{a'}$ is the smallest RSS value applied to a twinned plane that is consistent with a given stress tensor. A RSS of 10 MPa was used considering that the majority of twins measured in thin section are thin to moderate, straight, and rational, which suggests little deformation and temperatures below 200°C [*Burkhard*, 1993; *Lacombe*, 2010]. This value is also within the range of RSS values (~5 to 10 MPa) commonly used for inversion [*Lacombe*, 2010]. Mostly type 1 twins [*Burkhard*, 1993] (Figure 4) were measured from calcite crystals predominantly ~400 μm in size (measured along the longest axis) with an internal deformation of ~8% (Table 1).

As measurement errors and local heterogeneities at the crystal scale may contaminate data, it may be required to ignore a small percentage of untwinned planes when defining the tensor solution to increase the number of twinned planes used. Ignoring a portion of the untwinning planes in this manner is reflected by a slight increase in the penalization function, f, which describes how badly a trial stress tensor fails to explain a given data set [*Lacombe and Laurent*, 1996; *Amrouch et al.*, 2010a]. In this sense, the penalization function, f, describes the arrangement quality of the measured e planes for a given tensor solution. For more detail on the CSIT, see *Lacombe* [2010] and *Amrouch* [2010], and references therein.

3.3. Natural Fractures Obtained From Borehole Image Logs

As we only encounter mode 2 natural fractures from borehole image logs and core, we use the term fractures in a general sense to describe sliding-mode discontinuities measured on the mesoscale from borehole image logs [*Pollard and Aydin*, 1988]. Interpretation and analysis of natural fracture data are based on the statistical analysis of fracture strike and dip angle relative to bedding and the relative chronologies. As this region is not exposed at surface, natural fracture and bedding

planes were interpreted from 27 borehole image logs (Figure 2). The vertical length of image logs ranges from 50 to 900 m, for a total length of more than 7000 m across the 27 logs. Borehole images are generated by measuring the electrical resistivity or acoustic reflection of the borehole at centimeter scale or directly with downhole optical imaging tools. A typical Electro Imaging Tool contains six pads, each with 150 microelectrodes, which press against the borehole wall to measure the change in resistivity commonly associated with cement or fluid filled natural fractures. Digital data are converted into an oriented resistivity image log that highlights changes in micro resistivity. A large population of fractures ($n = 521$) were interpreted and correlated to core samples and thin sections where possible. Cross-cutting relationships, mode of deformation (opening or shear), and fracture strike and dip angle relative to the bedding plane geometry were also examined in both borehole image logs and core.

Fracture data, measured from borehole image logs, are divided into stratal units to assess variations in strike or dip angle with time, which can provide insights into the relative chronology. Fracture sets were identified based on common strike (30° bins) and dip angles (30° bins) prerotation and postrotation of the bedding plane to horizontal and considering their stratigraphic distribution. A principal stress orientation inversion tool (Wintensor) was used to assist in statistically defining fracture sets. Fracture measurements that do not fall within one of the regionally extensive fracture sets (less than 20% of fracture data) are not included in the final interpretations, as these outliers might represent local stress perturbations, rock heterogeneities, or measurement error that do not align with the direction of regional maximum principal stresses [*Faulkner et al*., 2010].

The fundamental rock failure principles that describe the geometry of rock failure relative to the principal stresses are used to interpret the development of these natural fracture sets. Natural fractures develop when the stress conditions reach the rock strength, typically associated with tectonic events [*Zoback et al*., 1989; *Dresen*, 1991; *Sibson*, 2003; *Zoback et al*., 2003], and form distinguishable strike and dip angles with respect to stress orientations (σ_1, σ_2, and σ_3) but also dependent on the mode of fracturing [*Anderson*, 1951; *Sibson*, 2003; *Zoback et al*., 2003]. Conjugate natural fracture sets will develop with 60° of separation and bisected by the σ_1 direction, with the direction of σ_3 bisecting the corresponding 120° angle made by the fracture pair and normal to σ_2 [*Anderson*, 1951; *Sibson*, 2003; *Zoback et al*., 2003]. In the case for tensile fractures, which are not encountered in this study, the interpretation of principal stresses is entirely different, highlighting the importance of understanding the fracturing mode. An understanding of the natural fracture strike and dip angle, while considering the bedding plane, allows us to predict the most likely principal stress orientation and stress regime responsible for their development [*Anderson*, 1951; *Zoback et al*., 2003]. A change in strike, dip angle, or intensity with depth can infer a change in tectonic activity [*Seeburger and Zoback*, 1982]. It is important to note that *Tavani et al*. [2015] and *Healy et al*. [2006] have shown that the geometry of fractures and faults relative to far-field stresses can vary due to the occurrence of precursory fractures and faults and from the folding of strata, which must be carefully considered during analysis.

A key to this analysis is identifying whether fracture sets developed prior to, during, or post tilting of the bedding plane, as well as the mode of fracturing present. In order to constrain the timing of fracture set development, the data are first divided into sets according to their present-day orientation and also after unfolding of the bedding plane. Ideally, fractures that require unfolding to horizontal bedding, in order to be consistent with the Andersonian system, developed prior to bedding tilting. Fracture planes that are consistent with being developed under the Andersonian system (±10°) with inclined bedding planes are treated as being developed after the bedding plane tilting event [e.g., *Hancock*, 1985; *Bellahsen et al*., 2006; *Amrouch et al*., 2010a, 2010b; *Arboit et al*., 2015]. This distinction can help with defining the relative chronology of natural fracture development. Considering that only shear fractures were encountered in this study, together with distinguishing between pretilting, syntilting, and posttilting fractures, enables fracture sets to be organized based on a relative chronological sequence and provide information on the stress regime and direction of maximum paleoprincipal stresses through time.

3.4. Faults Extracted From Seismic Data

Fault strikes and dip angles were obtained from depth-converted 3-D seismic surveys covering major petroleum fields located along the GMI and MN ridges and within the Patchawarra Trough (Figure 2). The seismic surveys cover the Swan Lake and Greater Tindilpie (acquired 2000), Gidgealpa (acquired 2002), Greater Strzelecki (acquired 2001), Dullingari (acquired 1997), Merrimelia (acquired 1998), and Fly Lake (acquired

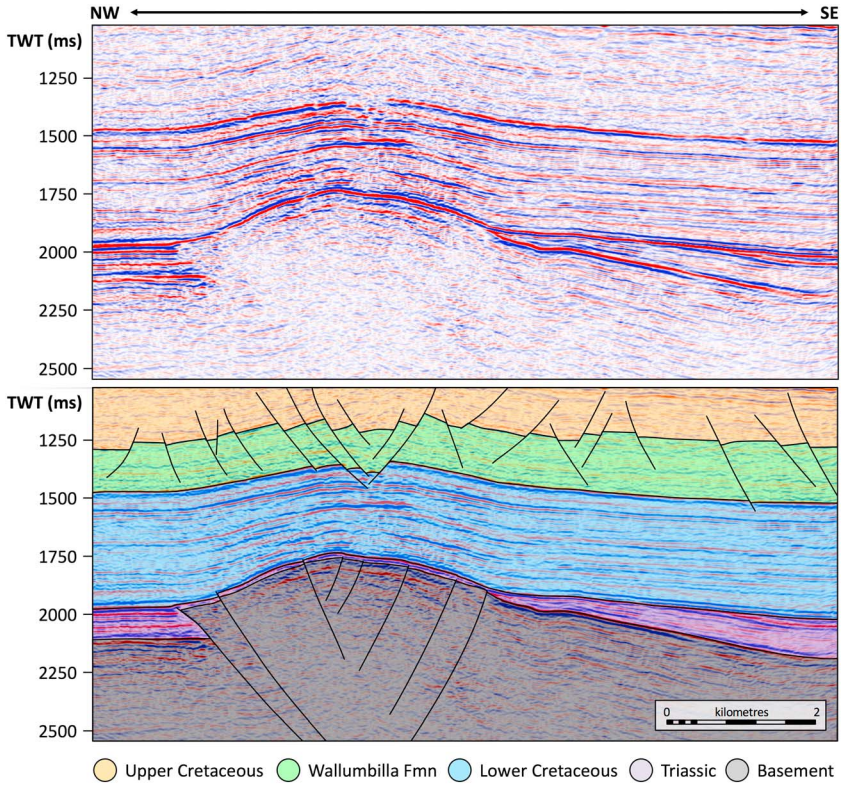


Figure 5. Examples of inverted basement normal faults and the distribution of Cretaceous polygonal faults in Merrimelia 3-D [after *Kulikowski et al*., 2017]. See Figure 2 for location.

2000) fields (Figure 2). Depth conversion ensured that true, rather than pseudo, fault geometries were measured [*Kulikowski et al*., 2016a, 2016b]. Seismic depth conversion in this study utilized well check shot data to create an interval velocity model that was corrected to true well depths. All fault interpretation was performed on the resultant depth-converted seismic volume.

Macroscale fault data measured from the six 3-D seismic surveys served as structural upscaling that would be integrated with calcite twin and natural fracture analysis results. The analysis of fault data followed the fundamental rock failure principles that state the geometry of rock failure relative to the orientation of principal stresses [*Anderson*, 1951; *Zoback et al*., 1989, 2003; *Sibson*, 2003]. This is similar to the methodology used for natural fracture analysis; however, when analyzing fault data the bedding plane is not taken into account. This is because large macroscale faults are considerably larger (up to 1 km) than mesoscale natural fractures and displace a number of seismic reflectors, preventing the measurement of a single representative bedding value. The fault analysis used here is somewhat primitive for paleostress orientation inversion, as striations could not be incorporated into the analysis, and poor seismic data quality prevents rigorous fault growth analysis. The relative density of newly formed faults through time is often significantly less compared to preexisting faults, as fault reactivation is often more stress economic than overcoming the cohesive strength of rocks required for new fault development [*Sibson*, 1985].

It is well known that inverted high-angle extensional faults and vertical strike-slip faults are extensive within this basin (Figure 5); however, there is little mention of low-angle reverse faults in literature [*Kuang*, 1985; *Apak et al*., 1997; *Gravestock and Jensen-Schmidt*, 1998; *Grant-Woolley et al*., 2014; *Kulikowski et al*., 2016a, 2017]. Recent works utilizing depth-converted 3-D seismic data have acknowledged the presence of vertical strike-slip faults [*Grant-Woolley et al*., 2014; *Kulikowski et al*., 2016a, 2017], low-angle reverse faults [*Kulikowski et al*., 2016a, 2017], and inverted high-angle extensional faults [*Grant-Woolley et al*., 2014; *Kulikowski et al*., 2016a, 2017] with no mention of non-Andersonian faults. The analysis of macroscale fault data therefore follows a more elementary methodology than mesoscale natural fracture analysis but remains in line with the fundamental rock failure principles [*Anderson*, 1951]: low angle (~30°) faults develop under a compressional stress regime parallel to the dip direction; high-angle faults (~60°) develop under an extensional stress

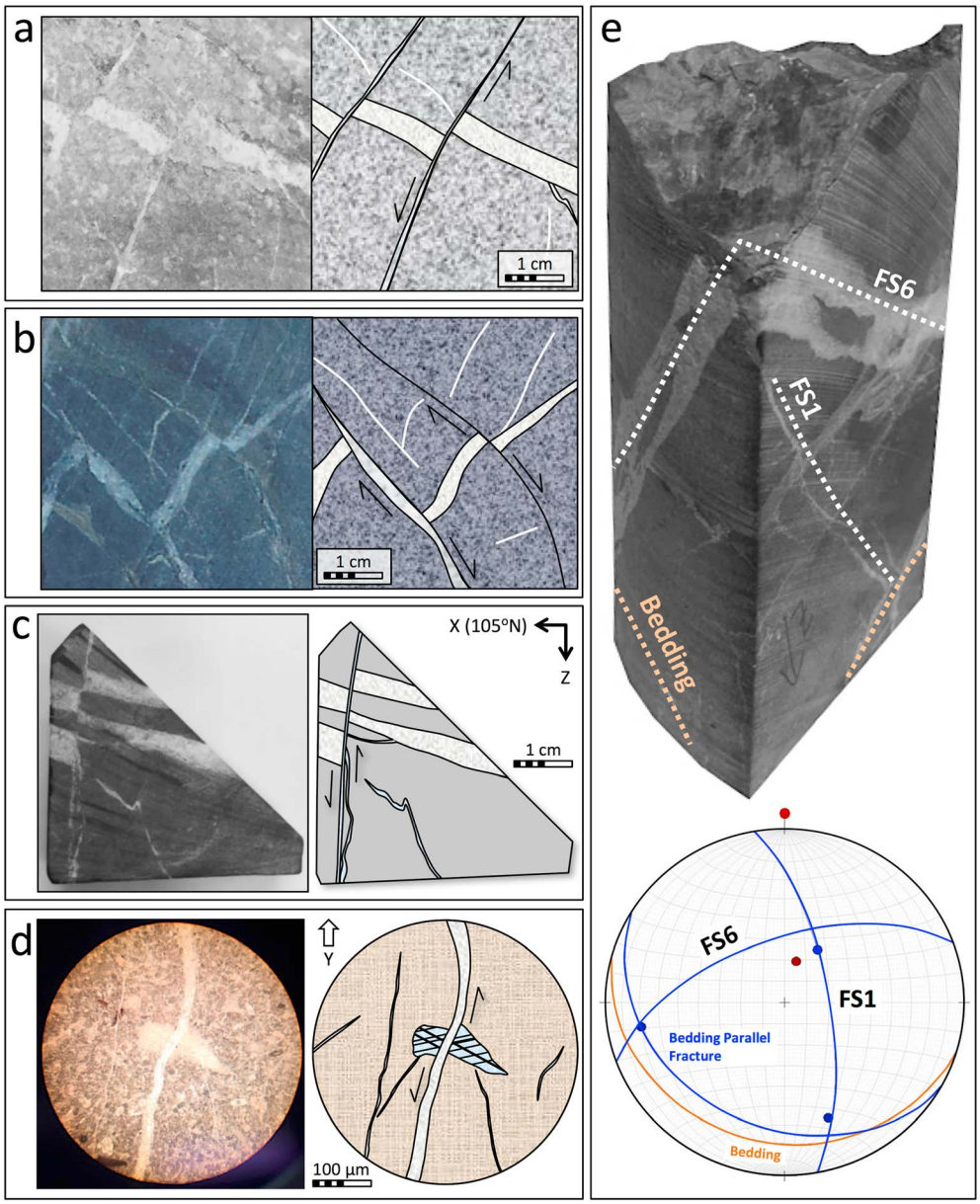


Figure 6. Evidence of shear fracturing observed in (a) core sample from the Merrimelia Formation in Gidgealpa 5; (b) core sample from the Merrimelia Formation in Gidgealpa 5; (c) core sample from the Kalladeina Formation in Gidgealpa 5; (d) thin section from the Merrimelia Formation in Gidgealpa 5; and (e) core sample from Gidgealpa 5 showing three natural fractures projected onto a lower hemisphere stereonet.

regime with the minimum horizontal stress oriented parallel to the dip direction; and near-vertical faults formed under a strike-slip stress regime 30° from the maximum principal stress direction [*Anderson*, 1951; *Zoback et al.*, 2003].

4. Results

4.1. Microscale Calcite Twin Data

Microstructural analysis was performed on six oriented core samples following the *Etchecopar* [1984] method, giving rise to 12 stress tensors. Each sample contained calcite that was coarse enough to measure the deformation twinning, either within the matrix or as fracture fill (Figures 4a and 6). Shear was observed in thin sections (Figures 4 and 6) and also evident in core samples (Figure 6). A universal stage microscope was used to

measure between 150 and 185 calcite twin planes per sample, for a total of over 1000 measured twin planes. The internal twinning deformation observed within all samples appeared to belong to the thin twin regime (Figure 4b), implying that temperatures remained below 200°C [*Burkhard*, 1993]. The calcite twin inversion process was demonstrated by *Lacombe et al*. [1990] to be entirely void of inversion errors when at least 90 crystals per sample were measured. As we systematically measured in excess of 90 crystals per sample, the results presented here are statistically accurate and reliable (Table 1).

To evaluate the relationship between deformation and layers' tilting, we examined calcite twin results in their present-day orientation as well as the orientation pretilting (orientation after bedding is rotated to horizontal). This is vital to accurate analysis as calcite crystals may have been subject to a given stress and subsequently rotated through folding or tilting of the bedding plane. In cases where rotating the bedding plane resulted in one of the principal stresses becoming vertical, we infer that the stress tensor was active prior to tilting. However, if a principal vertical stress exists without rotating the bedding plane, we assign the stress tensor as occurring after tilting. The bedding dip angle associated with calcite samples is 10–15°, which makes it difficult to constrain bedding tilt chronologies, particularly when considering the uncertainties associated with paleostress orientations [*Lacombe*, 2010]. However, for each of the results that required rotation of the bedding plane to horizontal, one principal stress was consistently within the bedding plane, and another was perpendicular to it. The differential stress ratio, differential stress magnitude, and stress regime of each stress tensor were also examined. This process permitted us to resolve 12 stress tensors existing either in the present-day orientation or after tilting (Table 1), which then formed six individual stress tensors (Figure 7).

The differential stress magnitudes ranged from 43 to 67 MPa (Table 1), with an average of 53 ± 11 MPa, which are on the same order as differential stresses found in other provinces [*Weathers et al*., 1979; *Ferrill*, 1998; *Lacombe*, 2001, 2007]. Interestingly, the present day differential stress magnitude within the Cooper-Eromanga Basin is 50 MPa [*Reynolds et al*., 2005, 2006] despite representing the local, instantaneous ambient crustal stress [*Lacombe*, 2007, 2012], in contrast to the paleostress magnitudes that represent the average of ancient crustal stresses over several thousands or millions of years [*Lacombe*, 2007]. Paleodepths are critical for paleostress constraints as they provide an indication into the magnitude of overburden stress; however, they are difficult to measure within the Cooper-Eromanga Basin because of the several episodes of exhumation and erosion.

Results from calcite twin principal stress orientation inversion are summarized in Table 1. Constraining whether calcite results occurred before or after tilting is difficult with this data set, as bedding plane dip angles are typically 15°. The first stress tensor was constrained from samples collected from the Warburton Basin (basement) (sample CalS5b) with the σ_1 striking N-S (172–352°N) and close to the bedding plane (Figure 7a). Upon rotating the bedding plane to horizontal, the σ_2 was near vertical with a differential stress ratio of 0.70. A SE-NW (129–309°N) oriented σ_1 was calculated from Kalladeina and Merrimelia formation samples (sample CalS1, CalS2, and CalS3) (Figure 7b). The σ_1 from each of these results became near horizontal when the bedding plane was rotated, with σ_2 becoming vertical in samples CalS2b and CalS1b, and horizontal in sample CalS3. The differential stress ratio ranges from 0.40 to 0.80. Samples from the Merrimelia and Kalladeina formations (sample CalS2b, CalS1b, and CalS4) also present an NE-SW (055–235°N) oriented σ_1 that is close to the bedding plane in samples CalS2b and CalS1b, and appear to be in a somewhat similar geometry with inclined bedding in sample CalS4 (Figure 7c). The σ_2 in these results is vertical and the differential stress ratio ranges from 0.40 to 0.60. An E-W (077–257°N) oriented σ_1 is recorded in a sample collected from the Kalladeina Formation (sample CalS5) that plots close to the bedding plane (Figure 7d). In this result the σ_3 becomes vertical when bedding is rotated to horizontal and the differential stress ratio is 0.50. An additional group of results with an E-W (85–265°N) striking σ_1 are recorded in samples CalS6b and CalS4b with inclined bedding, sampled from the Kalladeina and Merrimelia formations (Figure 7e). The σ_2 in these results is near vertical and the differential stress ratio ranges from 0.30 to 0.50. Finally, an N-S (174–354°N) striking horizontal σ_2 is recorded in samples CalS3b and CalS6, both with inclined bedding (Figure 7f). The σ_2 in these results is vertical and the differential stress ratio is 0.40 in both samples.

4.2. Mesoscale Natural Fracture Data

An important aspect of this analysis is distinguishing between the modes of fracturing present, as shear and tensile fractures must be treated differently when inferring the principal stress orientations and stress

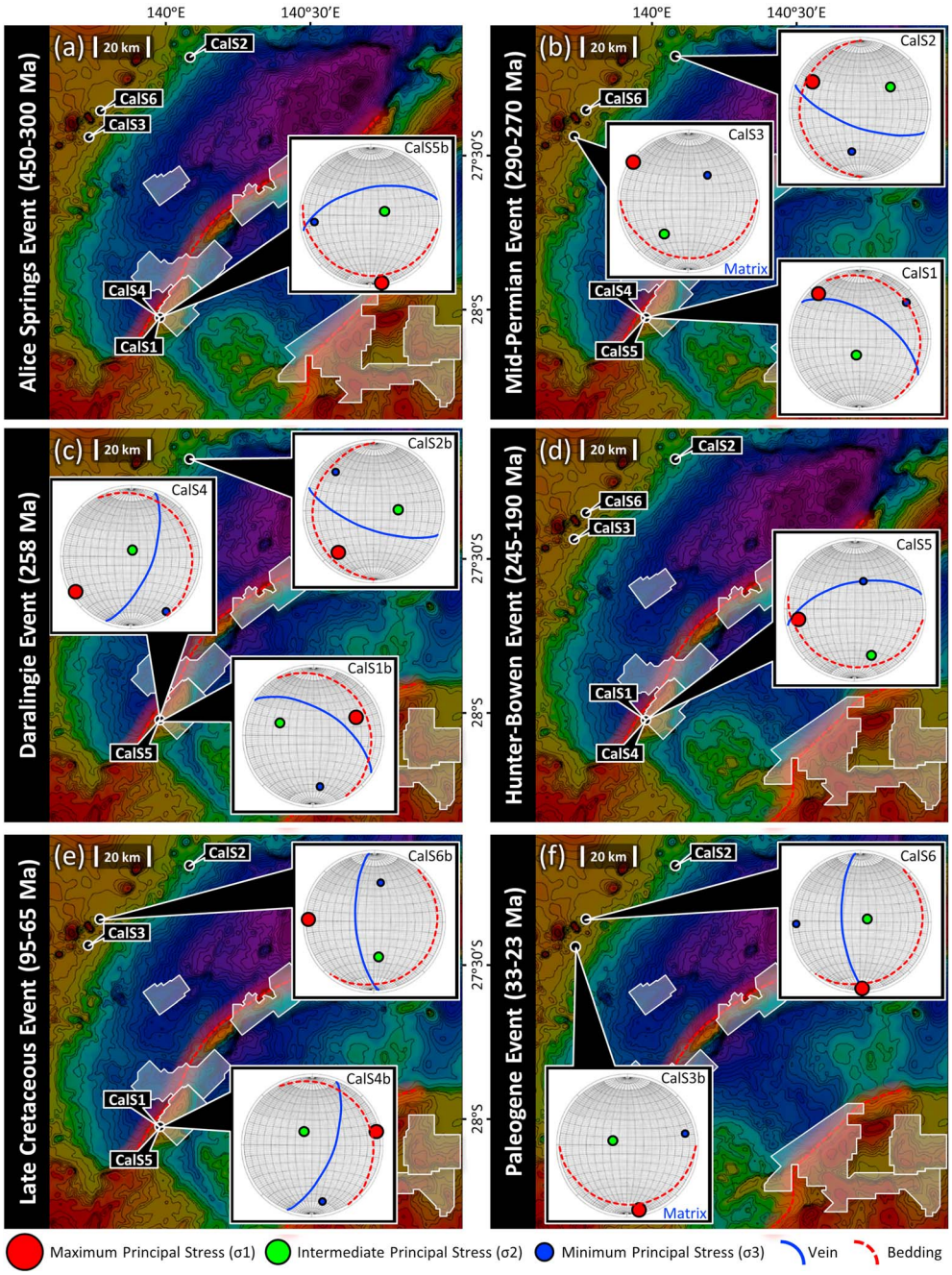


Figure 7. Calcite twin stress inversion results divided into six tectonic events that are arranged from (a) oldest to (f) youngest. Results are shown with inclined bedding (red dashed) and the sampled veins (blue solid).

regimes responsible for their development. Where possible, given that not all wells were cored, natural fractures interpreted from borehole image logs were correlated to core samples. During this process the vast majority of observed fractures from core were mode 2 (shear) (Figure 6) with fibrous growth of cement oblique to the vein wall also present (Figure 6c). This consistent sighting of shear fracturing and evidence of shearing (fibrous growth of cement) was used to infer that the entire natural fracture data set interpreted from borehole image logs are all likely to be mode 2. The stereographic projection of all measured natural fracture planes are presented for each well (Figure 8). The present day geometry of natural fractures across the 27 well locations shows a complex distribution with multiple clusters (Figure 8). The dominant strikes of natural fractures cluster at NE-SW, N-S, and SE-NW, with the natural fracture dip

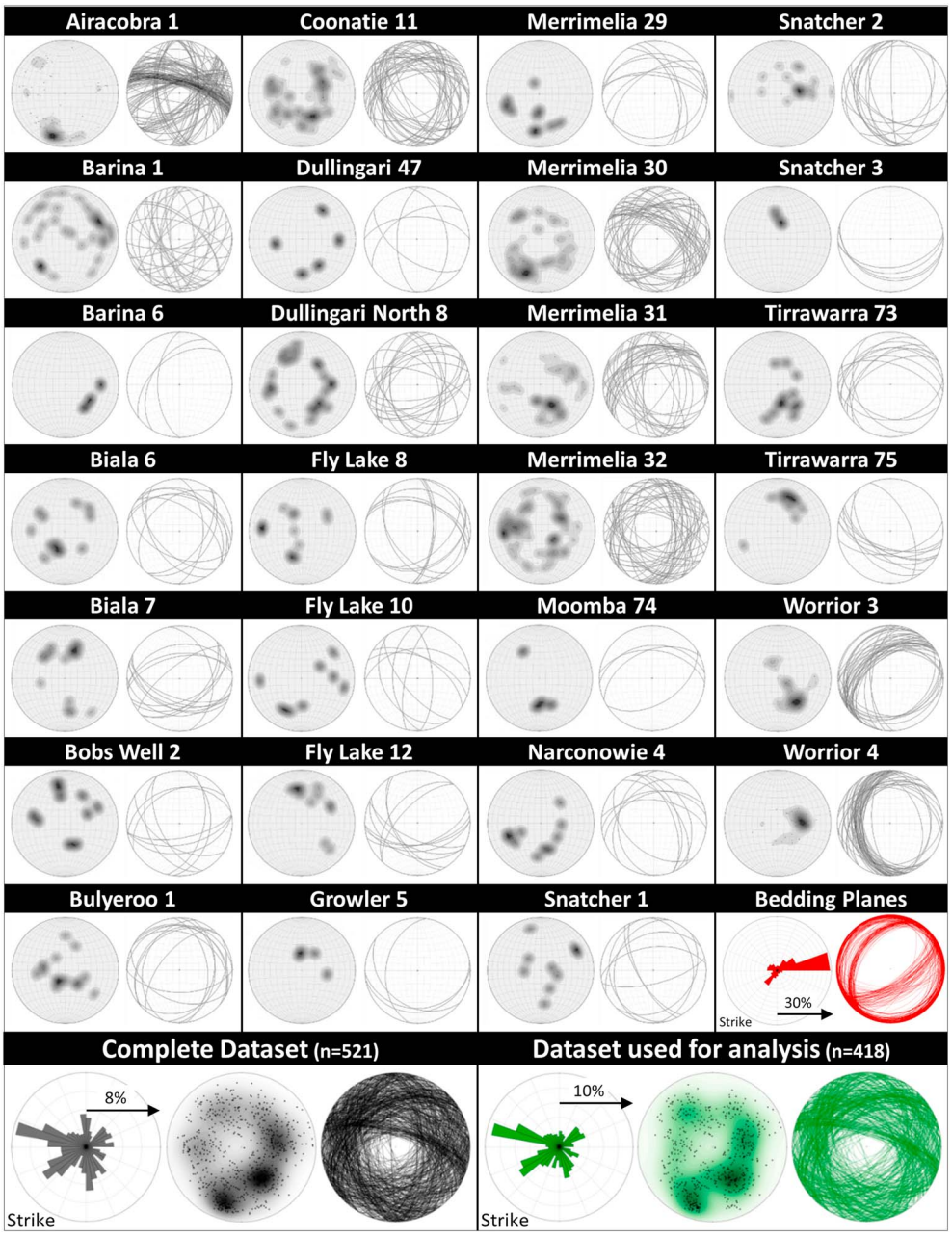


Figure 8. Interpreted borehole image log data showing fracture planes per well. Lower hemisphere stereonets shown. For well locations see Figure 2.

angles varying considerably from horizontal to vertical even within an individual well. These observations are important for hydrocarbon exploration and development; however, for the purpose of inferring paleostress orientations and regimes from natural fracture data, clustering of fracture sets must consider the geometry of the bedding plane. This is explored further in section 5.

Microfaults with centimeter to decimeter displacements were found in borehole image logs across the Merrimelia, Patchawarra, Birkhead, Cadna-owie, and Allura formations. Microfaults mimicked the geometry of high-angle fractures and faults striking NE-SW and SE-NW. The displacement across microfault planes ranges from 1.5 to 8 cm. Figure 9 shows an example of a fault interpretation on a borehole image log from Merrimelia 32 and the corresponding core sample highlighting normal fault growth in the Birkhead Formation.

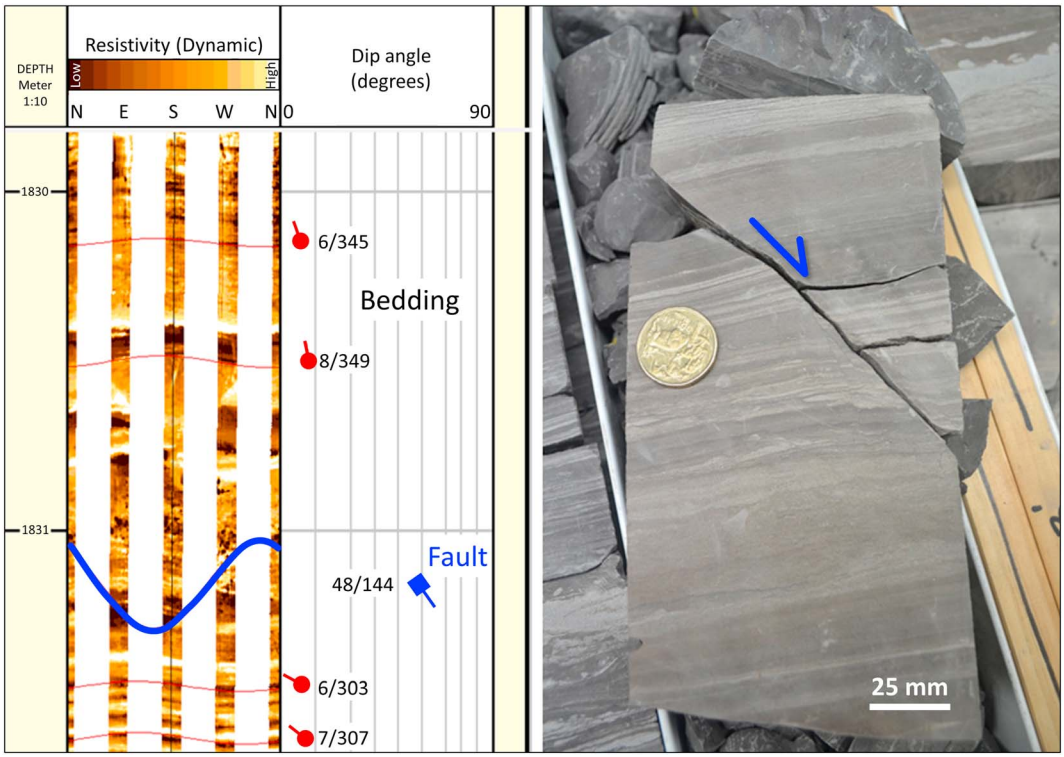


Figure 9. Normal microfault identified in the borehole image log from the Birkhead Formation in Merrimelia 32 and the corresponding core sample.

4.3. Macroscale Fault Data

A regional N-S cross section through the basin illustrates the basic structural architecture of the region, and the relationship between basement involved faults and structuring, while also illustrating a basin-wide system of normal faults within Middle Cretaceous sediments (Figure 10a). The majority of measured faults are basement involved with reverse sense of motion and typically terminate within the basement or the middle Patchawarra Formation; however, faults are also observed to extend to the top Nappamerri Group sediments (Figure 10a).

Fault geometries measured from the six depth-converted 3-D seismic surveys are presented in Figure 10. The majority of seismic surveys have a dominant NE-SW striking fault system dipping at angles of 55–70° with reflector displacement suggesting reverse fault motion (Figure 5). A significant number of SE-NW striking near vertical faults are identified, particularly within the Dullingari (Figure 10b), Swan Lake (Figure 10c), Gidgealpa (Figure 10d), and Greater Strzelecki (Figure 10e) areas. The complete fault data set is plotted on a stereonet (Figure 10h) and dip angle histogram (Figure 10i) to show the overwhelming dominance of NE-SW striking faults with dip angles of 50–70°. A secondary group of SE-NW striking faults is also present (Figure 10h). The dip angle of the data set shows a distinct subset of vertical faults (Figure 10i). Fault measurement was limited to strikes and dip angles, as slickensides could not be measured from seismic data. As such, the results from this portion of the study are primitive, but they provide a general understanding of the upscaled and regional stresses that have deformed the basin. Basement faults measured from the six depth-converted 3-D seismic surveys found four key points;

1. NE-SW striking faults with 50–70° dip are dominant in the basin (Figures 10b and 10c).
2. Small populations of N-S, E-W, and SE-NW striking faults with 50–70° dip are present.
3. Few NE-SW and N-S striking faults with 30° dip are present.
4. Near-vertical NNE-SSW and SE-NW striking fault sets with lateral offset are present.

The near-vertical SE-NW striking faults are more common than NNE-SSW striking vertical faults and typically terminate within basement but are occasionally observed to extend into the Middle Patchawarra Formation.

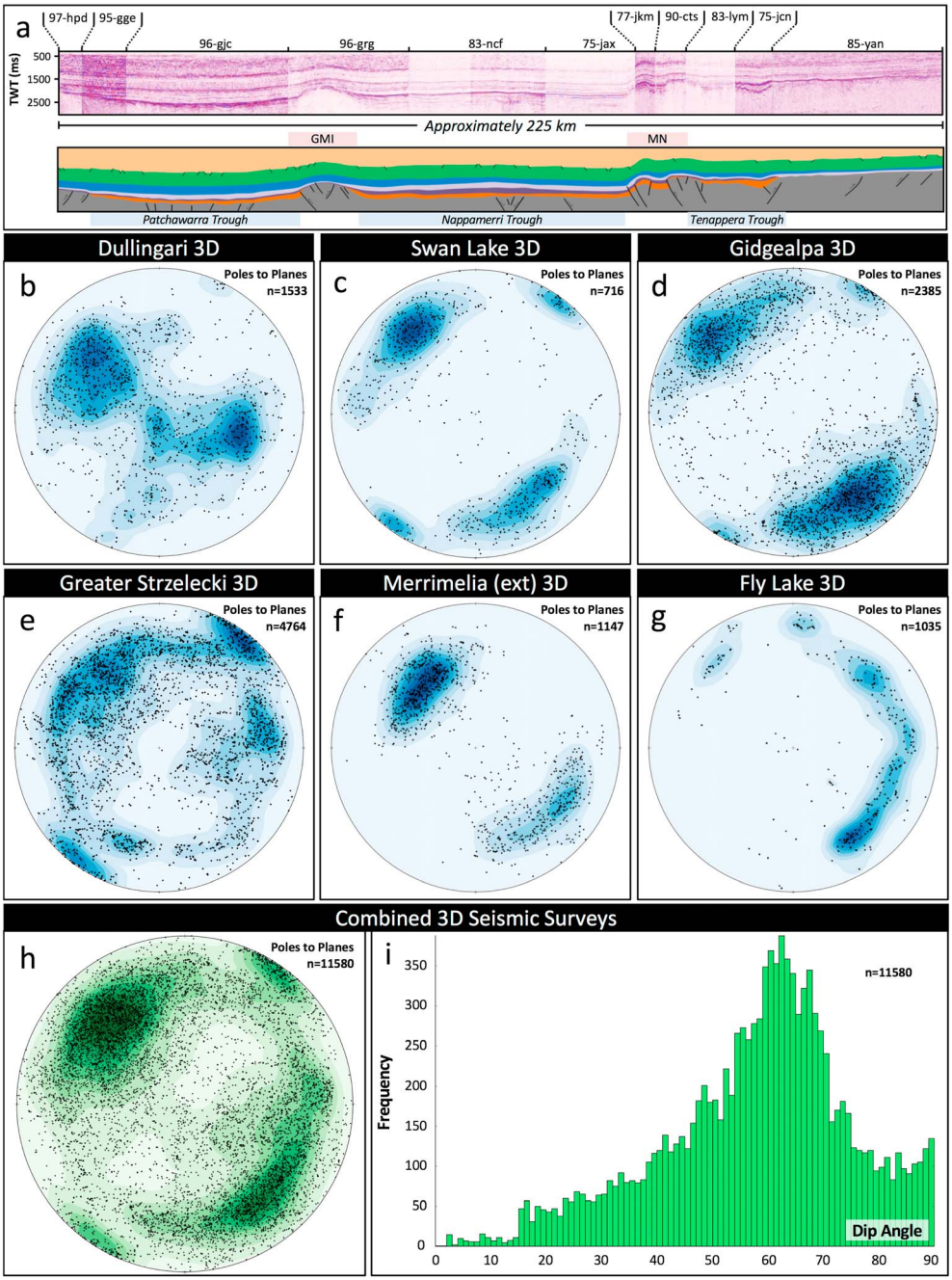


Figure 10. (a) N-S cross section of the Cooper Basin [after *Kulikowski et al*., 2016a]. See Figure 2 for location and Figure 3 for color scheme. Depth-converted faults from (b) Dullingari 3-D, (c) Swan Lake 3-D, (d) Gidgealpa 3-D, (e) Greater Strzelecki 3-D, (f) Merrimelia (extension) 3-D, and (g) Fly Lake 3-D. Combined fault data as (h) poles, and (i) dip angles. See Figure 2 for location of 3-D seismic surveys. Stereonets are equal-area lower hemisphere.

These vertical faults were not always visible in cross section, but more frequently interpreted from seismic depth slices. Considering that the seismic resolution is quite poor at this depth, it is possible that faults may extend into younger sediments at a subseismic resolution before terminating. The seismic resolution below the Permian coal measures rapidly decreases and prevents fault growth analysis; however, where the seismic resolution is comprehendible, seismic reflectors are displaced with reverse sense of motion across high-angle faults.

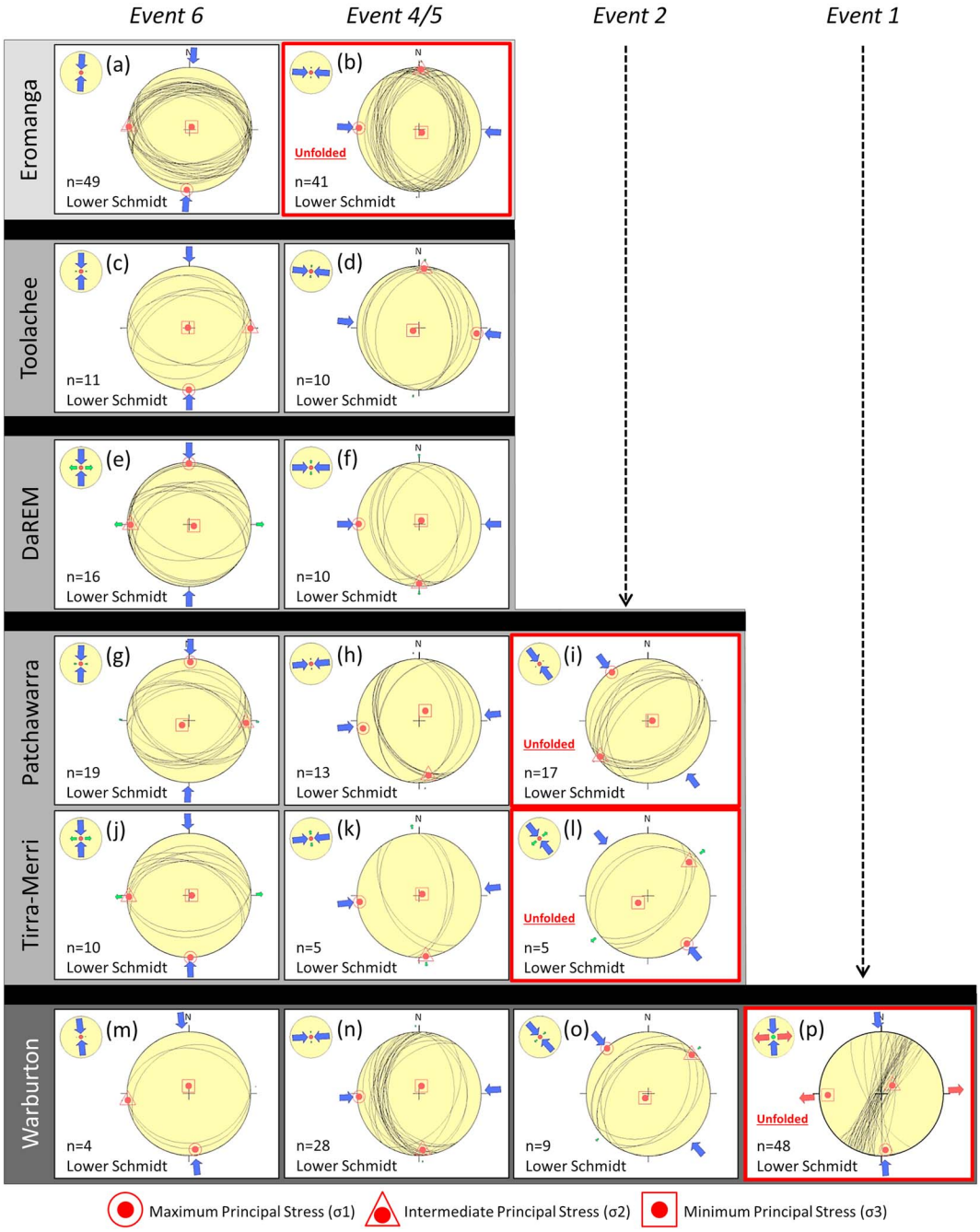


Figure 11. Dominant natural fracture sets identified per stratal package with inferred principal stress orientation shown as blue arrows. The fracture sets are ordered based on their stratigraphic distribution, ranging from (a) youngest to (p) oldest. All fracture planes contain inclined bedding unless specified. DaREM: Daralingie, Roseneath, Epsilon, and Murteree stratal unit; Tirra-Merri: Tirrawarra and Merrimelia stratal unit.

5. Interpretation and Discussion

Previous authors have shown conflicting evidence on the number and combination of events that have affected the Cooper-Eromanga Basin. These include (1) *Kuang* [1985] presented three compressional phases during the Carboniferous to Permian (unknown orientation), Upper Triassic oriented NE-SW, and Upper Cretaceous to Paleocene oriented E-W; (2) *Apak et al.* [1997] suggested four tectonic events including the first Mid-Permian uplift (273 Ma) (unknown orientation), the Second Mid-Permian uplift (270 Ma) (unknown

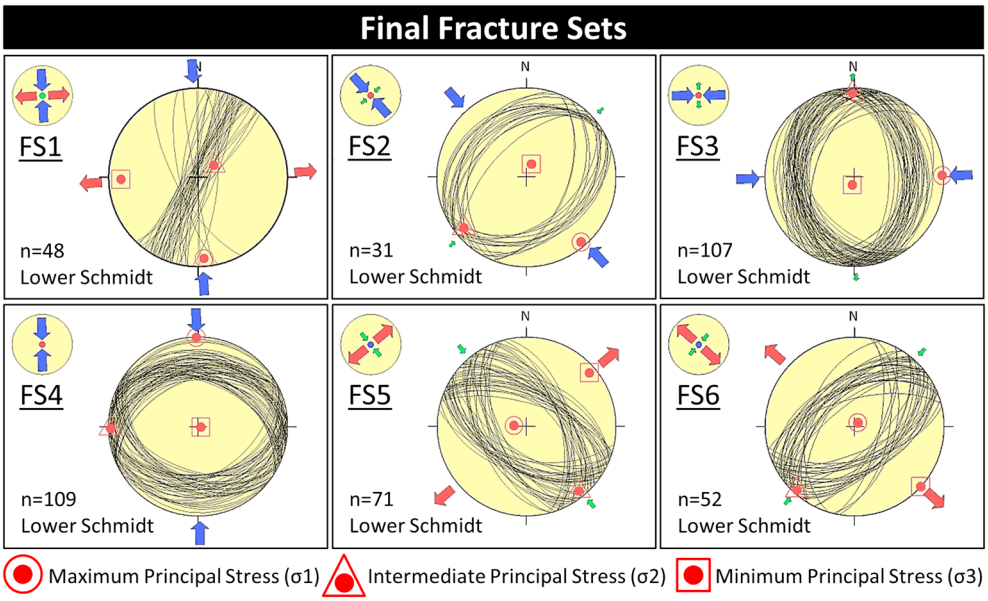


Figure 12. Interpreted regional natural fracture sets. Arrows denote the orientation of principal horizontal stress interpreted to have developed the given fracture set.

orientation), Late Permian uplift (258 Ma) (unknown orientation), and the E-W Middle Triassic uplift (245 Ma); and (3) *Gravestock and Jensen-Schmidt* [1998] showed the possibility of five events including the NW-SE oriented post-Ordovician compression caused by the cross vector of the N-S ASE and the E-W Kanimblan event, two periods of uplift during the Mid-Permian (unknown orientation), large collision during the Triassic (212–190 Ma) (unknown orientation), and an E-W oriented early Tertiary event. Not only is the number of events highly speculative between researchers, the stress orientation and regime are also uncertain.

To define the orientation and stress regime of tectonic events that have affected the Cooper-Eromanga Basin, calcite twins, natural fractures, and faults are independently analyzed prior to being integrated. Calcite twin and natural fracture results were examined in their present-day orientation as well as the orientation pretilting (orientation after bedding is rotated to horizontal) to determine whether the results were recorded pretilting or posttilting of the bedding plane. A stress inversion tool (Wintensor) was used to statistically define two low-angle N-S and E-W striking conjugate natural fracture sets present throughout the stratigraphic column (Figure 11). A low-angle conjugate natural fracture set striking NE-SW was also identified but limited to the Patchawarra Formation, Tirrawarra and Merrimelia, and Pando and Innamincka stratal units (Figures 11i, 11l, and 11o). This fracture geometry required rotation to horizontal bedding within the Patchawarra Formation and Tirrawarra and Merrimelia stratal unit to conform to the Andersonian system and is present within the Pando and Innamincka stratal unit with inclined bedding. A near-vertical NNE-SSW and SE-NW striking fracture set is present only within the Pando and Innamincka stratal unit (Figure 11p) and requires rotation to a horizontal bedding plane to align with the Andersonian system.

Calcite twin data resolved 12 stress tensors (Table 1) that align with the paleostress analysis of six systematically appearing regionally extensive natural fracture sets (Figure 12). These natural fracture sets represent the regionally pervasive fracture system within the Cooper-Eromanga Basin and exclude local anomalous fracture sets that formed through stress perturbation. The distinguishable fracture sets show evidence of shearing at the core and thin section scales (Figures 4, 6, and 9). Stress perturbation, commonly caused by faults, folds, topography, or lithology, can develop natural fractures and faults that are not representative of the far-field tectonic stresses [*Tavani et al.*, 2015]. *Tavani et al.* [2015] also discuss that regional scale stresses may slightly differ to the plate scale tectonic stresses. Considering that the regional natural fracture sets are present extensively throughout our study area, it is likely that these represent the true far-field stresses.

Two (FS5 and FS6) of the six regional conjugate natural fracture sets (Figure 12) are high angled (60°) striking SE-NW (FS5) and NE-SW (FS6) and present throughout the stratigraphic column with inclined bedding. For

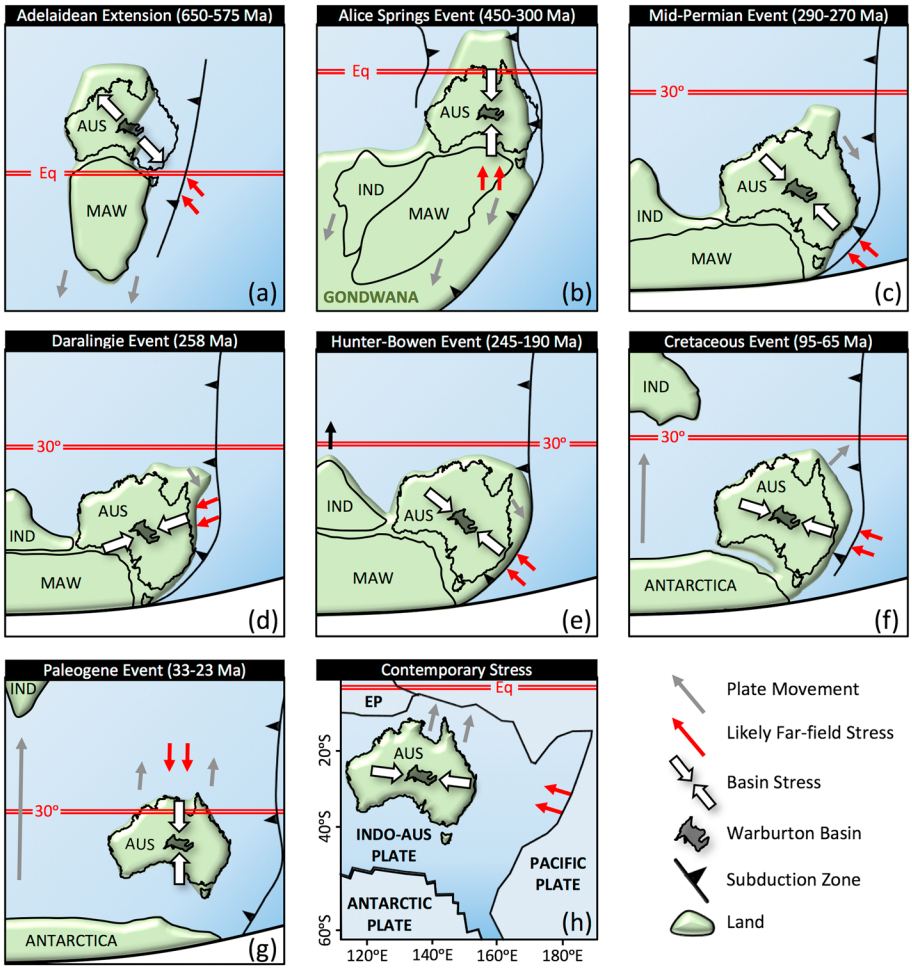


Figure 13. Schematic of the tectonic evolution of Australia from (a) 650 Ma to (h) the present day showing final paleostress results to determine far-field origins. AUS: Australia; IND: India; MAW: Mawson Block; EP: Eurasian Plate; Eq: Equator. Tectonic evolution maps derived from *Myers et al.* [1996], *Collins and Pisarevsky* [2005], *Reeves and De Wit* [2000], *Rees et al.* [2002], *Boger and Miller* [2004], *Gray and Foster* [2004], *Hillis et al.* [2008], *Li et al.* [2008], *Van der Meer et al.* [2012], *Metcalfe* [2013], and *Müller et al.* [2016].

these fracture sets to develop, an extensional stress regime must be present [*Anderson*, 1951]. Intermittent periods of flexural relaxation (sag) along faults, or lateral movement of strike-slip faults, may induce extensional stress regimes sufficient enough to induce extensional fracturing. The majority of calcite samples were obtained from these two fracture sets (Table 1), as they were more commonly calcite filled, particularly within basement formations. Extensional stresses are also supported with the presence of microfaults (Figure 9) parallel to fractures and regional faults.

Macroscale faults were difficult to analyze, given that the majority of faults were high angle in nature with reverse reactivation and inadequate seismic resolution at basement preventing rigorous fault growth analysis (Figure 5). Conjugate fault sets were also sparse throughout the study area (Figure 10), particularly for low-angle reverse faults, as much of the successive events were likely accommodated by reactivation of preexisting faults. As such, the complexities of tectonic stresses that have affected the basin do not appear to be present within fault data. Considering that faults measured from seismic data do not contain slickenside information, oblique reactivation is also difficult to constrain. However, fault data provided an indication of the likely stress regime and principal stress orientation responsible for initial and widespread basement fault development. The high-angle nature of measured faults infers that their development is related to an extensional stress regime event oriented SE-NW. These faults are prevalent throughout the basin and likely developed during the early stages of basin development during SE-NW Adelaidean (650–575 Ma) extension

(Figure 13a). Also, based on the presence of reverse and strike-slip faults, compressional and strike-slip stress regime events had likely affected the evolution of the basin.

The integration of microscale, mesoscale, and macroscale analyses demonstrates statistical and geological confidence in the results, which are discussed below for each event. The comparison between macroscale fault data (seismic data) and mesoscale fracture data (borehole image logs) does illustrate somewhat of a disconnect in terms of strike and dip geometries (Figures 10 and 12). The NE-SW striking inverted basement normal faults that are prevalent throughout the basin are believed to have developed during the Adelaidean extensional event (650–575 Ma) and accommodated much of the strain created by subsequent events (Figure 10). This accommodation of strain on the macroscale can explain the dominance of this pervasive fault set. Such accommodation is absent on the mesoscale and can explain the relatively larger variation in fracture set populations (Figure 12). The integration of results provides better constraints on the timing of tectonic events, the timing of fault and fracture development and reactivation, the evolution of stress orientations and stress regimes through time, and an overall better understanding of Australia's largest onshore hydrocarbon province (Figure 14). The final results are projected onto paleotectonic maps of Australia (Figure 13) to determine the likely origin of far-field paleostresses.

5.1. Carboniferous Alice Springs Event (ASE) (450–300 Ma) (Event 1)

A near-vertical conjugate natural fracture set (FS1) is present within the basement, striking NNE-SSW and SE-NW when the bedding planes are rotated to horizontal (Figure 11p) [*Grohmann and Campanha*, 2010]. Considering that this fracture set requires the corresponding bedding to be rotated to horizontal and that it is not present within younger sedimentary rocks, it is considered to be one of the oldest fracture sets present (Figure 11p). Although the number of fractures attributed to this set is high ($n = 48$), the distribution is unevenly biased and must be processed carefully. A NNE-SSW and SE-NW striking strike-slip fault set was also interpreted from four of the six 3-D seismic surveys (Figure 10). A NNW-SSE oriented strike-slip stress regime (Event 1) is required, under the Andersonian theory [*Anderson*, 1951], for the development of these fractures and faults; occurring between deposition of the Innamincka Formation (440 Ma) and Cooper Basin sediments (300 Ma). *Grant-Woolley et al*. [2014] identified strike-slip faults within a newly acquired 3-D seismic survey in the Cooper-Eromanga Basin, attributing their presence to reduced reservoir properties and poor well performance.

Sample CalS5b was collected from a calcite-filled natural fracture (fracture set 6) in the Late Cambrian Kalladeina Formation (485–505 Ma) that underlies the Cooper Basin (Figure 2). This fracture set corresponds to a calcite veins that developed during SE-NW oriented extension. Results from CalS5b show an N-S oriented strike-slip stress regime (Event 1) present pretilting of the bedding plane (Figure 7). Calcite samples collected from younger sediments are void of this event, inferring that an N-S oriented stress was present prior to the Early Permian (300 Ma). This event correlates to the ASE (Figure 13b), which has previously been described by authors as a compressional event in an N-S (or NE-SW) orientation [*Kuang*, 1985; *Gravestock and Jensen-Schmidt*, 1998]. However, the results presented here support an N-S oriented strike-slip stress regime event occurring concurrent with the southward movement of Gondwana (Figure 13b). The sampled calcite vein corresponds to natural fracture set 6 and was developed by a SE-NW oriented extensional stress.

5.2. Mid-Permian Event (290–270 Ma) (Event 2)

Previous structural analysis of the Cooper-Eromanga Basin has found a relatively small event occurring during the Mid-Permian (Figure 2) [*Kuang*, 1985; *Apak et al*., 1997; *Gravestock and Jensen-Schmidt*, 1998]. Low-angle NE-SW striking conjugate natural fractures (FS2) are present within the basement, Merrimelia Formation, Tirrawarra Formation, and the Patchawarra Formation, suggesting that their development was related to a postdepositional SE-NW oriented compressional stress (Event 2), but prior to deposition of the overlying Murteree Shale (268 Ma) (Figure 14). A distinct absence of FS1 within Permian and younger sedimentary rocks infers a chronology, such that FS1 is older than FS2 (Figures 11, 12, and 14). This fracture set also mimics large-scale fault geometries within the study area inferring that microscale, mesoscale, and macroscale deformation was taking place at this time. High- and low-angle NE-SW striking faults have been shown to reactivate during this time through a SE-NW oriented event [*Apak et al*., 1997].

Calcite twin data analyzed from both the Merrimelia and Kalladeina formations (samples CalS1, CalS2, and CalS3) were obtained from calcite filled extensional natural fractures (fracture set 5) and matrix (Table 1)

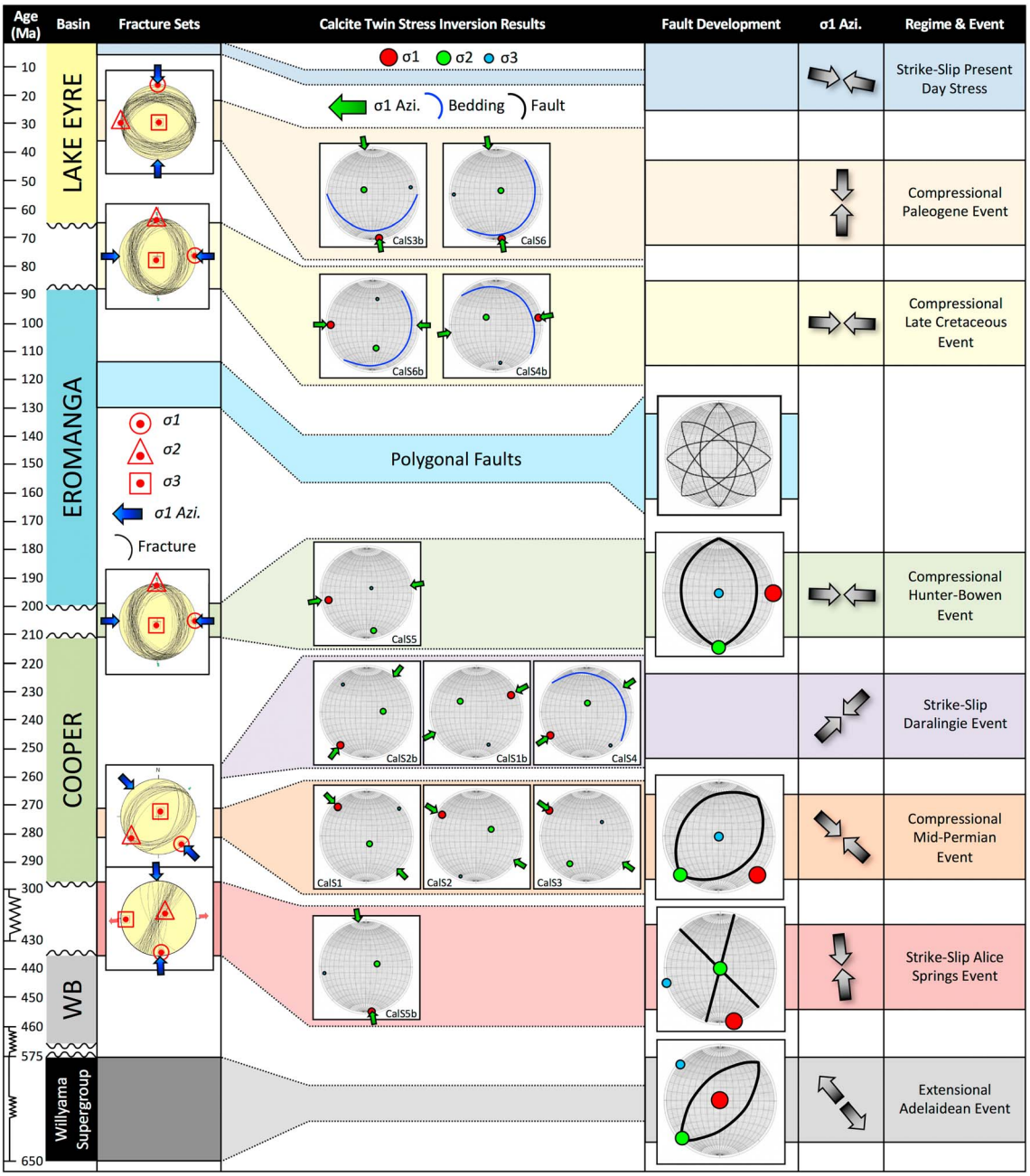


Figure 14. Integration of the final results obtained through paleostress analysis of calcite twin, natural fracture, and fault data. The timing of natural fracture and fault development is shown together with the corresponding structural event.

that were developed by a NE-SW oriented extensional stress (likely flexural relaxation post ASE) and subsequently calcite filled. The calcite twin data show evidence for a strike-slip to compressional stress regime event (Event 2) with σ_1 striking SE-NW (Figures 7 and 14). This event occurred pretilting of the bedding plane in each of the samples, since the σ_2 is mostly near vertical after rotation of the bedding plane to horizontal. This set of results strongly correlates to the compressional Mid-Permian event, which aligns with previous literature [*Apak et al.*, 1997; *Gravestock and Jensen-Schmidt*, 1998]. The orientation of this event is perpendicular to the NE-SW striking subduction zone that was present along eastern Australia (Figure 13c) and parallel to the strike of SE-NW oriented strike-slip faults that were likely reactivated. The differential stress ratio, *R*, (Table 1) obtained from CalS1 is significantly higher than CalS2 and CalS3; however,

considering that reverse and strike-slip faults are located adjacent to CalS1, and not CalS2 and ClaS3, it is likely that these affected the result (Figure 7).

5.3. Late Permian Daralingie Event (258 Ma) (Event 3)

This event peneplaned the entire Cooper Basin; however, the orientation and regime has been poorly constrained in literature. This event is reported to have reactivated preexisting basement involved faults and induced wrenching [*Apak et al*., 1997; *Gravestock and Jensen-Schmidt*, 1998]. Although this event does not appear to have developed a regional conjugate fracture set, interpretation of calcite results supports the presence of a NE-SW oriented strike-slip stress regime event occurring during the Late Permian correlating to the Daralingie event. Few low-angle faults were interpreted from the Greater Strzelecki 3-D seismic survey (Figure 10e), suggesting that this event preferentially reactivated preexisting basement-involved faults or caused widespread folding, rather than faulting.

An NE-SW oriented strike-slip phase (Event 3) is recorded in three calcite samples (CalS2b, CalS1b, and CalS4) collected from the Merrimelia and Kalladeina formations. Sample CalS4 records this event as posttilting, with the bedding plane inclined approximately parallel to the σ_1 direction of these results. The bedding dip angle associated with this sample is low, with tilting likely developed during this event and concurrent with calcite twins being formed. A relative chronology was established between this and the SE-NW oriented stress tensors, since rotating the low-angle bedding plane to horizontal brought one of the SE-NW principal axes closer to a near-vertical position within samples obtained from the same location. This chronology is in line with previous research that suggests a possible erosional event during the Late Permian that eroded much of the Daralingie Formation [*Apak et al*., 1997]. Importantly, the results in all three calcite samples show that this was a strike-slip stress regime event, which was not previously considered in literature (Figure 7).

These results were parallel to major NE-SW striking basement faults which perhaps accommodated much of the strain through lateral displacement rather than developing new faults. The origin of this stress can be explained to be the clockwise rotation of the Australia-Mawson Block and its interaction with the N-S striking subduction zone (Figure 13d). The differential stress magnitudes and the *R* value are consistent in all three tensors (Table 1). The differential stress magnitudes are similar to the previous Mid-Permian event (Table 1). These samples were obtained from calcite-filled natural fractures (fracture sets 5 and 6) that likely developed during repeated periods of postcompressional flexural relaxation creating SE-NW and NE-SW oriented extension (Table 1).

5.4. Upper Triassic Hunter-Bowen Event (245–190 Ma) (Event 4)

This compressional event developed a low-angle N-S striking conjugate fracture set (FS3), as well as sparse low-angle N-S striking faults interpreted from 3-D seismic data. Preexisting high-angle faults accommodated much of the strain during this time, as few low-angle reverse faults were identified when compared to the abundance of high-angle faults. Reactivation of preexisting basement-involved faults exhumed the Cooper Basin and generated the regional unconformity isolating the basin from the overlying Eromanga Basin.

A compressional stress phase oriented E-W (Event 4) was identified prior to the bedding plane being tilted within sample CalS5 from the Kalladeina Formation (Figure 7). The σ_3 becomes vertical when the bedding plane is unfolded to horizontal, suggesting a compressional stress regime prior to tilting. The timing and orientation of this event confirms previous research that proposed an E-W orientation for this event and correctly described it as a compressional stress regime [*Kuang*, 1985; *Apak et al*., 1997; *Gravestock and Jensen-Schmidt*, 1998]. The E-W compressional event recorded within calcite twin data correlates to the Upper Triassic Hunter-Bowen event, which is marked by a regional unconformity separating the Cooper and Eromanga basins. The calcite sample was obtained from a calcite-filled natural fracture belonging to fracture set 6 (Table 1), which also contained information on the ASE. This natural fracture set is associated with SE-NW oriented extensional stresses (typically postcompressional flexural relaxation) that were cyclically present throughout the evolution of the basin.

The likely far-field stress origin of the Hunter-Bowen event can be traced back to the subduction zone that was located along the eastern margin of Australia and normal to basin paleostress during the clockwise rotation and southward movement of the Australian plate (Figure 13e). The calcite sample that recorded this event (CalS5) has an inclined bedding plane that dips to the south (15/190), inferring a possible subsequent N-S event that inclined the bedding plane. The differential stress magnitude is again similar to the previous

two events (Table 1). After this event, there was a pronounced period of tectonic quiescence that is recorded in the uninterrupted deposition of the Eromanga Basin sediments. This event (Figure 13e) is notably different to the subsequent Upper Cretaceous event (Figure 13f), as the distinction defines the moment that the Australian plate ceased its clockwise rotation and southward movement, and starts its new journey moving toward the northeast. The change in stress regime (strike-slip to compressional) between this and previous events is likened to the intracratonic Paris basin, in terms of polyphase complexity, which transitions between strike-slip, extensional, and compressional stress regimes [*Lacombe et al*., 1994; *Rocher et al*., 2004].

5.5. Upper Cretaceous Event (95–65 Ma) (Event 5)

A low-angle N-S striking conjugate natural fracture set (FS3) (Figure 12) is present throughout the stratigraphic column (Figure 11). This fracture set is present in Pre-Jurassic formations with tilted bedding, suggesting that FS3 was developed when the bedding plane of Eromanga Basin sediments was horizontal, but after Pre-Triassic sediments were tilted. Again, as FS1 and FS2 (Figure 12) are not present in the Eromanga Basin (Figure 11), a relative chronology can be made, such that FS3 is younger than FS2. To develop FS3, an E-W oriented compressional stress regime event (Events 4 and 5) is required sometime after the Toolachee Formation was tilted, but before tilting of the Eromanga Basin sediments (Figure 11). This confirms previous research suggesting that an E-W oriented event formed en echelon anticlines elongate in a N-S direction, as well as forging the regional unconformity that separates the Eromanga and Lake Eyre basins during the Late Cretaceous (Figure 14) [*Lowe-Young et al*., 1997]. As this event (Event 5) has a similar orientation and stress regime to the Hunter-Bowen event (Event 4), it is likely that the faults and fractures developed during Event 4 were reactivated. Fault activity during Event 5 appears limited in seismic data with much of the deformation likely to be in the form of folds rather than faults or reactivation at a subseismic resolution scale.

This E-W oriented stress (Event 5) postdates the Hunter-Bowen event and is calculated from samples CalS6b (fracture set 1) and CalS4b (fracture set 6) collected from the Kalladeina and Merrimelia formations, respectively. These samples recorded a strike-slip to compressional stress phase after the bedding plane was tilted (Figure 7). As these samples are in close proximity to CalS5, which records pretilting events, we can infer that the results obtained from CalS6b and CalS4b succeed the Hunter-Bowen event. The R values of CalS6b and CalS4b are consistent, with the differential stress magnitudes showing some discrepancies; however, considering the greater depth of CalS6b, a larger differential stress magnitude is expected (Table 1). Integrating these results shows that the Late Cretaceous event was a compressional stress regime in an E-W direction, with the far-field stress likely originating from a similar location to the Hunter-Bowen event (Figure 13f); the N-S striking subduction zone along eastern Australia. The two samples were obtained from calcite-filled natural fractures belonging to fracture sets 1 and 6 (Table 1). Fracture set 6 was developed by SE-NW oriented extensional stresses, with this particular natural fracture becoming calcite filled prior to or during the Late Permian Daralingie event, as this event is recorded in the calcite veins from CalS4. This calcite vein corresponds to fracture set 1, which was developed by the ASE (Table 1). This may explain why the results obtained from this sample (CalS6) are void of older events (Table 1).

5.6. Paleogene Event (33–23 Ma) (Event 6)

The final low-angle conjugate natural fracture set (FS4) has an E-W strike with inclined bedding (Figure 12), which infers a posttilting event (Event 6) oriented N-S (Figure 11a). This is likely to be the youngest fracture sets as it is present throughout the stratigraphic column with inclined bedding. The development of FS4 therefore postdates the development of FS3 (Figures 11 and 14). New fault development was not evident; likely forming folds rather than faults, or reactivating preexisting faults at a subseismic resolution. These results are consistent with previous research suggesting the development of the Birdsville Track Ridge and the Innamincka Dome during a Paleogene N-S event [*Lowe-Young et al*., 1997].

A posttilting strike-slip to compressional stress phase oriented N-S (Event 6) was recorded in samples CalS3b and CalS6 collected from the Kalladeina Formation (Figure 7). As both samples record this event after tilting, and considering the relative chronology of calcite and fracture data, this was found to be the youngest event. As with all samples, local stress perturbations may have influenced the stress regime results obtained from calcite data; however, the natural fracture data irrefutably suggests that this was a compressional stress regime event. CalS3b and CalS6 were obtained from matrix and a calcite-filled natural fracture belonging

to fracture set 1, respectively (Table 1). As highlighted earlier, fracture set 1 was developed by the ASE and interestingly only recorded the earliest two events (Table 1). The timing of this event is in line with rapid northward movement of Australia as it is rifted from Antarctica (Figure 13g). The *R* values from CalS3b and CalS6 are equal ($R = 0.4$), with the differential stress magnitude showing some dissimilarity (Table 1) albeit from a similar location (Figure 7). However, CalS3b is sampled from a slightly greater depth that relates to a higher differential stress magnitude. This being said, the error associated with differential stress magnitude calculations (~20%) falls within the difference in magnitude between CalS3b and CalS6 [*Lacombe*, 2001].

6. Conclusion

The integration of geophysical data (seismic and well data) together with calcite twin data has refined the tectonic history of the subsurface Cooper-Eromanga Basin by confirming the presence, orientation and regime of six events. Previous research has provided a partial picture of basin evolution, with authors presenting conflicting or incomplete results. This study uses a holistic approach to provide more certainty on the tectonic evolution and timing of natural fracture and fault development, such that

1. The Carboniferous Alice Springs event was a strike-slip stress regime oriented N-S that developed vertical NNE-SSW and SE-NW striking conjugate fractures and potentially influenced the development, and/or reactivation, of the regionally extensive SE-NW and NNE-SSW striking strike-slip faults;
2. The Mid-Permian event was a compressional stress regime oriented SE-NW that developed low-angle NE-SW striking conjugate fractures and developed, and/or reactivated, NE-SW striking faults;
3. The Late Permian Daralingie event was a strike-slip stress regime oriented NE-SW that reactivated SE-NW striking high-angle faults;
4. The Upper Triassic Hunter-Bowen event was a compressional stress regime oriented E-W that developed low-angle N-S striking conjugate fractures and developed and/or reactivated low-angle N-S striking faults;
5. The Upper Cretaceous event was a compressional stress regime oriented E-W that developed and/or reactivated low-angle N-S striking conjugate fractures and formed regional N-S elongate en echelon anticlinal traps;
6. The Paleogene event was a compressional stress regime oriented N-S that developed low-angle E-W striking conjugate fractures and created folds rather than faults.

Fault interpretation and natural fracture analysis infers that successive periods of postcompressional flexural relaxation, or sag, oriented in a NE-SW and SE-NW direction (parallel to major structures) developed and/or reactivated high-angle NE-SW and SE-NW striking conjugate fractures. Fault interpretation from six 3-D seismic surveys identified high-angle (50–70°) NE-SW striking faults with reverse sense of motion extensively throughout the basin, which developed during Adelaidean (650–575 Ma) SE-NW extension and reactivated by successive compressional and strike-slip events.

This approach has refined the stress history of the subsurface Cooper-Eromanga Basin by utilizing geophysical and core data to constrain the principal stresses of six events and discuss their far-field origin through time. This analysis will lead to future work that will perform the final stage of the calcite twin stress inversion technique, which is to constrain the magnitude of individual events. For this reason, the differential magnitude component presented in this work has not been thoroughly discussed. This study presents an approach that can be utilized in other subsurface and offshore provinces with limited, or no, accessible outcrop that has prevented paleostress inversion analyses.

Acknowledgments
The authors would like to acknowledge the financial contribution made by the GeoFrac Consortium, which includes the program manager, Dennis Cooke, and the sponsoring companies: Santos, Beach Energy, Chevron, Halliburton and BG Group (QGC). We thank DUG Insight and Midland Valley (MOVE) for their generous donation of academic licenses for software. Thank you also to Michael Edward Gray and Ulrike Schacht for their input, Richard Allmendinger for Stereonet 8.8.8, Damien Delvaux for "Wintensor," and Carlos H. Grohmann and Ginaldo A.C. Campanha for "OpenStereo 0.1.2". DUG Insight software (v.3.1, 2015) was used for seismic visualization, interpretation, and analysis. Thank you to Claudio Faccenna (Editor), the anonymous Associate Editors, the anonymous reviewer, Nicolas Beaudoin (reviewer), and Atsushi Yamaji (reviewer) for their constructive feedback that has improved the quality and scientific impact of this research. This forms TRaX record 366. Additional information is available by contacting the corresponding author "david.kulikowski@adelaide.edu.au."

References

Alexander, E. M., D. I. Gravestock, C. Cubitt, and A. Chaney (1998), Lithostratigraphy and environments of deposition, in *Petroleum Geology of South Australia*, *Cooper Basin*, vol. 4, edited by D. I. Gravestock, J. E. Hibburt, and J. F. Drexel, pp. 69–116, Primary Industries and Resources, Adelaide, S. A.

Amrouch, K. (2010), Apport de l'analyse microstructurale à la compréhension des mécanismes de plissement. Exemples de structures plissées aux USA (Wyoming) et en Iran (Zagros), these, Univ. Pierre et Marie Curie—Paris 6, 2010-03, 477 p.

Amrouch, K., O. Lacombe, N. Bellahsen, J. M. Daniel, and J. P. Callot (2010a), Stress and strain patterns, kinematics and deformation mechanisms in a basement-cored anticline: Sheep Mountain Anticline, Wyoming, *Tectonics*, *29*, TC1005, doi:10.1029/2009TC002525.

Amrouch, K., P. Robion, J. P. Callot, O. Lacombe, J. M. Daniel, N. Bellahsen, and J. L. Faure (2010b), Constraints on deformation mechanisms during folding provided by rock physical properties: A case study at Sheep Mountain anticline (Wyoming, USA), *Geophys. J. Int.*, *182*(3), 1105–1123.

Amrouch, K., N. Beaudoin, O. Lacombe, N. Bellahsen, and J. M. Daniel (2011), Paleostress magnitudes in folded sedimentary rocks, *Geophys. Res. Lett.*, *38*, L17301, doi:10.1029/2011GL048649.
Anderson, E. M. (1951), *The Dynamics of Faulting and Dyke Formation with Applications to Britain*, Oliver and Boyd, Edinburgh.
Angelier, J., and P. Mechler (1977), Sur une method graphique de recherche des contraintes principals egalement utilisable en tectonique et en seismologie: La method des diedres droits, *Bull. Soc. Geol.*, *19*(6), 1309–1318.
Apak, S. N., W. J. Stuart, N. M. Lemon, and G. Wood (1997), Structural evolution of the Permian-Triassic Cooper Basin, Australia: Relation to hydrocarbon trap styles, *AAPG Bull.*, *81*(4), 533–555.
Arboit, F., K. Amrouch, A. S. Collins, R. King, and C. Morley (2015), Determination of the tectonic evolution from fractures, faults, and calcite twins on the southwestern margin of the Indochina Block, *Tectonics*, *34*, 1576–1599, doi:10.1002/2015TC003876.
Arboit, F., K. Amrouch, C. Morley, A. S. Collins, and R. King (2017), Palaeostress magnitudes in the Khao Khwang fold-thrust belt, new insights into the tectonic evolution of the Indosinian orogeny in central Thailand, *Tectonophysics*, doi:10.1016/j.tecto.2017.01.008, in press.
Baudon, C., and J. Cartwright (2008), The kinematics of reactivation of normal faults using high resolution throw mapping, *J. Struct. Geol.*, *30*(8), 1072–1084.
Beaudoin, N., R. Leprêtre, N. Bellahsen, O. Lacombe, K. Amrouch, J. P. Callot, L. Emmanuel, and J. M. Daniel (2012), Structural and microstructural evolution of the Rattlesnake Mountain Anticline (Wyoming, USA): New insights into the Sevier and Laramide orogenic stress build-up in the Bighorn Basin, *Tectonophysics*, *576*, 20–45.
Beaudoin, N., D. Koehn, O. Lacombe, A. Lecouty, A. Billi, E. Aharonov, and C. Parlangeau (2016), Fingerprinting stress: Stylolite and calcite twinning paleopiezometry reveal the complexity of progressive stress patterns during folding—The case of the Monte Nero anticline in the Apennines, Italy, *Tectonics*, *35*, 1687–1712, doi:10.1002/2016TC004128.
Bellahsen, N., P. Fiore, and D. D. Pollard (2006), The role of fractures in the structural interpretation of Sheep Mountain Anticline, Wyoming, *J. Struct. Geol.*, *28*(5), 850–867.
Bergbauer, S., and D. D. Pollard (2004), A new conceptual fold-fracture model including prefolding joints, based on the Emigrant Gap anticline, Wyoming, *Geol. Soc. Am. Bull.*, *116*(3–4), 294–307.
Boger, S. D., and J. M. Miller (2004), Terminal suturing of Gondwana and the onset of the Ross–Delamerian Orogeny: The cause and effect of an Early Cambrian reconfiguration of plate motions, *Earth Planet. Sci. Lett.*, *219*(1), 35–48.
Boreham, C. J., and A. J. Hill (1998), Source rock distribution and geochemistry, in *Petroleum Geology of South Australia*, *Cooper Basin*, vol. 4, edited by D. I. Gravestock, J. E. Hibburt, and J. F. Drexel, pp. 129–142, Primary Industries and Resources, Adelaide, S. A.
Bradshaw, M. T. (1993), Australian petroleum systems, *PESA J.*, *21*, 43–53.
Burkhard, M. (1993), Calcite twins, their geometry, appearance and significance as stress-strain markers and indicators of tectonic regime: A review, *J. Struct. Geol.*, *15*(3), 351–368.
Childs, C., A. Nicol, J. J. Walsh, and J. Watterson (1996), Growth of vertically segmented normal faults, *J. Struct. Geol.*, *18*(12), 1389–1397.
Collins, A. S., and S. A. Pisarevsky (2005), Amalgamating eastern Gondwana: The evolution of the Circum-Indian Orogens, *Earth Sci. Rev.*, *71*(3), 229–270.
Constantin, J., P. Laurent, P. Vergély, and J. Cabrera (2007), Paleo-deviatoric stress magnitudes from calcite twins and related structural permeability evolution in minor faults: Example from the toarcian shale of the French Causses Basin, Aveyron, France, *Tectonophysics*, *429*(1), 79–97.
Craddock, J. P., and B. A. Van Der Pluijm (1999), Sevier-Laramide deformation of the continental interior from calcite twinning analysis, west-central North America, *Tectonophysics*, *305*, 275–286.
Dresen, G. (1991), Stress distribution and the orientation of Riedel shears, *Tectonophysics*, *188*(3), 239–247.
Etchecopar, A. (1984), *Etude des e tats de Contraintes en Tectonique Cassante et Simulation de Formation Plastique (Approche Mathe Matique), the se Doctorates-Sciences*, 270 pp., Univ. Sci. et Tech. Du Langue-doc, Montpellier, Fr.
Etchecopar, A., G. Vasseur, and M. Daignieres (1981), An inverse problem in microtectonics for the determination of stress tensors from fault striation analysis, *J. Struct. Geol.*, *3*(1), 51–65.
Faulkner, D. R., C. A. L. Jackson, R. J. Lunn, R. W. Schlische, Z. K. Shipton, C. A. J. Wibberley, and M. O. Withjack (2010), A review of recent developments concerning the structure, mechanics and fluid flow properties of fault zones, *J. Struct. Geol.*, *32*(11), 1557–1575.
Ferrill, D. A. (1998), Critical re-evaluation of differential stress estimates from calcite twins in coarse-grained limestone, *Tectonophysics*, *285*(1), 77–86.
Friedman, M., and D. W. Stearns (1971), Relations between stresses inferred from calcite twin lamellae and macrofractures, Teton Anticline, Montana, *Geol. Soc. Am. Bull.*, *82*(11), 3151–3162.
Friedman, M., L. W. Teufel, and J. D. Morse (1976), Strain and stress analyses from calcite twin lamellae in experimental buckles and faulted drape-folds, *Philos. Trans. R. Soc. London, Ser. A*, *283*(1312), 87–107.
Gephart, J. W. (1990), Stress and the direction of slip on fault planes, *Tectonics*, *9*(4), 845–858, doi:10.1029/TC009i004p00845.
Glikson, A. Y., I. T. Uysal, J. D. Fitz Gerald, and E. Saygin (2013), Geophysical anomalies and quartz microstructures, Eastern Warburton Basin, North-east South Australia: Tectonic or impact shock metamorphic origin?, *Tectonophysics*, *589*, 57–76.
González-Casado, J. M., and C. García-Cuevas (2002), Strain analysis from calcite e-twins in the Cameros basin, NW Iberian Chain, Spain, *J. Struct. Geol.*, *24*(11), 1777–1788.
Grant-Woolley, L., A. Kong, B. Schoemaker, H. Nasreddin, and E. T. Montague (2014), Identification of strike-slip faults provides insights into the further development of mature Cooper Basin fields, in *SPE Asia Pacific Oil and Gas Conference and Exhibition*, pp. 1–12, Society of Petroleum Engineers, SPE 171492-MS, Adelaide, Australia.
Gravestock, D. I., and B. Jensen-Schmidt (1998), Structural setting, in *Petroleum Geology of South Australia*, *Cooper Basin*, vol. 4, edited by D. I. Gravestock, J. E. Hibburt, and J. F. Drexel, pp. 47–67, Primary Industries and Resources, Adelaide, S. A.
Gray, D. R., and D. A. Foster (2004), Tectonic evolution of the Lachlan Orogen, southeast Australia: Historical review, data synthesis and modern perspectives, *Aust. J. Earth Sci.*, *51*(6), 773–817.
Green, P. M., T. J. Brain, and B. H. John (1989), Possible stratigraphic controls on hydrocarbon distribution within the Jurassic-Early Cretaceous rocks, Eromanga Basin, southern Queensland, in *The Cooper and Eromanga Basins, Australia*, edited by B. J. O'Neil, pp. 251–264, Proceedings of Petroleum Exloration Society of Australia, Society of Petroleum Engineers, Australian Society of Exploration Geophysicists (SA Branches), Adelaide S. A.
Grohmann, C. H., and G. A. C. Campanha (2010), OpenStereo: Open source, cross-platform software for structural geology analysis, paper presented at 2010 Fall Meeting, AGU, San Francisco, Calif.
Groshong, R. H. (1972), Strain calculated from twinning in calcite, *Geol. Soc. Am. Bull.*, *83*(7), 2025–2038.
Groshong, R. H. (1974), Experimental test of least-squares strain gage calculation using twinned calcite, *Geol. Soc. Am. Bull.*, *85*(12), 1855–1864.

Haines, P. W., M. Hand, and M. Sandiford (2001), Palaeozoic synorogenic sedimentation in central and northern Australia: A review of distribution and timing with implications for the evolution of intracontinental orogens, *Aust. J. Earth Sci.*, *48*(6), 911–928.
Hancock, P. L. (1985), Brittle microtectonics: Principles and practice, *J. Struct. Geol.*, *7*, 437–457.
Healy, D., R. R. Jones, and R. E. Holdsworth (2006), Three-dimensional brittle shear fracturing by tensile crack interaction, *Nature*, *439*, 64–67.
Hillis, R. R., J. G. G. Morton, D. S. Warner, and R. K. Penney (2001), Deep basin gas: A new exploration paradigm in the Nappamerri Trough, Cooper Basin, South Australia, *Aust. Pet. Prod. Explor. Assoc. J.*, *41*, 158–200.
Hillis, R. R., M. Sandiford, S. D. Reynolds, and M. C. Quigley (2008), Present-day stresses, seismicity and Neogene-to-Recent tectonics of Australia's 'passive' margins: Intraplate deformation controlled by plate boundary forces, *Geol. Soc. London, Spec. Publ.*, *306*(1), 71–90.
Hoffman, K. L. (1989), The influence of pre-Jurassic tectonic regimes on the structural development of the southern Eromanga Basin, Queensland, in *The Cooper and Eromanga Basins, Australia*, edited by B. J. O'Neil, pp. 315–328, Proceedings of Petroleum Exploration Society of Australia, Society of Petroleum Engineers, Australian Society of Exploration Geophysicists (SA Branches), Adelaide S. A.
Jamison, W. R., and J. H. Spang (1976), Use of calcite twin lamellae to infer differential stress, *Geol. Soc. Am. Bull.*, *87*(6), 868–872.
Kantsler, A. J., T. J. C. Prudence, A. C. Cook, and M. Zwigulis (1984), Hydrocarbon habitat of the Cooper/Eromanga Basin, Australia, *Aust. Pet. Explor. Assoc. J.*, *23*, 75–92.
Khair, H. A., D. Cooke, and M. Hand (2013), The effect of present day in situ stresses and paleo-stresses on locating sweet spots in unconventional reservoirs, a case study from Moomba-Big Lake fields, Cooper Basin, South Australia, *J. Pet. Explor. Prod. Technol.*, *3*(4), 207–221.
Khair, H. A., D. Cooke, and M. Hand (2015), Paleo stress contribution to fault and natural fracture distribution in the Cooper Basin, *J. Struct. Geol.*, *79*, 31–41.
Kuang, K. S. (1985), History and style of Cooper–Eromanga Basin structures, *Explor. Geophys.*, *16*(2/3), 245–248.
Kulikowski, D., K. Amrouch, and D. Cooke (2016a), Geomechanical modelling of fault reactivation in the Cooper Basin, Australia, *Aust. J. Earth Sci.*, *63*(3), 295–314.
Kulikowski, D., C. Hochwald, D. Cooke, and K. Amrouch (2016b), A statistical approach to assessing depth conversion uncertainty on a regional dataset: Cooper-Eromanga Basin, Australia, ASEG-PESA-AIG 2016 Conference, Adelaide, Extended Abstract 200, 484–490.
Kulikowski, D., K. Amrouch, D. Cooke, and M. E. Gray (2017), Basement structural architecture and hydrocarbon conduit potential of polygonal faults in the Cooper-Eromanga Basin, Australia, *Geophys. Prospect.*, in press.
Lacombe, O. (2001), Paleostress magnitudes associated with development of mountain belts: Insights from tectonic analyses of calcite twins in the Taiwan Foothills, *Tectonics*, *20*(6), 834–849, doi:10.1029/2001TC900019.
Lacombe, O. (2007), Comparison of paleostress magnitudes from calcite twins with contemporary stress magnitudes and frictional sliding criteria in the continental crust: Mechanical implications, *J. Struct. Geol.*, *29*(1), 86–99.
Lacombe, O. (2010), Calcite twins, a tool for tectonic studies in thrust belts and stable orogenic forelands, *Oil Gas Sci. Technol.*–Revue d'IFP Energies Nouvelles, *65*(6), 809–838.
Lacombe, O. (2012), Do fault slip data inversions actually yield "paleostresses" that can be compared with contemporary stresses? A critical discussion, *C. R. Geosci.*, *344*(3), 159–173.
Lacombe, O., and P. Laurent (1996), Determination of deviatoric stress tensors based on inversion of calcite twin data from experimentally deformed monophase samples: Preliminary results, *Tectonophysics*, *255*(3), 189–202.
Lacombe, O., J. Angelier, P. Laurent, F. Bergerat, and C. Tourneret (1990), Joint analyses of calcite twins and fault slips as a key for deciphering polyphase tectonics: Burgundy as a case study, *Tectonophysics*, *182*(3), 279–300.
Lacombe, O., J. Angelier, and P. Laurent (1992), Determining paleostress orientations from faults and calcite twins: A case study near the Sainte-Victoire Range (southern France), *Tectonophysics*, *201*(1), 141–156.
Lacombe, O., P. Laurent, and J. Angelier (1994), Calcite twins as a key to paleostresses in sedimentary basins: Preliminary results from drill cores of the Paris basin, in *Peri-Tethyan Platforms*, edited by F. Roure, pp. 197–210, Revue Institut Français du Pétrole, Technip, Paris.
Lacombe, O., K. Amrouch, F. Mouthereau, and L. Dissez (2007), Calcite twinning constraints on late Neogene stress patterns and deformation mechanisms in the active Zagros collision belt, *Geology*, *35*(3), 263–266.
Lacombe, O., J. Malandain, N. Vilasi, K. Amrouch, and F. Roure (2009), From paleostresses to paleoburial in fold–thrust belts: Preliminary results from calcite twin analysis in the Outer Albanides, *Tectonophysics*, *475*(1), 128–141.
Laurent, P., H. Kern, and O. Lacombe (2000), Determination of deviatoric stress tensors based on inversion of calcite twin data from experimentally deformed monophase samples. Part II. Axial and triaxial stress experiments, *Tectonophysics*, *327*(1), 131–148.
Li, Z. X., et al. (2008), Assembly, configuration, and break-up history of Rodinia: A synthesis, *Precambrian Res.*, *160*(1), 179–210.
Lowe-Young, B. S., S. I. Mackie, and R. S. Heath (1997), The Cooper-Eromanga Petroleum System, Australia: Investigation of Essential Elements and Processes, in *Proceedings of the Petroleum Systems of SE Asia and Australasia Conference*, pp. 199–211, Indonesian Petroleum Association, Jakarta.
Mavromatidis, A. (2006), Burial/exhumation histories for the Cooper–Eromanga Basins and implications for hydrocarbon exploration, Eastern Australia, *Basin Res.*, *18*(3), 351–373.
Metcalfe, I. (2013), Gondwana dispersion and Asian accretion: Tectonic and palaeogeographic evolution of eastern Tethys, *J. Asian Earth Sci.*, *66*, 1–33.
Michael, A. J. (1984), Determination of stress from slip data: Faults and folds, *J. Geophys. Res.*, *89*(B13), 11,517–11,526, doi:10.1029/JB089iB13p11517.
Müller, R. D., S. Dyksterhuis, and P. Rey (2012), Australian paleo-stress fields and tectonic reactivation over the past 100 Ma, *Aust. J. Earth Sci.*, *59*(1), 13–28.
Müller, R. D., N. Flament, K. J. Matthews, S. E. Williams, and M. Gurnis (2016), Formation of Australian continental margin highlands driven by plate–mantle interaction, *Earth Planet. Sci. Lett.*, *441*, 60–70.
Myers, J. S., R. D. Shaw, and I. M. Tyler (1996), Tectonic evolution of Proterozoic Australia, *Tectonics*, *15*(6), 1431–1446, doi:10.1029/96TC02356.
Nemcok, M., and R. J. Lisle (1995), A stress inversion procedure for polyphase fault/slip data sets, *J. Struct. Geol.*, *17*(10), 1445–1453.
Pokalai, K., D. Kulikowski, R. L. Johnson Jr., M. Haghighi, and D. Cooke (2016), Development of a new approach for hydraulic fracturing in tight sand with pre-existing natural fractures, *Aust. Pet. Prod. Explor. Assoc. J.*, *56*, 225–238.
Pollard, D. D., and A. Aydin (1988), Progress in understanding jointing over the past century, *Geol. Soc. Am. Bull.*, *100*(8), 1181–1204.
Ramsay, J. G. (1962), The geometry of conjugate fold systems, *Geol. Mag.*, *99*(06), 516–526.
Rees, P. M., A. M. Ziegler, M. T. Gibbs, J. E. Kutzbach, P. J. Behling, and D. B. Rowley (2002), Permian phytogeographic patterns and climate data/model comparisons, *J. Geol.*, *110*(1), 1–31.
Reeves, C., and M. De Wit (2000), Making ends meet in Gondwana: Retracing the transforms of the Indian Ocean and reconnecting continental shear zones, *Terra Nova*, *12*(6), 272–280.

Reynolds, S. D., D. D. Coblentz, and R. R. Hillis (2002), Tectonic forces controlling the regional intraplate stress field in continental Australia: Results from new finite element modelling, *J. Geophys. Res.*, *107*(B7), 2131, doi:10.1029/2001JB000408.
Reynolds, S. D., S. D. Mildren, R. R. Hillis, J. J. Meyer, and T. Flottmann (2005), Maximum horizontal stress orientations in the Cooper Basin, Australia: Implications for plate-scale tectonics and local stress sources, *Geophys. J. Int.*, *160*(1), 331–343.
Reynolds, S. D., S. D. Mildren, R. R. Hillis, and J. J. Meyer (2006), Constraining stress magnitudes using petroleum exploration data in the Cooper–Eromanga Basins, Australia, *Tectonophysics*, *415*(1), 123–140.
Rezaee, M. R., and X. Sun (2007), Fracture-filling cements in the Palaeozoic Warburton Basin, South Australia, *J. Pet. Geol.*, *30*(1), 79–90.
Robson, A. G., R. C. King, and S. P. Holford (2016a), 3D seismic analysis of gravity-driven and basement influenced normal fault growth in the deepwater Otway Basin, Australia, *J. Struct. Geol.*, *89*, 74–87.
Robson, A. G., R. C. King, and S. P. Holford (2016b), Structural evolution of a gravitationally detached normal fault array: Analysis of 3D seismic data from the Ceduna Sub-Basin, Great Australian Bight, *Basin Res.*, 1–20, doi:10.1111/bre.12191.
Rocher, M., O. Lacombe, J. Angelier, and H. W. Chen (1996), Mechanical twin sets in calcite as markers of recent collisional events in a fold-and-thrust belt: Evidence from the reefal limestones of southwestern Taiwan, *Tectonics*, *15*(5), 984–996, doi:10.1029/96TC00625.
Rocher, M., O. Lacombe, J. Angelier, B. Deffontaines, and F. Verdier (2000), Cenozoic folding and faulting in the south Aquitaine Basin (France): Insights from combined structural and paleostress analyses, *J. Struct. Geol.*, *22*(5), 627–645.
Rocher, M., M. Cushing, F. Lemeille, Y. Lozac'h, and J. Angelier (2004), Intraplate paleostresses reconstructed with calcite twinning and faulting: Improved method and application to the eastern Paris Basin (Lorraine, France), *Tectonophysics*, *387*(1), 1–21.
Rowe, K. J., and E. H. Rutter (1990), Palaeostress estimation using calcite twinning: Experimental calibration and application to nature, *J. Struct. Geol.*, *12*(1), 1–17.
Sandiford, M., M. Wallace, and D. Coblentz (2004), Origin of the in situ stress field in south-eastern Australia, *Basin Res.*, *16*(3), 325–338.
Seeburger, D. A., and M. D. Zoback (1982), The distribution of natural fractures and joints at depth in crystalline rock, *J. Geophys. Res.*, *87*(B7), 5517–5534, doi:10.1029/JB087iB07p05517.
Sibson, R. H. (1985), A note on fault reactivation, *J. Struct. Geol.*, *7*(6), 751–754.
Sibson, R. H. (2003), Brittle-failure controls on maximum sustainable overpressure in different tectonic regimes, *AAPG Bull.*, *87*(6), 901–908.
Silliphant, L. J., T. Engelder, and M. R. Gross (2002), The state of stress in the limb of the Split Mountain anticline, Utah: Constraints placed by transected joints, *J. Struct. Geol.*, *24*(1), 155–172.
Sperner, B., and L. Ratschbacher (1994), A turbo program package for graphical presentation and stress analysis of calcite deformation, *Z. Dtsch. Geol. Ges.*, *145*, 414–423.
Sun, X. (1997), Structural style of the Warburton Basin and control in the Cooper and Eromanga Basins, South Australia, *Explor. Geophys.*, *28*(3), 333–339.
Tavani, S., F. Storti, O. Lacombe, A. Corradetti, J. A. Muñoz, and S. Mazzoli (2015), A review of deformation pattern templates in foreland basin systems and fold-and-thrust belts: Implications for the state of stress in the frontal regions of thrust wedges, *Earth Sci. Rev.*, *141*, 82–104.
Tourneret, C., and P. Laurent (1990), Paleo-stress orientations from calcite twins in the North Pyrenean foreland, determined by the Etchecopar inverse method, *Tectonophysics*, *180*(2), 287–302.
Tripathy, V., and D. Saha (2015), Inversion of calcite twin data, paleostress reconstruction and multiphase weak deformation in cratonic interior—Evidence from the Proterozoic Cuddapah basin, India, *J. Struct. Geol.*, *77*, 62–81.
Turner, F. J. (1953), Nature and dynamic interpretation of deformation lamellae in calcite of three marbles, *Am. J. Sci.*, *251*(4), 276–298.
Turner, F. J., D. T. Griggs, and H. Heard (1954), Experimental deformation of calcite crystals, *Geol. Soc. Am. Bull.*, *65*(9), 883–934.
Van der Meer, D. G., T. H. Torsvik, W. Spakman, D. J. J. Van Hinsbergen, and M. L. Amaru (2012), Intra-Panthalassa Ocean subduction zones revealed by fossil arcs and mantle structure, *Nat. Geosci.*, *5*(3), 215–219.
Weathers, M. S., J. M. Bird, R. F. Cooper, and D. L. Kohlstedt (1979), Differential stress determined from deformation-induced microstructures of the Moine Thrust Zone, *J. Geophys. Res.*, *84*(B13), 7495–7509, doi:10.1029/JB084iB13p07495.
Williams, G. D., C. M. Powell, and M. A. Cooper (1989), Geometry and kinematics of inversion tectonics, *Geol. Soc. London, Spec. Publ.*, *44*(1), 3–15.
Zoback, M. D., C. A. Barton, M. Brudy, D. A. Castillo, T. Finkbeiner, B. R. Grollimund, and D. J. Wiprut (2003), Determination of stress orientation and magnitude in deep wells, *Int. J. Rock Mech. Min. Sci.*, *40*(7), 1049–1076.
Zoback, M. L., et al. (1989), Global patterns of tectonic stress, *Nature*, *341*(6240), 291–298.

5.3. MANUSCRIPT 3: Basement structural architecture

Basement structural architecture and hydrocarbon conduit potential of polygonal faults in the Cooper-Eromanga Basin, Australia

This research forms a robust and much needed regional structural architecture study of Australia's largest onshore hydrocarbon province, the Cooper-Eromanga Basin. Previous structural work has utilised old and sparse two-dimensional (2D) seismic lines that remained in the time-domain. Our study structurally interprets all available 2D seismic lines and 12 three-dimensional (3D) seismic surveys within the study area to provide a modern, detailed and comprehensive basement fault map, which was not previously available in literature. In doing so, we identified a regional system of polygonal faults that has the potential to facilitate tertiary migration of hydrocarbons from known oil-rich reservoirs into shallow sediments. To constrain the polygonal fault geometry optimally oriented to reactivate and act as a hydrocarbon conduit, we calculated the Dilation Tendency and Leakage Factor of polygonal faults by developing a geomechanical model of the in situ stress. The distribution of permeable polygonal faults is presented for each of the 12 3D seismic surveys. This research has implications for future hydrocarbon exploration of shallow reservoirs and presents a detailed basement fault map of the basin, together with the complete and detailed structural interpretation of 12 3D seismic surveys.

CITATION:

Kulikowski, D., Amrouch, K., Cooke, D., & Gray, M.E. (2017). Basement Structural Architecture and Hydrocarbon Conduit Potential of Polygonal Faults in the Cooper-Eromanga Basin, Australia. Geophysical Prospecting, 65, in press, doi:10.1111/1365-2478.12531.

Statement of Authorship

Title of Paper:	Basement Structural Architecture and Hydrocarbon Conduit Potential of Polygonal Faults in the Cooper-Eromanga Basin, Australia
Publication Status:	**Manuscript Published**
Publication Details:	Kulikowski, D., Amrouch, K., Cooke, D., & Gray, M.E. (2017). Basement Structural Architecture and Hydrocarbon Conduit Potential of Polygonal Faults in the Cooper-Eromanga Basin, Australia. *Geophysical Prospecting*, in press, doi:10.1111/1365-2478.12531.

Principal Author

Principal Author (Candidate):	David Kulikowski		
Contribution to the Paper:	Data collection, depth-conversion, interpretation, measurement, analysis, and writing.		
Overall percentage (%):	75%		
Certification:	This paper reports on original research I conducted during the period of my Higher Degree by Research candidature and is not subject to any obligations or contractual agreements with a third party that would constrain its inclusion in this thesis. I am the primary author of this paper.		
Signature:		Date:	29 March 2017

Co-Author Contribution

By signing the Statement of Authorship, each author certifies that:

i. the candidate's stated contribution to the publication is accurate (as detailed above);

ii. permission is granted for the candidate to include the publication in the thesis; and

iii. the sum of all co-author contributions is equal to 100% less the candidate's stated contribution.

Name of Co-Author:	Khalid Amrouch (10%)		
Contribution to the Paper:	Provided feedback on analysis and a complete review of paper.		
Signature:		Date:	29 March 2017

Name of Co-Author:	Dennis Cooke (10%)		
Contribution to the Paper:	Provided feedback on analysis and a complete review of paper.		
Signature:		Date:	28 Mar 2017

Name of Co-Author:	Michael E. Gray (5%)		
Contribution to the Paper:	Some seismic interpretation, feedback on analysis and a complete review of paper.		
Signature:		Date:	29 March 2017

Geophysical Prospecting

EAGE EUROPEAN ASSOCIATION OF GEOSCIENTISTS & ENGINEERS

Geophysical Prospecting, 2017 doi: 10.1111/1365-2478.12531

Basement structural architecture and hydrocarbon conduit potential of polygonal faults in the Cooper-Eromanga Basin, Australia

David Kulikowski*, Khalid Amrouch, Dennis Cooke and Michael Edward Gray

Australian School of Petroleum, University of Adelaide, North Terrace, Adelaide 5005, Australia

Received August 2016, revision accepted March 2017

ABSTRACT

A thorough and complete understanding of the structural geology and evolution of the Cooper-Eromanga Basin has been hampered by low-resolution seismic data that becomes particularly difficult to interpret below the thick Permian coal measures. As a result, researchers are tentative to interpret the basement fault architecture within the basin, which is largely undefined. To provide a better understanding of the basement fault geometry, all available two-dimensional seismic lines together with 12 three-dimensional seismic surveys were structurally interpreted with assistance from seismic attribute analysis. The Upper Cretaceous Cadna-owie Formation and top Permian reflectors were analysed using a common seismic attribute technique (incoherency) that was used to infer the presence of faults that may have otherwise been overlooked. Detailed basement fault maps for each seismic survey were constructed and used in conjunction with two-dimensional seismic data interpretation to produce a regional basement fault map. Large north-northeast–south-southwest-striking sinistral strike–slip faults were identified within the Patchawarra Trough appearing to splay from the main northeast–southwest-striking ridge. These sinistral north-northeast–south-southwest-striking faults, together with field-scale southeast–northwest-striking dextral strike–slip faults, are optimally oriented to have potentially developed as a conjugated fault set under a south-southeast–north-northwest-oriented strike–slip stress regime. Geomechanical modelling for a regionally extensive system of Cretaceous polygonal faults was performed to calculate the Leakage Factor and Dilation Tendency of individual faults. Faults that extend into Lower Cretaceous oil-rich reservoirs with strikes of between 060°N and 140°N and a high to near-vertical dip angle were identified to most likely be acting as conduits for the tertiary migration of hydrocarbons from known Lower Cretaceous hydrocarbon reservoirs into shallow Cretaceous sediments. This research provides valuable information on the regional basement fault architecture and a more detailed exploration target for the Cooper-Eromanga Basin, which were previously not available in literature.

Key words: Cooper-Eromanga Basin, Seismic interpretation, Coherency, Fault.

1 INTRODUCTION

The structurally complex Cooper-Eromanga Basin is Australia's largest onshore hydrocarbon province with the first natural gas discovered in 1963 (Radke 2009; Mackie 2015). The region has numerous low-resolution three-dimensional (3D) seismic surveys that rapidly decrease in resolution below thick Permian coal measures. Due to the poor seismic quality, basement faults are difficult to interpret, and as a result, a thorough understanding of the structural architecture and the

*E-mail: david.kulikowski@adelaide.edu.au

© 2017 European Association of Geoscientists & Engineers

evolution of the basin is difficult to constrain. Early structural interpretation was performed on old sparse two-dimensional (2D) seismic lines, with only a few 3D seismic surveys used for research (Abul Khair, Cooke and Hand 2013, 2015; Grant-Woolley *et al.* 2014; Kulikowski, Amrouch and Cooke 2016b; Kulikowski and Amrouch 2017). The basin is known to have two major northeast–southwest (NE-SW)-striking ridges (Gidgealpa–Merrimelia–Innamincka (GMI) and Murteree–Nappacoongee (MN) ridges) that isolate the NE-SW elongate Patchawarra, Nappamerri, and Tenappera troughs; however, details beyond this are greatly unknown. The lack of basement fault information is one major reason for the poorly defined structural history of the basin.

Advancements in seismic data processing software and attribute analyses offer the opportunity to revisit 3D seismic data and extract information previously unavailable. Improvements in seismic time-to-depth conversion methods have also enabled more accurate interpretation of faults and structural closures. Seismic attribute analyses have developed to become a formidable tool in effective hydrocarbon exploration by highlighting subtle changes in seismic data that are not visible from the standard vertical section. Incoherency (also referred to as coherency and similarity) has become the most widely used seismic attribute due to its ability to visually enhance the discrepancies of adjacent seismic traces along a horizon, or time-slice, to infer the presence of faults (Neves, Zahrani and Bremkamp 2004; Mai, Marfurt and Chávez-Pérez 2009; Backé *et al.* 2011; Basir, Javaherian and Yaraki 2013; Kulikowski *et al.* 2016b). Following this rapid improvement in seismic imaging, this research revisits low-resolution seismic data to develop a modern structural model of the Cooper-Eromanga Basin consisting of basement faults that were previously difficult to identify and interpret.

To better understand the basement fault architecture on both a regional and seismic survey scale, we utilise a large regional dataset of all publicly available 2D seismic lines together with 12 3D seismic surveys located within the South Australian portion of the basin. The 2D seismic data enabled accurate interpretation of large basement faults between 3D seismic surveys. Interpretation, time-to-depth conversion, and incoherency analysis of the Upper Cretaceous, Cadna-owie Formation, and top Permian reflectors was performed in each 3D seismic volume. These horizon maps were fundamental to accurately interpret faults, particularly within the low-resolution basement, and to also constrain the distribution of a regionally extensive system of Cretaceous polygonal faults when incoherency analysis was applied. The potential for these Cretaceous polygonal faults to be acting as conduits for hydrocarbon migration into shallow Cretaceous reservoirs was first suggested by Watterson *et al.* (2000). Recent work (Kulikowski *et al.* 2016b) has investigated the reactivation potential of basement faults and the pore pressure increase required to induce movement; however, their results were calculated at much greater depths and considerable higher pore pressures than the conditions present in Cretaceous sediments. Therefore, we investigate the distribution of polygonal faults that extend into oil-rich Lower Cretaceous sediments (Heath, McIntyre and Gibbins 1989) and perform geomechanical modelling to calculate the optimum fault geometry for these shallow faults to dilate and leak hydrocarbon under present-day stress.

A regional basement fault map of the South Australian portion of the Cooper-Eromanga Basin is interpreted in this study from 2D and 3D seismic data. Seismic data interpretation identified a number of strike–slip faults with associated positive flower structures, constrained the optimum polygonal fault geometry with the highest potential to migrate hydrocarbons from oil-rich Lower Cretaceous sediments into shallow reservoirs (Heath *et al.* 1989), and identified the geometry of polygonal and basement faults in 12 3D seismic surveys. The results presented here will encourage the continued research into better understanding the structural and stress history of the structurally complex Cooper-Eromanga Basin and provide insights into the application of attribute analysis and geomechanical modelling of fault reactivation in other basins around the world.

2 GEOLOGICAL SETTING

The structurally complex intra-cratonic Cooper Basin extends across 130,000 km^2 of South Australia and Queensland (Fig. 1) and is unconformably isolated from the overlying Jurassic to Middle Cretaceous Eromanga Basin and the underlying Cambrian to Middle Silurian Warburton Basin (Kantsler *et al.* 1984; Kuang 1985; Bradshaw 1993; Apak *et al.* 1997; Gravestock and Jensen-Schmidt 1998; Mavromatidis 2006) (Fig. 2). These regional unconformities mark successive periods of exhumation and reactivation along pre-existing basement-involved faults (Apak *et al.* 1997; Mavromatidis 2006). The complex structural architecture of the basin is dominated by the northeast–southwest (NE-SW)-striking Gidgealpa–Merrimelia–Innamincka (GMI) and Murteree–Nappacoongee (MN) ridges that form prolific hydrocarbon fields within the South Australian portion of the basin and isolate the NE-SW elongate Patchawarra, Nappamerri, and Tenappera troughs (Kuang 1985; Apak

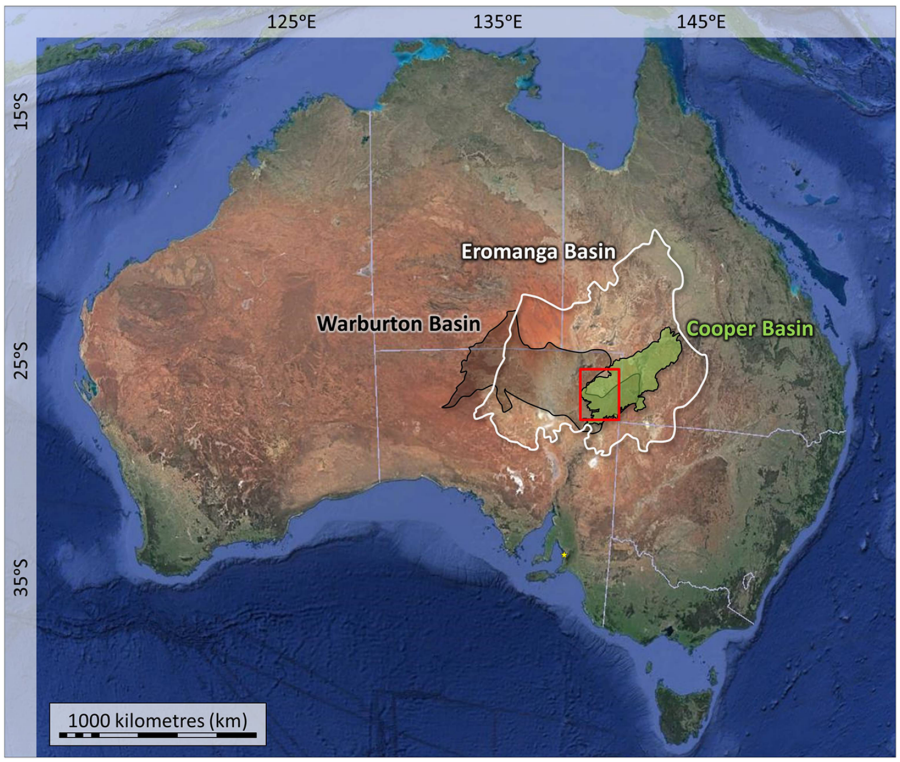


Figure 1 Location map of the Warburton, Cooper, and Eromanga basins with the study area shown in red (modified after Kulikowski *et al.* 2016b).

et al. 1997). Much of the original structural research explored the South Australian portion of the basin using sparsely spaced two-dimensional (2D) seismic data, with only very recent works utilising relatively new three-dimensional (3D) seismic surveys (Abul Khair *et al.* 2013, 2015; Grant-Woolley *et al.* 2014; Kulikowski *et al.* 2016b). However, there remains some uncertainty as to the absolute orientation and stress regime of structural events, which can be attributed to a lack of high-resolution 3D seismic volumes. As newly acquired 3D seismic data become available, and the seismic resolution and processing software continue to improve, it is likely that the structural evolution of the basin will become more tightly constrained through detailed fault growth analysis.

The accepted present-day basin evolution model suggests that initial accommodation space and NE-SW and southeast–northwest (SE-NW) lineaments were generated during Adelaidean (650 Ma) rifting along the NE-SW-striking Tasman Line in eastern Australia (Apak *et al.* 1997; Haines, Hand and Sandiford 2001; Müller, Dyksterhuis and Rey 2012). Subsequent structuring took place during the five major crustal shortening events; (1) north–south (N-S) (or SE-NW) Carboniferous Alice Springs Orogeny; (2) SE-NW (or east–west [E-W]) Sakmarian uplift event; (3) NE-SW (or E-W) Late Permian Daralingie unconformity event; (4) E-W Triassic Hunter-Bowen Orogeny; and (5) E-W Late Cretaceous crustal shortening (e.g., Gregory, Senior and Gallaway 1967; Senior *et al.* 1968; Kuang 1985; Apak *et al.* 1997; Abul Khair *et al.* 2013). These events are suggested to have formed compressive and strike–slip features and reactivated basement faults throughout the basin; a marked contrast to the early works suggesting concepts of basinwide continued extensional stress (e.g., Kuang 1985; Bradshaw 1993; Apak *et al.* 1997; Sun 1997; Gravestock and Jensen-Schmidt 1998; Grant-Woolley *et al.* 2014).

The regional unconformity isolating the Warburton and Cooper Basins was generated through the exhumation of sediments during the N-S (or SE-NW) Carboniferous Alice Springs Orogeny (Apak *et al.* 1997; Rezaee and Sun 2007; Glikson *et al.* 2013). This event is thought to have also exhumed the Carboniferous Big Lake Granite Suit and also applied a dextral rotation to faults striking SE-NW, and a sinistral rotation to faults striking NE-SW (Apak *et al.* 1997; Rezaee and Sun 2007; Glikson *et al.* 2013; Kulikowski, Cooke and Amrouch 2016a). Glacial sediments of the Merrimelia Formation were deposited onto this regional unconformity, with fluvially deposited Tirrawarra Formation

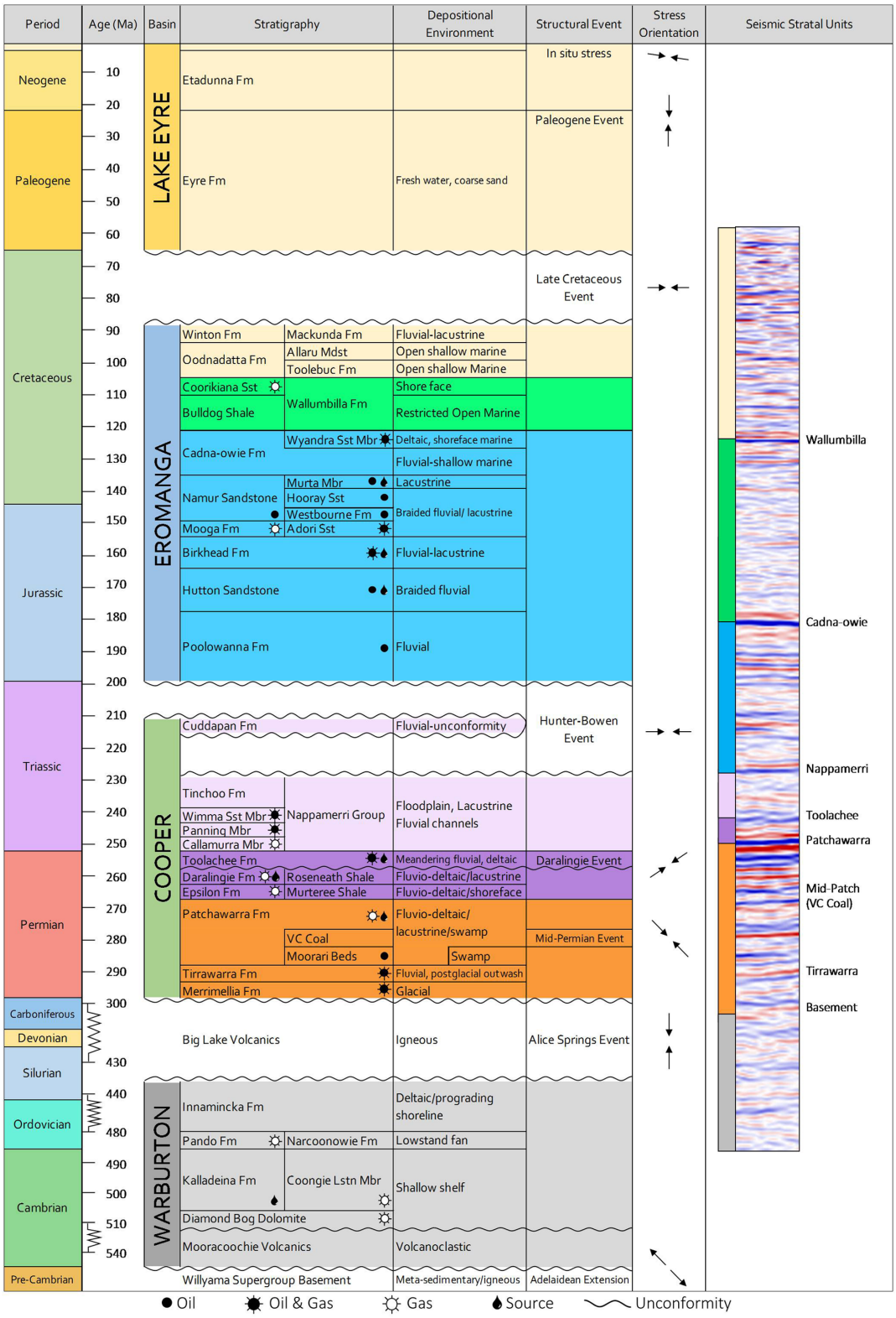


Figure 2 Stratigraphic column of the Warburton, Cooper, Eromanga, and Lake Eyre basins with the corresponding seismic reflection profile (Kulikowski *et al*. 2016b).

sediments soon following (Kantsler *et al*. 1984; Apak *et al*. 1997). Onlapping of the Late Carboniferous to Early Permian Merrimelia and Tirrawarra formations onto paleo-structural highs infers structural control during deposition and marks the initial period of flexural relaxation that generated accommodation space for the deposition of Cooper Basin sediments (Apak *et al*. 1997; Kulikowski *et al*. 2015). A transition into fluvial, peat swamp, and flood plain conditions deposited cycles of sand, shale, and coal to form the gas-rich Patchawarra Formation (Alexander *et al*. 1998; Boreham and Hill 1998). Evidence from seismic data suggests that two periods of uplift occurred within the middle Patchawarra Formation that resulted in onlapping of sediments (Kantsler *et al*. 1984; Apak *et al*. 1997; Kulikowski *et al*. 2015). Compression eased during the deposition of the upper Patchawarra Formation, and an east-to-west transgression raised sea level producing fluvio-deltaic, shoreface, and lacustrine environments, which deposited the Murteree Shale, Epsilon Formation, Roseneath Shale, and Daralingie Formation (Bradshaw 1993; Apak *et al*. 1997; Gravestock and Jensen-Schmidt 1998). Deposition of the Daralingie Formation was interrupted by NE-SW (or E-W) compression that reactivated basement faults and regionally eroded much of the Daralingie Formation (Kuang 1985; Apak *et al*. 1997; Mavromatidis 2006).

Post-compressional relaxation during the late Permian encouraged the cyclic deposition of sands, shales, and coals to form the Toolachee Formation. These fluvial conditions continued to deposit the Triassic Nappamerri Group sediments (Kantsler *et al*. 1984; Apak *et al*. 1997). Up to 500 m of upper Nappamerri Group sediments were eroded by the onset of the Upper Triassic E-W Hunter-Bowen Orogeny (Kantsler *et al*. 1984; Apak *et al*. 1997; Alexander *et al*. 1998; Mavromatidis 2006). A prolonged period of post-compressional sag between the Lower Jurassic and Upper Cretaceous created ample accommodation space to deposit the Eromanga Basin sediments under uninterrupted fluvio-deltaic and lacustrine conditions (Green, Brain and John 1989; Hoffmann 1989; Lowe-Young, Mackie and Heath 1997). The Jurassic to Lower Cretaceous sediments form prolific oil reservoirs that are currently one of the major hydrocarbon exploration targets in the basin.

Eromanga Basin sediment deposition ceased with the onset of the Upper Cretaceous E-W crustal shortening event that formed a regional unconformity isolating the Eromanga Basin from the overlying Paleogene to Quaternary Lake Eyre Basin (Kuang 1985; Apak *et al*. 1997; Gravestock and Jensen-Schmidt 1998; Mavromatidis 2006). After this event, the maximum horizontal stress orientation rotated to approximately N-S during the Paleogene to approximately E-W at present day (Müller *et al*. 2012; Pokalai *et al*. 2015a, 2015b, 2016). The present-day stress regime is oriented approximately 101°N under a strike–slip to compressional stress regime with a maximum horizontal stress magnitude of approximately 41.9 MPa at 1 km depth (Reynolds *et al*. 2006; Nelson *et al*. 2007; Pokalai *et al*. 2016). The minimum horizontal and vertical stress magnitudes are approximately 18 and 21.5 MPa at 1 km depth, respectively, but can change locally between strike–slip and compressional stress regimes (Nelson *et al*. 2007).

3 METHODOLOGY

3.1 Seismic data location

For the purpose of this research, publicly available three-dimensional (3D) seismic surveys were selected based on a wide range of acquisition ages, a good spatial distribution that covered a range of structural features, and the presence of strong Upper Cretaceous, Cadna-owie Formation, and top Permian seismic amplitude reflectors. These selection parameters resulted in 12 3D seismic surveys, which include Moomba 3D (acquired 1997), Spencer–Kiana–Muteroo 3D (acquired 2007), Greater Strzelecki 3D (acquired 2001), Dullingari 3D (acquired 1997), Gidgealpa 3D (acquired 2002), Greater Tindilpie and Swan Lake 3D (acquired 2000), Fly Lake 3D (acquired 2000), Coonatie 3D (acquired 2000), Merrimelia 3D (acquired 1998), Pondrinie 3D (acquired 1997), Sprigg (Extension) 3D (acquired 2005), and Cuttapirrie 3D (acquired 1981) (Fig. 3(a)). The seismic data quality and resolution within these surveys is consistently "good" between the surface and the top Patchawarra Formation before rapidly decreasing with depth below the Permian coal measures.

This dramatic decrease in seismic resolution has prevented detailed research on basement faults. The vertical seismic resolution can be calculated by dividing the seismic wavelength by 4, where the wavelength is calculated by dividing the velocity by the seismic frequency. Within the upper sections of the seismic surveys, where the seismic quality is consistently "good", the vertical seismic resolution ranges between 15 m and 35 m, before decreasing to between 50 m and 150 m within basement. The large two-dimensional (2D) seismic dataset used in this research covers the majority of the South Australian portion of the Cooper-Eromanga Basin with a similar seismic resolution to the 3D seismic data, but largely dependent on the acquisition age and depth of investigation (Fig. 3).

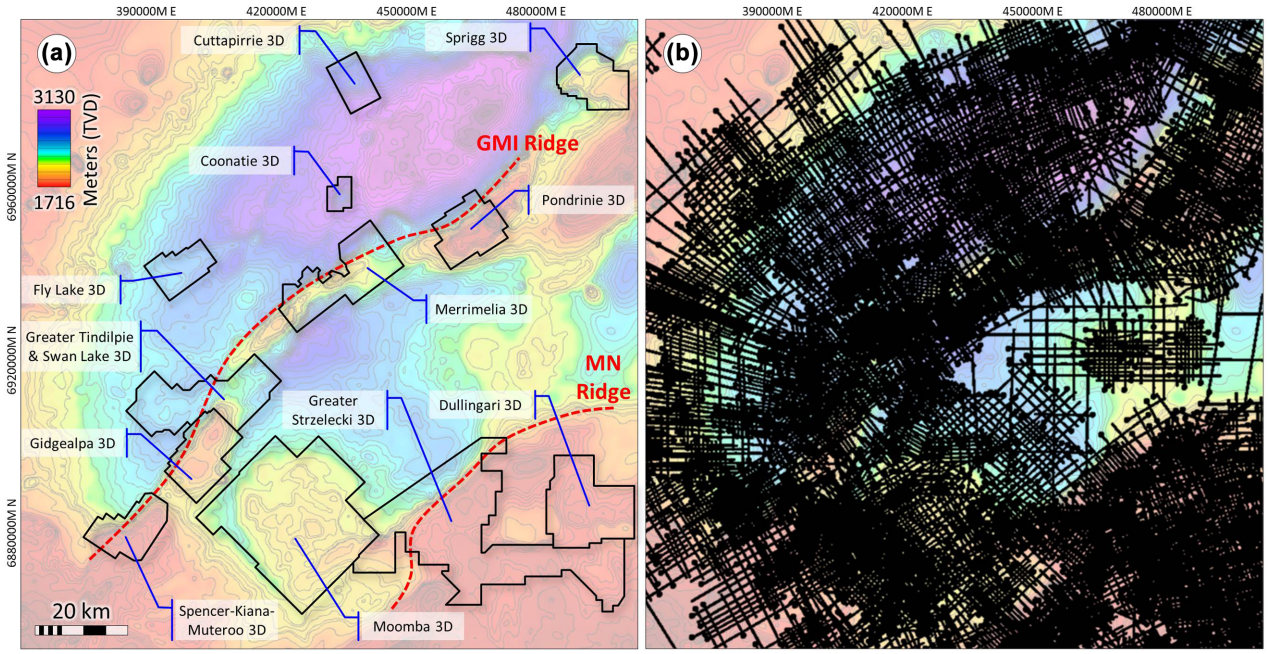


Figure 3 (a) Location of the 12 three-dimensional seismic surveys used in this study with the Gidgealpa–Merrimelia–Innamincka (GMI) and Murteree–Nappacoongee (MN) ridges shown; and (b) location of two-dimensional seismic lines used in this study. See Fig. 1 for location of study area.

3.2 Attribute analysis

This research exploits a commonly used seismic attribute called incoherency, which was first introduced by Bahorich and Farmer (1995) and further developed by Gersztenkorn and Marfurt (1999). Incoherency visually emphasises the discrepancy between adjacent seismic traces along any given horizon or time slice that may otherwise be overlooked (Neves *et al.* 2004; Mai *et al.* 2009; Backé *et al.* 2011; Basir *et al.* 2013). Incoherency is most useful for structural interpretation because of its ability to highlight abrupt changes in amplitude along a reflector typically corresponding to faults. All 3D seismic volumes were converted into incoherency volumes prior to loading the interpreted two-way-time (TWT) grids to display the incoherency along the reflector.

3.3 Seismic interpretation technique

The interpretation of three high-amplitude seismic reflectors (Upper Cretaceous, Cadna-owie Formation, and top Permian) was made in the time domain for each 3D seismic volume. The reflectors were picked every 20 seismic lines (400 m) and propagated using the seismic volume as a background drift to create a final TWT surface grid. These grids were used in the incoherency analysis process to assist with fault interpretation. This was used as a first-pass look into the expected fault strike and location prior to interpreting fault planes (fault sticks) in the seismic volume. Faults were interpreted at a line spacing of between 10 (200 m) and 20 (400 m) depending on their length and strike, but was largely dependent on the complexity of individual fault planes. Incoherency maps were used to guide fault interpretation only in areas of significantly poor seismic resolution and in zones of complex faulting to differentiate between various fault planes. The interpreted faults were transposed onto the TWT surfaces. To remain consistent, all field-scale basement faults are transposed onto the top Permian surface grid irrespective of whether they intersect the surface or not.

3.4 Seismic time-to-depth conversion

A recent study on the most accurate depth conversion method within the Cooper-Eromanga Basin highlighted that from the four most commonly used methods (average velocity method, time–depth trend method, kriging using a TWT grid as an external drift method, and kriging using a stacking velocity grid as an external drift method), the average velocity method was statistically the most accurate (Kulikowski *et al.* 2016c). All interpreted seismic amplitude reflectors were depth converted using the average velocity method. This method uses the depth (Δz metres) of a reflector at a well

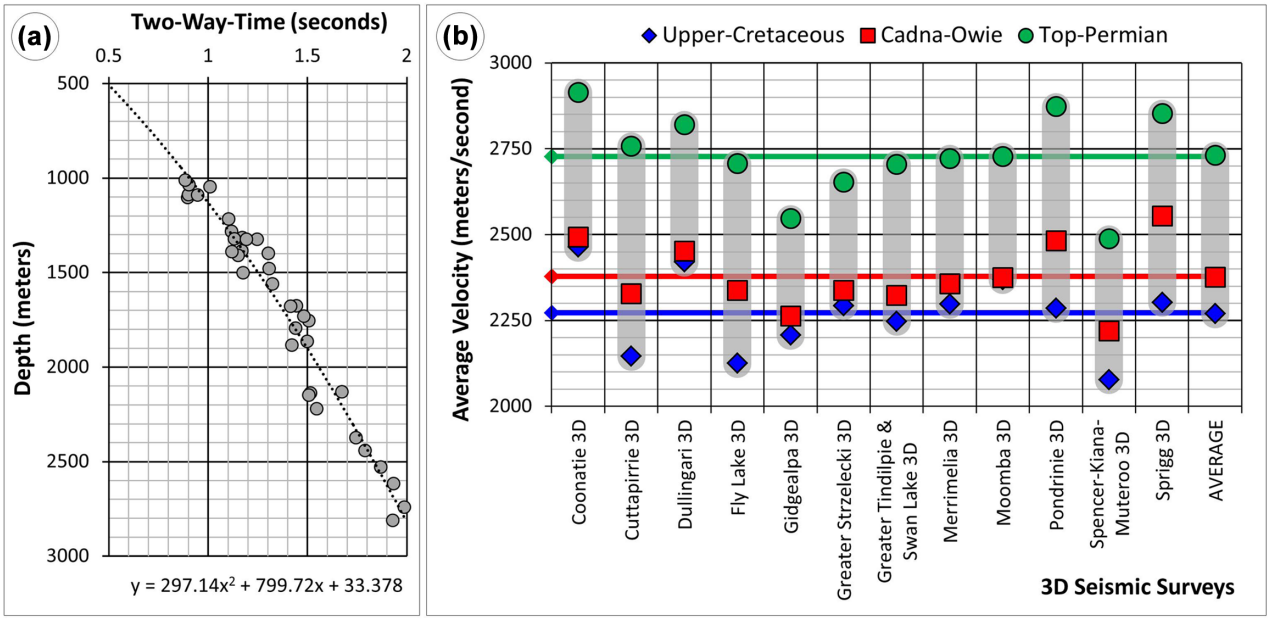


Figure 4 (a) The time (x)-to-depth (y) relationship obtained from three-dimensional seismic data; and (b) the average velocities used for seismic time-to-depth conversion within each of the seismic surveys and for each of the three reflectors. The mean average velocity is displayed for the Upper Cretaceous (blue line), Cadna-owie (red line), and top Permian (green line) reflectors for the entire study area.

control point together with the measured one-way-time (Δt seconds) value from seismic data to infer, or back-calculate, the average velocity required for a precise well tie at that given location by dividing Δz by Δt. An average velocity model is calculated for each seismic volume and for each TWT surface grid. The TWT surface grid (in the time domain) is multiplied by the velocity model to calculate the depth of the grid.

A seismic time-to-depth curve was constructed using data that were measured from each of the 12 3D seismic volumes (Fig. 4(a)). The equation that defines this curve can be used for quick seismic time-to-depth conversions. The average velocity from each seismic volume and for each seismic amplitude reflector is shown in Fig. 4(b), giving an overall average velocity from the surface to the Upper Cretaceous (~2280 m/s), Cadna-owie Formation (~2375 m/s), and top Permian (~2740 m/s) seismic amplitude reflectors.

3.5 Geomechanical modelling

A geomechanical model was developed by using rock mechanics data and *in situ* stress conditions present within the Cooper-Eromanga Basin, with a focus on the Cretaceous polygonal fault system present throughout the basin at approximately 1500 m depth. This polygonal fault system has potential of becoming a new exploration target within the basin, but little is known about the sealing and conduit potential of these faults (Watterson *et al.* 2000). Constraining the fault geometry most likely to be open to fluid flow is significant to this play, as these faults facilitate tertiary hydrocarbon migration from known reservoirs into shallow sandstones (Watterson *et al.* 2000). Therefore, the purpose of this model is to identify the polygonal fault geometry that is most likely to act as a fluid conduit under the present-day stress (Barton, Zoback and Moos 1995; Barton *et al.* 1997; Ferrill and Morris 2003; Jolie, Moeck and Faulds 2015).

Fundamental structural permeability concepts and equations have been developed and used extensively around the world to define the risk of fault slip (shear) and fault opening (dilation) (e.g., Barton *et al.* 1995, 1997; Morris, Ferrill and Henderson 1996; Wiprut and Zoback 2000, 2002; Ferrill and Morris 2003; Worum *et al.* 2004; van Ruth, Nelson and Hill 2006; Moeck, Kwiatek and Zimmermann 2009; Macdonald *et al.* 2012; Jolie *et al.* 2015; Kulikowski *et al.* 2016b). The two more common calculations used to assess hydrocarbon conduit potential of faults are the Leakage Factor and Dilation Tendency (Barton *et al.* 1995, 1997; Ferrill and Morris 2003; Jolie *et al.* 2015; Kulikowski *et al.* 2016b). The Leakage Factor (equation (1)) calculates the relative risk of failure by taking into account the pore pressure (P_p) and the difference between the normal (σ_n) and shear (T) stresses acting on a fault plane at a given depth. For the purpose of this research, a depth of 1500 m was selected,

Table 1 Present-day stress values used for geomechanical modelling at target depth (1500 m). SHmax = maximum horizontal stress; Shmin = minimum horizontal stress; Sv = vertical stress. Data obtained from Reynolds *et al.* (2005) and Nelson *et al.* (2007)

Input	Value at 1500 m
SHmax Azimuth	101°N
Stress Regime	Strike-slip
SHmax magnitude	62.85 MPa
Shmin magnitude	27 MPa
Sv magnitude	32.25 MPa
Pore Pressure	14.7 MPa
Angle of friction	25°
Cohesion	30 MPa

as mentioned earlier, and the present-day stress data were obtained from Reynolds *et al.* (2005) and Nelson *et al.* (2007) (Table 1). A maximum calculated Leakage Factor value of 0.24 corresponds to a high likelihood of failure:

$$Leakage\ Factor = \frac{P_p}{(\sigma_n - T)}\ . \tag{1}$$

The risk of a fault plane undergoing tensile reactivation (dilation) and acting as a fluid conduit is also assessed using the Dilation Tendency (T_d) attribute (equation (2)). This attribute is useful in petroleum reservoirs that are fault sealing or that have faults extending into, under, or overlying sealing units or reservoirs, as it can predict the potential of tertiary migration through a permeable conduit away from the accumulation (Barton *et al.* 1995, 1997; Ferrill and Morris 2003; Jolie *et al.* 2015; Kulikowski *et al.* 2016b). The T_d is largely governed by the effective normal stress magnitude that directly controls the fault aperture (Ferrill *et al.* 1999; Mildren *et al.* 2005; Kulikowski *et al.* 2016b). The equation for T_d (equation (2)) uses the effective maximum (σ_1') and minimum (σ_3') stress magnitudes, together with the effective normal (σ_n') stress magnitude acting on the fault plane. A maximum Dilation Tendency value of 1 suggests a high probability of a fault plane to undergo tensile reactivation:

$$Dilation\ Tendency(T_d) = \frac{\sigma_1' - \sigma_n'}{\sigma_1' - \sigma_3'}\ . \tag{2}$$

The output of this analysis includes two stereonets with the Leakage Factor and T_d attributes overlain to allow any unique fault or fracture plane at 1500 m depth to be plotted and assessed. Poles to fault planes that plot within high (T_d = 1.0; Leakage Factor = 0.24) values would have a greater likelihood of acting as conduit pathways, which therefore allows the optimum fault geometries to be constrained. These stereonets can be used as a first-pass screening tool for future hydrocarbon exploration in shallow Cooper-Eromanga Basin reservoirs and also to assess the sealing potential of faults in Jurassic and Lower Cretaceous reservoirs that may form fault-sealing trap. It is important to note, however, that in order to improve the accuracy of this analysis, local *in situ* stress and pore pressure data must be used, rather than basin-wide average values that are used here (Table 1). Rock mechanics data obtained specifically Cretaceous rocks must also be incorporated.

4 RESULTS

4.1 Three-dimensional seismic interpretation

4.1.1 Moomba 3D

The Moomba three-dimensional (3D) seismic survey covers the Moomba and Big Lake oil and gas fields located within the Nappamerri Trough (Fig. 3(a)). The Upper Cretaceous seismic amplitude reflector is found approximately 1000 m below surface. Incoherency analysis along this seismic amplitude reflector indicates significant faulting throughout the area with no obvious organisational pattern (Fig. 5(a)). The depth grid of this reflector highlights three main structural domes amongst the scatter of faults (Fig. 5(b)). These faults appear to be layer bound and largely remain in the Upper Cretaceous sediments; however, incoherency along the Cadna-owie Formation (Fig. 5(c)) suggests that some normal faults do occasionally extend into deeper sections to displace the Cadna-owie Formation at approximately 1600 m subsurface (Fig. 5(d)). The top Permian reflector is interpreted at approximately 2400 m subsurface. Incoherency along this reflector highlights a dominant northeast–southwest (NE-SW)-striking fault to the southeast of the survey (Fig. 5(e)). The depth grid of this reflector shows a series of small domes scattered throughout the survey with a large NE-SW elongate dome aligned parallel to the main fault strike (Fig. 5(f)). The majority of the major basement faults have a southeast–northwest (SE-NW) strike, perpendicular to the large NE-SW-striking fault, and with reverse sense of motion, and appear in conjunction with structural highs. Incoherency slightly increases at the edges of small domal culminations, inferring the presence of small-scale uninterpretable faults or reduced amplitude at a fold hinge.

4.1.2 Spencer–Kiana–Muteroo 3D

The Spencer–Kiana–Muteroo 3D seismic survey has the best seismic data quality of all surveys, which is likely due to

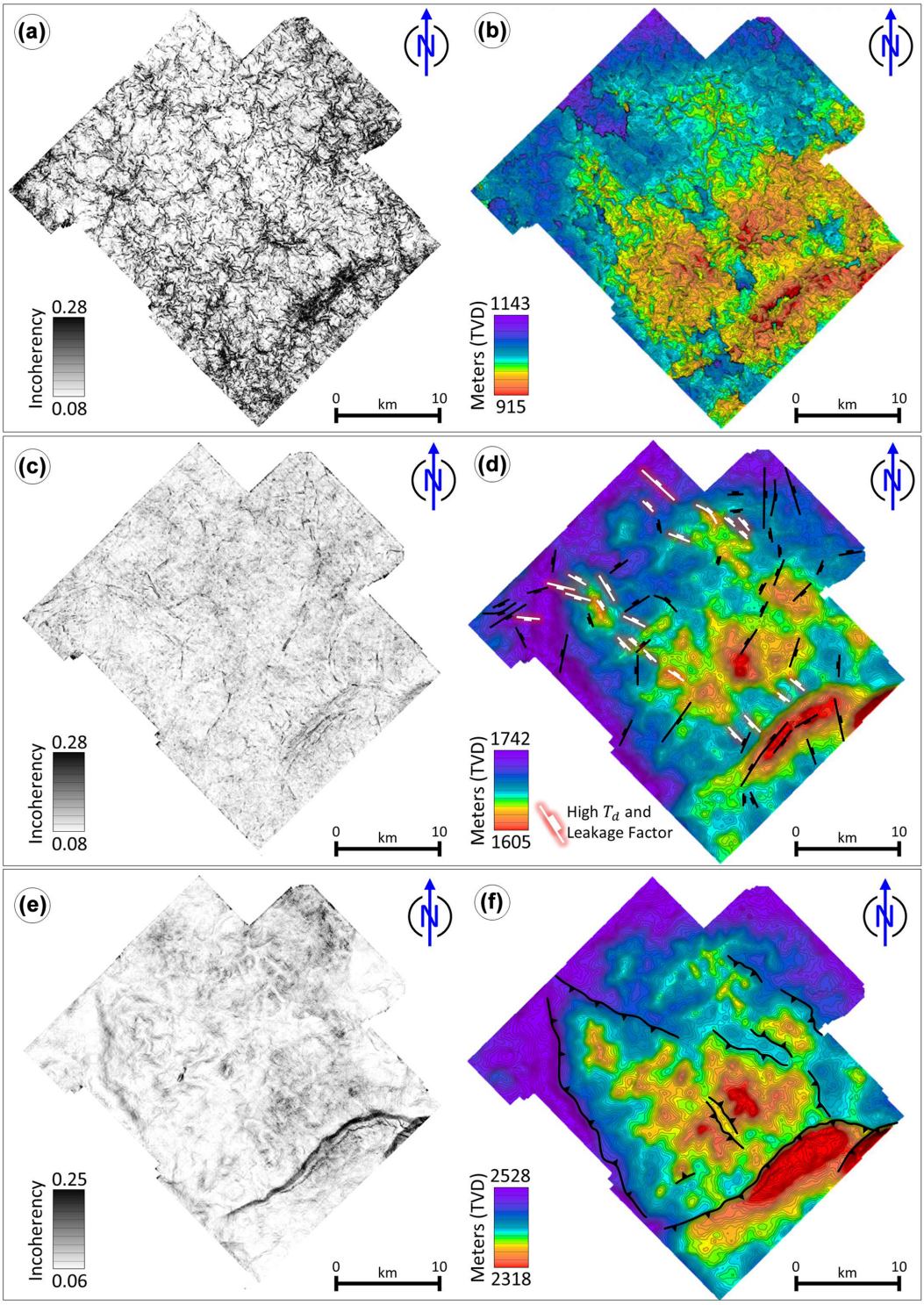


Figure 5 Structural analysis of Moomba 3D. (a) Incoherency analysis along the Upper Cretaceous reflector; (b) depth-converted Upper Cretaceous reflector; (c) incoherency analysis along the Cadna-owie Formation reflector; (d) depth-converted Cadna-owie Formation reflector showing location of normal faults that extend from Upper Cretaceous polygonal fault system to displace the Cadna-owie Formation reflector; (e) incoherency analysis along the top Permian reflector; and (f) depth-converted top Permian reflector showing location of basement reverse faults. See Fig. 3(a) for location.

the relatively recent acquisition. Spencer–Kiana-Muteroo 3D is located on the southern continuation of the Gidgealpa–Merrimelia–Innamincka (GMI) Ridge toward the basin margin (Fig. 3(a)). The Upper Cretaceous seismic amplitude reflector in this survey is approximately 1200 m subsurface, and incoherency analysis along this reflector highlights a large number of faults with irregular strike orientations (Fig. 6(a)). The depth grid of this reflector shows a large anticlinal structure with three individual domes (Fig. 6(b)). The contours show large displacement coinciding with the faults identified in incoherency. Faults were identified along the Cadna-owie Formation reflector at approximately 1500 m depth clearly highlighted using incoherency (Fig. 6(c)). Faults interpreted to displace the Cadna-owie Formation typically extend from the overlying system of faults and have normal displacement (Fig. 6(d)). The first-pass check of basement faults was made using incoherency along the top Permian reflector at approximately 2000 m depth (Fig. 6(e)). Incoherency highlighted a complex array of reverse faults largely with NE-SW strikes and within close proximity to structural highs (Fig. 6(f)).

An NW-SE cross-section through this survey targeting the Cretaceous section shows the complex system of normal faults appearing to be mostly layer bound with the exception of some faults that extend into the oil-rich Lower Cretaceous section (Fig. 7).

4.1.3 Greater Strzelecki 3D

The Greater Strzelecki 3D seismic survey covers a number of oil- and gas-producing fields, including Della, Marabooka, Strzelecki, Kidman, and Bagundi. The survey is located along the Murteree–Nappacoongee (MN) Ridge (Fig. 3(a)). A widespread distribution of randomly oriented faults is highlighted using incoherency along the Upper Cretaceous reflector (Fig. 8(a)). This reflector is approximately 1200 m subsurface and appears to have three large anticlinal structures with rapid change in contours coinciding with high values in incoherency (Fig. 8(b)). The Cadna-owie Formation reflector is located approximately 2200 m subsurface with incoherency showing the main NE-SW-striking MN Ridge reverse fault in the northwest of the survey (Fig. 8(e)). Normal faults were also interpreted to displace the Cadna-owie Formation reflector (Fig. 8(d)). The NE-SW-striking MN Ridge fault is more clearly defined in incoherency along the top Permian reflector (Fig. 8(e)). Interesting incoherency features are seen throughout the survey including a large north–south (N-S)-striking reverse fault in the southeast of the survey (Fig. 8(f)), en echelon lineaments extending from the main MN striking ridge fault in the southwest of the survey (Fig. 8(g)), and oddly shaped domes (Fig. 8(h)). The majority of the structural highs were interpreted to co-exist with basement reverse faults (Fig. 8(f)).

4.1.4 Dullingari 3D

The Dullingari 3D seismic survey covers the Dullingari, Dullingari North, and Burke oil and gas fields and is located to the northeast of the Greater Strzelecki 3D seismic survey along the MN Ridge (Fig. 3(a)). The Upper Cretaceous reflector is located approximately 1100 m subsurface. A high density of faults is highlighted by incoherency throughout the survey (Fig. 9(a)) with no particular relationship with the structure (Fig. 9(b)). A small number of faults extend into the deeper Cadna-owie Formation reflector located approximately 1400 m subsurface (Fig. 9(c)). These normal faults do not appear to conform to an organised pattern (Fig. 9(d)). A large east–west (E-W)-striking fault in the south of the survey is highlighted with incoherency along the top Permian reflector located approximately 2100 m subsurface (Fig. 9(e)). This fault has a zigzag pattern and curves to strike approximately N-S in the west of the survey (Fig. 9(f)). The survey contains primarily NE-SW-striking reverse faults, with secondary E-W-striking reverse faults and a major SE-NW-striking dextral strike–slip fault (Fig. 9(f)). The structural highs appear to coincide with basement faults (Fig. 9(f)).

4.1.5 Gidgealpa 3D

The Gidgealpa 3D seismic survey is located along the NE-SW-striking GMI Ridge and covers the Gidgealpa oil and gas field (Fig. 3(a)). Incoherency along the Upper Cretaceous reflector identified randomly oriented faults at approximately 1300 m depth (Fig. 10(a)). Contours on the depth-converted surface change rapidly in areas of high incoherency (Fig. 10(b)). The density of these faults appears to be unaffected by the structural highs. Large normal faults extending from Upper Cretaceous sediments into oil-rich lower Cretaceous sediments are highlighted by incoherency along the Cadna-owie Formation reflector (Fig. 10(c)). This reflector is located approximately 1500 m subsurface and is displaced extensively by normal faults (Fig. 10(d)). The NE-SW-striking GMI Ridge fault is seen to split into two parallel reverse faults when incoherency is applied to the top Permian reflector (Fig. 10(e)). The depth-converted surface shows two domes bound by NE-SW-striking reverse faults, with the northern dome being laterally displaced by SE-NW-striking dextral strike-slip faults (Fig. 10(f)).

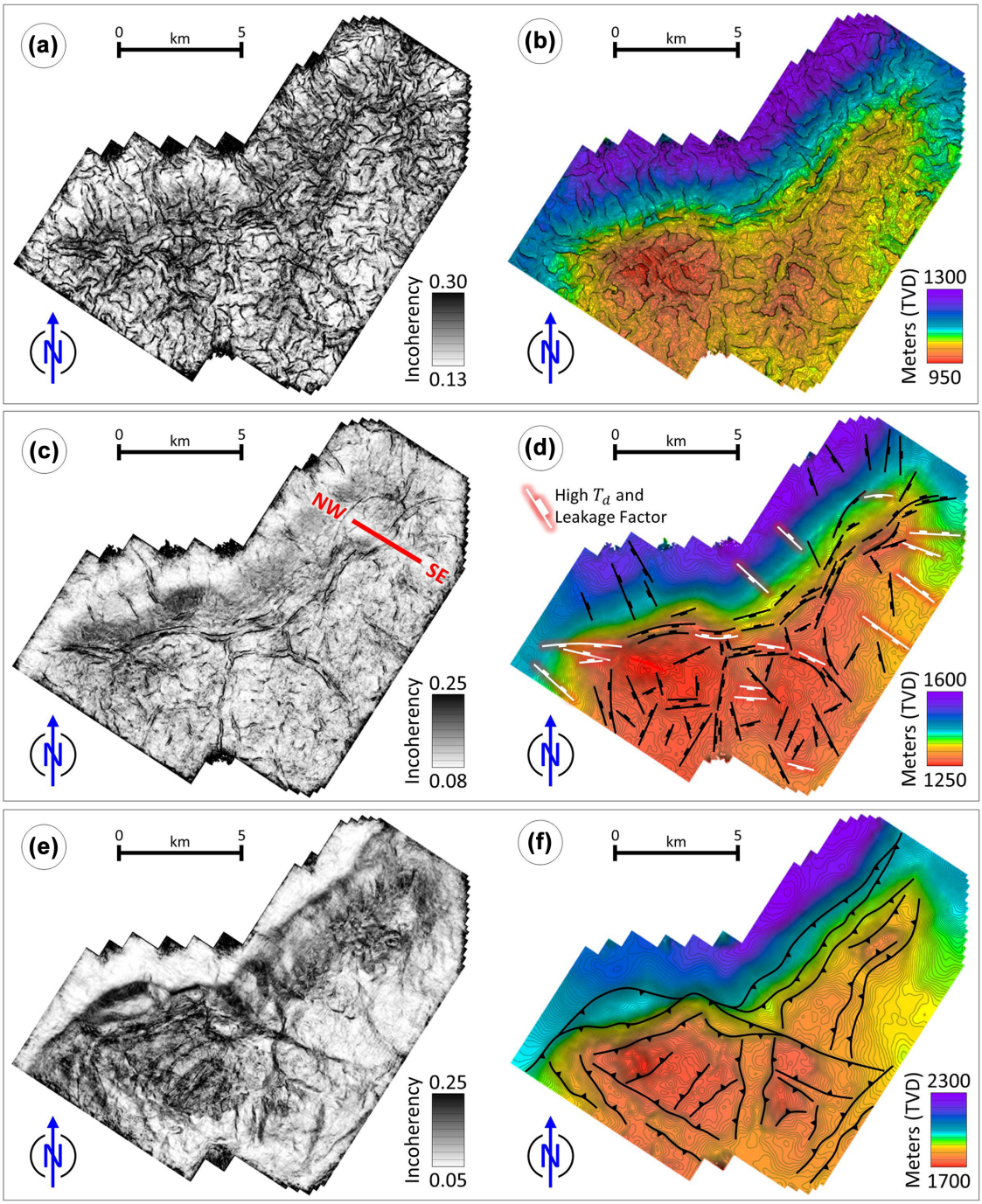


Figure 6 Structural analysis of Spencer–Kiana–Muteroo 3D. (a) Incoherency analysis along the Upper Cretaceous reflector; (b) depth-converted Upper Cretaceous reflector; (c) incoherency analysis along the Cadna-owie Formation reflector and location of cross-section (Fig. 7); (d) depth-converted Cadna-owie Formation reflector showing location of normal faults that extend from Upper Cretaceous polygonal fault system to displace the Cadna-owie Formation reflector; (e) incoherency analysis along the top Permian reflector; and (f) depth-converted top Permian reflector showing location of basement reverse faults. See Fig. 3(a) for location.

© 2017 European Association of Geoscientists & Engineers, *Geophysical Prospecting*, 1–31

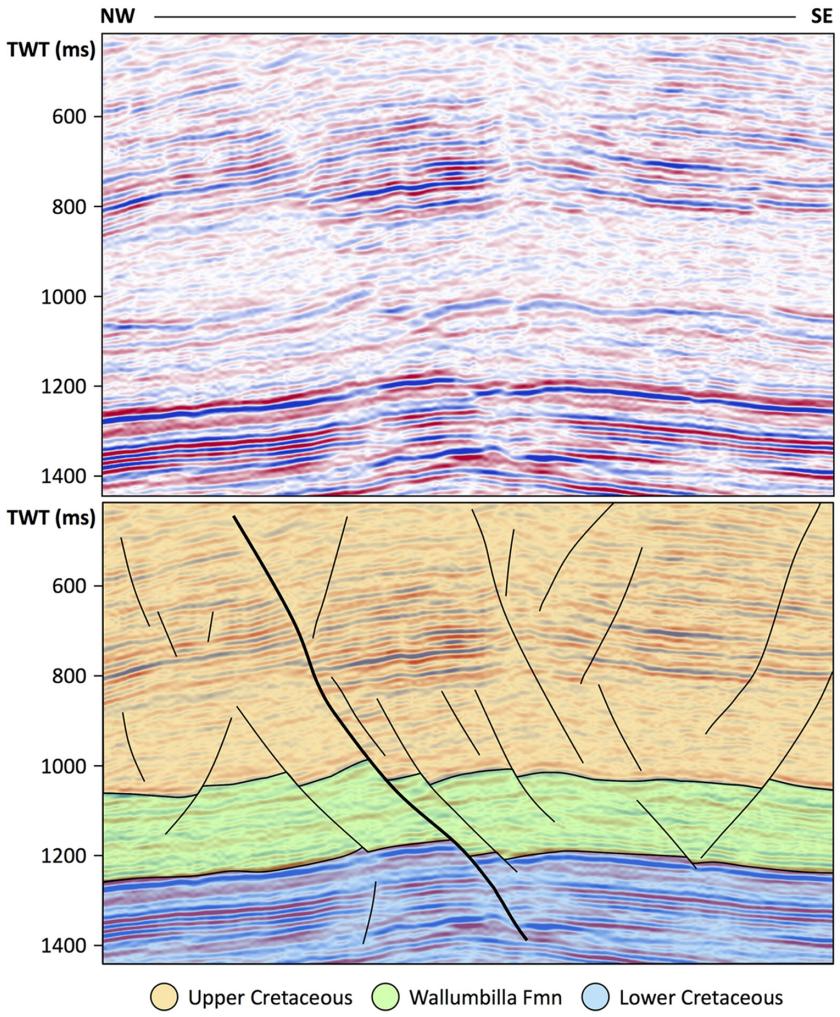


Figure 7 Cross-section showing the Cretaceous polygonal fault system with large normal faults seen to displace the Cadna-owie Formation reflector and extend into oil-rich Lower Cretaceous sediments. These large penetrative normal faults may have the potential to act as conduits to migrate hydrocarbons from Lower Cretaceous oil-rich reservoirs into Upper Cretaceous sediments. For location of cross-section (Inline 640), see Fig. 6(c).

4.1.6 Greater Tindilpie and Swan Lake 3D

The Greater Tindilpie and Swan Lake 3D seismic survey is located along the GMI Ridge north of the Gidgealpa 3D survey and covers the Tindilpie, Cowralli, Gidgealpa north, and Swan Lake gas fields (Fig. 3(a)). Incoherency along the Upper Cretaceous reflector shows a series of unorganised faults appearing to increase in density to the east of the survey (Fig. 11(a)). This seismic amplitude reflector is located approximately 950 m subsurface with high incoherency coinciding with rapid contour changes (Fig. 11(b)). These normal faults extend into Lower Cretaceous sediments as evidenced by displacement along the Cadna-owie Formation reflector at approximately 1600 m subsurface (Fig. 11(c)). The normal faults displacing this reflector increase in density to the east of the survey (Fig. 11(d)). Basement faults appear to splay from the main NE-SW-striking GMI Ridge fault seen along the top Permian reflector under incoherency (Fig. 11(e)). The reflector is approximately 2400 m subsurface and shows small domal culminations scattered around the main NE-SW elongate ridge with all structural highs coinciding with the presence of underlying basement faults (Fig. 11(f)).

4.1.7 Fly Lake 3D

The Fly Lake 3D seismic survey is located within the Patchawarra Trough and covers the Fly Lake and Brolga oil and gas fields (Fig. 3(a)). Incoherency along the Upper Cretaceous reflector shows high-incoherency lineaments dispersed randomly throughout the survey (Fig. 12(a)). The seismic amplitude reflector is approximately 950 m subsurface and when depth-converted shows rapid contour changes in high-incoherency areas (Fig. 12(b)). The Cadna-owie Formation

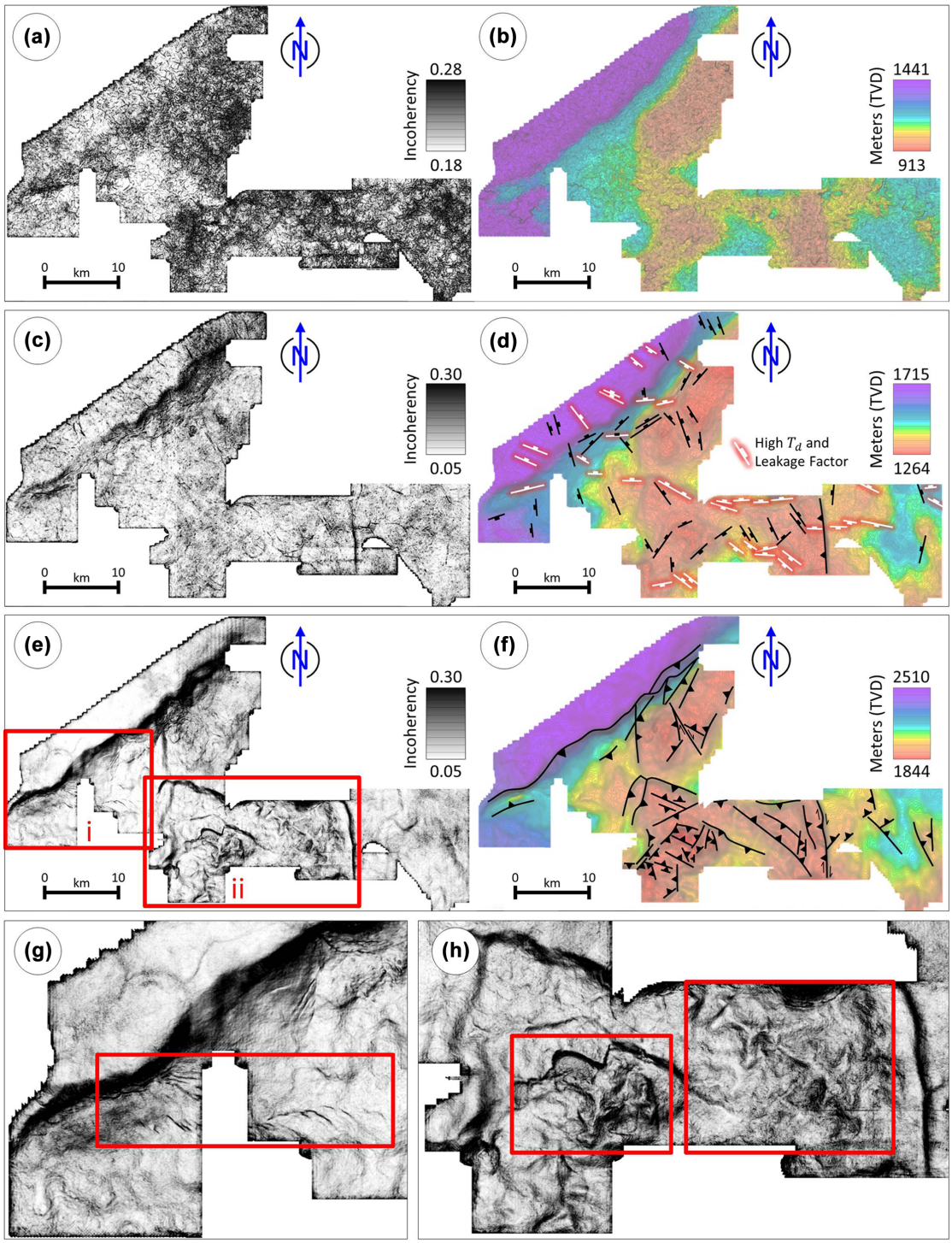


Figure 8 Structural analysis of Greater Strzelecki 3D. (a) Incoherency analysis along the Upper Cretaceous reflector; (b) depth-converted Upper Cretaceous reflector; (c) incoherency analysis along the Cadna-owie Formation reflector; (d) depth-converted Cadna-owie Formation reflector showing normal faults extending from Upper Cretaceous sediments to displace the Cadna-owie Formation reflector; (e) incoherency analysis along the top Permian reflector with location of Fig. 8(g) and (h) shown; (f) depth-converted top Permian reflector showing location of basement reverse faults; (g) interesting en echelon faults that were identified from Fig. 8(e) at location (i); and (h) irregularly shaped structural domes identified from Fig. 8(e) at location (ii). See Fig. 3(a) for location.

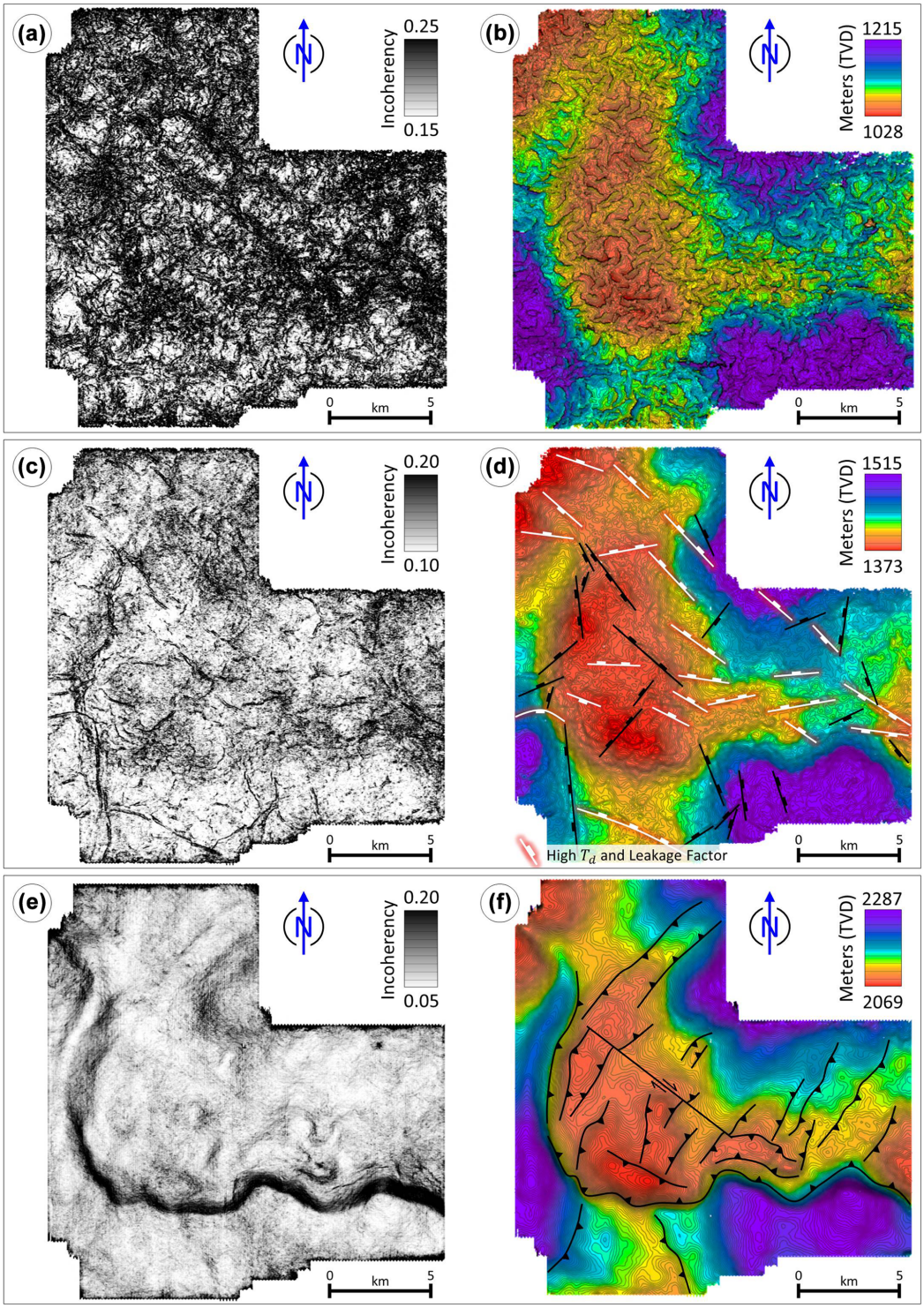


Figure 9 Structural analysis of Dullingari 3D. (a) Incoherency analysis along the Upper Cretaceous reflector; (b) depth-converted Upper Cretaceous reflector; (c) incoherency analysis along the Cadna-owie Formation reflector; (d) depth-converted Cadna-owie Formation reflector showing normal faults extending from Upper Cretaceous sediments to displace the Cadna-owie Formation reflector; (e) incoherency analysis along the top Permian reflector; and (f) depth-converted top Permian reflector showing location of basement reverse faults. See Fig. 3(a) for location.

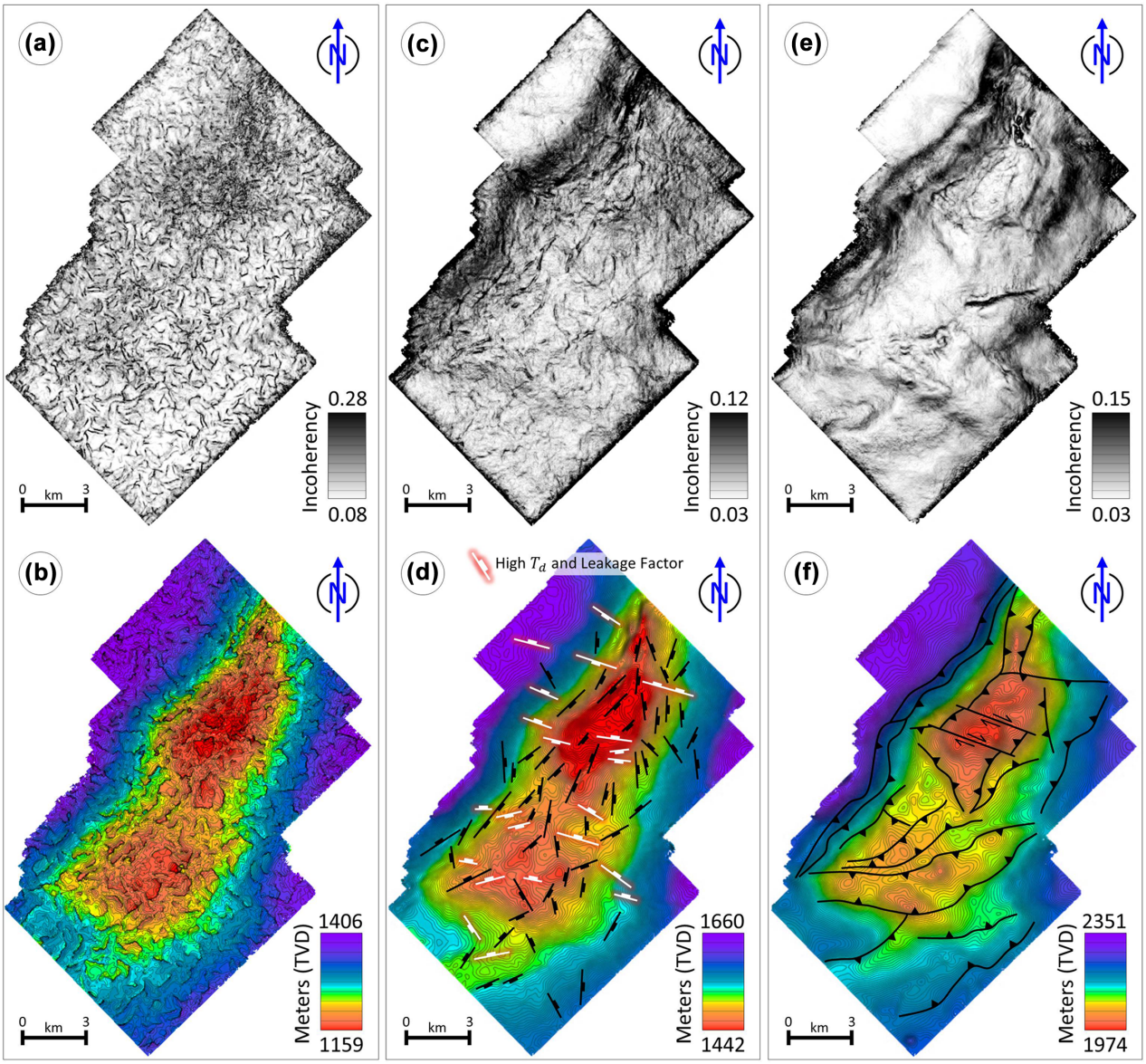


Figure 10 Structural analysis of Gidgealpa 3D. (a) Incoherency analysis along the Upper Cretaceous reflector; (b) depth-converted Upper Cretaceous reflector; (c) incoherency analysis along the Cadna-owie Formation reflector; (d) depth-converted Cadna-owie Formation reflector showing normal faults extending from Upper Cretaceous sediments to displace the Cadna-owie Formation reflector; (e) incoherency analysis along the top Permian reflector; and (f) depth-converted top Permian reflector showing location of basement reverse faults. See Fig. 3(a) for location.

reflector is displaced by normal faults, which are highlighted using incoherency (Fig. 12(c)). The displacement of these faults is significantly less than in Upper Cretaceous sediments, as evidenced in the contour spacing of the depth-converted reflector at approximately 1750 m depth (Fig. 12(d)). The distribution of these deep normal faults is randomly oriented and appears unaffected by the underlying structure. The top Permian reflector has low resolution, which is most apparent in incoherency (Fig. 12(e)). The incoherency along this reflector is relatively unclear but does highlight some major structures. The structural highs are bound from the south by an NE-SW-striking reverse fault (Fig. 12(f)). Depth conversion of this reflector shows one large dome with smaller domes to the northeast of the survey that parallel the main fault. The depth of this reflector is approximately 2600 m.

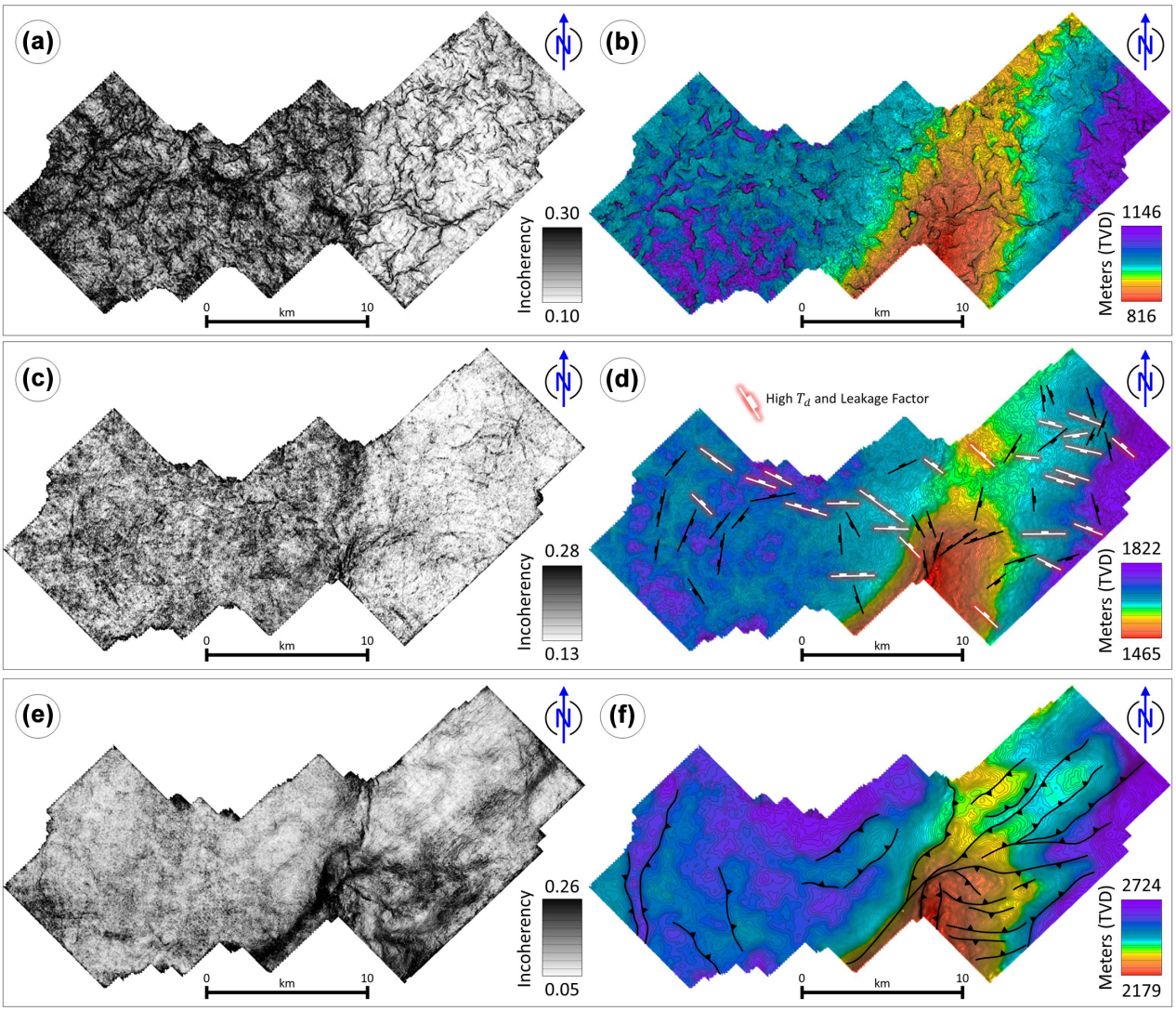


Figure 11 Structural analysis of Greater Tindilpie and Swan Lake 3D. (a) Incoherency analysis along the Upper Cretaceous reflector; (b) depth-converted Upper Cretaceous reflector; (c) incoherency analysis along the Cadna-owie Formation reflector; (d) depth-converted Cadna-owie Formation reflector showing normal faults extending from Upper Cretaceous sediments to displace the Cadna-owie Formation reflector; (e) incoherency analysis along the top Permian reflector; and (f) depth-converted top Permian reflector showing location of basement reverse faults. See Fig. 3(a) for location.

4.1.8 Coonatie 3D

The Coonatie 3D seismic survey is located centrally within the Patchawarra Trough covering the Coonatie gas field (Fig. 3(a)). Incoherency along the Upper Cretaceous reflector highlights large lineaments with high incoherency within the middle of the survey (Fig. 13(a)). This reflector is located at approximately 1100 m depth with sharp contour changes along high-incoherency sections (Fig. 13(b)). Some of these faults extend to normally displace the deeper Cadna-owie Formation reflector at approximately 1800 m depth (Fig. 13(c)). The normal faults are mostly present within the centre of the survey and can be argued to have a dominantly NE-SW strike (Fig. 13(d)). Basement faults can be identified in incoherency along the top Permian reflector and are seen to have a dominant north-northeast–south-southwest (NNE-SSW) strike (Fig. 13(e)). Fault interpretation shows a single structural high elongate in a NNE-SSW direction, which is bound entirely by reverse faults that appear to converge at the north and south of the structure (Fig. 13(f)).

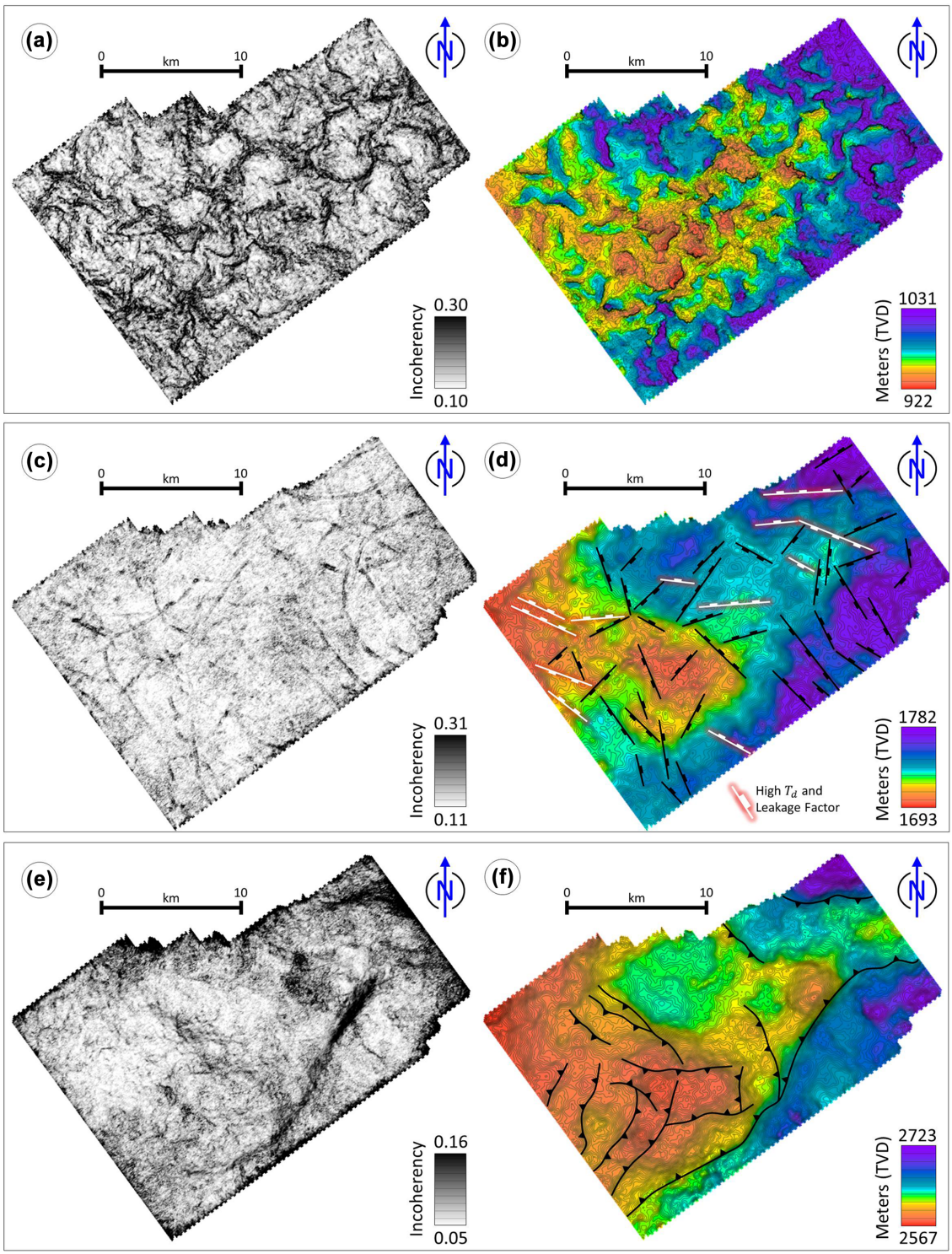


Figure 12 Structural analysis of Fly Lake 3D. (a) Incoherency analysis along the Upper Cretaceous reflector; (b) depth-converted Upper Cretaceous reflector; (c) incoherency analysis along the Cadna-owie Formation reflector; (d) depth-converted Cadna-owie Formation reflector showing normal faults extending from Upper Cretaceous sediments to displace the Cadna-owie Formation reflector; (e) incoherency analysis along the top Permian reflector; and (f) depth-converted top Permian reflector showing location of basement reverse faults. See Fig. 3(a) for location.

© 2017 European Association of Geoscientists & Engineers, *Geophysical Prospecting*, 1–31

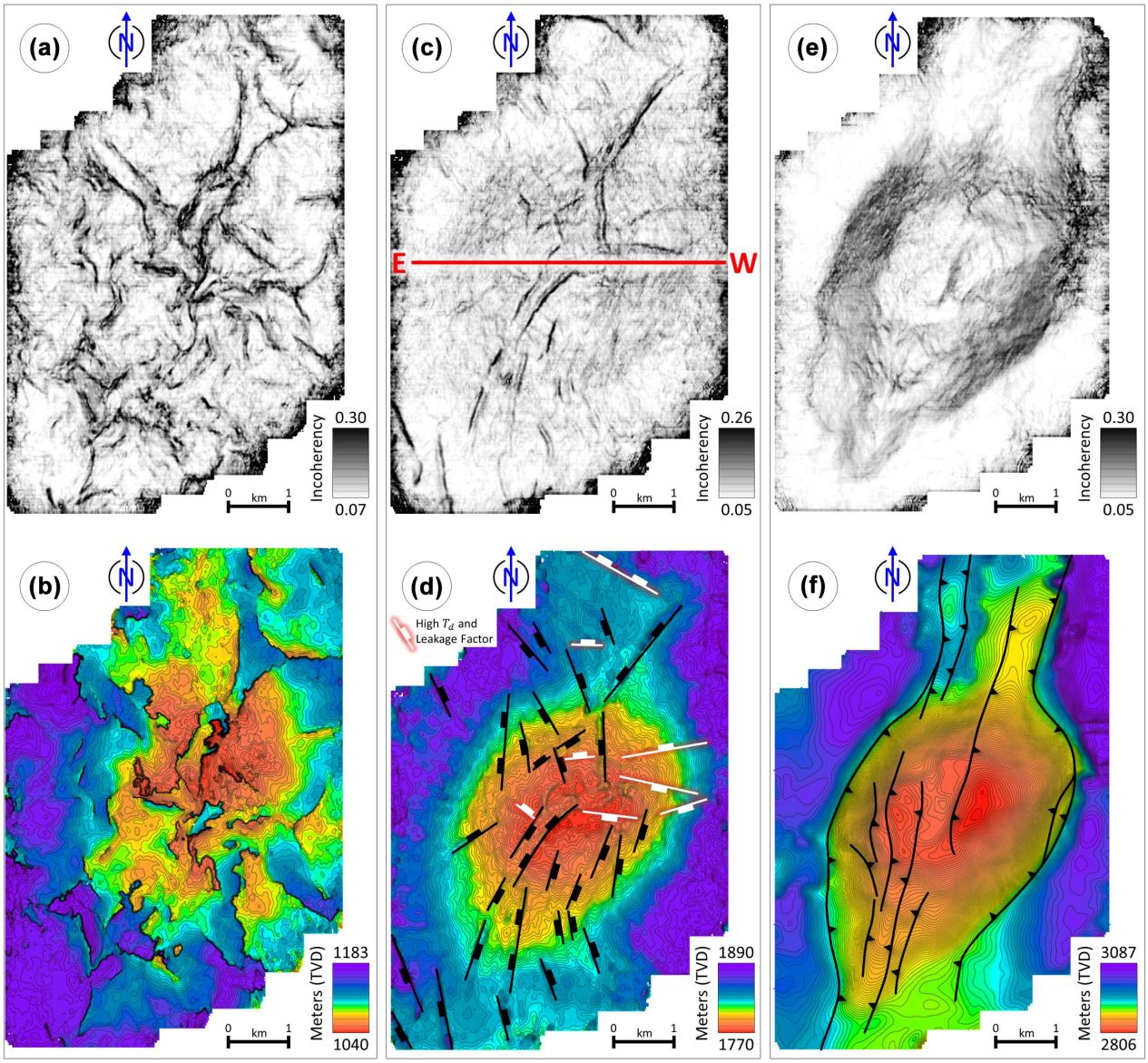


Figure 13 Structural analysis of Coonatie 3D. (a) Incoherency analysis along the Upper Cretaceous reflector; (b) depth-converted Upper Cretaceous reflector; (c) incoherency analysis along the Cadna-owie Formation reflector and location of cross-section (Fig. 14); (d) depth-converted Cadna-owie Formation reflector showing normal faults extending from Upper Cretaceous sediments to displace the Cadna-owie Formation reflector; (e) incoherency analysis along the top Permian reflector; and (f) depth-converted top Permian reflector showing location of basement reverse faults. See Fig. 3(a) for location.

An E-W cross-section across the Coonatie 3D seismic survey shows the structure bounding faults converging at the centre of the structure (Fig. 14). The faults are interpreted to have reverse sense of motion creating structural highs through the stratigraphic column. The high incoherency lineaments imaged along the Upper Cretaceous reflector were interpreted to be normal faults that extend from Upper Cretaceous sediments to displace the deeper Cadna-owie Formation reflector and continue into Lower Cretaceous and Jurassic sediments (Fig. 14).

4.1.9 Merrimelia (Extension) 3D

The Merrimelia (Extension) 3D seismic survey is located along the GMI Ridge covering the northern section of the Merrimelia structure, which, unlike the other seismic surveys,

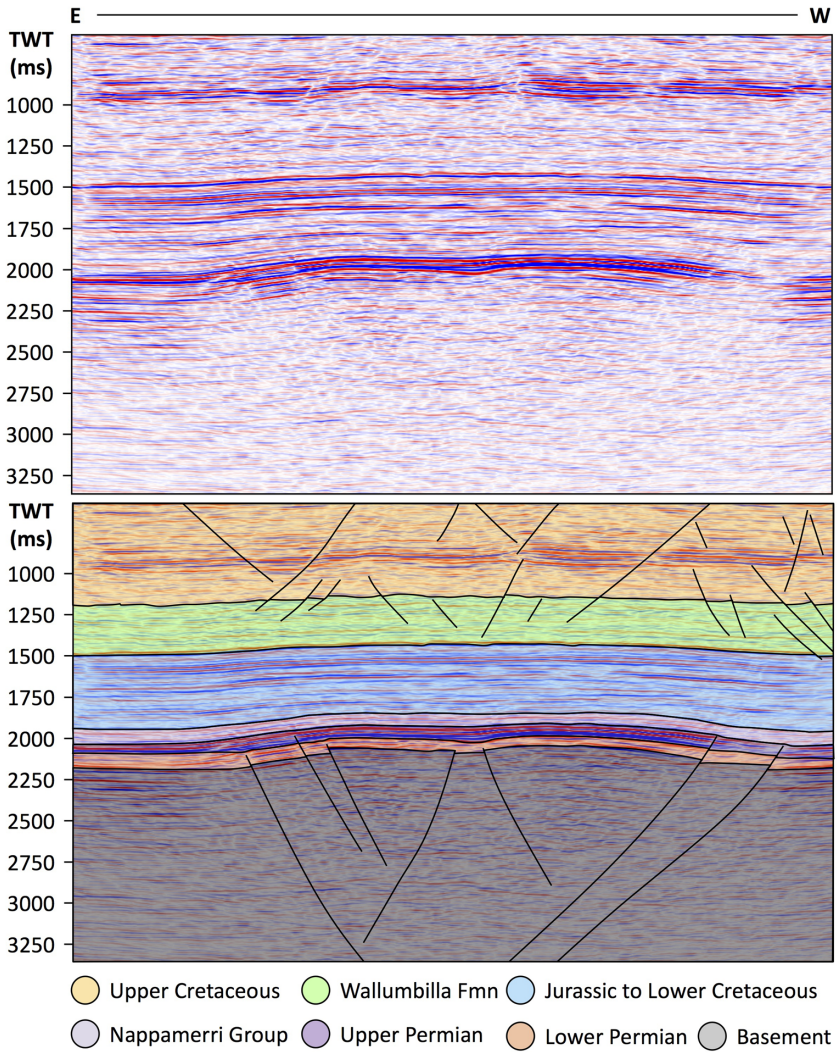


Figure 14 Cross-section through the main Coonatie structure showing a system of Cretaceous polygonal faults above basement reverse faults. The main basement faults are seen to converge to a central point and create a positive flower, or pop-up, structure in Permian and Triassic sediments. For location of cross-section (Inline 2203), see Fig. 13(c).

has no major oil and gas fields but rather a small scattering of oil and gas wells across the survey (Fig. 3(a)). The Upper Cretaceous reflector has a strong incoherency response showing a system of randomly oriented faults (Fig. 15(a)). The strong amplitude of this reflector clearly shows rapid changes in contours along these high-incoherency sections, which are found at approximately 1000 m depth (Fig. 15(b)). Extension of a number of these randomly oriented faults into Lower Cretaceous sediments can be seen along the Cadna-owie Formation reflector with incoherency (Fig. 15(c)). The strike of these normal faults appears to somewhat follow the major NE-SW elongate structural high at approximately 1700 m depth (Fig. 15(d)). A closer look at the basement faults using incoherency along the top Permian reflector highlights dominantly NE-SW-striking lineaments with a high degree of curvature in some faults, which is particularly evident along the NE-SW-striking GMI Ridge fault (Fig. 15(e)). The main NE-SW-striking GMI Ridge fault is observed to straddle the main structural high from the northwest and split into two reverse faults (Fig. 15(f)). The depth-converted top Permian reflector is approximately 2550 m subsurface and delineates two distinct fault-bound domes.

A SE-NW cross-section through the southern portion of the survey shows the underlying structure of the ridge (Fig. 16). Reverse faults extend from basement and control much of the overlying structure; they appear to control the depositional pattern of Triassic sediments with significant thinning evident across the present-day structural high. The system of randomly oriented faults evident in incoherency along the Upper Cretaceous reflector (Fig. 15(a)) can be seen

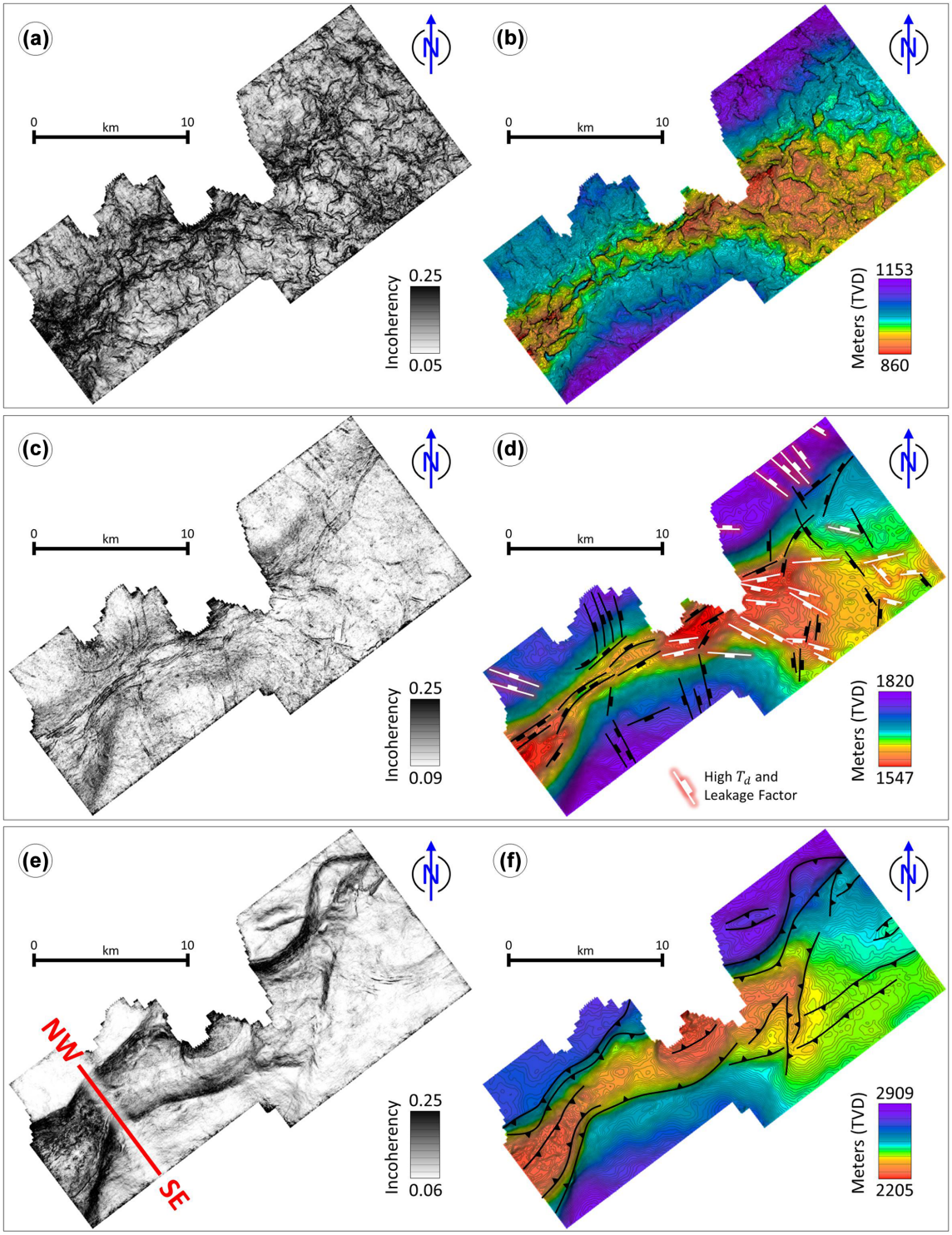


Figure 15 Structural analysis of Merrimelia (Extension) 3D. (a) Incoherency analysis along the Upper Cretaceous reflector; (b) depth-converted Upper Cretaceous reflector; (c) incoherency analysis along the Cadna-owie Formation reflector; (d) depth-converted Cadna-owie Formation reflector showing normal faults extending from Upper Cretaceous sediments to displace the Cadna-owie Formation reflector; (e) incoherency analysis along the top Permian reflector and location of cross-section (Fig. 16); and (f) depth-converted top Permian reflector showing location of basement reverse faults. See Fig. 3(a) for location.

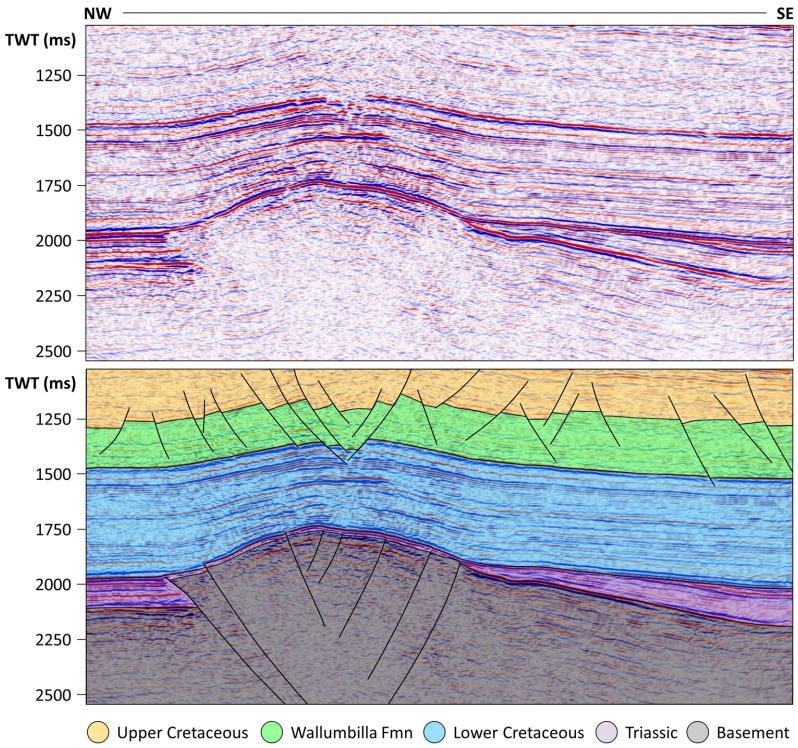


Figure 16 Cross-section through the main Merrimelia structure showing a dense system of Cretaceous polygonal faults above basement reverse faults. The structure appears to be controlled by a main reverse fault with multiple antithetic reverse faults. Movement along these faults appears to have limited the deposition of Permian and Triassic sediments to low-lying areas that fostered the formation of a large pinch-out on the southeast edge of the Merrimelia structure. For location of cross-section (Inline 4295), see Fig. 15(e).

in cross-section to be largely layer bound with the exception of large faults that displace the Cadna-owie Formation reflector and penetrate into the Lower Cretaceous sediments.

4.1.10 Pondrinie 3D

The Pondrinie 3D seismic survey is located along the northern portion of the GMI Ridge covering the Pondrinie and Packsaddle oil and gas fields (Fig. 3(a)). Incoherency analysis along the Upper Cretaceous reflector highlights the presence of randomly oriented faults scattered throughout the survey (Fig. 17(a)). This reflector is located approximately 1200 m subsurface and after depth conversion shows rapid contour changes along high-incoherency lineaments and a large NE-SW elongate dome spread across the survey (Fig. 17(b)). The Cadna-owie Formation reflector is located approximately 1550 m subsurface and shows significant faulting when incoherency is applied (Fig. 17(c)). The normal faults displacing this reflector appear to have a mostly NE-SW or SE-NW strike and are seen to slightly increase in density across the structural high. Basement faults are clearly resolved under incoherency along the top Permian reflector, which is located approximately 2450 m subsurface (Fig. 17(e)). Reverse faults are in close proximity to structural highs and have a dominant NE-SW strike.

4.1.11 Sprigg (Extension) 3D

The Sprigg (Extension) 3D seismic survey is located along the northernmost portion of the GMI Ridge covering the Sprigg and Acrasia oil and gas fields (Fig. 3(a)). Randomly oriented faults are identified using incoherency along the Upper Cretaceous reflector at approximately 1200 m depth (Fig. 18(a)). The density of these faults increases to the north of the survey. Post-depth conversion, the reflector is seen to rapidly change in depth along these high-incoherency sections, and the density and geometry of these faults appear to stay consistent despite the main structural high in the east of the survey (Fig. 18(b)). The larger normal faults that extend deeper in the stratigraphic column are clearly depicted along the Cadna-owie Formation reflector at approximately 1600 m depth when analysed using incoherency (Fig. 18(c)). The strike of these faults does not appear to conform to a regular pattern (Fig. 18(d)). The top Permian reflector is largely eroded from the Sprigg 3D area; hence, the base Triassic reflector was interpreted at approximately 2200 m depth. As such, the amplitude of this reflector is significantly decreased, which is evident when analysed with incoherency (Fig. 18(e)). The incoherency surface is unclear for majority of the survey; however, a number of dominantly E-W-striking reverse faults could still be resolved (Fig. 18(f)). Reverse faults are

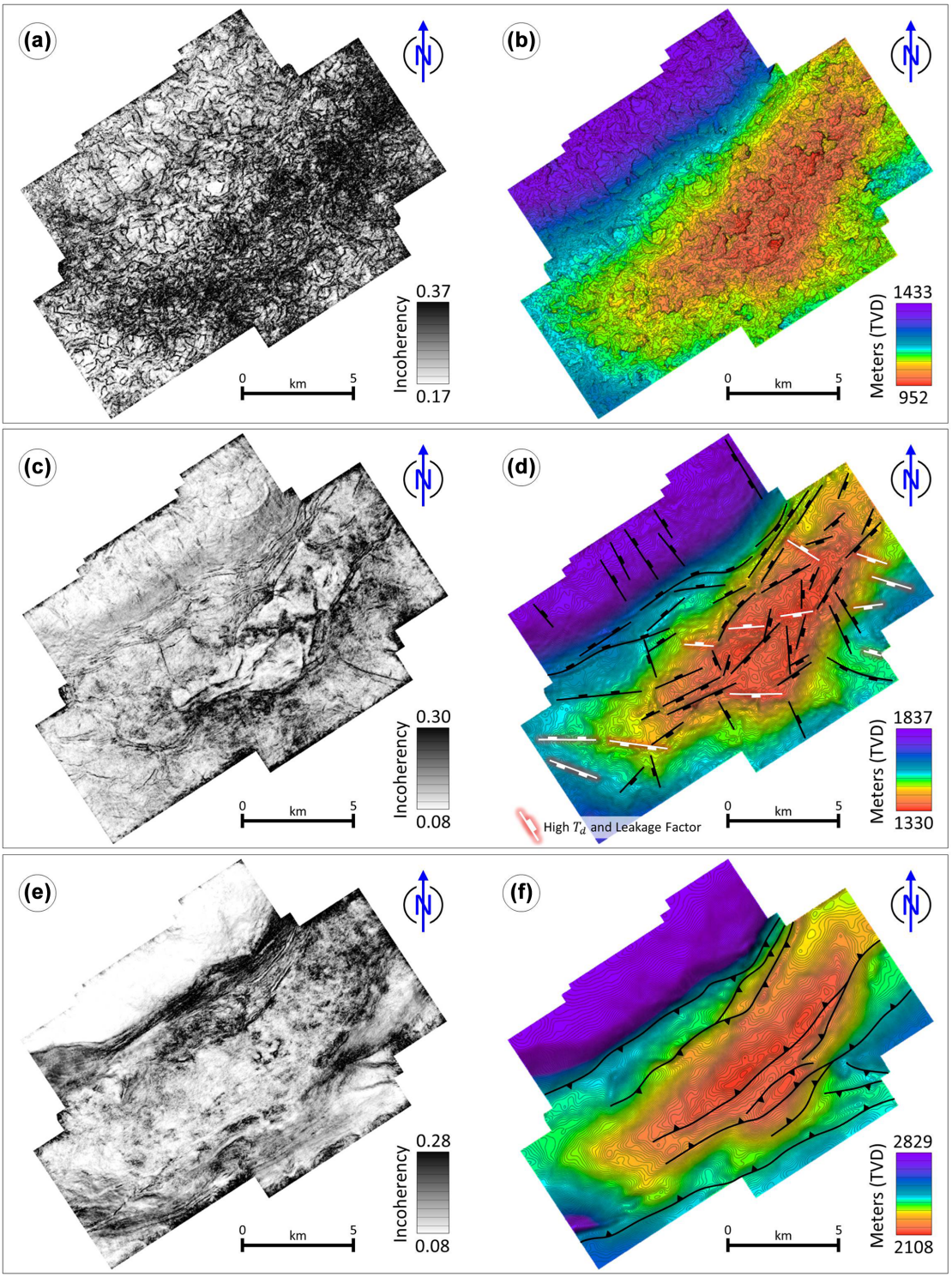


Figure 17 Structural analysis of Pondrinie 3D. (a) Incoherency analysis along the Upper Cretaceous reflector; (b) depth-converted Upper Cretaceous reflector; (c) incoherency analysis along the Cadna-owie Formation reflector; (d) depth-converted Cadna-owie Formation reflector showing normal faults extending from Upper Cretaceous sediments to displace the Cadna-owie Formation reflector; (e) incoherency analysis along the top Permian reflector; and (f) depth-converted top Permian reflector showing location of basement reverse faults. See Fig. 3(a) for location.

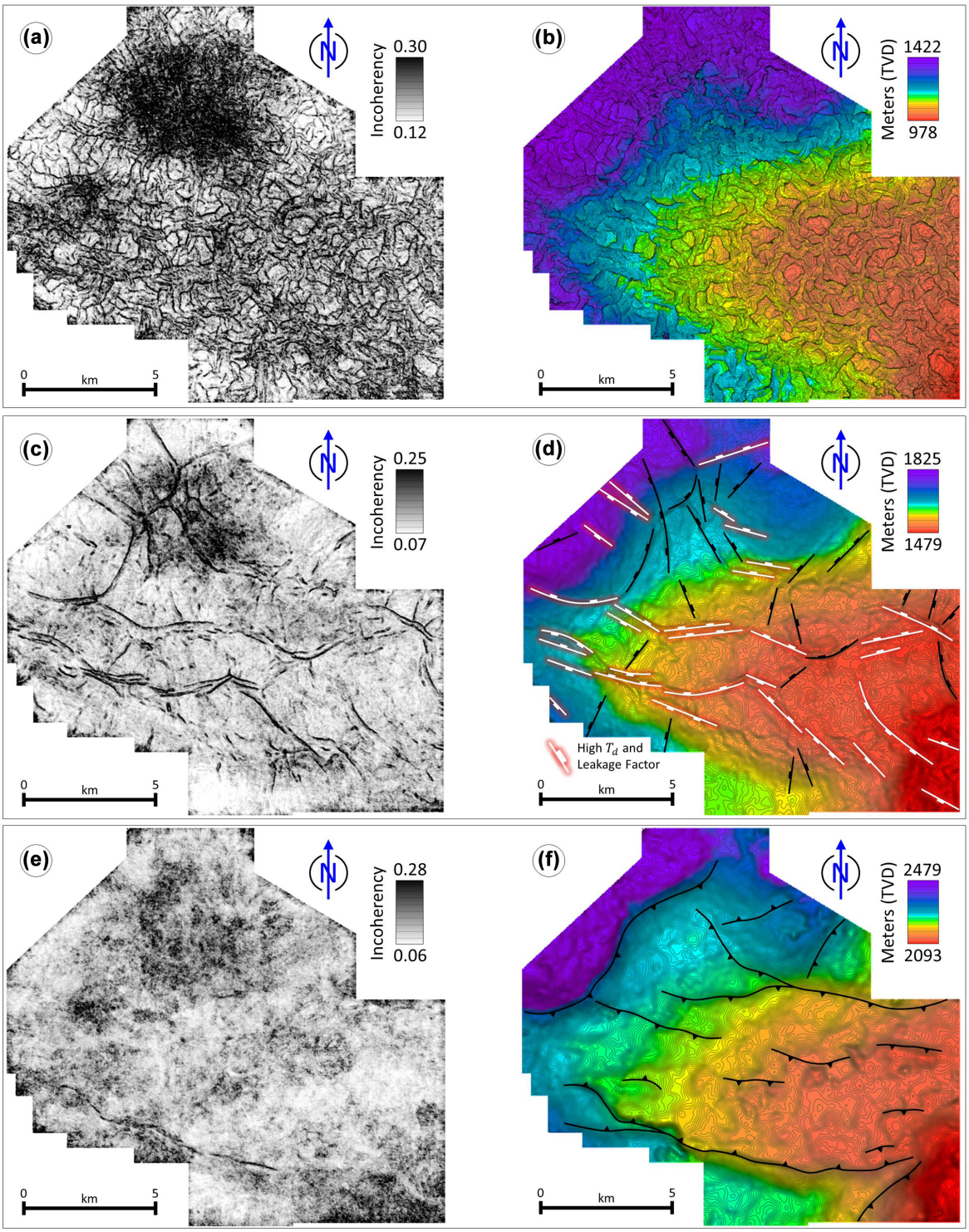


Figure 18 Structural analysis of Sprigg (Extension) 3D. (a) Incoherency analysis along the Upper Cretaceous reflector; (b) depth-converted Upper Cretaceous reflector; (c) incoherency analysis along the Cadna-owie Formation reflector; (d) depth-converted Cadna-owie Formation reflector showing normal faults extending from Upper Cretaceous sediments to displace the Cadna-owie Formation reflector; (e) incoherency analysis along the top Permian reflector; and (f) depth-converted top Permian reflector showing location of basement reverse faults. See Fig. 3(a) for location.

© 2017 European Association of Geoscientists & Engineers, *Geophysical Prospecting*, 1–31

interpreted at the base of a majority of the structural highs that are present.

4.1.12 Cuttapirrie 3D

The Cuttapirrie 3D seismic survey is located within the Patchawarra Trough covering the Cuttapirrie oil and gas field situated directly north of the Coonatie 3D seismic survey (Fig. 3(a)). The seismic survey is one of the oldest and, as such, has a much poorer resolution than the other seismic surveys. This is particularly noticeable when the Upper Cretaceous reflector, located at approximately 1450 m depth, is analysed using incoherency (Fig. 19(a)). Incoherency does highlight some major lineaments, but these are highly interpretable and difficult to visualise. Depth conversion of this reflector shows rapid contour changes similar to the other seismic surveys (Fig. 19(b)). The Cadna-owie Formation reflector is located approximately 1800 m subsurface and more clearly defines the presence of normal faults that extend from Upper Cretaceous sediments (Fig. 19(c)). The large normal faults appear to cluster above the centrally located dome and the structural high found to the north of the survey (Fig. 19(d)). Incoherency along the top Permian reflector shows a large approximately E-W-striking fault bounding the main dome from the south, and a series of NE-SW-striking faults (Fig. 19(e)). These reverse faults are in close proximity to the main structural highs (Fig. 19(f)).

4.2 Two-dimensional seismic interpretation

The top Permian/base Triassic reflector was regionally interpreted across the study area and depth converted using the mean of the average velocities, which was found to be approximately 2740 m/s (Figs. 3(a) and 20). All of the publicly available two-dimensional (2D) seismic lines (Fig. 3b) were used in conjunction with 3D seismic surveys (Fig. 3(a)) to interpret the major basement faults within the study area and projected onto the regional depth-converted top Permian/base Triassic surface (Fig. 20(a)). The majority of the faults have a NE-SW strike that parallels the GMI Ridge. Structural highs across the basin appear to be closely related to the presence of reverse faults and their antithetic pair. Near-vertical sinistral strike–slip faults splay from the main NE-SW-striking GMI Ridge fault system. These strike–slip faults have a NNE-SSW orientation and appear to terminate at the northern portion of the Patchawarra Trough. Reverse faults splay from one of the large strike–slip faults creating structural highs within the Patchawarra Trough that are covered by the Fly Lake and Greater Tindilpie and Swan Lake 3D seismic surveys. A second NNE-SSW-striking strike–slip fault trends through the Coonatie 3D seismic survey. Small-scale dextral strike–slip faults are present throughout the study area and are most prevalent in the Gidgealpa, Swan Lake, Della, and Dullingari fields. Due to the poor seismic resolution of old 2D seismic lines through the Nappamerri Trough, structural lineaments were difficult to interpret. As a result, the presence of faults shown as dotted lines is speculative; however, they do conform to the large-scale structural interpretation of the basin.

Anticlinal structures are observed to be in areas of known basement faults, with structural lows present along the footwall of major reverse faults and within sections of the major troughs. The present-day maximum horizontal stress orientation from various wells is plotted on the interpreted basement fault map to investigate whether the stress direction is being perturbed by basement faults (Fig. 20(b)). The stress direction from a majority of wells has an approximately E-W trend and slightly rotates to SE-NW within the Patchawarra Trough and on the southern and northern sections of the Ridge (Fig. 20(b)).

4.3 Geomechanical modelling of polygonal faults

Geomechanical modelling was performed at a depth of 1500 m and under the present-day stress tensor to calculate the optimum geometry of polygonal faults to be acting as possible fluid conduits. The calculations were performed using the Leakage Factor and Dilation Tendency equations, which can both be used as a guide to infer the relative likelihood of hydrocarbon migration through open faults. The Leakage Factor analysis found that faults with a strike of 076°N and 126°N with high dip angles record the largest Leakage Factor (Fig. 21(a)). Using the same present-day stress data, the Dilation Tendency analysis found that faults with a strike of 101°N and high to near-vertical dip angles are most likely to dilate (Fig. 21(b)). Both analyses found that approximately NNE-SSW-striking faults are least likely to leak or dilate under the present-day stress. The stereonets developed here can be used to assess the relative likelihood of faults being open to fluid flow at 1500 m under the average present-day stress data from the South Australia portion of the Cooper-Eromanga Basin and under hydrostatic pressure conditions.

5 DISCUSSION

The basement fault architecture within the South Australian portion of the Cooper-Eromanga Basin has historically been difficult to interpret due primarily to the rapid decrease in

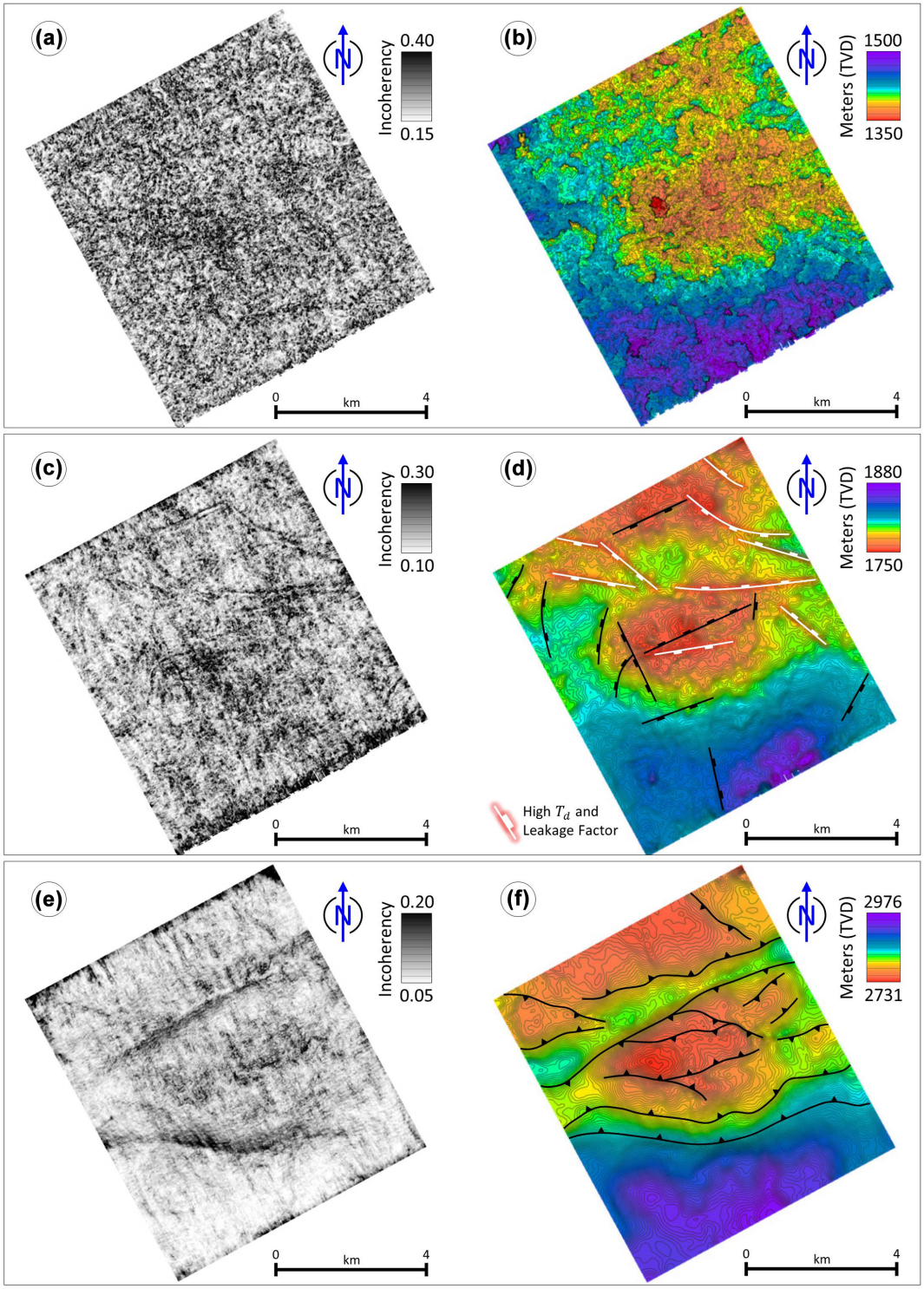


Figure 19 Structural analysis of Cuttapirrie 3D. (a) Incoherency analysis along the Upper Cretaceous reflector; (b) depth-converted Upper Cretaceous reflector; (c) incoherency analysis along the Cadna-owie Formation reflector; (d) depth-converted Cadna-owie Formation reflector showing normal faults extending from Upper Cretaceous sediments to displace the Cadna-owie Formation reflector; (e) incoherency analysis along the top Permian reflector; and (f) depth-converted top Permian reflector showing location of basement reverse faults. See Fig. 3(a) for location.

© 2017 European Association of Geoscientists & Engineers, *Geophysical Prospecting*, 1–31

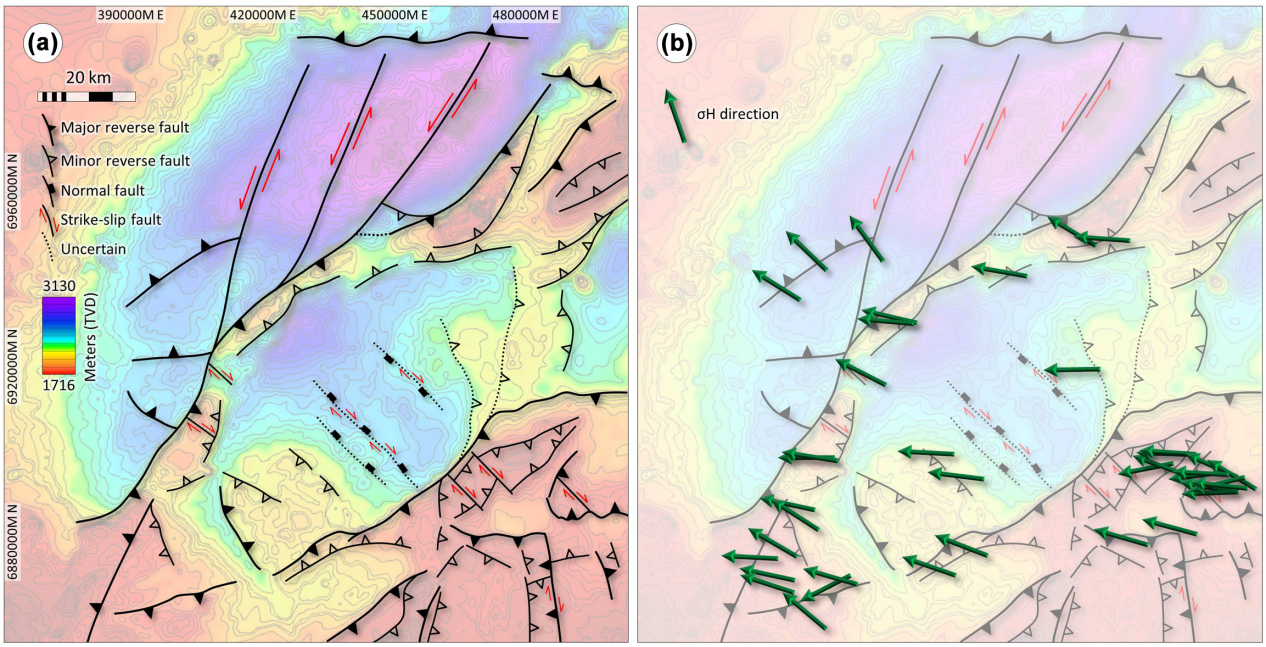


Figure 20 Results from the structural interpretation of 2D and 3D seismic interpretation showing (a) basement fault interpretation of the main reverse (secondary reverse faults are shown un-bold), strike–slip, and normal faults. Highly interpretative faults that could not be accurately measured due to poor seismic resolution are shown as dotted lines; and (b) distribution of present-day maximum horizontal stress (σ_H) orientations calculated from petroleum wells by Reynolds *et al.* (2004). For location of study area, see Fig. 1.

seismic resolution below the Permian coal measures. The introduction of attribute analysis and improved seismic interpretation and processing software has reinvigorated the value of vintage seismic data that can extract information that was previously not detectable. The value of seismic attribute analysis, such as incoherency, is realised in old and low-resolution seismic data that can reveal the presence of faults that may have otherwise been overlooked. The use of incoherency along the Upper Cretaceous, Cadna-owie Formation, and top Permian reflectors within 12 three-dimensional (3D) seismic surveys has improved the accuracy of fault interpretation by providing a first-pass look into the distribution of expected faults and as a quality control measure to ensure consistency with fault interpretation.

In each of the 3D seismic surveys, a system of polygonal faults was identified within Cretaceous sediments. A thorough description of the geometry and origin of polygonal faults in the Lake Hope 3D seismic survey has previously been reported (Watterson *et al.* 2000); however, the regional extent of this system away from the study area was not explored. These normal faults were largely layer bound, with the exception of faults occasionally extending to displace the deeper Cadna-owie Formation reflector and penetrating into oil-rich Lower Cretaceous reservoirs (Heath *et al.* 1989). This scenario is a common exploration target around the world, where hydrocarbons have migrated through fault conduits into shallow reservoirs (e.g., Faber and Stahl 1984; Horvitz and Ma 1988; Gay *et al.* 2006; Sun *et al.* 2010). Watterson *et al.* (2000) first identified this as a potential play in the Lake Hope 3D seismic survey region. Taking into account the regional distribution of this polygonal fault system, the potential for hydrocarbons to be migrating into shallow reservoirs is a real possibility. To assess the likelihood that polygonal faults are acting as hydrocarbon conduits, geomechanical modelling was used to calculate the Leakage Factor and Dilation Tendency. Polygonal faults that extend into oil-rich Lower Cretaceous reservoirs and with optimum Leakage Factor and Dilation Tendency values would theoretically be most likely to have oil accumulations in shallower reservoirs. These potentially permeable polygonal faults are highlighted in each of the 3D seismic surveys to aid in future exploration programs. Shallow Cretaceous sediments above the Cadna-owie Formation include the Wallumbilla Formation (restricted open-marine and shore-face sediments), Oodnadatta Formation (open shallow-marine sediments), Winton Formation (fluvial-lacustrine sediments), and Mackunda Formation (fluvial-lacustrine sediments), which can host hydrocarbon that has migrated through potentially permeable faults. Geomechanical analysis identified

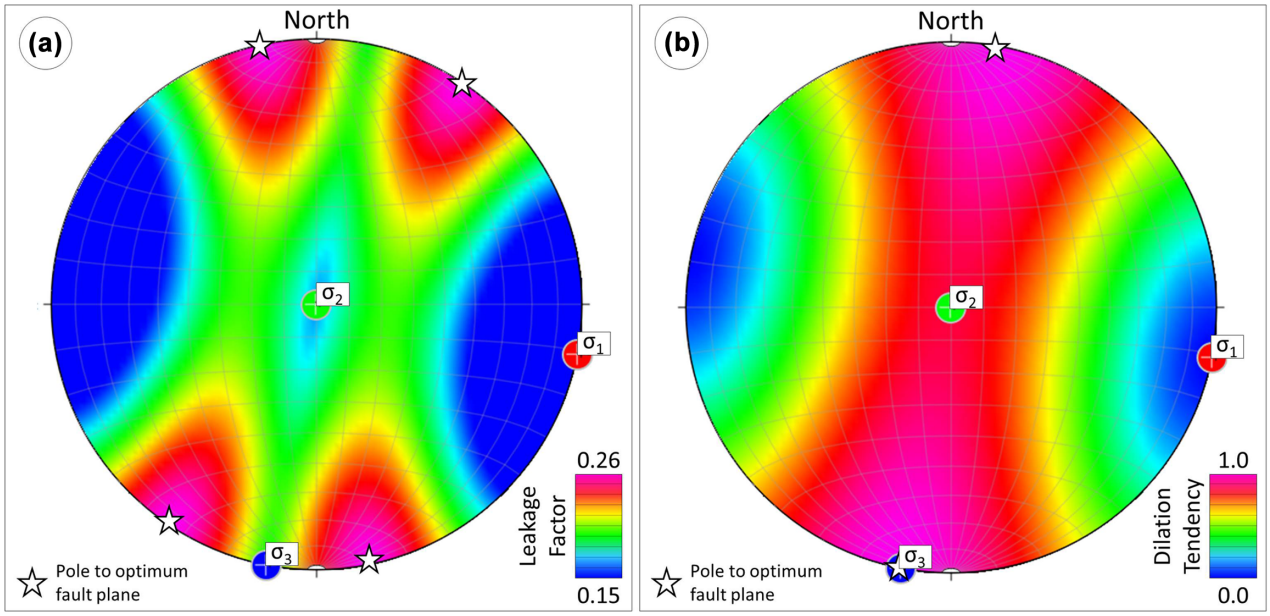


Figure 21 Results from the geomechanical modelling of polygonal faults using the (a) Leakage Factor (equation (1)) and (b) Dilation Tendency (equation (2)). Results show the relative likelihood of faults being open to fluid flow at 1500 m depth under the present-day stress. Data obtained from research conducted by Reynolds *et al.* (2005) and Nelson *et al.* (2007). See Table 1 for input data.

faults with high to near-vertical dip angles striking between 060°N and 140°N to be preferentially open to fluid flow and may act as conduits for the tertiary migration of hydrocarbons from Lower Cretaceous reservoirs into shallow Cretaceous sediments.

The detailed fault interpretation of each seismic volume showcased the complexity of the basin, governed by reverse faults that appear to control the development of structural highs. The deep basement faults have an overarching control on the present-day structure of not only Permian sediments, but also the younger Upper Cretaceous sediments. The broad structure of deeper reflectors is mimicked in a general sense by younger Eromanga Basin sediments. Although the major reverse faults have a dominant northeast–southwest (NE-SW) strike, the field-scale geometry of faults varies markedly depending on the particular 3D seismic survey location. Field-scale southeast–northwest (SE-NW)-striking dextral strike–slip faults have previously been interpreted (Grant-Woolley *et al.* 2014; Kulikowski *et al.* 2015, 2016b) and were also present within some of the 3D seismic surveys used for this study. Although their presence was not always well defined, it is possible that they may be present throughout the basin at a sub-seismic resolution level.

The SE-NW-striking strike–slip faults are ideally oriented relative to the large north-northeast–south-southwest (NNE-SSW)-striking sinistral strike–slip faults identified within the Patchawarra Trough to be part of a conjugated set. The sense of movement and geometry is consistent across the basin to support the notion that they potentially developed during an approximately south-southeast–north-northwest-oriented strike–slip stress regime event. Nonetheless, these NNE-SSW-striking strike–slip faults found only within the Patchawarra Trough form prolific positive flower, or pop-up, structures that create prolific hydrocarbon accumulations. The exploration of similar strike–slip features elsewhere in the basin, particularly within areas not covered with 3D seismic data, may prove to be a rewarding target. The structural highs within the eastern Nappamerri Trough are challenging to explain since only sparse low-resolution two-dimensional (2D) seismic data are available. It is interpreted that they developed in conjunction with reverse faults that splayed from the NE-SW-striking Murteree–Nappacoongee (MN) Ridge fault. Structural lineaments oriented SE-NW were identified in the central Nappamerri Trough; however, their displacement varied along the strike of the fault from strongly normal to no displacement evident. Considering the near-vertical nature of these faults, it is likely that they developed as strike–slip faults with normal displacement taking place during the successive periods of flexural relaxation, or sag. The sparse distribution of 2D seismic data over this area prevented any detailed analysis of these faults.

En echelon features were identified within the Greater Strzelecki 3D seismic survey that appeared to extend or splay from the large NE-SW-striking MN Ridge fault (Fig. 8(g)). These were found to have high to near-vertical dip angles and appear to be contained within the Permian to Triassic Cooper Basin sediments with normal displacement of reflectors; however, they may also extend into low-resolution basement at sub-seismic resolution. Their strike varies from 090°N proximal to the fault to 135°N as they move east. This strike falls within the optimal Leakage Factor and Dilation Tendency values when plotted on the geomechanical modelling stereonets (Fig. 21). Albeit they appear at approximately 2000 m depth, these faults would remain optimally oriented to act as conduits for hydrocarbon migration if geomechanical modelling was performed at 2000 m depth. Directly east of these extensional faults, incoherency analysis identified irregularly shaped domes that are known to be prolific oil and gas fields (Fig. 8(h)). The structure of these domes resembles that of ridges that have been extensively eroded by river channels and draped with sediments. Differential erosion of ridges and paleohighs has been shown to generate similar structural features elsewhere in South Australia, such as the Mount Buffalo area (Boucher 2001).

Onlapping of sediments onto paleo-structural highs can form pinch-out traps that, although much higher risk than anticline features with four-way dip closure, can generate substantial return. Large structures such as the Gidgealpa–Merrimelia–Innamincka (GMI) and MN ridges have endured successive periods of crustal shortening and flexural relaxation, which fosters the onlap of sediments (Fig. 16). As the low-risk anticline features with four-way dip closure become exploited within the Cooper-Eromanga Basin, a change in focus to pinch-out traps, fault-sealing anticlines, shallow prospects filled via tertiary migration, deep coal measures, and basin-centred gas will become the new exploration targets (Watterson *et al.* 2000; Hillis *et al.* 2001). Improved 3D seismic data acquisition and processing techniques will lead to higher-quality seismic data within the Cooper-Eromanga Basin, enabling a more thorough and detailed understanding of the structural architecture of the basin and more accurate risk assessments for the new wave of exploration targets expected to sweep through the basin.

6 CONCLUSION

The structurally complex Cooper-Eromanga Basin has been largely interpreted using sparse low-resolution two-dimensional (2D) seismic data that has only allowed a poor understanding of the underlying basement fault architecture. This research precisely maps the field-scale and regional distribution of basement faults using all publicly available 2D seismic lines and 12 three-dimensional (3D) seismic surveys. Interpretation, attribute analysis, and depth conversion of the Upper Cretaceous, Cadna-owie Formation, and top Permian reflectors were performed within each seismic volume to present the underlying structural configuration of the major oil- and gas-producing fields, as well as to provide a better understanding of the regionally extensive system of Cretaceous polygonal faults that may act as conduits for the tertiary migration of hydrocarbons into shallow reservoirs. The randomly oriented polygonal faults were geomechanically modelled to calculate the optimum fault geometry that would enable tertiary migration of hydrocarbons from Lower Cretaceous oil-rich sediments into shallow Cretaceous reservoirs. Faults with high to near-vertical dip angles striking between 060°N and 140°N were identified as the most likely to be open to fluid flow. As the humble anticlinal targets become exhausted within the basin, a secondary sweep of historically unconventional targets will become the focus, such as pinch-out traps, subtle structures, shallow reservoirs, deep coal measures, and basin-centred gas. It is critical that existing 3D seismic surveys are re-processed and re-interpreted to ensure all potential accumulations are identified, particularly considering the rapid developments in geophysics and well logging. Future work may investigate the relationship between the two main strike–slip fault sets that may have developed as a single conjugated set and use the detailed basement fault interpretation to guide the construction of a regional 3D model of the structural architecture of the basin and attempt to perform a balanced restoration.

ACKNOWLEDGEMENTS

The authors appreciate the financial contribution made by the GeoFrac Consortium, which includes the sponsoring companies: Santos, Beach Energy, Chevron, Halliburton, and BG Group (QGC). We thank DownUnder GeoSolutions (DUG Insight 3.1) and Midland Valley Exploration (MOVE 2016.2) for their generous donation of academic licences and software. DUG Insight software (v.3.1, 2015) was used for seismic visualisation, interpretation, and analysis. We also thank the Associate Editor and the two anonymous reviewers from *Geophysical Prospecting* who provided constructive feedback and suggestions to improve the quality of the manuscript.

REFERENCES

Abul Khair H., Cooke D. and Hand M. 2013. The effect of present day *in situ* stresses and paleo-stresses on locating sweet spots in unconventional reservoirs, a case study from Moomba-Big Lake fields, Cooper Basin, South Australia. *Journal of Petroleum Exploration and Production Technology* **3**, (4), 207–221.

Abul Khair H., Cooke D. and Hand M. 2015. Seismic mapping and geomechanical analyses of faults within deep hot granites, a workflow for enhanced geothermal system projects. *Geothermics* **53**, 46–56.

Alexander E.M., Gravestock D.I., Cubitt C. and Chaney A. 1998. Lithostratigraphy and environments of deposition. In: *The Petroleum Geology of South Australia: Cooper Basin*., Vol. **4** (eds. D.I. Gravestock, J.E. Hibburt and J.F. Drexel), pp. 69–115. South Australia: Department of Primary Industries and Resources. Report Book, 98/9.

Apak S.N., Stuart W.J., Lemon N.M. and Wood G. 1997. Structural evolution of the Permian–Triassic Cooper Basin, Australia: relation to hydrocarbon trap styles. *American Association of Petroleum Geologists Bulletin* **81**, 533–555.

Backé G., Abul Khair H., King R. and Holford S. 2011. Fracture mapping and modelling in shale-gas target in the Cooper Basin, South Australia. *The Australian Petroleum Production and Exploration Association Journal* **51**, 397–410.

Bahorich M. and Farmer S. 1995. 3-D seismic discontinuity for faults and stratigraphic features: the coherence cube. *The Leading Edge* **14**(10), 1053–1058.

Barton C.A., Zoback M.D. and Moos D. 1995. Fluid flow along potentially active faults in crystalline rock. *Geology* **23**, 683–686.

Barton C.A., Moos D., Peska P. and Zoback M.D. 1997. Utilizing wellbore image data to determine the complete stress tensor: application to permeability anisotropy and wellbore stability. *The Log Analyst* **38**(6), 21–33.

Basir H.M., Javaherian A. and Yaraki M.T. 2013. Multi-attribute ant-tracking and neural network for fault detection: a case study of an Iranian oilfield. *Journal of Geophysics and Engineering* **10**, 015009.

Boreham C.J. and Hill A.J. 1998. Source rock distribution and hydrocarbon geochemistry. In: *The petroleum geology of South Australia: Cooper Basin*, Vol. **4**. (eds. D.I. Gravestock, J.E. Hibburt and J.F. Drexel), pp. 129–142. South Australia: Department of Primary Industries and Resources. Report Book, 98/9.

Boucher R.K. 2001. Cooper Basin ridges: are they structural? *MESA Journal* **21**, 30–32.

Bradshaw M.T. 1993. Australian petroleum systems. *Petroleum Exploration Society of Australia Journal* **21**, 43–53.

Faber E. and Stahl W. 1984. Geochemical surface exploration for hydrocarbons in North Sea. *American Association of Petroleum Geologists Bulletin* **68**(3), 363–386.

Ferrill D.A. and Morris A.P. 2003. Dilational normal faults. *Journal of Structural Geology* **25**, 183–196.

Ferrill D.A., Winterle J., Wittmeyer G., Sims D., Colton S., Armstrong A. and Morris A.P. 1999. Stressed rock strains groundwater at Yucca Mountain, Nevada. *GSA Today* **9**(5), 1–8.

Gay A., Lopez M., Cochonnat P., Levaché D., Sermondadaz G. and Seranne M. 2006. Evidences of early to late fluid migration from an upper Miocene turbiditic channel revealed by 3D seismic coupled to geochemical sampling within seafloor pockmarks, Lower Congo Basin. *Marine and Petroleum Geology* **23**, 387–399.

Gersztenkorn A. and Marfurt K.J. 1999. Eigenstructure-based coherence computations as an aid to 3D structural and stratigraphic mapping. *Geophysics* **64**(5), 1468–1479.

Glikson A.Y., Uysal I.T., Fitz Gerald J.D. and Saygin E. 2013. Geophysical anomalies and quartz microstructures, eastern Warburton Basin, north-east South Australia: tectonic or impact shock metamorphic origin? *Tectonophysics* **589**, 57–76.

Grant-Woolley L., Kong A., Schoemaker B., Nasreddin H. and Montague E.T. 2014. Identification of strike–slip faults provides insights into the further development of mature Cooper Basin fields. SPE Asia Pacific oil and gas conference and exhibition, Adelaide, SPE 171492-MS.

Gravestock D.I. and Jensen-Schmidt B. 1998. Structural setting. In: *The petroleum geology of South Australia: Cooper Basin*, Vol. **4** (eds. D.I. Gravestock, J.E. Hibburt and J.F. Drexel), pp. 69–115. South Australia: Department of Primary Industries and Resources. Report Book, 98/9.

Green P.M., Brain T.J. and John B.H. 1989. Possible stratigraphic controls on hydrocarbon distribution within the Jurassic–Early Cretaceous rocks, Eromanga Basin, southern Queensland. In: *The Cooper and Eromanga Basins, Australia* (ed. B.J. O'Neil), pp. 251–264. Petroleum Exploration Society of Australia, Society of Petroleum Engineers, Australian Society of Exploration Geophysicists (S.A. Branches), Adelaide (Proceedings of Cooper and Eromanga Basins Conference).

Gregory C.M., Senior B.R. and Galloway M.C. 1967. The geology of the Connemara, Jundah, Canterbury, Windorah and Adavale 1:250,000 sheet areas, Queensland. Bureau of Mineral Resources.

Haines P.W., Hand M. and Sandiford M. 2001. Palaeozoic synorogenic sedimentation in central and northern Australia: a review of distribution and timing with implications for the evolution of intracontinental orogens. *Australian Journal of Earth Sciences* **48**, 911–928.

Heath R., McIntyre S. and Gibbins N. 1989. A Permian origin for Jurassic reservoired oil in the Eromanga Basin. In: *The Cooper and Eromanga Basins, Australia* (ed. B.J. O'Neil), pp. 405–416. Petroleum Exploration Society of Australia, Society of Petroleum Engineers, Australian Society of Exploration Geophysicists (S.A. Branches), Adelaide (Proceedings of Cooper and Eromanga Basins Conference).

Hillis R.R., Morton J.G.G., Warner D.S. and Penney R.K. 2001. Deep basin gas: a new exploration paradigm in the Nappamerri Trough, Cooper Basin, South Australia. *The Australian Petroleum Production and Exploration Association Journal* **41**(1), 185–200.

Hoffmann K.L. 1989. The influence of pre-Jurassic tectonic regimes on the structural development of the southern Eromanga Basin, Queensland. In: *The Cooper and Eromanga Basins, Australia* (ed. B.J. O'Neil), pp. 315–328. Petroleum Exploration Society of Australia, Society of Petroleum Engineers, Australian Society of Exploration Geophysicists (S.A. Branches), Adelaide (Proceedings of Cooper and Eromanga Basins Conference).

Horvitz E.P. and Ma S. 1988. Hydrocarbons in near-surface sand, a geochemical survey of the dolphin field in North Dakota.

Association of Petroleum Geochemical Explorationists Bulletin **4**(1), 30–46.

Jolie E., Moeck I. and Faulds J.E. 2015. Quantitative structural geological exploration of fault-controlled geothermal systems—A case study from the Basin-and-Range Province, Nevada (USA). *Geothermics* **54**, 54–67.

Kantsler A.J., Prudence T.J.C., Cook A.C. and Zwigulis M. 1984. Hydrocarbon habitat of the Cooper/Eromanga Basin, Australia. In: Petroleum geochemistry and basin evolution. *American Association of Petroleum Geologists Memoir*, Vol. **35** (eds. G. Demaison and R.J. Murris), pp. 373–390.

Kuang K.S. 1985. History and style of Cooper-Eromanga Basin structures. *Exploration Geophysics* **16**, 245–248.

Kulikowski D., Amrouch K., Al Barwani K. H., Liu W. and Cooke D. 2015. Insights into the tectonic stress history and regional 4D natural fracture distribution in the Australian Cooper Basin using Etchecopar's calcite twin stress inversion technique, 2D/3D seismic interpretation and natural fracture data from image logs and core. American Association of Petroleum Geologists International Conference and Exhibition, Melbourne, Victoria, Extended Abstract 2224164.

Kulikowski D., Cooke D. and Amrouch K. 2016a. Constraining the distribution and relationship between overpressure, natural fracture density and temperature in the Cooper Basin. *The Australian Petroleum Production and Exploration Association Journal* **56**, 11–28.

Kulikowski D., Amrouch K. and Cooke D. 2016b. Geomechanical modelling of fault reactivation in the Cooper Basin, Australia. *Australian Journal of Earth Sciences* **63**(3), 295–314.

Kulikowski D., Hochwald C., Cooke D. and Amrouch K. 2016c. A statistical approach to assessing depth conversion uncertainty on a regional dataset: Cooper-Eromanga Basin, Australia. ASEG-PESA-AIG 2016 Conference, Adelaide, Extended Abstract 200, 484–490.

Kulikowski D. and Amrouch K. 2017. Combining geophysical data and calcite twin stress inversion to refine the tectonic history of subsurface and offshore provinces: a case study on the Cooper-Eromanga Basin, Australia. *Tectonics* **36**, 1–27. https://doi.org/10.1002/2016TC004366

Lowe-Young B.S., Mackie S.I. and Heath R.S. 1997. The Cooper-Eromanga petroleum system, Australia: Investigation of essential elements and processes. Indonesian Petroleum Association. *Proceedings of the Petroleum Systems of SE Asia and Australasia Conference*, Jakarta, Indonesia, pp. 199–211.

Macdonald J., Backé G., King R., Holford S. and Hillis R. 2012. Geomechanical modelling of fault reactivation in the Ceduna Subbasin, Bight Basin, Australia. *Geological Society, London, Special Publications* **367**(1), 71–89.

Mackie S. 2015. History of petroleum exploration and development in the Cooper and Eromanga Basins. AAPG/SEG international conference and exhibition, Melbourne, Australia, Search and Discovery Article 10814.

Mai H.T., Marfurt K.J. and Chávez-Pérez S. 2009. Coherence and volumetric curvatures and their spatial relationship to faults and folds, an example from Chicontepec Basin. *Proceedings of the Society of Exploration Geophysicists International Exposition and Annual Meeting*, Houston, TX, pp. 1063–1067.

Mavromatidis A. 2006. Burial/exhumation histories for the Cooper-Eromanga Basins and implications for hydrocarbon exploration, Eastern Australia. *Basin Research* **18**, 351–373.

Mildren S.D., Hillis R.R., Lyon P.J., Meyer J.J., Dewhurst D.N. and Boult P.J. 2005. FAST: a new technique for geomechanical assessment of the risk of reactivation-related breach of fault seals. In: *Evaluating Fault and Cap Rock Seals. AAPG Hedberg Series*, no. 2 (eds. P. Boult and J. Kaldi), pp. 73–85. AAPG.

Moeck I., Kwiatek G. and Zimmermann G. 2009. Slip tendency analysis, fault reactivation potential and induced seismicity in a deep geothermal reservoir. *Journal of Structural Geology* **31**(10), 1174–1182.

Morris A., Ferrill D.A. and Henderson D.B. 1996. Slip-tendency analysis and fault reactivation. *Geology* **24**(3), 275–278.

Müller R.D., Dyksterhuis S. and Rey P. 2012. Australian paleo-stress fields and tectonic reactivation over the past 100 Ma. *Australian Journal of Earth Sciences* **59**, 13–28.

Nelson E.J., Chipperfield S.T., Hillis R.R., Gilbert J., McGowen J. and Mildren S.D. 2007. The relationship between closure pressures from fluid injection tests and the minimum principal stress in strong rocks. *International Journal of Rock Mechanics and Mining Sciences* **44**, 787–801.

Neves F.A., Zahrani M.S. and Bremkamp S.W. 2004. Detection of potential fractures and small faults using seismic attributes. *The Leading Edge* **23**(9), 903–906.

Pokalai K., Fei Y., Ahmad M., Haghighi M. and Gonzalez M. 2015a. Design and optimisation of multi-stage hydraulic fracturing in a horizontal well in a shale gas reservoir in the Cooper Basin, South Australia. *The Australian Petroleum Production and Exploration Association Journal* **55**, 1–14.

Pokalai K., Haghighi M., Sarkar S., Tyiasning S. and Cooke D. 2015b. Investigation of the effects of near-wellbore pressure loss and pressure dependent leakoff on flowback during hydraulic fracturing with pre-existing natural fractures. SPE/IATMI Asia Pacific oil and gas conference and exhibition, Nusa Dua, Bali, Indonesia, SPE-176440.

Pokalai K., Kulikowski D., Johnson Jr. R. L., Haghighi M. and Cooke D. 2016. Development of a new approach for hydraulic fracturing in tight sand with pre-existing natural fractures. *The Australian Petroleum Production and Exploration Association Journal* **56**, 225–238.

Radke B. 2009. Hydrocarbon and geothermal prospectivity of sedimentary basins in Central Australia; Warburton, Cooper, Pedirka, Galilee, Simpson and Eromanga Basins. Geoscience Australia Record 2009/25.

Reynolds S.D., Mildren S.D., Hillis R.R., Meyer J.J. and Flottmann T. 2005. Maximum horizontal stress orientations in the Cooper Basin, Australia. Implications for plate-scale tectonics and local stress sources. *Geophysical Journal International* **160**, 332–344.

Reynolds S.D., Mildren S.D., Hillis R.R. and Meyer J.J. 2006. Constraining stress magnitudes using petroleum exploration data in the Cooper-Eromanga Basins, Australia. *Tectonophysics* **415**, 123–140.

Rezaee M.R. and Sun X. 2007. Fracture-filling cements in the Palaeozoic Warburton Basin, South Australia. *Journal of Petroleum Geology* **30**(1), 79–90.

Senior B.R., Galloway M.C., Ingram J.A. and Senior D. 1968. The geology of the Barrolka, Eromanga, Durham Downs, Thargomindah, Tickalara and Bulloo 1:250,000 sheet areas, Queensland. Bureau of Mineral Resources.

Sun X. 1997. Structural style of the Warburton Basin and control in the Cooper and Eromanga Basins, South Australia. *Exploration Geophysics* **28**(3), 333–339.

Sun Q., Wu S., Lü F. and Yuan S. 2010. Polygonal faults and their implications for hydrocarbon reservoirs in the southern Qiongdongnan Basin, South China Sea. *Journal of Asian Earth Sciences* **39**(5), 470–479.

van Ruth P.J., Nelson E.J. and Hill R.R. 2006. Fault reactivation potential during CO_2 injection in the Gippsland Basin, Australia. *Exploration Geophysics* **37**(1), 50–59.

Watterson J., Walsh J., Nicol A., Nell P.A.R. and Bretan P.G. 2000. Geometry and origin of a polygonal fault system. *Journal of the Geological Society* **157**(1), 151–162.

Wiprut D. and Zoback M.D. 2000. Fault reactivation and fluid flow along a previously dormant normal fault in the northern North Sea. *Geology* **28**(7), 595–598.

Wiprut D. and Zoback M.D. 2002. Fault reactivation, leakage potential, and hydrocarbon column heights in the northern North Sea. *Norwegian Petroleum Society Special Publications* **11**, 203–219.

Worum G., van Wees J.D., Bada G., van Balen R.T., Cloetingh S. and Pagnier H. 2004. Slip tendency analysis as a tool to constrain fault reactivation: a numerical approach applied to three-dimensional fault models in the Roer Valley rift system (southeast Netherlands). *Journal of Geophysical Research: Solid Earth* **109**(B2), B02401.

5.4. MANUSCRIPT 4: Stratigraphic architecture and fault activity

3D seismic analysis investigating the relationship between stratigraphic architecture and structural activity in the intra-cratonic Cooper and Eromanga basins, Australia

The structurally complex Cooper-Eromanga Basin is Australia's largest onshore hydrocarbon province with large potential in unconventional energy. This region is known to have experienced a number of tectonic events; however, the intrinsic relationship between these six events and their effect on the stratigraphic architecture of the basin is presently unknown. We depth convert and interpret four three-dimensional seismic surveys to find that on-lapping features are abundant within the basin and closely related to the repeated reactivation of basement faults. Cross-sections, isopach maps, incoherency analysis, and fault interpretation are presented for each of the seismic surveys. This research presents new data that:
(1) can improve hydrocarbon exploration and development programs;
(2) better constrain the tectonostratigraphic evolution of this complex basin; and
(3) provides a working framework for future work that will investigate the sub-seismic resolution stratigraphic architecture (well correlations) of the prolific Patchawarra Formation.

CITATION:
Kulikowski, D., & Amrouch, K. (2017). 3D seismic analysis investigating the relationship between stratigraphic architecture and structural activity in the intra-cratonic Cooper and Eromanga basins, Australia. Marine and Petroleum Geology, under review.

Statement of Authorship

Title of Paper:	3D seismic analysis investigating the relationship between stratigraphic architecture and structural activity in the intra-cratonic Cooper and Eromanga basins, Australia
Publication Status:	**Manuscript Submitted**
Publication Details:	Kulikowski, D., & Amrouch, K. (2017). 3D seismic analysis investigating the relationship between stratigraphic architecture and structural activity in the intra-cratonic Cooper and Eromanga basins, Australia. Marine and Petroleum Geology, under review

Principal Author

Principal Author (Candidate):	David Kulikowski		
Contribution to the Paper:	Seismic interpretation, analysis, and writing.		
Overall percentage (%):	90%		
Certification:	This paper reports on original research I conducted during the period of my Higher Degree by Research candidature and is not subject to any obligations or contractual agreements with a third party that would constrain its inclusion in this thesis. I am the primary author of this paper.		
Signature:		Date:	29 March 2017

Co-Author Contribution

By signing the Statement of Authorship, each author certifies that:

i. the candidate's stated contribution to the publication is accurate (as detailed above);

ii. permission is granted for the candidate to include the publication in the thesis; and

iii. the sum of all co-author contributions is equal to 100% less the candidate's stated contribution.

Name of Co-Author:	Khalid Amrouch (10%)		
Contribution to the Paper:	Provided feedback on analysis and a complete review of paper.		
Signature:		Date:	29 March 2017

3D Seismic Analysis Investigating the Relationship Between Stratigraphic Architecture and Structural Activity in the Intra-cratonic Cooper and Eromanga Basins, Australia

*David **Kulikowski**[a] (david.kulikowski@adelaide.edu.au)

Khalid **Amrouch**[a] (khalid.amrouch@adelaide.edu.au)

[a]Australian School of Petroleum, University of Adelaide, North Tce, 5005, Adelaide, AUS.

*Corresponding author: David Kulikowski (+61 435 135 148)

ABSTRACT

This research uses four three-dimensional (3D) seismic surveys located in Australia's largest onshore hydrocarbon province, the intra-cratonic Cooper and Eromanga basins, to present an approach that extracts important structural and stratigraphic information from geophysical data that can then be used to define the tectonostratigraphic evolution of subsurface provinces. The methodology consists of: (1) analysing isopach maps; (2) cross-section interpretation of stratigraphic features, erosional surfaces, and faults; and (3) constraining the evolution of fault activity. Most faults within this province are basement-involved with high dip angles. The primary fault set is NE-SW striking, with secondary sets striking N-S, E-W and NW-SE. These high angled faults most likely developed as normal faults before being reactivated by five of the six major tectonic events. Field scale NW-SE strike-slip faults are prolific and can often be overlooked due to the low seismic resolution. A close relationship between on-lapping features and present-day structural highs was found during each of the major structural events, particularly within hydrocarbon-rich Permian stratigraphy, inferring that present-day structures were present throughout basin development and intermittently reactivated. Significant stratal-package thinning, and a high presence of on-lapping features, were associated with regional basement-involved faults, particularly along the Gidgealpa-Merrimelia-Innamincka and Murteree-Nappacoongee ridges. Initial structural trap development occurred during the early Permian, but was most significant during the Late Triassic. Hydrocarbon accumulations were unaffected by structural growth after the critical moment in the petroleum system (90 Ma), as the final period of fault activity was during the Late Cretaceous. This research constrains the tectonostratigraphic evolution of the intra-cratonic Cooper and Eromanga basins, while detailing an approach that extracts and analyses important structural and stratigraphic information from geophysical data, where outcrop is not accessible.

KEY WORDS: Seismic; Interpretation; Stratigraphy; Fault; Tectonics; Hydrocarbon; Cooper Basin; Eromanga Basin.

1. INTRODUCTION

Structural and stratigraphic studies are often accompanied by hard data measured directly from outcrop (e.g. Lacombe et al., 2007, 2009; Amrouch, 2010; Amrouch et al., 2010a, 2010b, 2011; Beaudoin et al., 2012, 2014; Lin and Yamashita, 2013; Arboit et al., 2015, 2017; Burgin et al., 2018); however, this is difficult in regions that are entirely subsurface. For such provinces, wellbore core and geophysical data analysis are the only means of obtaining important structural and stratigraphic information and can be equally as representative as direct measurements from outcrop (e.g. Cartwright et al., 1998; Wiprut and Zoback, 2000; Manzi et al., 2015; Szalaiová et al., 2015; Kulikowski et al., 2017; Kulikowski and Amrouch, 2017; Ryan et al., 2017). Three-dimensional (3D) seismic surveys covering the subsurface Cooper and Eromanga (Cooper-Eromanga) Basins (Fig. 1), Australia, are used as a case study for this work to present a methodological approach for constraining the relative timing of structural activity through the interpretation and analysis of the present-day stratigraphic architecture of the region. Development of accurate 3D tectonic and stratigraphic models are fundamental to gain a better understanding of the evolution of subsurface provinces, as they: (1) present the influence of structural growth, or subsidence, on the depositional patterns within a basin; (2) assist in constraining the periods of structural movement, fault reactivation and timing of structural trap development; (3) can be used to develop hydrocarbon migration pathway and accumulation models; (4) constrain the preferred location of sediment deposition through time; and (5) assist in the exploration and development of hydrocarbons.

Insert Fig. 1

The structural and stratigraphic complexity of the Cooper-Eromanga Basin (Fig. 1) has been conjectural since its first commercial hydrocarbon discovery in 1963 (Gravestock and Jensen-Schmidt, 1998). The majority of hydrocarbons in this province are reservoired within Permian fluvial sediments with exploration companies currently exploring for stratigraphic traps that have a close association with paleo-structural highs (Fig. 2) (Gravestock et al., 1998). Although significant research has been made to better understand the evolution of this basin (Kantsler et al., 1983; Kuang, 1985; Apak et al., 1997; Sun, 1997; Kulikowski and Amrouch, 2017), the intricate relationship between fault movement and the stratigraphic architecture remains poorly defined, and is in part due to a conservative approach when drawing conclusions from old, poor resolution and sparse two-dimensional (2D) seismic lines that were not time-to-depth converted. The difficulty of interpreting old and poor resolution 2D seismic data within the Cooper-Eromanga Basin is showcased in the transition between fault models, alternating between interpretations of extensive normal faulting (Gatehouse, 1986; Gravestock and Jensen-Schmidt, 1998), to interpreting the same structures as

reverse faults (Sun, 1997), and to relatively more recent models that accept the presence of strike-slip features amongst inverted faults (Kuang, 1985; Apak et al., 1997; Grant-Wooley et al., 2014; Kulikowski and Amrouch, 2017; Kulikowski et al., 2017).

Insert Fig. 2

This study uses four 3D seismic surveys, located along major structural features, to define the tectonostratigraphic evolution of the intra-cratonic Cooper-Eromanga Basin (Fig. 3). Seismic data was depth converted, re-processed into incoherency volumes, interpreted for faults, stratigraphically interpreted, and divided into key stratal-units to create isopach maps. Cross-sections are interpreted through each of the 3D seismic surveys to constrain the timing and distribution of stratigraphic features related to structural growth, and to define the distribution and geometry of faults. To improve the accuracy of fault interpretation and assist in determining the depth of fault termination, seismic incoherency analysis is incorporated into the methodology and extracted along four key seismic reflector surfaces. The results are presented for seven hydrocarbon producing field to ensure minor details are not overlooked and to make it simple for readers to access data. The results are also discussed in a basin-wide context through time to provide regional relationships between structural growth and the distribution of stratigraphic features within hydrocarbon-rich stratal-units. The six structural events are finally linked to their influence on sediment deposition, erosion, and the timing of structural and stratigraphic trap development.

Insert Fig. 3

The structurally complex Cooper-Eromanga Basin has been affected by numerous regional tectonic events (Alice Springs: 450-300 Ma; Mid-Permian: 290-270 Ma; Daralingie: 258 Ma; Hunter-Bowen: 245-190 Ma; Late Cretaceous: 95-65 Ma; and Paleogene: 33-23 Ma) and undergone local stages of compression and flexural relaxation, which has developed a tectonostratigraphic architecture that is difficult to determine (Kulikowski and Amrouch, 2017). The difficulty is further compounded by the absence of outcrop and the previous use of poor resolution and sparse 2D seismic data (Kuang, 1985; Apak et al., 1997; Gravestock and Jensen-Schmidt, 1998). The uncertainty of seismic interpretation below the thick Permian coal measures enhances the difficulty of stratigraphic interpretation. Results from this study provide insights into the intricate relationship between structural movement, sediment deposition, and structural trap development that can be used for future hydrocarbon exploration and development programs and highlights the benefit of such studies to subsurface provinces where measurable outcrop is not available.

2. GEOLOGICAL SETTING

The Late Carboniferous to Middle Triassic Cooper Basin is a structurally complex intra-cratonic basin that is separated by unconformities to the overlying Jurassic to Cretaceous Eromanga Basin, and the underlying Cambrian to Silurian Warburton Basin (basement) (Fig. 2) (Kantsler et al., 1983; Bradshaw, 1993; Apak et al., 1997; Gravestock and Jensen-Schmidt, 1998; Kulikowski et al., 2016a, 2016b). Understanding the evolution of this province has proven a difficult task, with early works providing contradicting results (Kantsler et al., 1983; Kuang, 1985; Bradshaw, 1993; Apak et al., 1997; Sun, 1997; Gravestock and Jensen-Schmidt, 1998), which was largely due to the use of poor resolution and sparse 2D seismic lines that remained in the time domain.

Literature does show that initial accommodation space developed during the NW-SE Adelaidean Extensional Event (650 Ma), which created a regional NE-SW striking normal fault set (Apak et al., 1997; Haines et al., 2001). This fault set was reactivated by subsequent events give their present-day geometry (Apak et al., 1997; Haines et al., 2001). Recent work (Kulikowski and Amrouch, 2017) has applied stress inversion techniques to calcite twin, natural fracture and fault data to constrain the evolution of the province to six events, which follow on from initial extension; (1) N-S Carboniferous Alice Springs Event; (2) NW-SE Mid-Permian Event; (3) NE-SW Late Permian Daralingie Event; (4) E-W Late Triassic Hunter-Bowen Event; (5) E-W Late Cretaceous Event; and (6) N-S Paleogene Event.

The N-S Alice Springs Event is believed to have applied dextral motion along some NW-SE striking pre-existing basement-involved faults and facilitated exhumation of the Carboniferous Big Lake Granite Suit (Shaw et al., 1991; Apak et al., 1997; Rezaee and Sun, 2007; Glikson et al., 2013; Kulikowski et al., 2016b). This event created a regional unconformity upon which late Carboniferous sediments were deposited (Fig. 2) (Kuang, 1985; Apak et al., 1997; Sun, 1997; Mavromatidis, 2006). As the Australian continent began to escape glaciation, glacial sediments were deposited onto this regional unconformity forming the Merrimelia Formation (Kantsler et al., 1983; Apak et al., 1997). Based on sparse 2D seismic lines, the early Permian Merrimelia Formation, together with the overlying, fluvially deposited, early Permian Tirrawarra Formation, show signs of structural control on deposition (Apak et al., 1997). A transition from a fluvial to a peat swamp and floodplain environment encouraged deposition of the middle Permian Patchawarra Formation, which cycles between coals, shales and sands (Alexander et al., 1998; Boreham and Hill, 1998).

Onset of the NW-SE Mid-Permian Event is evidenced in 2D seismic data as the early to middle Patchawarra Formation onlaps onto major paleo-highs (Kantsler et al., 1983; Apak et al., 1997). Mild compression continued until the upper Patchawarra Formation deposition (Apak et al., 1997).

Regional sag promoted the deposition of the fluvial Late Permian Toolachee Formation, which cycles in coal, shale and sands, and the Triassic Nappamerri Group, consisting of sands, shales and a distinct lack of coals (Kantsler et al., 1983; Apak et al., 1997). The Late Permian Murteree Shale, Epsilon Formation, Roseneath Shale and Daralingie Formation were deposited during an east to west transgression that facilitated regional sea level rise (Bradshaw, 1993; Apak et al., 1997; Gravestock and Jensen-Schmidt, 1998). Much of the Daralingie Formation was eroded post deposition during the NE-SW Daralingie Event, which peneplaned the basin (Apak et al., 1997).

Prior to the E-W Late Triassic Hunter-Bowen Event, Permian to Triassic sediments reached their maximum burial depth, before being exhumed up to 2700 m at the onset of compression (Apak et al., 1997; Mavromatidis, 2006). This event eroded up to 500 m of Nappamerri Group sediments and is marked as a regional unconformity (Kantsler et al., 1983; Apak et al., 1997; Alexander et al., 1998; Mavromatidis, 2006). The top-Permian to basement sediment thickness increases in the South Australian portion of the basin, particularly within the Nappamerri Trough (Fig. 1).

Significant post-compressional flexural relaxation (or sag) vastly increased accommodation space between the Lower Jurassic and the upper Cretaceous, allowing fluvio-deltaic and lacustrine sediment deposition (Green et al., 1989; Lowe-Young et al., 1997). This extensive period of uninterrupted deposition seized with the onset of the E-W Late Cretaceous Event that regionally eroded the upper Cretaceous Winton Formation, and is marked by the regional unconformity (Kantsler et al., 1983; Apak et al., 1997; Gravestock and Jensen-Schmidt, 1998; Mavromatidis, 2006). This is the critical moment in the Cooper-Eromanga petroleum system (90 Ma), where major hydrocarbon accumulation commenced, and NE-SW trending anticlinal traps likely formed (Lowe-Young et al., 1997; Gravestock and Jensen-Schmidt, 1998; Müller et al., 2012).

3. SEISMIC REFLECTION DATA

3.1 DATASET

This study utilises four publicly available 3D seismic surveys covering the Swan Lake Field (Swan Lake 3D), Gidgealpa Field (Gidgealpa 3D), Dullingari Field (Dullingari 3D), and the Della, Marabooka, and Strzelecki fields (Greater Strzelecki 3D) (Fig. 3). The Swan Lake (acquired 2000), Gidgealpa (acquired 2002), Dullingari (acquired 1997) and Greater Strzelecki (acquired 2001) 3D seismic surveys were chosen based on their high well density (well check-shot and formation top data), and their relative locations to major structural features, including the Gidgealpa-Merrimelia-Innamincka (GMI) and Murteree-Nappacoongee (MN) ridges that would provide the most insights into the relationship between structural movement and sediment deposition.

3.2 DEPTH CONVERSION

Correlation of seismic reflectors to stratigraphic well markers was made possible by importing check-shot and formation top well data to convert the 3D seismic data from two-way-time (TWT) to depth (m). The seismic time-to-depth conversion used the time to depth relationship and average velocity data to generate a unique velocity model for each of the 3D seismic surveys (Fig. 4). Seismic time-to-depth conversion ensured that a 1:1 (horizontal: vertical) scale was used to accurately interpret structural and stratigraphic features. Error is introduced into isopach maps and fault geometry measurements during the seismic time-to-depth conversion process as there are many methods that can be used; average velocity, interval velocity, stacking velocity and time-depth trend methods. Recent work investigated the accuracy of seismic time-to-depth conversion methods on a regional scale within the Cooper-Eromanga Basin and showed that the accuracy of these methods changes by 10's of feet depending on the unique dataset being used (Kulikowski et al., 2016c). The major cause for the variation in average velocity is difficult to identify; however, may be associated with local changes in fault density, stratigraphy, cementation, compaction, or near surface statics (Al-Chalabi et al., 1974; Lowe-Young et al., 1998; Kulikowski et al., 2016c).

Insert Fig. 4

3.3 INTERPRETATION TECHNIQUE

The depth converted 3D seismic surveys were structurally and stratigraphically interpreted using a 1:1 scale to ensure that all interpretations were made using true angles and true thicknesses. The interpretation utilised standard interpretation techniques (e.g. Mitchum et al., 1977; Vail et al., 1977) that included seismic reflector tracing, calculating chrono-stratigraphic thickness, and incoherency (i.e. coherency or similarity) and reflectivity mapping. Horizons were initially picked from well formation tops and tied together along arbitrary lines to give an initial framework. A framework of 6 seismic reflectors (top Wallumbilla Formation, top Cadna-owie Formation, top Nappamerri Group, top Toolachee Formation, top Patchawarra Formation, and top VC Coal) (Fig. 2) was used to divide the seismic volume into five seismic packages. This approach is commonly used to define the thickening trends of individual packages across a study area. Increases in sediment thickness may infer an increase in the accommodation space, and an obvious thinning may infer erosion post deposition, or restricted accommodation space during deposition. It is difficult to constrain fluctuation of sediment supply during basin evolution and also to consider the effect of compaction on Permian stratigraphy, where sands, shales, and coals can alternate (<1 foot) at a sub-

seismic resolution scale. These were not considered in this study and presents an opportunity for future research. Any attempt to de-compact the stratigraphy would provide misleading results.

Fault interpretation was governed by the present day structural model for the Cooper-Eromanga Basin, in that extensive, compressive and strike-slip stress regimes have dominated its structural evolution (Kulikowski and Amrouch, 2017). The interpretation of strike-slip faults, which are vague or not present in cross-section, required the creation of depth-slices through the seismic volumes to resolve lateral offsets. Offset along inclined faults is best resolved in cross-section, with reactivation interpreted in areas that show either: (1) an erosional feature along a given reflector to suggest inversion; (2) reduced stratal unit thickness across paleo-highs to infer a structural influence on deposition; or (3) thickening of packages towards a fault to infer normal reactivation (Mitchum et al., 1977; Kuang, 1985; Stanmore and Johnstone, 1988; Apak et al., 1997; Gravestock and Jensen-Schmidt, 1998; Giba et al., 2012; Jackson and Rotevatn, 2013; Robson et al., 2017a, 2017b). However, seismic interpretations such as these become difficult with increasing depth, particularly below the Permian coal measures where seismic resolution is significantly reduced and prevents fault growth analysis, which may only become possible with improved seismic acquisition and processing techniques.

3.4 ATTRIBUTE ANALYSIS

A useful seismic attribute for fault interpretation is incoherency (i.e. coherency or similarity). Incoherency visually enhances the discrepancies along a seismic horizon or depth-slice to assist in identifying faults that may have otherwise been overlooked (Neves et al., 2004; Mai et al., 2009; Basir et al., 2013). Incoherency analysis was used as a first-pass look into the expected fault distribution and geometries before interpretation. Isopach maps were generated between five of the key seismic reflectors within each 3D seismic survey by subtracting the depth of one reflector surface from a second reflector surface. Four key stratal-packages (SP) were used for analysis: (1) SP1: top Cadna-owie Formation to top Nappamerri Group reflectors; (2) SP2: top Nappamerri Group to top Toolachee Formation reflectors; (3) top Toolachee Formation to top Patchawarra Formation reflectors; and (4) SP4: top Patchawarra Formation to top VC Coal reflectors (Fig. 2). The output isopach maps allowed inferences to be made regarding the depositional and erosional trends of individual stratigraphic packages. Although not a complex seismic attribute, the change in amplitude along reflectors can also provide information on the lateral changes in the relative rock properties. This information can be used to infer reduced accommodation space or erosion where amplitude decreases, or unrestricted sediment deposition where amplitude is high. This type of analysis is used to accompany the results and does not form the core component of evidence.

4. 3D SEISMIC DATA INTERPRETATION

The results presented here highlight the key changes in the stratigraphic architecture for four stratal-packages (SP1, SP2, SP3, and SP4) (Fig. 2) with commentary on the present-day structural architecture. Depth-slices and incoherency mapping along key seismic reflector surfaces are used to identify the main structural features. Stratigraphic features are interpreted in cross-sections and the fault distribution and geometry within each of the seven hydrocarbon fields is presented.

4.1 SWAN LAKE FIELD

The Swan Lake Field is located along the GMI Ridge, northeast of the Gidgealpa Field (Fig. 3). The anticlinal structure is bound from the northwest and southeast by inverted faults (Fig. 5a). A cross-section through the field depicts a dominant array of high angle faults within basement that periodically penetrate overlying sediments (Fig. 5c and 5d). Vertical NW-SE striking faults were also interpreted within the basement and lower Patchawarra Formation (Fig. 5). The main fault strike in this field is NE-SW, with minor fault sets striking E-W, N-S, and NW-SE (Fig. 6). Faults are observed to have a high dip angle (60°), with NW-SE strike-slip faults also present (Fig. 6c). The majority of NE-SW striking faults terminate after displacing the top VC Coal reflector, with N-S striking faults extending into the Nappamerri Group. A system of layer bound normal faults exists within upper Cretaceous sediments, enhanced using incoherency along the top Wallumbilla Formation reflector and visible in cross-section (Fig. 5 and 7).

Insert Fig. 5

Insert Fig. 6

Insert Fig. 7

A cross-section view of the Swan Lake Field shows considerable thinning of Permian and Triassic sediments above the present day structural high, with on-lapping of the middle Patchawarra Formation evident (Fig. 5). Isopach maps were generated to visually show the variation in sediment thickness (Fig. 8). Each of the isopach maps show relative thinning above the present day structural high along the GMI Ridge. The isopach map for SP1 shows thinning in the east of the study area and thickens to the west. The SP2 isopach map (Fig. 8b) shows thinning in the west of the study area near the Tindilpie group of wells. The amplitude of the top Wallumbilla and top Cadna-Owie formation reflectors remain consistently strong across the study area unless intersected by a fault. The amplitude of the top Nappamerri Group reflector is reduced in all areas with underlying faults,

similarly with the Toolachee Formation, Patchawarra Formation and VC Coal reflectors, which have a much more rapid decrease in amplitude adjacent to basement faults.

Insert Fig. 8

4.2 GIDGEALPA FIELD

The Gidgealpa Field is located along the GMI Ridge (Fig. 3) and comprises of a northern and southern dome, both producing oil and gas and elongated in a NE-SW direction (Fig. 9a). The field is held to the west by the main NE-SW striking inverted fault that terminates below the top Cadna-owie Formation reflector (Fig. 9b). Most of the interpreted faults are basement involved and have a NE-SW strike with high dip angles (60°) (Fig. 6d) and generally terminate within the Patchawarra Formation (Fig. 9). Near vertical faults striking NW-SE are interpreted to terminate prior to the top Patchawarra Formation and have a dextral sense of motion when viewed in depth-slice (Fig. 9e). A system of randomly oriented and layer bound faults were interpreted within upper Cretaceous sediments (Fig. 9) and are visually enhanced using incoherency along the top Wallumbilla Formation (Fig. 10a).

Insert Fig. 9

Insert Fig. 10

On-lapping of the Merrimelia, Tirrawarra and intra-Patchawarra formations is evident across the main structural highs. The SP4 isopach map (Fig. 11d) thins across the structural high, with on-lapping evident in cross-section (Fig. 9). The cross-sections through the northern dome (Fig. 9b and 9c) depict intra-formational on-lapping of the lower Jurassic sediments, which is again evidenced through an isopach map of SP2 (Fig. 11). The sedimentation between these successive on-lapping events does not vary in thickness and shows strong amplitude throughout the survey along the top Wallumbilla Formation, top Cadna-owie Formation and top Nappamerri Group reflectors. The amplitude along the top Toolachee Formation, top Patchawarra Formation and top VC Coal reflectors are strongest above underlying faults and decrease away from the present day structural high, implying that normal reactivation of major faults may have generated accommodation space.

Insert Fig. 11

4.3 DELLA FIELD

The Della Field is a NE-SW elongate fault-bounded anticline located along the MN Ridge (Fig. 3 and 12a). The interpreted faults are presented as strikes (Fig. 6g), poles to planes (Fig. 6h), and planes

(Fig. 6i). NE-SW striking faults with high dip angles (60º) are most common, with few NW-SE striking near vertical faults also present (Fig. 6i and 12b). Most high angle faults extend from basement and terminate in the middle Patchawarra Formation; only NW-SE striking faults terminate between the top Patchawarra and top Toolachee formation reflectors (Fig. 12).

Insert Fig. 12

North of the Della Field, the main NE-SW striking fault divides into two inverted faults (Fig. 12a). Cross-sections through the field show this fault displacing the top Nappamerri Group reflector and terminating prior to the top Cadna-owie Formation (Fig. 12c and 12d). Incoherency along the top Cadna-owie Formation and top Nappamerri Group supports that the fault does not displace the top Cadna-owie Formation (Fig. 13a and 13b). The southern segment of this NE-SW striking fault appears to divide, or split, from the main fault between the Patchawarra and Toolachee formations. This is clear when comparing the top Toolachee Formation and top Patchawarra formation incoherency maps (Fig. 13c and 13d), which may indicate a fault relay zone or coherent fault growth.

Insert Fig. 13

Incoherency along the top Wallumbilla Formation reflector shows an array of layer bound normal faults that have no obvious organisational pattern (Fig. 13a). The cross-sections through the field (Fig. 12) show high angle normal faults present within upper Cretaceous sediments. Periodically, these normal faults displace the top Cadna-owie Formation, which is evident in the incoherency map along the top Cadna-owie Formation reflector (Fig. 13b). The isopach map of SP1 shows thinning in the southwest portion of the field (Fig. 14a). Substantial thinning is observed between the top Toolachee Formation to top VC Coal, and also in the SP2 isopach map (Fig. 14). Sediment thickness of packages is better observed in cross-section (Fig. 12) where on-lapping was interpreted during the Tirrawarra Formation and Merrimelia Formation deposition, as well as during the deposition of the middle Patchawarra Formation. Amplitude is consistently strong through the Della Field along each of the reflectors. A strong amplitude channel-like feature is identified along the top Nappamerri Group reflector (Fig. 14f) and is also observed in the SP1 isopach map (Fig. 14b). The top Toolachee Formation reflector is strongest in the north Della Field region.

Insert Fig. 14

4.4 MARABOOKA FIELD

The Marabooka Field is located less than 5 km northwest of the Strzelecki Field and less than 10 km south of the Della Field (Fig. 3). The field contains dominantly NW-SE and NNE-SSW striking faults

with high to near vertical dip angles evident when projected on stereonets (Fig. 6u). Large scale NW-SE, NNE-SSW, and NE-SW striking faults contain the Marabooka Field from the north, west and southeast, respectively (Fig. 12a). NW-SE striking dextral strike-slip faults were also identified in a depth-slice (Fig. 14e).

Cross-sections through the field shows the fault angle and the termination points of faults (Fig. 15). Several NW-SE striking high angle (60°) faults terminate between the top Toolachee and top Patchawarra formations, while the majority of NE-SW striking high angle (60°) faults terminate within the Patchawarra Formation (Fig. 15). Incoherency along the top VC Coal reflector visually highlights the dominance of NE-SW striking faults (Fig. 13d). The main NW-SE striking fault is observed to extend into the Nappamerri Group, together with the northern segment of the main NNE-SSW striking fault (Fig. 15). A system of layer bound normal faults was interpreted within upper Cretaceous sediments, as illustrated in cross-section (Fig. 15). Incoherency along the top Wallumbilla Formation illustrates the variable geometry of these normal faults (Fig. 13a).

Insert Fig. 15

Isopach maps for the key stratal-packages highlights areas of sediment thinning and the location of local depocenters through time (Fig. 14). The SP1 isopach map forms a channel-like feature through the centre of the field with thinning evident on either side (Fig. 14b). This feature is highlighted using amplitude mapping (Fig. 14f). Isopach maps for the remaining stratal-packages show thinning across the present day structural high (Fig. 14) with non-deposition of the Tirrawarra and Merrimelia formations on the present day structural high evident from cross-sections (Fig. 15). Intra-formational on-lapping of the Patchawarra Formation was also interpreted in cross-section (Fig. 15). The amplitude along the top Toolachee Formation and top VC Coal reflectors are significantly weaker when compared to adjacent areas, such as the Della Field.

4.5 STRZELECKI FIELD

The Strzelecki Field is an NE-SW striking anticline 5 km southeast of the Marabooka Field (Fig. 12). The field contains NE-SW and NW-SE striking basement faults below major anticlinal structures. NW-SE strike-slip faults were interpreted from seismic depth-slices. The dominant strike of faults interpreted from this field is WNW-ESE with high dip angles (60°) (Fig. 6p and 6r). The majority of interpreted high angle faults begin from basement and terminate prior to early Permian sediments (Fig. 16). The major NE-SW striking fault bounding the Strzelecki Field from the north terminates after displacing the top VC Coal reflector (Fig. 16). An N-S striking high angle (60°) fault with reverse displacement that contains the field from the west (Fig. 12a) extends into the top Nappamerri Group

(Fig. 16). A system of layer bound normal faults can be identified along the top Wallumbilla Formation reflector when viewed in incoherence (Fig. 13a). The randomly oriented geometry of these normal faults is better observed in cross-section (Fig. 16) and shows a number of these normal faults extending from the Wallumbilla Formation to displace the underlying top Cadna-owie Formation reflector (Fig. 16).

The isopach maps show significant thinning above the present day structural high (Fig. 14). The cross-sections through the field show significant on-lapping of the Merrimelia and Tirrawarra, and Patchawarra formations (Fig. 16). Intra-formational on-lapping features are again present within the Patchawarra Formation (Fig. 16). Each of the interpreted reflectors decrease in amplitude above the present day structural high, with a large strong amplitude channel-like feature bisecting the field along the top Nappamerri Group reflector (Fig. 14f).

Insert Fig. 16

4.6 KIDMAN-BAGUNDI FIELDS

The Kidman-Bagundi Fields are situated 15 km east of the Strzelecki Field and southwest of the Dullingari Field (Fig. 12a). Structural highs coincide with underlying basement faults, which have a dominant N-S strike, as well as NW-SE, E-W and NE-SW striking faults (Fig. 6m). The stereographic projection of faults shows high dip angle (60°), with some N-S and NW-SE striking faults plotted close to vertical (Fig. 6o). A cross-section through the field shows the fault geometry (Fig. 17). Basement faults rarely penetrate Permian strata, but can be found to displace middle Patchawarra Formation sediments. The main N-S striking near vertical fault that bounds the fields from the east extends into the Cadna-owie Formation when viewed in cross-section (Fig. 17b and 17c).

Incoherency along the top Cadna-owie Formation highlights this fault in the southern portion of the study area, which appears to gradually fade to the north (Fig. 13b). An irregular surface feature is observed along the top Toolachee Formation reflector when viewed in incoherence (Fig. 13c). This feature is a system of curved structural highs with a smooth erosional-like surface that trends parallel to adjacent NW-SE striking faults. Incoherency along the top Wallumbilla Formation visually enhances a system of layer bound normal faults present within Cretaceous stratigraphy (Fig. 13a). Cross-sections through the field show the dip angle of these faults and identify a several faults extending into the Cadna-owie Formation (Fig. 17). Figure 14f shows the continuation of the strong amplitude channel-like feature from the Della, Marabooka, and Strzelecki fields. Reflector amplitude is strongest along the top Toolachee Formation and much weaker along the top VC Coal reflector.

Although the relative thinning of isopach maps in this study area are not to the same degree as the Strzelecki Field (Fig. 14), the Kidman-Bagundi area shows significant thinning of the Tirrawarra and Merrimelia formations, Patchawarra Formation, and Nappamerri Group adjacent to underlying basement faults. This is also observed in cross-sections through the area (Fig. 17). Intra-formational on-lapping features are observed within the Patchawarra Formation (Fig. 17a).

Insert Fig. 17

4.7 DULLINGARI FIELD

The Dullingari Field is an oil and gas producing field that is divided into the northern and main domes by a structural saddle. The Dullingari Field is bound from the south by the major E-W striking saw-tooth-like fault (Fig. 12a and 18a). This fault curves to strike N-S in the western portion of the study area and increases in throw to the east. Incoherency mapping of the top Toolachee and top Cadna-owie formations (Fig. 19b and 19c), together with a cross-section through the main field (Fig. 18c and 18d), show that the main fault terminates in the Middle Triassic after displacing the top Toolachee Formation reflector. NE-SW striking high angle (60º) faults are observed throughout the Dullingari Field, with fewer faults striking E-W and N-S (Fig. 6j). The E-W and N-S striking faults displace the top Patchawarra Formation reflector and terminate prior to the top Toolachee Formation (Fig. 18c). Dextral NW-SE strike-slip faults are interpreted from depth-slices and picked in cross-section to show that they generally terminate in the middle Patchawarra Formation after displacing the top VC Coal reflector (Fig. 18b). A layer bound system of normal faults was again interpreted in upper Cretaceous sediments (Fig. 18c and 18d) and visually enhanced using incoherency along the top Wallumbilla Formation reflector (Fig. 19a).

Insert Fig. 18

Insert Fig. 19

Wells drilled in this area do not intersect the Tirrawarra and Merrimelia formations, inferring their non-deposition or erosion (Fig. 18c and 18d). The top Toolachee to top VC Coal isopach map shows substantial thinning along the eastern edge of the main fault and along NE-SW striking lineaments (Fig. 20d). A cross-section through the Dullingari Field shows obvious on-lapping of the middle Patchawarra Formation after VC Coal deposition (Fig. 18c). The SP2 isopach map shows thinning along the entire main E-W fault and isolated areas in Dullingari North (Fig. 20c). When viewed in cross-section, the lower Nappamerri Group sediments on-lap onto the Toolachee Formation (Fig. 18d). The thickness of SP1 shows thickening from the east (440 m) to the west (530 m), appearing as though the eastern edge of the survey has been uplifted relative to the western edge (Fig. 20b).

The amplitude along reflectors, particularly within the Permian section, changes between strong and weak very rapidly to form isolated sections of strong amplitude. The amplitude along the top Patchawarra Formation reflector is strongest on the southern side of the main E-W striking fault and significantly weaker above the present day structural highs. The amplitude of the top VC Coal reflector is highly variable throughout the survey, showing strong amplitude in the east and south of the survey and significantly weak amplitude in the north. The top Toolachee Formation reflector increases in amplitude in the south and east of the survey and is consistently high across sections of the E-W striking fault in the western half of the survey.

Insert Fig. 20

5. DISCUSSION

The link between the stratigraphic architecture and tectonic activity in the Cooper-Eromanga Basin is poorly defined in literature, often presented in as separate research topics. To better understand this complex relationship in the intra-cratonic basin, we present new data detailing the effect that each of the six structural events has had on the stratigraphic architecture, fault activity, and structural trap development.

The fault strike across all 7 fields is shown to trend NE-SW, with generally high dip angles (60º) (Fig. 6v). A smaller sample size of N-S, E-W and NW-SE striking faults were also interpreted. These faults typically extend from basement into younger sediments and can be seen to broadly mimic the regionally pervasive natural fracture geometry within the basin (Pokalai et al., 2016; Kulikowski et al., 2016b, 2017; Kulikowski and Amrouch, 2017). A high proportion of interpreted faults have reverse sense of motion albeit their high angle. Due to poor seismic resolution at this depth, fault growth analysis is not possible to constrain the precise movement of these faults through time. However, Andersonian faulting theory (Anderson, 1905) demonstrates that these high angle (60º) faults developed under an extensional stress regime. This fault set is now inverted suggesting that it was critically oriented to reactivate under shear during subsequent compressional and strike-slip stress regime events. Given the absence of low dip angle faults, the reactivation of pre-existing faults was likely to be more stress economic than developing new faults during the four compressional stress regime events (Anderson, 1905).

A near vertical fault set striking approximately NW-SE with dextral lateral offset was also interpreted. This strike-slip fault set is interpreted within most of the seven fields and consistently terminates either in Pre-Permian or middle Patchawarra Formation sediments. Recent works have also interpreted near vertical NW-SE and NNE-SSW strike-slips faults on both the regional and field

scale (Grant-Woolley et al., 2014; Kulikowski et al., 2016a, 2017; Kulikowski and Amrouch, 2017) that are believed to have developed, or reactivated, during the N-S Alice Springs Event. The relationship between structural movement and the stratigraphic architecture of the basin is analysed for the following six events.

5.1 CARBONIFEROUS ALICE SPRINGS EVENT (400-300 Ma)

The N-S Alice Springs Event developed and/or reactivated NW-SE and NNE-SSW strike-slip faults that exhumed the Big Lake Granodiorite and formed a regional unconformity that separates the Cambrian to Silurian basement to the overlying stratigraphy (Fig. 2) (Kantsler et al., 1983; Kuang, 1985; Apak et al., 1997; Sun, 1997; Kulikowski and Amrouch, 2017; Kulikowski et al., 2017). Reduced accommodation space during this time is evident in each of the 3D seismic surveys as NE-SW striking high angle faults are reactivated to prevent or inhibit the deposition of the Tirrawarra and Merrimelia formations along present-day structural highs. These formations on-lap onto basement in the Gidgealpa (Fig. 9b, 9c and 9d), Della (Fig. 12c and 12d), Marabooka (Fig. 15a and 15b), Strzelecki (Fig. 16a), and Kidman-Bagundi (Fig. 17a and 17b) fields. This stratigraphic package shows subtle thinning above the Swan Lake Field (Fig. 5c and 5d) and non-deposition within the Dullingari Field (Fig. 18c and 18d). The Alice Springs Event had a substantial impact on the deposition of the Tirrawarra and Merrimelia formations along the GMI and MN ridges, inferring that these were prominent pre-Permian features.

5.2 MID-PERMIAN EVENT (273-270 Ma)

Small, field scale NE-SW striking high angle (60^{o}) faults generally terminate during the deposition of the middle Patchawarra Formation and likely reactivated by the NW-SE Mid-Permian Event. The NW-SE Mid-Permian Event was optimally oriented to have reactivated these NE-SW striking faults, which appear to have interacted with the paleo-free surface and exhumed sediments (Anderson, 1905). Reduced accommodation space is evident through the on-lapping of the VC Coal (Fig. 5, 9, 12, 15, 16, 17 and 18) and thinning of isopach maps (Fig. 8d, 11d, 14d and 20d) in each of the 3D seismic surveys. Intra-formational on-lapping within the Patchawarra Formation was a result of the Mid-Permian Event that reactivated NE-SW striking high angle faults and was most severe alongside the GMI and MN ridges. Therefore, the initial stage of structural trap development of Permian sediments began during the Mid-Permian Event, forming low relief anticlines associated with basement faults.

To better define the effect of this event on the stratigraphic architecture of the Patchawarra Formation, well wireline logs should be used to correlate individual sands across the basin. Sub-seismic resolution detail may provide evidence to support previous research (Apak et al., 1997)

suggesting that numerous events occurred during this short period of time. The upper Patchawarra Formation shows evidence of structural quiescence in the Dullingari, Swan Lake, Marabooka, Kidman-Bagundi, Della, and portions of the Gidgealpa fields, with reflectors maintaining thickness and amplitude across these areas.

5.3 LATE PERMIAN DARALINGIE EVENT (258 Ma)

High angle NW-SE striking faults (60^{o}) terminate between the top Toolachee and top Patchawarra formations within the Marabooka, Strzelecki and Dullingari fields, affected by the NE-SW Daralingie Event that deformed much of the province during this time (Kuang, 1985; Apak et al., 1997; Mavromatidis, 2006; Kulikowski and Amrouch, 2017). Cross-sections through each of the fields, together with thinning of the SP3 isopach maps, illustrate that accommodation space was reduced during this time. The effect of this event appears most severe in the Gidgealpa, Della and Strzelecki fields (Fig. 11c and 14c), evident through substantial thinning of isopach maps. Again, as with previous events, the effect of the Daralingie Event was focused along the major GMI and MN ridges. The basement fault controlled anticlines developed by this event would have begun accumulating the initial hydrocarbon generated during the Late Permian to Early Triassic (Deighton and Hill, 1998). Although only relatively small volumes of hydrocarbons were generated at this time, this marks the first point of possible hydrocarbon accumulation within the Cooper-Eromanga petroleum system.

Depositions of Triassic fluvial to lacustrine sediments appear unaffected by structural highs as the base of these sediments does not show evidence of on-lap. This is further substantiated as a large channel system is interpreted along the top Nappamerri Group reflector within the Greater Strzelecki 3D seismic survey spanning the Della, Marabooka, Strzelecki, and Kidman-Bagundi fields (Fig. 14f). The upper portion of SP2 begins showing evidence of exhumation and erosion.

5.4 LATE TRIASSIC HUNTER-BOWEN EVENT (245-190 Ma)

The E-W Late Triassic Hunter-Bowen Event is known to have significantly affected the structural development of the basin (Apak et al., 1997; Mavromatidis, 2006). Large NE-SW striking faults along the GMI and MN ridges were interpreted to displace the Nappamerri Group sediments before terminating in Upper Triassic sediments (Fig. 9b and 9d), which were likely reactivated by the E-W Hunter-Bowen Event. Based on our interpretations, this event reactivated the main NE-SW striking faults along the GMI and MN ridges to exhume sediments and form the regional erosional unconformity between Upper Triassic and Jurassic sediments. The N-S striking faults within the Swan Lake Field, on the north-eastern-most portion of the Gidgealpa Field, and the western edge of the Strzelecki Field also show movement during this time. This period of regional structural growth can

be observed in the thinning of the upper Nappamerri Group above present-day structural highs (Fig. 5d, 9d, 12c, 15a, 16a, 17b) and movement along N-S striking field scale faults.

Isopach maps of SP2 show significant thinning above present day structural highs in each of the 3D seismic surveys (Fig. 8b, 11b, 14b and 20b), but was most significant within the Gidgealpa 3D seismic survey (Fig. 11b). The isopach map of SP2 in the Dullingari 3D seismic survey (Fig. 20a) shows an increase in thickness to the west, inferring uplift and tilting towards the west. Fault reactivation caused by this event likely enhanced pre-existing Permian anticlinal structures and formed low relief anticlines within Triassic sediments (Lowe-Young et al., 1997). Most structures were developed during this event as it caused the complete Permian to Triassic stratigraphy to fold. Subsequent deposition of Jurassic sediments is observed to be impacted by reduced accommodation space, as shown by thinning of SP1 isopach maps within the Swan Lake (Fig. 8a), Greater Strzelecki (Fig. 14a), and Dullingari (Fig. 20a) 3D seismic surveys.

5.5 MIDDLE CRETACEOUS POLYGONAL FAULT SYSTEM

Layer bound normal faults are evident across each of the seismic surveys and are mostly contained within the open marine Wallumbilla Formation, with few faults extending into the underlying and hydrocarbon-rich Lower Cretaceous sediments. The geometry of these faults closely resembles that of polygonal faults typical to passive continental margins and within intracratonic basins (Watterson et al., 2000; Davies et al., 2009). A system of polygonal faults was previously interpreted within the Lake Hope 3D seismic survey, Eromanga Basin (Cartwright and Lonergan, 1997; Watterson et al., 2000), with the regional extent of this system only recently discovered (Kulikowski et al., 2017). The mechanism for their formation is not well understood; however, all genetic models involve dewatering of the host rock. Previous research found that the polygonal fault system within the Lake Hope 3D may have developed through a density inversion, as the low-density and over pressured layer was buried by normally pressured sediments (Watterson et al., 2000).

These faults pose a major risk to preservation of Lower Cretaceous and Jurassic hydrocarbon reservoirs, and to the increased likelihood of contaminating the Great Artesian Basin, which is also hosted within these sediments. Faults that penetrate the hydrocarbon-rich Murta Member may also facilitate hydrocarbon migration and accumulation within low relief and shallow structural traps that are present within Cretaceous sediments. Geomechanical modelling of this fault system (Kulikowski et al., 2017) concluded that polygonal faults with high to near vertical dip angles striking between 60°N and 140°N were optimally oriented to leak hydrocarbons.

5.6 LATE CRETACEOUS EVENT (95-55 Ma)

The final period of fault activity was interpreted during the Late Cretaceous and is recorded as a regional unconformity between Upper Cretaceous and Paleogene sediments (Fig. 2). A N-S striking fault within the Kidman-Bagundi Field extends from basement into Cretaceous sediments (Fig. 17b), inferring likely reactivation during the Late Cretaceous Event. This is the only interpreted fault that extends from basement into Cretaceous sediments and suggests that fault activity did not continue past the Cretaceous. This event caused significant folding within the Gidgealpa 3D seismic survey, where Paleogene aged sediments thin above the present day structural highs (Fig. 9b, 9c and 9d). The thinning of sediments is not as significant elsewhere in the basin as it is at Gidgealpa; however, a cross-section through the Della Field (Fig. 12c) shows substantial sediment thickening to the east into the Nappamerri Trough, suggesting that the region was tilted. The results show that crustal folding dominated during this time and hydrocarbon accumulations were not compromised by fault activity. Importantly, although initial hydrocarbon generation began during the Late Permian to Lower Triassic, significant volumes were not generated until the Cretaceous (Deighton and Hill, 1998; Borazjani et al., 2018). This suggests that structural traps that were developed prior to the Late Cretaceous Event were not accumulating significant volumes of hydrocarbons.

5.7 PALEOGENE EVENT (33-23 Ma)

This structural movement had little visible effect on the reactivation of faults, but movement may be at a sub-seismic resolution scale. A regionally pervasive natural fracture set was developed during this event (Kulikowski and Amrouch, 2017) providing some arguments to suggest that fault reactivation might also have occurred, but perhaps below seismic resolution. A cross-section through the Swan Lake Field (Fig. 5c) presents a polygonal fault extending from Cretaceous sediments into Paleogene to Quaternary sediments and may be related to reactivation during this event. No thinning or on-lapping of sediments was observed during this period, suggesting that the magnitude was relatively smaller than the previous events.

6. CONCLUSION

The Cooper-Eromanga Basin is a structurally complex province that has been affected by numerous structural events and is subject to poor resolution seismic data below Permian coal measures, making it difficult to analyse the key stages of basin evolution. This research utilised 3D seismic data to investigate the relationship between known structural events and the present day stratigraphic architecture of the basin.

Results show that: (1) present day hydrocarbon-filled structures were developed as early as the Permian before succumbing to intermittent periods of sag and reactivation along basement faults; (2) the geometry of basement faults is closely linked to the timing of reactivation and exhumation; (3) stratigraphic pinch-outs and sediment on-lapping are prolific within the basin, present during five major structural event, and could form hydrocarbon targets for future exploration programs; (4) subtle NW-SE dextral strike-slip faults are interpreted throughout the basin; and (5) the proposed critical moment (90 Ma) in the Cooper-Eromanga Basin petroleum system is generally unaffected by fault reactivation, as the final period of fault activity was interpreted during the Late Cretaceous.

The results provide a better understanding of the intricate relationship between fault reactivation through time and the stratigraphic architecture of the basin. The distribution of on-lapping features presented here will provide a working framework for future hydrocarbon exploration programs that begin targeting the underdeveloped stratigraphic traps that are prevalent throughout the basin and found to increase in intensity within the hydrocarbon-rich Permian stratigraphy. The approach used to extract subtle structural and stratigraphic information from geophysical data can be highly beneficial if applied to other subsurface provinces, where direct measurements from outcrop is not possible and the tectonostratigraphic evolution model remains undefined.

7. ACKNOWLEDGMENTS

The authors would like to acknowledge the financial contribution made by the GeoFrac Consortium, which includes the program manager, Dennis Cooke, and the sponsoring companies: Santos, Beach Energy, Chevron, Halliburton and BG Group (QGC). We thank DUG Insight for their generous donation of academic licence. DUG Insight software (v.4.2, 2017) was used for seismic visualisation, interpretation and analysis. Thank you also to the reviewers and editorial staff at Marine and Petroleum Geology for their constructive feedback.

8. REFERENCES

Al-Chalabi, M., 1974. An analysis of stacking, RMS, average, and interval velocities over a horizontally layered ground. *Geophysical Prospecting* **22** (3), 458-475.

Alexander, E.M., Gravestock, D.I., Cubitt, C., Chaney, A., 1998. Lithostratigraphy and Environments of Deposition. In: The petroleum geology of South Australia. Vol. 4: Cooper Basin (eds. D.I. Gravestock, J.E. Hibburt and J.F. Drexel), pp 69-115. South Australia. Department of Primary Industries and Resources. Report Book, 98/9.

Amrouch, K., Lacombe, O., Bellahsen, N., Daniel, J.M., Callot, J.P., 2010a. Stress and strain patterns, kinematics and deformation mechanisms in a basement-cored anticline: Sheep Mountain Anticline, Wyoming. *Tectonics* **29**, TC1005, doi:10.1029/2009TC002525.

Amrouch, K., Robion, P., Callot, J.P., Lacombe, O., Daniel, J.M., Bellahsen, N., Faure, J.L., 2010b. Constraints on deformation mechanisms during folding provided by rock physical properties: a case study at Sheep Mountain anticline (Wyoming, USA). *Geophysical Journal International* **182** (3), 1105-1123.

Amrouch, K., Beaudoin, N., Lacombe, O., Bellahsen, N., Daniel, J.M., 2011. Paleostress magnitudes in folded sedimentary rocks. *Geophysical Research Letters* **38** (17), L17301.

Amrouch, K., 2010. Apport de l'analyse microstructurale à la comprehension des mécanismes de plissement. Exemples de structures plissées aux USA (Wyoming) et en Iran (Zagros). Thèse, Université Pierre et Marie Curie – Paris 6, 2010-03, 477 p.

Anderson, E.M., 1905. The dynamics of faulting. *Transactions of the Edinburgh Geological Society* **8** (3), 387-402.

Apak, S.N., Stuart, W.J., Lemon, N.M., Wood, G., 1997. Structural evolution of the Permian-Triassic Cooper Basin, Australia: relation to hydrocarbon trap styles. *AAPG Bulletin* **81** (4), 533-555.

Arboit, F., Amrouch, K., Collins, A.S., King, R., Morley, C., 2015. Determination of the tectonic evolution from fractures, faults, and calcite twins on the southwestern margin of the Indochina Block. *Tectonics* **34** (8), 1576-1599, doi:10.1002/2015TC003876.

Arboit, F., Amrouch, K., Morley, C., Collins, A.S., King, R., 2017. Palaeostress magnitudes in the Khao Khwang fold-thrust belt, new insights into the tectonic evolution of the Indosinian orogeny in central Thailand. *Tectonophysics* **710**, 266-276.

Basir, H.M., Javaherian, A., Yaraki, M.T., 2013. Multi-attribute ant-tracking and neural network for fault detection: a case study of an Iranian oilfield. *Journal of Geophysics and Engineering* **10** (1), 1-10, 015009.

Beaudoin, N., Leprêtre, R., Bellahsen, N., Lacombe, O., Amrouch, K., Callot, J.P., Emmanuel, L., Daniel, J.M., 2012. Structural and microstructural evolution of the Rattlesnake Mountain Anticline (Wyoming, USA): New insights into the Sevier and Laramide orogenic stress build-up in the Bighorn Basin. *Tectonophysics* **576**, 20-45.

Beaudoin, N., Lacombe, O., Bellahsen, N., Amrouch, K., Daniel, J.M., 2014. Evolution of pore-fluid pressure during folding and basin contraction in overpressured reservoirs: Insights from the Madison–Phosphoria carbonate formations in the Bighorn Basin (Wyoming, USA). *Marine and Petroleum Geology* **55**, 214-229.

Borazjani, S., Kulikowski, D., Amrouch, K., McCabe, P., Bedrikovetsky, P., 2018. Composition changes of hydrocarbons during secondary petroleum migration. *The APPEA Journal* **58**, abstract, accepted.

Boreham, C.J., Hill, A.J., 1998. Source rock distribution and hydrocarbon geochemistry. In: The petroleum geology of South Australia. Vol. 4: Cooper Basin (eds. D.I. Gravestock, J.E. Hibburt and J.F. Drexel), pp 129-142. South Australia. Department of Primary Industries and Resources. Report Book, 98/9.

Bradshaw, M.T., 1993. Australian petroleum systems. *Petroleum Exploration Society of Australia Journal* **21**, 43-53.

Burgin, H.B., Amrouch, K., Rajabi, M., Kulikowski, D., Holford, S.P., 2018. Determining structural environments through natural fracture and calcite twin analysis: A case study in the Otway Basin. *The APPEA Journal* **58**, accepted.

Cartwright, J., Lonergan, L., 1997. Seismic expression of layer-bound fault systems of the Eromanga and North Sea Basins. *Exploration Geophysics* **28** (3), 323-331.

Cartwright, J., Bouroullec, R., James, D., Johnson, H., 1998. Polycyclic motion history of some Gulf Coast growth faults from high-resolution displacement analysis. *Geology* **26**, 819-822.

Davies, R.J., Ireland, M.T., Cartwright, J.A., 2009. Differential compaction due to the irregular topology of a diagenetic reaction boundary: a new mechanism for the formation of polygonal faults. *Basin Research* **21** (3), 354-359.

Deighton, I., Hill, A.J., 1998. Thermal and Burial History. In: The petroleum geology of South Australia. Vol. 4: Cooper Basin (eds. D.I. Gravestock, J.E. Hibburt and J.F. Drexel), pp 143-156. South Australia. Department of Primary Industries and Resources. Report Book, 98/9.

Gatehouse, C.G., 1986. The geology of the Warburton Basin in South Australia. *Australian Journal of Earth Sciences* **33** (2), 161-180.

Giba, M., Walsh, J.J., Nicol, A., 2012. Segmentation and growth of an obliquely reactivated normal fault. *Journal of Structural Geology* **39**, 253-267.

Glikson, A.Y., Uysal, I.T., Fitz Gerald, J.D., Saygin, E., 2013. Geophysical anomalies and quartz microstructures, Eastern Warburton Basin, North-east South Australia: Tectonic or impact shock metamorphic origin? *Tectonophysics* **589**, 57-76.

Grant-Woolley, L., Kong, A., Schoemaker, B., Nasreddin, H., Montague, E.T., 2014. Identification of Strike-Slip Faults Provides Insights into the Further Development of Mature Cooper Basin Fields. In SPE Asia Pacific Oil & Gas Conference and Exhibition, Adelaide, SPE 171492-MS.

Gravestock, D.I., Jensen-Schmidt, B., 1998. Structural setting. In: The petroleum geology of South Australia. Vol. 4: Cooper Basin (eds. D.I. Gravestock, J.E. Hibburt and J.F. Drexel), pp 69-115. South Australia. Department of Primary Industries and Resources. Report Book, 98/9.

Gravestock, D.I., Alexander, E.M., Morton, J.G.G., Sun, X., 1998. Reservoirs and Seals. In: The petroleum geology of South Australia. Vol. 4: Cooper Basin (eds. D.I. Gravestock, J.E. Hibburt and J.F. Drexel), pp 157-180. South Australia. Department of Primary Industries and Resources. Report Book, 98/9.

Green, P.M., Brain, T.J., John, B.H., 1989. Possible stratigraphic controls on hydrocarbon distribution within the Jurassic-Early Cretaceous rocks, Eromanga Basin, southern Queensland. In: The Cooper and Eromanga Basins, Australia (ed. B.J. O'Neil), pp. 251-264. Petroleum Exploration Society of Australia, Society of Petroleum Engineers, Australian Society of Exploration Geophysicists (S.A. Branches), Adelaide (Proceedings of Cooper and Eromanga Basins Conference).

Haines, P.W., Hand, M., Sandiford, M., 2001. Palaeozoic synorogenic sedimentation in central and northern Australia: A review of distribution and timing with implications for the evolution of intracontinental orogens. *Australian Journal of Earth Sciences* **48**, 911-928.

Jackson, C.A.L., Rotevatn, A., 2013. 3D seismic analysis of the structure and evolution of a salt-influenced normal fault zone: a test of competing fault growth models. *Journal of Structural Geology* **54**, 215-234, doi:10.1016/j.jsg.2013.06.012.

Kantsler, A.J., Prudence, T.J.C., Cook, A.C., Zwigulis, M., 1984. Hydrocarbon habitat of the Cooper/Eromanga basin, Australia. In: Petroleum geochemistry and basin evolution (eds. G. Demaison and R. J. Murris), pp 373-390. *American Association of Petroleum Geologists Memoir* **35**.

Kuang, K.S., 1985. History and style of Cooper-Eromanga Basin structures. *Exploration Geophysics* **16**, 245-248.

Kulikowski, D., Amrouch, K., Cooke, D., 2016a. Geomechanical Modelling of Fault Reactivation in the Cooper Basin, Australia. *Australian Journal of Earth Sciences* **63** (3), 295-314, doi:10.1080/08120099.2016.1212925.

Kulikowski, D., Cooke, D., Amrouch, K., 2016b. Constraining the distribution and relationship between overpressure, natural fracture density and temperature in the Cooper Basin. *The Australian Petroleum Production and Exploration Association Journal* **56**, 11-28, doi:10.1071/AJ15002.

Kulikowski, D., Hochwald, C., Cooke, D., Amrouch, K., 2016c. A Statistical Approach to Assessing Depth Conversion Uncertainty on a Regional Dataset: Cooper-Eromanga Basin, Australia. ASEG-PESA-AIG 2016 Conference, Adelaide. Extended Abstract #200, 484-490.

Kulikowski, D., Amrouch, K., 2017. Combining Geophysical Data and Calcite Twin Stress Inversion to Refine the Tectonic History of Subsurface and Offshore Provinces: A Case Study on the Cooper-Eromanga Basin, Australia. *Tectonics* **36**, 515-541, doi:10.1002/2016TC004366.

Kulikowski, D., Amrouch, K., Cooke, D., Gray, M.E., 2017. Basement Structural Architecture and Hydrocarbon Conduit Potential of Polygonal Faults in the Cooper-Eromanga Basin, Australia. *Geophysical Prospecting*, doi:10.1111/1365-2478.12531.

Lacombe, O., Amrouch, K., Mouthereau, F., Dissez, L., 2007. Calcite twinning constraints on late Neogene stress patterns and deformation mechanisms in the active Zagros collision belt. *Geology* **35** (3), 263-266.

Lacombe, O., Malandain, J., Vilasi, N., Amrouch, K., Roure, F., 2009. From paleostresses to paleoburial in fold–thrust belts: Preliminary results from calcite twin analysis in the Outer Albanides. *Tectonophysics* **475** (1), 128-141.

Lin, A., Yamashita, K., 2013. Spatial variations in damage zone width along strike-slip faults: An example from active faults in southwest Japan. *Journal of Structural Geology* **57**, 1-15.

Lowe-Young, B.S., Mackie, S.I., Heath, R.S., 1997. The Cooper-Eromanga petroleum system, Australia: Investigation of essential elements and processes. Indonesian Petroleum Association. Proceedings of the Petroleum Systems of SE Asia and Australasia Conference, Jakarta, 199-211.

Mai, H.T., Marfurt, K.J., Chávez-Pérez, S., 2009. Coherence and volumetric curvatures and their spatial relationship to faults and folds, an example from Chicontepec basin. Proceedings of the Society of Exploration Geophysicists International Exposition and Annual Meeting, Houston, 1063-1067.

Manzi, M., Cooper, G., Malehmir, A., Durrheim, R., Nkosi, Z., 2015. Integrated interpretation of 3D seismic data to enhance the detection of the gold-bearing reef: Mponeng Gold mine, Witwatersrand Basin (South Africa). *Geophysical Prospecting* **63** (4), 881-902.

Mavromatidis, A., 2006. Burial/exhumation histories for the Cooper-Eromanga Basins and implications for hydrocarbon exploration, Eastern Australia. *Basin Research* **18**, 351-373.

Mitchum, R.M., Vail, P.R., Sangree, J.B., 1977. Stratigraphic interpretation of seismic reflection patterns in depositional sequences. In: Seismic Stratigraphy-Application to Hydrocarbon Exploration, Part 6, AAPG, Tulsa, Okla **8**, 117-133.

Müller, R.D., Dyksterhuis, S., Rey, P., 2012. Australian paleo-stress fields and tectonic reactivation over the past 100 Ma. *Australian Journal of Earth Sciences* **59**, 13-28.

Neves, F.A., Zahrani, M.S., Bremkamp, S.W., 2004. Detection of potential fractures and small faults using seismic attributes. *The Leading Edge* **23** (9), 903-906.

Pokalai, K., Kulikowski, D., Johnson, Jr., R.L., Haghighi, M., Cooke, D., 2016. Development of a new approach for hydraulic fracturing in tight sand with pre-existing natural fractures. *The Australian Petroleum Production and Exploration Association Journal* **56**, 225-238.

Rezaee, M.R., Sun, X., 2007. Fracture-Filling Cements in the Palaeozoic Warburton Basin, South Australia. *Journal of Petroleum Geology* **30** (1), 79-90.

Robson, A.G., King, R.C., Holford, S.P., 2017a. Structural evolution of a gravitationally detached normal fault array: Analysis of 3D seismic data from the Ceduna Sub-Basin, Great Australian Bight. *Basin Research* **29** (5), 605-624, doi:10.1111/bre.12191.

Robson, A.G., Holford, S.P., King, R.C., 2017b. Structural evolution of a normal fault array in the Gambier Embayment, offshore Otway Basin, South Australia: insights from 3D seismic data. *Australian Journal of Earth Sciences* **64** (5), 611-624, doi:10.1080/08120099.2017.1324822.

Ryan, L., Magee, C., Jackson, C.A.L., 2017. The kinematics of normal faults in the Ceduna Subbasin, offshore southern Australia: Implications for hydrocarbon trapping in a frontier basin. *AAPG Bulletin* **101** (3), 321-341.

Shaw, R.D., Etheridge, M.A., Lambeck, K., 1991. Development of the Late Proterozoic to Mid-Paleozoic, intracratonic Amadeus Basin in central Australia: A key to understanding tectonic forces in plate interiors. *Tectonics* **10** (4), 688-721.

Stanmore, P.J., Johnstone, E.M., 1988. The search for stratigraphic traps in the southern Patchawarra trough, South Australia. *The Australian Petroleum Exploration Association Journal* **28** (1), 156-166.

Sun, X., 1997. Structural style of the Warburton Basin and control in the Cooper and Eromanga Basins, South Australia. *Exploration Geophysics* **28** (3), 333-339.

Szalaiová, E., Iwanowski-Strahser, K., Rabbel, W., 2015. 3D fracture networks in the crystalline upper crust-A new seismic model of the Continental Deep Drilling Site (South Germany). *Geophysical Prospecting* **63** (4), 937-956.

Vail, P.R., Mitchum, R.M., Thompson, S., 1977. Seismic stratigraphy and global changes of sea-level. Part 3: Relative changes of sea level from coastal onlap, in Seismic Stratigraphy-Applications to Hydrocarbon Exploration. AAPG Memoirs, Tulsa, Okla **26**, 63-81.

Watterson, J., Walsh, J., Nicol, A., Nell, P.A.R., Bretan, P.G., 2000. Geometry and origin of a polygonal fault system. *Journal of the Geological Society* **157** (1), 151-162.

Wiprut, D., Zoback, M.D., 2000. Fault reactivation and fluid flow along a previously dormant normal fault in the northern North Sea. *Geology* **28**, 595-598.

9. FIGURES

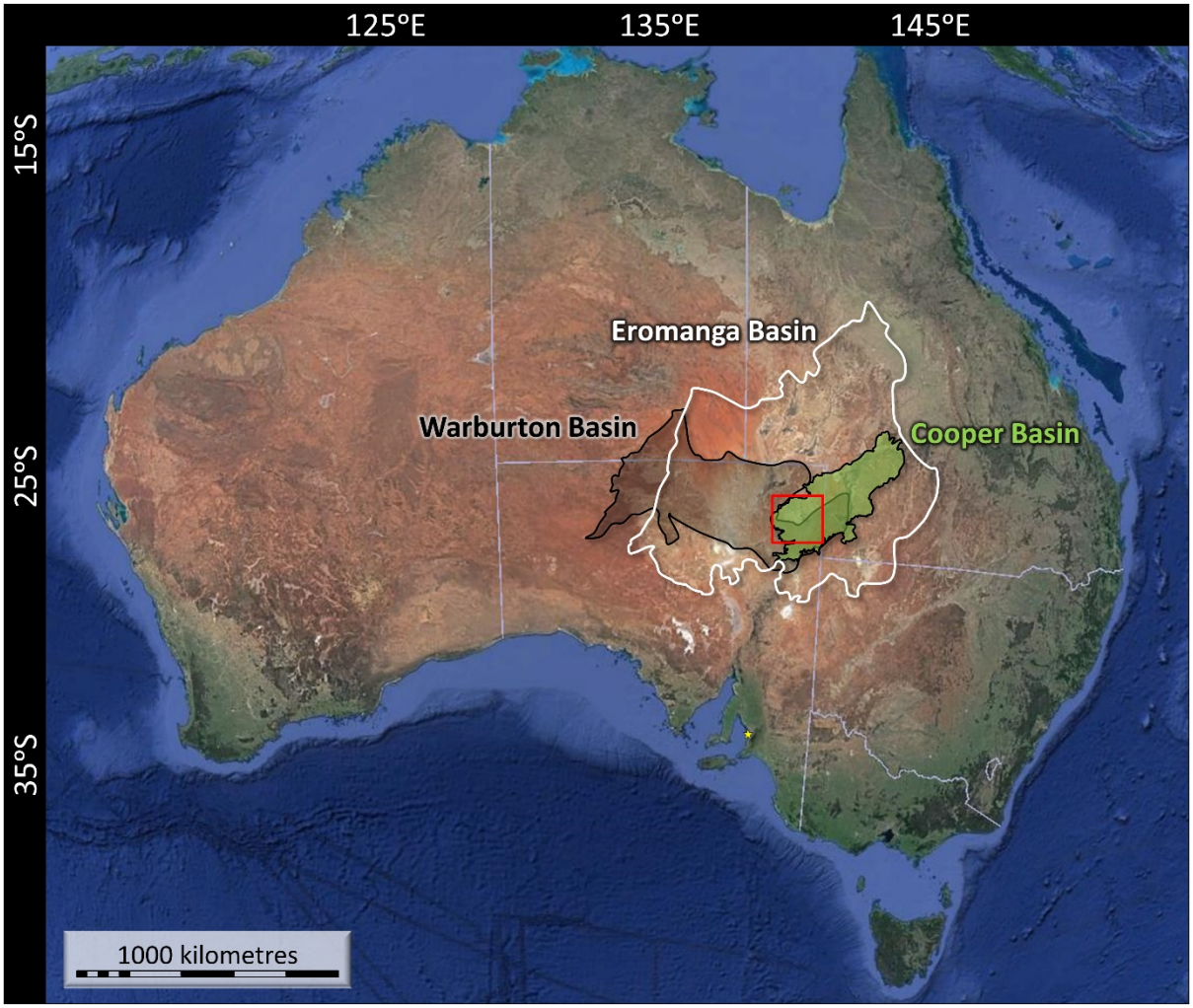


Figure 1. Location of the Warburton, Cooper and Eromanga basins, Australia (Kulikowski *et al.*, 2016a). Study area shown in red.

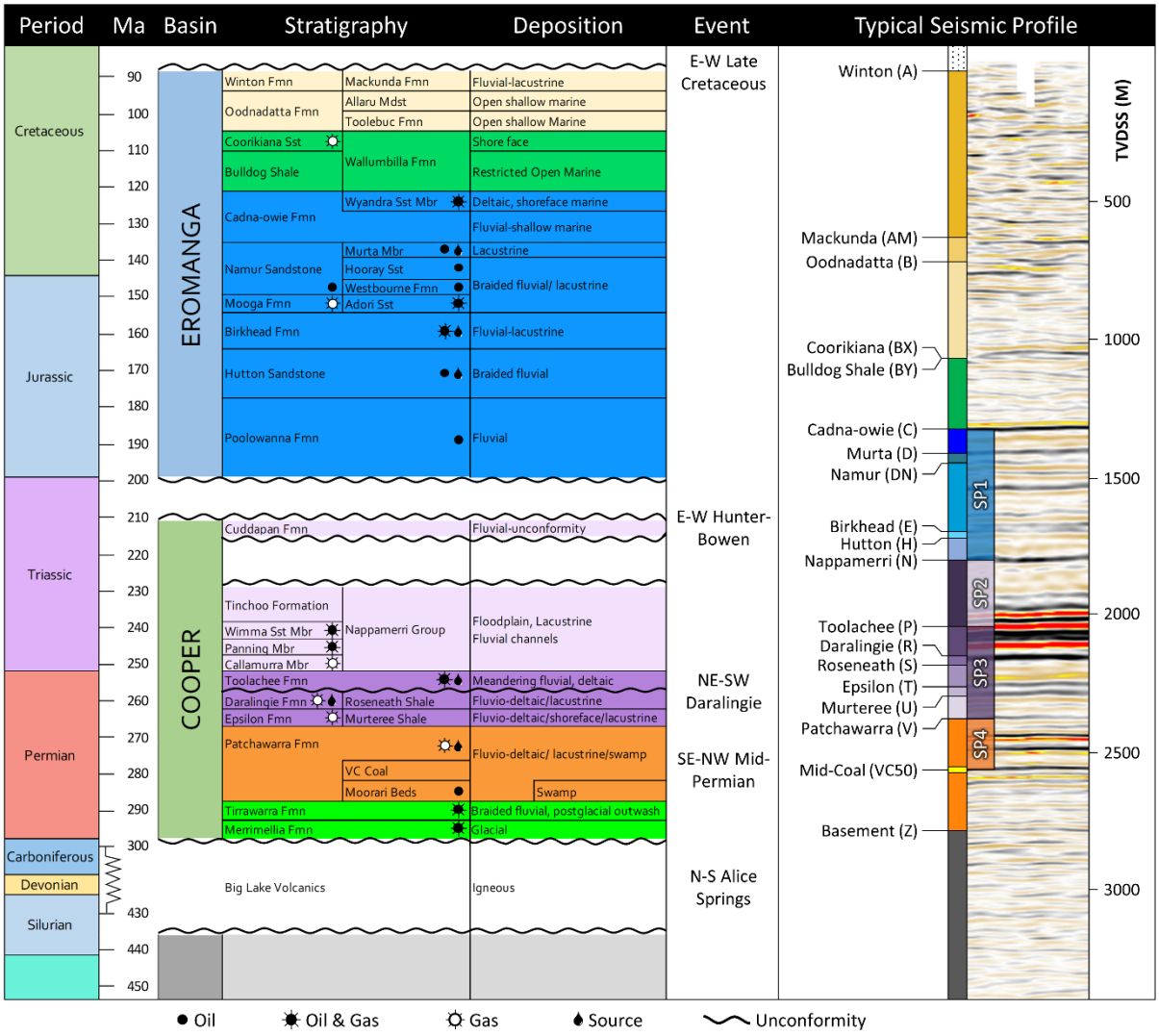


Figure 2. A summary of the Warburton, Cooper, Eromanga, and Lake Eyre basins. A typical seismic reflection profile is shown together with the stratal-packages (SP) and colour scheme.

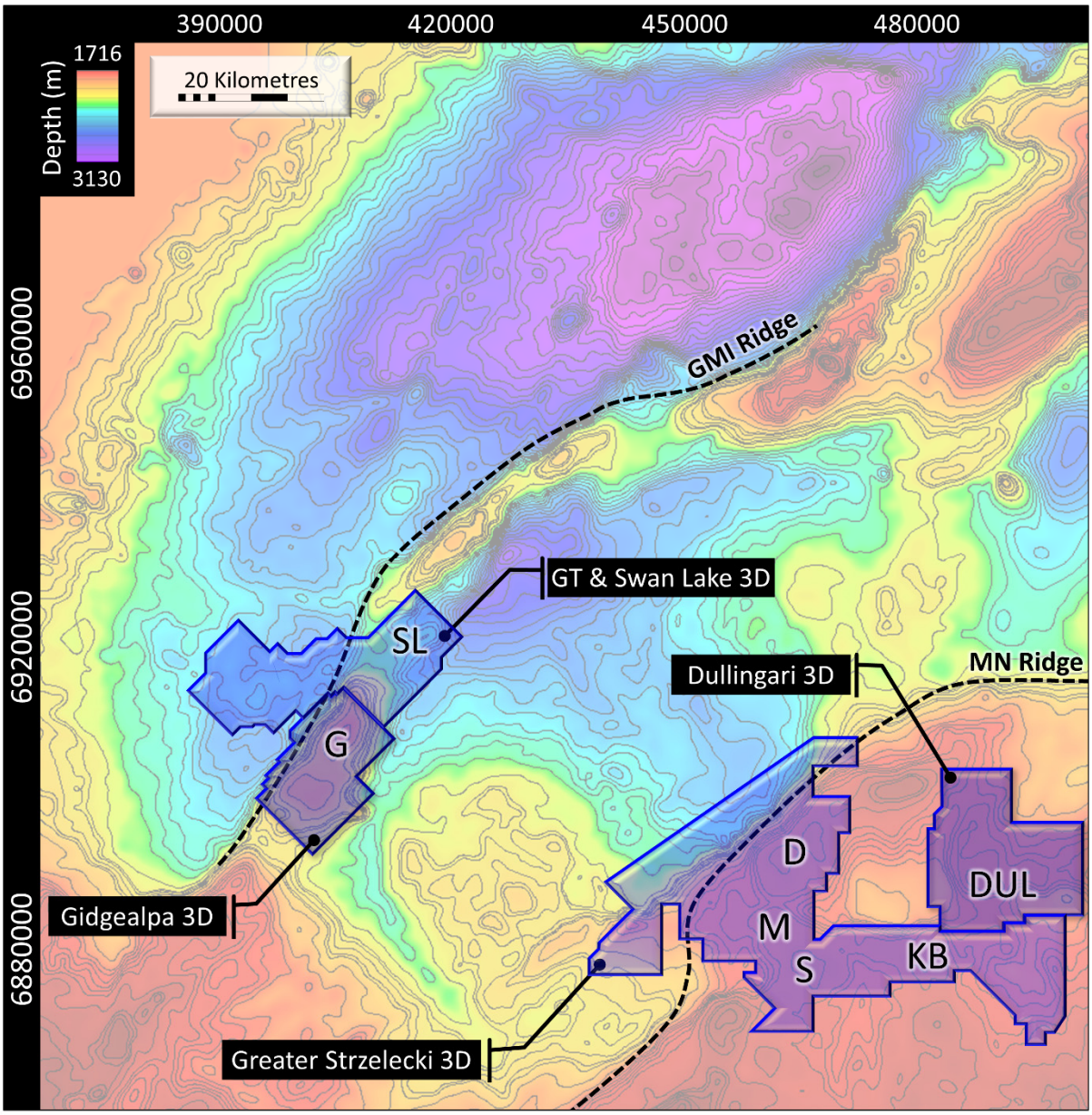


Figure 3. Location of the four 3D seismic surveys used for this study. The location of the Swan Lake (SL), Gidgealpa (G), Dullingari (DUL), Della (D), Marabooka (M), Strzelecki (S), and Kidman-Bagundi (KB) fields is shown. Base Triassic/top Permian depth map shown (after Kulikowski et al., 2017). GT: Greater Tindilpie.

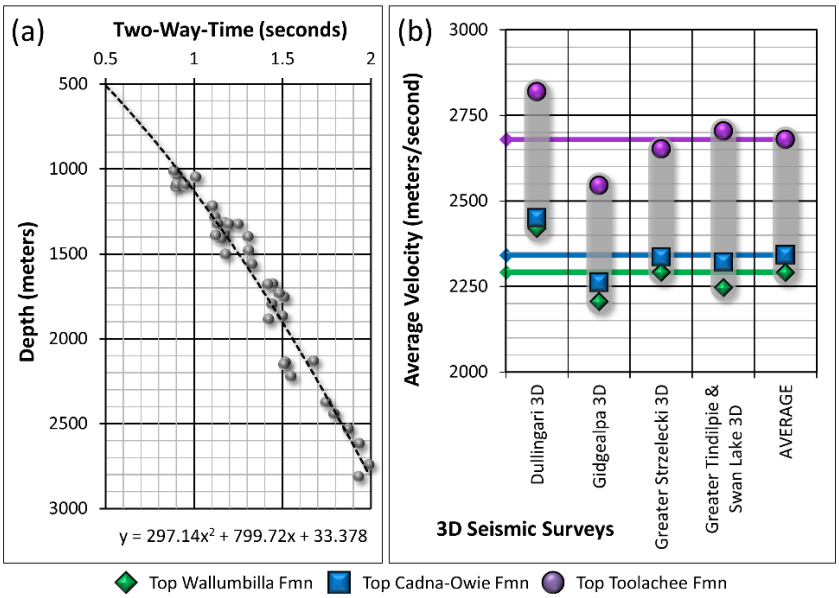


Figure 4. Seismic velocity data showing: (a) time-to-depth relationship; and (b) average velocities for key reflectors (after Kulikowski et al., 2017).

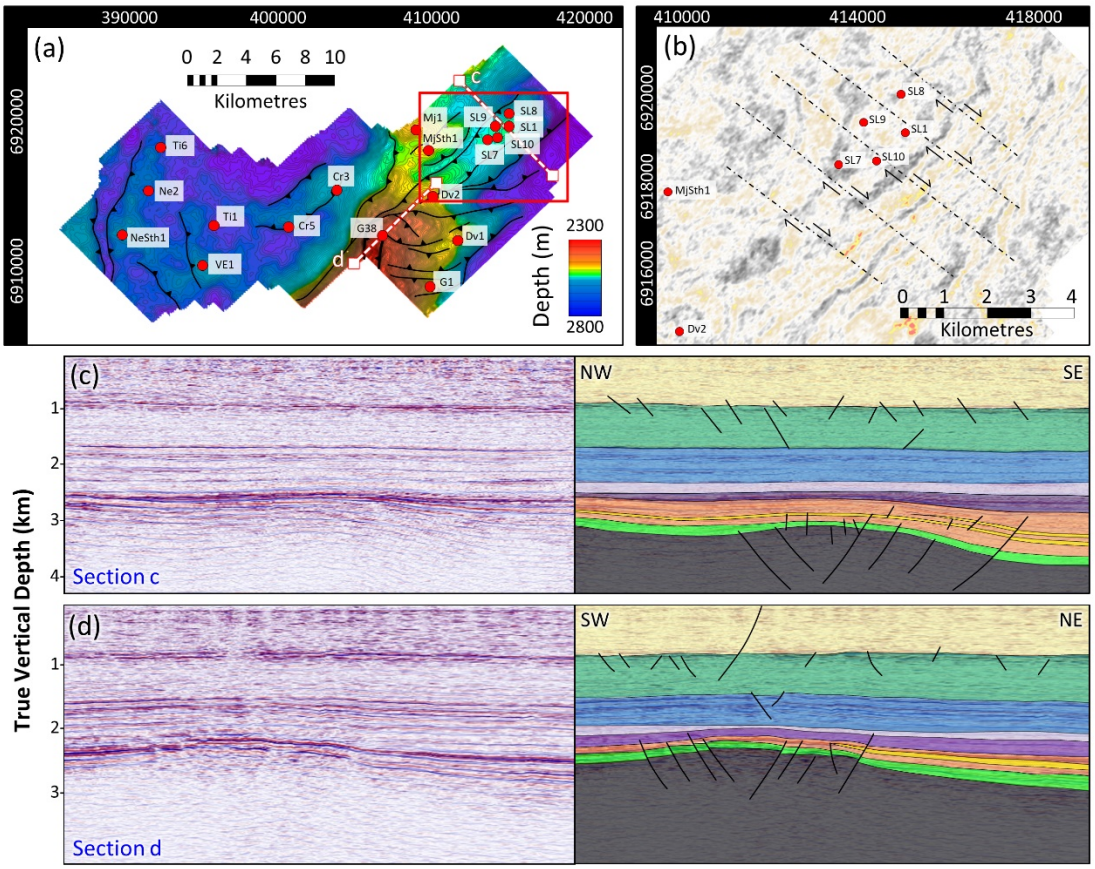


Figure 5. Structural interpretation of the Swan Lake Field. (a) Fault interpretation projected onto the top Permian depth map with the location of cross-sections 'c' and 'd' shown (after Kulikowski et al., 2017). Location of depth-slice (see Fig. 5b) is shown in red. (b) Interpretation of approximately NW-SE striking dextral strike-slip faults on a depth-slice (3,001 MTVD) in the Swan Lake Field (see Fig. 5a for location). (c) Cross-section 'c'; (d) Cross-section 'd'. See Fig. 2 for colour scheme and Fig. 3 for survey location.

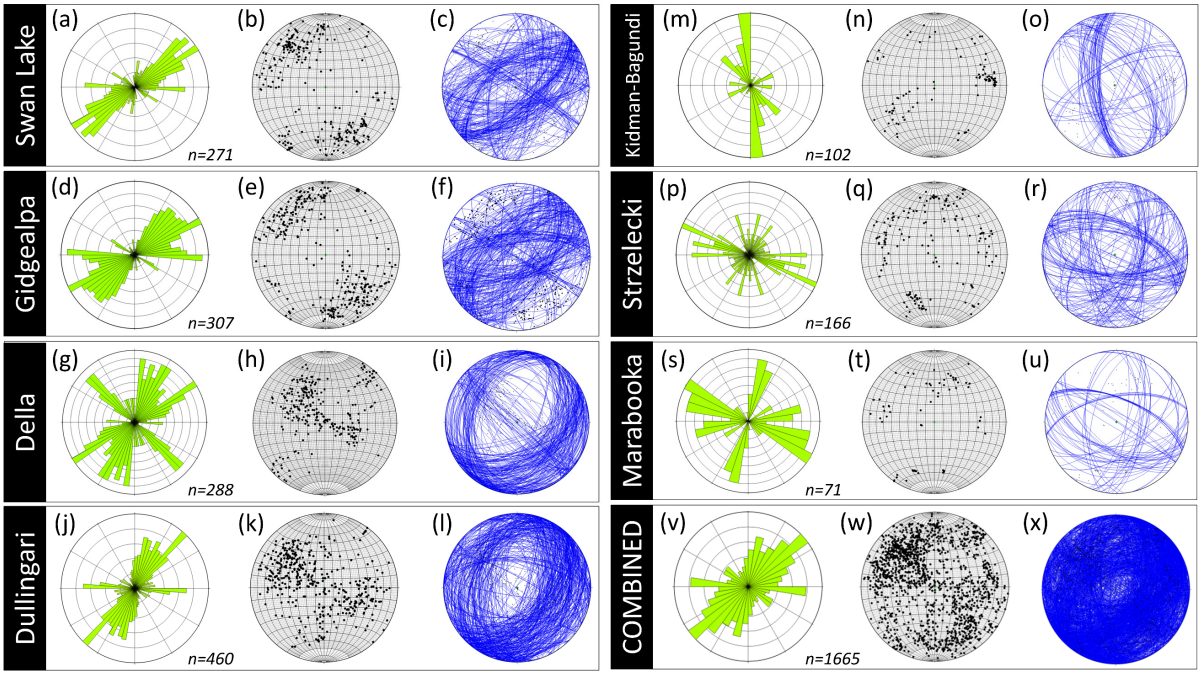


Figure 6. Basement fault geometry interpreted from each of the seven fields. Strike, pole to plane, and stereographic projection of all faults is shown on lower hemisphere plots.

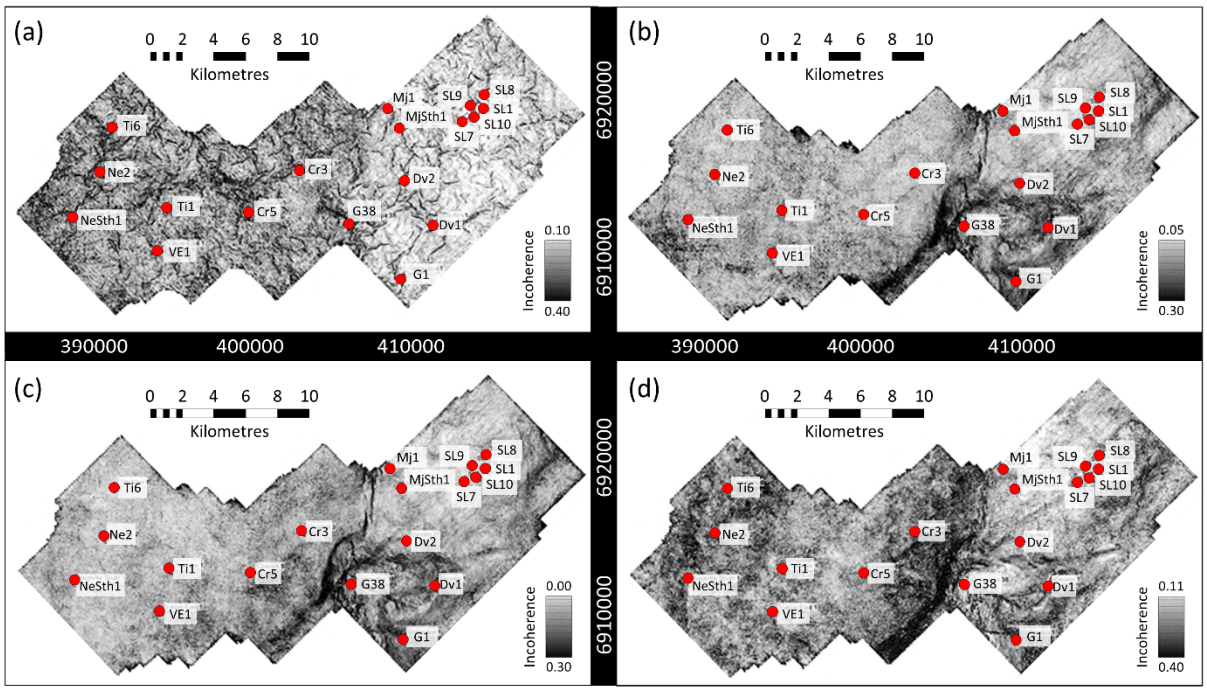


Figure 7. Incoherency analysis maps in the Swan Lake Field along the: (a) top Wallumbilla Formation; (b) top Toolachee Formation; (c) top Patchawarra Formation; and (d) top VC Coal. Faults are shown in black. See Fig. 3 for seismic survey location.

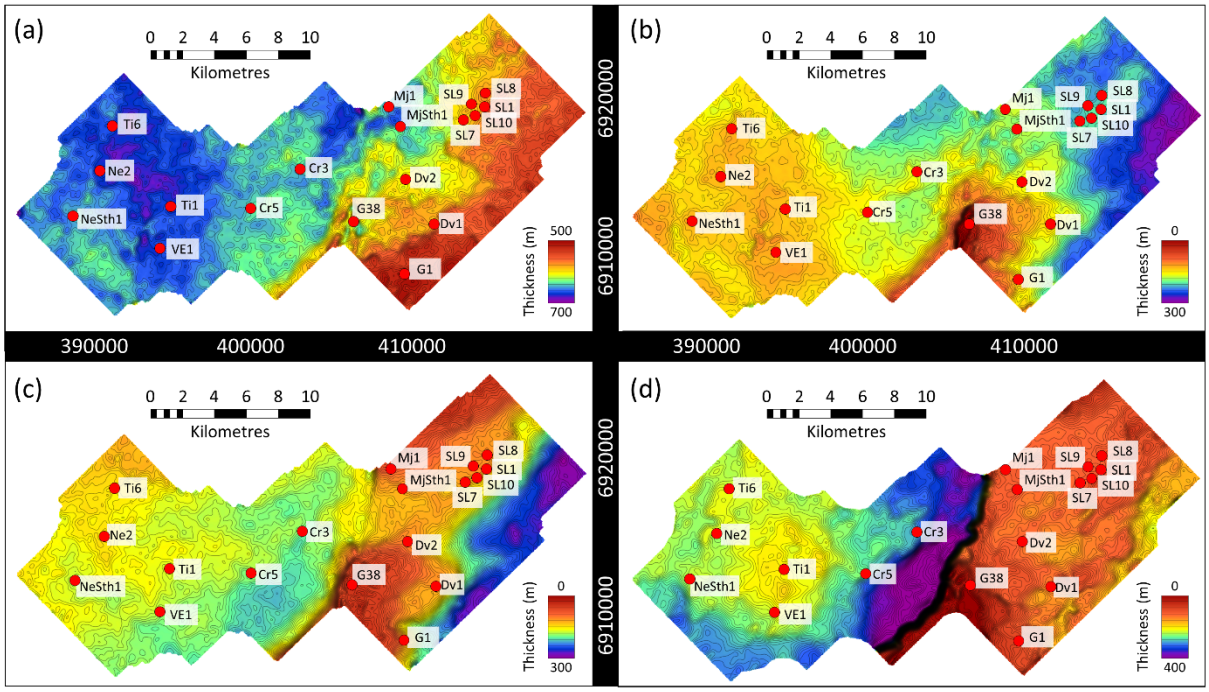


Figure 8. Isopach maps in the Swan Lake Field showing: (a) SP1; (b) SP2; (c) SP3; and (d) SP4. See Fig. 3 for seismic survey location and Fig. 2 for stratal-package (SP) description.

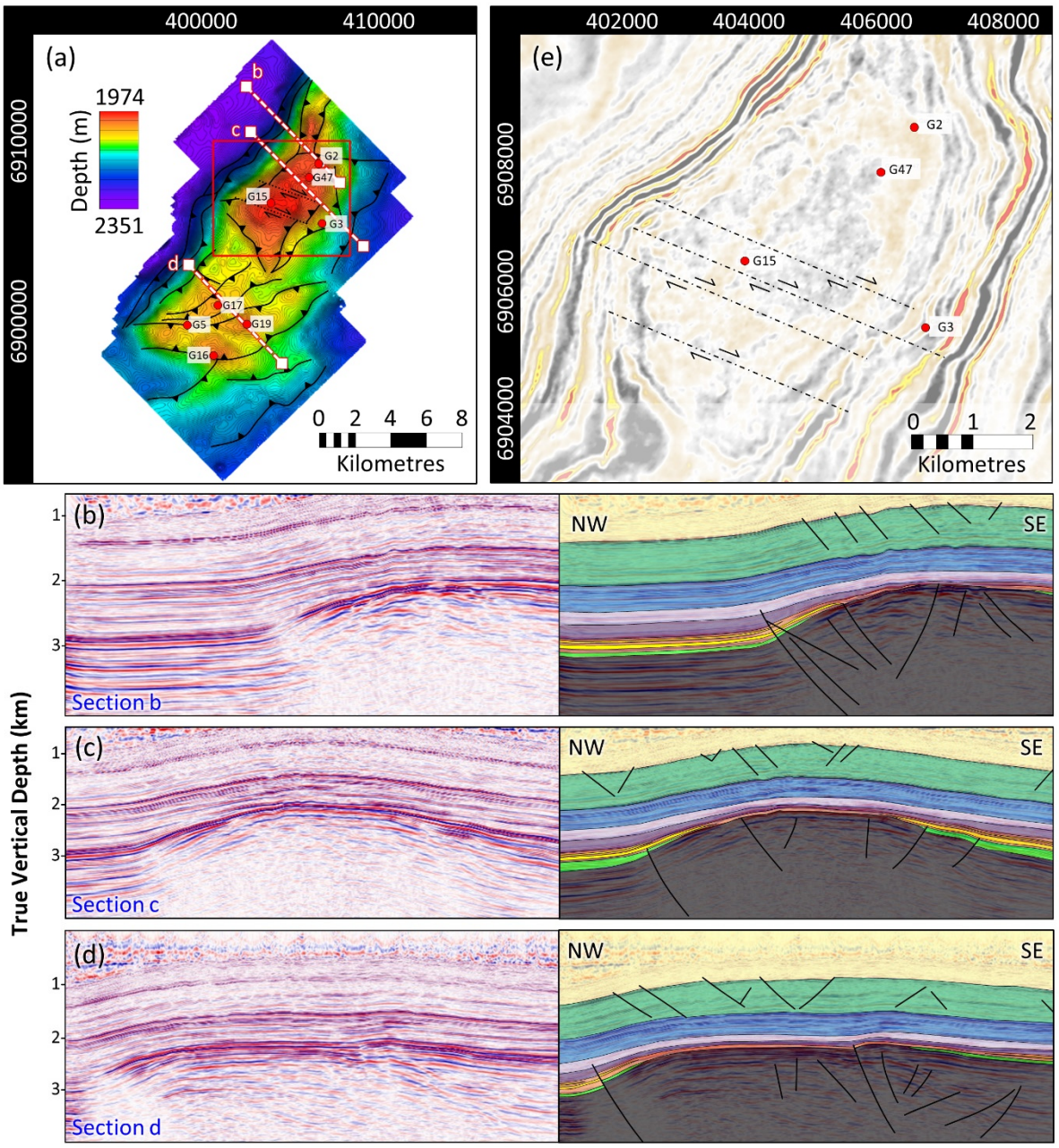


Figure 9. Structural interpretation of the Gidgealpa 3D seismic survey showing: (a) Structural map projected onto the top Permian depth map with the location of cross-section 'b', 'c', and 'd' with the location of depth-slice (see Fig. 9e) shown in red (after Kulikowski et al., 2017); (b) Cross-section 'b' through the northern dome; (c) Cross-section 'c' through the northern dome; (d) Cross-section 'd' through the southern dome; and (e) Interpretation of approximately NW-SE striking dextral strike-slip faults on a depth-slice (2,399 MTVD) in the Gidgealpa Field. Location of depth-slice is shown in Fig. 9a. Refer to Fig. 2 for colour scheme. See Fig. 3 for seismic survey location.

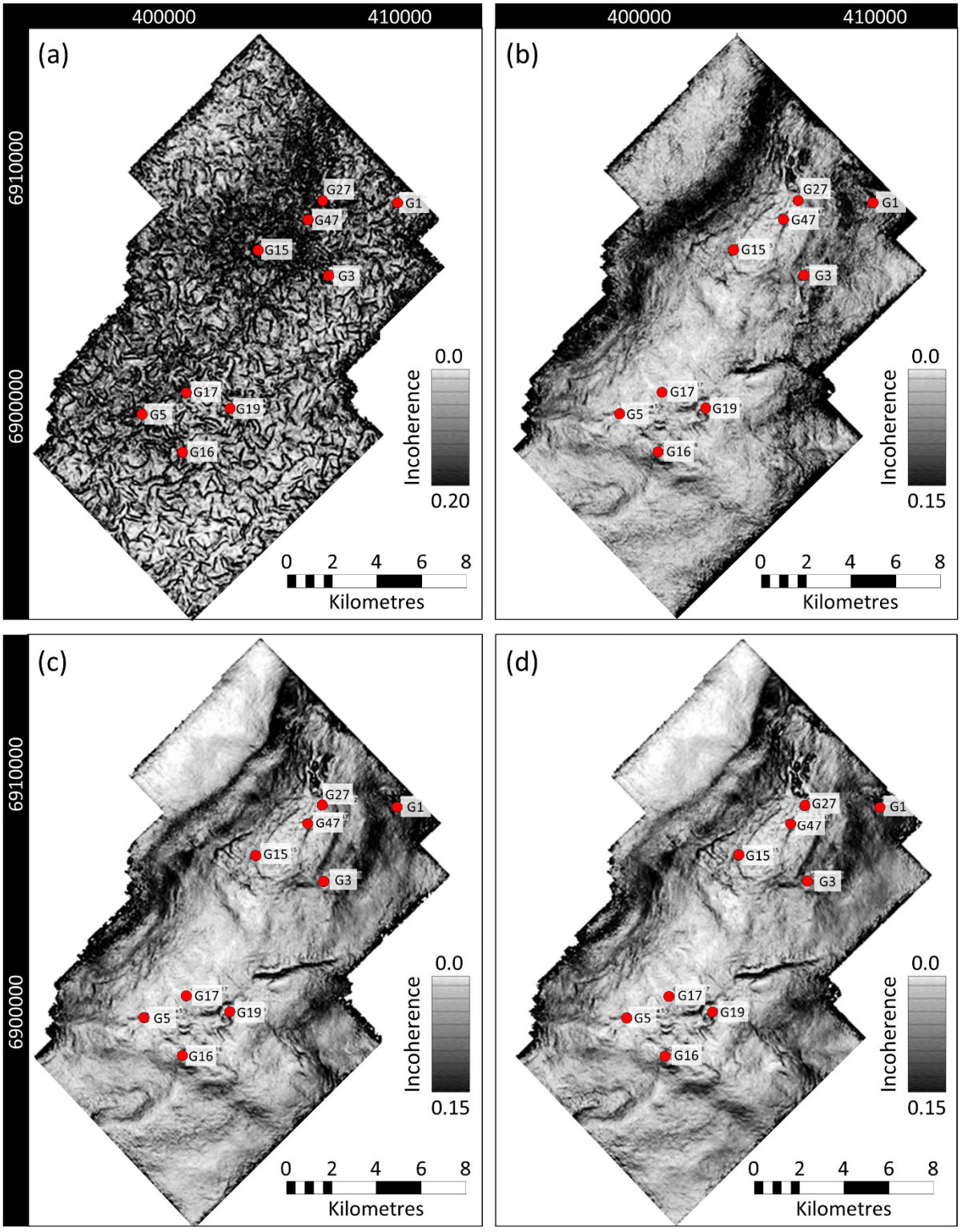


Figure 10. Incoherency maps in the Gidgealpa Field along the: (a) top Wallumbilla Formation; (b) top Toolachee Formation; (c) top Patchawarra Formation; and (d) top VC Coal. Faults are shown in black. See Fig. 3 for seismic survey location.

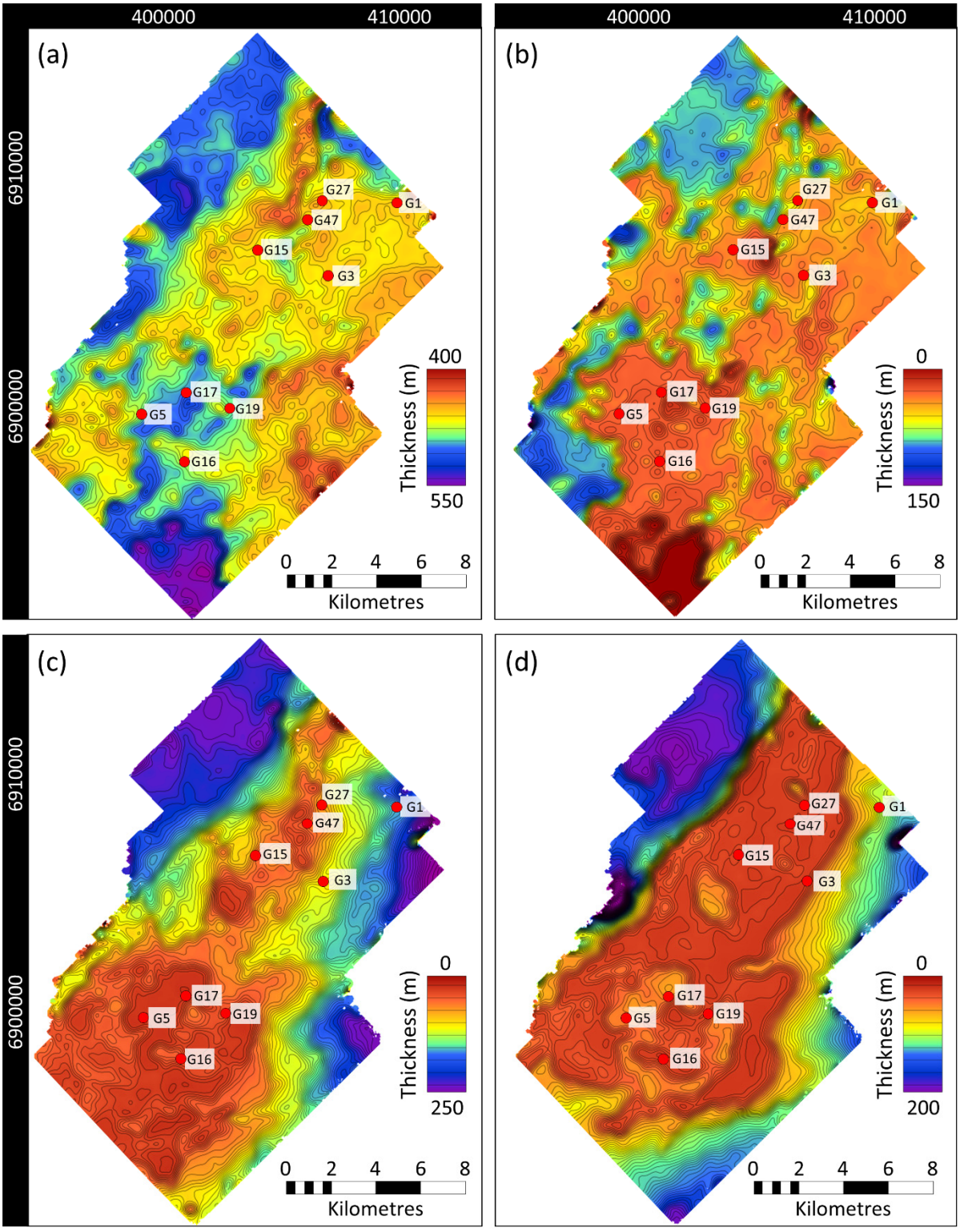


Figure 11. Isopach maps in the Gidgealpa Field showing: (a) SP1; (b) SP2; (c) SP3; and (d) SP4. See Fig. 3 for seismic survey location and Fig. 2 for stratal-package (SP) description.

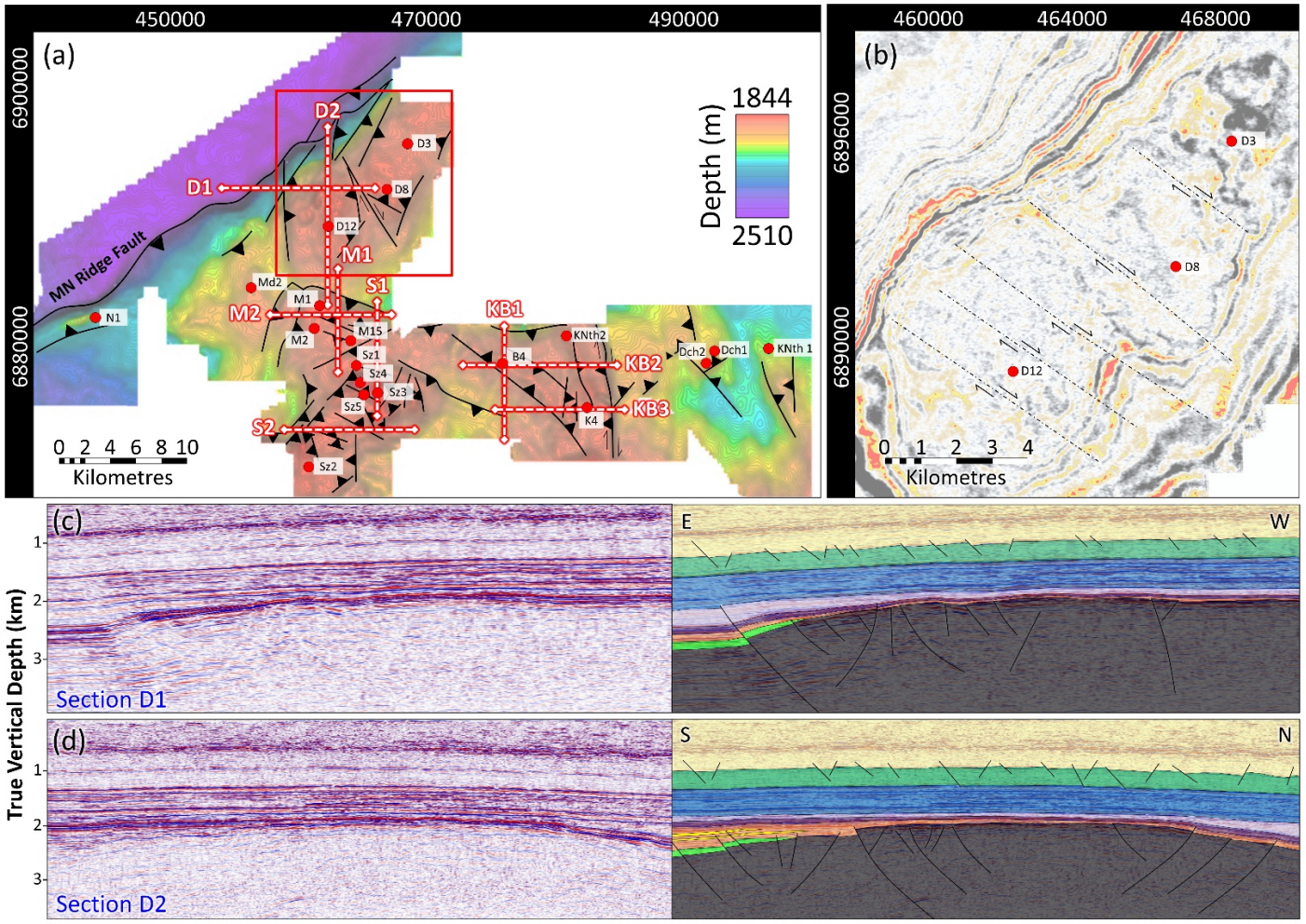


Figure 12. (a) Structural interpretation of the Greater Strzelecki 3D seismic survey projected onto the top Permian depth map (after Kulikowski et al., 2017). Location of cross-sections through the Della (cross-sections D1 and D2), Marabooka (cross-sections M1 and M2), Strzelecki (cross-sections S1 and S2), and Kidman-Bagundi Fields (cross-sections KB1, KB2, and KB3) shown. Location of depth-slice (Fig. 12b) shown in red. (b) Interpretation of NW-SE dextral strike-slip faults on a depth-slice (1,586 m) in the Della Field (see Fig. 12a for location). (c) Cross-section 'D1' through the Della Field. (d) Cross-section 'D2' through the Della Field. See Fig. 2 for colour scheme and Fig. 3 for location.

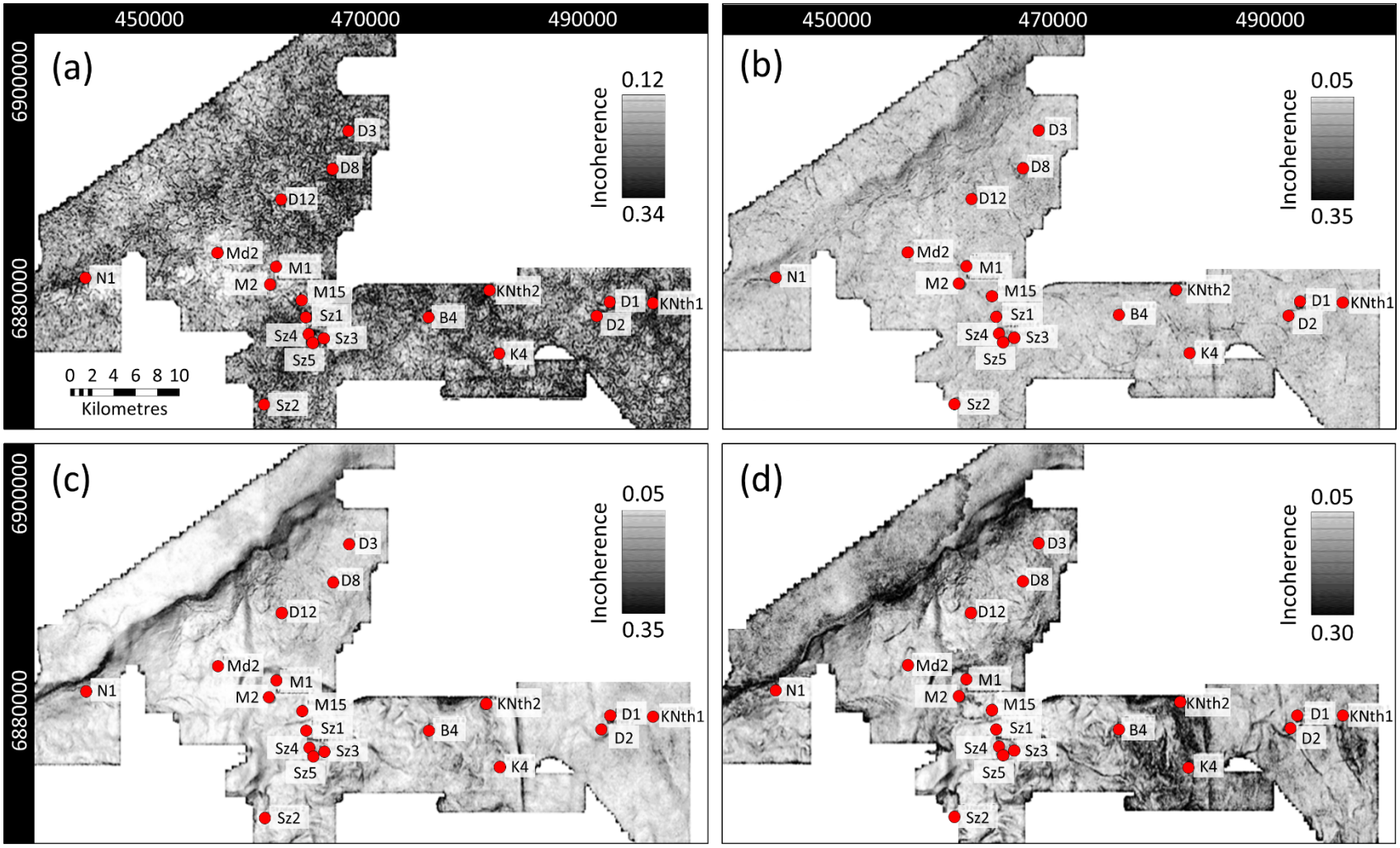


Figure 13. Incoherency analysis across the Greater Strzelecki 3D seismic survey along the: (a) top Wallumbilla Formation; (b) top Cadna-Owie Formation; (c) top Toolachee Formation; and (d) top VC Coal. Faults are shown in black. See Fig. 3 for seismic survey location.

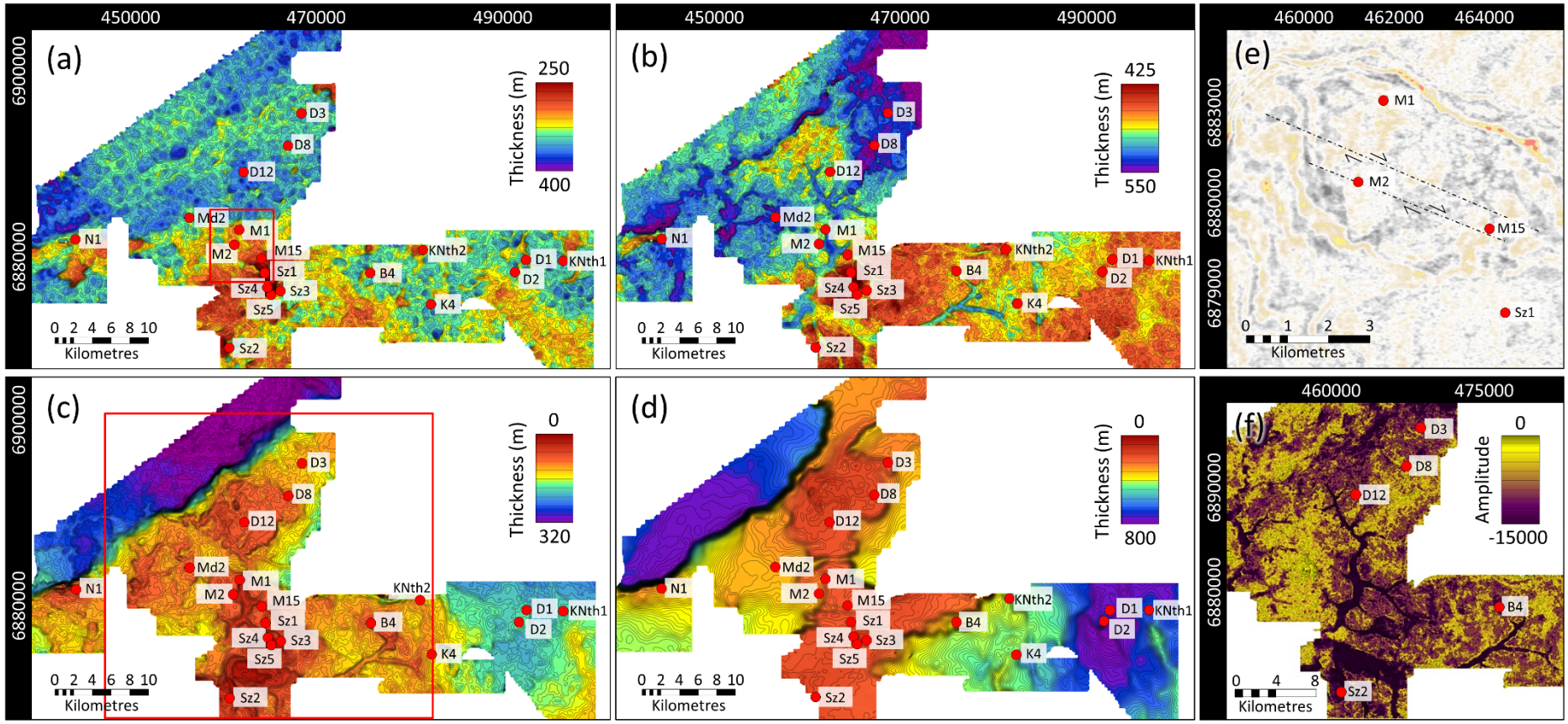


Figure 14. Isopach maps within the Greater Strzelecki 3D seismic survey between the: (a) top Wallumbilla and top Cadna-Owie formations with the location of the depth-slice in Fig. 14e shown in red; (b) SP1; (c) SP2 with the location of Fig. 14f outlined; (d) top Toolachee Formation and top VC Coal; (e) NW-SE dextral strike-slip faults on a depth-slice (2,194 m) in the Marabooka Field area. See Fig. 14a for location. (f) Amplitude map along the top Nappamerri Group reflector showing fluvial channel systems. Fig. 3 for seismic survey location and Fig. 2 for stratal-package (SP) description.

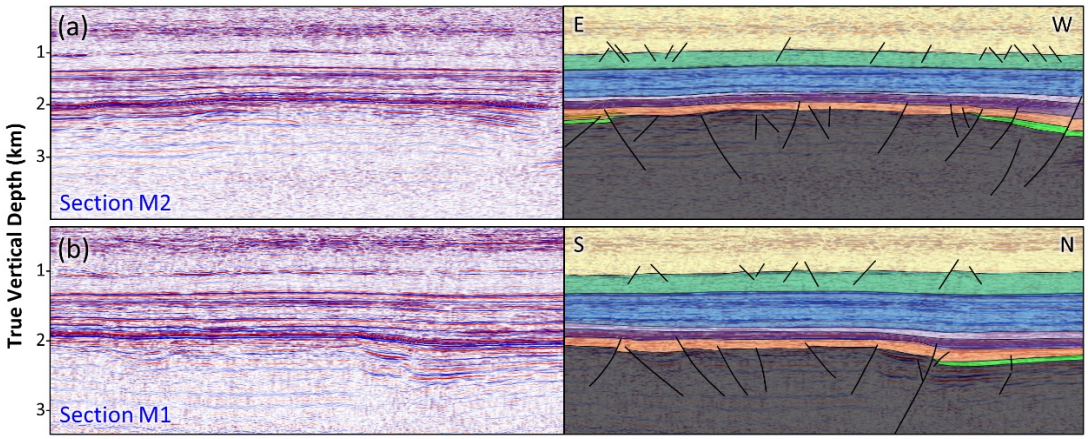


Figure 15. Interpretation of cross-sections through the Marabooka Field at location: (a) M2; and (b) M1. Location of cross-sections is shown in Fig. 12a. See Fig. 2 for colour scheme.

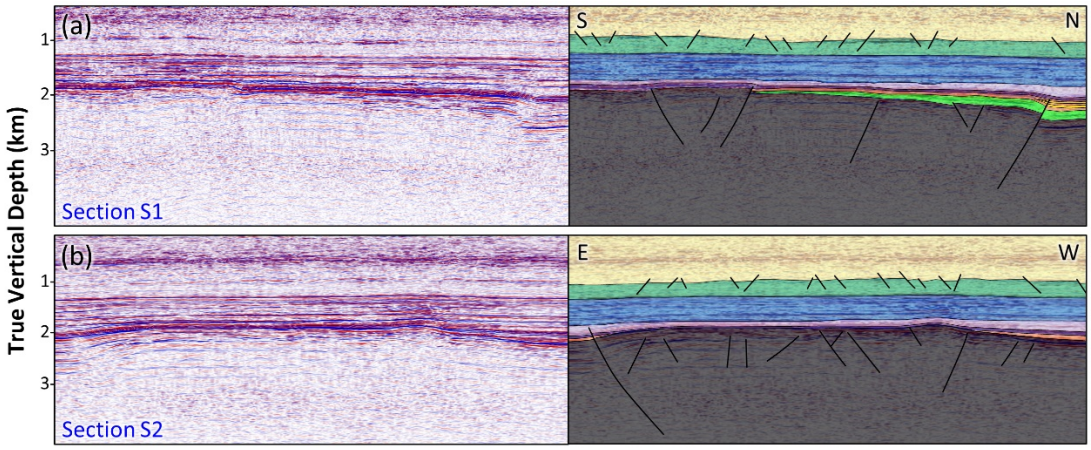


Figure 16. Interpretation of cross-sections through the Strzelecki Field at location: (a) S1; and (b) S2. Location of cross-sections is shown in Fig. 12a. See Fig. 2 for colour scheme.

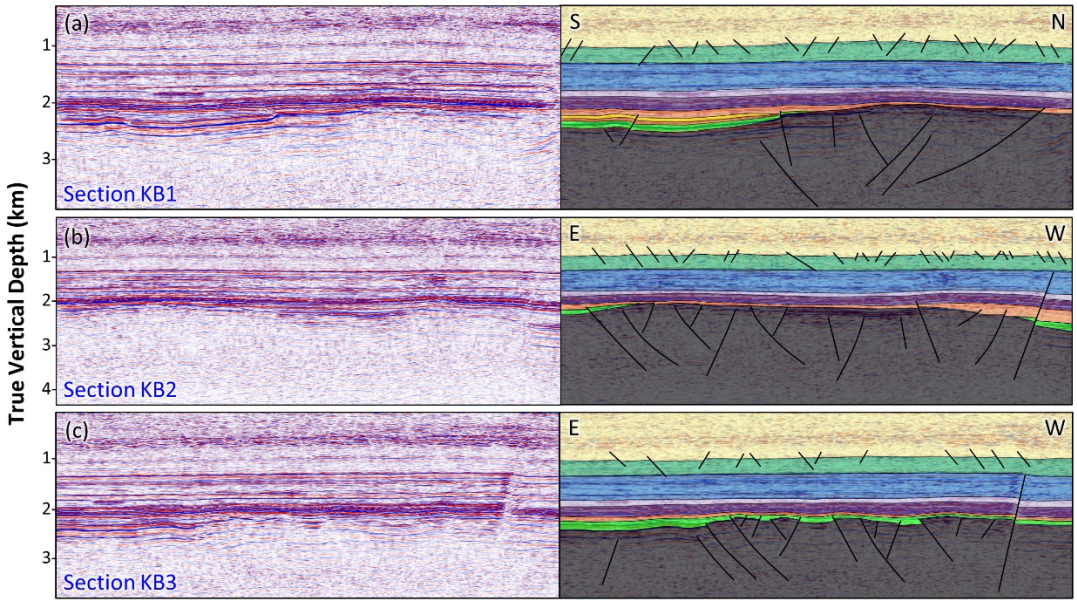


Figure 17. Interpretation of cross-sections through the Kidman-Bagundi Fields at location: (a) KB1; (b) KB2; and (c) KB3. See Fig. 12a for location. See Fig. 2 for colour scheme.

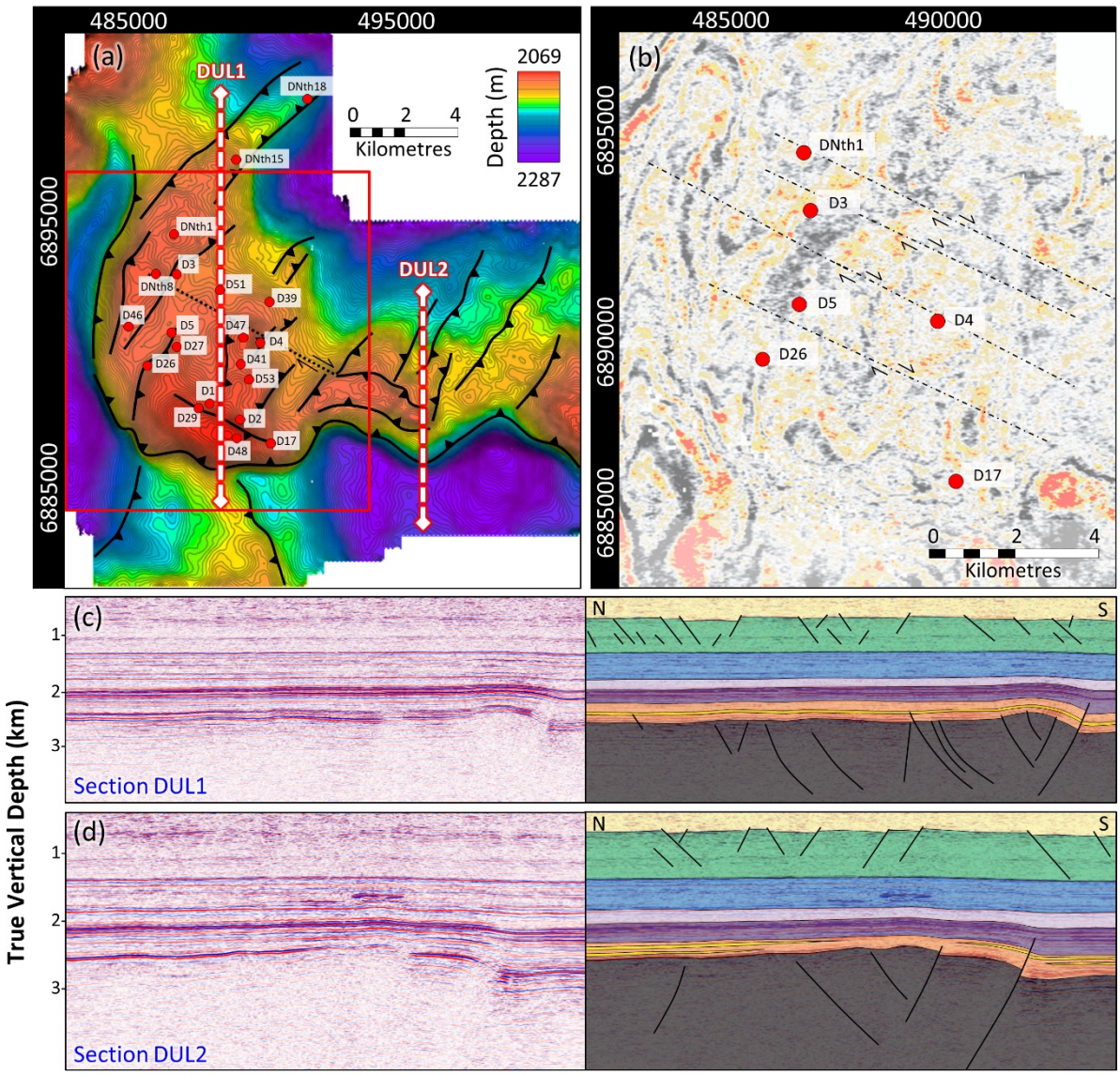


Figure 18. Structural interpretation of the Dullingari Field showing: (a) Detailed structural map of the Dullingari Field projected onto the top Permian depth map with the location of cross-sections DUL1 and DUL2 and depth-slice (red outline) shown (after Kulikowski et al., 2017); (b) Interpretation of approximately NW-SE dextral strike-slip faults on a depth-slice (2,907 m) in the Dullingari Field (See Fig. 18a for location); (c) Cross-section DUL1; and (d) Cross-section DUL2. Location of cross-sections shown in Fig. 18a. See Fig. 2 for colour scheme and Fig. 3 for seismic survey location.

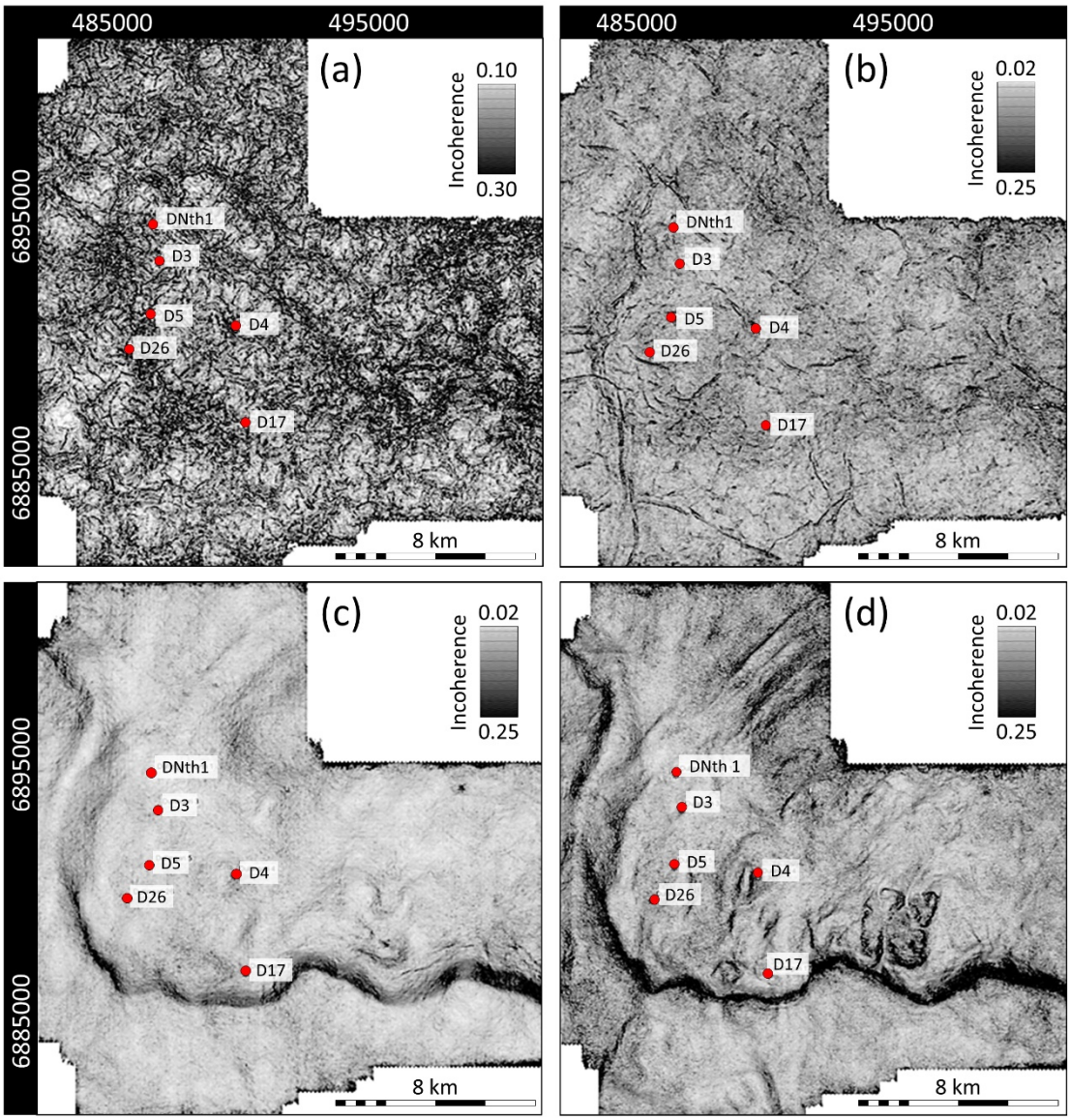


Figure 19. Incoherency maps in the Dullingari Field along the: (a) top Wallumbilla Formation; (b) top Cadna-Owie Formation; (c) top Toolachee Formation; and (d) top VC Coal (after Kulikowski et al., 2017). Faults are shown in black. See Fig. 3 for seismic survey location.

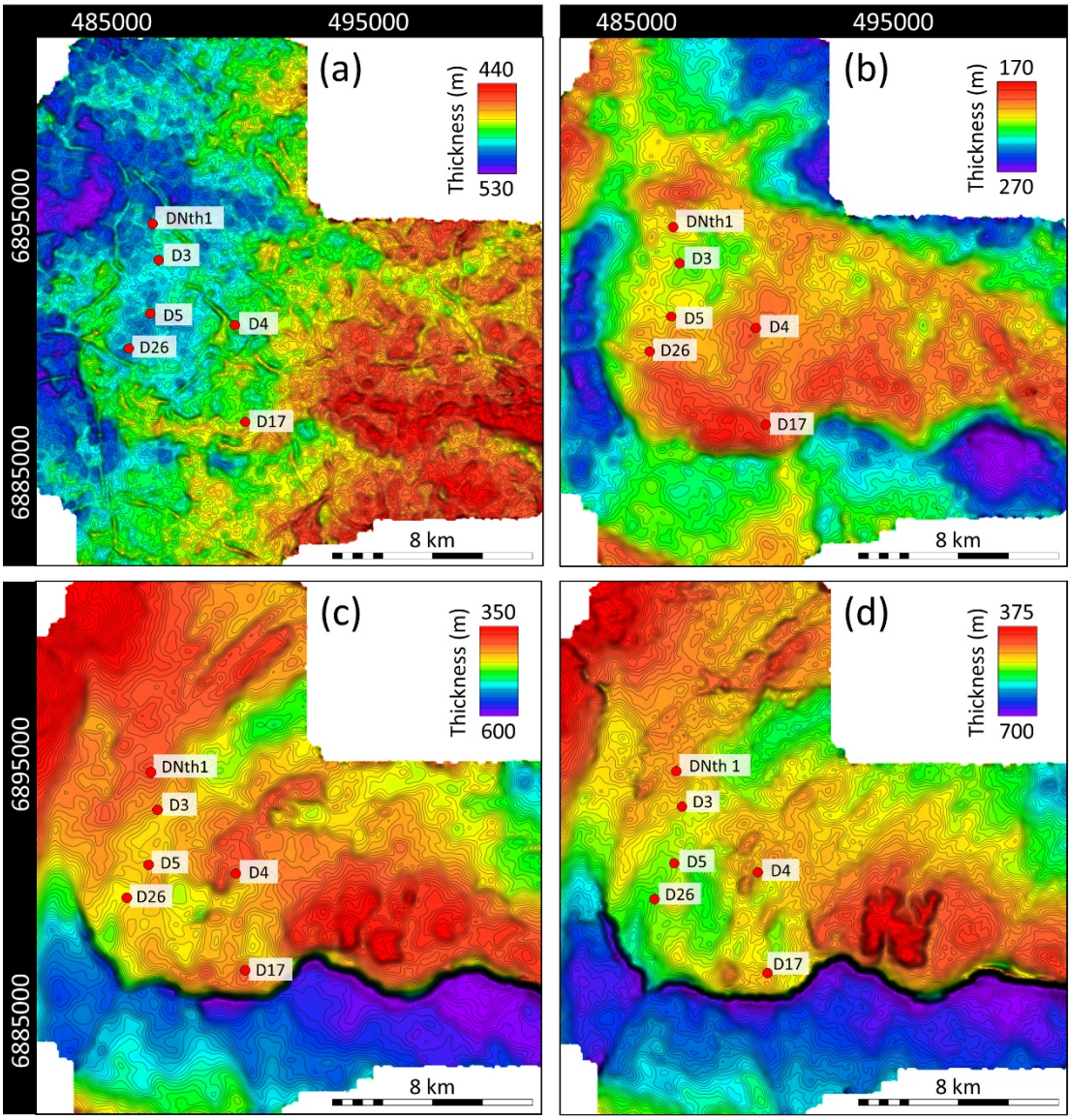


Figure 20. Isopach maps in the Dullingari Field showing: (a) SP1; (b) SP2; (c) SP3; and (d) top Toolachee Formation to top VC Coal thickness. See Fig. 3 for seismic survey location and Fig. 2 for stratal-package (SP) description.

5.5. MANUSCRIPT 5: Fault reactivation with in situ stress

Geomechanical modelling of fault reactivation in the Cooper Basin, Australia

For the first time in the Cooper-Eromanga Basin, Australia, we model the risk of fault reactivation in four ways; [1] fault slip tendency; [2] fault dilation tendency; [3] fault reactivation (shear fracture) with increased pore pressure; and [4] fault reactivation (shear reactivation) with increased pore pressure. Similar analyses have been performed in basins around the world to predict the potential for faults to reactivate and act as fluid conduits. This analysis is particularly beneficial to this basin because of its high dependency on hydraulic fracture stimulation treatments, which is known to encourage fault reactivation. We analysed the depth converted Dullingari and Swan Lake three-dimensional seismic surveys to find that near vertical SE-NW striking faults are most susceptible to slip, dilate, and reactivate under the present-day stress regime. The pore pressure increase during fracture stimulation treatments may be sufficiently high to reactivate this regional fault set and lead to cataclasis, compartmentalisation of the reservoir, and hydrocarbon leakage.

CITATION:

Kulikowski, D., Amrouch, K., & Cooke, D. (2016). Geomechanical Modelling of Fault Reactivation in the Cooper Basin, Australia. Australian Journal of Earth Sciences, 63(3), 295-314, doi:10.1080/08120099.2016.1212925.

Statement of Authorship

Title of Paper:	Geomechanical Modelling of Fault Reactivation in the Cooper Basin, Australia
Publication Status:	**Manuscript Published**
Publication Details:	Kulikowski, D., Amrouch, K., & Cooke, D. (2016). Geomechanical Modelling of Fault Reactivation in the Cooper Basin, Australia. *Australian Journal of Earth Sciences*, 63(3), 295-314, doi:10.1080/08120099.2016.1212925.

Principal Author

Principal Author (Candidate):	David Kulikowski		
Contribution to the Paper:	Seismic interpretation, geomechanical modelling, analysis, and writing.		
Overall percentage (%):	80%		
Certification:	This paper reports on original research I conducted during the period of my Higher Degree by Research candidature and is not subject to any obligations or contractual agreements with a third party that would constrain its inclusion in this thesis. I am the primary author of this paper.		
Signature:		Date:	29 March 2017

Co-Author Contribution

By signing the Statement of Authorship, each author certifies that:

i. the candidate's stated contribution to the publication is accurate (as detailed above);

ii. permission is granted for the candidate to include the publication in the thesis; and

iii. the sum of all co-author contributions is equal to 100% less the candidate's stated contribution.

Name of Co-Author:	Khalid Amrouch (10%)		
Contribution to the Paper:	Provided feedback on analysis and a complete review of paper.		
Signature:		Date:	29 March 2017

Name of Co-Author:	Dennis Cooke (10%)		
Contribution to the Paper:	Provided feedback on analysis and a complete review of paper.		
Signature:		Date:	28 Mar 2017

AUSTRALIAN JOURNAL OF EARTH SCIENCES, 2016
VOL. 63, NO. 3, 295–314
http://dx.doi.org/10.1080/08120099.2016.1212925

Geomechanical modelling of fault reactivation in the Cooper Basin, Australia

D. Kulikowski, K. Amrouch and D. Cooke

Australian School of Petroleum, University of Adelaide, 5005, North Terrace, Adelaide, Australia

ABSTRACT

The Australian Cooper Basin is a structurally complex intra-cratonic basin with large unconventional hydrocarbon potential. Fracture stimulation treatments are used extensively in this basin to improve the economic feasibility; however, such treatments may induce fault activity and risk the integrity of hydrocarbon accumulations. Fault reactivation may not only encourage tertiary fluid migration but also decrease porosity through cataclasis and potentially compartmentalise the reservoir. Relatively new depth-converted three-dimensional seismic surveys covering the Dullingari and Swan Lake 3D seismic surveys were structurally interpreted and geomechanically modelled to constrain the slip tendency, dilation tendency and fracture stability of faults under the present-day stress. A field-scale pore pressure study found a maximum pressure gradient of 11.31 kPa/m within the Dullingari 3D seismic survey, and 11.14 kPa/m within the Swan Lake 3D seismic survey. The present-day stress tensor was taken from previously published work, and combined with local pore pressure gradients and depth-converted field-scale fault geometries, to conclude that SE–NW-striking strike-slip faults are optimally oriented to reactivate and dilate. High-angle faults striking approximately E–W appear most likely to dilate, and act as fluid conduits irrespective of being modelled under a strike-slip or compressional stress regime. Near-vertical SE–NW and NE–SW-striking faults were modelled to be preferentially oriented to slip and reactivate under a strike-slip stress regime. Considering that SE–NW-striking strike-slip faults have only recently been interpreted in the literature, it is possible that many reservoir simulations and development plans have overlooked or underestimated the effect that fault reactivation may have on reservoir properties. Future work investigating the likelihood that fracture stimulation treatments may be interacting, and reactivating, pre-existing faults and fractures would benefit field development programs utilising high-pressure hydraulic fracture stimulation treatments.

ARTICLE HISTORY
Received 9 November 2015
Accepted 25 June 2016

KEYWORDS
Cooper Basin; fault reactivation; structural geology; seismic interpretation; stress; geomechanical modelling; geomechanics

Introduction

This study utilises two-dimensional (2D) and three-dimensional (3D) seismic data from Australia's largest onshore hydrocarbon province, the Cooper Basin (Figure 1), to analyse the slip tendency, dilation tendency and fracture stability of field-scale faults under the present-day stress field based on fundamental structural permeability concepts (Morris, Ferrill, & Henderson, 1996; Sibson, 1996). These analyses define the risk of fault slip, fault opening (or dilation) and fault reactivation, which provide insights into the potential escape, or tertiary migration, of hydrocarbons through recently active faults. The relative risk of fault reactivation can be accurately assessed given that the complete present-day stress tensor, fault geometry, pore pressure and rock failure envelope are well constrained. Similar risk assessments have been conducted in many basins around the world but never in the Australian Cooper Basin (Macdonald, Backé, King, Holford, & Hillis, 2012; Moeck, Kwiatek, & Zimmermann, 2009; Morris et al., 1996; Swierczek et al., 2013; van Ruth, Nelson, & Hill, 2006; Wiprut & Zoback, 2000, 2002; Worum et al., 2004). Our research models the reactivation potential of reverse and strike-slip faults in a highly complex stress field that can alternate between a compressive and strike-slip stress regime between adjacent fields. Our structural interpretation of field-scale faults within the Dullingari and Swan Lake 3D seismic surveys (Figure 2) was performed on relatively new (acquired 2001 and 2000, respectively) depth-converted 3D seismic data utilising cutting-edge seismic processing and interpretation software. The results highlight the fault geometry optimally oriented to dilate, slip and reactivate within the present-day stress regime.

The structurally complex intra-cratonic Cooper Basin is located across central Australia (Figure 1). Unconformable boundaries isolate the basin from the overlying Jurassic to Cretaceous Eromanga Basin, and underlying Cambrian to Silurian Warburton Basin (basement) (Figure 3). Researchers have linked the reactivation of basement-involved faults with the development of present-day structures such as the major NE–SW-striking Gidgealpa–Merrimelia–Innamincka (GMI) and Murteree–Nappacoongee (MN) Ridges (Apak, Stuart, Lemon, & Wood, 1997; Kuang, 1985; Mavromatidis, 2006).

CONTACT D. Kulikowski david.kulikowski@adelaide.edu.au
Editorial handling: Keyu Liu

© 2016 Geological Society of Australia

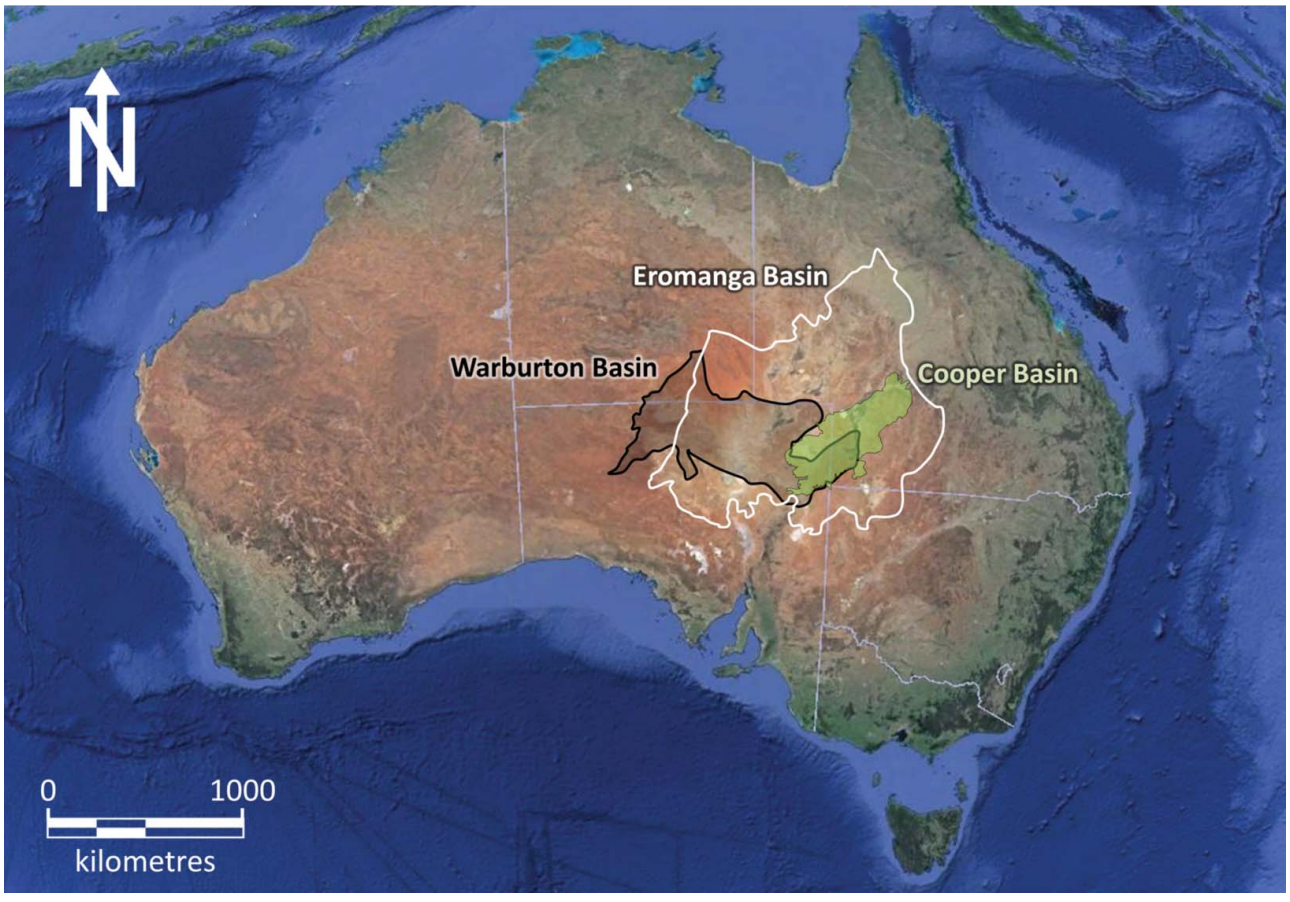


Figure 1. Location of the Eromanga, Cooper and Warburton basins within central Australia.

However, it is unclear whether the present-day stress regime, coupled with high-formation pore pressure, has the potential to reactivate existing faults. The basin has large potential in unconventional hydrocarbon production; however, low permeability hydrocarbon reservoirs require multi-stage fracture stimulation treatments, which are commonly complex, in order to be economically feasible (Durant et al., 2013; Pokalai, Kulikowski, Johnson, Haghighi, & Cooke, 2016). The effect of

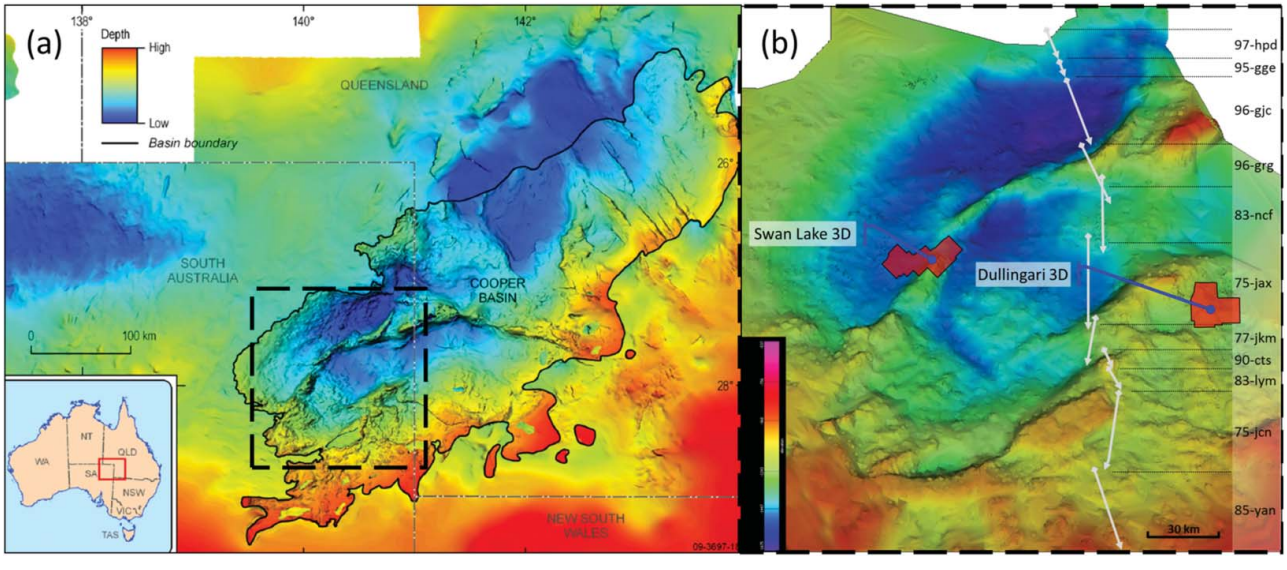


Figure 2. (a) Location of the study area relative to the entire Cooper Basin. (b) Inset map of the study area showing the location and orientation of the Swan Lake 3D seismic survey and the Dullingari 3D seismic survey, and the location of 2D seismic lines used for the regional N—S cross-section. (Figure 2a modified after Radke, 2009).

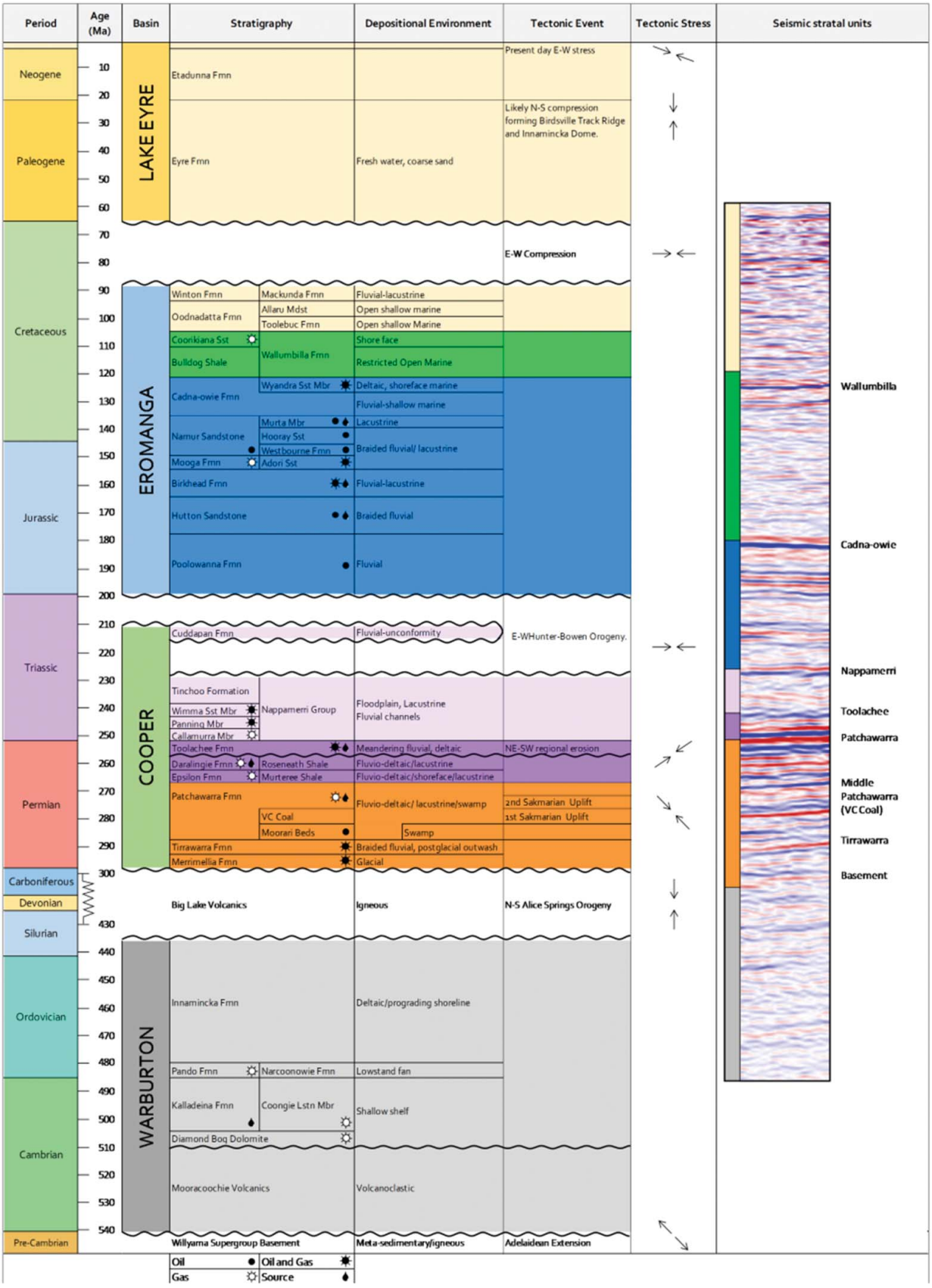


Figure 3. Stratigraphy of the Lake Eyre, Eromanga, Cooper and Warburton basins. A typical seismic reflection profile is shown together with the colour scheme for cross-sections.

increasing pore pressure at depth during fluid injection has benefits in improving structural permeability within a reservoir, but has also been reported to result in seismicity, or fault reactivation (Healy, Rubey, Griggs, & Raleigh, 1968; Raleigh, Healy, & Bredehoeft, 1976; Rutqvist, Rinaldi, Cappa, & Moridis, 2013; Wiprut & Zoback, 2000; Zoback & Harjes, 1997). It is well understood that increasing pore pressure at depth reduces the effective stress and therefore increases the risk of fault and fracture reactivation, which may lead to hydrocarbons leaking to the surface and potentially contaminating Australia's natural aquifer; the Great Artesian Basin. This research constrains the fault geometries that are optimally oriented to reactivate under the present-day stress and investigates the conditions that may encourage reactivation.

Geological setting

The structurally complex Carboniferous to Triassic Cooper Basin is located within central Australia and is isolated from the overlying Eromanga Basin and underlying Warburton Basin by regional unconformities (Figure 3). Initial accommodation space was developed during SE–NW-oriented Adelaidean (540 Ma) extension, which developed NE–SW-striking normal faults and SE–NW-striking strike-slip faults (Apak et al., 1997; Haines, Hand, & Sandiford, 2001; Müller, Dyksterhuis, & Rey, 2012). It is difficult to analyse fault growth as seismic data are poor below thick Permian coal; however, normal and reverse faults can be seen within basement (Figure 4). This extensional phase continued through the deposition of Warburton Basin sediments, which consist of volcanics and carbonates within shallow shelf and deltaic sediments (Gatehouse, 1986). The regional unconformity separating the Cambrian to Silurian Warburton Basin from the Cooper Basin is thought to have developed during the reactivation of pre-existing faults caused by the Carboniferous N–S Alice Springs Orogeny. This erosional unconformity event is associated with the emplacement of the Carboniferous Big Lake Granites and is believed to have facilitated a dextral sense of motional along pre-existing SE–NW-striking vertical faults, as well as increased the local geothermal gradient in areas where uranium-rich basement was uplifted (Apak et al., 1997; Glikson, Uysal, Fitz Gerald, & Saygin, 2013; Khair, Cooke, & Hand, 2015; Kulikowski, Cooke, & Amrouch, 2016a; Rezaee & Sun, 2007).

Post-compressional flexural relaxation is recorded during the deposition of the glacial Merrimelia Formation and fluvial Tirrawarra Formation, which on-lap onto major structures including the NE–SW-striking GMI and MN Ridges (Apak et al., 1997; Kantsler, Prudence, Cook, & Zwigulis, 1983). The Patchawarra Formation was cyclically deposited in fluvio-deltaic, lacustrine and swamp conditions during the middle Permian (Alexander, Gravestock, Cubitt, & Chaney, 1998; Boreham & Hill, 1998). Two periods of intra-formational on-lapping are evidenced within the Patchawarra Formation and align with SE–NW-oriented Sakmarian compression (Apak et al., 1997; Kantsler et al., 1983; Kulikowski, Amrouch, Al Barwani, Liu, & Cooke, 2015). As compression eased towards the upper Patchawarra Formation, an east-to-west regional transgression raised sea-level, and fluvio-deltaic, shoreface and lacustrine sediments were deposited as the Murteree Shale, Epsilon Formation, Roseneath Shale, and Daralingie Formation (Apak et al., 1997; Bradshaw, 1993; Gravestock & Jensen-Schmidt, 1998). Sedimentation was interrupted post-Daralingie Formation deposition, as a NE–SW-oriented stress regime reactivated basement faults and eroded much of the Daralingie Formation (Apak et al., 1997; Kuang, 1985; Mavromatidis, 2006).

As compression eased in the late Permian, the fluvial Toolachee Formation was deposited as cyclic sands, shales and coals (Apak et al., 1997; Kantsler et al., 1983). Fluvial conditions continued with the deposition of the Nappamerri Group sediments (Apak et al., 1997; Kantsler et al., 1983). The upper Nappamerri Group sediments mark an erosional unconformity that separates the Cooper Basin from the overlying Jurassic to Cretaceous Eromanga Basin. Erosion of up to 500 m of Nappamerri Group sediments was facilitated by the reactivation of basement faults during the Upper Triassic E–W Hunter-Bowen Orogeny (Alexander et al., 1998; Apak et al., 1997; Kantsler et al., 1983; Mavromatidis, 2006). Subsequent flexural relaxation (or sag) dominated during a pronounced period of

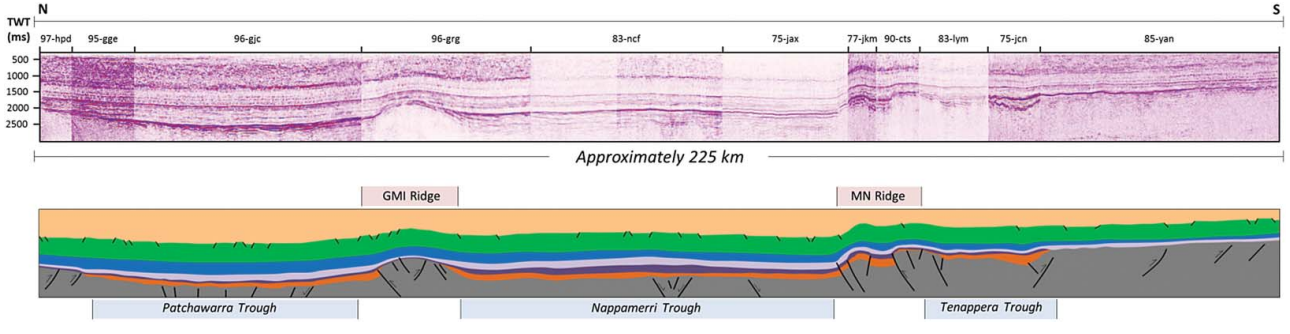


Figure 4. Regional N–S cross-section through the South Australian portion of the Cooper Basin interpreted from 2D seismic lines. The NE–SW-striking Gidgealpa–Merrimelia–Innamincka (GMI) and Murteree–Nappacoongee (MN) Ridges are seen to isolate the Patchawarra, Nappamerri and Tenappera troughs. A system of polygonal faults is regionally identified within Cretaceous-aged sediments, and a combination of extensional, reverse and strike-slip faults are interpreted within basement and Permian strata. The location of 2D seismic lines is shown in Figure 2b. Please refer to Figure 3 for colour scheme.

tectonic quiescence between the Jurassic and Upper Cretaceous (Lowe-Young, Mackie, & Heath, 1997). Deposition of fluvio-deltaic and lacustrine sediments was uninterrupted throughout Eromanga Basin deposition (Green, Brain, & John, 1989; Hoffman, 1989; Lowe-Young et al., 1997). These sediments not only hold the Great Artesian Basin but also are presently being targeted by hydrocarbon exploration companies along basin margins.

A Late Cretaceous E−W compressional event is recorded as a regional unconformity that isolates the Eromanga Basin from the overlying Paleogene to Quaternary Lake Eyre Basin (Apak et al., 1997; Gravestock & Jensen-Schmidt, 1998; Kuang, 1985; Mavromatidis, 2006). The critical point in the Cooper Basin petroleum system has been constrained to this time (90 Ma) (Lowe-Young et al., 1997). Hydrocarbon generation, migration and entrapment within structural traps (NE−SW-trending anticlines and fault-bounded anticlines) are thought to have commenced (Gravestock & Jensen-Schmidt, 1998; Lowe-Young et al., 1997; Müller et al., 2012). This would suggest that subsequent structural movement and fault reactivation would increase the risk of seal breach, and the tertiary migration of hydrocarbons through conductive faults.

The present-day stress tensor has been researched by many authors through the measurement of leak of tests, hydraulic fracture-type (minifrac) tests, and the interpretation and analysis of borehole break out and drilling-induced tensile fractures (Hillis, Sandiford, Reynolds, & Quigley, 2008; Müller et al., 2012; Nelson et al., 2007; Reynolds, Coblentz, & Hillis, 2002; Reynolds, Mildren, Hillis, & Meyer, 2006; Sandiford, Wallace, & Coblentz, 2004); however, there is some uncertainty on the stress regime, as it can alternate between strike-slip and compressional depending on the location. The maximum stress (σ_H) is oriented approximately 101°N with a magnitude of approximately 38−41 kPa/m (e.g. Flottmann, Campagna, Hillis, & Warner, 2004; Nelson et al., 2007; Reynolds et al., 2006; Reynolds, Mildren, Hillis, & Meyer, 2004; van Ruth, Hillis, Tingate, & Swarbrick, 2003). The minimum horizontal stress magnitude (σ_h) ranges between 12 and 27 kPa/m, and the vertical stress magnitude (σ_v) overlaps this range recording between 17 and 20 kPa/m (Flottmann et al., 2004; Nelson et al., 2007; Reynolds et al., 2006; Reynolds, Mildren, Hillis, Meyer, & Flottmann, 2005; Roberts, Chipperfield, & Miller, 2000).

Methods

Seismic reflection data

Location and data quality

This study utilises publicly available 2D and 3D seismic surveys covering the Swan Lake (acquired 2000) and Dullingari (acquired 2001) fields in the South Australian portion of the Cooper Basin (Figure 2b). These fields contain a high density of wells with a large volume of adequate well control (well check-shot and formation top) data. These data are vital for accurate depth conversion and precise fault interpretation and analysis. The 3D seismic surveys are adjacent to the two major structural trends; the GMI Ridge (Swan Lake 3D seismic survey) and the MN Ridge (Dullingari 3D seismic survey). A regional N−S cross-section (Figure 4) was interpreted from several 2D seismic lines (Figure 2b) to show the general structural architecture of the basin. Seismic resolution is good between surface and top Patchawarra Formation, but the quality drastically decreases below the thick Permian coal measures. As a result, fault growth analysis is not possible within basement, making it difficult to comment on whether basement faults originated as normal faults during the Adelaidean (540 Ma) extensional event with subsequent reactivation, or whether they developed as high-angle reverse faults.

The Dullingari Field was discovered in 1979 along the NE−SW-striking MN Ridge (Kantsler et al., 1983). The field comprises two structurally isolated domes; a N−S-striking anticlinal ridge in the north and a conical dome elongate in a NW−SE direction in the south (Mount, 1981). A NE−SW-striking structural grain exists through the field, with E−W, SE−NW and N−S-striking faults also present (Kulikowski et al., 2015). The field is an oil and gas producer requiring hydraulic fracture stimulation treatments. The Swan Lake Field consists of an elongate anticlinal structure with four-way dip closure and fault bound from the northwest and southeast. High-angle reverse faults striking NE−SW are abundant in this field, with vertical SE−NW-striking strike-slip faults also present (Kulikowski et al., 2015). These fields were chosen because of their relatively high-quality 3D seismic surveys, abundance of well control and large variety of fault geometries.

Seismic time-to-depth conversion

A vital component of this research is ensuring the 3D seismic data are converted from two-way time to true depth. This allows true fault geometries to be interpreted and analysed, which will in most cases be different to faults interpreted on two-way-time seismic data. There are many methods of depth conversion that could be used (interval velocity, mean velocity, kriging with external drift, stacking velocity); however, determining the accuracy of these methods on data in the Cooper Basin is not straightforward, as many data specific variables can have a large impact on accuracy (Kulikowski, Hochwald, Cooke, & Amrouch, 2016b). Therefore, we utilise the most straightforward and basic of these methods; a time−depth trend with well check-shot data from each 3D seismic survey used as a quality control. Individual velocity models were generated for the Swan Lake and Dullingari seismic surveys using well check-shot and formation top data. Time−depth curves are shown in Figure 5.

Fault interpretation

Structural and stratigraphic interpretation from 3D seismic data is typically one of the most significant stages in the hydrocarbon exploration and development process. Correct interpretation of regional and field-scale faults is imperative to accurate reservoir modelling and production strategies; however, these may appear as subtle changes in the seismic volume that can easily be overlooked. Seismic attributes such

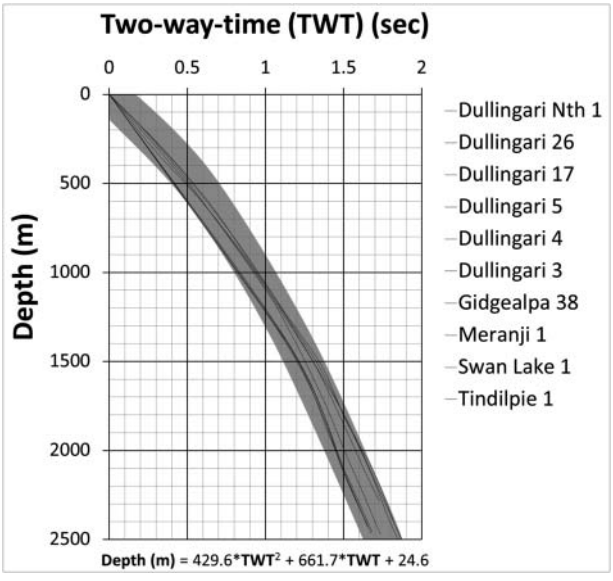


Figure 5. Time-to-depth relationship used for seismic depth conversion in the Swan Lake and Dullingari 3D seismic surveys.

as coherency, curvature and dip highlight these subtle discontinuities in seismic data and have therefore become a staple to the seismic interpreter (Basir, Javaherian, & Yaraki, 2013). These fault-enhancement attributes were used as an initial glance to better understand the fault geometry within the Dullingari and Swan Lake 3D seismic surveys. Incoherency analysis was performed on both seismic surveys as an initial pass prior to structural interpretation to gain a high level understanding of the main structural features. Incoherency visually enhances discrepancies of adjacent seismic traces to successfully identify faults that displace a given reflector or time-slice (Backé, Abul Khair, King, & Holford, 2011; Basir et al., 2013; Mai, Marfurt, & Chavez-Perez, 2009; Neves, Zahrani, & Bremkamp, 2004).

The Dullingari Field (Figure 6a) is an oil- and gas-producing field that is divided into the north and main structural domes, which are separated by a NE−SW elongate structural saddle (Figure 6b). Incoherency was applied to the VC Coal (Figure 6c) and Wallumbilla Formation (Figure 6d) reflectors to visualise the dominant fault orientation prior to interpretation. Incoherency along the VC Coal reflector highlighted a dominant NE−SW-striking fault system throughout the area, and a large E−W-striking fault that bounds the Dullingari Field from the south. This E−W-striking fault appears to form a saw-tooth-like geometry with throw decreasing to the east where it begins to rotate and strike N−S (Figure 6a−c). Incoherency along the Wallumbilla Formation reflector presented an array of randomly oriented faults. Cross-sections through the field were interpreted to show that these randomly oriented faults occur as a system of layer-bound normal faults that occur only within Cretaceous-aged sediments (Figure 6d, e). These cross-sections also show that the main basement-involved faults have a mean fault angle of approximately 60° (Figure 6d, e). Near-vertical SE−NW-striking strike-slip faults are present below the Cooper Basin strata (Figure 6d), but can be seen to penetrate into Permian sediments.

The Swan Lake Field is located along the GMI Ridge (Figure 2b) and can be described as a fault bound anticlinal structure with four-way dip closure and elongate in a NE−SW direction (Figure 7a). Fault orientation is predominantly in a NE−SW orientation (Figure 7a). The Swan Lake Field is down dip of the Gidgealpa Field and structurally isolates the Patchawarra and Nappamerri troughs (Figure 7b). Incoherency along the VC Coal (Figure 7c) and Wallumbilla Formation (Figure 7d) reflectors was used to highlight fault orientations. Figure 7d shows similar results to incoherency along the Wallumbilla Formation within the Dullingari 3D seismic survey, inferring that the layer-bound system of normal faults may be pervasive throughout the Cooper Basin (Figure 6d). Cross-sections through the Swan Lake 3D seismic survey (Figure 7e, f) show basement-involved faults dipping approximately 60° with vertical strike-slip faults present within the Swan Lake 3D seismic survey that extend into the middle Patchawarra Formation (Figure 7e). Normal faults are seen to displace the Cadna-Owie Formation and even extend into Jurassic-aged sediments (Figure 7f).

Geomechanical modelling

Overview

Structural interpretation of the 3D seismic surveys was performed on depth-converted seismic data with picks every 100−300 m depending on the length and strike of faults, but was largely dependent on the complexity of individual fault planes. Meshing artefacts were largely removed but may be present along the base of faults as seismic uncertainty and resolution decreases. The seismic data quality in the basin is a function of the thick Permian coal measures that reflect much of the signal before reaching the lowermost Cooper Basin sediments and basement formations. This has limited the detail of research possible on fault growth analysis and stratigraphic analysis that would have provided valuable details into the structural evolution of the basin.

To precisely analyse the fault planes, a thorough understanding of the present-day stress tensor is required. Input data was collated from authors who have comprehensively constrained the complete present-day stress tensor (Table 1) (Nelson et al., 2007; Reynolds et al., 2006). Each study area was modelled under both a compressive and strike-slip stress regime. The Cooper Basin exhibits a mostly strike-slip stress regime between approximately 900 and 3050 m depth; however, it has been shown through stress magnitude calculations that some areas are subject to alternating stress regimes between strike-slip and compressional (Nelson et al., 2007; Reynolds et al., 2006). The minimum horizontal stress and vertical stress were found to be equal at these depths, making it feasible to alternate stress regimes on local scales. To encapsulate all possible variations of stress, the authors model fault reactivation under both a strike-slip and compressional stress regime.

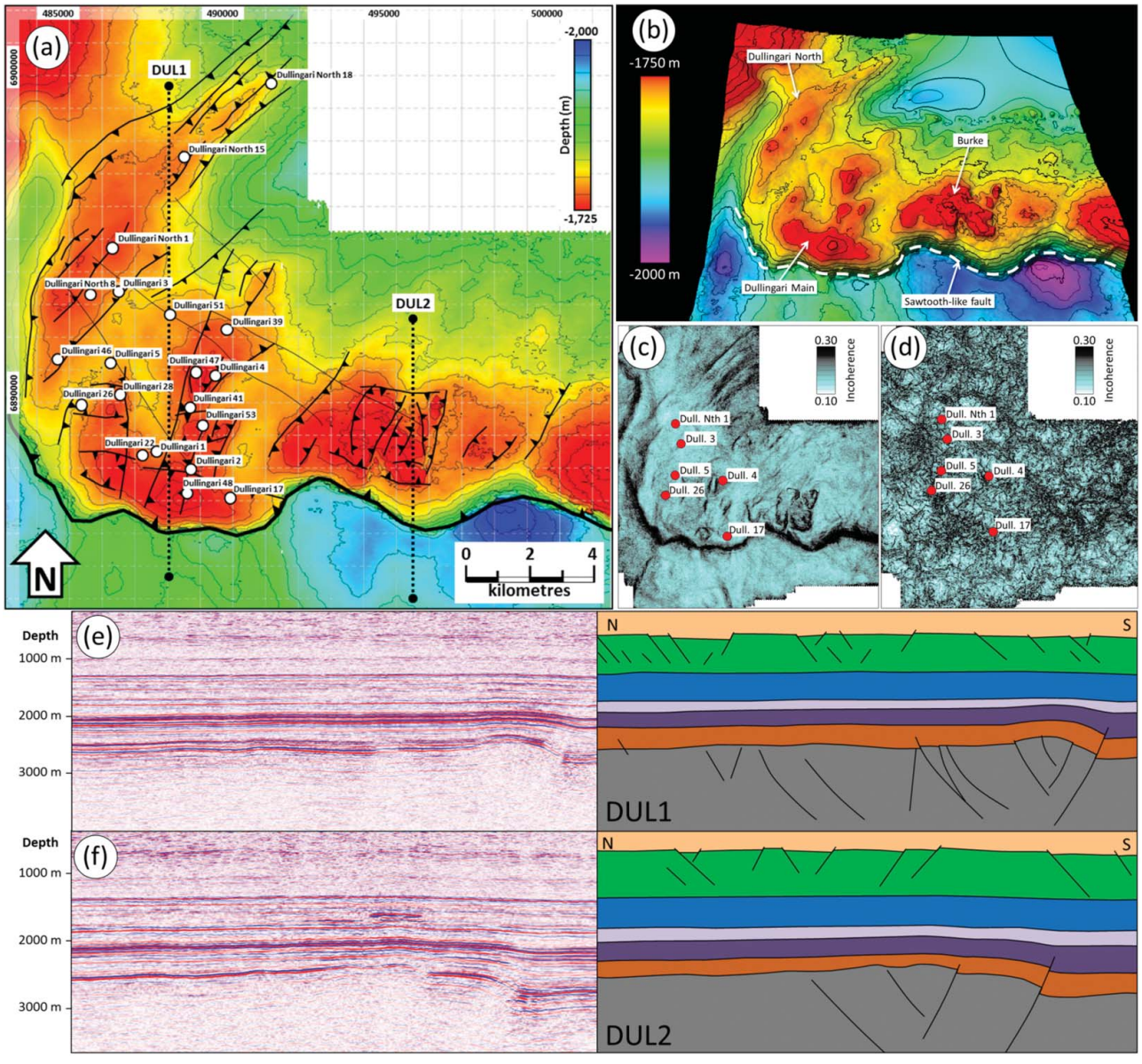


Figure 6. (a) Structural interpretation of reverse and strike-slip faults within the Dullingari 3D seismic survey with the location of two N—S cross-sections shown (DUL1 and DUL2). Wells used as horizon depth ties during the depth conversion process are shown. (b) Three-dimensional view of the Dullingari 3D seismic survey highlighting the main structural features including the main E—W-striking sawtooth-like fault. (c) Incoherency attribute analysis of the VC Coal reflector highlighting faults in black. Wells highlighted in red here contain check-shot data used for depth conversion. (d) Incoherency attribute analysis along the Wallumbilla reflector highlighting a system of polygonal faults in black. (e) N—S seismic cross-section (DUL1) through Dullingari North and Dullingari Main with structural and stratigraphic interpretation showing true fault geometries. (f) N—S seismic cross-section (DUL2) through the Burke Field and across the main E—W-striking sawtooth-like fault. Please refer to Figure 2b for location of 3D seismic survey, Figure 3 for colour scheme and Figure 6a for cross-section locations.

Geomechanical modelling of fault reactivation is performed under three equations, each providing a unique description on the likelihood of a fault plane to be active. The slip tendency, dilation tendency and fracture stability are modelled for each of the 3D seismic surveys and on every fault plane. The reactivation of faults can be undesirable within the petroleum industry as movement may increase fault permeability resulting in unwanted tertiary migration of hydrocarbons, and may promote cataclasis within a reservoir resulting in reduced reservoir properties and potential for reservoir compartmentalisation. A high-level pore pressure analysis was performed within each of the 3D seismic surveys, using various well-test data, to determine whether the study areas deviate from the hydrostatic gradient. A friction angle (μ) of 0.6 was consistently applied to each of the fault reactivation models. This value was taken from previous geomechanical research performed on the Cooper Basin (Khair et al., 2015; Nelson et al., 2007; Reynolds et al., 2006).

Slip tendency

The slip tendency (T_s) generates an assessment of the relative risk of fault slip given the present-day stress tensor and is

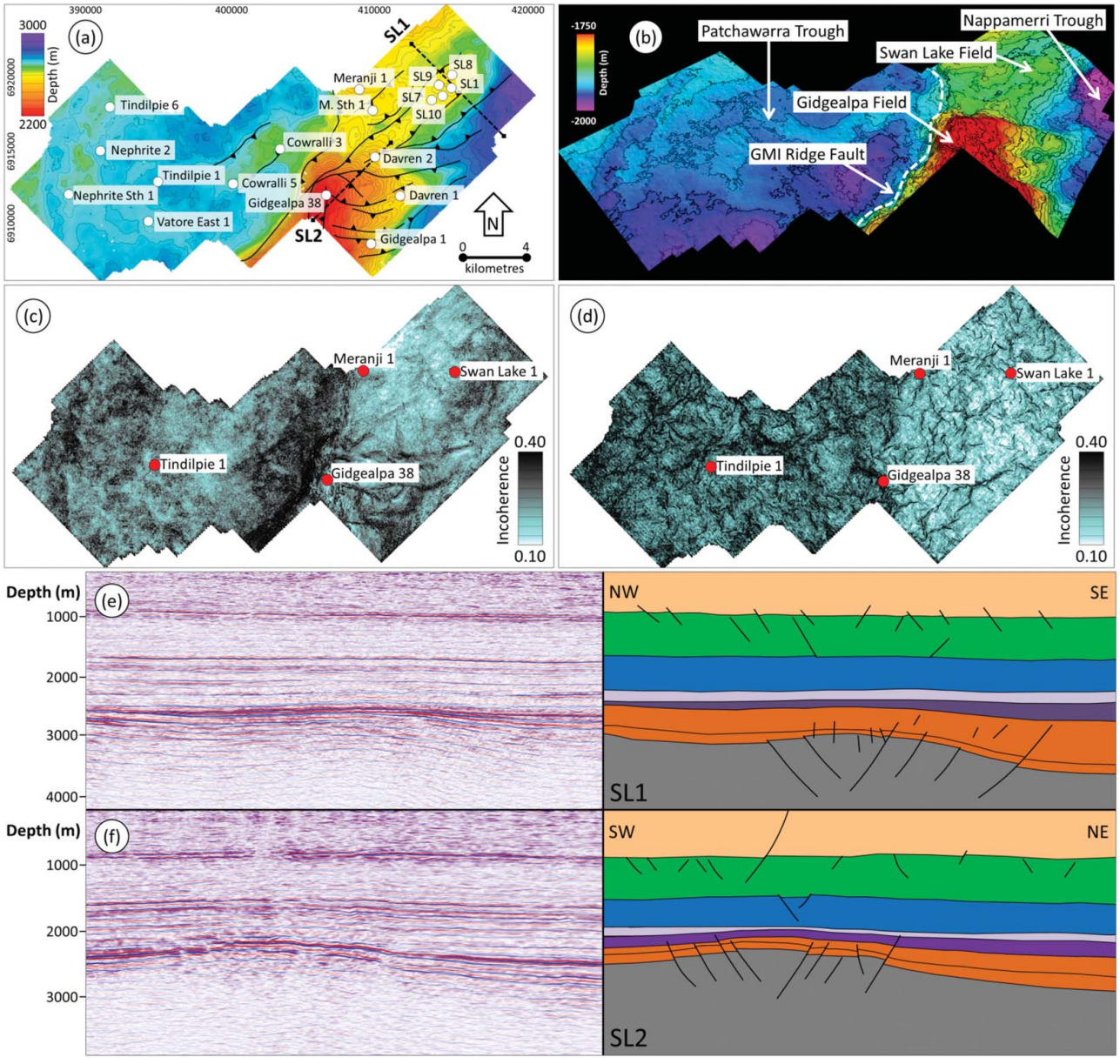


Figure 7. (a) Structural interpretation of reverse and strike-slip faults within the Swan Lake 3D seismic survey with the location of two cross-sections shown (SL1, SL2). Wells used as horizon depth ties during the depth conversion process are shown. (b) Three-dimensional view of the Swan Lake 3D seismic survey highlighting the main structural features including the regional NE—SW-striking GMI Ridge Fault that isolates the Patchawarra and Nappamerri troughs. (c) Incoherency attribute analysis of the VC Coal reflector highlighting faults in black. Wells highlighted in red here contain check-shot data used for depth conversion. (d) Incoherency attribute analysis along the Wallumbilla reflector highlighting a system of polygonal faults in black, similar to the Dullingari Field. (e) NW—SW seismic cross-section (SL1) through the Swan Lake Field with structural and stratigraphic interpretation showing true fault geometries. (f) SW—NE seismic cross-section (SL2) through the Gidgealpa Field towards the Swan Lake Field. Please refer to Figure 2b for location of 3D seismic survey, Figure 3 for colour scheme and Figure 7a for cross-section locations.

Table 1. Present-day stress data used for modelling the slip tendency, dilation tendency and fracture stability of fault planes in the Cooper Basin (Nelson et al., 2007; Reynolds et al., 2006).

Stress regime	S_{Hmax} (kPa/m)	S_{Hmax} (azi)	S_{hmin} (kPa/m)	S_v (kPa/m)	P_p (kPa/m)	Friction angle (μ)	Fault rock scenario	Cohesion (MPa)
Strike-slip	38.0	101°N	17.3	19.0	9.8	0.6	Healed	10.0
							Cohesionless	0.0
Compressional	38.0	101°N	19.0	17.3	9.8	0.6	Healed	10.0
							Cohesionless	0.0

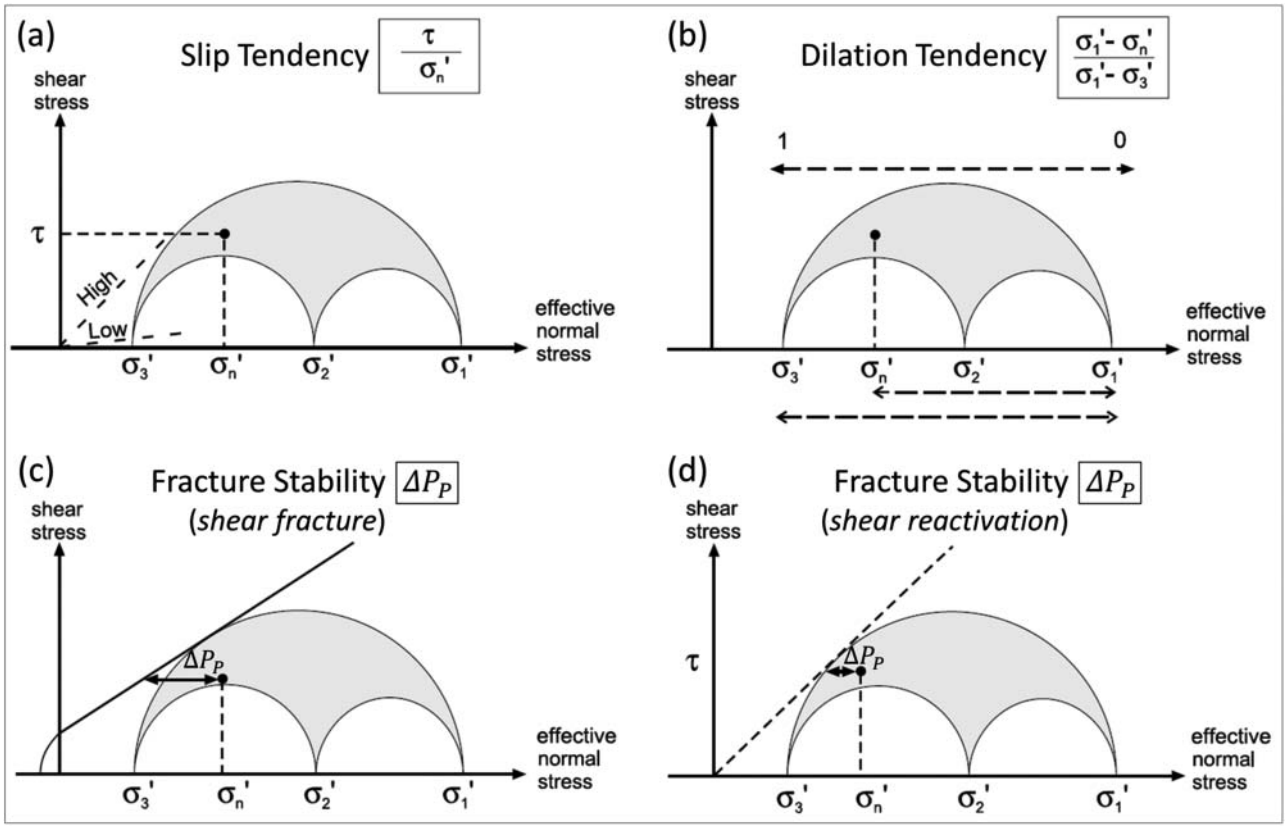


Figure 8. Definition of: (a) slip tendency; (b) dilation tendency; (c) fracture stability for shear fracture; and (d) fracture stability for shear reactivation when plotting a fault plane on the Mohr circle (modified after Mildren et al., 2005).

largely used as a tool for earthquake risk assessment (Morris et al., 1996; Sibson, 1996). This is calculated using the effective normal stress (σ'_n) and shear stress (τ) magnitudes, with the sense of motion strongly dictated by the direction of the maximum resolved shear stress relative to the fault plane (Morris et al., 1996). The equation used to measure the likelihood that a fault will slip is given below (Equation 1). This is further illustrated in Figure 8a, which visually emphasises the relationship between the fault plane geometry and the normal and shear stress magnitudes. In a broad sense, fault slip will occur when the resolved shear stress applied to a fault plane exceeds the frictional resistance to sliding (Morris et al., 1996; Swierczek et al., 2013). An increase in pore pressure creates a net decrease in the normal stress applied to a given fault plane, which relates to increased slip tendency (Jolie, Moeck, & Faulds, 2015). Morris et al. (1996) presents a thorough derivation of the slip tendency.

$$T_s = \frac{\tau}{\sigma'_n} \quad (1)$$

Dilation tendency

The ability of a fault plane to act as a fluid conduit under the present-day stress regime, or undergo tensile reactivation, is modelled using the dilation tendency attribute. This attribute is most applicable to petroleum reservoirs that are fault sealing or that have faults extending from the reservoir and penetrating through overlying sealing units, as this analysis predicts the likelihood of tertiary migration of hydrocarbons through a potentially permeably conduit away from the accumulation (Barton, Zoback, & Moos, 1995; Ferrill & Morris, 2003; Jolie et al., 2015). The relative dilation tendency is governed by the effective normal stress acting on the fault plane when normalised to the differential stress, which directly influences the fault aperture (Ferrill et al., 1999; Mildren et al., 2005). Equation 2 is a normalised relative measure used to calculate the dilation tendency (T_d) of a given fault plane and data set (Equation 2) (Ferrill et al., 1999; Jolie et al., 2015). A visual representation of how this simple equation is derived with respect to the maximum (σ'_1) and minimum (σ'_3) effective normal (σ'_n) stresses, and the projection of fault planes in a 3D Mohr circle is shown in Figure 8b. This equation shows how an existing fault plane has an increased tendency to dilate and remain open to potential fluid flow as σ'_n approaches σ'_3.

$$T_d = \frac{\sigma'_1 - \sigma'_n}{\sigma'_1 - \sigma'_3} \quad (2)$$

Fracture stability

Fracture stability analysis is used to illustrate the relative increase in pore pressure required to initiate fault reactivation on a given fault plane. The increase in pore pressure (ΔP_P)

effectively shifts the Mohr circle to the left until the projected fault plane intersects the composite failure envelope (Figure 8c). Hung and Wu (2012) showed that fluid injection technologies (hydraulic fracture stimulation, carbon dioxide sequestration, natural gas storage, etc.) have sufficient mobility to interact with nearby fault planes and influence their reactivation potential by effectively increasing the horizontal stress magnitude. This relationship is described in Equation 3.

$$\Delta S_{\mathrm{Hor}} = \alpha\left(\frac{1-2v}{1-v}\right)\Delta P_{\mathrm{P}} \quad (3)$$

where ΔS_{Hor} is the horizontal stress, α is Biot's coefficient that describes the difference between the total stress and the effective stress, v is the Poisson ratio, and ΔP_{P} is the pore pressure increase (Hung & Wu, 2012). It is clear how closely the change in pore pressure relates to an increase in horizontal stress; therefore, fracture stability analysis would be beneficial in the Cooper Basin, considering that hydraulic fracture stimulation treatments are used extensively throughout the basin (Rutqvist et al., 2013).

Fracture stability is calculated using the complete present-day stress tensor, pore pressure, fault geometry, composite failure envelope, and fault surface cohesion (Swierczek et al., 2013). Two cases were considered for each stress regime when calculating the fracture stability: (1) fault planes with a cohesion of 10 MPa modelling healed fault planes (Figure 8c); and (2) cohesionless fault planes to isolate areas of a fault plane that are relatively more likely to reactivate than others given the present-day stress (Figure 8d).

Results

Pore-pressure analysis

Understanding the pore pressure among faults is fundamental to accurate geomechanical modelling, as the effective stress changes with a change in pore pressure. Significant over pressures have been recorded throughout the Cooper Basin, increasing as high as 14.5 MPa in excess of the hydrostatic gradient (Kulikowski et al., 2016a; van Ruth et al., 2003). Over pressure in the Nappamerri Trough has been attributed to an increase in mean stress of up to 50 MPa since the Late Cretaceous (van Ruth et al., 2003). Pressure profiles within the Nappamerri Trough follow the hydrostatic gradient until approximately 2700 m depth, where significant over pressure is observed (Reynolds et al., 2006). Field-scale pore pressure analyses outside the Nappamerri Trough have not been previously explored, and considering that the Dullingari and Swan Lake 3D seismic surveys are on structural highs, research conducted exclusively in the Nappamerri Trough cannot be confidently extrapolated to our study areas. In order to accurately analyse the reactivation potential of faults, we collate reservoir pressure data from the Dullingari and Swan Lake 3D seismic surveys. Pressure data from drill stem tests (DSTs), repeat formation tests (RFTs), and formation multi-testers (FMTs) are plotted against the hydrostatic gradient (9.80 kPa/m) to determine the degree of over pressure.

Reservoir pressures within the Dullingari 3D seismic survey reach a maximum pressure gradient of 11.31 kPa/m sampled from the Patchawarra Formation (Figure 9a). A number of pressure data points are plotted above the hydrostatic gradient, particularly within the Toolachee and Patchawarra formations. Temperature data were also plotted with depth giving a mean temperature gradient in the Dullingari 3D seismic survey of 4.55°C/100 m (Figure 9b). Pressure data within the Swan Lake 3D seismic survey are also plotted above the hydrostatic gradient reaching a maximum of 11.14 kPa/m (Figure 10a).

Dullingari 3D seismic survey

The Dullingari 3D seismic survey contains a dominant NE–SW-striking structural grain (Figure 11a–c), with N–S, E–W and SE–NW-striking faults also present (Figures 6a, 11c). Fault planes typically have a high angle (Figure 11a) with two dominant fault strike clusters (Figure 11b); high-angle NE–SW-striking faults, and near vertical SE–NW-striking faults. The mean fault plane dip angle of these fault sets is shown in Table 2, with high-angle reverse faults typically dipping at approximately 55–60°, and near vertical SE–NW-striking strike-slip faults dipping at approximately 80–85°. These fault geometries are known to be present on a regional-scale; however, they have not been measured at field-scale. Near vertical SE–NW-striking field-scale faults have only recently appeared in literature and may have a substantial impact on reservoir properties through cataclasis and compartmentalisation of reservoirs (Grant-Woolley, Kong, Schoemaker, Nasreddin, & Montague, 2014). High-angle faults show reverse displacement; however, owing to decreased seismic resolution with depth, it is not possible to comment on whether these faults originated as normal faults and were reactivated, or simply formed during a compressional stress regime. A main E–W-striking fault bounds the 3D seismic survey from the south and has a unique sawtooth-like geometry (Figure 6b). The fault angle decreases with depth and appears to shallow to near horizontal, which can be seen in Figure 11a where poles to planes are plotted in the centre of the stereonet (Allmendinger, Cardozo, & Fisher, 2012; Cardozo & Allmendinger, 2013).

Fault planes were analysed for their slip tendency, dilation tendency and fracture stability using fundamental

Table 2. Results from the geomechanical modelling of fault reactivation potential performed on the main fault sets within the Dullingari 3D seismic survey, where T_s = slip tendency; S_f = fracture stability with cohesion factor of 10 MPa; T_d = dilation tendency.

Main fault sets	Mean dip (angle)	Mean T_s	Mean S_f (MPa)	Mean T_d
NE–SW striking faults	57.244	0.348	5.921	0.494
SE–NW strike-slip faults	83.553	0.384	5.066	0.543
N–S striking faults	57.601	0.270	22.626	0.312
E–W striking faults	58.482	0.230	14.127	0.900

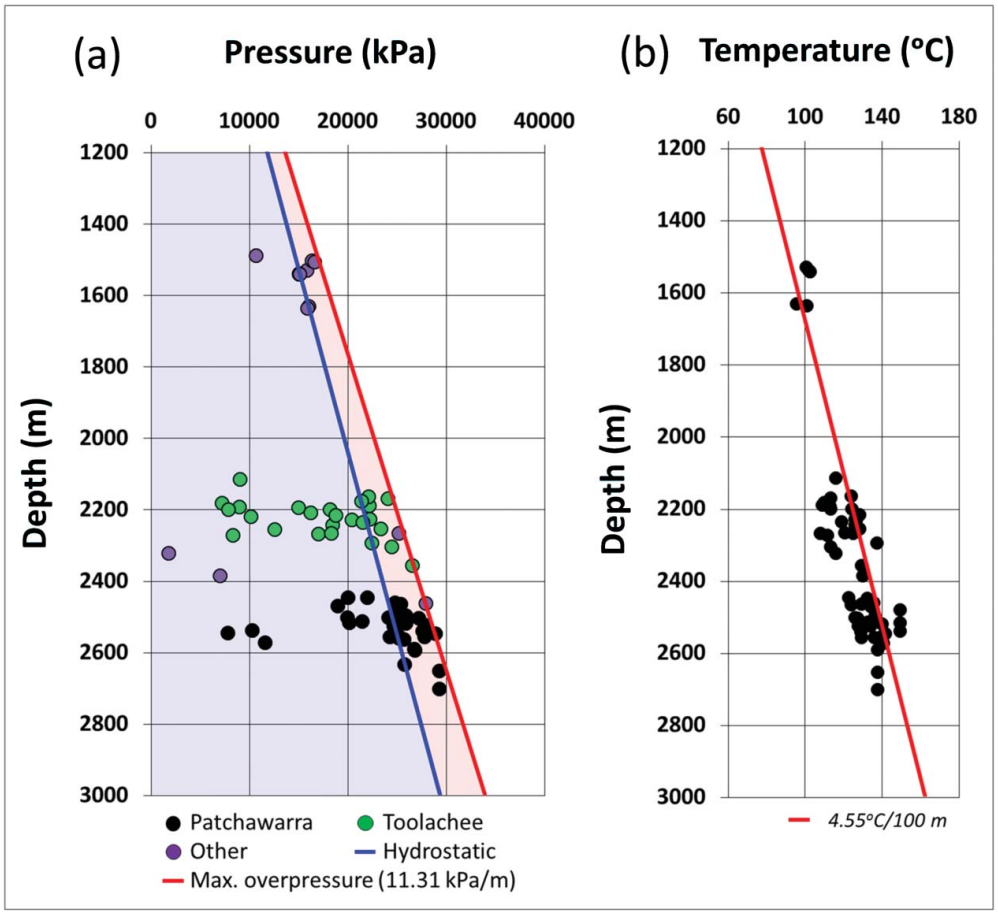


Figure 9. (a) Reservoir pressure profile of the Dullingari 3D seismic survey plotted with the hydrostatic gradient to suggest that certain reservoirs may be over pressured; reaching a maximum pressure gradient of 11.31 kPa/m in the Patchawarra Formation at approximately 2550 m. (b) Temperature profile within the Dullingari 3D seismic survey giving a mean temperature gradient of 4.55°C/100 m, assuming a surface temperature of 21°C.

geomechanical properties coupled with data on the present-day stress tensor. The fracture stability analysis simulated two scenarios; fault planes with a cohesion factor of 10 MPa to represent shear fracture, and fault planes with a cohesion factor of 0 MPa, or cohesionless fault planes, to highlight areas along individual fault planes that are relatively more likely to reactivate when the pore pressure (ΔP_P) is sufficiently increased. As such, the true fracture stability using a true cohesion factor of 10 MPa is presented in Table 2, together with the mean slip tendency and dilation tendency of the main fault sets present within the Dullingari 3D seismic survey. SE—NW strike-slip faults were found to be the most prone to reactivate with a mean fracture stability of only 5.066 MPa and a relatively large slip tendency of 0.384 (Table 2). The E—W-striking fault set was found to be most prone to dilate with a dilation tendency of 0.900, with SE—NW strike-slip faults also showing a high-dilation tendency of 0.543 (Table 2). The true depth, geometry and spatial relationship of these fault sets is presented in Figure 12a, with geomechanical modelling results shown visually by overlaying fault planes with a results colour bar shown in Figure 12b—i. The poles to planes are also plotted on a stereonet and Mohr circle with the results colour bar overlain to better visualise the analysis (Figure 13).

Swan Lake 3D seismic survey

Analysis of the depth-converted Swan Lake 3D seismic survey faults shows two distinct clusters; near-vertical striking approximately SE—NW and high-angle striking approximately NE—SW (Figure 11d). Figure 11e shows the dominant nature of NE—SW-striking faults. This dominant NE—SW strike of faults present in the Swan Lake 3D seismic survey (Figure 11e) mimics the large-scale regional structural architecture in the Cooper Basin. A secondary fault set striking approximately 300° can be seen in Figure 11f. These SE—NW-striking faults were interpreted in seismic data as strike-slip faults (Figure 7a, e). Incoherency analysis along the VC Coal reflector, together with structural and stratigraphic interpretation of cross-sections, highlights the dominant fault strike and fault density within the Swan Lake 3D seismic survey (Figure 7c). The main NE—SW-striking fault that contains the Swan Lake Field from the west is part of the large GMI Ridge that isolates the Nappamerri Trough from the Patchawarra Trough (Figures 4, 7b). The 3D seismic survey contains a series of NE—SW-striking reverse and antithetic faults that are associated with positive displacement and a system of layer-bound polygonal faults within Cretaceous-aged sediments (Figure 7e, f).

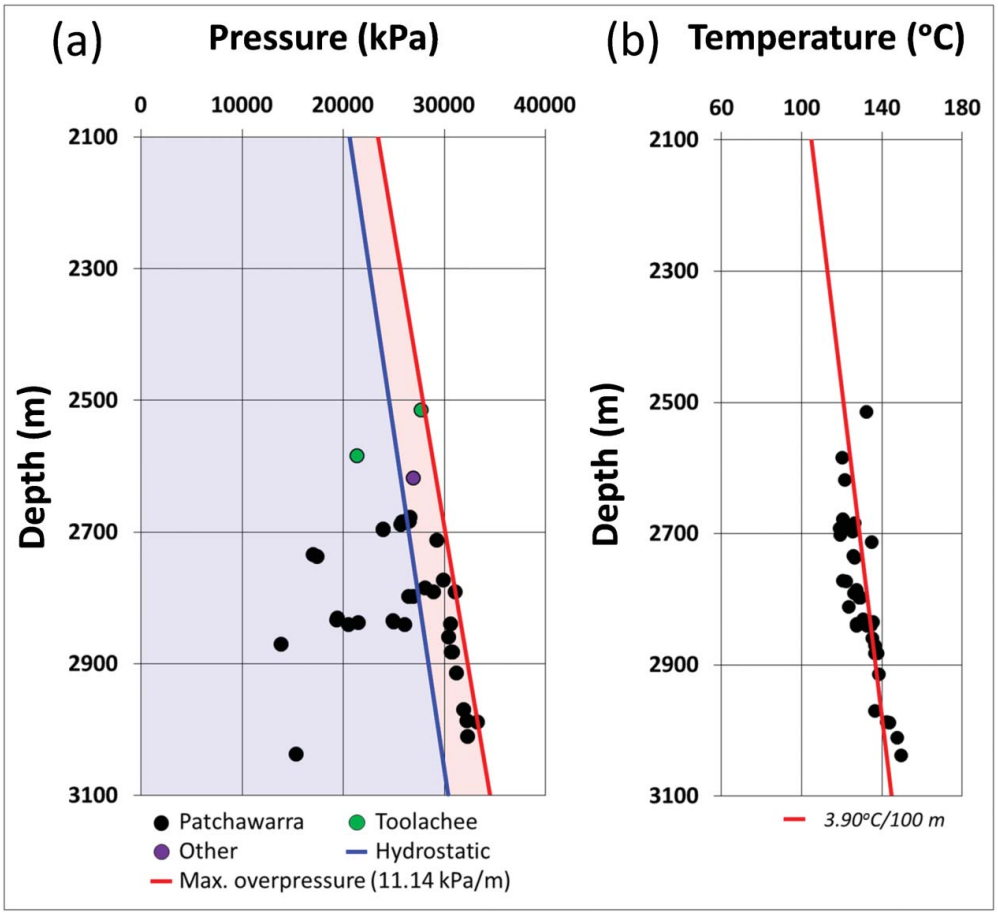


Figure 10. (a) Reservoir pressure profile of the Swan Lake 3D seismic survey plotted with the hydrostatic gradient to suggest that certain reservoirs may be over pressured; reaching a maximum pressure gradient of 11.14 kPa/m in the Patchawarra Formation at approximately 3000 m. (b) The temperature profile within the Swan Lake 3D seismic survey giving a mean temperature gradient of 3.90°C/100 m, assuming a surface temperature of 21°C.

The geomechanical modelling of this fault set utilises slip tendency, dilation tendency, and fracture stability attributes to analyse the relative risk of fault reactivation under the present-day stress regime (Figure 14). The poles to fault plane are plotted on a stereonet and Mohr circle with stress overlays to more accurately illustrate the analysis (Figure 15). In order to model the relative risk of fault reactivation on a given fault plane, we re-model the fracture stability attribute with the assumption that the fault plane is cohesionless by applying a cohesion factor of 0 MPa (Table 1). The results for the main fault sets within the Swan Lake 3D seismic survey are displayed in Table 3, illustrating the high risk of reactivation (S_f = 0.45 MPa), dilation (T_d = 0.697) and slip (T_s = 0.734) of high-angle SE−NW-striking faults.

Table 3. Results from the geomechanical modelling of fault reactivation potential performed on the main fault sets within the Swan Lake 3D seismic survey, where T_s = slip tendency; S_f = fracture stability with cohesion factor of 10 MPa; and T_d = dilation tendency.

Main fault sets	Mean dip (angle)	Mean T_s	Mean S_f (MPa)	Mean T_d
NE−SW striking faults	59.959	0.559	6.899	0.495
SE−NW strike-slip faults	85.569	0.734	0.450	0.697

Discussion

To understand the general risk of fault reactivation within the Cooper Basin, we present a detailed geomechanical analysis of faults within the Dullingari and Swan Lake 3D seismic surveys. Utilising the complete present-day stress tensor calculated by previous authors (Nelson et al., 2007; Reynolds et al., 2006), together with a field-scale pore pressure analysis, the slip tendency, dilation tendency, and fracture stability (shear fracture and shear reactivation) was modelled.

A regional N−S cross-section through the major structural features of the Cooper Basin highlighted several normal faults occurring in the basement of the Patchawarra and Nappamerri troughs (Figure 4). There are some uncertainties regarding the original nature of basement faults within the basin: whether they are reactivated normal faults or purely high-angle reverse faults. The occurrence of normal faults within basement may infer that an extensional stress regime was apparent; however, owing to rapid decrease in seismic quality with depth, accurate fault growth analysis is not possible.

Incoherency analysis along the along the Patchawarra VC Coal reflector highlighted a dominant NE−SW-striking structural grain in both 3D seismic surveys (Figures 6c, 7c), which

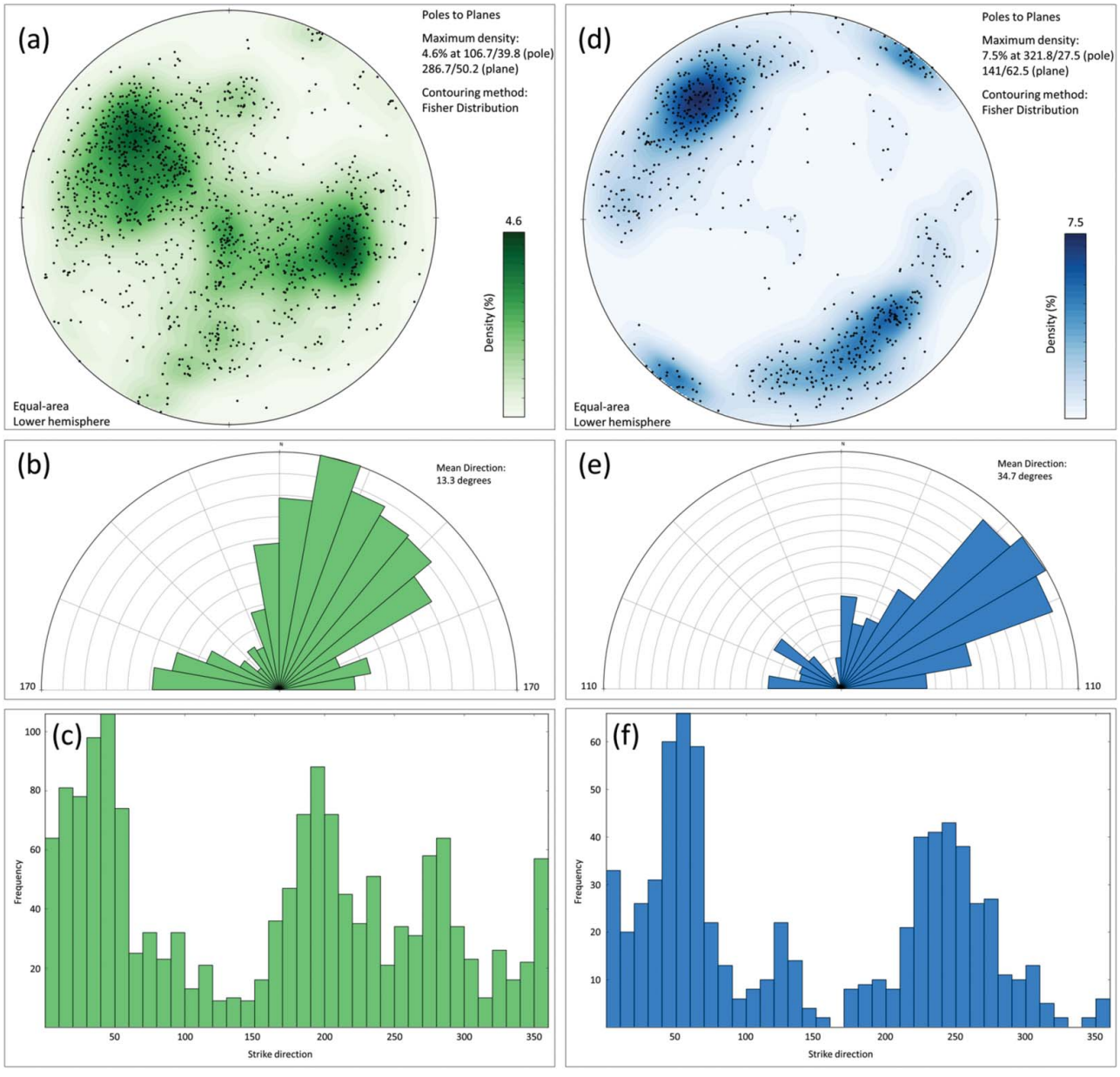


Figure 11. Detailed presentation of the faults interpreted from the Dullingari and Swan Lake 3D seismic surveys. (a) Stereographic projection of poles to fault planes from the Dullingari 3D seismic survey; (b) rose diagram showing dominant strike direction of faults from the Dullingari 3D seismic survey; (c) bar graph presenting strike direction of faults from the Dullingari 3D seismic survey against frequency to easily identify fault sets based on strike direction alone; (d) stereographic projection of poles to fault planes from the Swan Lake 3D seismic survey; (e) rose diagram showing dominant strike direction of faults from the Swan Lake 3D seismic survey; and (f) bar graph presenting strike direction of faults from the Swan Lake 3D seismic survey against frequency to easily identify fault sets based on strike direction alone.

closely resembles the regional structural architecture of the basin (Figure 2a). The Dullingari and Swan Lake 3D seismic surveys both contained near-vertical SE–NW-striking faults extending from the basement and terminating within the middle Patchawarra Formation sediments. These are interpreted to be strike-slip faults that have only recently become a focal point for field-scale reservoir development research (Grant-Woolley et al., 2014). Grant-Woolley et al. (2014) invoke that the field-scale strike-slip faults that we interpreted within the Dullingari and Swan Lake 3D seismic surveys may reduce reservoir properties through cataclasis and could potentially compartmentalise reservoirs. There is potential that these previously undetected strike-slip faults may be compartmentalising hydrocarbon fields and may also be subject to present-day reactivation.

Reservoir pressure data frequently plotted along, or slightly above, the hydrostatic gradient reaching a maximum of 11.31 kPa/m in the Dullingari 3D seismic survey, and 11.14 kPa/m in the Swan Lake 3D seismic survey. As the mean pressure gradients for the 3D seismic surveys were

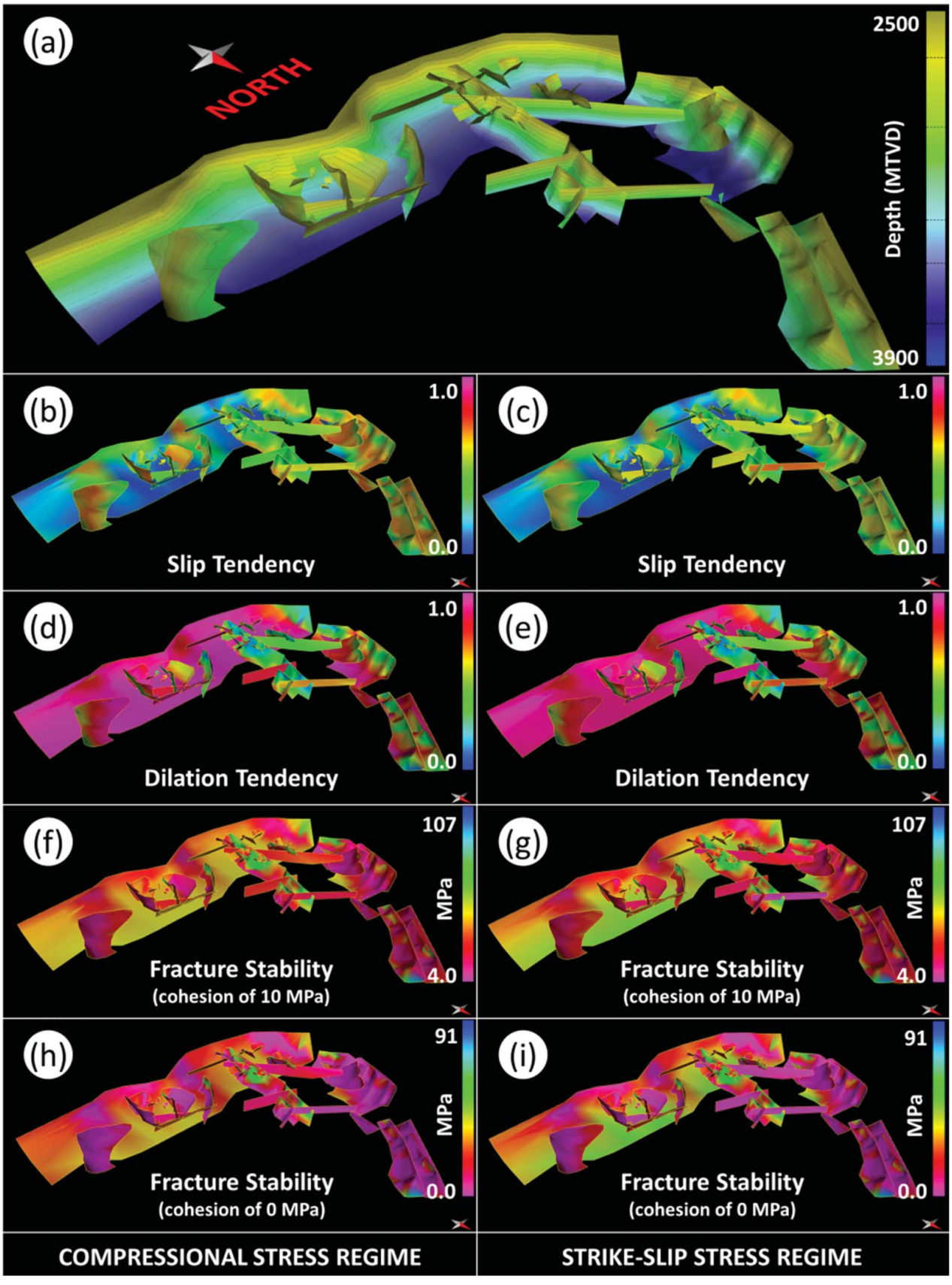


Figure 12. (a) Three-dimensional view of depth-converted faults within the Dullingari 3D seismic survey. Geomechanical modelling results for the slip tendency, dilation tendency and fracture stability (with a cohesion of 10 MPa and 0 MPa) under a compressional (b, d, f, h) and strike-slip (c, e, g, i) stress regime.

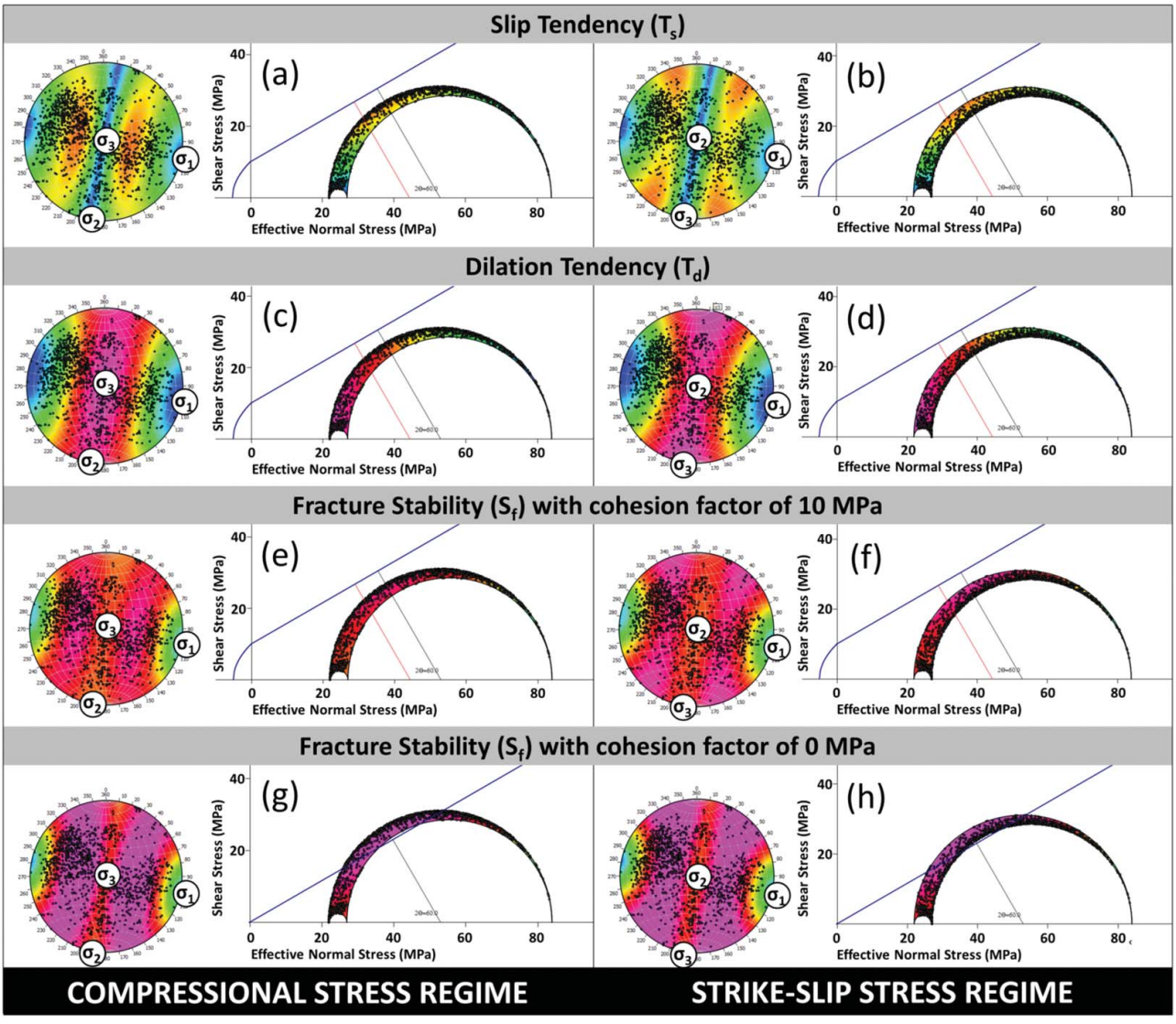


Figure 13. Projection of poles to fault planes on a stereonet and Mohr circle with the geomechanical modelling results overlayed as a colour bar highlighting high fault reactivation potential in pink, and low reactivation potential in blue; 1341 sample points were collected from faults within the Dullingari 3D seismic survey.

approximately hydrostatic with few outliers, geomechanical modelling was performed using a hydrostatic gradient of 9.80 kPa/m.

Geomechanical modelling results within both the Dullingari and Swan Lake 3D seismic surveys identified a strong relationship between SE—NW strike-slip faults and a relatively high risk of reactivation (Tables 2, 3), particularly when modelled to assess the fracture stability and slip tendency. This fault geometry is optimally oriented not only to reactivate, but also to dilate and potentially act as fluid conduit (Figures 12, 14). A relatively high-dilation tendency of 0.697 may have substantial implications to reservoir engineering and field development programs, as not only do these faults appear to pose the largest risk to seal integrity and hydrocarbon preservation if they become reactivated, but also they have been reported to potentially be acting as baffles to compartmentalise the reservoir (Grant-Woolley et al., 2014).

Analysis of the dilation tendency of faults found a common trend between E—W to SE—NW-striking faults and a relatively high chance to dilate under the present-day stress (Figures 12, 14). As the dilation tendency is strongly weighted on the orientation of the maximum horizontal stress, the stress regime itself had a nominal effect on results (Figures 12d, e, 14d, e). The main E—W-striking fault within the Dullingari 3D seismic survey and small-scale faults within the Dullingari and Swan Lake 3D seismic surveys, and SE—NW-striking strike-slip faults, show similar dilation tendencies and appear the most likely to be open to fluid flow. This main E—W-striking fault within the Dullingari 3D seismic survey (Figure 6a, b) also poses a relatively lower risk to shear reactivate when pore pressure is increased, recording a mean fracture stability of 14.127 MPa (Table 2). Again, SE—NW-striking strike-slip faults appear vulnerable to reactivate under a strike-slip stress when pore pressure is increased (Figures 13, 15), with fracture stabilities of

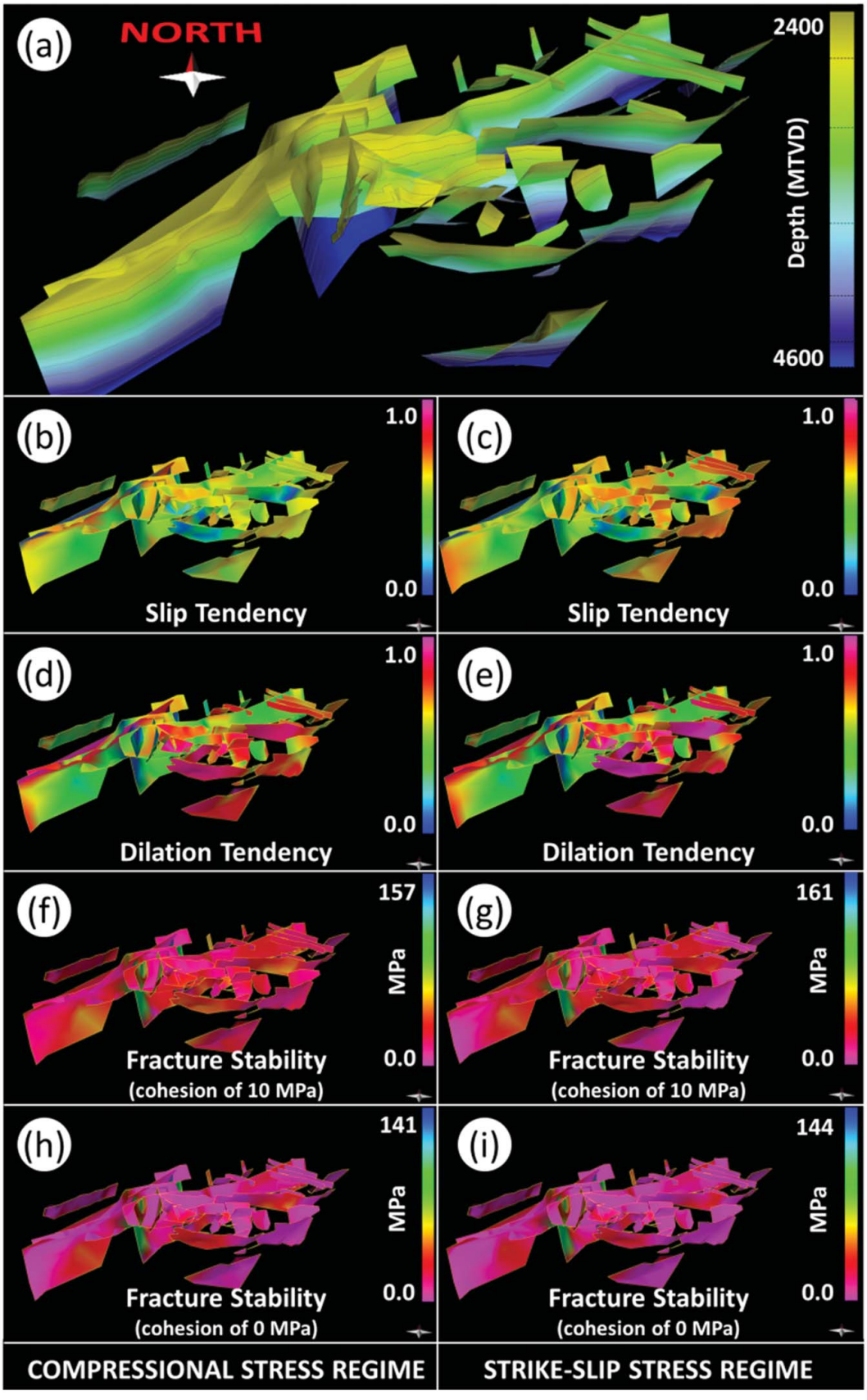


Figure 14. (a) Three-dimensional view of depth-converted faults within the Swan Lake 3D seismic survey. Geomechanical modelling results for the slip tendency, dilation tendency and fracture stability (with a cohesion of 10 MPa and 0 MPa) under a compressional (b, d, f, h) and strike-slip (c, e, g, i) stress regime.

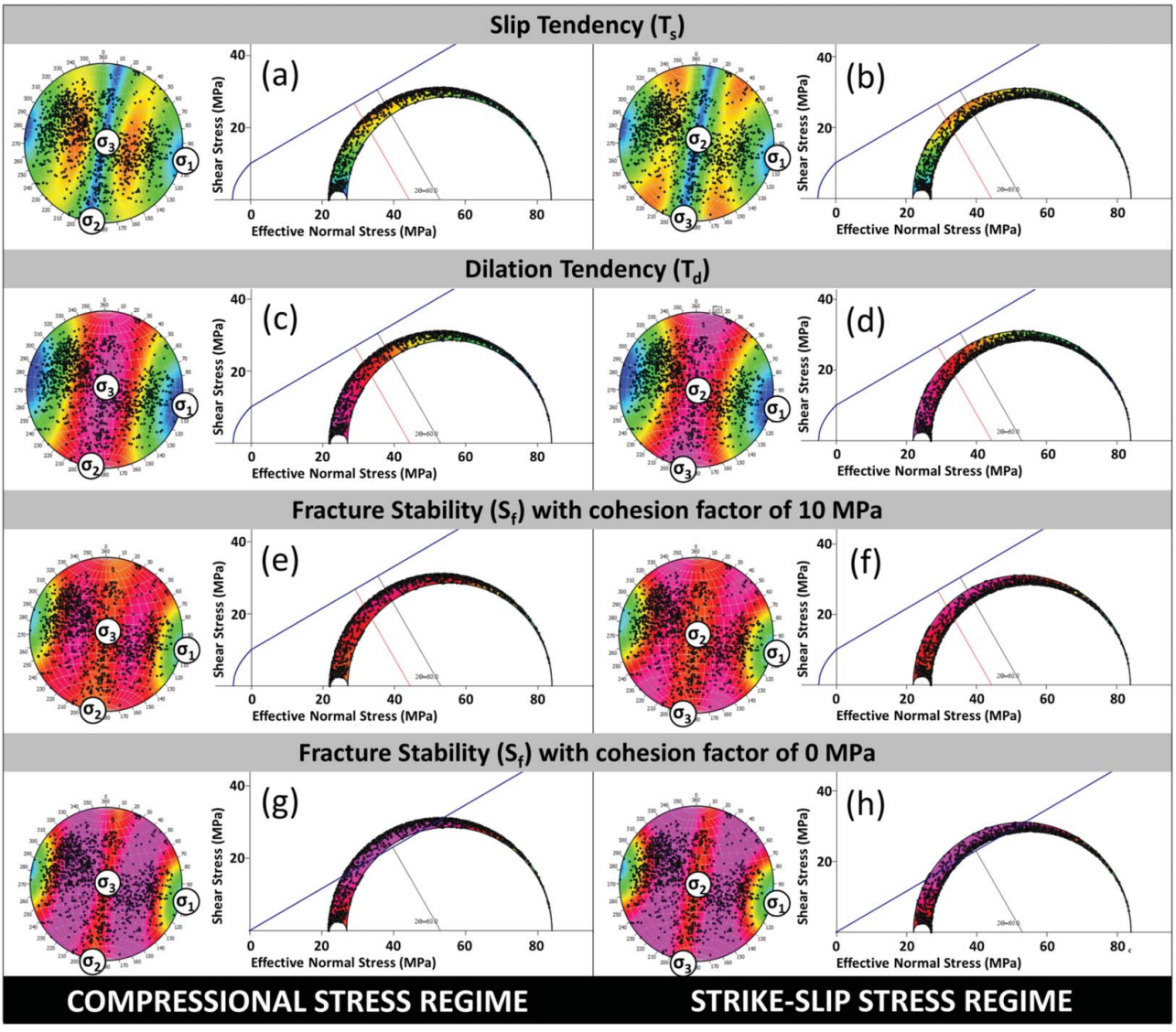


Figure 15. Projection of poles to fault planes on a stereonet and Mohr circle with the geomechanical modelling results overlayed as a colour bar highlighting high fault reactivation potential in pink, and low reactivation potential in blue; 713 sample points were collected from faults within the Swan Lake 3D seismic survey.

5.066 and 0.450 MPa within the Dullingari and Swan Lake 3D seismic surveys, respectively (Tables 2, 3). Results predicting the dilation tendency and fracture stability of faults appear to be similar irrespective of being modelled under strike-slip or compressional stress regime. Considering that the major contribution factors for these two modelling techniques (effective normal stress and differential pore pressure) remain similar irrespective of being modelled under either stress regime, the results are as expected.

Near vertical SE—NW and NE—SW-striking faults were measured to have the greatest risk of reactivation under a strike-slip stress, with low-angle NNE—SSW-striking faults being most prone to reactive under a compressional stress (Figures 13, 15). The fracture stability of faults, both the shear fracture and shear reactivation, are fundamentally important in reservoir characterisation and development, particularly in low permeability and overpressured petroleum basins such as the Cooper Basin, which rely on fracture stimulation treatments. A fracture stimulation model that incorporates the fault sets most prone to reactive (in this case SE—NW-striking strike-slip faults) should be incorporated within reservoir development programs to model the likelihood of fracture stimulation treatments interacting and possibly reactivating pre-existing faults and fractures. Increased pore pressure associated with fracture stimulation treatments may prove to be substantial enough to reactivate pre-existing faults and fractures to cause fracture propagation difficulties during the treatments.

Although there may be similar fault geometries elsewhere in the basin, these may not necessarily contain comparable reactivation potentials. Considering that the present-day stress regime, and the orientation and magnitude of principal stresses, can change locally, extrapolating results to a much broader scale is fraught with danger. As such, individual

geomechanical models predicting fault reactivation must be created for individual fields within the Cooper Basin and, where possible, should be coupled with field-scale stress and pore-pressure data. This technique of predicting the reactivation potential of faults may be used in subsequent research to predict the relative movement of faults through basin evolution by altering the stress parameters to match that of paleo-structural events. This would require accurate paleo-stress orientation and magnitude data not currently available within the Cooper Basin but may be applicable to other regions around the world.

Conclusions

For the first time in the Cooper Basin, we geomechanically model the slip tendency, dilation tendency and fracture stability of faults within the Dullingari and Swan Lake 3D seismic surveys. This research provides a better understanding of the possible risks of hydrocarbon leakage, cataclasis along faults and the potential of compartmentalisation, which are all associated with the reactivation potential of faults. The geomechanical stability of faults within the Cooper Basin identified SE−NW-striking strike-slip faults to be optimally oriented to reactivate, and also dilate, to become potentially open to fluid flow. Considering that this fault set is difficult to interpret in seismic data owing to small lateral offsets that can be undetectable in cross-section, and given that these faults have been found to also potentially be acting as baffles to compartmentalise reservoirs and reduce vital reservoir properties, a significant effort must be spent to accurately interpret and measure this fault set during reservoir development programs. High-angle E−W-striking faults also appear to be optimally oriented to dilate, irrespective of being modelled under a strike-slip or compressional stress regime, and therefore pose a large risk of reactivation and in becoming potential fluid conduits.

The large volume of fracture stimulation treatments being performed within the basin could potentially be interacting with pre-existing faults and fractures, with little research currently available in literature attempting to model this intrinsic relationship within the Cooper Basin. Research that investigates the likelihood that fracture stimulation treatments may be interacting, and reactivating, pre-existing faults and fractures would benefit field development programs that utilise high-pressure hydraulic fracture stimulation treatments to improve economics. Future geomechanical modelling within the Cooper Basin would benefit from more recently acquired 3D seismic data that may have better seismic resolution with depth, which will enable more accurate interpretation of the fault plane roughness and hence the heterogeneities along the fault plane surface.

Acknowledgements

The authors appreciate the financial contribution made by the GeoFrac Consortium, which includes the sponsoring companies: Santos, Beach Energy, Chevron, Halliburton and BG Group (QGC). We thank DUG Insight, Midland Valley Exploration (MOVE), Schlumberger (Petrel), and the creators of 'OpenStereo 0.1.2', Carlos H. Grohmann and Ginaldo A.C. Campanh, for their generous donation of academic licences and software. DUG Insight software (v.3.1, 2015) was used for seismic visualisation, interpretation and analysis. Thank you also to the Australian Journal of Earth Sciences and the reviewers, who provided valuable comments and suggestions to improve the scientific impact of this research article.

Disclosure statement

No potential conflict of interest was reported by the authors.

ORCID

D. Kulikowski http://orcid.org/0000-0002-1761-7598

References

Alexander, E. M., Gravestock, D. I., Cubitt, C., & Chaney, A. (1998). Lithostratigraphy and Environments of Deposition. Petroleum Geology of South Australia, Cooper Basin, Primary Industries and Resources, *4*, 69−116.

Allmendinger, R. W., Cardozo, N. C., & Fisher, D. (2012). *Structural geology algorithms: Vectors & tensors*. Cambridge: Cambridge University Press, 289 p.

Apak, S. N., Stuart, W. J., Lemon, N. M., & Wood, G. (1997). Structural evolution of the Permian−Triassic Cooper Basin, Australia: Relation to hydrocarbon trap styles. *AAPG Bulletin, 81*, 533−555.

Backé, G., Abul Khair, H., King, R., & Holford, S. (2011). Fracture mapping and modelling in shale-gas target in the Cooper basin, South Australia. *The APPEA Journal, 51*, 397−410.

Barton, C. A., Zoback, M. D., & Moos, D. (1995). Fluid flow along potentially active faults in crystalline rock. *Geology, 23*, 683−686.

Basir, H. M., Javaherian, A., & Yaraki, M. T. (2013). Multi-attribute ant-tracking and neural network for fault detection: A case study of an Iranian oilfield. *Journal of Geophysics and Engineering, 10*, 1−10, 015009.

Boreham, C. J., & Hill, A. J. (1998). Source rock distribution and geochemistry. In D. I. Gravestock, J. E. Hibburt & J. F. Drexel (Eds.) *Petroleum Geology of South Australia, v. 4 Cooper Basin* (pp. 129−142). Adelaide SA: Primary Industries and Resources.

Bradshaw, M. T. (1993). Australian petroleum systems. *PESA Journal, 21*, 43−53.

Cardozo, N., & Allmendinger, R. W. (2013). Spherical projections with OSX-Stereonet. *Computers & Geosciences, 51*, 193−205. doi:10.1016/j.cageo.2012.07.021

Durant, R., Woodroof, R., Stephens, T., Thom, W., McGowen, J., & Scott, M. P. (2013). Investigating Hydraulic fracturing in tight gas sand and shale gas reservoirs in the Cooper Basin. In SPE Unconventional Resources Conference and Exhibition-Asia Pacific. (pp. 1−26). Tulsa Ok: Society of Petroleum Engineers, SPE 167073.

Ferrill, D. A., Winterle, J., Wittmeyer, G., Sims, D., Colton, S., Armstrong, A., & Morris, A. P. (1999). Stressed rock strains groundwater at Yucca Mountain, Nevada. *GSA Today*, *9*(5), 1−8.

Ferrill, D. A., & Morris, A. P. (2003). Dilational normal faults. *Journal of Structural Geology, 25*, 183−196.

Flottmann, T., Campagna, D. J., Hillis, R., & Warner, D. (2004). Horizontal microfractures and core discing in sandstone reservoirs, Cooper Basin, Australia. In PESA Eastern Australasian Basins Symposium II, Adelaide, Australia, pp. 689−694.

Gatehouse, C. G. (1986). The geology of the Warburton Basin in South Australia. *Australian Journal of Earth Sciences, 33*, 161−180.

Glikson, A. Y., Uysal, I. T., Fitz Gerald, J. D., & Saygin, E. (2013). Geophysical anomalies and quartz microstructures, Eastern Warburton Basin, North-east South Australia: Tectonic or impact shock metamorphic origin? *Tectonophysics, 589*, 57−76.

Grant-Woolley, L., Kong, A., Schoemaker, B., Nasreddin, H., & Montague, E. T. (2014). Identification of strike-slip faults provides insights into the further development of mature Cooper Basin fields. In SPE Asia Pacific Oil & Gas Conference and Exhibition. (pp 1–12). Adelaide, Australia Society of Petroleum Engineers, SPE 171492-MS.

Gravestock, D. I., & Jensen-Schmidt, B. (1998). Structural setting. *Petroleum Geology of South Australia, 4*, 47–67.

Green, P. M., Brain, T. J., & John, B. H. (1989). Possible stratigraphic controls on hydrocarbon distribution within the Jurassic–Early Cretaceous rocks, Eromanga Basin, southern Queensland. In B. J., O'Neil (Ed.) *The Cooper and Eromanga Basins, Australia* (pp. 251–264). Adelaide SA: Proceedings of Petroleum Exloration Society of Australia, Society of Petroleum Engineers, Australian Society of Exploration Geophysicists (SA Branches).

Haines, P. W., Hand, M., & Sandiford, M. (2001). Palaeozoic synorogenic sedimentation in central and northern Australia: A review of distribution and timing with implications for the evolution of intracontinental orogens. *Australian Journal of Earth Sciences, 48*, 911–928.

Healy, J. H., Rubey, W. W., Griggs, D. T., & Raleigh, C. B. (1968). The Denver earthquakes: Disposal of waste fluids by injection into a deep well has triggered earthquakes near Denver, Colorado. *Science, 161*, 1301–1310.

Hillis, R. R., Sandiford, M., Reynolds, S. D., & Quigley, M. C. (2008). Present-day stresses, seismicity and Neogene-to-Recent tectonics of Australia's 'passive' margins: Intraplate deformation controlled by plate boundary forces. *Geological Society, London, Special Publications*, *306*, 71–90.

Hoffman, K. L. (1989). The influence of pre-Jurassic tectonic regimes on the structural development of the southern Eromanga Basin, Queensland. In B. J. O'Neil (Ed.), *The Cooper and Eromanga Basins, Australia* (pp. 315–328). Proceedings of the Petroleum Exploration Society of Australia, Society of Petroleum Engineers, Australian Society of Exploration Geophysicists (S.A. Branches). Adelaide: Cooper and Eromanga Basins Conference.

Hung, J. H., & Wu, J. C. (2012). In-situ stress and fault reactivation associated with LNG injection in the Tiechanshan gas field, fold-thrust belt of Western Taiwan. *Journal of Petroleum Science and Engineering, 86*, 37–48.

Jolie, E., Moeck, I., & Faulds, J. E. (2015). Quantitative structural–geological exploration of fault-controlled geothermal systems—A case study from the Basin-and-Range Province, Nevada (USA). *Geothermics, 54*, 54–67.

Kantsler, A. J., Prudence, T. J. C., Cook, A. C., & Zwigulis, M. (1983). Hydrocarbon habitat of the Cooper/Eromanga basin, Australia. *Australian Petroleum Exploration Association Journal, 23*, 75–92.

Khair, H. A., Cooke, D., & Hand, M. (2015). Seismic mapping and geomechanical analyses of faults within deep hot granites, a workflow for enhanced geothermal system projects. *Geothermics, 53*, 46–56.

Kuang, K. S. (1985). History and style of Cooper–Eromanga Basin structures. *Exploration Geophysics, 16*, 245–248.

Kulikowski, D., Amrouch, K., Al Barwani, K. H., Liu, W., & Cooke, D. (2015). Insights into the tectonic stress history and regional 4D natural fracture distribution in the Australian Cooper Basin using Etchecopar's calcite twin stress inversion technique, 2D/3D seismic interpretation and natural fracture data from image logs and core. AAPG ICE, Melbourne, Victoria, 13–16 September, extended abstract #2224164.

Kulikowski, D., Cooke, D., & Amrouch, K. (2016a). Constraining the distribution and relationship between overpressure, natural fracture density and temperature in the Cooper Basin. *The APPEA Journal, 56*, 11–28.

Kulikowski, D., Hochwald, C., Cooke, D., & Amrouch, K. (2016b). A statistical approach to assessing depth conversion uncertainty on a regional dataset: Cooper-Eromanga Basin, Adelaide, Australia. ASEG-PESA-AIG 2016 Conference, Extended Abstract, in press.

Lowe-Young, B. S., Mackie, S. I., & Heath, R. S. (1997). The Cooper-Eromanga petroleum system, Australia: Investigation of essential elements and processes. In Proceedings of the Petroleum Systems of SE Asia and Australasia Conference (pp. 199–211). Jakarta, Indonesia: Indonesian Petroleum Association.

Macdonald, J., Backé, G., King, R., Holford, S., & Hillis, R. (2012). Geomechanical modelling of fault reactivation in the Ceduna Sub-basin, Bight Basin, Australia. *Geological Society, London, Special Publications, 367*, 71–89.

Mai, H. T., Marfurt, K. J., & Chavez-Perez, S. (2009). Coherence and volumetric curvatures and their spatial relationship to faults and folds, an example from Chicontepec basin. Proceedings of the International Exposition and Annual Meeting, Mexico, *28*, pp. 1063–1067 (SEG Expanded Abstracts).

Mavromatiis, A. (2006). Burial/exhumation histories for the Cooper–Eromanga Basins and implications for hydrocarbon exploration, Eastern Australia. *Basin Research, 18*, 351–373.

Mildren, S. D., Hillis, R. R., Dewhurst, D. N., Lyon, P. J., Meyer, J. J., & Boult, P. J. (2005). FAST: A new technique for geomechanical assessment of the risk of reactivation-related breach of fault seals. In P. Boult & J. Kaldi (Eds.), *Evaluating fault and cap rock seals* (Vol. **2**, pp. 73–85). Proceedings of the AAPG Hedberg conference, Barossa Valley, South Australia, Australia AAPG Hedberg Series.

Moeck, I., Kwiatek, G., & Zimmermann, G. (2009). Slip tendency analysis, fault reactivation potential and induced seismicity in a deep geothermal reservoir. *Journal of Structural Geology, 31*, 1174–1182.

Morris, A., Ferrill, D. A., & Henderson, D. B. (1996). Slip-tendency analysis and fault reactivation. *Geology, 24*, 275–278.

Mount, T. J. (1981). Dullingari North 1–an oil discovery in the Murta Member of the Eromanga Basin. *Australian Petroleum Exploration Association Journal, 21*, 71–77.

Müller, R. D., Dyksterhuis, S., & Rey, P. (2012). Australian paleo-stress fields and tectonic reactivation over the past 100 Ma. *Australian Journal of Earth Sciences, 59*, 13–28.

Nelson, E. J., Chipperfield, S. T., Hillis, R. R., Gilbert, J., McGowen, J., & Mildren, S. D. (2007). The relationship between closure pressures from fluid injection tests and the minimum principal stress in strong rocks. *International Journal of Rock Mechanics and Mining Sciences, 44*, 787–801.

Neves, F. A., Zahrani, M. S., & Bremkamp, S. W. (2004). Detection of potential fractures and small faults using seismic attributes. *The Leading Edge, 23*, 903–906.

Pokalai, K., Kulikowski, D., Johnson, Jr., R. L., Haghighi, M., & Cooke, D. (2016). Development of a new approach for hydraulic fracturing in tight sand with pre-existing natural fractures. *The APPEA Journal, 56*, 225–238.

Radke, B. (2009). Hydrocarbon and geothermal prospectivity of sedimentary basins in central Australia: Warburton, Cooper, Pedirka, Galilee, Simpson and Eromanga basins. Braidwood, New South Wales, Australia. Canberra ACT: Geoscience Australia Record 2009/25, 161 p.

Raleigh, C. B., Healy, J. H., & Bredehoeft, J. D. (1976). An experiment in earthquake control at Rangeley, Colorado. *Science, 191*, 1230–1237.

Reynolds, S. D., Coblentz, D. D., & Hillis, R. R. (2002). Tectonic forces controlling the regional intraplate stress field in continental Australia: Results from new finite element modeling. *Journal of Geophysical Research: Solid Earth (1978–2012), 107*(B7), ETG–1–15.

Reynolds, S. D., Mildren, S. D., Hillis, R. R., & Meyer, J. J. (2004). The in situ stress field of the Cooper Basin and its implications for hot dry rock geothermal energy development. In PESA Eastern Australasian Basins Symposium II, Adelaide, South Australia, pp. 431–440.

Reynolds, S. D., Mildren, S. D., Hillis, R. R., Meyer, J. J., & Flottmann, T. (2005). Maximum horizontal stress orientations in the Cooper Basin, Australia. implications for plate-scale tectonics and local stress sources. *Geophysical Journal International, 160*, 331–343.

Reynolds, S. D., Mildren, S. D., Hillis, R. R., & Meyer, J. J. (2006). Constraining stress magnitudes using petroleum exploration data in the Cooper–Eromanga Basins, Australia. *Tectonophysics, 415*, 123–140.

Rezaee, M. R., & Sun, X. (2007). Fracture–filling cements in the Palaeozoic Warburton Basin, South Australia. *Journal of Petroleum Geology, 30*, 79–90.

Roberts, G. A., Chipperfield, S. T., & Miller, W. K. (2000). The evolution of a high near-well bore pressure loss treatment strategy for the Australian Cooper Basin. In SPE Annual Technical Conference Exhibition, Dallas, pp. 1–12, SPE 63029.

Rutqvist, J., Rinaldi, A. P., Cappa, F., & Moridis, G. J. (2013). Modeling of fault reactivation and induced seismicity during hydraulic fracturing

of shale-gas reservoirs. *Journal of Petroleum Science and Engineering*, *107*, 31−44.

Sandiford, M., Wallace, M., & Coblentz, D. (2004). Origin of the in situ stress field in south−eastern Australia. *Basin Research, 16*, 325−338.

Sibson, R. H. (1996). Structural permeability of fluid-driven fault-fracture meshes. *Journal of Structural Geology, 18*, 1031−1042.

Swierczek, E., Zhen-dong, C., Holford, S., Backé, G., King, R., & Mitchell, A. (2013). Quantifying fault reactivation risk in the western Gippsland Basin using geomechanical modelling. *The APPEA Journal, 53*, 255−272.

van Ruth, P., Hillis, R., Tingate, P., & Swarbrick, R. (2003). The origin of overpressure in 'old' sedimentary basins: An example from the Cooper Basin, Australia. *Geofluids, 3*, 125−131.

van Ruth, P. J., Nelson, E. J., & Hill, R. R. (2006). Fault reactivation potential during CO_2 injection in the Gippsland Basin, Australia. *Exploration Geophysics, 37*, 50−59.

Wiprut, D., & Zoback, M. D. (2000). Fault reactivation and fluid flow along a previously dormant normal fault in the northern North Sea. *Geology, 28*, 595−598.

Wiprut, D., & Zoback, M. D. (2002). Fault reactivation, leakage potential, and hydrocarbon column heights in the northern North Sea. *Norwegian Petroleum Society Special Publications, 11*, 203−219.

Worum, G., van Wees, J. D., Bada, G., van Balen, R. T., Cloetingh, S., & Pagnier, H. (2004). Slip tendency analysis as a tool to constrain fault reactivation: A numerical approach applied to three−dimensional fault models in the Roer Valley rift system (southeast Netherlands). *Journal of Geophysical Research: Solid Earth (1978−2012), 109*(B2), 1−16.

Zoback, M. D., & Harjes, H. P. (1997). Injection-induced earthquakes and crustal stress at 9 km depth at the KTB deep drilling site, Germany. *Journal of Geophysical Research, 102*, 18 477−418 491.

5.6. MANUSCRIPT 6: Fault reactivation with paleo-stress

4D modelling of fault reactivation using complete paleo-stress tensors from the Cooper-Eromanga Basin, Australia

This research presents a new approach for determining the evolution of fault reactivation (tensile and shear) by integrating complete paleo-stress tensors with geomechanical modelling. The purpose of this study is to: (1) present a new approach that can be replicated in other provinces to determine the evolution of fault reactivation; (2) constrain the complete paleo-stress tensors of six tectonic events; and (3) provide valuable information on the fault sets that were most likely to dilate and shear reactivate at six key stages during basin development. Considering that the Cooper-Eromanga Basin is Australia's largest onshore hydrocarbon province, a thorough understanding of hydrocarbon migration pathways through time is invaluable for future exploration and development activity.

CITATION:

Kulikowski, D., & Amrouch, K. (2017). 4D Modelling of Fault Reactivation using Complete Paleo-Stress Tensors from the Cooper-Eromanga Basin, Australia. Australian Journal of Earth Sciences, under review.

Statement of Authorship

Title of Paper:	4D Modelling of Fault Reactivation using Complete Paleo-Stress Tensors from the Cooper-Eromanga Basin, Australia
Publication Status:	**Manuscript Submitted**
Publication Details:	Kulikowski, D., & Amrouch, K. (2017). 4D Modelling of Fault Reactivation using Complete Paleo-Stress Tensors from the Cooper-Eromanga Basin, Australia. *Australian Journal of Earth Sciences*, under review.

Principal Author

Principal Author (Candidate):	David Kulikowski		
Contribution to the Paper:	Data collection, Mohr's circle construction, depth-conversion, geomechanical modelling, interpretation, analysis, and writing.		
Overall percentage (%):	85%		
Certification:	This paper reports on original research I conducted during the period of my Higher Degree by Research candidature and is not subject to any obligations or contractual agreements with a third party that would constrain its inclusion in this thesis. I am the primary author of this paper.		
Signature:		Date:	29 March 2017

Co-Author Contribution

By signing the Statement of Authorship, each author certifies that:

i. the candidate's stated contribution to the publication is accurate (as detailed above);

ii. permission is granted for the candidate to include the publication in the thesis; and

iii. the sum of all co-author contributions is equal to 100% less the candidate's stated contribution.

Name of Co-Author:	Khalid Amrouch (15%)		
Contribution to the Paper:	Technical feedback of Mohr's construction, feedback on interpretation/analysis and a complete review of paper.		
Signature:		Date:	29 March 2017

4D Modelling of Fault Reactivation using Complete Paleo-Stress Tensors from the Cooper-Eromanga Basin, Australia

David **Kulikowski**[a] (david.kulikowski@adelaide.edu.au)

Khalid **Amrouch**[a] (khalid.amrouch@adelaide.edu.au)

[a]Australian School of Petroleum, University of Adelaide, North Terrace, 5005, Australia.

Corresponding author: David Kulikowski (+61 435 135 148)

ABSTRACT

Determining the fault activity through time has typically utilised high resolution seismic data to identify stratigraphic thickness changes or displacement to distance plots; however, this approach is not possible in regions with low resolution seismic data. We present a new approach for determining fault reactivation (tensile and shear) through time by integrating three-dimensional seismic data, geomechanical modelling, and complete paleo-stress tensors from calcite twin stress inversion. The Cooper-Eromanga Basin is used as a case study to model the stress conditions present during the six tectonic events that have affected the basin, and in doing so, constrain the effective paleo-stress magnitudes through time. Results show that the likelihood of dilation and shear reactivation of individual fault sets varies through time, with N-S and E-W striking faults likely to have been open to fluid flow after the critical moment in the hydrocarbon system. These results have substantial implications for hydrocarbon migration pathway models and structural and stratigraphic models for the Cooper-Eromanga Basin. This approach would benefit other provinces with low resolution seismic data preventing fault growth analysis, or in regions where hydrocarbon migration pathways are poorly defined.

KEY WORDS: Stress; Calcite; Tectonic; Geomechanics; Structural Evolution; Fault Reactivation; Hydrocarbon Migration; Cooper Basin; Eromanga Basin.

1. INTRODUCTION

This work presents an approach that incorporates geomechanical modelling of faults, interpreted from low resolution three-dimensional (3D) seismic data, with paleo-stress tensors, obtained from the application of a calcite twin stress inversion technique (CSIT), to evaluate the four-dimensional (4D) evolution of fault reactivation (tensile and shear). The key application of this novel approach is in constraining the dynamic evolution of permeable fault conduits that can facilitate fluid migration. The typical approach to assessing fault growth and fault activity during basin development is through the analysis of high resolution three-dimensional (3D) seismic data to identify changes in stratigraphic thickness across a fault, or by generating displacement to distance plots (e.g. Williams, Powell, & Cooper, 1989; Childs, Nicol, Walsh, & Watterson, 1996; Baudon & Cartwright, 2008). However, in regions where seismic data quality is poor, such as the Cooper-Eromanga Basin, Australia, this becomes a difficult task, particularly as lateral (or oblique) shear reactivation is not easily recognised in fault growth analysis. Geomechanical modelling has successfully predicted the reactivation potential of faults under the present day stress (e.g. Morris, Ferrill, & Henderson, 1996; Sibson, 1996; Wiprut & Zoback, 2000, 2002; Moeck, Kwiatek, & Zimmermann, 2009; Kulikowski, Amrouch, & Cooke, 2016c); however, considering that CSIT results have never been integrated with fault reactivation models, this study presents a new approach for determining the fault geometries most likely to facilitate fluid migration at key stages during basin development. This has direct implications for hydrocarbon migration and structural evolution models in basins subject to poor resolution seismic data that prevents fault growth analyses, and also in subsurface provinces where structural data cannot be obtained directly from outcrop.

The CSIT has been applied to many regions around the world (e.g. Lacombe, Angelier, & Laurent, 1992; Amrouch, Lacombe, Mouthereau, & Dissez, 2005; Lacombe, Amrouch, Mouthereau, & Dissez, 2007; Amrouch, Lacombe, Bellahsen, Daniel, & Callot, 2010a; Amrouch, Robion, Callot, Lacombe, Daniel, Bellahsen, & Faure, 2010b; Amrouch, Beaudoin, Lacombe, Bellahsen, & Daniel, 2011; Beaudoin et al., 2012; Arboit, Amrouch, Collins, King, & Morley, 2015; Tavani et al., 2015; Arboit, Amrouch, Morley, Collins, & King, 2017), which includes the Cooper-Eromanga Basin, Australia (Kulikowski & Amrouch, 2017). This basin is subject to poor resolution seismic data and has an incomplete understanding of fault activity and hydrocarbon migration pathways through time and as such, is an ideal case study for this approach.

Results from the previous application of the CSIT in this basin provide valuable information on the stress orientations, stress regimes, stress ellipsoid shape ratio (R; $where\ R = (\sigma_2 - \sigma_3)/(\sigma_1 - \sigma_3)$) and maximum differential stress ($\sigma_1 - \sigma_3$) magnitudes of tectonic events; however, the precise

magnitudes of these events remains unknown. We incorporate these previous CSIT results with rock mechanics measurements and Mohr's circle construction to define the effective stress magnitudes recorded by 12 calcite samples that define the six individual events (Kulikowski and Amrouch, 2017). This aspect of the study is independent of the geomechanical models and follows a well-established methodology that has been presented by several previous studies (e.g. Lacombe, 2007; Amrouch, 2010; Amrouch et al., 2011; Arboit et al., 2017). The portion of the study that presents a novel approach is the subsequent integration of completed CSIT results with geomechanical modelling to identify the geometry of critically oriented faults during the six key stages of basin development. These results provide relative measures of the dilation and shear reactivation potential that can be used to infer the fault geometry optimally oriented to migrate fluids through time.

Insert Fig. 1

Faults were interpreted from six depth converted 3D seismic surveys to determine the most common fault geometries present across the basin and plotted on the Mohr's circles to identify the fault geometries that would preferentially develop with changing stress conditions (Anderson, 1905). The Gidgealpa 3D seismic survey was geomechanically modelled under six unique stress conditions to assess the Dilation Tendency (ability to act as a permeable conduit) and the Slip Tendency (shear reactivation potential) of faults at key periods in time. The results aim to constrain the variation in Dilation Tendency and Slip Tendency between faults, which will be used to infer migration pathways along potentially permeable fault conduits. This new approach improves hydrocarbon migration pathway and structural evolution models by identifying fault sets that were critically oriented (most likely to reactivate) at specific periods of time. This approach can be replicated in other provinces with uncertain geological evolution and hydrocarbon migration pathway models.

2. TECTONOSTRATIGRAPHIC EVOLUTION

The Permian to Triassic intra-cratonic Cooper Basin is located in central Australia (Fig. 1) and is unconformably isolated from the overlying Jurassic to Cretaceous Eromanga Basin, and the underlying Cambrian to Silurian Warburton Basin (basement) (Fig. 2). The province consists of the NE-SW striking Gidgealpa-Merrimelia-Innamincka (GMI) and Murteree-Nappacoongee (MN) ridges that divide the NE-SW elongate Patchawarra, Nappamerri and Tenappera troughs (Fig. 3). The NW-SE Adelaidean (650-575 Ma) Extensional Event developed NE-SW striking normal faults and NW-SE striking strike-slip faults at the earliest stage of basin development. The regional distribution of these normal faults generated accommodation space for the deposition of calcareous and clastic Warburton Basin sediments (Apak, Stuart, Lemon, & Wood, 1997; Haines, Hand, & Sandiford, 2001;

Muller, Dyksterhuis, & Rey, 2012). Deposition of volcanics and carbonates within shallow-shelf and deltaic sediments continued until the Silurian Alice Spring Event (Gatehouse, 1986).

The NNW-SSE oriented strike-slip Alice Springs Event (ASE) reactivated pre-existing basement faults between the Silurian and Carboniferous periods, and developed a regional erosional unconformity between the Warburton and Cooper Basins (Apak et al., 1997; Kulikowski & Amrouch, 2017). This event also facilitated a dextral motion along pre-existing NW-SE striking faults and may have developed a set of conjugate strike-slip faults striking NW-SE and NNE-SSW (Kulikowski & Amrouch, 2017). Uranium-rich Big Lake Granodiorite was emplaced during this prolonged period of fault reactivation, which increased the geothermal gradient across the basin to levels higher than the typical geothermal gradient of continental crust (Glikson, Uysal, Fitz Gerald, & Saygin, 2013; Kulikowski, Cooke, & Amrouch, 2016a). This known spike in the geothermal gradient may have resulted in an increase in paleo-pore pressure, which may affect paleo-stress calculations (Lacombe, 2001; Amrouch, 2010).

Insert Fig. 2

Insert Fig. 3

Post compressional flexural relaxation, or thermal sag caused by the Big Lake Granodiorite intrusion, enabled Upper Carboniferous glacial sediments (Merrimelia Formation) to deposit onto the regional unconformity, followed by the deposition of Lower Permian braided fluvial sediments (Tirrawarra Formation). The Merrimelia and Tirrawarra Formations on-lap onto the GMI and MN ridges suggesting that these were pronounced structural features at this time (Kantsler, Prudence, Cook, & Zwigulis, 1983; Apak et al., 1997). Cycles of fluvio-deltaic, lacustrine and swamp conditions deposited middle Permian sandstones, shales and coals (Patchawarra Formation) (Alexander, Gravestock, Cubitt, & Chaney, 1998; Boreham & Hill, 1998). On-lapping is observed in the Middle Patchawarra Formation and is attributed to the NW-SE compressional Mid-Permian Event that reactivated pre-existing faults and created a NE-SW striking conjugate fracture set (Apak et al., 1997; Kulikowski & Amrouch, 2017).

As compression from the Mid-Permian Event eased during the deposition of the top Patchawarra Formation, an east to west Late Permian transgression deposited fluvio-deltaic, shoreface and lacustrine sediments (Murteree Shale, Epsilon Formation, Roseneath Shale, and Daralingie Formation) (Bradshaw, 1993; Apak et al., 1997; Gravestock & Jensen-Schmidt, 1998). Deposition of the Upper Permian Daralingie Formation was interrupted by the NE-SW strike-slip Daralingie Event that reactivated pre-existing basement faults and eroded much of the Daralingie Formation (Apak et

al., 1997; Kuang, 1985; Mavromatidis, 2006). Meandering fluvial to deltaic sediments (Toolachee Formation) were deposited onto this unconformity, and were followed by the overlying Triassic Nappamerri Group consisting of floodplain, lacustrine and fluvial channel sediments (Kantsler et al., 1983; Apak et al., 1997).

Up to 500 meters of Nappamerri Group sediments were subsequently uplifted and eroded along pre-existing basement faults as a results of the Late Triassic E-W compressional Hunter-Bowen Event. This exhumation and erosion formed the regional unconformity that separates the Cooper and Eromanga Basins (Apak et al., 1997; Kantsler et al., 1983; Alexander et al., 1998; Mavromatidis, 2006; Kulikowski, Amrouch, Al Barwani, Liu, & Cooke, 2015; Kulikowski & Amrouch, 2017). This event also developed a regional set of N-S striking conjugate fractures (Kulikowski and Amrouch, 2017). The deposition of Jurassic to Cretaceous Eromanga Basin sediments was uninterrupted and transitioned between fluvial, deltaic, lacustrine and shallow marine depositional environments (Lowe-Young, Mackie, & Heath, 1997). Jurassic and Lower Cretaceous sediments are currently being targeted for hydrocarbon exploration along the basin margins, where the Triassic sealing units pinch-out exposing the Permian source rocks to the Jurassic reservoirs (Lowe-Young et al., 1997). A polygonal fault system exists within Cretaceous stratigraphy with faults shown to periodically penetrate oil-rich Lower Cretaceous reservoirs, which may be facilitating tertiary migration of hydrocarbon into shallow sandstones (Watterson, Walsh, Nicol, Nell, & Bretan, 2000; Kulikowski, Amrouch, Cooke, & Gray, 2017).

A Late Cretaceous E-W compressional event enhanced structures and formed the regional unconformity separating the Eromanga Basin from the overlying Paleogene to Quaternary Lake Eyre Basin (Kuang, 1985; Apak et al., 1997; Gravestock & Jensen-Schmidt, 1998; Mavromatidis, 2006; Kulikowski & Amrouch, 2017). This marks the critical moment in the Cooper-Eromanga Basin petroleum system, where hydrocarbon accumulation and preservation commenced (Lowe-Young et al., 1997; Gravestock & Jensen-Schmidt, 1998; Muller et al., 2012). Subsequent N-S compression during the Paleogene Event and the present day ESE-WNW compression are believed to have a negligible effect on hydrocarbon preservation, forming folds rather than reactivating pre-existing faults (Lowe-Young et al., 1997). Geomechanical modelling of fault reactivation under contemporary stresses found that NW-SE striking strike-slip faults are most likely to dilate and reactivate under shear (Kulikowski et al., 2016c).

3. METHODS

3.1. Introduction

The three key aspects of this study are: (1) accurate fault interpretation from seismic data; (2) completing the paleo-stress tensors by combining data from 12 calcite samples with fault and fracture sets that define the complete tensors of six events (Lacombe, 2007; Amrouch, 2010); and (3) combining the calculated paleo-stress tensors with geomechanical and fault models to infer potential migration pathways through time. To complete the paleo-stress tensors, an understanding of rock mechanics or paleo-depths are required, and does not involve geomechanical modelling. Geomechanical modelling is combined with completed paleo-stress tensors to present a novel approach that is used to quantify the relative likelihood of fault reactivation for four commonly encountered fault sets.

3.2. Three-dimensional Seismic Reflection Data

3.2.1. LOCATION AND SEISMIC DATA QUALITY

Six 3D seismic surveys (Fly Lake, Merrimelia, Greater Tindilpie (GT) and Swan Lake, Gidgealpa, Greater Strzelecki, and Dullingari) were used to measure faults and determine the fault geometries that are most common across the basin (Fig. 3). These 3D seismic surveys are spatially distributed across the basin and provide a wide range of fault geometries. The Gidgealpa 3D seismic survey was acquired in 2002 and covers the Gidgealpa oil and gas field, which is located along one of the main structural ridges of the basin; the GMI Ridge (Fig. 3 & Fig. 4). This seismic survey was chosen as a case study for geomechanical modelling because of the large portion of paleo-stress results obtained from within the survey area, the relatively high seismic resolution, and the wide range of fault geometries present. This allows the study to analyse a number of individual fault sets that are not present, or at sub-seismic resolution, elsewhere in the basin.

The Gidgealpa Field is comprised of two NE-SW elongate domes located in the northern and southern sections of the survey, and are separated from the west by the main NE-SW striking high angle inverted normal fault (GMI Ridge) (Fig. 4). The vertical seismic resolution varies from <20m above the Permian Toolachee Formation (from surface to approximately 2.3km depth), to >40m below thick Permian coal measures (between approximately 2.4 and 6km). Due to the poor seismic resolution at basement level, accurate fault growth studies are not possible, and small-scale faults are either sub-seismic resolution or difficult to interpret.

Insert Fig. 4

3.2.2. TIME TO DEPTH CONVERSION OF SEISMIC DATA

An important aspect of this study is ensuring that seismic data is accurately converted from the time domain to true depth. This allows true fault geometries to be analysed and interpreted, and as is the case within the Cooper-Eromanga Basin, fault geometries will be vastly different between the time and depth domains. There are a number of methods that can be used to convert between domains, including the average velocity, time-depth trend, stacking velocity, and interval velocity methods. A depth conversion study assessing the accuracy of these methods in the Cooper-Eromanga Basin found that the most accurate method and the expected error will depend on the unique dataset, showing that it is not practical to use a single method for the entire basin as this can incur large errors (Kulikowski, Hochwald, Cooke, & Amrouch, 2016b). For the purpose of this study, a time-depth trend and well check-shot data are used to generate an interval velocity model for depth conversion due to its simplicity and its ability to be easily replicated in the future if required.

Well check-shot data provides a time-depth pair for several key depths. These check-shots were used as a quality control for the time (seismic) vs depth (formation top) trend used to generate an interval velocity model. The interval velocity model consisted of three layers: (1) surface and Upper Cretaceous (velocity of 2400 m/s); (2) Upper Cretaceous to Toolachee Formation (velocity of 3250 m/s); and (3) below Toolachee Formation (velocity of 3900 m/s).

3.3. Fault Interpretation from Seismic Reflection Data

All fault interpretation was performed on time-to-depth converted seismic volumes in both cross-section (in-line and cross-line) and depth-slice views. Major faults affecting the evolution of the Cooper-Eromanga Basin are mostly basement-involved and developed as extensional faults, but have since undergone numerous stages of reactivation as described in the tectonic section of this paper. These faults typically terminate between basement and middle Permian sediments. A regional system of polygonal faults exists within Upper Cretaceous sediments; however, these were not included in the analysis because they developed through a density inversion of sediments rather than through structural activity (Watterson et al., 2000). Basement-involved faults were interpreted with picks every 100-200 meters depending on the complexity of individual fault planes. Faults interpreted from the six seismic surveys consisted of a wide range of strikes with dip angles mostly either 50-70° or near vertical (Fig. 5). The dominant fault geometry within the Gidgealpa 3D seismic survey is NE-SW striking with dip angles of 50-70° (Fig. 5), which likely developed during the NW-SE extensional Adelaidean Event as normal faults and subsequently inverted. Three additional fault sets were identified within the survey: (1) E-W striking faults with dip angles of 50-70°; (2) N-S striking

faults with dip angles of 50-70°; and (3) NW-SE striking faults with dip angles of 80-90° (Fig. 5) (Grohmann & Campanha, 2010; Grohmann, Campanha, & Soares, 2011).

Delaunay Triangulation (Delaunay, 1934) was used to generate continuous mesh surfaces of each fault with the gridding artefacts largely removed, but may be present at the base of faults where seismic resolution is particularly low (Fig. 4c). Difficulties arose in interpreting deep basement faults due to the rapidly decreasing seismic resolution. The low seismic resolution below Permian coals not only prevents fault growth analysis, but also reduces the accuracy of interpreting fault plane roughness and the heterogeneities along the fault plane surface.

Insert Fig. 5

3.4. Completing the Paleo-stress Tensors

3.4.1. INTRODUCTION

The CSIT has become more widely used in recent years after its continued success in accurately defining the stress orientations and magnitudes of tectonic events (Constantin, Laurent, Vergély, & Cabrera, 2007; Amrouch, Lacombe, Bellahsen, Daniel, & Callot, 2010a; Amrouch et al., 2010b; 2011; Arboit, Amrouch, Collins, King, & Morley, 2015; Tavani et al., 2015; Tripathy and Saha, 2015; Arboit et al., 2017). This method of stress inversion, using measured calcite twin data, was previously performed on the Cooper-Eromanga Basin as a case study (Kulikowski & Amrouch, 2017); however, they provided incomplete stress tensors by only constraining five stress parameters for each of the six tectonic events (Alice Springs Event, Mid-Permian Event, Daralingie Event, Hunter-Bowen Event, Late Cretaceous Event, and Paleogene Event) that have affected the basin; (1) maximum principal stress orientation; (2) intermediate principal stress orientation; (3) minimum principal stress orientation; (4) stress ellipsoid shape ratio (R; $where\ R = (\sigma_2 - \sigma_3)/(\sigma_1 - \sigma_3)$; $and\ 0 \leq \mathrm{R} \leq 1$); and (5) maximum differential stress ($\sigma_1 - \sigma_3$) magnitude. To complete these tensors, the effective paleo-stress magnitudes are calculated in this study by constructing 12 Mohr's circles that represent the incomplete stress tensor results obtained from Kulikowski & Amrouch (2017).

3.4.2. CALCITE TWIN STRESS INVERSION TECHNIQUE

Twinning is a plastic deformation mechanism that occurs in calcite crystals at temperatures of between 25 and 400°C, in low confining pressures and when subject to a critical resolved shear stress (τ_a) of approximately 10±4 MPa (e.g. Turner, 1953; Turner, Griggs, & Heard, 1954; Lacombe and Laurent, 1996; Lacombe, 2001, 2007; Amrouch, 2010; Amrouch et al., 2010a, 2011; Arboit et al., 2017; Kulikowski and Amrouch, 2017). An individual twin (e) plane is the result of dislocation gliding,

or the re-alignment of atoms, towards the optical axis of a calcite crystal, giving unique optical axes for the calcite crystal and the zone of calcite twinning (Turner et al., 1954; Lacombe and Laurent, 1996; Ferrill, 1998). The orientation of twin development follows well defined geometric laws that only permit three potential twin planes $[01\bar{1}2]$ for a given calcite crystal, which are arranged symmetrically around the optical axis (Amrouch, 2010). Twin planes can therefore be liked to a pre-existing fault plane that experiences subsequent reactivation to develop slickensides, which can be measured and analysed to determine the shear direction. For a given calcite sample, three orthogonal thin sections are created and each twin (met conditions required for twinning) and un-twinned (did not meet conditions required for twinning) are measured.

Stress inversion of calcite twin data computes the three principal stress orientations and R. These four parameters define the reduced stress tensor, T', where the completed stress tensor, T, is $T = kT' + lI$ (where k ($k = \sigma_1 - \sigma_3 > 0$) and l ($l = \sigma_3$) are scalars, and I is the unit matrix) (Lacombe, 2007). By scaling the maximum differential stress ($\sigma_1 - \sigma_3$) to be equal to 1, the value of the resolved shear stress acting on a given plane (τ_a) lies between -0.5 (-$[\sigma_1 - \sigma_3]/2$) and +0.5 (+$[\sigma_1 - \sigma_3]/2$) (Jamison and Spang, 1976; Etchecopar, 1984). Several trial stress tensors are then applied to the dataset and an optimum reduced stress tensor is obtained by including the maximum number of twinned planes and ideally zero un-twinned planes. This reduced stress tensor defines the three principal stress orientations and the R value. By incorporating the τ_a value (typically 10±4 MPa), and using $(\sigma_1 - \sigma_3) = \tau_a/\tau_a{}'$ and $(\sigma_2 - \sigma_3) = R(\sigma_1 - \sigma_3)$, the maximum differential stress magnitude ($\sigma_1 - \sigma_3$) can be calculated (where $\tau_a{}'$ is the minimum τ_a applied to a twin plane that is compatible with the optimum stress tensor solution). As these values are known for the six events in Cooper-Eromanga Basin (Kulikowski and Amrouch, 2017), we complete the paleo-stress tensors from 12 calcite samples by determining the effective stress magnitudes.

3.4.3. QUANTIFICATION OF PALEO-STRESS MAGNITUDES

The deviatoric stress tensor, T_D, where $T_D = T - [(\sigma_1 + \sigma_2 + \sigma_3)/3]I$, can be broken down into three parts; (i) $\sigma_{1D} = [(2 - R)(\sigma_1 - \sigma_3)]/3$; (ii) $\sigma_{2D} = [(2R - 1)(\sigma_1 - \sigma_3)]/3$; and (iii) $\sigma_{3D} = -[(1 + R)(\sigma_1 - \sigma_3)]/3$ (Lacombe, 2001). However, to complete the stress tensors the isotropic component is required and cannot be obtained from calcite twin data alone (Lacombe, 2001). CSIT results are therefore often left incomplete, as paleo-Mohr's circle construction is required. To place a given paleo-Mohr's circle in the correct location, one of the three effective principal stress magnitudes needs to be known (Lacombe, 2001, 2007; Amrouch, 2010), as the minimum ($\sigma_2 - \sigma_3$) and maximum ($\sigma_1 - \sigma_3$) differential stress magnitudes, the R value and stress regime are already known. By assuming the Andersonian system (Anderson, 1905), where one principal stress is

vertical, the paleo-vertical stress magnitude can be calculated through simple density and stratigraphic thickness relationships, while considering paleo-pore pressures (Lacombe, 2007; Amrouch, 2010). Alternatively, the failure and reactivation envelopes can be used as a guide to place the Mohr's circle at the maximum effective stress conditions prior to rock failure or reactivation occurring (Lacombe and Laurent, 1992; Lacombe, 2001, 2007; Amrouch, 2010). This location would correspond to the intersection between the maximum differential stress circle and the failure envelope. Using the failure and reactivation envelopes therefore requires an understanding of fracture and fault development and/or reactivation at specific periods of time (Lacombe and Laurent, 1992; Lacombe, 2001, 2007; Amrouch, 2010; Arboit et al., 2017).

The Mohr's circle construction was based on previous literature that provides a comprehensive summary of rock mechanics measurements for the Cooper Basin and the limestone-rich Warburton Basin (basement) (Goodman, 1980; Nelson, Chipperfield, Hillis, Gilbert, & McGowen, 2007). Rock mechanics measurements for the Cooper Basin includes a rock cohesion (S_o) of 15 MPa, tensile rock strength (T_o) of 7.5 MPa, and an angle of internal friction (μ) of 43° (Fig. 6) (Nelson et al., 2007). Rock mechanics measurements for the limestone-rich Kalladeina Formation uses mean rock mechanics measurements for limestone formations, which includes an angle of internal friction (μ) of 37° and a rock cohesion (S_o) of 6.7 MPa (Goodman, 1980). For additional constraints on existing CSIT data (Kulikowski & Amrouch, 2017), friction and failure envelopes are also incorporated (Lacombe, 2001, 2007).

Knowing that calcite twins record the maximum stress magnitude at a given time, the maximum differential stress magnitude obtained from the inversion of calcite twins corresponds to the stress magnitudes that induced initial crack development, or peak magnitude, which occurs when the Mohr's circle first meets the failure envelope and would also correspond to new fault and fracture development in the region (Lacombe, 2001, 2007). Placement of the Mohr's circle in this way can also use previous knowledge of whether pre-existing faults and fractures reactivated during the individual events, where during placement of the Mohr's circle, all points that represent reactivated planes will lie above the friction curve (Lacombe, 2001, 2007; Amrouch, 2010). This is a common approach for completing stress tensor results obtained from the inversion of fault slip data (e.g. Bergerat, 1985; Reches, Baer, & Hatzor, 1992; Angelier, 1989) and calcite twin data (e.g. Jamison & Spang, 1976; Rowe & Rutter, 1990; Lacombe & Laurent, 1992, 1996; Lacombe, 2001, 2007; Amrouch, 2010; Amrouch et al., 2010a, 2011; Arboit et al., 2017). As a change in pore pressure may affect the vertical and horizontal stresses differently, the calculated differential stress magnitudes ($\sigma_1 - \sigma_3$ and $\sigma_2 - \sigma_3$) may change when simply shifting the Mohr's circle, perhaps presenting a

slight oversimplification of reality (Biot, 1941; Green and Wang, 1986). However, as the maximum differential stress magnitudes ($\sigma_1 - \sigma_3$) have a ±20% error, the poroelastic effect is negligible and not considered during Mohr's circle constructions (Lacombe, 2001, 2007; Amrouch, 2010).

Insert Fig. 6

3.5. Geomechanical Modelling

3.5.1. OVERVIEW

The Dilation Tendency (T_d) and Slip Tendency (T_s) of faults are common geomechanical modelling calculations used in the petroleum industry to assess the present-day risk of faults dilating and acting as potential permeable conduits for hydrocarbon migration, and assessing the risk of shear reactivation, respectively. Geomechanical modelling is also a commonplace technique for earthquake risk assessment (Morris et al., 1996; Sibson, 1990; Zoback & Harjes, 1997). This study uses the meshed fault model interpreted from the Gidgealpa 3D seismic survey to geomechanically model the T_d and T_s of faults using six individual and complete paleo-stress tensors. These complete paleo-stress tensors were used to develop six unique geomechanical models, which assumed that a hydrostatic pore pressure gradient (0.0098 MPa/m) was present throughout basin development, as paleo-pore pressure estimates are not presently available in literature. The results provide fault geometries that were optimally (critically) oriented to undergo tensile and shear reactivation under each of the six stress conditions, providing information on the evolution of fault activity and the likely hydrocarbon migration pathways through time. The results are converted to colour bars that are overlain onto the fault model for visual emphasis and are also incorporated with stereonets. These stereonets can be used to plot additional fault geometries, that could be present elsewhere in the basin, to measure their unique Dilation Tendency and Slip Tendency.

Insert Table 1

3.5.2. DILATION TENDENCY OF FAULTS

The Dilation Tendency (T_d) is a measure of a faults ability to tensile reactivate (dilate) and can be used to broadly infer the likelihood of unique fault sets acting as potential fluid conduits (high T_d) or seals (low T_d), or to identify zones within an individual fault plane with high or low T_d (Eq. 1) (Barton, Zoback, & Moos, 1995; Ferrill & Morris, 2003).

$$T_d = \frac{\sigma'_1 - \sigma'_n}{\sigma'_1 - \sigma'_3} \qquad \text{(Eq. 1)}$$

The T_d is a manipulation of the components of the stress tensor as plotted on the Mohr circle diagram (Fig. 7a), involving the effective maximum (σ'_1) and minimum (σ'_3) principal stresses, and the effective normal (σ'_n) stress (Eq. 1). The measure is largely controlled by the effective normal stress (σ'_n) acting on a fault plane, with the likelihood of tensile reactivation increasing as the σ'_n approaches the σ'_3 (Ferrill et al., 1999; Mildren et al., 2005). The application of T_d is particularly important in hydrocarbon fields that are interpreted to have sealing faults, or fields that depend on hydrocarbon migration through fault conduits to charge reservoirs (Barton et al., 1995; Ferrill & Morris, 2003; Jolie, Moeck, & Faulds, 2015; Kulikowski et al., 2016c). The T_d values are dimensionless and range from one (high probability) to zero (low probability) and is used in this study to generate a relative ranking between the four unique fault sets during the key stages of basin development.

Insert Fig. 7

3.5.3. SLIP TENDENCY OF FAULTS

Slip Tendency (T_s) is a measure incorporating the effective normal (σ'_n) and shear (τ) stresses acting on a fault plane (Eq. 2), and describes the shear reactivation potential of faults (Ferrill et al., 1999). Shear reactivation will occur when the resolved shear stress acting on a fault plane is equal to, or exceeds, the frictional resistance to sliding (Ferrill et al., 1999). The T_s results will range from one (high shear potential) to zero (low shear potential).

$$T_S = \frac{\tau}{\sigma' n} \qquad \text{(Eq. 2)}$$

As the frictional resistance to sliding is related to the normal stress (Jaeger, Cook, & Zimmerman, 2007), the T_s was measured as the ratio between the τ and σ'_n (Eq. 2) (Morris et al., 1996). We assume a hydrostatic pore pressure gradient (0.0098 MPa/m) throughout basin evolution as accurate pore pressure evolution models are not available. This forms the main uncertainty with geomechanical modelling because sufficient increases in pore pressure can induce rock failure by reducing the effective stresses. For these reasons, geomechanical modelling is traditionally focused on the present-day reactivation potential of faults within hydrocarbon fields, rather than investigating the effect of paleo-stress conditions on the evolution of fault reactivation. Overpressures may have existed during the 650 million year history of the basin and influenced the effective stress magnitudes; however, this data is not available in literature and presents an opportunity for future work to investigate. As such, the evolution of pore pressure, and therefore constraints on absolute stress magnitudes, are not considered in this work. The aim of the study is to

present a new approach and discuss the fault reactivation of four unique fault sets through time in a relative sense throughout basin development.

4. RESULTS

4.1. Overview

Mohr's circles were constructed from each of the 12 calcite samples that define the six events (Fig. 8) with results shown in Table 1. The effective stress magnitudes presented in Table 1 were not converted to absolute stress magnitudes as the evolution of paleo-pore pressure and exhumation/erosion is not well understood in the basin. For this reason, the geomechanical models that are developed for each event assume a hydrostatic pore pressure gradient throughout basin development, which does not affect the modelling results because only relative (not absolute) results are obtained. A fault model from the Gidgealpa 3D seismic survey was used to determine the relative risk of fault dilation and shear reactivation as it is located along the major NE-SW trending GMI Ridge (Fig. 3), hosts a major oil and gas field, and contains four commonly occurring fault sets (striking N-S, NE-SW, and E-W with high (50-70°) dip angle, and striking NW-SE with near vertical (80-90°) dip angle). This variation of fault geometries allowed us to model the evolution of Dilation Tendency (T_d) and Slip Tendency (T_s) for four unique fault sets.

Insert Fig. 8

Results from T_d (Fig. 9) and T_s (Fig. 10) analysis are converted to colour bars and overlay the fault model to visually emphasise the changes between fault geometries. Stereonets with poles to fault planes and the results colour bars are included to enable the theoretical optimum fault geometries to be calculated by plotting poles to fault planes in high T_d and T_s regions. These stereonets can be used to better understand the evolution of fault reactivation elsewhere in the basin, and can also provide insights into natural fracture reactivation through time. Future basin exhumation studies that constrain the true sample depths prior to erosion and pore pressure evolution models will improve the accuracy of this approach.

4.2. Evolution of the Effective Paleo-Stress Magnitudes

Mohr circles were constructed from 12 calcite samples to complete the paleo-stress results from previous work (Kulikowski & Amrouch, 2017). These were placed to intersect the failure envelope, which provided the effective paleo-stress magnitudes at the first point of crack development for 9 out of the 12 calcite samples (Fig. 8). The Daralingie Event did not reach the stress conditions necessary for fault development, as presented by previous works (Kuang, 1985; Apak et al., 1997;

Kulikowski and Amrouch, 2017), but rather reactivated pre-existing NE-SW striking high angle faults. Therefore, the Mohr's circle for this event can be placed between the failure and reactivation envelopes (Lacombe, 2001, 2007) (Fig. 8e, 8f, & 8g). This placement is independent of the geomechanical models and uses established understandings of whether new faults and fractures were developed, or pre-existing faults and fractures were reactivated at key stages in the development of the Cooper-Eromanga Basin. For a more detailed summary on this approach, refer to Lacombe (2001, 2007) and Amrouch (2010).

The effective maximum stress magnitudes ranged from 49 MPa during the Alice Springs Event, to 64 MPa during the Paleogene Event (Table 1). These magnitudes remained relatively constant for most of the basin evolution before decreasing to the present-day magnitude of 42 MPa (Nelson et al., 2007) (Fig. 8m). Strike-slip stress regimes existed during the Silurian, Late Permian, and also during the present day, with compressional stress regimes present during all other periods (Kulikowski and Amrouch, 2017). Differential stress ratios (R; $where\ R = (\sigma_2 - \sigma_3)/(\sigma_1 - \sigma_3)$) also decreased through time from 0.70 during the Alice Springs Event (ASE) to 0.35 during the Paleogene, before deceasing further to 0.10 at present day (Fig. 8m). The maximum differential stress ($\sigma_1 - \sigma_3$) magnitudes ranges from 44 MPa during the ASE, to 55 MPa during the Daralingie, Late Cretaceous, and Paleogene events (Fig. 8m).

4.3. Fault Reactivation during the Alice Springs Event (450-300 Ma)

The Carboniferous Alice Springs Event was a NNW-SSE oriented strike-slip stress regime event (Table 1). Modelling the T_d of faults (Eq. 1) under the stress conditions present during this time (Table 1) found that N-S striking high angle faults (T_d=0.78) were critically oriented to dilate and E-W striking high angle faults were the least likely to dilate (T_d=0.09) (Table 2). N-S (T_s=0.96) and NW-SE (T_s=0.75) striking faults have similar values and were both likely to reactivate under shear (Table 2). E-W striking faults were relatively least likely to reactivate under shear (T_s=0.16) (Table 2). The Mohr's circle construction found that near-vertical faults with strikes NNE-SSW and NW-SE would preferentially develop during this time (Fig. 8a).

Insert Table 2

4.4. Fault Reactivation during the Mid-Permian Event (290-270 Ma)

The Mid-Permian Event was a NW-SE oriented compressional stress regime (Table 1). Modelling the T_d of faults under this stress (Table 1) found NW-SE striking strike-slip faults (T_d=0.43) and E-W striking faults (T_d=0.44) were moderately oriented to dilate (Table 2). NE-SW (T_d=0.26) and N-S

(T_d=0.31) striking high angle faults were less likely to dilate (Table 2). Modelling the T_s found that E-W striking faults (T_s=0.70) had a high probability to reactivate under shear under this stress (Table 2). NW-SE striking strike-slip faults were unlikely to reactivate under shear (T_s=0.08) (Table 2). The Mohr's circles for this event found that low angle faults striking NE-SW were most likely to develop (Fig. 8b, 8c, & 8d).

4.5. Fault Reactivation during the Daralingie Event (258 Ma)

The Late Permian Daralingie Event was oriented in a NE-SW direction under a strike-slip stress regime (Table 1). Modelling the T_d of faults under the stress condition present at this time found that NE-SW striking high angle faults (T_d=0.85) were highly likely to dilate, with NW-SE striking strike-slip faults (T_d=0.12) the least likely (Table 2). Analysis of the T_s found that NE-SW (T_s=1.00), E-W (T_s=0.98) and N-S (T_s=0.81) striking faults were most likely to reactivate under shear, with NW-SE striking faults (T_s=0.36) being the most stable (Table 2). Near-vertical NE-SW and E-S striking faults would have preferentially developed during this time, as highlighted in the Mohr's circle (Fig. 8e, 8f, & 8g).

4.6. Fault Reactivation during the Hunter-Bowen Event (245-190 Ma)

The Late Triassic Hunter-Bowen Event was a compressional stress regime oriented E-W (Table 1). The T_d of faults under the stress conditions present during this time found that E-W (T_d=0.58) and NE-SW (T_d=0.45) striking faults were moderately oriented to dilate, with NW-SE (T_d=0.25) and N-S (T_d=0.26) striking faults least likely to dilate (Table 2). NE-SW striking faults (T_s=0.79), together with E-W (T_s=0.70) and N-S (T_s=0.64) striking faults had the highest tendency to reactivate under shear during this event (Table 2). NW-SE striking faults (T_s=0.38) were relatively least likely to reactivate under shear at this time (Table 2). The Mohr's circle construction found that N-S striking low angle faults would preferentially develop under this stress tensor (Fig. 8h).

4.7. Fault Reactivation during the Late Cretaceous Event (95-65 Ma)

An E-W oriented compressional event occurred during the Late Cretaceous (Table 1). Modelling the T_d of faults at this stage of basin development presents E-W (T_d=0.582) and NE-SW (T_d=0.45) striking faults with the highest T_d, and N-S (T_d=0.24) and NW-SE (T_d=0.28) striking faults with the lowest values (Table 2). NE-SW (T_s=0.74) and E-W (T_s=0.63) striking faults were found to be the most likely to reactivate under shear at this time (Table 2). NW-SE striking faults (T_s=0.35) were relatively least likely to reactivate under shear (Table 2). N-S striking faults with low dip angles would have preferentially developed during this time given by the Mohr's circle analysis (Fig. 8i & 8j).

4.8. Fault Reactivation during the Paleogene Event (33-23 Ma)

The Paleogene Event was a compressional stress regime oriented N-S (Table 1). The T_d of faults under the stress conditions present during this time found that N-S striking faults (T_d=0.66) were optimally oriented to dilate (Table 2). E-W (T_d=0.23) and NW-SE (T_d=0.26) striking faults were the least likely to dilate (Table 2). The relative likelihood of faults to reactivate under shear using the T_s measure found that NE-SW (T_s=0.79) and N-S (T_s=0.76) striking faults had the highest probabilities (Table 2). Again, NW-SE striking faults (T_s=0.44) were relatively least likely to reactivate under shear at this time (Table 2). The Mohr's circle for this event shows that E-W striking faults with low dip angles would have preferentially developed (Fig. 8k & 8l), but these were not commonly encountered in seismic data.

5. DISCUSSION

The application of geomechanical modelling to petroleum basins is more easily applied to faults under the present-day stress because stress tensors are easily calculated and fault geometries are known (e.g. Morris et al., 1996; Wiprut & Zoback, 2000, 2002; Moeck et al., 2009; Kulikowski et al., 2016c). This approach is important in understanding the risk of seal breach and the potential for faults to act as potential leak paths at present day; however, this does not utilise the full potential of geomechanical modelling and does not provide information on potential hydrocarbon migration pathways through time. In petroleum basins where seismic data quality is not sufficiently high to analyse fault growth, the tectonic evolution of the basin, and hence hydrocarbon migration pathways, can be unclear. Even with mainstream fault growth analysis, the inability of these techniques to detect lateral (or oblique) shearing can oversimplify fault activity by overlooking key structural periods. For such regions, the integration of the CSIT with geomechanical modelling can determine the evolution of fault development and reactivation during basin evolution, providing fault geometries that are optimally oriented to dilate and reactivate under shear at key periods in time. This study utilises 12 incomplete paleo-stress tensor results from previous research (Kulikowski & Amrouch, 2017) to determine the effective stress magnitudes of each event, and thus completing the paleo-stress tensors. These completed stress-tensors are then used to model the Dilation Tendency (T_d) and Slip Tendency (T_s) of faults within the Gidgealpa 3D seismic survey, Cooper-Eromanga Basin, Australia.

As expected, the results show that individual fault sets will dynamically dilate and reactivate under shear through time and are strongly controlled by the changing paleo-stress conditions. This reiterates the importance of understanding the evolution of fault activity, and highlights the

uncertainty of hydrocarbon migration pathway models that use the present-day fault geometries without considering their T_d and T_s evolution through time. Although a particular fault set may be open to hydrocarbon migration under contemporary stresses, it is important to understand that stress conditions change through time. Considering that Permian Cooper Basin source rocks were early mature (%Ro=0.5-0.7) during the Triassic, and mid mature (%Ro=0.7-1.0) during the Jurassic, hydrocarbon migration models are unaffected by pre-Triassic events (Kantsler et al., 1983; Mavromatidis, 2006).

Additionally, Kantsler et al. (1983) and Deighton and Hill (1998) show that although Permian source rock maturation began between the Triassic and Jurassic, most oil and gas expulsion occurred during the Cretaceous. This suggests that during the major period of hydrocarbon expulsion and migration, fault conduits could have been affected by two tectonic events: (1) the compressional Late Cretaceous Event, and (2) the compressional Paleogene Event. Nonetheless, basin evolution models require a complete understanding of the structural history to predict paleo-highs that may have affected the depositional environment through time. As such, we model the stress conditions present during each of the six tectonic events that have affected the evolution of the basin, not including the present-day stress conditions as investigated by Kulikowski et al. (2016c).

Although the Cooper-Eromanga Basin has been affected by numerous compressional and strike-slip stress regime events, a large volume of faults have high dip angles (>50°), with a dominant NE-SW strike. This fault geometry likely developed under an extensional stress regime (Adelaidean Event) oriented in a NW-SE direction (Anderson, 1905), and subsequently reactivated to give their present-day inverted geometry. The relatively smaller volume of low angle faults (typical to compressional stress regime events) is likely attributed to the preferential reactivation of old pre-existing high angle normal faults, rather than the development of new faults (Kulikowski and Amrouch, 2017). The stress required to reactivate a pre-existing fault is almost always considerably less than that required to develop a new fault, but may depend on the stress orientations relative to the pre-existing fault geometry and the presence of precipitates or cements. This is also consistent with previous research that infers the successive reactivation of NE-SW striking high angle faults, rather than the development of new low angle thrust faults (Kuang, 1985; Apak et al., 1997). Additionally, stress perturbation can be caused by folds, faults, topography, or lithology, and can develop fault geometries that are not representative of the far-field tectonic stress orientation or regime (Tavani et al., 2015). However, three regionally pervasive and low dipping conjugate natural fracture sets have been found to exist throughout the basin, confirming the presence of compressional stress regimes (Kulikowski & Amrouch, 2017).

The NNW-SSE oriented strike-slip Alice Spring Event (ASE) was responsible for the development of NNE-SSW and NW-SE striking conjugate fracture set (Kulikowski and Amrouch, 2017) and has one of the lowest maximum differential stress ($\sigma_1 - \sigma_3$) magnitudes (44 MPa) of the six events, which reduces the likelihood of faults to fall within high T_d and T_s areas (Fig. 9a and 10a). Small maximum differential stress ($\sigma_1 - \sigma_3$) magnitudes reduce the diameter of the Mohr circle and require higher overpressures to induce failure or reactivation. This is clear when comparing the stereonet results from the ASE (Fig. 9a and 10a) with the N-S oriented Paleogene Event (Fig. 9f and 10f), the latter of which has a maximum differential stress ($\sigma_1 - \sigma_3$) magnitude of 55 MPa (Table 1). High reactivation values are limited to a smaller area of the stereonet within the ASE. Ultimately, only N-S striking high angle faults would dilate (Fig. 9g) and shear (Fig. 10g) reactivate during this time; however, the optimum fault geometries based on the stereonet are NNE-SSW and NNW-SSE striking strike-slip faults (Fig. 10a).

Under compressive stress regime conditions, such as during the Mid-Permian Event, the T_d of faults is greatest for low angle to horizontal fault planes. However, the intensity of low angle faults within the Gidgealpa 3D seismic survey, and also the Cooper-Eromanga Basin, is relatively low when compared to high angle (50-70°) faults (Fig. 5b). The reason for this is likely due to it being more stress economic to reactivate the original basement normal faults (60° dip angle) than to develop new faults. This event did however create a low angle (<30°) NE-SW striking conjugate fracture set across the basin (Kulikowski & Amrouch, 2017). Nonetheless, the sub-horizontal faults that are most likely to dilate during this time will have a greater influence on the lateral migration of hydrocarbons rather than vertical. The T_d of faults during the Mid-Permian Event, as well as other compressional stress regime events, is therefore considerably lower than during the ASE or Daralingie Event (Fig. 9g). The faults that are most likely to dilate during this time are E-W striking high angle and NW-SE striking strike-slip faults (Fig. 9b and 9g) with high angle E-W striking faults most likely to reactivate under shear (Fig. 10b and 10g; Table 2). NW-SE striking strike-slip faults are found to terminate within the middle Patchawarra Formation, coinciding with the Mid-Permian Event, and can pose detrimental effects on hydrocarbon production and reservoir quality through significant compartmentalisation of the reservoir (Kulikowski & Amrouch, 2017. These faults can be easily overlooked in reservoir models, as strike-slip faults are difficult to identify and interpret in cross-section, particularly in poor quality seismic data common to the Cooper-Eromanga Basin.

Faults are rarely seen to penetrate past the Permian into younger sediments. This may suggest that faults were dormant after the Mid-Permian Event and stress was largely accommodated by folding rather than faulting, or that faults were active during subsequent events but grew as blind

faults (Yan et al., 2009). It is also possible that fault tips extend into younger sediments at a sub-seismic resolution scale as the seismic resolution is 20 meters at best, and particularly if reactivation is lateral (or oblique) where reflector offsets cannot be observed. The Late Permian Daralingie Event was a strike-slip stress regime oriented in an NE-SW direction that did not record natural fracture or fault development (Kulikowski & Amrouch, 2017). As such, the Mohr's circle cannot be accurately placed in a single location, but most exist between the failure and reactivation envelopes (Fig. 8e, 8f & 8g). The relatively high maximum differential stress ($\sigma_1 - \sigma_3$) magnitude (55 MPa) of this event (Table 1) can be seen to affect the results by expanding the high T_d and T_s zones (Fig. 9c and 10c). High angle NE-SW striking faults are optimally oriented to dilate (Fig. 9g) and shear (Fig. 10g) reactivate under these stress conditions. High angle E-W striking faults are also optimally oriented to dilate (Fig. 9g) and act as potential hydrocarbon conduits (Table 2).

The remaining three tectonic events were compressional stress regimes that created their own set of low angle (30^o) conjugate fracture sets (Kulikowski & Amrouch, 2017). Under these stress conditions, near horizontal to shallow dipping faults would record high T_d and T_s results. However, the maximum differential stress ($\sigma_1 - \sigma_3$) magnitudes of these three events are relatively high compared to the previous events and enlarge the stereonet zones of high T_d and T_s. In the case of the E-W oriented Hunter-Bowen Event (Fig. 9d and 10d), this increase puts E-W and NE-SW striking high angle faults as relatively most likely to dilate; however, when compared to previous stress conditions such as the Daralingie Event, the Dilation Tendency value is relatively low with a differential Dilation Tendency of 0.25 (Fig. 9g; Table 2). This infers that faults were relatively less likely to dilate during the Hunter-Bowen Event when compared to the Daralingie Event and ASE (Fig. 9g). This is equally the case for Slip Tendency results (Fig. 10g; Table 2). Elsewhere in the basin, faults striking ENE-WSW with low dip angle are critically oriented to have dilated (Fig. 9d), and low angle NE-SW and E-W striking faults are critically oriented to have reactivated under shear (Fig. 10d) during the Hunter-Bowen Event. However, these low angled to sub-horizontal faults will contribute mostly to the lateral migration of hydrocarbons, whereas high angled to sub-vertical faults can have significant influence on vertical migration of hydrocarbons into overlying, and potentially unsealed stratigraphic intervals. Important to note is that fault surfaces are highly textured and will have high fluid conductivity fairways within a certain zone, rather than the entire plane acting as a conduit.

The paleo-stress results calculated for the Late Cretaceous Event show some dissimilarity between the two samples, which was detailed in the original works (Kulikowski and Amrouch, 2017) and attributed to a nearby fault that perturbed stresses. Geomechanical modelling results using the stress from the Late Cretaceous Event found that the fault geometries most likely to dilate and

reactivate under shear are similar to the geometries mentioned under the Hunter-Bowen Event stress conditions and with similar values (Fig. 9g & 10g; Table 2). This result is vital for hydrocarbon migration models as it identifies that E-W and NE-SW striking faults were most likely to dilate (Fig. 9g) and shear (Fig. 10g) reactivate after the critical moment in the Cooper-Eromanga Basin hydrocarbon system. Subsequently, the stress conditions present during the Paleogene Event encouraged N-S striking faults to preferentially dilate (Fig. 9f and 9g; Table 2) and NE-SW and N-S striking faults to preferentially reactivate under shear (Fig. 10f and 10g; Table 2) during this time. After the Paleogene Event, the σ_1 direction has rotated to 101°N at present-day with a maximum horizontal stress magnitude of 42 MPa at 1 km depth (Fig. 8m) (Reynolds, Mildren, Hillis, Meyer, & Flottmann, 2005; Reynolds, Mildren, Hillis, & Meyer, 2006; Nelson et al., 2007). The present-day stress conditions have increased the T_d of NW-SE striking strike-slip faults, making this fault geometry the most likely to act as a permeable conduit for tertiary migration of hydrocarbons at present day (Kulikowski et al., 2016c).

Determining the paleo-burial depth of samples is difficult in the Cooper-Eromanga Basin, as five of the six events are recorded as unconformable surfaces inferring some degree of exhumation and erosion. The degree of erosion is not well understood in the basin so any attempt to assume a paleo-depth based on the present-day stratigraphy would need to be highly critical and involve careful consideration of many aspects. Considering that the evolution of pore pressure is also unknown in the basin, the effective stress magnitudes presented for the six events cannot be easily converted to the absolute stress magnitudes. From the individual sample results, one effective stress magnitude (σ'_v or σ'_h) is negative in four of the 12 results (Table 1), which can infer significant overpressure during these events (Amrouch, 2010; Amrouch et al., 2011; Arboit et al., 2017). This aligns well with previous research (Flottman, Campagna, Hillis, & Warner, 2004; Cooke, Tyiasning, & Abul Khair, 2015) that has presented significant horizontal fracturing and potential opening of the bedding plane throughout the basin, which would be geomechanically favourable if σ'_v is negative.

Future work could investigate the applicability of using these measured T_d and T_s results to calculate the potential volume of hydrocarbon migration along semi-conductive faults through time, which may then be directly incorporated into hydrocarbon migration models and used for exploration and development programs. Insights into the exhumation/erosion and pore pressure evolution could also be carefully investigated from these results (Amrouch, 2010; Amrouch et al., 2011; Arboit et al., 2017). As this is the first study of its kind to incorporate geomechanical modelling of fault reactivation with the complete paleo-stress tensors, a similar approach can be applied to any

other petroleum basin or province that requires a better understanding of the 4D evolution of fault reactivation.

6. CONCLUSIONS

This research presents a unique approach in determining the structural evolution of provinces where seismic data quality is poor, using the hydrocarbon-rich Cooper-Eromanga Basin as a case study. The integration of complete paleo-stress tensors, obtained from calcite twin stress inversion (CSIT), with geomechanical modelling provides a more defined look-back at the evolution of fault activity where fault growth modelling is inhibited by poor resolution seismic data. We provide more constraints on previous CSIT results by incorporating rock mechanics measurements to define the effective paleo-stress magnitudes from 12 previously incomplete stress tensors that combine to define six tectonic events. These stress conditions were modelled to evaluate the fault geometries most likely to dilate (act as potential hydrocarbon conduits) and reactivate under shear at key periods of time during basin development. The findings of this research show that during each of the six structural stages of basin development, the main regional fault sets will have unique and dynamic hydrocarbon conduit potential. The fault sets that are most likely to reactivate and facilitate fluid migration at key stages of basin development include:

(1) Alice Springs Event: NNW-SSE striking faults (>60° dip);
(2) Mid Permian Event: E-W striking faults (<50° dip);
(3) Daralingie Event: NE-SW striking faults (>60° dip);
(4) Hunter-Bowen Event: E-W and NE-SW striking faults (<50° dip);
(5) Late Cretaceous Event: E-W and NE-SW striking faults (<50° dip);
(6) Paleogene Event: N-S and NE-SW striking faults (<50° dip);
(7) Present day: E-W and NW-SE striking faults (>60° dip).

Since the critical moment in the Cooper-Eromanga Basin hydrocarbon system (90 Ma), the theoretical fault geometries most likely to have acted as permeable hydrocarbon conduits are E-W (during the Upper Cretaceous Event) and N-S (during the Paleogene Event) striking low (<50°) dip angle faults. Future work constraining the exhumation of this province should incorporate the effective vertical stress magnitudes present here to calculate the maximum burial depth prior to exhumation and erosion and quantify the evolution of pore pressure. The complete paleo-stress tensors of the six events will also benefit future work attempting to model the structural and stratigraphic evolution of this basin.

7. ACKNOWLEDGEMENTS

The authors appreciate the financial contribution made by the GeoFrac Consortium, which includes the Program Manager Dennis Cooke, and the sponsoring companies: Santos, Beach Energy, Chevron, Halliburton and BG Group (QGC). We thank Midland Valley (MOVE 2016.2), DownUnder Geosolutions (DUG Insight) and the creators of OpenStereo 0.1.2 (Carlos H. Grohmann and Ginaldo A.C. Campanh) for their generous donation of academic licences. DUG Insight software (v.3.1, 2015) was used for seismic visualisation, interpretation and analysis. We appreciate the feedback provided by Jozina Dirkzwager, Scott Mildren, and the editorial team at the AJES.

8. REFERENCES

Alexander, E. M., Gravestock, D. I., Cubitt, C., & Chaney, A. (1998). Lithostratigraphy and Environments of Deposition. In: Gravestock, D. I., Hibburt, J. E., & Drexel, J. F. (Eds). (1998). The petroleum geology of South Australia. Vol. 4: Cooper Basin. South Australia. Department of Primary Industries and Resources. Report Book, 98/9.

Amrouch, K., Lacombe, O., Mouthereau, F., & Dissez, L. (2005). Quantification of orientations and magnitudes of the late Cenozoic paleostresses in the Zagros folded belt from calcite twin analysis. *In* Thrust Belts and Foreland Basins, International Meeting, Rueil-Malmaison, 31-35.

Amrouch, K., Lacombe, O., Bellahsen, N., Daniel, J. M., & Callot, J. P. (2010a). Stress and strain patterns, kinematics and deformation mechanisms in a basement-cored anticline: Sheep Mountain Anticline, Wyoming. Tectonics, 29, TC1005, doi:10.1029/2009TC002525.

Amrouch, K., Robion, P., Callot, J. P., Lacombe, O., Daniel, J. M., Bellahsen, N., & Faure, J. L. (2010b). Constraints on deformation mechanisms during folding provided by rock physical properties: a case study at Sheep Mountain anticline (Wyoming, USA). Geophysical Journal International, 182(3), 1105-1123.

Amrouch, K. (2010). Apport de l'analyse microstructurale à la comprehension des mécanismes de plissement. Exemples de structures plissées aux USA (Wyoming) et en Iran (Zagros). Thèse, Université Pierre et Marie Curie – Paris 6, 2010-03, 477 p.

Amrouch, K., Beaudoin, N., Lacombe, O., Bellahsen, N., & Daniel, J. M. (2011), Paleostress magnitudes in folded sedimentary rocks, Geophysical Research Letters, 38, L17301, doi:10.1029/2011GL048649.

Anderson, E. M. (1905). The dynamics of faulting. Transactions of the Edinburgh Geological Society, 8(3), 387-402.

Angelier, J. (1989). From orientation to magnitudes in paleostress determinations using fault slip data. Journal of Structural Geology, 11(1), 37–50.

Apak, S. N., Stuart, W. J., Lemon, N. M., & Wood, G. (1997). Structural evolution of the Permian-Triassic Cooper Basin, Australia: Relation to hydrocarbon trap styles. AAPG Bulletin, 81, 533-555.

Arboit, F., Amrouch, K., Collins, A. S., King, R., & Morley, C. (2015). Determination of the tectonic evolution from fractures, faults, and calcite twins on the southwestern margin of the Indochina Block. Tectonics, 34, doi:10.1002/2015TC003876.

Arboit, F., Amrouch, K., Morley, C., Collins, A. S., & King, R. (2017), Palaeostress magnitudes in the Khao Khwang fold-thrust belt, new insights into the tectonic evolution of the Indosinian orogeny in central Thailand, Tectonophysics, doi:10.1016/j.tecto.2017.01.008.

Barton, C. A., Zoback, M. D., & Moos, D. (1995). Fluid flow along potentially active faults in crystalline rock. Geology, 23, 683-686.

Baudon, C., & Cartwright, J. (2008). The kinematics of reactivation of normal faults using high resolution throw mapping. Journal of Structural Geology, 30(8), 1072–1084.

Beaudoin, N., Leprêtre, R., Bellahsen, N., Lacombe, O., Amrouch, K., Callot, J. P., Emmanuel, L., & Daniel, J. M. (2012). Structural and microstructural evolution of the Rattlesnake Mountain Anticline (Wyoming, USA): new insights into the Sevier and Laramide orogenic stress build-up in the Bighorn Basin. Tectonophysics, 576, 20-45.

Bergerat, F. (1985). Déformations cassantes et champs de contrainte tertiaires dans la plate-forme européenne (Doctoral dissertation, Université Pierre et Marie Curie-Paris VI).

Biot, M. A. (1941). General theory of three-dimensional consolidation. Journal of Applied Physics, 12(2), 155-164.

Boreham, C. J., & Hill, A. J. (1998). Source rock distribution and hydrocarbon geochemistry. In: Gravestock, D. I., Hibburt, J. E., & Drexel, J. F. (Eds). (1998). The petroleum geology of South Australia. Vol. 4: Cooper Basin. South Australia. Department of Primary Industries and Resources. Report Book, 98/9.

Bradshaw, M. T. (1993). Australian petroleum systems. PESA Journal, 21, 43-53.

Childs, C., Nicol, A., Walsh, J. J., & Watterson, J. (1996). Growth of vertically segmented normal faults. Journal of Structural Geology, 18(12), 1389–1397.

Constantin, J., Laurent, P., Vergély, P., & Cabrera, J. (2007). Paleo-deviatoric stress magnitudes from calcite twins and related structural permeability evolution in minor faults: Example from the toarcian shale of the French Causses Basin, Aveyron, France. Tectonophysics, 429(1), 79-97.

Cooke, D., Tyiasning, S., & Abul Khair, H. (2016). Unexpected behaviors of stimulated fractures in the high-stress Cooper Basin. The Leading Edge, 35(1), 78-84.

Delaunay, B. (1934). Sur la sphère vide. Bulletin de l'Académie des Sciences de L'URSS, Classe des sciences mathématiques et naturelles, 6, 793–800.

Deighton, I., & Hill, A. J. (1998). Thermal and Burial History. In: Gravestock, D. I., Hibburt, J. E., & Drexel, J. F. (Eds). (1998). The petroleum geology of South Australia. Vol. 4: Cooper Basin. South Australia. Department of Primary Industries and Resources. Report Book, 98/9.

Etchecopar, A. (1984). Etude des e tats de Contraintes en Tectonique Cassante et Simulation de Formation Plastique (Approche Mathe Matique), the se Doctorates-Sciences, 270 pp., Univ. Sci. et Tech. Du Langue-doc, Montpellier, Fr.

Ferrill, D. A. (1998). Critical re-evaluation of differential stress estimates from calcite twins in coarse-grained limestone, Tectonophysics, 285(1), 77-86.

Ferrill, D. A., Winterle, J., Wittmeyer, G., Sims, D., Colton, S., Armstrong, A., & Morris, A. P. (1999). Stressed rock strains groundwater at Yucca Mountain, Nevada. GSA Today, 9(5), 1-8.

Ferrill, D. A., & Morris, A. P. (2003). Dilational normal faults. Journal of Structural Geology, 25, 183-196.

Flottmann, T., Campagna, D. J., Hillis, R., & Warner, D. (2004). Horizontal microfractures and core discing in sandstone reservoirs, Cooper Basin, Australia. PESA Eastern Australian Basins Symposium II, Adelaide, 19-22 September, 689-694.

Gatehouse, C. G. (1986). The geology of the Warburton Basin in South Australia. Australian Journal of Earth Sciences, 33, 161-180.

Glikson, A. Y., Uysal, I. T., Fitz Gerald, J. D., & Saygin, E. (2013). Geophysical anomalies and quartz microstructures, Eastern Warburton Basin, North-east South Australia: Tectonic or impact shock metamorphic origin? Tectonophysics, 589, 57-76.

Goodman, R. E. (1980). Introduction to Rock Mechanics. John Wiley & Sons, New York, 2, 576.

Gravestock, D. I., & Jensen-Schmidt, B. (1998). Structural setting. Petroleum Geology of South Australia, 4, 47-67.

Grohmann, C. H., & Campanha, G. A. C. (2010). OpenStereo: Open source, cross-platform software for structural geology analysis. In AGU Fall Meeting, San Francisco, California, Abstracts, 1, 6.

Grohmann, C. H., Campanha, G. A. C., & Soares, Jr, A. V. (2011). OpenStereo: um programa Livre e multiplataforma para análise de dados estruturais. In: XIII Simpósio Nacional de Estudos Tectônicos.

Haines, P. W., Hand, M., & Sandiford, M. (2001). Palaeozoic synorogenic sedimentation in central and northern Australia: A review of distribution and timing with implications for the evolution of intracontinental orogens. Australian Journal of Earth Sciences, 48, 911-928.

Jaeger, J. C., Cook, N. G., & Zimmerman, R. (2007). Fundamentals of rock mechanics. 4th ed., Blackwell Publishing, Oxford, United Kingdom.

Jamison, W. R., & Spang, J. H. (1976). Use of calcite twin lamellae to infer differential stress. Geological Society of America Bulletin, 87(6), 868–872.

Jolie, E., Moeck, I., & Faulds, J. E. (2015). Quantitative structuralgeological exploration of fault-controlled geothermal systems—A case study from the Basin-and-Range Province, Nevada (USA). Geothermics, 54, 54-67.

Kantsler, A. J., Prudence, T. J. C., Cook, A. C., & Zwigulis, M. (1983). Hydrocarbon habitat of the Cooper/Eromanga basin, Australia. Australian Petroleum Exploration Association Journal, 23, 75-92.

Kuang, K.S. (1985). History and style of Cooper-Eromanga Basin structures. Exploration Geophysics, 16, 245-248.

Kulikowski, D., Cooke, D., & Amrouch, K. (2016a). Constraining the distribution and relationship between overpressure, natural fracture density and temperature in the Cooper Basin. The APPEA Journal, 56, 11-28, doi:10.1071/AJ15002.

Kulikowski, D., Hochwald, C., Cooke, D., & Amrouch, K. (2016b). A Statistical Approach to Assessing Depth Conversion Uncertainty on a Regional Dataset: Cooper-Eromanga Basin, Australia. ASEG-PESA-AIG 2016 Conference, Adelaide, extended abstract #200, 484-490, doi:10.1071/ASEG2016ab200.

Kulikowski, D., Amrouch, K., & Cooke, D. (2016c). Geomechanical Modelling of Fault Reactivation in the Cooper Basin, Australia. Australian Journal of Earth Sciences, 63(3), 295-314, doi:10.1080/08120099.2016.1212925.

Kulikowski, D., & Amrouch, K. (2017). Combining Geophysical Data and Calcite Twin Stress Inversion to Refine the Tectonic History of Subsurface and Offshore Provinces: A Case Study on the Cooper-Eromanga Basin, Australia. Tectonics, 36(3), 515-541, doi:10.1002/2016TC004366.

Kulikowski, D., Amrouch, K., Cooke, D., & Gray, M.E. (2017). Basement Structural Architecture and Hydrocarbon Conduit Potential of Polygonal Faults in the Cooper-Eromanga Basin, Australia. Geophysical Prospecting, doi:10.1111/1365-2478.12531.

Lacombe, O., Angelier, J., & Laurent, P. (1992). Determining paleostress orientations from faults and calcite twins: A case study near the Sainte-Victoire Range (southern France). Tectonophysics, 201(1), 141–156.

Lacombe, O., & Laurent, P. (1992). Determination of principal stress magnitudes using calcite twins and rock mechanics data. Tectonophysics, 202(1), 83-93.

Lacombe, O., & Laurent, P. (1996). Determination of deviatoric stress tensors based on inversion of calcite twin data from experimentally deformed monophase samples: Preliminary results. Tectonophysics, 255(3), 189–202.

Lacombe, O. (2001). Paleostress magnitudes associated with development of mountain belts: Insights from tectonic analyses of calcite twins in the Taiwan Foothills. Tectonics, 20(6), 834–849, doi:10.1029/2001TC900019.

Lacombe, O. (2007). Comparison of paleostress magnitudes from calcite twins with contemporary stress magnitudes and frictional sliding criteria in the continental crust: Mechanical implications. Journal of Structural Geology, 29(1), 86–99.

Lacombe, O., Amrouch, K., Mouthereau, F., & Dissez, L. (2007). Calcite twinning constraints on late Neogene stress patterns and deformation mechanisms in the active Zagros collision belt. Geology, 35(3), 263–266.

Lowe-Young, B. S., Mackie, S. I., & Heath, R. S. (1997). The cooper-eromanga petroleum system, Australia: Investigation of essential elements and processes. Indonesian Petroleum Association. Proceedings of the Petroleum Systems of SE Asia and Australasia Conference, Jakarta, Indonesia (pp. 199-211).

Mavromatidis, A. (2006). Burial/exhumation histories for the Cooper-Eromanga Basins and implications for hydrocarbon exploration, Eastern Australia. Basin Research, 18, 351-373.

Mildren, S. D., Hillis, R. R., Dewhurst, D. N., Lyon, P. J., Meyer, J. J., & Boult, P. J. (2005). FAST: A new technique for geomechanical assessment of the risk of reactivation-related breach of fault seals. In

P. Boult & J. Kaldi (Eds.), Evaluating fault and cap rock seals (Vol. 2, pp. 73-85). AAPG Hedberg Series, Barossa Valley, South Australia.

Moeck, I., Kwiatek, G., & Zimmermann, G. (2009). Slip tendency analysis, fault reactivation potential and induced seismicity in a deep geothermal reservoir. Journal of Structural Geology, 31, 1174-1182.

Morris, A., Ferrill, D. A., & Henderson, D. B. (1996). Slip-tendency analysis and fault reactivation. Geology, 24, 275-278.

Muller, R. D., Dyksterhuis, S., & Rey, P. (2012). Australian paleo-stress fields and tectonic reactivation over the past 100 Ma. Australian Journal of Earth Sciences, 59, 13-28.

Nelson, E. J., Chipperfield, S. T., Hillis, R. R., Gilbert, J., & McGowen, J. (2007). Using geological information to optimize fracture stimulation practices in the Cooper Basin, Australia. Petroleum Geoscience, 13(1), 3-16.

Pokalai, K., Kulikowski, D., Johnson, Jr., R. L., Haghighi, M., & Cooke, D. (2016). Development of a new approach for hydraulic fracturing in tight sand with pre-existing natural fractures. The APPEA Journal, 56, 225-238, doi:10.1071/AJ15017.

Reches, Z. E., Baer, G., & Hatzor, Y. (1992). Constraints on the strength of the upper crust from stress inversion of fault slip data. Journal of Geophysical Research: Solid Earth, 97(B9), 12481-12493.

Reynolds, S. D., Mildren, S. D., Hillis, R. R., Meyer, J. J., & Flottmann, T. (2005). Maximum horizontal stress orientations in the Cooper Basin, Australia. implications for plate-scale tectonics and local stress sources. Geophysical Journal International, 160, 331-343.

Reynolds, S. D., Mildren, S. D., Hillis, R. R., & Meyer, J. J. (2006). Constraining stress magnitudes using petroleum exploration data in the Cooper-Eromanga Basins, Australia. Tectonophysics, 415, 123-140.

Rowe, K. J., & Rutter, E. H. (1990). Palaeostress estimation using calcite twinning: Experimental calibration and application to nature. Journal of Structural Geology, 12(1), 1–17.

Rutqvist, J., Rinaldi, A. P., Cappa, F., & Moridis, G. J. (2013). Modeling of fault reactivation and induced seismicity during hydraulic fracturing of shale-gas reservoirs. Journal of Petroleum Science and Engineering, 107, 31-44.

Sibson, R. H. (1990). Conditions for fault-valve behaviour. Geological Society, London, Special Publications, 54(1), 15-28.

Sibson, R. H. (1996). Structural permeability of fluid-driven fault-fracture meshes. Journal of Structural Geology, 18, 1031-1042.

Tavani, S., Storti, F., Lacombe, O., Corradetti, A., Muñoz, J. A., & Mazzoli, S. (2015). A review of deformation pattern templates in foreland basin systems and fold-and-thrust belts: Implications for the state of stress in the frontal regions of thrust wedges. Earth-Science Reviews, 141, 82-104.

Tripathy, V., & Saha, D. (2015). Inversion of calcite twin data, paleostress reconstruction and multiphase weak deformation in cratonic interior–Evidence from the Proterozoic Cuddapah basin, India. Journal of Structural Geology, 77, 62-81.

Turner, F. J. (1953). Nature and dynamic interpretation of deformation lamellae in calcite of three marbles. American Journal of Science, 251(4), 276-298.

Turner, F. J., Griggs, D. T., & Heard, H. (1954). Experimental deformation of calcite crystals, Geological Society of the American Bulletin, 65(9), 883–934.

Watterson, J., Walsh, J., Nicol, A., Nell, P. A. R., & Bretan, P. G. (2000). Geometry and origin of a polygonal fault system. Journal of the Geological Society, 157(1), 151-162.

Williams, G. D., Powell, C. M., & Cooper, M. A. (1989). Geometry and kinematics of inversion tectonics. Geological Society, London, Special Publications, 44(1), 3-15.

Wiprut, D., & Zoback, M. D. (2000). Fault reactivation and fluid flow along a previously dormant normal fault in the northern North Sea. Geology, 28, 595-598.

Wiprut, D., & Zoback, M. D. (2002). Fault reactivation, leakage potential, and hydrocarbon column heights in the northern North Sea. Norwegian Petroleum Society Special Publications, 11, 203-219.

Yan, D. P., Zhang, B., Zhou, M. F., Wei, G. Q., Song, H. L., & Liu, S. F. (2009). Constraints on the depth, geometry and kinematics of blind detachment faults provided by fault propagation folds: An example from the Mesozoic fold belt of South China. Journal of Structural Geology, 31, 150–162, doi:10.1016/j.jsg.2008.11.005.

Zoback, M. D., & Harjes, H. P. (1997). Injection-induced earthquakes and crustal stress at 9 km depth at the KTB deep drilling site, Germany. Journal of Geophysical Research, 102(B8), 18477-18491.

9. TABLES AND FIGURES.

Table 1. Completed effective paleo-stress results based on the incomplete results from Kulikowski & Amrouch (2017a). The present-day stress and rock mechanics measurements were taken from Nelson et al. (2007) and Goodman (1980).

Event	Sample#	Formation	σ_H Azimuth	Stress Regime	R	Max. Differential Stress (MPa)	S_o (MPa)	T_o (MPa)	μ	σ'_H (MPa)	σ'_h (MPa)	σ'_v (MPa)	**Final Event Magnitudes** σ_H Azimuth	σ'_H (MPa)	σ'_h (MPa)	σ'_v (MPa)
Alice Springs Event	CalS5b	Kalladeina	172°N	S-S	0.70	43 ± 9	6.7	3.2	37°	49	5	36	**172°N**	**49**	**5**	**36**
Mid-Permian Event	CalS1	Merrimelia	318°N	Comp.	0.80	52 ± 10	15	7.5	43°	48	38	-4	**128°N**	**56**	**33**	**4**
	CalS2	Kalladeina	301°N		0.40	55 ± 11	6.7	3.2	37°	64	31	9				
	CalS3	Kalladeina	306°N		0.50	50 ± 10	6.7	3.2	37°	57	32	7				
Daralingie Event	CalS2b	Kalladeina	219°N	S-S	0.40	53 ± 11	6.7	3.2	37°	61*	8*	29*	**234°N**	**56***	**1***	**26***
	CalS1b	Merrimelia	065°N		0.60	57 ± 11	15	7.5	43°	56*	-1*	33*				
	CalS4	Merrimelia	238°N		0.40	53 ± 11	15	7.5	43°	50*	-3*	18*				
Hunter-Bowen Event	CalS5	Kalladeina	260°N	Comp	0.50	52 ± 10	6.7	3.2	37°	60	34	8	**080°N**	**60**	**34**	**8**
Late Cretaceous Event	CalS6b	Kalladeina	272°N	Comp.	0.50	67 ± 13	6.7	3.2	37°	80	47	13	**085°N**	**59**	**28**	**4**
	CalS4b	Merrimelia	078°N		0.30	45 ± 9	15	7.5	43°	39	8	-5				
Paleogene Event	CalS3b	Kalladeina	170°N	Comp.	0.40	63 ± 13	6.7	3.2	37°	75	37	12	**174°N**	**64**	**28**	**9**
	CalS6	Kalladeina	178°N		0.40	46 ± 9	6.7	3.2	37°	52	18	6				
Present-day	-	-	*101°N*	*S-S*	*0.10*	*26*	-	-	-	*42*	*16*	*18*	***090°N***	***42***	***16***	***18***

σ_H: maximum horizontal stress azimuth; σ'_H: effective maximum horizontal stress magnitude; σ'_h: effective minimum horizontal stress magnitude; σ'_v: effective vertical stress magnitude; R: stress ellipsoid shape ratio ($R = [\sigma_2 - \sigma_3]/[\sigma_1 - \sigma_3]$); S_o: cohesive rock strength; T_o: tensile rock strength; μ: angle of internal friction. Where a range of possible stress magnitudes exists, the minimum stress magnitudes are used and annotated with an asterisk (*).

Table 2. Mean Dilation (T_d) and Slip (T_s) Tendency results for the four main fault sets within the Gidgealpa 3D seismic survey modelled under the six unique stress conditions (Table 1).

Fault Strike (dip angle)	Tendency	Alice Springs Event	Mid-Permian Event	Daralingie Event	Hunter-Bowen Event	Late Cretaceous Event	Paleogene Event
NE-SW (50-70°)	Dilation	0.34	0.26	**0.85**	0.48	0.46	0.42
	Slip	0.53	0.63	**1.00**	**0.79**	**0.74**	**0.79**
N-S (50-70°)	Dilation	**0.78**	0.31	0.45	0.26	0.24	**0.66**
	Slip	**0.96**	0.65	0.81	0.64	0.60	0.76
E-W (50-70°)	Dilation	0.09	**0.44**	0.65	**0.60**	**0.58**	0.23
	Slip	0.16	**0.70**	0.98	0.70	0.63	0.59
NW-SE (80-90°)	Dilation	0.47	0.43	0.12	0.25	0.28	0.26
	Slip	0.75	0.08	0.36	0.38	0.35	0.44

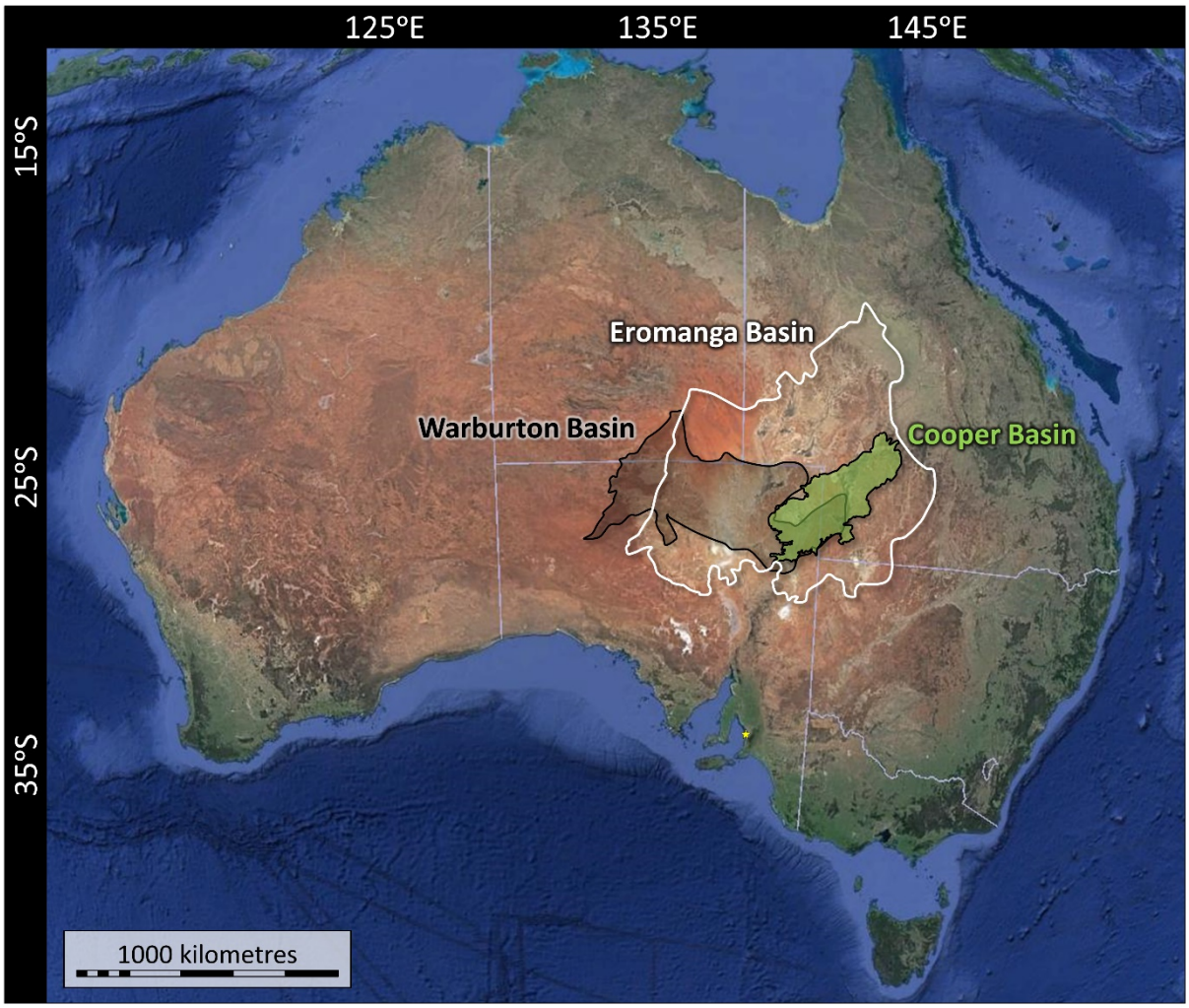


Figure 1. Location of the Warburton, Cooper and Eromanga basins (Kulikowski & Amrouch, 2017).

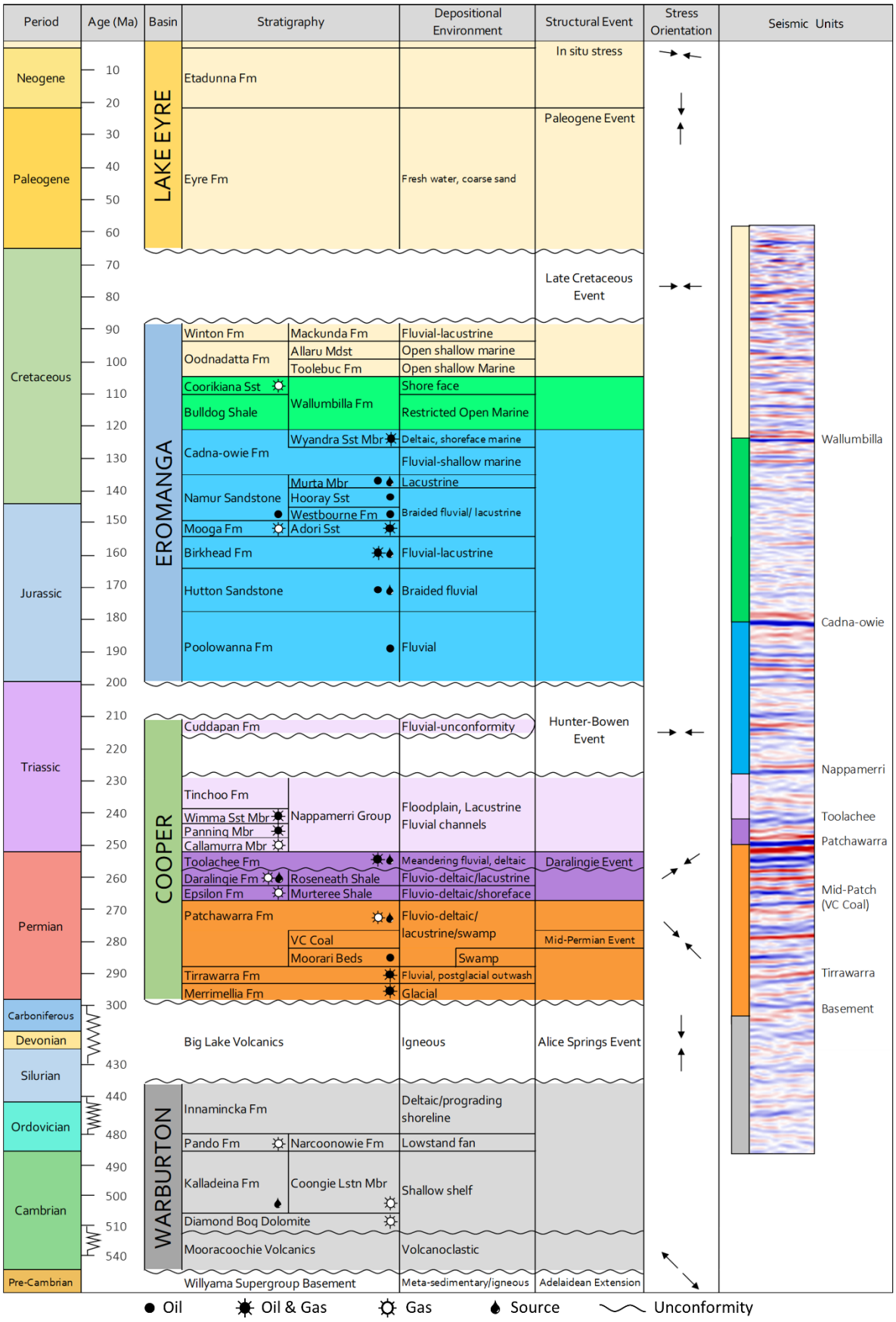


Figure 2. Stratigraphy, tectonic events and typical seismic reflection profile of the Warburton, Cooper, Eromanga, and Lake Eyre basins (Kulikowski et al., 2017).

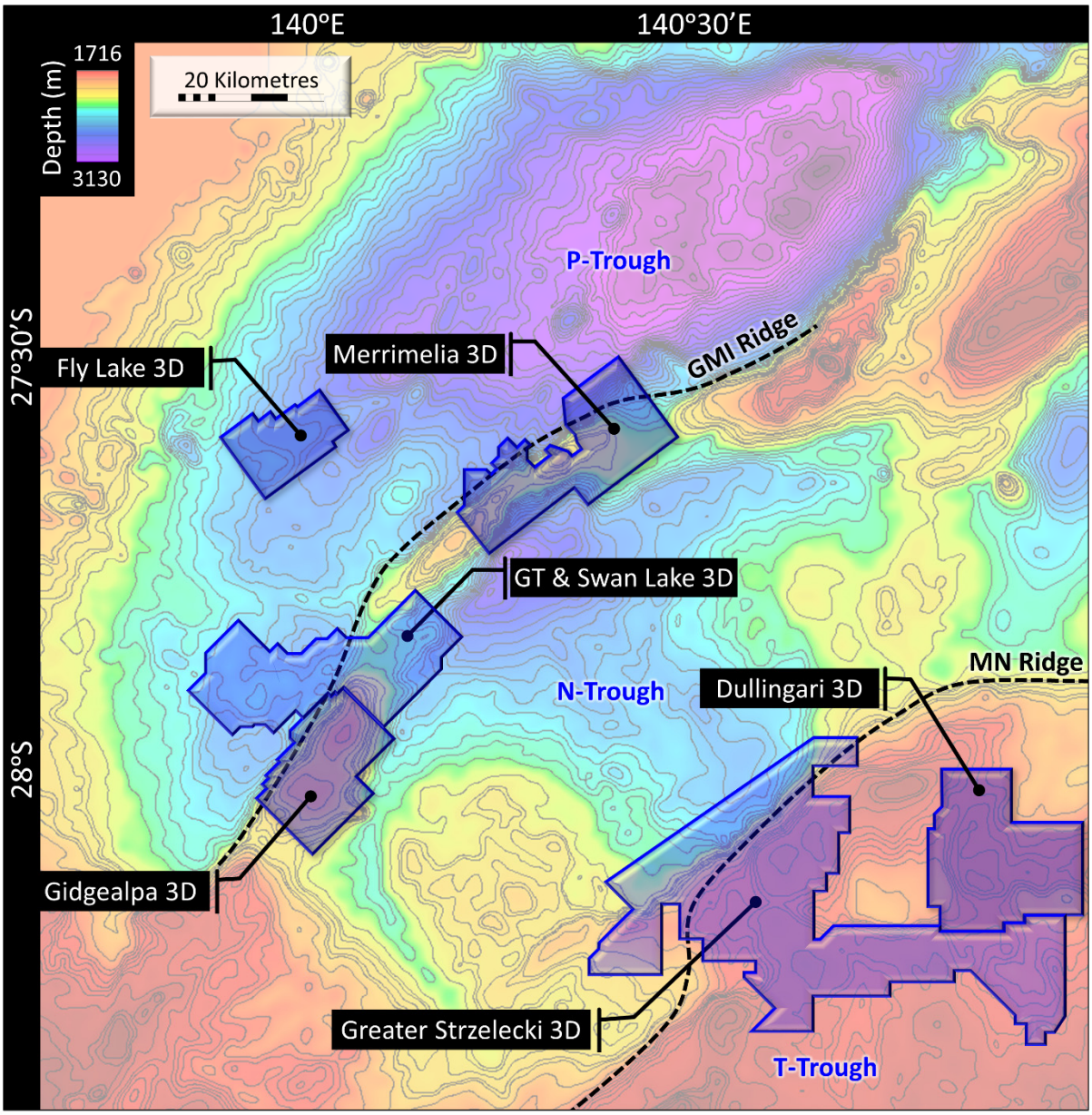


Figure 3. Location of the 3D seismic surveys covering the Gidgealpa-Merrimelia-Innamincka (GMI) and Murteree-Nappacoongee (MN) ridges. Top Permian depth grid showing the location of the Patchawarra (P-Trough), Nappamerri (N-Trough), and Tenappera (T-Trough) troughs (after Kulikowski & Amrouch, 2017; Kulikowski et al., 2017).

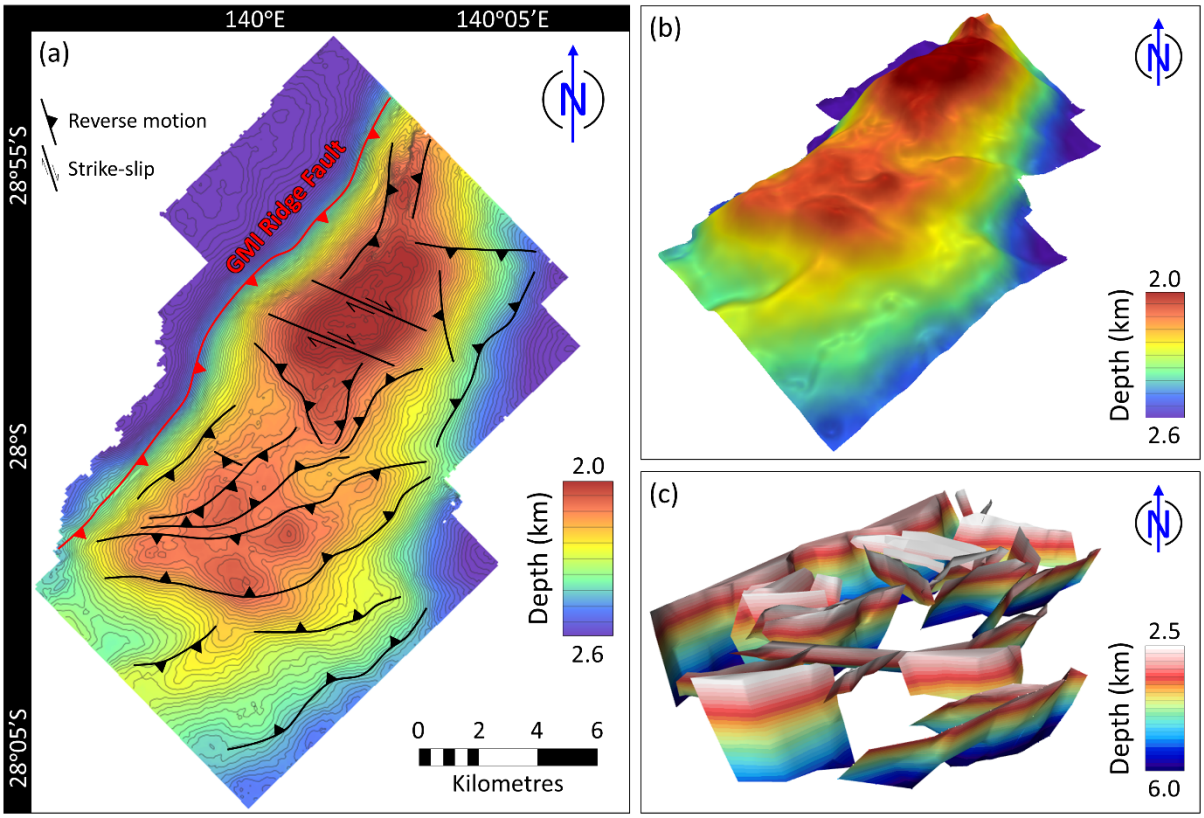


Figure 4. Interpretation of the Gidgealpa 3D seismic survey showing: (a) Interpreted faults projected onto the top Permian reflector (after Kulikowski et al., 2017); (b) 3D view of the interpreted top Permian reflector; and (c) 3D view of the interpreted fault model. For location of seismic survey see Figure 3.

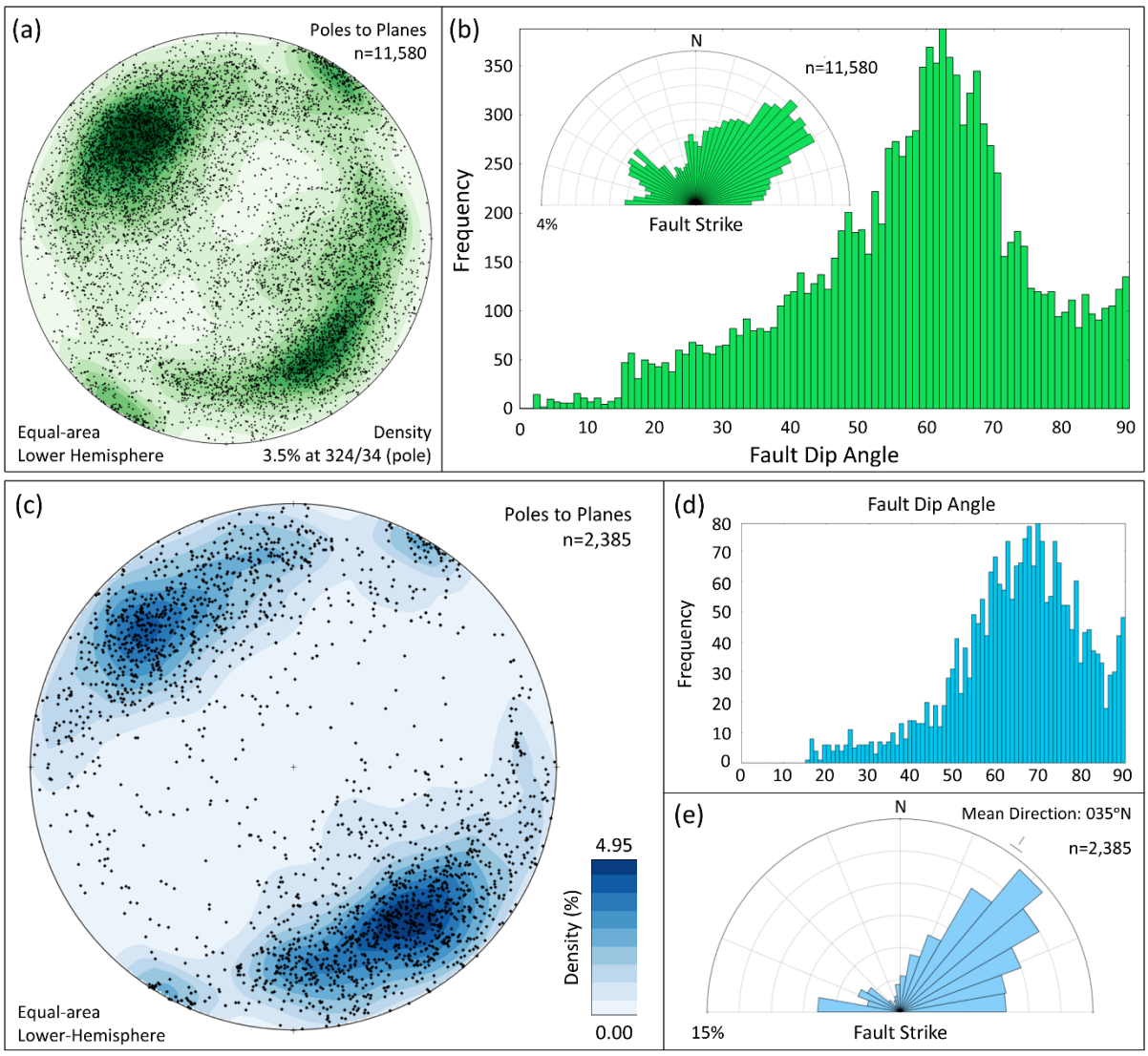


Figure 5. Fault interpretation from all 3D seismic surveys displayed as: (a) Stereographic projection of poles to fault planes; and (b) Bar graph showing dip angle of faults and rose diagram showing fault strike (after Kulikowski & Amrouch, 2017). Faults from the Gidgealpa 3D seismic survey shown as: (c) Stereographic projection of poles to fault planes; (d) Bar graph showing dip angle of faults; and (e) Rose diagram of fault strike.

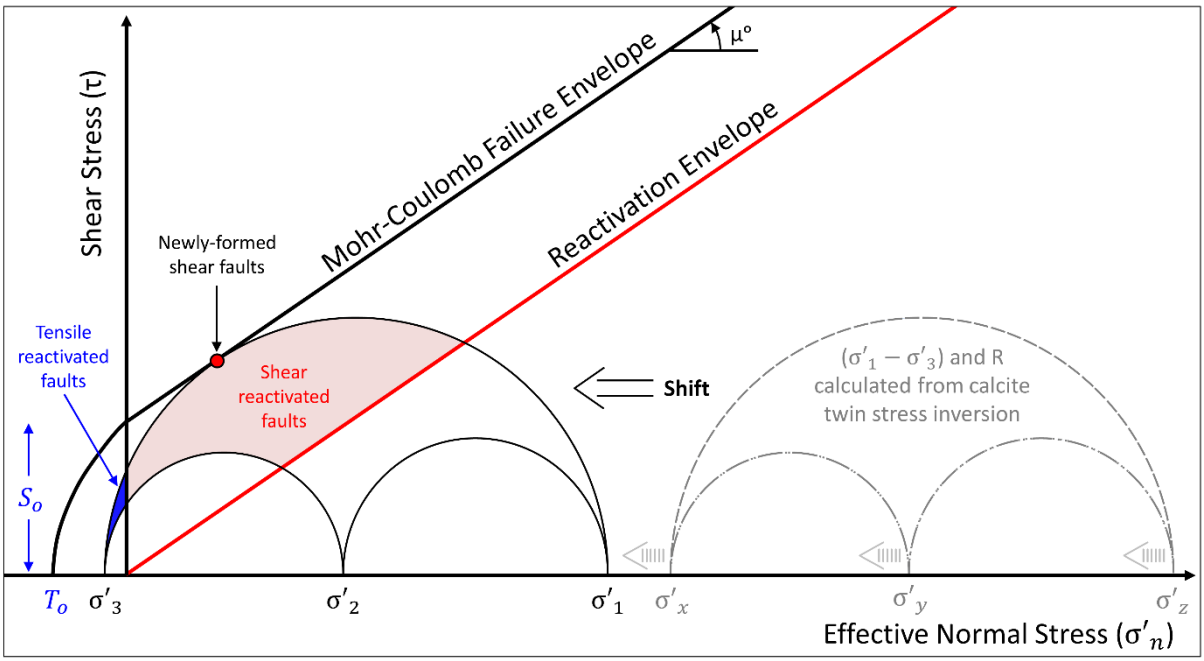


Figure 6. Approach used to determine the effective paleo-stress magnitudes when the stress regime, maximum differential stress $(\sigma_1 - \sigma_3)$ magnitude, stress ellipsoid shape ratio $(R; where\ R = (\sigma_2 - \sigma_3)/(\sigma_1 - \sigma_3))$ and frictional failure through time are known (after Lacombe, 2001; Lacombe and Laurent, 1992; Amrouch, 2010). The Mohr circle is shifted to intersect the failure envelope (slope defined by the coefficient of internal friction), with reactivated faults above the reactivation envelope (slope defined by the coefficient of sliding friction). Where T_o is the tensile strength, S_o is the inherent shear strength (or cohesion), and μ is the angle of internal friction.

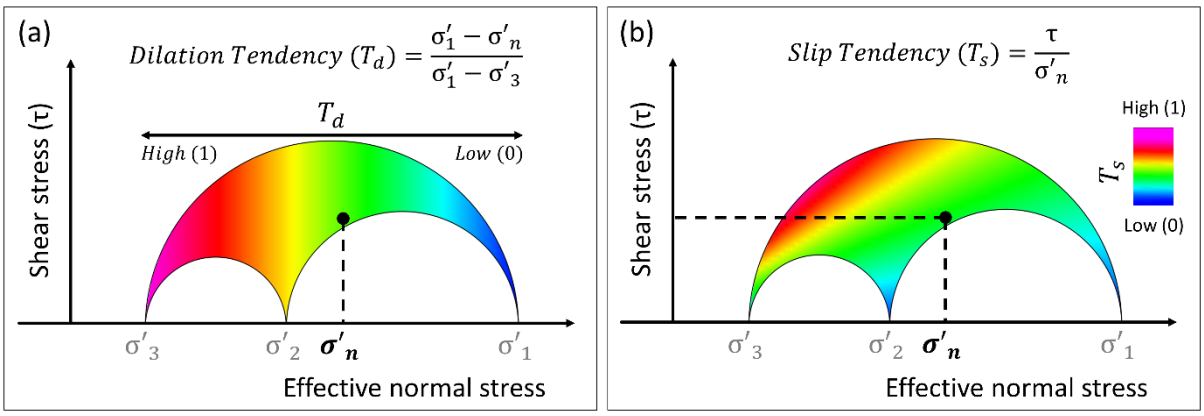


Figure 7. Illustration of the (a) Dilation Tendency (T_d) and (b) Slip Tendency (T_s) measures (after Mildren et al., 2005).

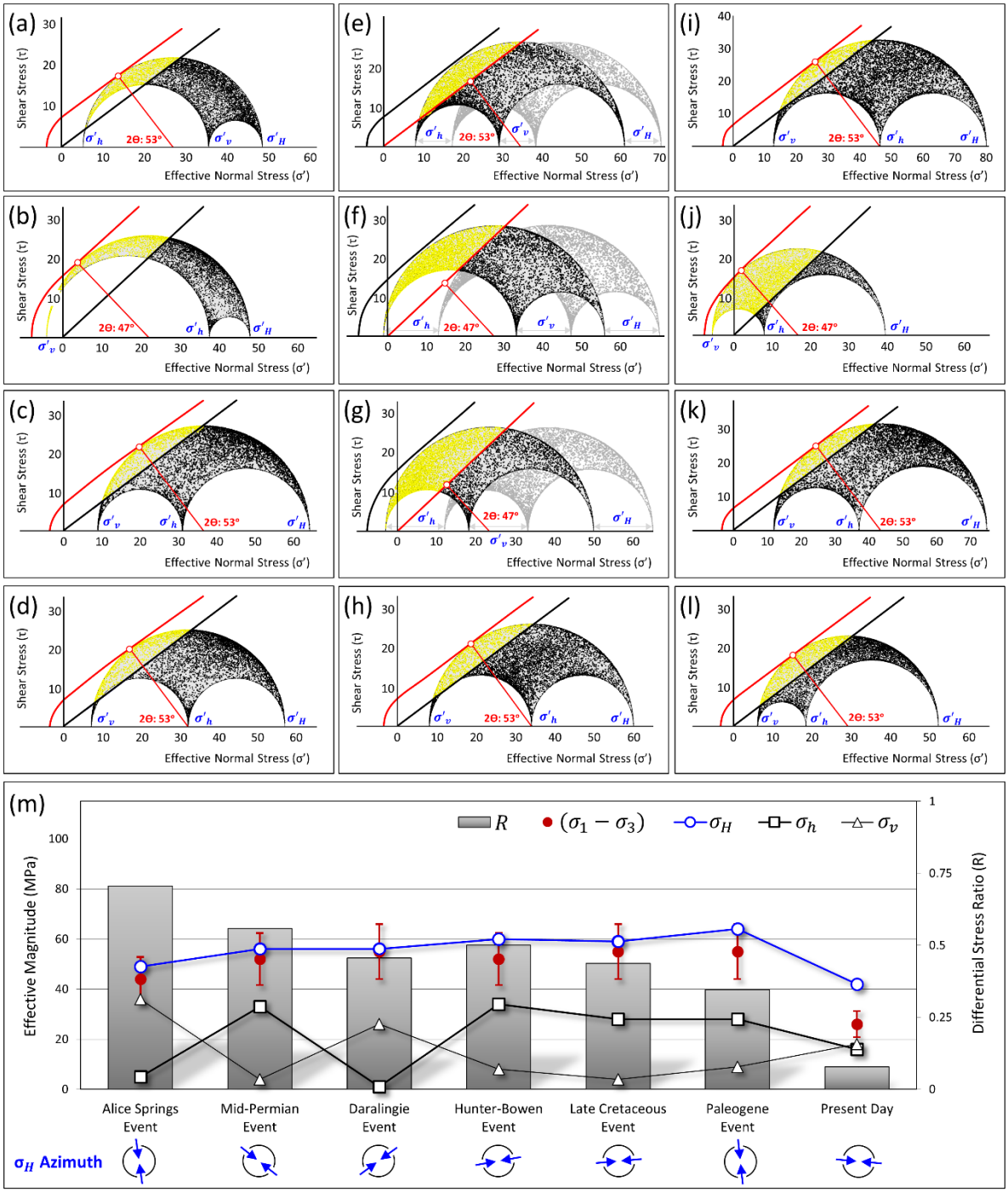


Figure 8. Mohr's circles showing effective paleo-stress magnitudes and critically oriented fault geometries (highlighted) for calcite sample: (a) CalS5b (Alice Springs Event); (b) CalS1 (Mid-Permian Event); (c) CalS2 (Mid-Permian Event); (d) CalS3 (Mid-Permian Event); (e) CalS2b (Daralingie Event); (f) CalS1b (Daralingie Event); (g) CalS4 (Daralingie Event); (h) CalS5 (Hunter-Bowen Event); (i) CalS6b (Late Cretaceous Event); (j) CalS4b (Late Cretaceous Event); (k) CalS3b (Paleogene Event); and (l) CalS6 (Paleogene Event). A range is given for the Daralingie Event as precise placement is unknown; however, the Mohr's circle is known to intersect the reactivation envelope but not intersect the failure envelope. (m) Evolution of effective paleo-stress magnitudes, maximum differential stress $(\sigma_1 - \sigma_3)$ magnitudes, stress ellipsoid shape ratio (R; $where\ R = (\sigma_2 - \sigma_3)/(\sigma_1 - \sigma_3)$), and maximum horizontal stress (σ_H) azimuths through time. The effective maximum (σ'_H) and minimum (σ'_h) horizontal stresses, and the effective vertical stress (σ'_v) are presented to easily distinguish between stress regimes. See Table 1 for results.

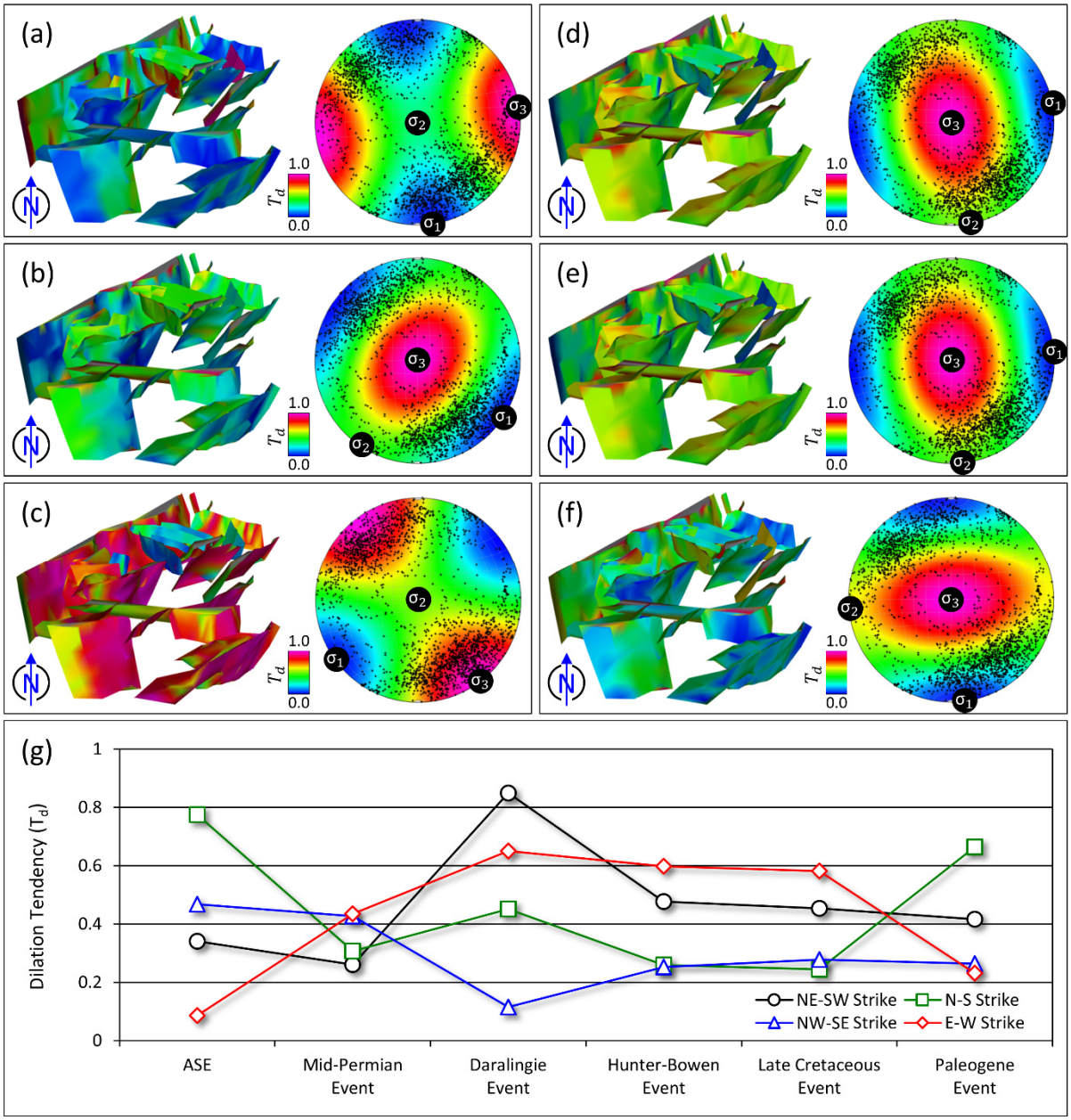


Figure 9. Results of Dilation Tendency (T_d) analysis performed on the Gidgealpa 3D fault model using paleo-stress results (Table 1) from the: (a) Alice Spring Event (ASE); (b) Mid-Permian Event; (c) Daralingie Event; (d) Hunter-Bowen Event; (e) Late Cretaceous Event; and (f) Paleogene Event. (g) Results for the main fault sets through time. See Fig. 4 for model location.

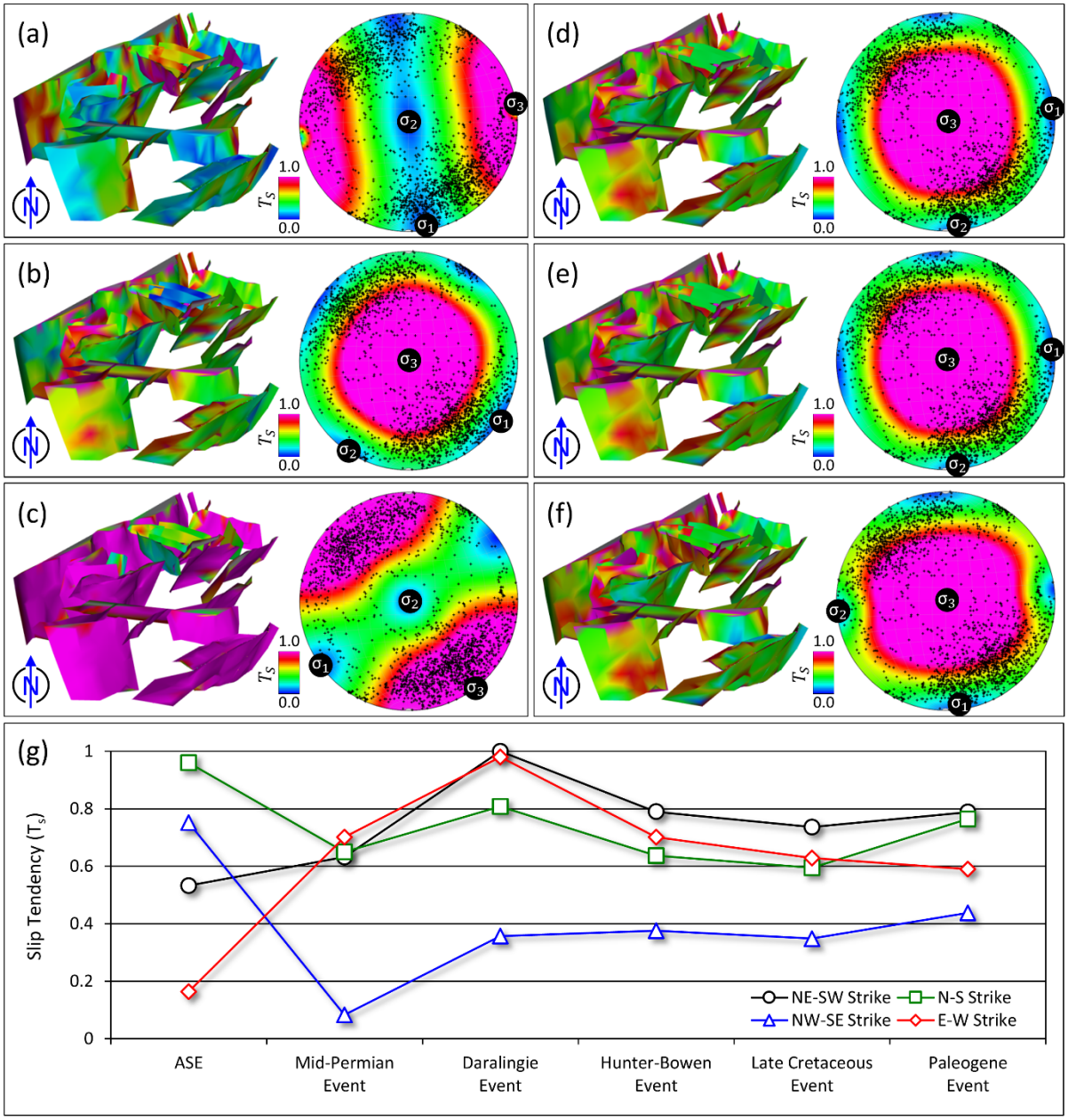


Figure 10. Results of Slip Tendency (T_s) analysis performed on the Gidgealpa 3D fault model using paleo-stress results (Table 1) from the: (a) Alice Spring Event (ASE); (b) Mid-Permian Event; (c) Daralingie Event; (d) Hunter-Bowen Event; (e) Late Cretaceous Event; and (f) Paleogene Event. (g) Results for the main fault sets through time. See Fig. 4 for model location.

5.7. MANUSCRIPT 7: Fracture networks in 3D seismic data

Mapping permeable subsurface fracture networks: A case study on the Cooper Basin, Australia

This study investigates the distribution of permeable subsurface natural fracture networks within Australia's largest onshore hydrocarbon province; the Cooper Basin. Previous research has shown the effectiveness of using curvature analysis for mapping subsurface structural features. The purpose of the following research is to: (1) show the relationship between wellbore derived fractures and curvature results; and (2) apply curvature analysis to five 3D seismic surveys in the Cooper Basin to provide structural "sweet-spots" in the hydrocarbon-rich and low permeability Patchawarra Formation. Natural fractures were interpreted from borehole image logs and compared to curvature analyses to discuss the risk of extrapolating borehole data to the wider reservoir. Geomechanical modelling was used to measure the Dilation Tendency of interpreted natural fractures to identify the geometry most likely to act as a hydrocarbon conduit under in situ stresses. The results provide permeable natural fracture networks, or "sweet-spots", in major oil and gas producing fields that can be exploited by future hydrocarbon exploration and development programs. This study presents new integration of methods that will form a frame-work for future research investigating permeable fracture distributions in other provinces.

CITATION:

Kulikowski, D., Amrouch, K., & Burgin, H.B. (2017). Mapping permeable subsurface fracture networks: A case study on the Cooper Basin, Australia. Journal of Structural Geology, under review.

Statement of Authorship

Title of Paper:	Mapping permeable subsurface fracture networks: A case study on the Cooper Basin, Australia
Publication Status:	**Manuscript Submitted**
Publication Details:	Kulikowski, D., Amrouch, K., Burgin, H.B. (2017). Mapping permeable subsurface fracture networks: A case study on the Cooper Basin, Australia. Journal of Structural Geology, under review.

Principal Author

Principal Author (Candidate):	David Kulikowski		
Contribution to the Paper:	Data collection, interpretation, analysis, and writing.		
Overall percentage (%):	80%		
Certification:	This paper reports on original research I conducted during the period of my Higher Degree by Research candidature and is not subject to any obligations or contractual agreements with a third party that would constrain its inclusion in this thesis. I am the primary author of this paper.		
Signature:		Date:	29 March 2017

Co-Author Contribution

By signing the Statement of Authorship, each author certifies that:

i. the candidate's stated contribution to the publication is accurate (as detailed above);

ii. permission is granted for the candidate to include the publication in the thesis; and

iii. the sum of all co-author contributions is equal to 100% less the candidate's stated contribution.

Name of Co-Author:	Khalid Amrouch (10%)		
Contribution to the Paper:	Supported with the structure, writing and review of paper.		
Signature:		Date:	29 March 2017

Name of Co-Author:	Hugo B. Burgin (10%)		
Contribution to the Paper:	Supported with the research and review of paper.		
Signature:		Date:	29 March 2017

Mapping permeable subsurface fracture networks: A case study on the Cooper Basin, Australia

*David **KULIKOWSKI**[a] (david.kulikowski@adelaide.edu.au)

Khalid **AMROUCH**[a] (khalid.amrouch@adelaide.edu.au)

Hugo B. **BURGIN**[a] (hugo.burgin@adelaide.edu.au)

[a]Australian School of Petroleum, University of Adelaide, North Terrace, 5005, Adelaide, Australia

***Corresponding Author**: David Kulikowski (+61 435 135 148)

Key Words: Cooper Basin; Fracture; Fault; Seismic; Curvature.

Abstract

The distribution of subsurface fracture networks can have implications for effective petroleum production, carbon dioxide storage, water injection for geothermal energy, and precise mining operations. However, the distribution of subsurface fracture networks is often dictated by fractures measured in outcrop or from well data, which are then assumed to represent the entire stratigraphic interval. This study uses geophysical data (3D seismic surveys and borehole image logs) and a geomechanical model to predict the distribution of permeable natural fracture networks in the entirely subsurface Cooper Basin, Australia. The dilation tendency of wellbore derived fractures was measured under the present-day strike-slip stress regime to identify SE-NW and E-W striking high angle (>50°) fractures as optimally oriented to undergo tensile reactivation. Seismic curvature results were processed into the semblance attribute to remove noise and highlight structural lineaments. Results identified the presence of SE-NW and E-W striking permeable fracture sets along the hydrocarbon-rich Patchawarra Formation within each of the five seismic surveys and at a higher density than that captured at the wellbore. The integration of geophysical data with a geomechanical model provides the arrangement of permeable fracture networks in the subsurface that can be applied across many different industries.

1. Introduction

Determining the distribution and density of natural fractures and faults in the subsurface is often limited to measurements from borehole image logs, cores, or seismic data, which are then analysed or extrapolated to the area of interest (Kulikowski and Amrouch, 2017). This approach has several limitations (i.e. sparse and non-representative data) that can lead to incorrect models and ultimately result in unsafe mining practices, inefficient hydrocarbon recovery, poor carbon dioxide sequestration, or unsecured geothermal activities. Recent work on geophysical fracture characterisation (Kremor and Amrouch, 2017; Kremor et al., 2017) and advancements in three-dimensional (3D) seismic data analysis (Roberts, 2001; Chopra and Marfurt, 2007) has enabled the use and application of seismic attributes, such as curvature and coherency, to provide high density structural data in the subsurface that does not require physical measurements. The Most Positive Curvature (K_+) seismic attribute has been shown to correlate with physically measured natural fractures (e.g. Murray, 1968; Lisle, 1995; Stewart and Podolski, 1999; Hakami et al., 2004; Al-Dosary and Marfurt, 2006; Chopra and Marfurt, 2007), and provides a more complete understanding of the subsurface. This study improves upon previous research in subsurface Cooper Basin (Australia) by providing high density structural data along the hydrocarbon-rich Patchawarra Formation, which is calibrated by measured natural fracture data (borehole image log) and compared to an in situ geomechanical model to determine which fracture geometry is critically oriented to dilate and act as a possible fluid conduit.

Previously, Backe et al. (2011) attempted to explore the relationship between high K_+ and measured natural fractures in the Cooper Basin, Australia. Their study, however, applied the analysis technique to seismic time-slices, rather than along a given seismic reflector, and they omitted a key limitation from their discussion, which is the inability to distinguish between high and low dipping fracture sets. To follow on from this previous research, we integrate a large geophysical database (five 3D seismic surveys and 28 borehole image logs) with a present-day geomechanical model to investigate the distribution of permeable natural fracture networks in the entirely subsurface Cooper Basin. To visually improve the results, the K_+ data are processed into a semblance (similarity) attribute volume to remove noise and highlight structural lineaments before being extracted along the hydrocarbon-rich and low permeability Patchawarra Formation. This integration presents an approach that can benefit other subsurface or offshore provinces, given adequate geophysical data coverage, to provide important structural data that would otherwise not be measurable.

Insert Fig. 1

2. Geological Setting

The Permian to Triassic intra-cratonic Cooper Basin is located in central Australia (Fig. 1) and is unconformably overlain by the Jurassic to Cretaceous Eromanga Basin (Apak et al., 1997; Alexander et al., 1998). The South Australian portion of this region is defined by the NE-SW striking Gidgealpa-Merrimelia-Innamincka (GMI) and Murteree-Nappacoongee (MN) ridges that bound the NE-SW elongate Patchawarra, Nappamerri and Tenappera troughs (Fig. 1) (Kulikowski et al., 2017). The SE-NW oriented Adelaidean (650-575 Ma) extensional event created these ridges together with regionally extensive NE-SW and SE-NW striking basement faults. These NE-SW striking normal faults created early accommodation space for calcareous and siliciclastic Warburton Basin sediments to be deposited before they were inverted by subsequent compressional and strike-slip stress regime events (Gatehouse, 1986; Kulikowski and Amrouch, 2017).

The unconformity between the Warburton and Cooper basins was created by the N-S Carboniferous Alice Springs Event that reactivated pre-existing basement faults (Apak et al., 1997; Kulikowski and Amrouch, 2017). Upper Carboniferous glacial sediments (Merrimelia Formation) and Lower Permian braided fluvial sediments (Tirrawarra Formation) were deposited during a period of tectonic quiescence. Repeated cycles sands, shales and coals were deposited to form the Middle Permian Patchawarra Formation (Alexander et al., 1998). On-lapping and erosional features are present in the middle Patchawarra Formation along the GMI and MN ridges, and coincide with the Mid-Permian Event (Apak et al., 1997; Kulikowski and Amrouch, 2017).

As compression from the Mid-Permian Event eased during the deposition of the top Patchawarra Formation, an east to west transgression deposited the Late Permian Murteree Shale, Epsilon Formation, Roseneath Shale, and Daralingie Formation (Apak et al., 1997). Deposition of the Upper Permian Daralingie Formation was interrupted by the NE-SW Daralingie Event, which eroded much of the Daralingie Formation and created a regional unconformity (Kuang, 1985; Apak et al., 1997; Mavromatidis, 2006; Kulikowski and Amrouch, 2017). The Late Permian Toolachee Formation and the Triassic Nappamerri Group were deposited under meandering fluvial to deltaic, and floodplain, lacustrine and fluvial channel conditions, respectively (Apak et al., 1997; Alexander et al., 1998).

The Late Triassic E-W Hunter-Bowen Event eroded up to 500 meters of Nappamerri Group sediments to create the unconformity between the Cooper and Eromanga basins (Alexander et al., 1998; Mavromatidis, 2006). Jurassic to Cretaceous deposition of Eromanga Basin units was uninterrupted, transitioning between fluvial, deltaic, lacustrine and shallow marine conditions

(Alexander et al., 1998). Later, the E-W Late Cretaceous Event and N-S Paleogene Event created folds and were succeeded by the present-day ESE-WNW strike-slip stress regime (Pokalai et al., 2016).

3. Methodology

3.1 Dataset

Most positive curvature analysis was performed on five depth converted 3D seismic surveys from the South Australian portion of the Cooper Basin (Fig. 1). These include the Moomba-Big Lake 3D (acquired 1997), Dullingari 3D (acquired 1997), Merrimelia (Extension (ext)) 3D (acquired 1998), Greater Tindilpie (GT)-Swan Lake 3D (acquired 2000), and Fly Lake 3D (acquired 2000) seismic surveys. All data is publicly available and covers major oil and gas producing fields. A total of 28 borehole image logs were used to measure 917 natural fractures. These wells are present throughout the study area, with 7 wells located within the 3D seismic data (Fig. 1). Prior to analysis, the seismic data was converted from the time-domain to the depth-domain using the average velocity method, which is one of the more accurate methods for the basin (Kulikowski et al., 2016b, 2017). After depth conversion, a 3D subsurface dip field volume was created to provide the dip angle of all reflectors. The five 3D seismic volumes were individually analysed using the most positive curvature attribute, which was then processed into a semblance (similarity) attribute volume and finally extracted along the Middle Patchawarra Formation reflector. The semblance attribute volume used a half-window vertical distance of ~50 meters, which visually emphasises the curvature results by removing noise (high semblance values) and highlighting structural discontinuities (low semblance values).

3.2 Curvature Attribute (K)

The value for curvature is defined as the rate of change of the direction of a curve (Roberts, 2001), such that for any point (P) the curvature (K) is defined as the rate of change of the dip angle ($d\omega$) with respect to the arc length (dS) (Roberts, 2001). The arc length (dS) is obtained from the osculating circle that has a common tangent to P and makes the greatest possible contact with the curve (Roberts, 2001). The radius of the osculating circle forms the radius of curvature (R); where in two-dimensions the value for K is defined as (Roberts, 2001);

$$K = \frac{d\omega}{dS} = \frac{2\pi}{2\pi R} = \frac{1}{R} \qquad Eq.(1)$$

However, when dealing with 3D seismic data the curvature can be calculated in an infinite number of directions all with unique values, but, for any P there exists a single intersecting plane normal to

the surface that defines the largest absolute curvature value, which is termed the maximum curvature (K_{max}) (Roberts, 2001). Perpendicular to this plane, the minimum curvature (K_{min}) value is obtained, which defines the smallest absolute curvature value (Roberts, 2001). The K_{max} and K_{min} attributes are collectively termed the principal curvatures and can be used to derive any curvature value for planes that are normal to the given surface (normal curvature) (Roberts, 2001), such that;

$$K_i = (K_{max})cos^2\delta + (K_{min})sin^2\delta \qquad Eq.(2)$$

Where δ is the angle between a normal curvature plane (K_i) and the K_{max} plane (Roberts, 2001). Significant curvature values are often associated with reflector displacement, which can be indicative of fracturing or faulting (Roberts, 2001; Al-Dossary and Marfurt, 2006). The distribution of natural fractures along anticlinal traps can therefore be predicted by calculating the most positive curvature (K_+) (Eq. 3) that uses a local quadratic surface with a 3x3 grid cell approach (Fig. 2a).

$$K_+ = (a+b) + \sqrt{(a-b)^2 + c^2} \qquad Eq.(3)$$

Where,

$$a = \frac{1}{2}\frac{\delta^2 z}{\delta x^2} = \left(\frac{Z_1 + Z_3 + Z_4 + Z_6 + Z_7 + Z_9}{12\Delta x^2}\right) - \left(\frac{Z_2 + Z_5 + Z_8}{6\Delta x^2}\right) \qquad Eq.(4)$$

$$b = \frac{1}{2}\frac{\delta^2 z}{\delta y^2} = \left(\frac{Z_1 + Z_2 + Z_3 + Z_7 + Z_8 + Z_9}{12\Delta x^2}\right) - \left(\frac{Z_4 + Z_5 + Z_6}{6\Delta x^2}\right) \qquad Eq.(5)$$

$$c = \frac{\delta^2 z}{\delta x \delta y} = \left(\frac{Z_3 + Z_7 - Z_1 - Z_9}{4\Delta x^2}\right) \qquad Eq.(6)$$

Insert Fig. 2

Here, Z_i refers to the location of grid nodes along the local quadratic surface and Δx is the distance between grid nodes (Fig. 2a; Roberts, 2001). The equation for K_+ given in Eq. (3) uses the combination of Eq. (4), (5), and (6) (Roberts, 2001). Calculation of the K attribute has been used extensively in delineating and visually exaggerating structural features that are not obvious in seismic amplitude volumes (e.g. Murray, 1968; Lisle, 1995; Al-Dosary and Marfurt, 2006; Chopra and Marfurt, 2007; Backe et al., 2011).

The relationship between curvature and the presence of natural fractures is in the stress re-distribution when a stratal-unit (or bed) is folded or bent (i.e. anticline). Folding alters the bed lengths and exerts compressional and extensional stresses towards the base and crest of the anticline, respectively (Ferrill and Groshong, 1993; Roberts, 2001; Amrouch et al., 2010a, 2010b, 2011). As the observed geometry of reflectors can also be caused by mechanism other than folding, such as erosion, depositional environments (dunes, on-lapping, clinoforms, etc.), an understanding of the structural and stratigraphic history of the region must be well understood. This relationship between folding and curvature is an important aspect that Backe et al. (2011) didn't discuss in their study, as they extracted results along horizontal time-slices rather than along seismic reflector surfaces. In doing so, they combine structural information across several stratigraphic intervals and time periods.

3.3 Borehole Image Logs

The South Australian Cooper Basin is entirely overlain by loose sediment preventing direct measurements from outcrop; therefore, direct natural fracture measurements can only be made from borehole image logs or core. These methods of obtaining natural fracture data can be selective in the natural fracture sets that they encounter, as high angled sets will be less likely to be intersected by vertical wells than low angle sets. This study uses 28 borehole image logs (Fig. 1) to measure the natural fracture geometries present across the basin and to then determine which of the fracture sets is most likely to be open to fluid flow under present-day stress (Fig. 2b). Both conductive (open to fluid flow) (Fig. 2c) and resistive (closed to fluid flow) (Fig. 2d & 2e) natural fractures were interpreted and geomechanically analysed based on the strike and dip angle.

3.4 Dilation Tendency

To determine the likelihood of natural fractures undergoing tensile reactivation, and hence more likely to be hydraulically conductive under present-day stresses, the Dilation Tendency (T_d) is measured from a geomechanical model using Eq. (8) and illustrated in Figure 2b (Ferrill et al., 1999; Mildren et al., 2005; Jolie et al., 2015). This attribute is commonly used in the petroleum industry to determine the sealing or conduit potential of faults (Barton et al., 1995; Ferrill and Morris, 2003; Jolie et al., 2015; Kulikowski et al., 2016a). The T_d is used in preference to measuring the Slip (shear) Tendency, as the latter predicts the shear potential and not the ability of natural fractures to remain open to fluid flow (Ferrill et al., 1999; Mildren et al., 2005). The T_d is governed by the effective normal stress acting on a plane, which directly affects the natural fracture aperture (Ferrill et al.,

1999; Mildren et al., 2005). Therefore, the maximum (σ'_1), minimum (σ'_3), and normal (σ'_n) effective stresses are used to measure the T_d (Ferrill et al., 1999; Mildren et al., 2005);

$$T_d = \left(\frac{\sigma'_1 - \sigma'_n}{\sigma'_1 - \sigma'_3}\right) \qquad Eq.(8)$$

The T_d results are normalised to the differential stress, giving values that range from a maximum of one (inferring high likelihood of tensile reactivation) to a minimum of zero (inferring little to no chance of tensile reactivation). To model the present-day stress conditions, a maximum horizontal stress orientation of 101°N was used together with a hydrostatic pore pressure gradient and a strike-slip stress regime with a low stress ellipsoid shape ratio (~0.10) (Nelson et al., 2007; Pokalai et al., 2016).

4. Results

Natural fracture data measured from borehole image logs are presented on a stereonet and rose plot to show the regional natural fracture sets (Fig. 3a). Natural fractures measured from wells that lie within the seismic surveys are also shown (Fig. 3b, 3c, 3d, 3e, & 3f). The complete natural fracture data (Fig. 3a) is projected onto the Dilation Tendency results (Fig. 4a) to identify the critically oriented sets, which are then found in seismic curvature results.

Insert Fig. 3

4.1 Natural Fractures at the Wellbore

Borehole image log data was interpreted from 28 wells, which included 7 wells present within the 3D seismic data (Fig. 1). These 917 measured natural fractures (Fig. 3) were used to: (1) act as quality control to check that the features observed in seismic data are in the same geometry as measured fractures; and (2) to determine the natural fracture geometry most likely to dilate under present-day stress. The wellbore data has a dominant N-S, NE-SW and E-W strike (Fig. 3a). A previous study, investigating the regional natural fracture sets present in the Cooper Basin, found five conjugate fracture sets within the Patchawarra Formation, which include two high angle (>50°) sets striking NE-SW and SE-NW, and three low angle (<30°) sets striking NE-SW, N-S, and E-W (Kulikowski and Amrouch, 2017).

The T_d results found that high angle (>50°) natural fractures striking 101°N (±20°) are optimally oriented to dilate ($T_d = 1.0$) and act as potential fluid conduits (Fig. 4a), with natural fractures striking normal to this geometry (011°N strike) being least likely to dilate ($T_d = 0$). This is also

observed in borehole image logs, with examples of conductive (open) and resistive (closed) natural fractures are presented from Cowralli 13 (Fig. 2c), and Merrimelia 32 (Fig. 2d) and Merrimelia 29 (Fig. 2e), respectively. These results infer that E-W striking high angled natural fractures have the least resistance to closing, making this set the most valuable for improved hydraulic conductivity.

4.2 Natural Fractures from Seismic Data

The seismic curvature (semblance) results are extracted along the Patchawarra Formation in each of the seismic surveys (Fig. 4b, 4c, 4d, 4e, & 4f). The strength of this attribute in identifying subsurface natural fracture distributions is illustrated for the Cowralli 13 well (Fig. 5). The well was drilled on an NE-SW elongate anticline with a high density of N-S striking natural fractures commonly interpreted in the borehole image log (Fig. 5a). A close look at the curvature results (Fig. 5b) shows a dominant N-S strike, which coincides with the mean natural fracture strike interpreted from the borehole image log (Fig. 5c). The high number of measured natural fractures in this well appears to coincide with high curvature results. Most other wells covered by seismic data also show this relationship; however, their relatively low natural fracture density could be correlated to low curvature results.

Insert Fig. 4

Insert Fig. 5

4.2.1 Fly Lake 3D

Structural interpretation of Fly lake 3D shows a structural high in the west that is bound from the east by a NE-SW striking fault (Fig. 3c). The K_+ results show a considerable natural fracture network consisting of lineaments striking NE-SW, E-W, and N-S, with fewer striking SE-NW (Fig. 4c). The results along the Middle Patchawarra Formation show high fracture density (high K_+) in the northeast of the survey within the vicinity of Fly Lake 10 and Fly Lake 12. Strong K_+ results are also present above known basement faults (Fig. 3c and 4c).

4.2.2 Dullingari 3D

The Dullingari 3D seismic survey contains two well controls; Dullingari North 8 and Dullingari 47, which are in the Dullingari North and Dullingari Main culminations, respectively (Fig. 3d and 4d). The K_+ analysis delineates a NE-SW and SE-NW striking natural fracture network present throughout the survey (Fig. 4d), with secondary N-S striking features present within the Dullingari Main area (Fig. 3d and 4d). The E-W strike of fractures appears in regions with E-W striking basement faults and increases in density (high K_+) along E-W elongate anticlines (Fig. 3d and 4d). The results along the Middle Patchawarra Formation shows the detailed distribution of structural lineaments, such as the

NE-SW striking features in Dullingari North and the saw-tooth-like geometry of the E-W striking fault bounding Dullingari Main from the south (Fig. 3d and 4d).

4.2.3 Moomba-Big Lake 3D

The Moomba 74 borehole image log is located on the outer edge of the 3D seismic survey along the flank of a small Permian structure corresponding to low K_+ density (Fig. 3e and 4e). E-W trending K_+ lineaments are present within the Moomba 47 well location, with large SE-NW trending lineaments present elsewhere in the seismic survey that are subparallel to the basement faults (Fig. 3e and 4e). The major NE-SW elongate Big Lake structure is expressed with high K_+ values in the southeast of the survey along the Middle Patchawarra Formation horizon (Fig. 3e and 4e). The K_+ results in this area have a wide distribution of strikes and appear highly complex.

4.2.4 Merrimelia (Extension) 3D

Three borehole image logs are located slightly outside of the Merrimelia (Extension) 3D seismic survey, but remain along the GMI Ridge (Fig. 1). The Merrimelia structure is a NE-SW elongate anticline bound from the west by the GMI Ridge fault (Fig. 3f). Significantly high K_+ values are present along this structure and increase in density to the northeast and southwest (Fig. 4f). The general trend of this dense natural fracture network is mostly NE-SW, with secondary N-S, SE-NW, and E-W striking features also present (Fig. 4f). The results present a large N-S striking feature along the Middle Patchawarra Formation in the centre of the survey (Fig. 4f), which coincides with basement faults and an abrupt increase in depth of the Top Permian reflector (Fig. 3f).

4.2.5 Greater Tindilpie-Swan Lake 3D

The Greater Tindilpie-Swan Lake 3D seismic survey contains the Cowralli 13 well, which is located on a subtle NE-SW elongate anticlinal closure on the footwall side of the GMI Ridge (Fig. 3b). The K_+ analysis presents high natural fracture density (high K_+) within the Cowralli 13 well location, and along the NE-SW striking GMI Ridge and the approximately E-W striking splays in the east of the survey (Fig. 3b and 4b). The results present a dominant SE-NW and NE-SW network throughout the Middle Patchawarra Formation surface, that increase in density (high K_+) in regions of known basement faults (Fig. 3b and 4b).

5. Discussion

To facilitate safe and effective subsurface operations in the petroleum, geothermal, carbon sequestration, water injection and mining industries, an understanding of the subsurface natural fracture network, geometry, density, hydraulic conductivity and distribution is fundamental. Curvature analysis using 3D seismic data has become an important tool for predicting the distribution of natural fractures away from the wellbore (e.g. Murray, 1968; Lisle, 1995; Al-Dosary and Marfurt, 2006; Chopra and Marfurt, 2007). Although borehole image logs and cores can provide the natural fracture distribution at the wellbore, assuming that this data is representative of the basin can be incorrect and result in significant errors. This research constrains the location of high density and hydraulically conductive fracturing in the subsurface by integrating curvature (and semblance) analysis with borehole image log data and Dilation Tendency (T_d) modelling.

Previous research on the regional natural fracture distribution in the basin found that NE-SW and SE-NW striking high (>50°) dip angle sets dominate the region and likely developed through extensional stress regime events (Kulikowski et al., 2016c; Kulikowski and Amrouch, 2017). These fracture sets are present within the Patchawarra Formation together with low angle (<30°) sets striking NE-SW, N-S, and E-W. The subsurface natural fracture distributions in each of the five seismic surveys shows a dominant NE-SW and SE-NW strike in the curvature (semblance) results, supporting previous works that suggested their regional presence (Kuang, 1985; Apak et al., 1997; Kulikowski et al., 2017; Kulikowski and Amrouch 2017). Amongst this dominant fracture network, N-S and E-W striking lineaments are also identified in each seismic survey, and may embody the regional sets described by Kulikowski and Amrouch (2017) that are linked to the compressional E-W Hunter Bowen and Late Cretaceous Events, and compressional N-S Paleogene Event, respectively.

Borehole image log interpretation found resistive (closed) natural fractures typically striking N-S and NE-SW with high dip angle (>50°), with examples shown from Merrimelia 32 (Fig. 2d) and Merrimelia 29 (Fig. 2e). Alternatively, conductive fractures typically strike SE-NW and E-W with high dip angles (>50°), as shown in Cowralli 13 (Fig. 2c). Regional NE-SW and SE-NW striking faults and fractures have been shown to preferentially shear reactivate under present-day stress (Kulikowski et al., 2016a); however, it is important to understand whether they will remain open after shearing. We examine this by developing a geomechanical model of the present-day stress to measure the T_d of natural fractures, with results showing that near vertical E-W striking natural fractures will preferentially dilate (T_d=1.0), as will the pervasive SE-NW striking natural fracture set ($T_d = 0.7 - 0.8$) (Fig. 4a).

These conductive natural fracture sets are present in each seismic survey and most pervasive within the Fly Lake (Fig. 4c), Dullingari (Fig. 4d), and Moomba-Big Lake (Fig. 4e) 3D seismic surveys. The density of these sets increases rapidly along SE-NW and E-W elongate anticlines, such as those found in the Moomba-Big Lake (Fig. 3e and 4e) and Dullingari (Fig. 3d and 4d) 3D seismic surveys. Targeting these regionally pervasive high angle E-W and SE-NW striking natural fractures can be highly beneficial for many industries including, petroleum, geothermal, and carbon sequestration as these are critically oriented to dilate and act as permeable fluid conduits under present-day stresses.

Wells that were drilled in high seismic curvature results were found to have an increased number of natural fractures measured from wellbore image logs. This relationship is also found in wells that were drilled in low seismic curvature regions, which have relatively less natural fractures measured from borehole image logs. A low fracture density in the Cooper Basin has previously been described and can be attributed to the inability of vertical wells to intersect the high angled (>50°) fracture sets that dominate the province (Kulikowski et al., 2016c; Kulikowski and Amrouch, 2017). Seismic K_+ analysis combats this limitation to widely present the fracture density within the five seismic surveys, suggesting that the density may be much higher than previously thought. An important limitation of K_+ results is its inability to distinguish between high and low angle fractures, which has a fundamental effect on the geomechanical modelling results (Ferrill et al., 1999; Ferrill and Morris, 2003; Maerten et al., 2016). The K_+ results must therefore consider that fractures defined in seismic data may have a wide range of dip angles.

The additional processing of K_+ results into semblance (similarity) has better defined the natural fracture networks, which would have otherwise been overlooked. High density fracture zones are compared with the location of known dry wells in each of the seismic surveys (Fig. 4), showing a noticeable absence of dry wells from high density locations in all cases. Although drilling within high density zones may not be the single factor involved in a well failing to produce hydrocarbons, it can have a significant impact on the efficiency of hydraulic fracture stimulation treatments and in well design. Ultimately, the approach presented here is applicable to several important industries that require insights into the distribution of permeable subsurface fracture networks for safe and effective operations.

6. Conclusion

The importance of understanding subsurface fracture networks is often negated by over simplistic models that extrapolate fracture data from the wellbore or outcrop to the area of interest. In instances where this assumption is false, there can be significant implications to the safety and effectiveness of programs that can span many important industries (e.g. petroleum, geothermal, mining, carbon sequestration). This study follows on from other works that have exploited the relationship between the seismic curvature attribute and measured fracture data. Through the integration of geophysical data and a geomechanical model, the distributions of permeable fracture networks are presented for the entirely subsurface Cooper Basin, Australia. This approach identified the regionally pervasive high angle (>50°) SE-NW and E-W striking natural fracture sets as optimally oriented to dilate and be hydraulically conductive under present-day stresses. These natural fracture sets are identified in each of the five seismic surveys and provide a target for future drilling programs exploiting high fracture density zones. The density of fracturing in the study area is shown to be underestimated in wellbore derived fractures when compared to seismic curvature analysis, as wells are commonly drilled in regions of low seismic curvature results. This approach can benefit other subsurface or offshore provinces in need of a refined understanding of the permeable subsurface fracture networks.

7. Acknowledgements

We thank the financial contribution made by the GeoFrac Consortium, which includes the sponsoring companies: Santos, Beach Energy, Chevron, Halliburton and BG Group (QGC). Thank you to Midland Valley (MOVE), DownUnder Geosolutions (DUG Insight), and Paradigm (Geolog) for academic licencing. Thank you to Carlos H. Grohmann and Ginaldo A.C. Campanha for the "OpenStereo 0.1.2" stereonet software.

8. References

Al-Dossary, S., Marfurt, K.J., 2006. 3D volumetric multispectral estimates of reflector curvature and rotation. Geophysics 71(5), 41-51.

Alexander, E.M., Gravestock, D.I., Cubitt, C., Chaney, A., 1998. Lithostratigraphy and environments of deposition. In: Gravestock, D.I., Hibburt, J.E., Drexel, J.F., (Eds.), The Petroleum Geology of South Australia. Vol. 4: Cooper Basin, South Australia. Department of Primary Industries and Resources. Report Book, 98/9, 69-116.

Amrouch, K., Lacombe, O., Bellahsen, N., Daniel, J.M., Callot, J.P., 2010a. Stress and strain patterns, kinematics and deformation mechanisms in a basement-cored anticline: Sheep Mountain Anticline, Wyoming. Tectonics 29, TC1005, doi:10.1029/2009TC002525.

Amrouch, K., Robion, P., Callot, J.P., Lacombe, O., Daniel, J.M., Bellahsen, N., Faure, J.L., 2010b. Constraints on deformation mechanisms during folding provided by rock physical properties: A case study at Sheep Mountain anticline (Wyoming, USA). Geophysical Journal International 182(3), 1105-1123.

Amrouch, K., Beaudoin, N., Lacombe, O., Bellahsen, N., Daniel, J.M., 2011. Paleostress magnitudes in folded sedimentary rocks. Geophysical Research Letters 38, L17301, doi:10.1029/2011GL048649.

Apak, S.N., Stuart, W.J., Lemon, N.M., Wood, G., 1997. Structural evolution of the Permian-Triassic Cooper Basin, Australia: Relation to hydrocarbon trap styles. AAPG Bulletin 81, 533-555.

Backe, G., Khair, H.A., King, R., Holford, S., 2011. Fracture mapping and modelling in shale-gas target in the Cooper basin, South Australia. The APPEA Journal 51, 397-410.

Barton, C.A., Zoback, M.D., Moos, D., 1995. Fluid flow along potentially active faults in crystalline rock. Geology 23, 683-686.

Chopra, S., Marfurt, K., 2007. Curvature attribute applications to 3D surface seismic data. The Leading Edge 26(4), 404-414.

Ferrill, D.A., Groshong, R.H., 1993. Kinematic model for the curvature of the northern Subalpine Chain, France. Journal of Structural Geology 15(3-5), 523-541.

Ferrill, D.A., Winterle, J., Wittmeyer, G., Sims, D., Colton, S., Armstrong, A., Morris, A.P., 1999. Stressed rock strains groundwater at Yucca Mountain, Nevada. GSA Today 9(5), 1-8.

Ferrill, D.A., Morris, A.P., 2003. Dilational normal faults. Journal of Structural Geology 25, 183-196.

Jolie, E., Moeck, I., Faulds, J.E., 2015. Quantitative structural geological exploration of fault-controlled geothermal systems—A case study from the Basin-and-Range Province, Nevada (USA). Geothermics 54, 54-67.

Kremor, J., Amrouch, K., 2017. Anisotropy parameter inversion from sonic and density logs in horizontally transverse isotropic media. The APPEA Journal 57(2), 772-775.

Kremor, J., Taylor, R., Amrouch, K., 2017. Polynomial amplitude versus azimuth inversion in horizontally transverse isotropic media, as tested on fractured coal seams in the Surat Basin. The APPEA Journal 57(2), 776-780.

Kuang, K.S., 1985. History and style of Cooper-Eromanga Basin structures. Exploration Geophysics 16, 245-248.

Kulikowski, D., Amrouch, K., Cooke, D., 2016a. Geomechanical modelling of fault reactivation in the Cooper Basin, Australia. Australian Journal of Earth Sciences 63(3), 295-314, doi:10.1080/08120099.2016.1212925.

Kulikowski, D., Hochwald, C., Cooke, D., Amrouch, K., 2016b. A Statistical Approach to Assessing Depth Conversion Uncertainty on a Regional Dataset: Cooper-Eromanga Basin, Australia. Proceedings of the ASEG-PESA-AIG Conference, Adelaide, abstract #200, 484-490.

Kulikowski, D., Cooke, D., Amrouch, K., 2016c. Constraining the distribution and relationship between overpressure, natural fracture density and temperature in the Cooper Basin. The APPEA Journal 56, 11-28, doi:10.1071/AJ15002.

Kulikowski, D., Amrouch, K., 2017. Combining Geophysical Data and Calcite Twin Stress Inversion to Refine the Tectonic History of Subsurface and Offshore Provinces: A Case Study on the Cooper-Eromanga Basin, Australia. Tectonics 36(3), 515-541, doi:10.1002/2016TC004366.

Kulikowski, D., Amrouch, K., Cooke, D., Gray, M.E., 2017. Basement Structural Architecture and Hydrocarbon Conduit Potential of Polygonal Faults in the Cooper-Eromanga Basin, Australia. Geophysical Prospecting, doi:10.1111/1365-2478.12531.

Lisle, R.J., 1994. Detection of zones of abnormal strains in structures using Gaussian curvature analysis. AAPG Bulletin 78(12), 1811-1819.

Maerten, L., Maerten, F., Lejri, M., Gillespie, P., 2016. Geomechanical paleostress inversion using fracture data. Journal of Structural Geology 89, 197-213.

Mavromatidis, A., 2006. Burial/exhumation histories for the Cooper-Eromanga Basins and implications for hydrocarbon exploration, Eastern Australia. Basin Research 18, 351-373.

Mildren, S.D., Hillis, R.R., Dewhurst, D.N., Lyon, P.J., Meyer, J.J., Boult, P.J., 2005. FAST: A new technique for geomechanical assessment of the risk of reactivation-related breach of fault seals. In: Boult, P., Kaldi, J., (Eds.), Evaluating fault and cap rock seals. AAPG Hedberg Series, Barossa Valley, South Australia 2, 73-85.

Murray, G.H., 1968. Quantitative fracture study-Spanish Pool, McKenzie County, North Dakota. AAPG Bulletin 52(1), 57-65.

Nelson, E.J., Chipperfield, S.T., Hillis, R.R., Gilbert, J., McGowen, J., 2007. Using geological information to optimize fracture stimulation practices in the Cooper Basin, Australia. Petroleum Geoscience, 13(1), 3-16.

Pokalai, K., Kulikowski, D., Johnson, Jr., R.L., Haghighi, M., Cooke, D., 2016. Development of a new approach for hydraulic fracturing in tight sand with pre-existing natural fractures. The APPEA Journal 56, 225-238, doi:10.1071/AJ15017.

Price, N.J., Cosgrove, J.W., 1990. Analysis of geological structures. Cambridge University Press, Cambridge.

Roberts, A., 2001. Curvature attributes and their application to 3D interpreted horizons. First Break 19(2), 85-100.

9. Figures

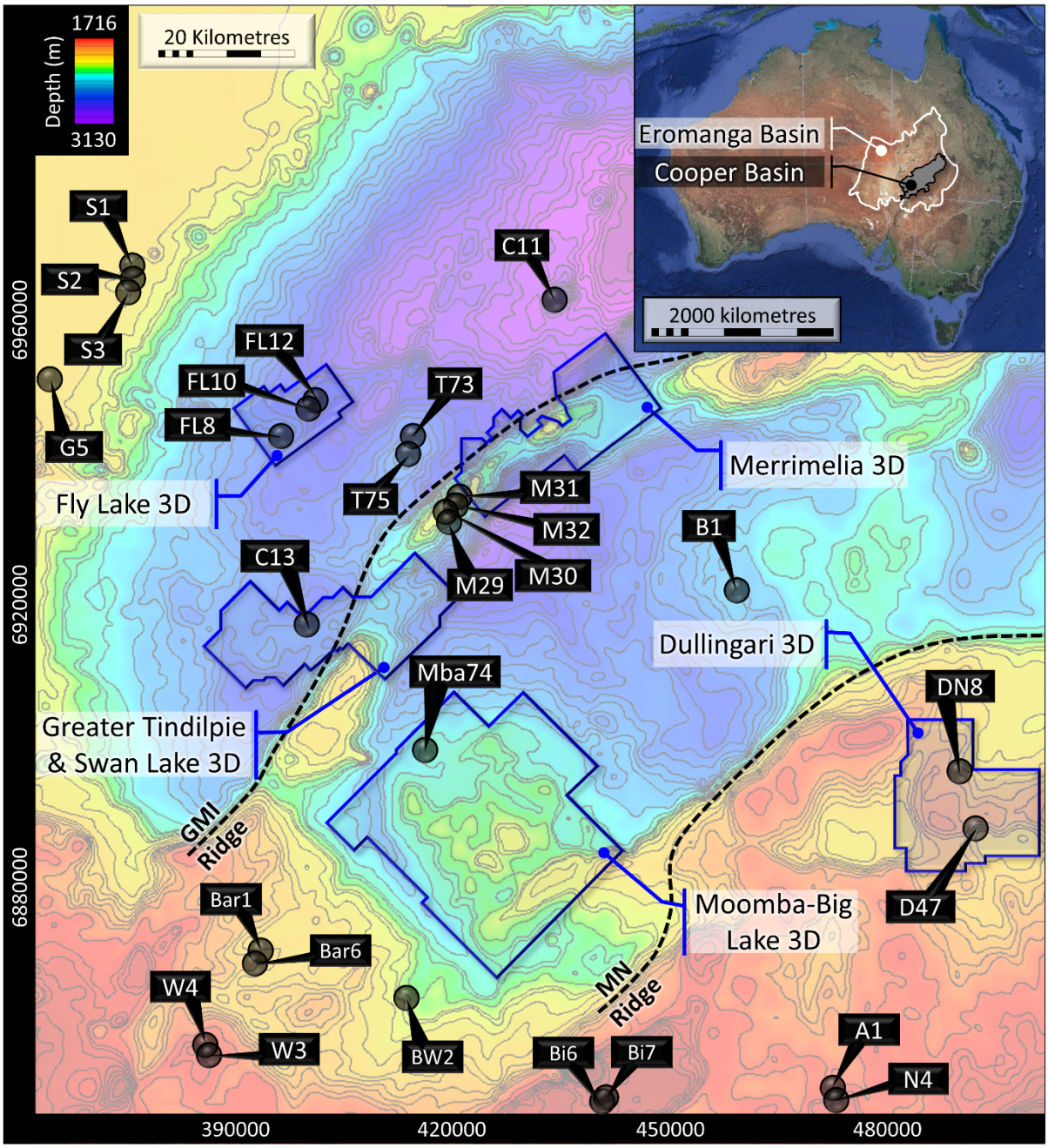


Figure 1. Location of 3D seismic surveys, borehole image logs, and the Gidgealpa-Merrimelia-Innamincka (GMI) and Murteree-Nappacoongee (MN) ridges within the South Australian Cooper Basin. Top Permian depth map shown (Kulikowski and Amrouch, 2017). Inset location of the Eromanga and Cooper basins, Australia (after Kulikowski et al., 2016a).

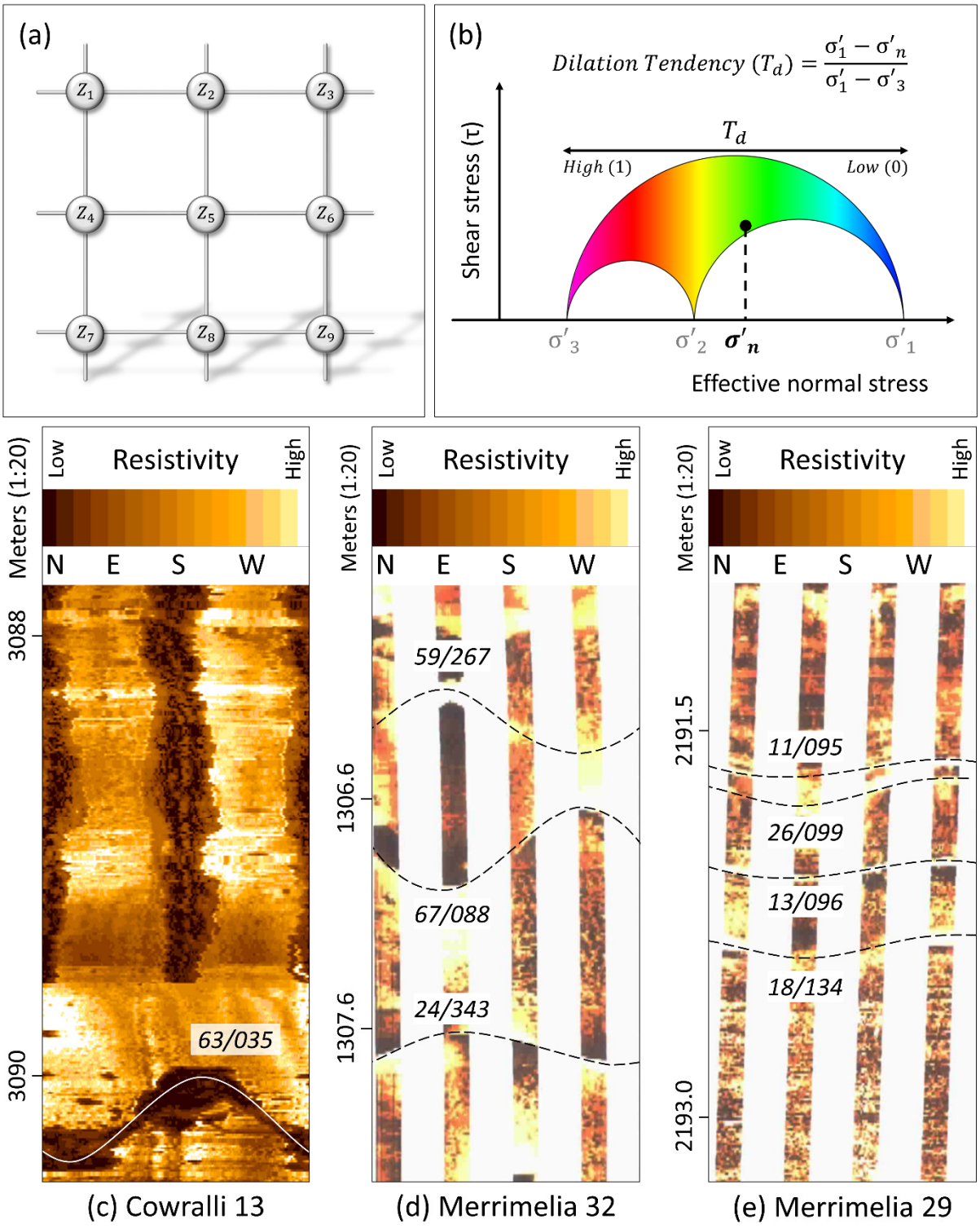


Figure 2. (a) Example of a 3x3 grid cell containing grid nodes (Z_i) used to compute curvature (Roberts, 2001); (b) The Dilation Tendency (T_d) in terms of maximum (σ'_1), minimum (σ'_3), and normal (σ'_n) effective stresses (Mildren et al., 2005). Conductive (solid line) and resistive (dashed line) natural fractures interpreted in borehole image logs from: (c) Cowralli 13; (d) Merrimelia 32; and (e) Merrimelia 29. See Figure 1 for location.

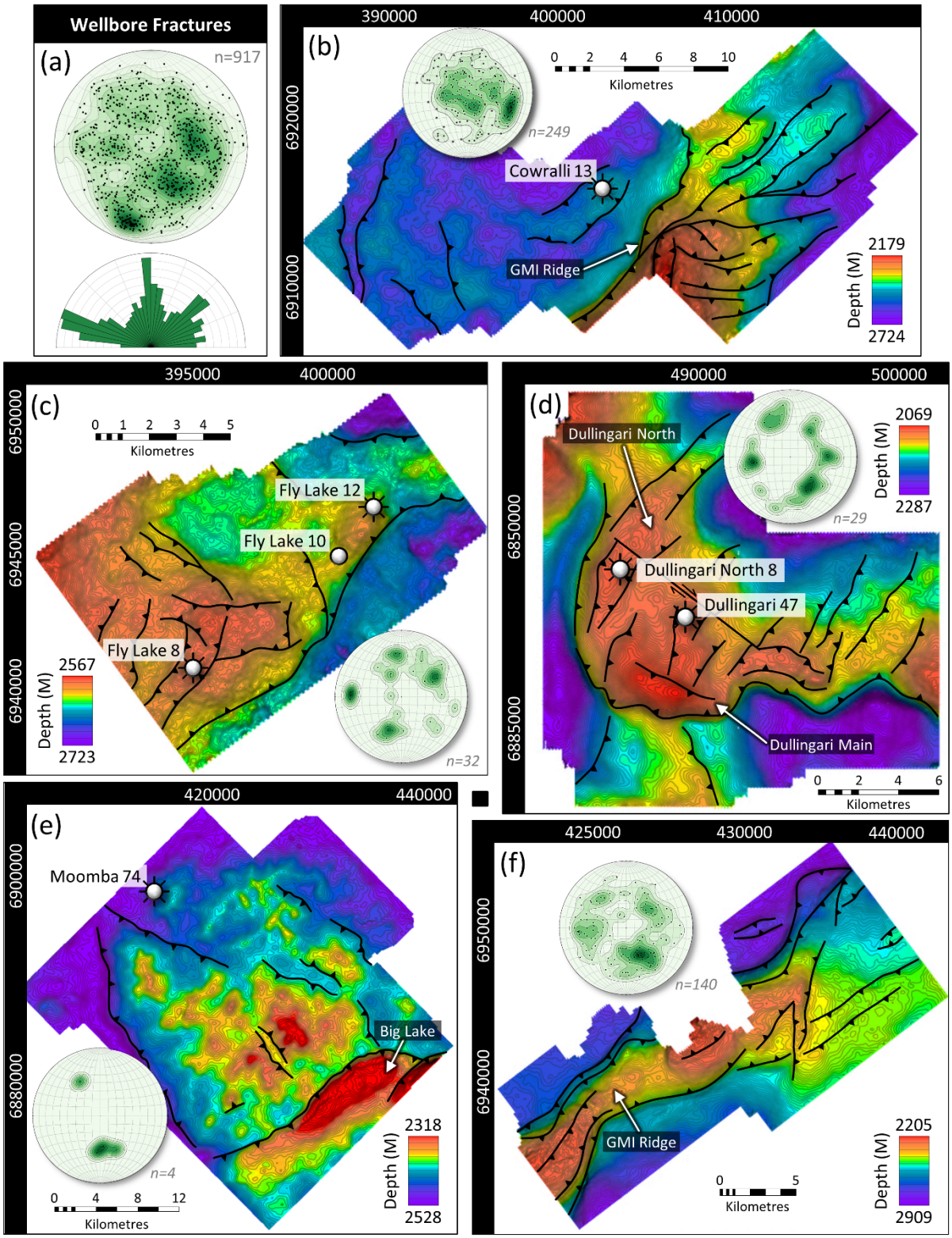


Figure 3. Basement faults projected onto Top Permian depth maps and the geometry of natural fractures interpreted from image logs in (adjacent to) the: (a) combined natural fracture data from all wells. See Figure 1 for seismic survey location. (b) Greater Tindilpie-Swan Lake 3D (after Kulikowski et al., 2017). (c) Fly Lake 3D; (d) Dullingari 3D; (e) Moomba-Big Lake 3D; and (f) Merrimelia (ext) 3D.

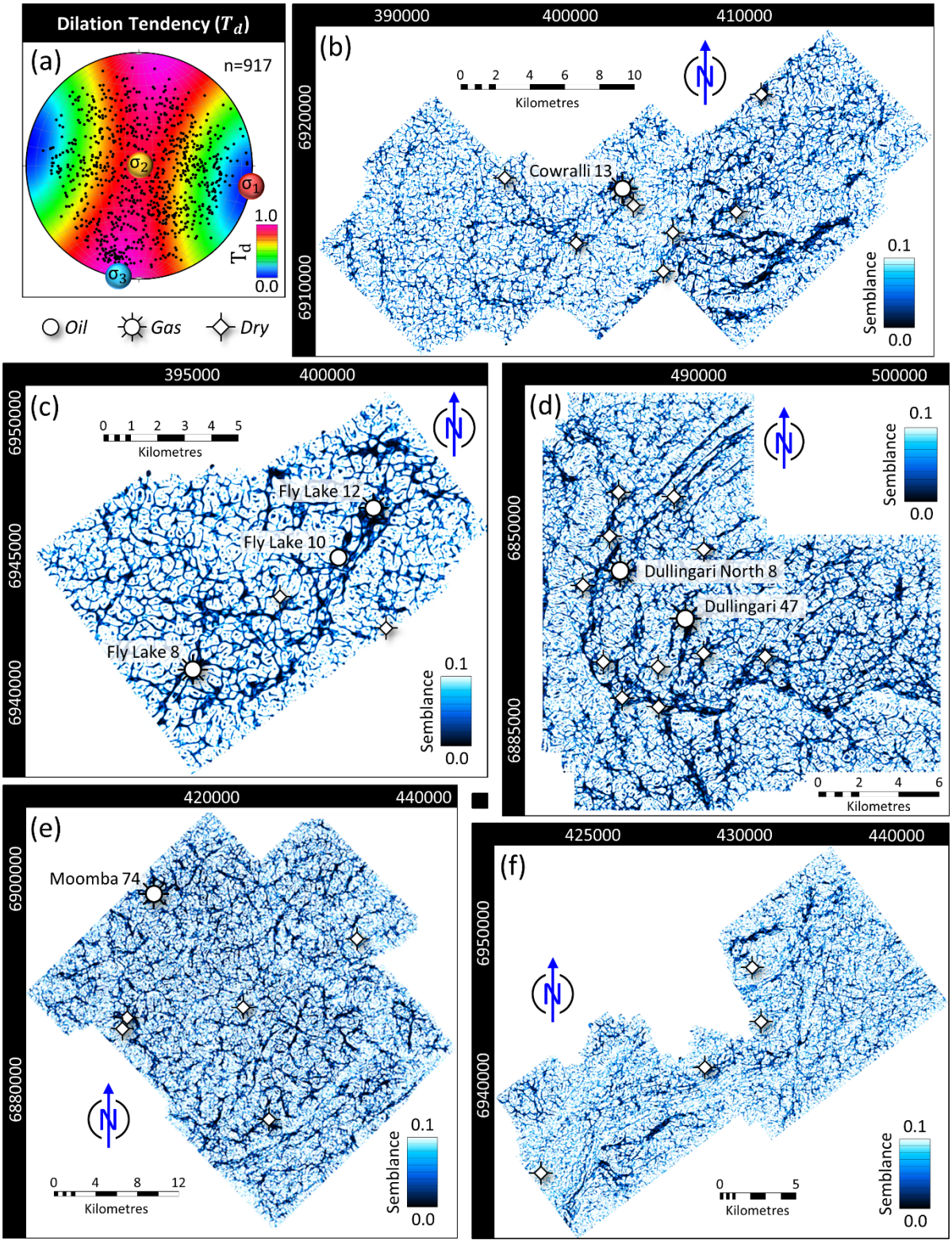


Figure 4. Most positive curvature displayed as semblance (zero semblance=fractures) along the Middle Patchawarra Formation in: (a) Dilation Tendency results at 1500 m. Equal-area lower hemisphere stereonet is shown. Stress data from Pokalai et al. (2016). (b) Greater Tindilpie-Swan Lake 3D. (c) Fly Lake 3D; (d) Dullingari 3D; (e) Moomba-Big Lake 3D; and (f) Merrimelia (ext) 3D. See Figure 1 for location.

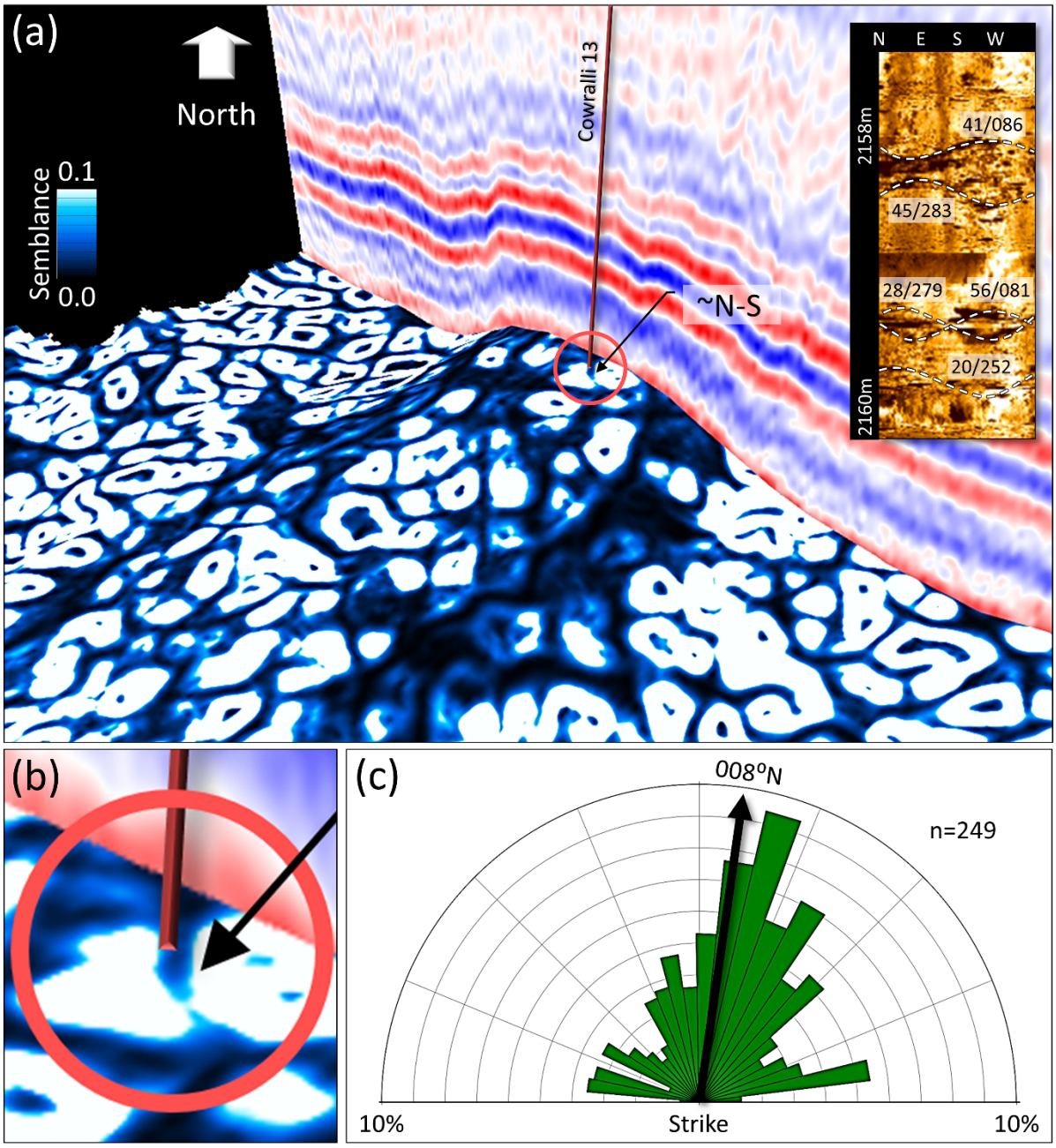


Figure 5. (a) Seismic curvature (displayed as semblance) at the Cowralli 13 well location showing N-S striking results correlating well to interpreted N-S striking natural fractures. (b) Zoomed in image of the N-S striking seismic curvature results (displayed as semblance) at the Cowralli 13 well location. (c) Rose diagram of interpreted natural fractures from the Cowralli 13 borehole image log showing a mean N-S strike direction. See Fig. 1 for location.

5.8. MANUSCRIPT 8: Temperature, pressure and fracture distribution

Constraining the distribution and relationship between overpressure, natural fracture density and temperature in the Cooper Basin, Australia.

The purpose of this study was to present the temporal and spatial variation in natural fracture intensity, temperature, and pressure across the Cooper-Eromanga Basin. Natural fractures were interpreted from 28 borehole image logs and integrated with pore pressure (>8,000 samples) and temperature (>6,000 samples) data from 1095 petroleum wells. This research found a relationship between the presence of volcanics, high temperatures, and overpressure and confirmed that natural fracture density has a negligible relationship to overpressure. This inferred that the development of natural fracture sets is likely attributed to tectonic events.

CITATION:

Kulikowski, D., Cooke, D., & Amrouch, K. (2016). Constraining the Distribution and Relationship between Overpressure, Natural Fracture Density and Temperature in the Cooper Basin, Australia. The Australian Petroleum Production & Exploration Association Journal, 56, 11-28, doi:10.1071/AJ15002.

Statement of Authorship

Title of Paper:	Constraining the distribution and relationship between overpressure, natural fracture density and temperature in the Cooper Basin, Australia
Publication Status:	**Manuscript Published**
Publication Details:	Kulikowski, D., Cooke, D., & Amrouch, K. (2016). Constraining the distribution and relationship between overpressure, natural fracture density and temperature in the Cooper Basin, Australia. *The APPEA Journal*, 56, 11-28, doi:10.1071/AJ15002.

Principal Author

Principal Author (Candidate):	David Kulikowski		
Contribution to the Paper:	Data collection, data conditioning, interpretation, analysis, and writing.		
Overall percentage (%):	80%		
Certification:	This paper reports on original research I conducted during the period of my Higher Degree by Research candidature and is not subject to any obligations or contractual agreements with a third party that would constrain its inclusion in this thesis. I am the primary author of this paper.		
Signature:		Date:	29 March 2017

Co-Author Contribution

By signing the Statement of Authorship, each author certifies that:

i. the candidate's stated contribution to the publication is accurate (as detailed above);

ii. permission is granted for the candidate to include the publication in the thesis; and

iii. the sum of all co-author contributions is equal to 100% less the candidate's stated contribution.

Name of Co-Author:	Dennis Cooke (10%)		
Contribution to the Paper:	Provided feedback on analysis and a complete review of paper.		
Signature:		Date:	28 Mar 2017

Name of Co-Author:	Khalid Amrouch (10%)		
Contribution to the Paper:	Provided feedback on analysis and a complete review of paper.		
Signature:		Date:	29 March 2017

Constraining the distribution and relationship between overpressure, natural fracture density and temperature in the Cooper Basin, Australia



Lead author
David Kulikowski

D. Kulikowski, D. Cooke and K. Amrouch
Australian School of Petroleum
The University of Adelaide
Adelaide, SA 5005
david.kulikowski@adelaide.edu.au

ABSTRACT

To effectively and safely extract hydrocarbon from low permeability and overpressured reservoirs in the Cooper Basin, a thorough understanding of the regional and field scale distribution of overpressure, temperature and fracture density is essential. Previous research omitted the effect of fluid expansion and hydrocarbon generation mechanisms for overpressure generation in the basin, albeit reservoir temperatures have sharply increased in the past five million years.

The authors collate pressure (>8,000 samples) and temperature (>6,000 samples) data from 1,095 wells across the SA portion of the Cooper Basin and incorporate natural fracture densities from 28 interpreted borehole image logs to investigate the spatial variation, and potential relationship, between pressure, temperature and natural fracture density. Results show significantly lower geothermal gradients within the Patchawarra Trough, likely attributed to a lack of shallow volcanics, blanketing coals or low uranium content. Shallow volcanics are common in high-temperature areas such as the Moomba/Big Lake and Gidgealpa fields and deeper portions of the Nappamerri Trough, with overpressured wells (>0.45 psi/ft) appearing to cluster in these areas, particularly south of the Gidgealpa-Merrimelia-Innamincka Ridge. Fracture density shows no obvious relationship to pressure, inferring a dominant structural origin for natural fracture development. Although the authors cannot exclusively attribute fluid expansion and hydrocarbon expansion mechanisms to overpressure, they likely have a profound effect.

Future work should investigate the feasibility of integrating pressure, vertical stress and sonic velocity to constrain the overpressure generation mechanism within the basin while incorporating field scale seismic attribute analysis for natural fracture detection and overpressure analysis.

KEYWORDS

Cooper Basin, natural fractures, reservoir pressure, geothermal gradient, structural geology.

INTRODUCTION

The mechanisms involved in generating overpressure in sedimentary basins have been well documented, with disequilibrium compaction and hydrocarbon generation being the most commonly cited (Bowers, 1995; Osborne and Swarbrick, 1997; van Ruth et al, 2003; Tingay et al, 2009). Overpressure describes a pore fluid that exceeds the hydrostatic gradient (0.433 psi/ft) at a given depth, requiring some mechanism other than the buoyancy force of a continuous column of static fluid (Osborne and Swarbrick, 1997). The dominant mechanisms range from hydrocarbon generation, disequilibrium compaction, fluid expansion from an increased geothermal gradient, an increase in mean compressive stress (tectonic loading), and vertical and lateral overpressure transfer (e.g. Grauls and Baleix, 1994; Bowers, 1995; Wangen, 2001; Tingay et al, 2007, 2009). The fundamental geomechanical rock failure properties state that overpressure effectively shifts the Mohr's circle to the left, promoting the development and reactivation of natural fractures and faults (Anderson, 1951; Barton et al, 1995). In this paper the authors explore the potential relationship between overpressure and natural fracture density within the SA portion of the Cooper Basin by collating numerous well tests and interpreting natural fractures from 28 borehole image logs, while also investigating the spatial variation of pore pressure and temperature.

The Permian to Triassic aged Cooper Basin is recognised as an overpressured sedimentary basin with a complex structural history and a relatively high geothermal gradient (Apak et al, 1997; Geotrack, 1997; van Ruth et al, 2003). Although some work has explored the origin of overpressure within local areas (van Ruth and Hillis, 2000; van Ruth et al, 2003), a regional assessment of pressure, temperature and natural fracture distribution has yet to be studied. The authors explore the variation in overpressure and temperature across the study area and attempt to integrate measured natural fracture density distributions to explore a potential high-level correlatable relationship. The authors collated pore pressure and formation temperature data from 1,095 wells located in the SA portion of the Cooper Basin. Pressure and temperature tests varied from repeat formation tests (RFTs), drill stem tests (DSTs), formation multi-tests (FMTs), modular formation dynamics tests (MDTs), and compact formation pressure tests (MFTs). Natural fractures were interpreted from 28 borehole image logs and converted to fracture densities based on the frequency of occurrence and the formation thickness.

Results from this study will enhance the understanding of the regional overpressure and temperature distributions in the basin, while integrating natural fracture density data to ascertain a possible relationship. Maps showcase a potential relationship between relatively high pressure and high temperature gradients, while also providing valuable information on likely natural fracture and pressure sweet spots that may be targeted by future exploration and development drilling. This assessment allowed the authors to deduce that overpressure may not directly be linked with natural fracture development, inferring that overpressures may not always be significant enough to induce fracturing, and that perhaps structural events have a dominant control on natural fracture development. Relatively high temperatures are found along, and south of, the Gidgealpa-Merrimelia-Innamincka (GMI) Ridge, with relatively high natural fracture density observed along the basin margins and along the main structural features, as well as in the Moomba and Coonatie fields. This preliminary analysis provides a working platform for future work investigating the prospect of using formation pressure, vertical stress and sonic velocity relationships to better constrain the overpressure generation mechanism in the basin, while incorporating field scale seismic attribute analysis for natural fracture detection and overpressure analysis with depth.

GEOLOGICAL SETTING

The intra-cratonic Permian to Upper Triassic aged Cooper Basin spans an area of approximately 130,000 km^2 across SA and Queensland (Apak et al, 1997). The basin is unconformably isolated from the overlying Jurassic to Upper Cretaceous aged Eromanga Basin, and underlying Cambrian to Ordovician aged Warburton Basin (Fig. 1) (Kantsler et al, 1983; Kuang, 1985; Bradshaw, 1993; Apak et al, 1997; Gravestock and Jensen-Schmidt, 1998; Mavromatidis, 2006). These unconformities mark successive periods of structural movement and exhumation during the Carboniferous aged Alice Springs Orogeny, followed by the Upper Triassic aged Hunter-Bowen Orogeny (Kuang, 1985; Apak et al, 1997; Mavromatidis, 2006). Between these major structural events, minor compression was experienced during the Sakmarian and late Permian (Apak et al, 1997). The structurally complex Cooper Basin was dominated by fluvial, lacustrine and swamp environments depositing sediments that now form the largest onshore hydrocarbon province in Australia (Kantsler et al, 1983; Apak et al, 1997; Gravestock and Jensen-Schmidt, 1998).

Initial accommodation space and northeast–southwest and southeast–northwest striking structural lineaments developed during southeast–northwest oriented Precambrian (Adelaidean) aged extension (Apak et al, 1997). This period of extension exhumed the Mooracoochie Volcanics to form the base of the Warburton Basin, upon which shallow shelf, low stand fan and deltaic/prograding shoreline sediments were deposited (Sun, 1997; Rezaee and Sun, 2007). The north–south oriented Alice Springs Orogeny exhumed the Warburton Basin sediments, developing a regional unconformity that isolates the overlying Cooper Basin. The Alice Springs Orogeny is concurrent with the exhumation of the Carboniferous aged Big Lake Granites and is believed to have reactivated pre-existing structural lineaments (Kuang, 1985; Apak et al, 1997; Mavromatidis, 2006). Following this period of structural re-organisation and increase in local hydrothermal activity, the glacial Late Carboniferous to Early Permian Merrimelia Formation and braided fluvial Early Permian Tirrawarra Formation were deposited, marking the base of the Cooper Basin (Kantsler et al, 1983; Apak et al, 1997).

The Early Permian Patchawarra Formation was deposited onto the Tirrawarra Formation during cycles of fluvio-deltaic, lacustrine and swamp environments (Boreham and Hill, 1998). Onlap of the lower Patchawarra Formation onto the northeast–southwest striking GMI and Murteree-Nappacoongee (MN) ridges marks the onset of the first Sakmarian aged uplift event (273 Ma) (Apak et al, 1997). A second period of structural movement during the Sakmarian (270 Ma) is notable along the GMI and MN ridges, and the northern flank of the Patchawarra Trough, where middle Patchawarra Formation sediments markedly pinch out (Kantsler et al, 1983; Apak et al, 1997). An easterly regression lowered water levels in the western and southern portions of the basin depositing the Murteree Shale, Epsilon Formation, Roseneath Shale and Daralingie Formation in shoreline, distributary and deltaic environments (Apak et al, 1997).

This period of deposition was interrupted by a compressional pulse during the late Permian (258 Ma) that reactivated pre-existing structural lineaments and eroded much of the Daralingie Formation (Apak et al, 1997). Post compressional relaxation and structural quiescence is marked by the deposition of channel sands, siltstones and coals in the meandering fluvial Toolachee Formation onto the regional Daralingie unconformity (Apak et al, 1997). Fluvial channels, floodplain and lacustrine sediments were deposited onto the Toolachee Formation in an oxidising, warm and humid environment, as evidenced by a distinct lack of coals, forming the Nappamerri Group sediments (Kantsler et al, 1983; Apak et al, 1997). Maximum burial depth was reached (235 Ma) prior to the Upper Triassic aged Hunter-Bowen Orogeny, which exhumed up to 500 m of sediment from the southern portion of the Cooper Basin (Kantsler et al, 1983; Apak et al, 1997; Mavromatidis, 2006).

The Hunter-Bowen Orogeny (245–190 Ma) rejuvenated pre-existing structural lineaments and induced major downwarping of the eastern portion of the Cooper Basin, as well as regionally eroding the upper Nappamerri Group sediments to create the regional unconformity that isolates the Cooper Basin from the overlying Eromanga Basin (Kantsler et al, 1983; Apak et al, 1997; Mavromatidis, 2006; Alexander et al, 1998). Post compressional relaxation and structural quiescence was pronounced during the uninterrupted deposition of Jurassic to Upper Cretaceous aged Eromanga Basin sediments in fluvial, lacustrine and open marine environments (Moore, 1986; Green et al, 1989; Hoffman, 1989; Lowe-Young et al, 1997). The Upper Cretaceous aged Winton Formation was deposited at a rate of 200 m/million years prior to regional exhumation and erosion, which marks the upper boundary of the Eromanga Basin before transitioning into the overlying Cenozoic aged Lake Eyre Basin (Lowe-Young et al, 1997; Apak et al, 1997; Mavromatidis, 2006).

MECHANISM FOR OVERPRESSURE GENERATION

Disequilibrium compaction

Increases in pore pressure can result from an increase in the horizontal (tectonic forces) and vertical (burial) stresses acting on the rock (Osborne and Swarbrick, 1997). Such overpressures can occur at a very rapid rate and, at an equally high rate, decreases in pore pressure can occur through fluid venting processes along fractures and faults (Sibson, 1990; Osborne and Swarbrick, 1997).

The mechanism of overpressure generation through disequilibrium compaction involves the relationship between increased vertical stress caused by rapid sedimentation and the inability of a given formation to expel fluids (Osborne and Swarbrick, 1997; van Ruth et al, 2003; Tingay et al, 2009). Under slow burial conditions, where the rate of sedimentation and the rate of reduced pore-fluid volume are at equilibrium, a hydrostatic gradient of approximately 0.43 psi/ft is maintained (Osborne and Swarbrick, 1997). As such, pore fluids that are not expelled during periods of increased sedimentation rate can experience significant overpressures in excess of the typical hydrostatic gradient (Tingay et al, 2009). This form of overpressure generation has been correlated to increased pressures in the Caspian Sea and North Sea basins (Bredehoeft et al, 1988; Mann and Mackenzie, 1990).

Tectonic compression

In the same way that disequilibrium compaction can increase pore pressure due to increased vertical stress, pore pressures can increase rapidly with an increase in horizontal, or tectonic, stress (Osbourne and Swarbrick, 1997). High pore pressures resulting from increased lateral compression have been found to be a possible cause of overpressure along the San Andreas Fault, within the North American craton, and within the Niger Delta fold and thrust belt (Ge and Garven, 1989; Bethke and Marshak, 1990; Bilotti and Shaw, 2005). Although this relationship is well-known (Berry, 1973; Yassir and Bell; 1996), accurately modelling or calculating the effect of this mechanism is difficult, given that the maximum horizontal stress magnitude is difficult to constrain (van Ruth et al, 2003).

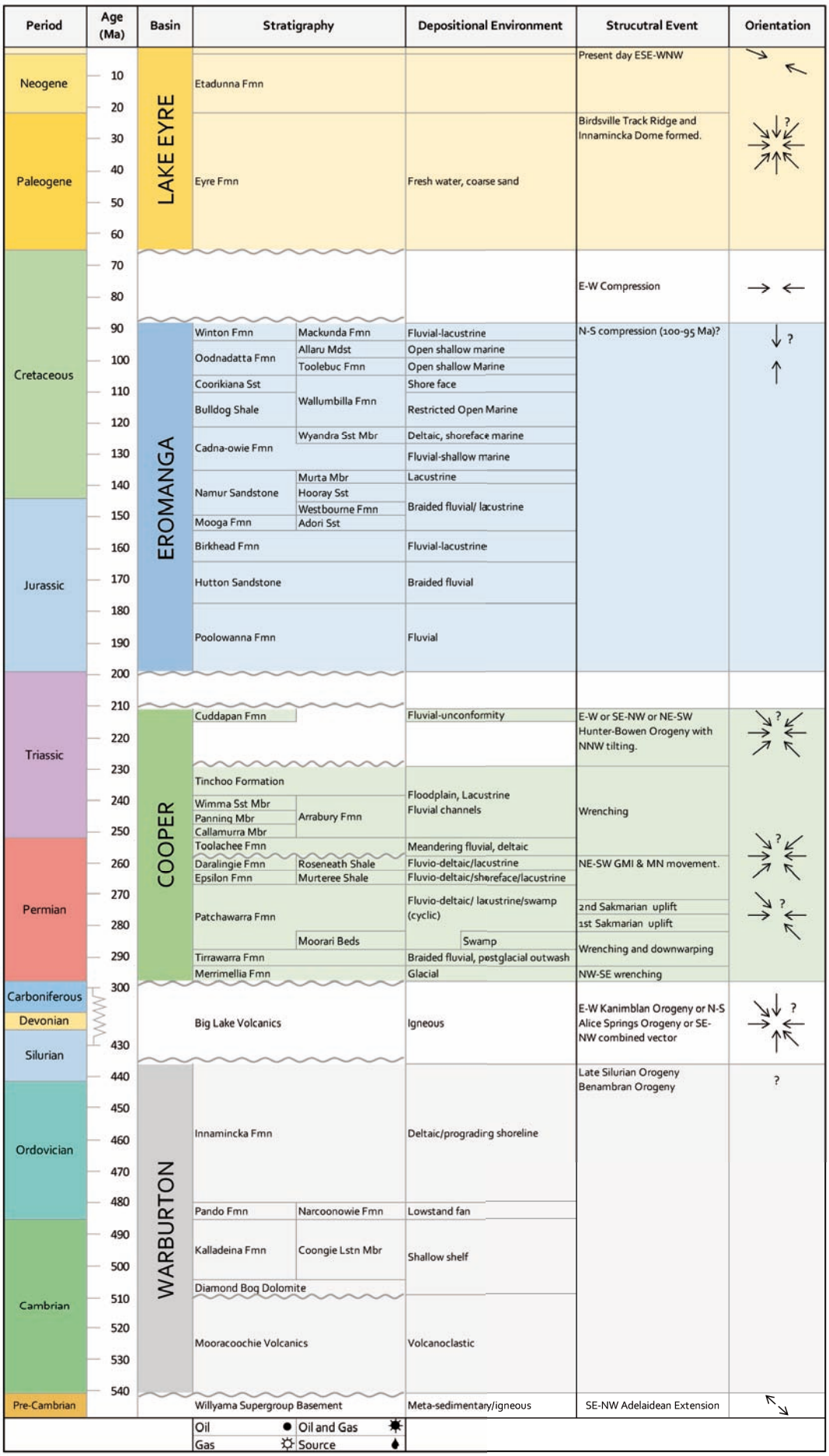


Figure 1. Summary of the age, stratigraphy, depositional environment and structural events of the Warburton, Cooper, Eromanga and Lake Eyre basins (modified after Kulikowski et al, 2015).

To accurately predict the effect that tectonic compression has on a given basin, the tectonic history and present-day stress regime must be well constrained. In many basins, the magnitude of paleo-structural events is poorly constrained, therefore, creating large uncertainty on the evolution of pore pressure. Van Ruth et al (2000 and 2003) have suggested that the overpressures observed in the Cooper Basin may be related to an increase in the mean stress (50 MPa) since the Late Cretaceous; however, they conclude that burial or temperature-driven mechanisms may also be possible.

Hydrocarbon generation

The conversion of kerogen to liquid or gas has been estimated to involve an increase in total volume by up to 25% (Meissner, 1978). Given a closed system, this increase in volume may lead to significant overpressures and can directly influence natural fracture development (Osborne and Swarbrick, 1997). Osborne and Swarbrick (1997) state that for overpressures to be generated through this mechanism on a basin-wide scale, a thick and mature source rock must be regionally extensive and rapid generation must take place in low permeability rocks. Such conditions are typical of the low permeability and high coal-bearing Cooper Basin strata. Interestingly, as pore pressures increase, the endomorphic reaction that converts kerogen to liquid or gas is inhibited and hence requires higher temperatures than a normally pressured system (Osborne and Swarbrick, 1997). Such cases of overpressure generation through hydrocarbon generation are recorded in the Rocky Mountains region (Spencer, 1987) and Bakken Shale (Burrus et al, 1998), with abnormally immature source rocks at high temperatures occurring in the Yinggehai and Qiongdongnan basins (China) (Fang et al, 1995).

The critical moment in the Cooper/Eromanga Basin hydrocarbon system occurred during the Upper Cretaceous (approximately 90 Ma), after major structural reconfiguration caused by a Late Cretaceous aged east–west compressional event (Lowe-Young et al, 1997). Maximum heat flow within Permian source rocks occurred during the Cretaceous, reaching average temperatures of approximately 192°F before cooling to the present-day temperature of 142°F (Geotrack, 1997). The conversion of oil to light gas, and ultimately methane, has the potential to produce extreme overpressures, requiring a temperature of approximately 248–284°F, which can be found in portions of the Cooper Basin (Osborne and Swarbrick, 1997). Local high-temperature anomalies will also cause sealed water bodies to expand, subject to the relationship with pore pressure and pore volume (Osborne and Swarbrick, 1997).

Fluid expansion

A body of water that is within a closed system will expand in volume, causing high internal pressures given that temperatures are above approximately 40°F (Osborne and Swarbrick, 1997). Fluid expansion as a mechanism for overpressure is subject to the pressure, temperature and volume relationship, as well as pore fluid properties such as compressibility and composition (Osborne and Swarbrick, 1997). Although the fluid expansion mechanism can generate extreme overpressure with a relatively small increase in temperature (an increase of approximately 100°F may increase internal pressure by 8,000 psi), the likelihood of preserving such high pressures for prolonged periods of time without vertical or lateral transfer of pressure may be unrealistic, as overpressures strongly seek hydrostatic equilibrium (Osborne and Swarbrick, 1997; Tingay et al, 2009).

The transfer of overpressure through faults, fractures or hydraulically connected pressure compartments may lead to a vertical or lateral redistribution of overpressure, which has been well documented in the Gulf of Mexico, Brunei, and in a Tertiary basin in Southeast Asia (Grauls and Baleix, 1994; Finkbeiner et al, 2001; Tingay et al, 2007, 2009). As such, fluid expansion mechanisms, other than hydrocarbon generation, are considered as secondary processes that may contribute to local variations in overpressure; however, this must be analysed on a case-by-case basis as ignoring this mechanism in some regions may lead to large errors in pore pressure predictions (Bowers, 1995; Osborne and Swarbrick, 1997; Wangen, 2001; Tingay et al, 2009).

METHODOLOGY

Pressure and temperature distribution

This research attempts to better understand the regional overpressure and temperature distribution in the Cooper Basin to support future exploration and development drilling campaigns. Drilling wells into overpressured or high geothermal gradient rocks not only presents risks associated with blow outs or fluid kicks, but also with completions, logging and optimisation processes. The authors collated pressure and temperature tests from 1,095 wells in the SA portion of the Cooper Basin to investigate trends or regions with anomalously high geothermal gradient or overpressure (Fig. 2).

The authors assumed a surface temperature of 70°F for all wells and calculated a geothermal gradient based on individual temperature tests performed within a well. The maximum geothermal gradient for a well was used and plotted on a base map (red-high; orange-intermediate; green-low) depending on whether the value was relatively high (>3.0°F/100 ft) intermediate (2.5–3.0°F/100 ft), or relatively low (<2.5°F/100 ft). A similar approach was taken with pressure data, with maximum pressure gradients used to describe individual wells. Pore pressure data was plotted according to the calculated pressure gradient of the well (green-depleted; blue-hydrostatic; orange-slightly overpressured; red-highly overpressured). Slightly overpressured wells contain pressure gradients between 0.45–0.50 psi/ft, while highly overpressured wells exhibit pressure gradients above 0.50 psi/ft. By maintaining a similar base map of the study area and similar display properties, data can be integrated to easily make inferences and locate possible relationships.

Natural fracture density distribution

The Cooper Basin is completely overlain by younger sediment and does not outcrop in the study area, requiring the use of borehole image logs to interpret natural fractures at depth. Borehole images are generated by measuring the electrical resistivity or acoustic reflection of the borehole at a centimeter scale, or more directly with the use of downhole optical imaging tools. A typical electro imaging tool contains six pads, each with 150 microelectrodes, which press against the borehole wall to measure the change in resistivity (Nie et al, 2013). Natural fractures may image as either high (open to fluid flow) or low (cemented and closed to fluid flow) resistivity. Appropriate processing techniques and filters are used to convert digital data from the available 28 borehole image logs into oriented and interpretable images (Fig. 3).

Natural fractures are plotted according to their dip, azimuth, fracture density and absolute frequency (Fig. 4a). The interpreted natural fractures are synthesised into a normalised natural fracture density for a given well based on the number of natural fractures interpreted and the length of the image log (number of fractures [f]/total image log length [m]) (Fig. 4B). Relative natural fracture density values are plotted on a base map with

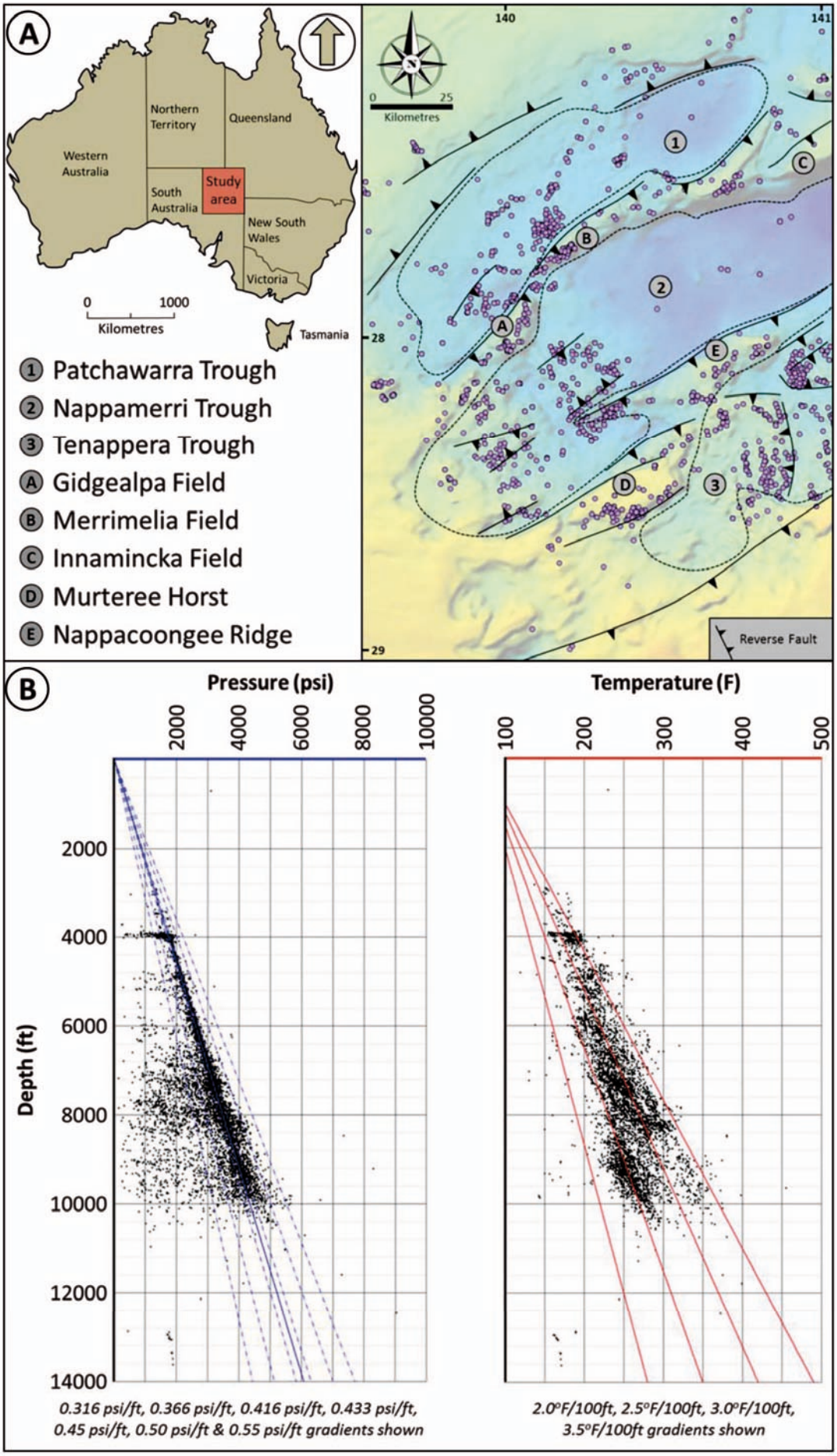


Figure 2. [A] Location of the 1,095 wells used to collate pressure and temperature data in the study area. Well location map shows major structural features of the basin. [B] Collated pressure and temperature data plotted with depth.

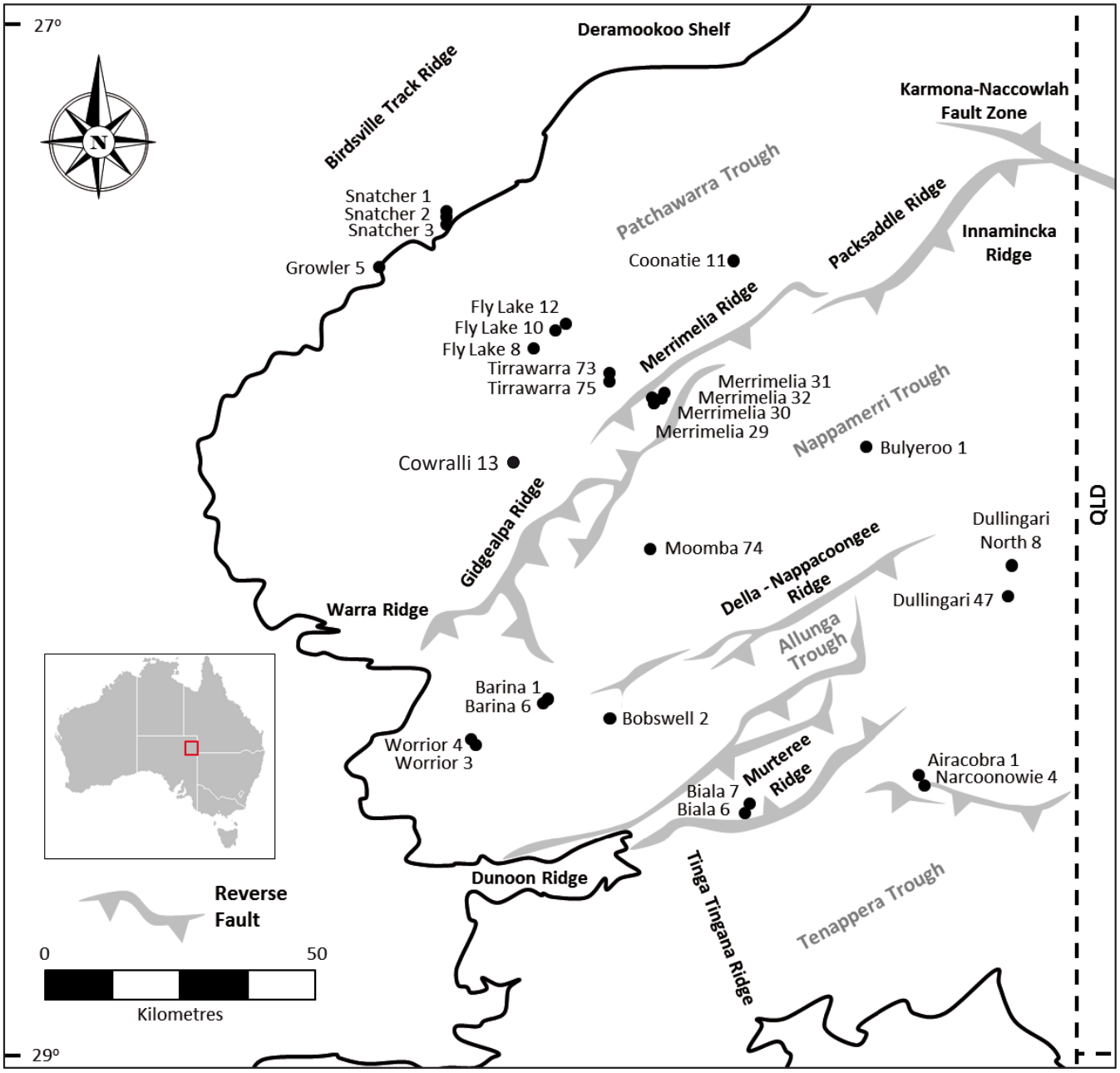


Figure 3. Location of borehole image logs used for this study (modified after Kulikowski et al, 2015; Razaee and Sun, 2007).

cut-offs arbitrarily chosen based on the range of data; relatively high (>0.1 f/m) (red), intermediate (0.05–0.1 f/m) (orange), or low (<0.05 f/m) (blue) natural fracture density (Fig. 5d). This methodology allows for a straight-forward comparison of fracture frequency with pressure and temperature gradients within wells, to ultimately investigate whether increased temperature in the basin correlates to increased pore pressure, which in turn may lead to increased natural fracture density as the effective stresses acting on the rock are reduced and effectively shift the Mohr's circle closer to the failure envelope.

RESULTS

Distribution of overpressure and temperature

The regional distribution of overpressure and temperature in the Cooper Basin has remained under-studied, with researchers pursuing more technical research on topics such as pore pressure prediction, rather than constraining the fundamental distributions (Meixner et al, 2000; van Ruth and Hillis, 2000; van Ruth et al, 2003; Reynolds et al, 2006). To better understand the regional distribution of pressure, temperature and natural fracture density, the authors collated a large number of pore pressure and formation temperature data from 1,095 wells to assess the lateral distributions and relationships in the basin (Fig. 2). This research may prove to be useful for exploration and development companies presently operating in the basin, to better quantify the risks associated with drilling greenfield exploration wells and to optimise well placement. It is well-known in the basin that borehole stability is a key risk. Drilling wells into highly stressed and potentially fractured reservoirs may in some instances provide increased flow; however, to maintain wellbore stability and achieve the objectives of the well, these locations may increase the risk of borehole instability.

Overpressured tests (exceeding the hydrostatic gradient of approximately 0.45 psi/ft) were recorded in 385 wells and the average geothermal gradient was found to be between 2.5°F/100 ft and 3.5°F/100 ft assuming a surface temperature of 70°F. Pore pressure and temperature data were collected from various well tests (DSTs, FMTs, RFTs, MDTs, and MDTs) and plotted with depth to extract possible trends or anomalies (Fig. 2). The authors began observing overpressures at approxi-

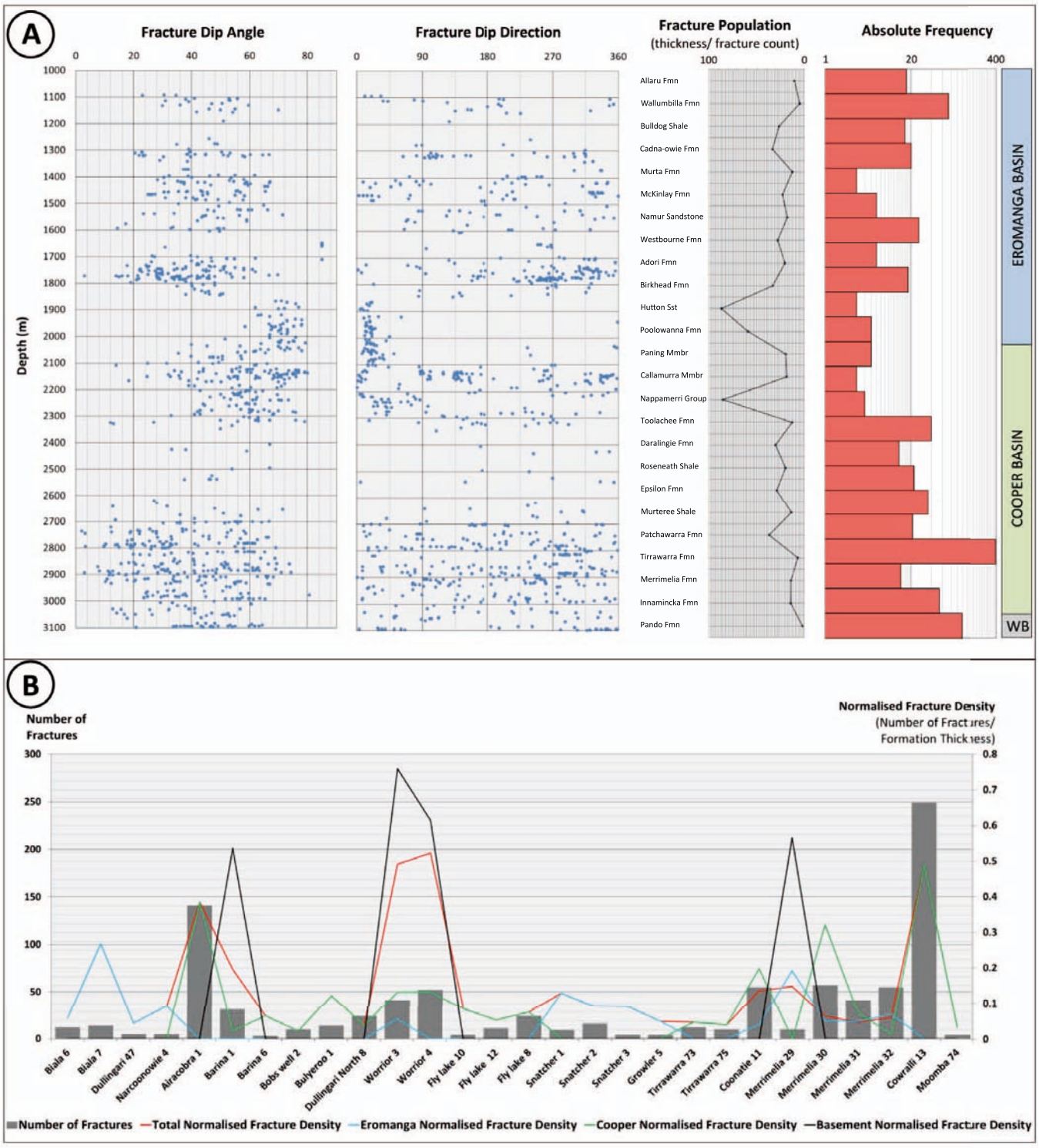


Figure 4. [A] Natural fracture data shown as dip angle, dip direction, distance between fractures (t/f) and absolute frequency versus depth. [B] Number of fractures and normalised (fracture count/total formation thickness) fracture density shown per well. Normalised fracture density is given for the Warburton (black), Cooper (green) and Eromanga (blue) basins, as well as a combined curve (red).

mately 7,000 ft, with considerable overpressures (>0.50 psi/ft) observed from 8,000 ft (Fig. 2). A large portion of pore pressure data is also plotted below the hydrostatic gradient, inferring that a majority of tests are most likely recording invalid tests or measuring pressure depleted reservoirs. Reservoirs can become depleted through the production of nearby wells targeting the same laterally continuous reservoir.

Spatial maps of maximum pore pressure and temperature gradients measured within wells illustrates a few key points.

1. Considerable overpressure appears in the Moomba/Big Lake and Coonatie fields, as well as in the deeper portions of the Nappamerri Trough.
2. Overpressure is present within structural lows and along structural highs.
3. Relatively low temperatures exist within the Patchawarra Trough.
4. Relatively high temperatures exist within the deeper portions of the Nappamerri Trough, within the Moomba/Big Lake and Dullingari fields, and along the Murteree-Nappacoongee Ridge.
5. Relatively low temperatures within the Cooper Basin (~2.5°F/100 ft) are still higher than the average geothermal gradient for the continents (approximately 2.3°F/100 ft) (Fig. 5) (Beardsmore and Cull, 2001).

The authors isolated data to show maximum overpressure and temperature gradients within the Toolachee-Daralingie-Roseneath-Epsilon-Murteree (TDREM) stratal unit and the Patchawarra Formation to observe possible changes with lithology (Fig. 6). Similar trends are observed within the Patchawarra Trough, with both the TDREM stratal unit and Patchawarra Formation showing consistently low relative temperatures and overpressure gradients within the Coonatie Field (overpressure in the Patchawarra Formation intersection in Beanbush–1). Overpressures within the Tirrawarra and Tindilpie/Nephrite/Coonatie fields, however, are more evident within the Patchawarra Formation than within the TDREM stratal unit (Fig. 5d). Overpressure and temperature gradients appear similar in the deeper portions of the Nappamerri Trough; however, the westernmost portion of the Nappamerri Trough (west of the Moomba/Big Lake Field) shows an increase in the pore pressure and temperature gradient. Pressure and temperature profiles for both stratal units are shown in Figure 7. To compare the pressure, temperature and fracture density across the basin, the authors collated data to within individual fields and calculated the minimum, average and maximum pressures, temperatures and pressure test depths. The calculations here exclude depleted reservoir pressures and invalid tests to show only virgin pressure data because inclusion of this data would skew the averages to lower than actual and could potentially mislead final conclusions. The average pressure (Fig. 8a) and temperature (Fig. 8b) of individual fields was calculated and plotted on a regional map. The investigation into a possible relationship between overpressure and high temperature within the basin is graphed in Figure 8c, showing individual well tests as well as average field values, and a very low R^2 value of 0.1.

Distribution of fracture density

Natural fractures interpreted from borehole image logs are given in Figure 9, showing the dominant strike orientations within the study area. A high volume of measured data appears to have a strike of north–south, northeast–southwest or southeast–northwest (Fig. 9). Normalised natural fracture densities (fracture count/sediment thickness) are illustrated in Figure 5d, with red highlighting relatively high normalised fracture density, orange showing relatively intermediate normalised natural fracture density, and blue indicating relatively low normalised natural fracture density. Relatively high normalised natural fracture densities were found along the GMI Ridge and along the basin flanks, as well as in the Moomba and Coonatie fields. Relatively low normalised natural fracture densities were found within the Tirrawarra, Dullingari and Barina fields. Future work will investigate the true natural fracture geometry across the basin and attempt to constrain the timing of individual natural fracture set development, and ultimately attempt to attribute their development to individual structural events. Understanding the true natural fracture geometry can be key to low permeability hydrocarbon production in the Cooper Basin, as production wells can be oriented to intersect the largest number of natural fractures possible in an attempt to improve recovery or, alternatively, can be placed in areas with low fracture density to maintain wellbore stability.

DISCUSSION

The structurally complex intracratonic Cooper Basin is a low permeability and overpressured hydrocarbon basin with a high geothermal gradient that commonly requires hydraulic fracture stimulation treatment of tight sandstones to produce economic flow rates (McGowen et al, 2007; Pokalai et al, 2015; Pokalai et al, 2016). To better understand the distribution of overpressure and temperature in the basin, the authors collated various well tests from 1,095 wells to calculate the maximum gradients occurring within individual wells. The study also assesses the relationship between overpressured wells and the natural fracture density calculated from borehole image log interpretation. The temperature and overpressure distribution within the basin is presented and the spatial variation in natural fracture density across the area is shown. These findings will enhance understanding for hydrocarbon exploration companies that are operating within the basin that may be seeking new field discoveries by targeting temperature, pressure and natural fracture density sweet spots for improved hydrocarbon recovery.

The authors analysed more than 8,000 pressure data points and more than 6,000 temperature data points to construct pressure and temperature versus depth profiles for the SA portion of the Cooper Basin (Fig. 2). A majority (50.4%) of pore pressure data was found to plot along the hydrostatic gradient (0.42–0.45 psi/ft). A further 14.3% of data was considered to be under pressured (<0.42 psi/ft), which the authors infer to be caused by depletion by hydrocarbon production in earlier drilled and adjacent wells. A large portion of pressure data (35.3%) plotted above the hydrostatic gradient (>0.45 psi/ft), and is considered to be overpressured. From the 35.3% of overpressured data, 14.3% plotted above 0.50 psi/ft. This portion of highly overpressured data poses a significant risk to new drilling campaigns due to the high potential of a blowout or fluid kick occurring. Highly overpressured sediments may also promote natural fracture development. Areas that are significantly overpressured occur in the Moomba/Big Lake and Coonatie fields, as well as in the deeper portion of the Nappamerri Trough (Fig. 5). Interestingly, these areas of overpressure also exhibit a relatively high geothermal gradient, exceeding 3.0°F/100 ft in some areas.

It is evident that relatively low temperature gradients (<2.5°F/100 ft) exist within the Patchawarra Trough when compared to the remaining study area (Fig. 5b and Fig. 8b). It is important to note that the relatively low temperature gradient of 2.5°F/100 ft remains considerably higher than the average temperature gradient of continents (approximately 2.3°F/100 ft) and still holds the potential to convert kerogen to hydrocarbons, or hydrocarbons to carbon dioxide (CO_2), given sufficient depth. The work of Meixner et al (2000) on the nature of basement to the Cooper Basin identified an extensive array of plutonic rocks throughout the Nappamerri Trough, as well as calcareous-rich sediments that are poor conductors of temperature. Relatively shallow Big Lake Granodiorite exists below the Moomba/Big Lake Field and the deeper section of the Nappamerri Trough (granite below the Nappamerri trough up to 3,500 m) (Fig. 10) (Meixner et al, 2000). Basement within the Patchawarra Trough is largely composed of calcareous Warburton Basin sediments that may form a temperature blanketing effect to overlying Cooper Basin sediments, as well as potentially increasing the CO_2 concentration (Fig. 10) (Meixner et al, 2000). Mooracoochie Volcanics are Early Cambrian Age and lost any heating potential long before the Cooper Basin sediments were deposited, and are found along the Gidgealpa Field region and the northernmost portion of the Patchawarra Trough, with calcareous-rich Warburton Basin sediments intersected elsewhere in the basin (Fig. 10) (Meixner et al, 2000). Some authors suggest that increased geothermal gradients may be linked to high uranium content in basement rock, and potentially controlled by thick coal measures that act as thermal blankets that retain heat at depth (Holgate, 2005; Khair et al, 2015). This is most evident within the Patchawarra Trough, which is known to contain much thicker coal measures than the Nappamerri Trough and, as such, these areas are seen to have contrasting geothermal gradients.

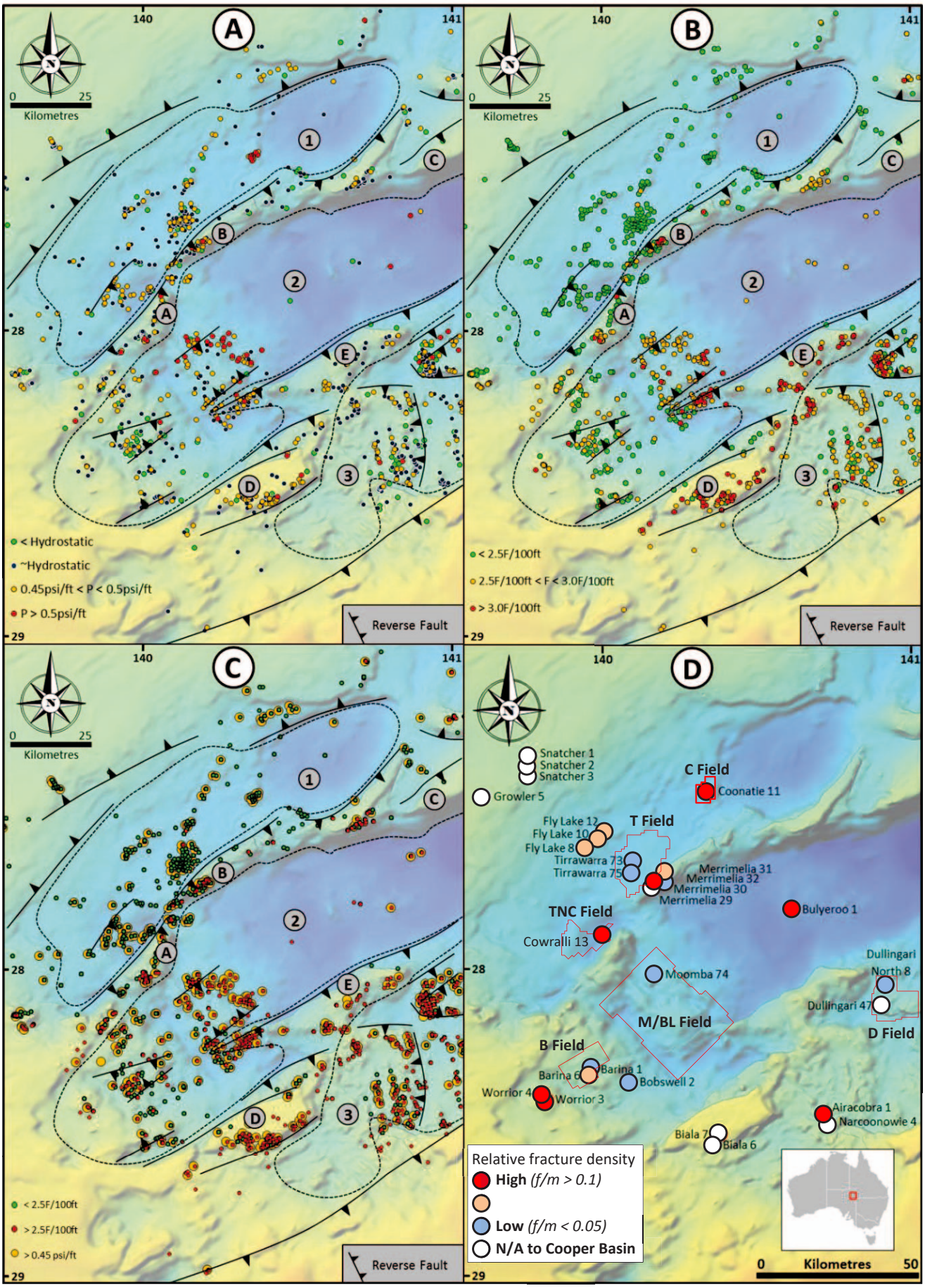


Figure 5. [A] Maximum pressure gradient per well. [B] Maximum temperature gradient per well. [C] Displaying overpressured (>0.45 psi/ft) wells overlain by maximum temperature gradients per well. [D] Relative natural fracture density per well for the Cooper Basin (fracture count/thickness). Locations of the Moomba/Big Lake (M/BL) Field, Coonatie (C) Field, Dullingari (D) Field, Tindilpie/Nephrite/Cowralli (TNC) Field, Barina (B) Field, and Tirrawarra (T) Field are shown.

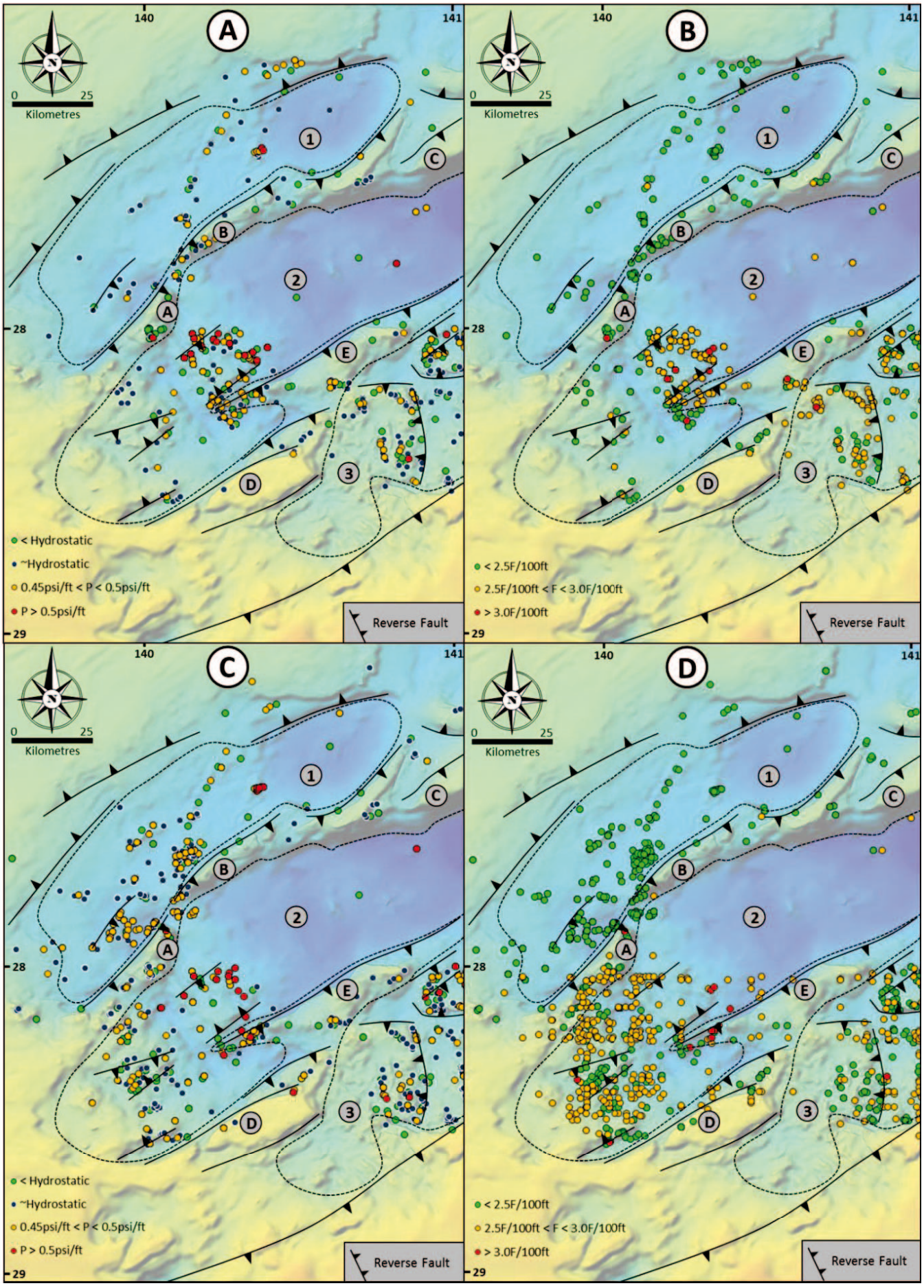


Figure 6. [A] TDREM stratal unit maximum pressure gradient per well. [B] TDREM maximum temperature gradient per well. [C] Patchawarra Formation maximum pressure gradient per well. [D] Patchawarra Formation maximum temperature gradient per well.

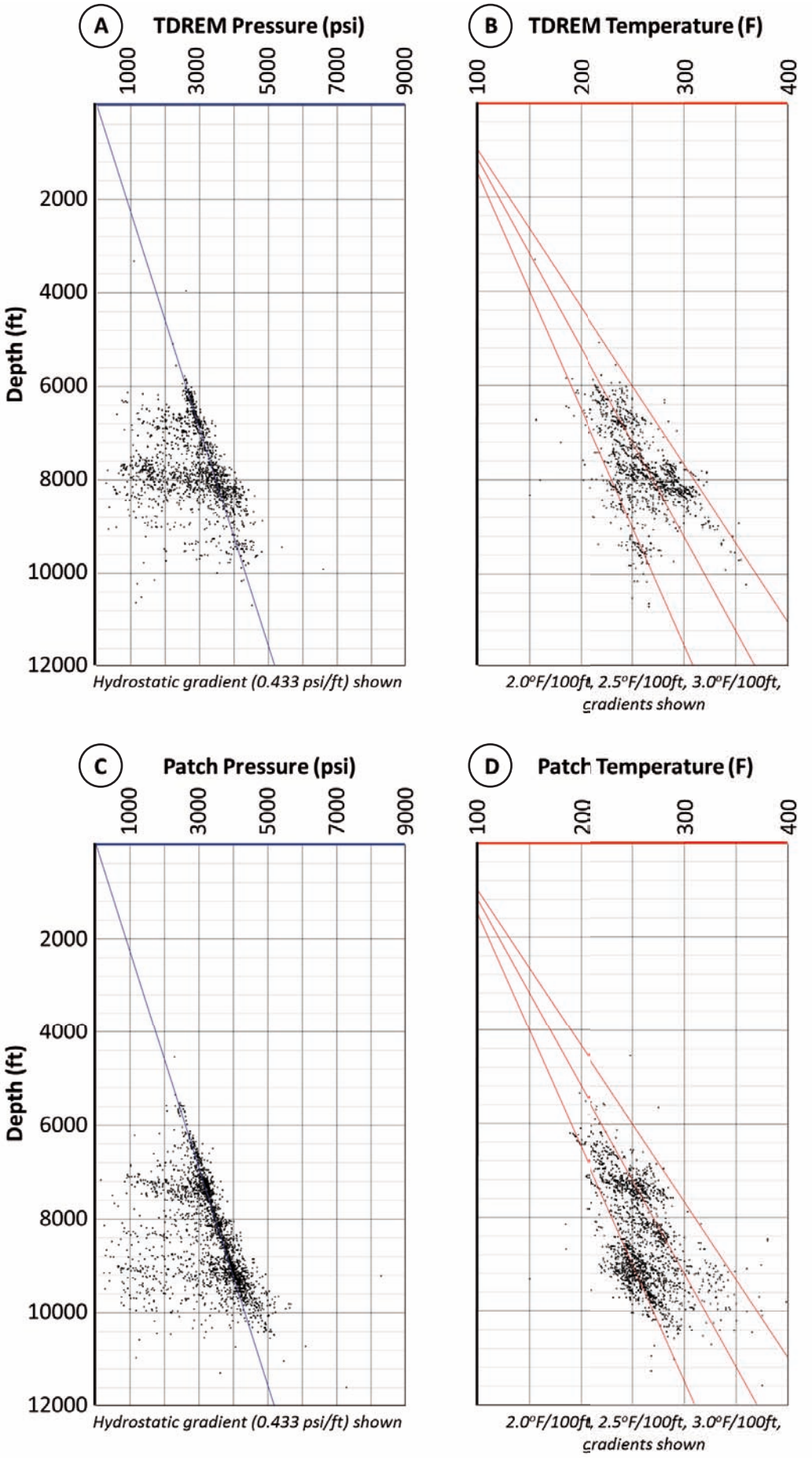


Figure 7. [A] TDREM stratal unit pressure profile. [B] TDREM stratal unit temperature profile. [C] Patchawarra Formation pressure profile. [D] Patchawarra Formation temperature profile.

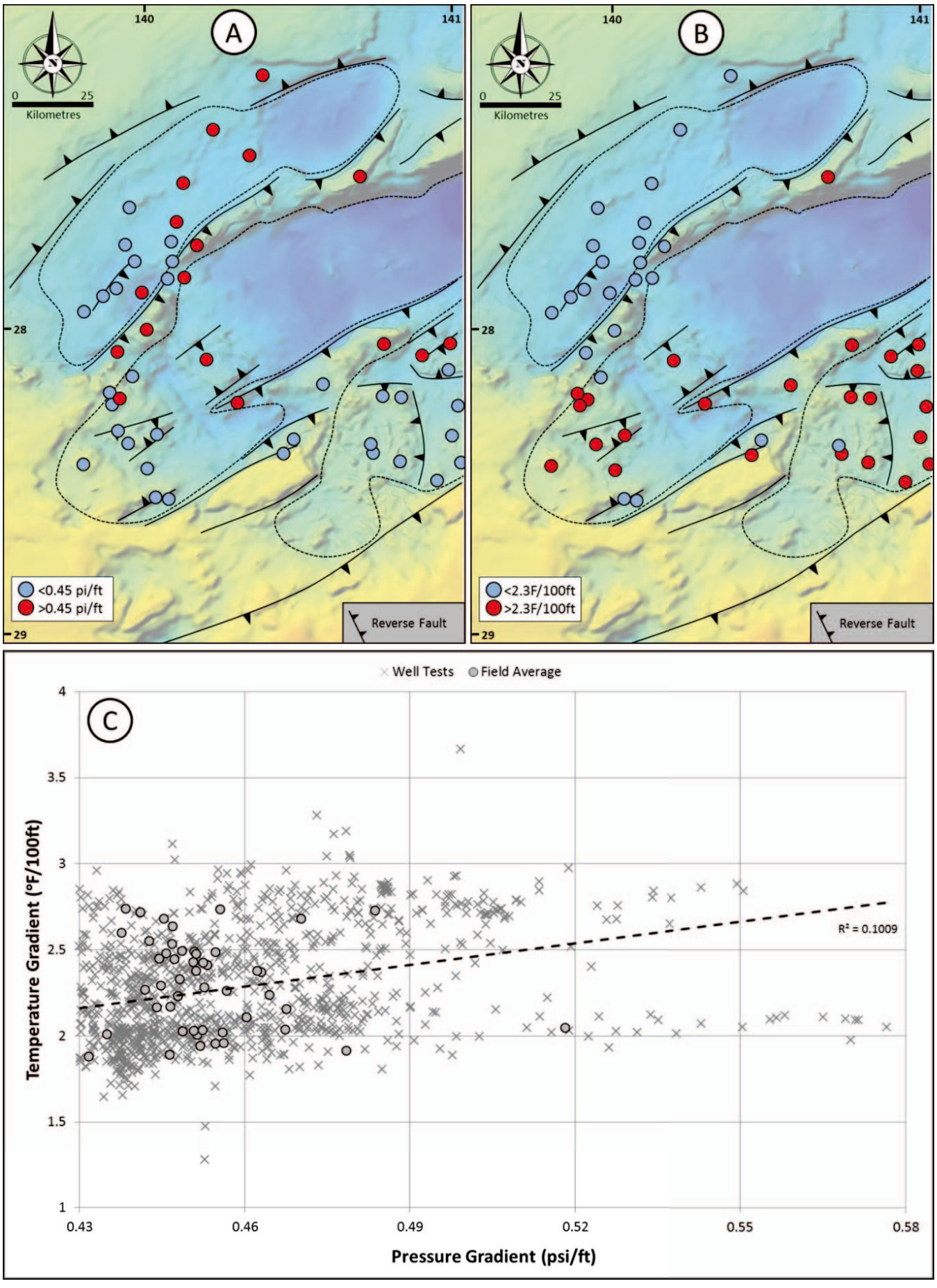


Figure 8. [A] The average pressure gradient distribution of individual fields. [B] The average temperature gradient distribution of individual fields. [C] A cross plot of pressure and temperature gradients of individual well tests and average field values. There appears to be little correlation between the two variables, evident by a low R^2 value.

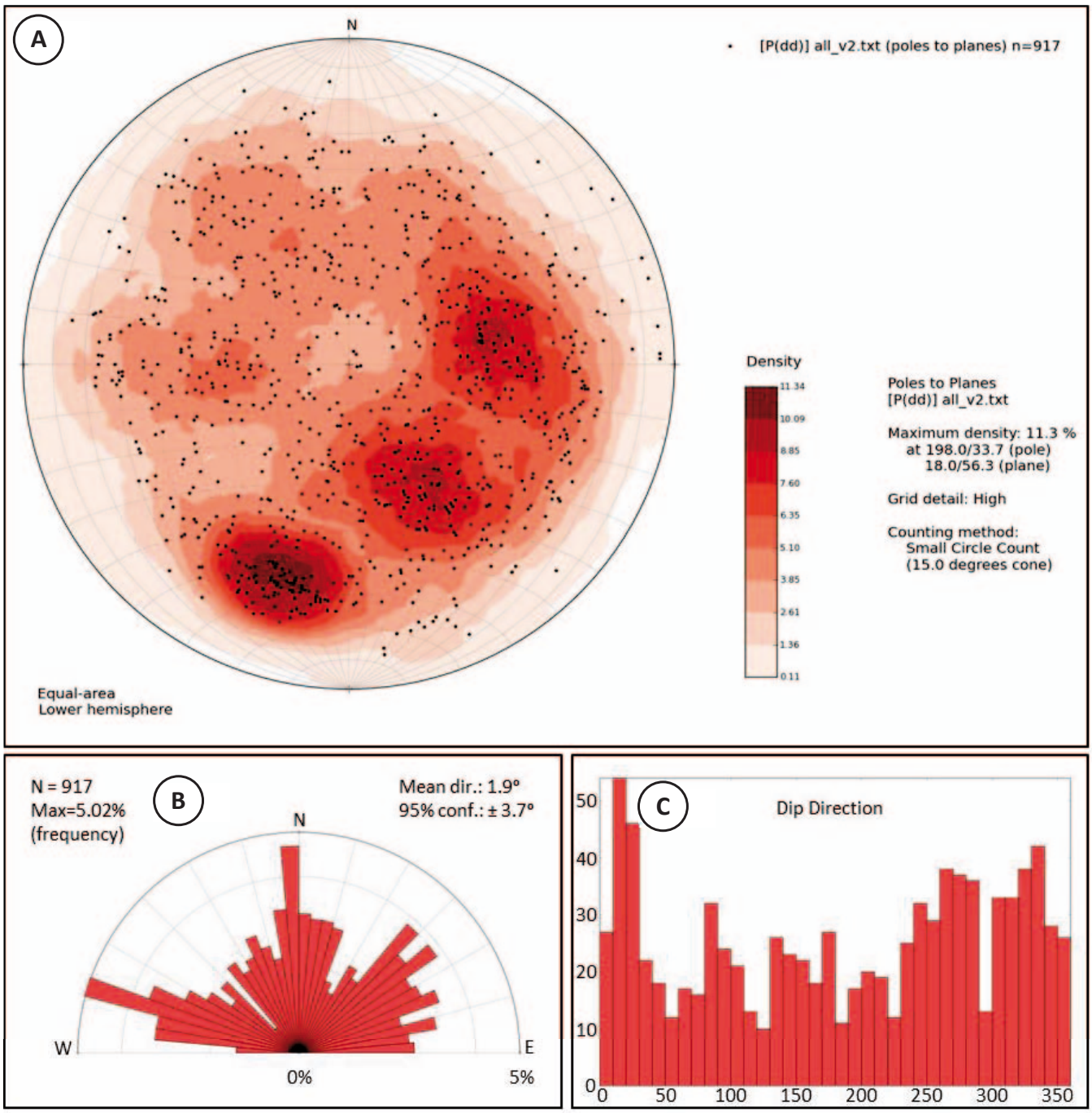


Figure 9. Complete natural fracture data shown as: [A] poles to planes; [B] strike; and, [C] a bar graph showing the frequency distribution of dip directions. Analysis performed using OpenStereo (Grohmann and Campanha, 2010).

The temperature distribution within this study area appears to somewhat correlate with the distribution of these plutonic rocks, particularly their noticeable absence within the relatively low geothermal gradient Patchawarra Trough (Fig. 10). Geothermal gradients across the basin also appear to change with changing pressure gradients. To better illustrate a potential relationship between increased geothermal gradient and overpressure, the authors integrate the data to only show overpressured (>0.45 psi/ft) locations (Fig. 5c). Overpressure appears to occur in regions of high geothermal gradient in some areas; however, there does not appear to be a substantial relationship between the two variables, made obvious by cross-plotting pressure and temperature gradients (Fig. 8c). The low correlation ($R^2 = 0.1$) infers that overpressure generation is not linked to increased temperature gradients within the basin. Previous work on overpressure generation in the Cooper Basin (van Ruth and Hillis, 2000; van Ruth et al, 2003) has found that an increase in mean stress of 50 MPa since the Late Cretaceous may be a dominant mechanism for overpressure. It is important to note that the influence of fluid expansion and hydrocarbon generation mechanisms at present day may have a substantial contribution to overpressure, particularly as the heat flow of the basin has substantially increased by up to 20 mW/m^2 in the past five million years, which has resulted in a 122°F increase in the average temperature of Permian sediments (Deighton and Hill, 1998). The potential for organic rich rocks to be generating under present-day conditions has been explored by Mavromatidis (2006) through vitrinite reflectance analysis, concluding that the Patchawarra Formation reached a vitrinite reflectance equivalent to that of mid maturity for oil generation (0.7% Ro) in the Cenozoic prior to the present-day increase in heat flow. It is possible that this relatively recent increase in the geothermal gradient of the basin may be linked to areas of overpressure

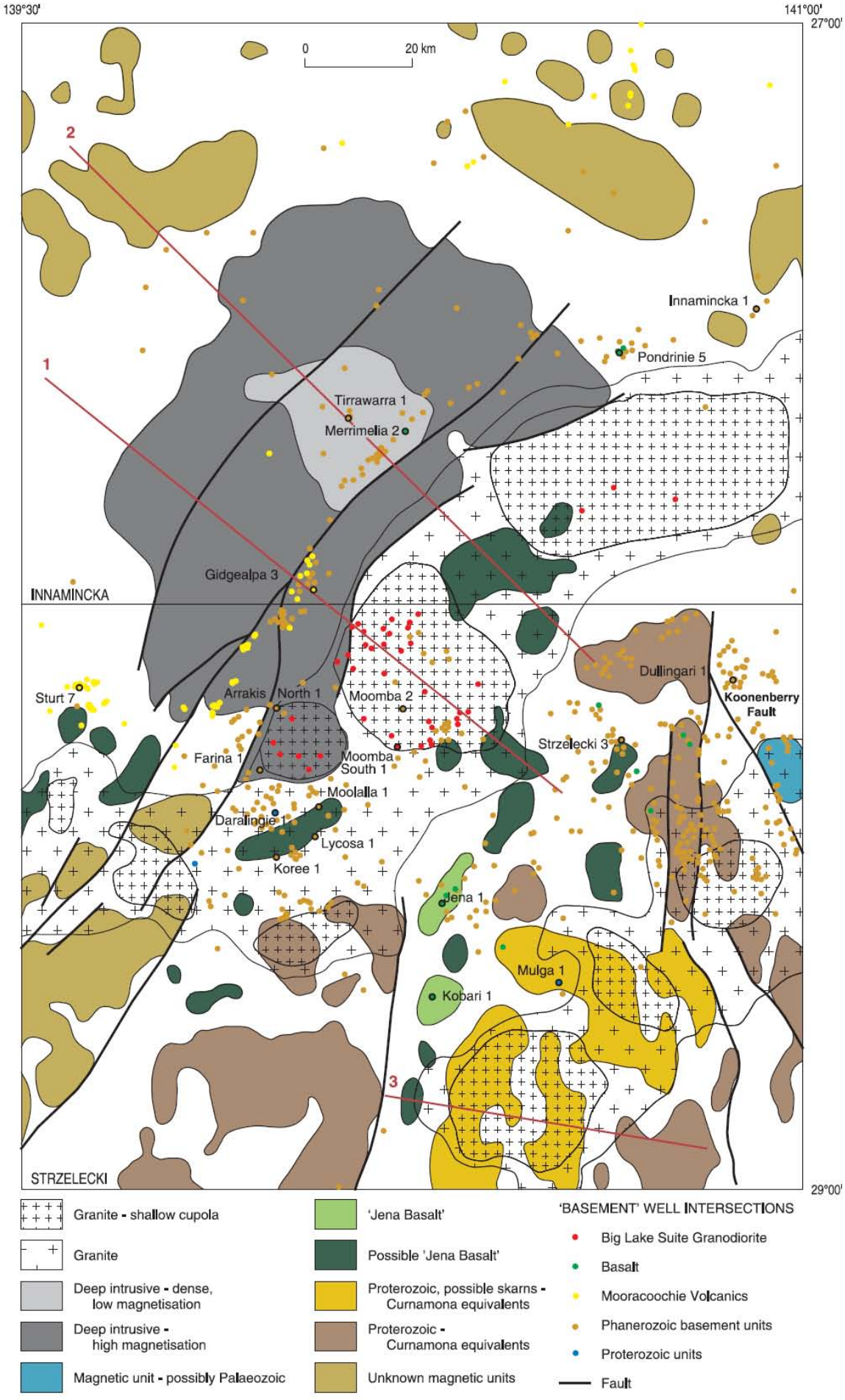


Figure 10. The basement rock units and structure below the Cooper Basin (Meixner et al, 2000).

through fluid expansion or hydrocarbon generation mechanisms, as well as the possibility of hydrocarbons being converted to CO_2. To better understand and potentially constrain the origin of overpressure within the basin, future work should investigate the feasibility of using pressure, vertical stress and sonic velocity relationships (Bowers, 1995).

Irrespective of the mechanism for overpressure generation, the fundamental rock failure principals state that the likelihood of rocks to undergo shear failure or reactivation are enhanced with increased pore pressure, effectively shifting the Mohr's circle closer to the failure envelope (Anderson, 1951; Barton et al, 1995). Under the typical stress conditions exhibited in the basin, coupled with increased pore pressure, it is well known that shear failure is likely (Nelson et al, 2007). The authors, however, do not observe an obvious relationship between relatively high normalised natural fracture density and overpressure (Fig. 5). This may infer that the effect of overpressure is relatively small and is not sufficiently high to induce shear failure in these areas when compared to the relative magnitude of structural events that have affected the basin through time. This high-level view of the relationship between high geothermal gradient and overpressure will encourage researchers and operating companies to investigate the field scale applicability of this study, while also investigating the potential for use of seismic attribute analysis for natural fracture detection and identifying lateral and vertical trends in overpressure.

CONCLUSIONS

The Cooper Basin is Australia's largest onshore hydrocarbon basin, with tremendous potential in unconventional reserves; however, to safely and effectively extract hydrocarbons from these low permeability reservoirs, a thorough understanding of the regional distribution of overpressure, temperature and fracture density is needed. This research presents a collation of pressure and temperature data from 1,095 wells from across the SA portion of the basin, and presents natural fracture densities from 28 interpreted borehole image logs. The authors' results show a significantly high geothermal gradient exceeding 2.5°F/100 ft across a majority of the study area. The Patchawarra Trough, however, appears to contain a much lower geothermal gradient than other areas, likely due to the lack of Big Lake Granites, which are rich in uranium. High geothermal gradient areas such as the Moomba/Big Lake Field and deeper portions of the Nappamerri Trough contain Big Lake Granodiorite and appear to have a close association with overpressures. Although the authors cannot confirm a direct relationship between overpressure and increased geothermal gradient, it should be noted that there is potential for fluid expansion and hydrocarbon generation mechanisms to contribute to the observed overpressures found in the Cooper Basin, particularly as the regional average heat flow has increased by approximately 20mW/m^2 in the past five million years. Although no obvious relationships exist between natural fracture density and pressure at such a high-level view, research into constraining the timing of natural fracture development would be useful for assessing the risk of natural fractures being open to fluid flow and acting as migration pathways during periods of hydrocarbon generation and migration. A complete natural fracture study showcasing the various natural fracture geometries throughout the basin could benefit operating companies with optimising well trajectories and hydraulic fracture stimulation treatments.

This research presents an initial and high-level analysis of the relationships between overpressure, geothermal gradient and natural fracture density in the Cooper Basin to provide a basic understanding of the spatial distributions and variability within the region. Future work should investigate the feasibility of using pressure, vertical stress and sonic velocity relationships to better constrain the overpressure generation mechanism within the basin, while incorporating field scale seismic attribute analysis for natural fracture detection and locating overpressure.

ACKNOWLEDGEMENTS

The authors would like to acknowledge the financial contribution made by the GeoFrac Consortium, which includes the sponsoring companies Santos, Beach Energy, Chevron, Halliburton, and BG Group (QGC). The authors would also like to thank Paradigm (Geolog) for their generous donation of academic licensing, and Carlos H. Grohmann and Ginaldo A.C. Campanh for OpenStereo 0.1.2.

REFERENCES

ALEXANDER, E.M., GRAVESTOCK, D.I., CUBITT, C. AND CHANEY, A., 1998—Lithostratigraphy and environments of deposition. In: Gravestock, D.I., Hibburt, J.E. and Drexel, J.F. (eds) Petroleum Geology of South Australia. Volume 4: Cooper Basin. Adelaide: Department of Primary Industries and Resources.

ANDERSON, E.M., 1951—The dynamics of faulting. Edinburgh: Oliver and Boyd.

APAK, S.N., STUART, W.J., LEMON, N.M. AND WOOD, G., 1997—Structural evolution of the Permian Triassic Cooper Basin, Australia: relation to hydrocarbon trap styles. AAPG Bulletin, 81 (4), 533–55.

BARTON, C.A., ZOBACK, M.D. AND MOOS, D., 1995—Fluid flow along potentially active faults in crystalline rock. Geology, 23 (8), 683–6.

BEARDSMORE, G.R. AND CULL, J.P., 2001—Crustal heat flow: a guide to measurement and modelling. Cambridge: Cambridge University Press.

BERRY, F.A., 1973—High fluid potentials in California Coast Ranges and their tectonic significance. AAPG Bulletin, 57 (7), 1,219–49.

BETHKE, C.M. AND MARSHAK, S., 1990—Brine migrations across North America-the plate tectonics of groundwater. Annual Review of Earth and Planetary Sciences, 18, 287–315.

BILOTTI, F. AND SHAW, J.H., 2005—Deep-water Niger Delta fold and thrust belt modelled as a critical-taper wedge: the influence of elevated basal fluid pressure on structural styles. AAPG Bulletin, 89 (11), 1,475–91.

BOREHAM, C.J. AND HILL, A.J., 1998—Source rock distribution and geochemistry. In: Gravestock, D.I., Hibburt, J.E. and Drexel, J.F. (eds) Petroleum Geology of South Australia. Volume 4: Cooper Basin. Adelaide: Department of Primary Industries and Resources.

BOWERS, G.L., 1995—Pore pressure estimation from velocity data: accounting for overpressure mechanisms besides undercompaction. SPE Drilling & Completion, 10 (2), 89–95.

BRADSHAW, M.T., 1993—Australian petroleum systems. PESA Journal, 21, 43–53.

BREDEHOEFT, J.D., DJEVANSHIR, R.D. AND BELITZ, K.R., 1988—Lateral fluid flow in a compacting sand-shale sequence, south Caspian Sea. AAPG Bulletin, 72 (4), 416–24.

BURRUS, J., 1998—Overpressure models for clastic rocks, their relation to hydrocarbon expulsion: a critical re-evaluation. In: Law B.E., Ulmishek G.F. and Slavin V.I. (eds) Abnormal Pressures in Hydrocarbon Environments. AAPG Memoir 70, 35–63.

DEIGHTON, I. AND HILL, A.J., 1998—Thermal and burial history. In: Gravestock, D.I., Hibburt, J.E. and Drexel, J.F. (eds) Petroleum Geology of South Australia. Volume 4: Cooper Basin. Adelaide: Department of Primary Industries and Resources.

FANG, H., YONGCHUAN, S., SITIAN, L. AND QIMING, Z., 1995—Overpressure retardation of organic-matter maturation and petroleum generation: a case study from the Yinggehai and Qiongdongnan Basins, South China Sea. AAPG Bulletin, 79 (4), 551–62.

FINKBEINER, T., ZOBACK, M., STUMP, B.B. AND FLEMINGS, P.H., 2001—Stress, pore pressure, and dynamically constrained hydrocarbon columns in the south Eugene Island field, Gulf of Mexico. AAPG Bulletin, 85 (6), 1,007–31.

GE, S. AND GARVEN, G., 1989—Tectonically induced transient groundwater flow in foreland basin. In Price, R.A. (ed.) Origin and Evolution of Sedimentary Basins and their Energy and Mineral Resources. Washington, D.C.: American Geophysical Union.

GEOTRACK, 1997—Apatite fission track analysis from several Cooper and Eromanga wells, South Australia. Geotrack Report 668 prepared for Mines and Energy South Australia. Open file Envelope, 8426. Adelaide: Department of Primary Industries and Resources.

GRAULS, D.J. AND BALEIX, J.M., 1994—Role of overpressures and in situ stresses in fault-controlled hydrocarbon migration: a case study. Marine and Petroleum Geology, 11 (6), 734–42.

GRAVESTOCK, D.I. AND JENSEN-SCHMIDT, B., 1998—Structural setting. In: Gravestock, D.I., Hibburt, J.E. and Drexel, J.F. (eds) Petroleum Geology of South Australia. Volume 4: Cooper Basin. Adelaide: Department of Primary Industries and Resources.

GREEN, P.M., BRAIN, T.J. AND JOHN, B.H., 1989—Possible stratigraphic controls on hydrocarbon distribution within the Jurassic-Early Cretaceous rocks, Eromanga Basin, southern Queensland. In: O'Neil, B.J. (ed.) The Cooper and Eromanga Basins, Australia. Proceedings of the Cooper and Eromanga Basins Conference. Adelaide: PESA, SPE, ASEG (SA branches).

GROHMANN, C.H. AND CAMPANHA, G.A.C., 2010—OpenStereo: Open Source, Cross-Platform Software for Structural Geology Analysis. 2010 AGU Fall Meeting, San Francisco, California, 13–17 December, IN31C-06.

HOFFMAN, K.L., 1989—The influence of pre-Jurassic tectonic regimes on the structural development of the southern Eromanga Basin, Queensland. In: O'Neil, B.J. (ed.) The Cooper and Eromanga Basins, Australia. Proceedings of the Cooper and Eromanga Basins Conference. Adelaide: PESA, SPE, ASEG (SA branches).

HOLGATE, F., 2005—Exploration and evaluation of the Australian geothermal resource. PhD thesis. Canberra: Australian National University.

KANTSLER, A.J., PRUDENCE, T.J.C., COOK, A.C. AND ZWIGULIS, M., 1983—Hydrocarbon habitat of the Cooper/Eromanga basin, Australia. The APEA Journal, 23 (1), 75–92.

KHAIR, H.A., COOKE, D. AND HAND, M., 2015—Seismic mapping and geomechanical analyses of faults within deep hot granites, a workflow for enhanced geothermal system projects. Geothermics, 53 (January 2015), 46–56.

KUANG, K.S., 1985—History and style of Cooper–Eromanga Basin structures. Exploration Geophysics, 16 (2/3), 245–8.

KULIKOWSKI, D., AMROUCH, K., AL BARWANI, K.H.M., LIU, W. AND COOKE, D., 2015—Insights into the tectonic stress history and regional 4D natural fracture distribution in the Australian Cooper Basin using Etchecopar's calcite twin stress inversion technique, 2D/3D seismic interpretation and natural fracture data from image logs and core. AAPG ICE, Melbourne, Victoria, 13–16 September, extended abstract #2224164.

LOWE-YOUNG, B.S., MACKIE, S.I. AND HEATH, R.S., 1997—The Cooper-Eromanga petroleum system, Australia: investigation of essential elements and processes. Proceedings of an International Conference on Petroleum Systems of SE Asia and Australasia, 199–211.

MANN, D.M. AND MACKENZIE, A.S., 1990—Prediction of pore fluid pressures in sedimentary basins. Marine and Petroleum Geology, 7 (1), 55–65.

MAVROMATIDIS, A., 2006—Burial/exhumation histories for the Cooper–Eromanga Basins and implications for hydrocarbon exploration, Eastern Australia. Basin Research, 18 (3), 351–73.

MCGOWEN, J.M., GILBERT, J.V. AND SAMARI, E., 2007—Hydraulic Fracturing Down Under. Hydraulic Fracturing Technology Conference, College station, Texas, 29–31 January, SPE-106051-MS.

MEISSNER, F.F., 1978—Petroleum geology of the Bakken Formation. Williston Basin Symposium, Montana Geological Society 24th Annual Conference, 207–27.

MEIXNER, T.J., GUNN, P.J., BOUCHER, R.K., YEATES, T.N., RICHARDSON, L.M. AND FREARS, R.A., 2000—The nature of the basement to the Cooper Basin region, South Australia. Exploration Geophysics, 31 (1/2), 24–32.

MOORE, P.S., 1986—An exploration overview of the Eromanga Basin. In: Gravestock, D.I., Moore, P.S. and Pitt, G.M. (eds) Contributions to the Geology and Hydrocarbon Potential of the Eromanga Basin. Geological Society of Australia Special Publication, 12. Sydney: Geological Society of Australia.

NELSON, E.J., CHIPPERFIELD, S.T., HILLIS, R.R., GILBERT, J. AND MCGOWEN, J., 2007—Using geological information to optimize fracture stimulation practices in the Cooper Basin, Australia. Petroleum Geoscience, 13 (1), 3–16.

NIE, X., ZOU, C., PAN, L., HUANG, Z. AND LIU, D., 2013—Fracture analysis and determination of in-situ stress direction from resistivity and acoustic image logs and core data in the Wenchuan Earthquake Fault Scientific Drilling Borehole-2 (50–1370 m). Tectonophysics, 593 (8 May 2013), 161–71.

OSBORNE, M.J. AND SWARBRICK, R.E., 1997—Mechanisms for generating overpressure in sedimentary basins: a re-evaluation. AAPG Bulletin, 81 (6), 1,023–41.

POKALAI, K., FEI, Y., AHMED, M., HAGHIGHI, M. AND GONZALEZ PERDOMO, M.E., 2015—Design and optimisation of multi-stage hydraulic fracturing in a horizontal well in a shale gas reservoir in the Cooper Basin, South Australia. The APPEA Journal, 55, 1–14.

POKOLAI, K., KULIKOWSKI, D., JOHNSON, Jr., R.L., HAGHIGHI, M. AND COOKE, D., 2016—Development of a new approach for hydraulic fracturing in tight sand with pre-existing natural fractures. The APPEA Journal, in review.

REYNOLDS, S.D., MILDREN, S.D., HILLIS, R.R. AND MEYER, J.J., 2006—Constraining stress magnitudes using petroleum exploration data in the Cooper–Eromanga Basins, Australia. Tectonophysics, 415 (1), 123–40.

REZAEE, M.R. AND SUN, X., 2007—Fracture - filling cements in the Palaeozoic Warburton Basin, South Australia. Journal of Petroleum Geology, 30 (1), 79–90.

SIBSON, R.H., 1990—Conditions for fault-valve behaviour. Geological Society, London, Special Publications, 54 (1), 15–28.

SPENCER, C.W., 1987—Hydrocarbon generation as a mechanism for overpressuring in Rocky Mountain region. AAPG Bulletin, 71 (4), 368–88.

SUN, X., 1997—Structural style of the Warburton Basin and control in the Cooper and Eromanga Basins, South Australia. Exploration Geophysics, 28 (3), 333–9.

TINGAY, M., HILLIS, R., SWARBRICK, R., MORLEY, C. AND DAMIT, A., 2007—"Vertically transferred" overpressures in Brunei: evidence for a new mechanism for the formation of high magnitude overpressures. Geology, 35 (11), 1,023–6.

TINGAY, M.R., HILLIS, R.R., SWARBRICK, R.E., MORLEY, C.K. AND DAMIT, A.R., 2009—Origin of overpressure and pore-pressure prediction in the Baram province, Brunei. AAPG Bulletin, 93 (1), 51–74.

VAN RUTH, P. AND HILLIS, R., 2000—Estimating pore pressure in the Cooper Basin, South Australia: sonic log method in an uplifted basin. Exploration Geophysics, 31 (1/2), 441–7.

VAN RUTH, P., HILLIS, R., TINGATE, P. AND SWARBRICK, R., 2003—The origin of overpressure in 'old' sedimentary basins: an example from the Cooper Basin, Australia. Geofluids, 3 (2), 125–31.

WANGEN, M., 2001—A quantitative comparison of some mechanisms generating overpressure in sedimentary basins. Tectonophysics, 334 (3–4), 211–34.

YASSIR, N.A. AND BELL, J.S., 1996—Abnormally high fluid pressures and associated porosities and stress regimes in sedimentary basins. SPE Formation Evaluation, 11 (1), 5–10.

Authors' biographies next page.

THE AUTHORS



David Kulikowski holds a BSc (Honours) in petroleum geoscience and geophysics, and is now completing a PhD by publication in structural geology at the Australian School of Petroleum, University of Adelaide. David's main research interests are in better understanding the structural and stress history of the Cooper Basin through the integration of micro- (calcite twinning), meso- (natural fractures) and macro-scale (faults) structural data.

David is a recipient of the 2015 American Association of Petroleum Geologists (AAPG) Grants-in-Aid Foundation Scholarship. He was also a team member in the first Australian team to win the prestigious Asia-Pacific Region AAPG Imperial Barrel Award (IBA) in 2014. During the early stages of his PhD, David was employed as a part-time technical assistant at Santos in the gas production and optimisation engineering team.

david.kulikowski@adelaide.edu.au



Dennis Cooke has a PhD in geophysics from the Colorado School of Mines, and more than 25 years of experience in oil and gas exploration and development. He is a past-president of the Australian Society of Exploration Geophysicists (ASEG), and a former vice president of the Society of Exploration Geophysicists (SEG).

Dennis owns and operates ZDAC Geophysical Technology, which provides technology and services for seismic inversion and reservoir characterisation. He is an Adjunct Assistant Professor at the University of Adelaide's Australian School of Petroleum.

dennis.cooke@adelaide.edu.au



Khalid Amrouch is a Lecturer/researcher at the Australian School of Petroleum. He joined the University of Adelaide in 2013.

He started his career by working for five years as a structural geologist in the IFPEN (Institut Français du Pétrole Énergies Nouvelles), and he was also a member of the crustal deformation team of the tectonic laboratory at Paris VI University (Pierre and Marie Curie). He also worked in Mines PariTech as a geologist engineer, where his main objective was to study the chronological history of fractures evolution using a field geotechnical analysis of different fracture sets.

Khalid's main research interests relate to stress/strain patterns and the understanding of the kinematics and (micro/meso) deformation mechanisms of folded and fractured sedimentary formations, timing of deformation and tectonic history. Recently he has focused his interests on fractures chronology and on the principal paleostress, and strain quantification and fracture stimulation in sedimentary rocks.

khalid.amrouch@adelaide.edu.au

5.9. MANUSCRIPT 9: Review of the Cooper and Eromanga Basins

A comprehensive review of the Cooper and Eromanga Basins, Australia

The purpose of this study is to provide readers with a holistic insight into Australia's largest hydrocarbon province, the Cooper-Eromanga Basin, that includes: (1) a modern tectonostratigraphic evolution model; (2) a summary of geomechanical modelling results that predict fault and fracture reactivation (tensile and shear) through time to better understand hydrocarbon migration pathways; (3) a synthesis of the petroleum system processes and elements; (4) the spatial and temporal distributions of permeable natural fracture networks away from the wellbore; (5) common hydraulic fracturing and well surveillance programs contrast with the common difficulties and risks; (6) a discussion on the seismic time-to-depth conversion methods that are being used and their individual accuracies and limitations; (7) current and future hydrocarbon exploration and development targets; and (8) future research opportunities that will directly impact exploration and development programs.

This review forms a knowledge platform that can be disseminated by operating companies to provide employees with a modern overview of this highly prospective basin. The detailed methodologies and collation of cutting-edge research and novel approaches also forms a research framework that can be applied to other hydrocarbon provinces.

CITATION:

Kulikowski, D., Amrouch, K., Pokalai, K., & Gray, M.E. (2017). A Comprehensive Review of the Cooper and Eromanga Basins, Australia. Unsubmitted.

Statement of Authorship

Title of Paper:	A Comprehensive Review of the Intracratonic Cooper and Eromanga Basins, Australia
Publication Status:	**Manuscript Unsubmitted**
Publication Details:	Kulikowski, D., Amrouch, K., Pokalai, K., & Gray, M.E. (2017). A Comprehensive Review of the Intracratonic Cooper and Eromanga Basins, Australia. Earth-Science Reviews, Unsubmitted.

Principal Author

Principal Author (Candidate):	David Kulikowski		
Contribution to the Paper:	Data collection, interpretation, analysis, and writing.		
Overall percentage (%):	75%		
Certification:	This paper reports on original research I conducted during the period of my Higher Degree by Research candidature and is not subject to any obligations or contractual agreements with a third party that would constrain its inclusion in this thesis. I am the primary author of this paper.		
Signature:		Date:	29 March 2017

Co-Author Contribution

By signing the Statement of Authorship, each author certifies that:

i. the candidate's stated contribution to the publication is accurate (as detailed above);
ii. permission is granted for the candidate to include the publication in the thesis; and
iii. the sum of all co-author contributions is equal to 100% less the candidate's stated contribution.

Name of Co-Author:	Khalid Amrouch (10%)		
Contribution to the Paper:	Supported with the structure, writing and review of paper.		
Signature:		Date:	29 March 2017

Name of Co-Author:	Kunakorn Pokalai (10%)		
Contribution to the Paper:	Writing hydraulic fracture stimulation chapter and support with the writing and review of paper.		
Signature:		Date:	28 March 2017

Name of Co-Author	Michael E. Gray (5%)		
Contribution to the Paper:	Supported with the structure, writing and review of paper.		
Signature:		Date:	29 March 2017

A Comprehensive Review of the Cooper and Eromanga Basins, Australia

David **Kulikowski**[a] (david.kulikowski@adelaide.edu.au)

Khalid **Amrouch**[a] (khalid.amrouch@adelaide.edu.au)

Kunakorn **Pokalai**[a] (kunakorn.pokalai@adelaide.edu.au)

Michael E. **Gray**[a] (michael.e.gray@adelaide.edu.au)

[a]Australian School of Petroleum, University of Adelaide, North Terrace, 5005, Adelaide, Australia.

CORRESPONDING AUTHOR: David Kulikowski

KEY WORDS: Cooper Basin; Eromanga Basin; Tectonic; Seismic; Fault; Fracture; Geomechanics; Geophysics; Hydrocarbon.

ABSTRACT

This review focuses on integrating old literature with present-day models to provide a modern summary of Australia's largest onshore hydrocarbon province, the Cooper-Eromanga Basin, with a focus on structural geology and geophysics. A rapid rise in cutting-edge research has been facilitated by exploration companies transitioning away from the nearly extinct anticlinal theory, to technically more challenging plays within the basin. The purpose of this review is to provide new and existing operating companies, and researchers, with a summary of the recent research developments, together with the fundamentals of the basin, to ensure that the tremendous unconventional hydrocarbon potential is effectively extracted. A modern tectonostratigraphic evolution model is presented alongside the stress magnitude, regime and orientation of the six events that have affected the province (N-S Carboniferous Alice Springs Event; SE-NW Mid-Permian Event; NE-SW Late Permian Daralingie Event; E-W Triassic Hunter-Bowe Event; E-W Late Cretaceous Event; N-S Paleogene Event). Integration of these complete paleo-stress tensors with geomechanical models has constrained the dynamic reactivation (shear and tensile) of faults through time to find that since the critical moment (90 Ma), N-S and E-W striking high angle (50-70°) faults were most likely to facilitate hydrocarbon migration. These form the major topics of discussion; however, the temporal and spatial distribution of natural fractures away from the wellbore, seismic time-to-depth conversion methods and accuracies, petroleum systems elements and processes, current and future exploration programs, common hydraulic fracturing and well surveillance programs, and recommendations for future research are also discussed. This review provides a knowledge platform that can be disseminated by new and existing operating companies to provide employees with a broad and up to date overview of this highly prospective basin. The methodologies, cutting-edge research and novel approaches presented here form a framework that can be applied to other hydrocarbon provinces around the world.

1. INTRODUCTION

The Cooper-Eromanga Basin is Australia's largest onshore hydrocarbon province (Fig. 1) and has been producing oil and gas from tight reservoirs since the first natural gas discovery at Gidgealpa in 1963 (Gravestock et al., 1998a; Radke, 2009; Mackie, 2015). The basin is oil and gas saturated and requires the simplest of structural traps, an anticline, for effecting accumulation and preservation (Apak et al., 1997; Gravestock et al., 1998b; Mackie, 2015). As such, much of the early research has focused on basic structural interpretation of sparse two-dimensional (2D) seismic data that remained in the time-domain, with the primary focus of identifying these anticlinal closures (e.g. Stuart, 1976; Veevers et al., 1982; Elliot, 1983; Kuang, 1985; Stanmore, 1989; Apak et al., 1997; Sun, 1997; Gravestock & Jensen-Schmidt, 1996). The lack of detailed research has been further compounded by the limited expose of rocks at surface, particularly within the South Australian portion of the basin, which has ultimately restricted much of the research to wellbore derived data. However, recent advancements in seismic data acquisition and processing, coupled with novel software applications and approaches, have enabled researchers to better constrain the structural geology and tectonic evolution of the Cooper-Eromanga Basin. A detailed and modern synthesis of this prospective province, with a focus on the structural geology and geophysics, will provide fundamental and up to date understandings that will benefit future hydrocarbon exploration and development programs and highlight the present day research gaps that can be further investigated.

The significantly reduced seismic resolution below Permian coal measures has made research difficult in the past. As a result, the structural and stratigraphic evolution of the province has received conflicting arguments through time, evolving from original models that display normal faults (Kuang, 1985; Gravestock & Jensen-Schmidt, 1996), followed by researchers interpreting the same structures as reverse faults (Apak et al., 1997; Sun et al., 1997), to most recent studies that have presented evidence for extensive, compressional, and strike-slip faulting (Radke, 2009; Grant-Wooley et al., 2014; Kulikowski et al., 2016c, 2017a; Kulikowski & Amrouch, 2017a, 2017b, 2017c). These models are discussed and integrated with recent research to provide a modern tectonostratigraphic evolution model, which includes paleo-stress orientations, magnitudes and stress regimes that have affected the province through time.

This transition of structural models can also be linked to the improvement, and the use, of seismic time-to-depth conversion methods, which can have a significant impact on: (1) the true measurable fault dip angle; (2) the presence or absence of shallow low relief structures; and (3) pseudo structures resulting from high or low velocity heterogeneities. To promote the use and accuracy of high resolution 3D seismic data in future research, we describe the most commonly used seismic

time-to-depth conversion methods, discuss their individual limitations and accuracies, identify the key seismic reflector profiles, and highlight the importance of accurate seismic time-to-depth conversion for future hydrocarbon exploration and research purposes.

Similarly, the improvement of petrophysics, drilling, and hydraulic fracture stimulation technologies has fostered exciting new research on geomechanics, optimisation of drilling programs, and in modelling the intrinsic relationship between hydraulic fracture stimulations and pre-existing natural fractures and faults (Chipperfield et al., 2000; Roberts et al., 2000; Johnson et al., 2002; Johnson and Greenstreet, 2003; McGowen et al., 2007; Scott et al., 2013; Johnson et al., 2015; Pokalai et al., 2016, 2017). Understanding the growth of hydraulic fractures, both temporally and spatially away from the wellbore, has been a strongly debated topic within the province (Scott et al., 2013; Cooke et al., 2015). The high stress environment, the effect of pre-existing natural fractures, the influence of near wellbore pressure loss, and the complexity of intra-formational heterogeneity have contributed to ineffective hydraulic fracture programs in the past (Scott et al., 2013; Cooke et al., 2015; Pokalai et al., 2016; 2017). These issues, together with current hydraulic fracturing practises and well surveillance programs, are discussed to provide fundamental background information for companies, both existing and new, that are investing in the basin.

This recent influx of high quality detailed research has been driven by the transition to a more technically challenging hydrocarbon exploration strategy. Few undrilled anticlinal traps remain within the basin, facilitating the shift to technically more challenging exploration that is focused on identifying new targets such as stratigraphic traps, basin centred gas, deep coals and polygonal fault related accumulations (Lowe-Young et al., 1997; Morton, 1998; Watterson et al., 2000; Hillis et al., 2001; Radke, 2009; Mackie, 2015). This paradigm shift has tremendous opportunities for new investors and existing companies targeting hydrocarbons within this prolific basin. To facilitate this transition, the purpose of this research is to collate and critically discuss published works and integrate the key findings into a single document that provides: (1) a modern tectonostratigraphic evolution model; (2) a summary of geomechanical modelling results that predict fault and fracture reactivation (tensile and shear) through time to better understand hydrocarbon migration pathways; (3) a synthesis of the petroleum system processes and elements; (4) the spatial and temporal distributions of permeable natural fracture networks; (5) common hydraulic fracturing and well surveillance programs contrast with the common difficulties and risks; (6) a discussion on the seismic time-to-depth conversion methods that are being used and their accuracies and limitations; (7) current and future hydrocarbon exploration and development targets; and (8) a discussion on the future research opportunities that can impact the success of future hydrocarbon programs.

This review paper collates and integrates previous research with modern understandings to form a knowledge platform that can be disseminated by new and existing operating companies to provide employees with a broad and up to date overview of this highly prospective basin. The detailed methodologies, cutting-edge research and novel approaches form a framework that can be applied to other hydrocarbon provinces around the world.

Insert Fig. 1

2. MODERN TECTONOSTRATIGRAPHIC EVOLUTION MODEL

Unique to this province, the Silurian to Cambrian Warburton Basin, Triassic to Permian Cooper Basin, Cretaceous to Jurassic Eromanga Basin, and Paleogene to Quaternary Lake Eyre Basin are separated in time by regional unconformities that were developed through successive reactivation of pre-existing faults (Fig. 2) (Kantsler et al., 1984; Bradshaw, 1993; Apak, 1997; Gravestock & Jensen-Schmidt, 1998; Mavromatidis, 2006). These vertically stacked basins have unique spatial extents and unique stratigraphy and hydrocarbon potential. The Warburton Basin is considered basement within this region and consists of volcanic, shallow shelf, deltaic and prograding shoreline deposits (Gatehouse, 1986). The Cooper Basin is the most hydrocarbon-rich, with a large volume of Permian coals that cycle with intra-formational sandstone and shale (Kantsler et al., 1984; Apak et al., 1997; Alexander et al., 1998). The Cooper Basin consists mostly of sediments deposited by fluvial, lacustrine, and swamp conditions. The Eromanga Basin is also hydrocarbon-rich with many of the present day exploration programs targeting oil-rich Jurassic and Early Cretaceous sediments primarily along the western flank of the basin (Lowe-Young et al., 1997). The depositional environment during this time transitioned from fluvial, lacustrine, deltaic, shoreface marine, and open shallow marine (Lowe-Young et al. 1997). The Lake Eyre Basin is presently exposed at surface with no hydrocarbon potential.

The Permian coals are the major hydrocarbon source rock of the basin, and increase in thickness in the South Australian portion of the basin. As such, the major exploration and development targets are located within South Australia (Reynolds et al., 2006). This portion of the basin contains two NE-SW striking ridges; the Gidgealpa-Merrimelia-Innamincka (GMI) Ridge and the Murteree-Nappacoongee (MN) Ridge (Fig. 3b) (Kuang, 1985; Apak et al., 1997; Gravestock & Jensen-Schmidt, 1998). These prominent ridges form the major hydrocarbon fields in the basin and also separate the NE-SW elongate Patchawarra, Nappamerri and Tenappera troughs (Fig. 3). In the following sections, the structural and stratigraphic evolution of this intra-cratonic region will be discussed, with emphasis on the most up-to-date research.

Insert Fig. 2

Insert Fig. 3

2.1 Pre-Cambrian Extension (650-575 Ma)

During the Late Proterozoic much of the worlds landmass was submerged by ocean with a relatively small landmass exposed at surface, consisting of portions of Antarctica, India, South Africa, Congo, and the western portion of Australia (Fig. 4a) (Myers et al., 1996; Boger & Miller, 2003; Collins & Pisarevsky, 2005; Kulikowski and Amrouch, 2017). The ancient Australian landmass was in a similar geometry to present day; slightly rotated in a clockwise direction and bisected in an NNE-SSW direction by the paleo-tectonic plate boundary (Myers et al., 1996; Boger & Miller, 2003; Collins & Pisarevsky, 2005). This boundary is now referred to as the Tasman Line that separates the younger land mass in eastern Australia from the rest of the continent (Haines et al., 2002). Rifting within the Panthalassic Ocean, east of ancient plate, began in the Late Proterozoic (650 Ma) in an approximately SE-NW direction. This regional rifting event affected the then Centralian Superbasin as well as the Warburton Basin, developing SE-NW striking strike-slip faults and NE-SW striking normal faults within the Igneous Meta-sedimentary rocks named the Willyama Supergroup (Veevers & Powell, 1984; Evan, 1988; Apak et al., 1997). These basin- to continent-scale SE-NW strike-slip faults are present within many other Australian provinces (Myers et al., 1996; Gibson et al., 2013).

Deep fault development during the Early Cambrian was concurrent with exhumation of the Mooracoochie Volcanics, which marks the base of the Warburton Basin stratigraphy (Gatehouse, 1986; Sun, 1997; Meixner et al., 2000). Continued extension developed accommodation space for the deposition of shallow shelf sediments that became the Diamond Bog Dolomite (~510 Ma), Coongie Limestone Member (~505-497 Ma), and Kalladeina Formation (~508-485 Ma) (Gatehouse, 1986). As relative sea levels rose, the depositional environment transitioned into low-stand fan, deltaic, and prograding shoreline, which deposited the Narcoonowie Formation (~490 Ma), Pando Formation (~488 Ma), and Innamincka Formation (~485-435 Ma) (Gatehouse, 1986; Rezaee & Sun, 2007). Regional erosion of the upper Innamincka Formation represents the unconformable boundary to the overlying Permian to Triassic Cooper Basin.

Insert Fig. 4

2.2 Carboniferous Alice Springs Event (450-300 Ma)

The Alice Springs Event (ASE) has had a significant influence on the tectonic development of central and northern Australia (Haines et al., 2002). Its effect has been recorded in a number of petroleum

basins and structural provinces, including the Amadeus, Ngalia, Georgina, Wiso, Officer, and Warburton basins, as well as the Arunta and Musgrave inliers (Haines et al., 2002). Calcite twin, natural fracture and fault data from within the South Australian portion of the Warburton Basin has constrained this regional tectonic event to have occurred under a strike-slip stress regime with maximum principal stress in an N-S direction in this region (Fig. 4b) (Kulikowski & Amrouch, 2017a). The effective maximum principal stress magnitude was also calculated (49 MPa) through calcite twin stress inversion (Fig. 4i) (Kulikowski & Amrouch, 2017c). Geomechanical modelling of fault reactivation under this paleo-stress tensor identified N-S and NE-SW striking high angle (50-70°), and SE-NW striking strike-slip faults to be the most likely to reactivate (Kulikowski & Amrouch, 2017c). A NNE-SSW and SE-NW striking vertical conjugate natural fracture set was developed during this event and is present only within the Warburton Basin stratigraphy (Kulikowski & Amrouch, 2017a).

As mentioned earlier, the stratigraphy of this region contains a regional unconformity that separates the Warburton and Cooper basins and is a result of basement fault reactivation, exhumation and erosion of upper Warburton Basin sediments. Carboniferous Big Lake Granodiorite was also exhumed during this event in local regions south of the GMI Ridge and provides elevated contemporary temperature gradients due to their high uranium content (Meixner et al., 2000; Kulikowski et al., 2016a). The Australian continent remained connected to Antarctica during this time and exposed to plate scale glaciation (Collins & Pisarevsky, 2000; Gray & Foster, 2004; Metcalfe, 2013).

As the continent began to escape glaciation during the Late Carboniferous to Early Permian, the glacial Merrimelia Formation (~290 Ma) was deposited onto the regional unconformity, marking the base of the Cooper Basin. The overlying Tirrawarra Formation (~287 Ma) was deposited under a postglacial outwash to braided fluvial depositional environment (Lowe-Young et al., 1997; Mavromatidis, 2006). The Tirrawarra Formation is produced for oil, albeit being deeper and under higher temperatures and pressures than the gas-rich middle to upper Permian and Triassic reservoirs (Gravestock et al., 1998a). The depositional environment transitioned into fluvio-deltaic, lacustrine and swamp during the middle Permian, and deposited repeated cycles of sandstone, shale, and coal to compose the predominantly gas-rich Patchawarra Formation (~285-260 Ma) (Kantsler et al., 1984; Apak et al., 1997; Alexander et al., 1998).

2.3 Mid-Permian Event (290-270 Ma)

During deposition of the Patchawarra Formation, intra-formational on-lapping is observed from seismic data along paleo-structural highs, which are more often than not also the present day

structures (Apak et al., 1997; Gravestock & Jensen-Schmidt, 1998). On-lap is observed between 273 and 270 Ma, inferring that structural highs were present during the Mid-Permian and limited the accommodation space (Apak et al., 1996; Kulikowski & Amrouch, 2017a, 2017b). Seismic interpretation aligns with stress inversion of calcite twin, natural fracture and fault data, which demonstrate a compressional SE-NW oriented event with an effective maximum principal stress magnitude of 56 MPa (Fig. 4i) (Kulikowski & Amrouch, 2017a, 2017c). The far-field stresses likely originated from the approximately NE-SW to N-S striking subduction line along the eastern margin of Australia (Fig. 4c). The paleo-stress conditions likely reactivated E-W, NE-SW and N-S striking high angle (50-70°) faults and developed a regional NE-SW striking low dip angle (30°) conjugate natural fracture set within the Patchawarra, Tirrawarra and Merrimelia formations and also within basement (Kulikowski & Amrouch, 2017a, 2017c).

As compression from the short lived Mid-Permian Event eased, the upper Patchawarra Formation became finer grained and more shale dominated (Apak et al., 1997). An east to west transgression ended the deposition of the Patchawarra Formation, transitioning into a shoreface and lacustrine dominated environment that deposited the Murteree Shale (~264 Ma), Epsilon Formation (~262 Ma), Roseneath Shale (~260 Ma), and Daralingie Formation (~258 Ma) (Bradshaw, 1993; Apak et al., 1997; Lowe-Young et al., 1997; Gravestock & Jensen-Schmidt, 1998; Mavromatidis, 2006). The Roseneath-Epsilon-Murteree (REM) stratal unit represents the major shale gas play in the region with total organic carbon (TOC) values ranging between 1.0 and 4.1% (Jadoon et al., 2016).

2.4 Late Permian Daralingie Event (258 Ma)

Following the deposition of the Daralingie Formation, an erosional unconformity was first identified in 2D seismic data (Apak et al., 1996) and later confirmed through calcite twin stress inversion analysis (Kulikowski & Amrouch, 2017a). This SE-NW oriented strike-slip stress regime event recorded an effective maximum principal stress magnitude of approximately 56 MPa (Fig. 4i) that reactivated NE-SW striking high angle (50-70°) faults (Kulikowski & Amrouch, 2017c). This event is most notable along the NE-SW striking GMI and MN ridges, as a significant portion of the Daralingie Formation was eroded from these areas (Kuang, 1985; Apak et al. 1997; Mavromatidis, 2006). New fracture and fault development was absent during this time, with the stress preferentially accommodated along pre-existing faults (Kulikowski et al., 2017a). The far-field stress was likely related to the N-S striking subduction zone east of Australia during this time (Fig. 4d) (Kulikowski & Amrouch, 2017a).

2.5 Upper Triassic Hunter-Bowen Event (245-190 Ma)

Post-compressional flexural relaxation, or sag, followed the Daralingie Event and generated accommodation space for the deposition of the Toolachee Formation (~250 Ma) that consists of sands, shales and coals deposited under meandering fluvial to deltaic conditions (Kantsler et al. 1984; Apak et al. 1997; Lowe-Young et al., 1997). The depositional environment transitioned to a floodplain, lacustrine and fluvial channel system in the Triassic, depositing the Nappamerri Group, which includes the Callamurra Member (~245 Ma), Panning Member (~243 Ma), Wimma Sandstone Member (~241 Ma), Tinchoo Formation (~238 Ma), and the Cuddapan Formation (~210 Ma) (Kantsler et al. 1984; Apak et al. 1997; Lowe-young et al., 1997; Alexander et al. 1998; Mavromatidis, 2006). The early Nappamerri Group was likely charged with oil and gas from the underlying Toolachee Formation, and perhaps along fault conduits from the deeper early Permian source rocks (Lowe-Young et al., 1997).

A regional erosional unconformity is carved into the upper Tinchoo Formation and the majority of the Cuddapan Formation, which is only present in local areas of the basin (Lowe-Young et al., 1997). This unconformity separates the Cooper and Eromanga basins and marks the timing of the Hunter-Bowen Event. The maximum principal stress was horizontal and in an E-W direction (Fig. 4e) (Kuang, 1985; Apak et al., 1997; Gravestock & Jensen-Schmidt, 1998; Kulikowski & Amrouch, 2017a). The regional erosional boundary was first interpreted from 2D seismic data (Kuang, 1985; Apak et al., 1997) and later confirmed through calcite twin stress inversion, and natural fracture and fault stress inversion (Kulikowski & Amrouch, 2017a). Calcite twin stress inversion results identified an E-W oriented compressional event with an effective maximum principal stress magnitude of 60 MPa (Fig. 4i) corresponding to the Hunter-Bowen Event (Kulikowski & Amrouch, 2017a, 2017c). Geomechanical modelling using this stress tensor identified that NE-SW striking high angle (50-70°) faults were most likely to shear reactivate at this time (Kulikowski & Amrouch, 2017c). Reactivation of predominantly this fault set exhumed and eroded up to 500 meters of Nappamerri Group sediments (Apak et al., 1997; Kantsler et al., 1983; Alexander et al., 1998; Mavromatidis, 2006).

2.6 Late Cretaceous Event (95-55 Ma)

As the Hunter-Bowen Event subsided, flexural relaxation generated accommodation space and a fluvial depositional environment transcended, which deposited the Poolowanna Formation (~200-180 Ma) onto the regional unconformity (Green et al. 1989; Hoffman, 1989; Lowe-Young et al. 1997). Tectonic quiescence continued with the deposition of the braided fluvial Hutton Sandstone (~178-160 Ma), fluvial to lacustrine Birkhead Formation (~157 Ma), and braided fluvial to lacustrine

Mooga Formation (~152 Ma) and Adori Sandstone (~152 Ma) (Green et al. 1989; Hoffman, 1989; Lowe-Young et al. 1997). The braided fluvial to lacustrine depositional environment continued within the region, depositing the Namur Sandstone (~152-140 Ma), Westbourne Formation (~150 Ma), Hooray Sandstone (~141 Ma), and the oil-rich Murta Member (~140 Ma) (Lowe-Young et al., 1997). Jurassic units contain abundant oil (and gas) reservoirs at a shallower depth than Permian reservoirs, and primarily targeted on the western flank of the Cooper Basin (Lowe-Young et al., 1997).

The depositional environment transitioned into fluvial to shallow marine conditions and deposited the Cadna-owie Formation (~140-126 Ma) (Lowe-Young et al., 1997). The overlying Wyandra Sandstone Member (~125 Ma) was deposited under deltaic to shoreface marine conditions and contains some oil and gas potential (Lowe-Young et al., 1997). Following this, the Bulldog Shale (~125-108 Ma) and Wallumbilla Formation (~125-104 Ma) were deposited in restricted open marine conditions, which transitioned into a shoreface depositional environment to deposit the Coorikiana Sandstone (~105 Ma) (Lowe-Young et al., 1997). Shallow open marine conditions developed and deposited the Oodnadatta Formation (~104-98 Ma), Toolebuc Formation (~103 Ma), and Allaru Mudstone (~100 Ma) (Lowe-Young et al., 1997). Finally, the Winton Formation (~97-93 Ma) and Mackunda Formation (~97 Ma) were deposited by fluvial-lacustrine conditions to mark the final period of sediment deposition within the Eromanga Basin (Lowe-Young et al., 1997). These Middle to Late Cretaceous marine sediments also host the regionally extensive polygonal fault system that may present a new target for future exploration (Watterson et al., 2000). The critical moment in the Cooper-Eromanga Basin hydrocarbon system, which marks the time of major hydrocarbon generation, migration, accumulation and preservation, occurred at 90 Ma (Lowe-Young, et al., 1997).

The Winton and Mackunda formations were significantly eroded following their exhumation by the E-W Late Cretaceous compressional Event (Fig. 4f) (e.g. Kuang, 1985; Green et al. 1989; Hoffman, 1989; Apak et al. 1997; Lowe-Young et al. 1997; Gravestock & Jensen-Schmidt, 1998; Mavromatidis, 2006; Kulikowski & Amrouch, 2017a, 2017b). Folding related to pre-existing NE-SW striking faults, rather than reactivation, facilitated the development of this erosional boundary, which separates the Eromanga and Lake Eyre basins (Fig. 2). An effective maximum principal stress magnitude of 59 MPa was measured from calcite twin stress inversion analysis (Fig. 4i) (Kulikowski & Amrouch, 2017c). N-S striking low angle (30°) conjugate natural fractures were developed during this time (Kulikowski & Amrouch, 2017a). Considering that this event occurred during and after the critical moment, understanding the dilation and shear tendency of faults is vital for accurate migration pathway modelling. Under these stress conditions, E-W and NE-SW striking high angle (60°) faults were the most likely to act as hydrocarbon conduits (Kulikowski & Amrouch, 2017c).

2.7 Paleogene Event (33-23 Ma)

During deposition of the Lake Eyre Basin, which is presently at surface, an N-S oriented Paleogene compressional event developed E-W striking low angle (30°) conjugate natural fractures throughout the stratigraphic column (Kulikowski & Amrouch, 2017a). This event is attributed to the northwards movement of the Australian plate (Fig. 4g). The effective maximum principal stress magnitude of this event was calculated from calcite twin stress inversion analysis and found to be 64 MPa (Fig. 4i) (Kulikowski & Amrouch, 2017c). Interestingly, this event does not appear to have reactivated or developed faults; however, N-S and NE-SW striking high angle (50-70°) faults are considered to have been likely to dilate and act as permeable hydrocarbon conduits (Kulikowski & Amrouch, 2017c).

3. PETROLEUM SYSTEM

3.1 Hydrocarbon Source Rocks

Hydrocarbons in the Cooper Basin are principally sourced from intra-formational Permian coals and Permian to Jurassic carbonaceous shales, and reservoired within fluvial sandstones (Fig. 5) (Boreham & Hill, 1998). The petroleum system is largely gas saturated with small volumes of liquids found in localised areas (Kantsler et al., 1984). As such, the isotopic composition of intra-formational coals and carboniferous shales indicates fresh water origin and dominated by high order plants (Kantsler et al., 1984; Boreham & Hill, 1998). The Toolachee, Daralingie, Epsilon and Patchawarra formations contain an average total organic content (TOC) of 3.9% and 6.9 kg/tonne of hydrocarbon (Smyth, 1983; Boreham and Hill, 1998). The most organic-rich source rock is within the Toolachee Formation, averaging 214 kg/tonne (Hydrogen index) across the Cooper Basin (Boreham & Hill, 1998). Liquid hydrocarbon yields are low in Permian reservoirs due to high vitrinite and inertinite (Type III kerogens) composition in shale and coal measures, and are absent within the over mature Nappamerri Trough, which contributes only dry gas (Kantsler et al., 1984; Boreham & Hill, 1998).

Insert Fig. 5

The hydrocarbon source for the overlying Eromanga Basin is more uncertain, and likely to be sourced from: (1) non-marine Jurassic aged rocks (Powell et al., 1989; Lowe-Young et al., 1997); (2) Permian shales and coals that migrated through reactivated faults (Heath et al., 1989; Lowe-Young et al., 1997); and (3) a combination of both Jurassic and Permian source rocks (Fig. 6c) (Kantsler et al., 1984; Gilby et al., 1989; Jennkins et al., 1989; Lowe-Young et al., 1997). Jurassic aged units contain oil and gas; however, only gas has been discovered in Cretaceous aged reservoirs in the Strzelecki, Packsaddle and Nappacoongee regions (Kantsler et al., 1984). Permian aged source rocks

are currently within the gas window, with Jurassic to Cretaceous source rocks currently at peak oil generation (Kantsler et al., 1984).

Insert Fig. 6

3.2 Hydrocarbon Generation

Permian and Triassic source rocks reached the hydrocarbon generation window as early as the Permian to Middle Triassic during maximum burial (Fig. 6), and peaked during a secondary sag period in the Middle Cretaceous (Deighton & Hill, 1998; Mavromatidis, 2006). Relatively minor hydrocarbon generation and expulsion commenced in the Permian to Middle Triassic, before peaking in the Middle to Late Cretaceous and potentially continues today (Fig. 6a & 6b) (Pitt, 1986; Duddy, 1987; Gallagher, 1988; Lowe-Young et al., 1997; Mavromatidis, 2006; Deighton & Hill, 2009). Minor volumes of hydrocarbons were also generated in the Nappamerri Trough during the Permian, and, given sufficient residual kerogen, the effect of Late Tertiary elevated temperatures and Tertiary deposition may have led to secondary (late-stage) hydrocarbon generation and expulsion in certain parts of the basin (Fig. 6b) (Deighton & Hill, 2009).

Although a rare phenomenon, the concentration of carbon dioxide (CO_2) within the Cooper-Eromanga Basin is significantly higher (10-30 v/v%) than typical sedimentary basins (Rigby & Smith, 1981; Kantsler et al., 1984; Wycherley et al., 1999). However, the origin remains somewhat questionable, but likely to be related to magmagenesis or metamorphic reactions, which is supported by the correlation between raised CO_2 levels and the presence of Carboniferous Uranium-rich Moomba-Big Lake Granodiorite (Gatehouse et al., 1995; Wycherley et al., 1999).

3.3 Hydrocarbon Migration

Hydrocarbon generation and expulsion is divided into three phases: (1) early expulsion between the Late Permian and Early Triassic; (2) primary expulsion within the Cretaceous; (3) and a possible secondary expulsion during the Late Cenozoic (Fig. 6) (Lowe-Young et al., 1997; Radke, 2009). These three phases of expulsion coincide with the timing of hydrocarbon migration (Fig. 6c) (Lowe-Young et al., 1997; Radke, 2009). Hydrocarbon generated from Permian source rocks migrated short distances to the vertically stacked overlying or underlying intra-formational reservoirs, or alternatively along deep seated and reactivated basement-involved faults into overlying Eromanga Basin reservoirs (Boreham & Hill, 1998; Gravestock et al., 1998; Radke, 2009). Tertiary hydrocarbon migration through stacked intra-formational seals into overlying reservoirs has also been discussed (Heath et al., 1989; Boult et al., 1998; Gravestock et al., 1998; Hillis et al., 2001; Radke, 2009).

Geomechanical modelling of fault reactivation (dilation and shear) through time highlighted the changing conduit potential of individual fault sets as stress conditions changed (Kulikowski et al., 2016c; Kulikowski & Amrouch, 2017c). See chapter 10 for more detail.

Secondary hydrocarbon migration from Permian source rocks into overlying Jurassic Eromanga Basin reservoirs has been suggested by numerous authors after observing oil compositions that were not consistent with a Jurassic origin (Heath et al., 1989; Hallmann et al., 2007). The origin of Jurassic oils has been found to be from either: (1) Permian source rocks; (2) Jurassic source rocks; or (3) a combination of the two (Smyth, 1983; Heath et al., 1989; Lowe-Young et al., 1997; Hallmann et al., 2007). In the case of Permian source rock origin, secondary migration of oil was through: (1) permeable fault conduits into shallow Eromanga Basin reservoirs; or (2) through a permeable carrier bed in the up-dip direction towards the western Cooper Basin flank, where overlying Triassic sealing units effectively pinch-out and allow the oil to migrate into directly overlying reservoir rocks (Heath et al., 1989; Lowe-Young et al., 1997; Borazjani et al., 2017a, 2017b). This western flank region hosts many large producing oil fields (Heath et al., 1989; Lowe-Young et al., 1997; Borazjani et al., 2017a, 2017b). In these two migration pathway cases, the oil composition between source and reservoir has shown to be different due to the effects of deep bed filtration (Borazjani et al., 2017a, 2017b), or water-washing (Heath et al., 1989) of hydrocarbons.

The ability of a fault to act as a potential hydrocarbon conduit can be measured by calculating the Dilation Tendency, or the likelihood of faults to undergo tensile reactivation. Alternatively the likelihood of faults to shear reactivate can be measured by calculating Slip Tendencies. These likelihoods were calculated for four regional fault sets, which were modelled under six unique paleo-stress tensors (Alice Springs Event, Mid-Permian Event, Daralingie Event, Hunter-Bowen Event, Late Cretaceous Event, and Paleogene Event), as well as the present day stress conditions (Kulikowski et al., 2016c; Kulikowski & Amrouch, 2017c). The results of these studies found that early expulsion of hydrocarbons would have preferentially migrated along NE-SW striking high angle (50-70°) faults during the Late Permian and along E-W striking high angle (50-70°) faults during the Late Triassic. Since the critical moment (90 Ma) hydrocarbons would have preferentially migrated along E-W striking high angle (50-70°) faults during the Late Cretaceous and N-S striking high angle (50-70°) faults during the Paleogene. Hydrocarbons generated during the secondary phase, or present day, would likely be migrating along E-W striking high angle (50-70°) faults or SE-NW strike-slip faults. See Chapter 6.2 for more detail.

3.4 Hydrocarbon Seals and Trap Development

Intra-formational fluvial-lacustrine to lacustrine shales and coal measures form cyclically deposited impermeable seals to underlying reservoirs, while also acting as potential source rocks to overlying reservoirs (Bradshaw, 1993; Gravestock & Jensen-Schmidt, 1998). These vertically stacked intra-formational shales and coals have the highest influence on sealing hydrocarbons within the four-way closing anticlinal traps that are present throughout the basin (Gravestock et al., 1998). The Murteree and Roseneath shales are highly efficient seals to the Patchawarra and Epsilon formations respectively; however, intra-formational shales hold back hydrocarbon to individual and compartmentalised intra-formational sandstone reservoirs (Gravestock et al., 1998). Cretaceous marine sediments and the Late Jurassic Birkhead Formation form regional seals for Jurassic to Early Cretaceous Eromanga Basin reservoirs (Gravestock et al., 1998; Radke, 2009).

The regional Murteree Shale and intra-formational Patchawarra Formation seals are eroded along the western margin of the basin contributing to the significant number of oil discoveries made along the western flank, as oil migrates from the deep sections of the Patchawarra Trough into shallow Eromanga Basin reservoirs (Radke, 2009). Low amplitude structural closures within the Eromanga Basin are sealed by the regional Birkhead and Wallumbilla formations, facilitating the accumulation of hydrocarbons (Radke, 2009; Kulikowski et al., 2016b, 2017c). A regional polygonal fault system is present within Cretaceous sediments and is observed to occasionally penetrate into the hydrocarbon-rich Murta Member (Fig. 7) (Watterson et al., 2000; Kulikowski et al., 2017a). Where these normal faults are approximately E-W striking and penetrate into the Murta Member, hydrocarbons may be migrating through permeable fault conduits into shallow reservoirs, possibly presenting a new exploration strategy (Watterson et al., 2000; Kulikowski et al., 2017a).

Insert Fig. 7

Structural trap development occurred as early as the Mid-Permian Event and Late Permian Daralingie Event, coinciding with the early phase of hydrocarbon generation and expulsion (Deighton & Hill, 1998; Kulikowski & Amrouch, 2017b). Key anticlinal traps were developed by two subsequent events; the E-W Hunter-Bowen Event and E-W Late Cretaceous Event (Kulikowski & Amrouch, 2017a, 2017b). These two events reactivated basement-involved faults to create broad anticlinal domes within the Permian, and low amplitude anticlines within Cretaceous sediments prior to the primary phase of hydrocarbon generation and expulsion (Deighton & Hill, 1998). The N-S Paleogene Event (33-23 Ma) may have contributed to a late-stage of structural trap development; however, this occurred significantly after the critical moment in the hydrocarbon system and may have negatively

influenced the preservation of existing hydrocarbon accumulations (Lowe-Young et al., 1997; Kulikowski & Amrouch, 2017b, 2017c). Although the majority of accumulations are trapped by anticlines, there does exists an opportunity to begin targeting higher risk stratigraphic pinch-out traps and on-lapping features that are common within the basin, particularly within the hydrocarbon-rich Patchawarra Formation (Apak et al., 1997; Kulikowski & Amrouch, 2017b).

3.5 Hydrocarbon Accumulation and Preservation

Hydrocarbons are primarily reservoired within the Tirrawarra Formation, Patchawarra Formation, Murteree Shale, Epsilon Formation, Roseneath Shale, Daralingie Formation, and Toolachee Formation of the Cooper Basin, and the Hutton Formation and Namur Sandstone of the Eromanga Basin (Kantsler et al., 1984; Alexander et al., 1998; Gravestock et al., 1998a; Mackie, 2015). Although these are the dominant oil and gas producers, with the Hutton Sandstone contributing greater than 50% of oil discoveries (by volume) in the Eromanga Basin, hydrocarbons can be found in virtually all reservoir-quality zones older than the Late Cretaceous (Kantsler et al., 1984; Lowe-Young et al., 1997; Radke, 2009). The majority of hydrocarbon discoveries are located within the South Australian portion of the Cooper Basin, reflecting the significantly greater volume of Permian source rocks (Kantsler et al., 1984; Reynolds et al., 2006). Primary hydrocarbon accumulation commenced during the Late Cretaceous critical moment (90 Ma), with existing fields withstanding the Late Cretaceous Event (95-55 Ma), Paleogene Event (33-23 Ma), and the present day stress environment (Fig. 6c) (Kantsler et al., 1984; Lowe-Young et al., 1997; Mackie, 2015; Kulikowski & Amrouch, 2017a).

The preservation of accumulations appears to be unaffected by these three events, as seismic data shows that basement-involved faults were not reactivated; however, sub-seismic resolution faulting may be possible considering that resolution is not better than 15 m (Kulikowski et al., 2017a; Kulikowski and Amrouch, 2017c). Fault reactivation causing less than 15 m of displacement can be sufficient to cause seal breach and facilitate tertiary migration of hydrocarbons, particularly if fault geometries are optimally oriented to tensile reactivate (dilate). Geomechanical modelling of fault reactivation has shown that the most common fault set, NE-SW striking high angle (50-70°), was the most likely to shear reactivate during the four most recent (Daralingie Event, Hunter-Bowen Event, Late Cretaceous Event, Paleogene Event) tectonic events (Kulikowski & Amrouch, 2017c). Under contemporary stresses, SE-NW strike-slip faults are most likely to shear reactivate and must be accurately interpreted because of the high likelihood of interacting with, and complicating, hydraulic fracture stimulations (Pokalai et al., 2016, 2017; Kulikowski et al., 2016c).

4. GEOPHYSICS

4.1 Significant Seismic Reflectors

With the majority of hydrocarbons reservoired within Permian rocks, the top Toolachee Formation, top Patchawarra Formation, and VC Coal seismic reflectors are mostly commonly interpreted. The Cretaceous Cadna-owie Formation reflector (C-reflector) is an easily identifiable and regional strong amplitude reflector typically found at 1000-1500 m (Fig. 8a). Its interpretation provides the structural trap geometry for Jurassic and Cretaceous reservoirs, as well as providing broad insights into the underlying structures. This reflector also shows intermittent normal displacement caused by polygonal faults extending from the Mackunda Formation (AM-reflector) into the deeper hydrocarbon-rich Murta Member (D-reflector) (Fig. 7). The top Nappamerri Group reflector (N-reflector) shows a similar characteristic to the Cadna-owie Formation reflector, although with variable amplitude due to the erosional boundary that it represents at 1500-2000 m (Fig. 8a). This reflector marks the boundary between the Cooper and Eromanga basins.

Insert Fig. 8

Top Permian stratigraphy is identified by an abrupt strong amplitude package at approximately 2000 m that represents the fluvial to deltaic Toolachee Formation (P-reflector) (Fig. 8a). The top Patchawarra Formation (V-reflector) is notoriously bland, attributed to the relatively more transitional boundary between the upper Patchawarra Formation and the Murteree Shale (U-reflector) that results in a low acoustic impedance boundary. As such, the stronger amplitude reflector immediately below the top Patchawarra Formation is typically interpreted (Fig. 8a). Within the Patchawarra Formation, the VC30 and VC50 coal measures produce strong amplitude (soft-kick) reflectors; however, the reflectors commonly split and merge (Fig. 8a). Middle Patchawarra Formation reflectors have been shown to on-lap onto paleo-structures correlating to the Mid-Permian Event (290-270 Ma) (Apak et al., 1997; Kulikowski & Amrouch, 2017b). Below the Permian coal measures, seismic resolution rapidly decays and the interpretation of reflectors and faults becomes difficult (Fig. 8a). The Tirrawarra and Merrimelia formation reflectors are absent in some parts of the basin and require high well control to be interpreted accurately.

Seismic interpretation of the basement (Z-reflector) is again difficult throughout the basin, commonly requiring phantom interpretation through significant fault shadow (Fig. 8a). Seismic resolution has been calculated to be upwards of 150 m, in contrast to Cretaceous reflectors that can be between 15-20 m (Kulikowski et al., 2017a). Recently acquired 3D seismic surveys have much

greater resolution below Permian coal measures, with broadband and full-azimuthal seismic data expected to significantly improve the resolution in the near future.

4.2 Seismic Time-to-Depth Conversion Methods

The seismic time-to-depth conversion process can incur large (10's of feet) errors caused by local velocity anomalies, incorrect well ties, or more commonly from a poor understanding of the near surface ground variation, or statics. Although errors cannot be removed entirely, selecting the most accurate depth conversion method for the given study area can have noticeable effects. For example, the presence of low relief hydrocarbon-rich structural traps within the Eromanga Basin can depend on the depth conversion method being used (Kulikowski et al., 2016b, 2017c). Additionally, fault analysis may lead to incorrect results if seismic data remains in the time-domain, as fault geometries will change once in the depth-domain (Fig. 8b & 8c).

Complete seismic volume time-to-depth conversion is often time consuming and not necessary for generating simply reflector maps. As such, time-to-depth conversion is often performed using gridding software, or horizon maths tools built into seismic processing and interpretation software. For the purpose of generating reflector maps, only the interpreted two-way-time (TWT) seismic reflector grid, rather than the seismic volume, is converted. In the simplest sense, the TWT grid is multiplied by a constant velocity to generate a depth grid. Three seismic time-to-depth conversion methods are commonly used within the Cooper-Eromanga Basin, including the: (1) average velocity method (Fig. 9a); (2) time-depth trend method (Fig. 9b); and (3) interval velocity method (Fig. 9c).

Insert Fig. 9

4.2.1 Average (Pseudo) Velocity Method

The average (pseudo) velocity (V_a) method is one of the more simple, yet most commonly used, seismic time-to-depth conversion methods within the Cooper-Eromanga Basin. This simple approach does not explicitly consider velocity anomalies. Rather, for any given well location and for any given reflector, the true depth (Δz: depth in feet) is obtained from well data and the interpreted time (Δt: one-way-time in seconds) obtained from seismic data (Fig. 9a). The ratio of the two measured values provides the V_a at the well location, such that;

$$V_a = \frac{\sum_{k=1}^{n} z_k}{\sum_{k=1}^{n} t_k} = \frac{\Delta Z\ (ft)}{\Delta t\ (s)}$$

Where *k* is the k^{th} reflector measured from *n* well locations. The time-to-depth conversion process involves multiplying the resultant V_a with the seismic data (one-way-time: OWT in seconds), to give true depth (ft), such that;

$$True\ Depth = V_a * OWT$$

For seismic data that contains an abundance of well control, the V_a for each well location can be summed to determine the overall mean V_a of the entire survey. Alternatively, the V_a values at each well location can be gridded to produce a spatial contour map of V_a, which can take into account spatial velocity anomalies. The V_a from the surface to the Upper Cretaceous, Cadna-owie Formation, and Top Permian seismic reflectors was measured from 12 3D seismic surveys (Fig. 3b) to give a basin wide V_a value (Fig. 9d). The basin wide V_a from the surface to the: (1) Upper Cretaceous reflector is 2,280 m/s, (2) Cadna-owie Formation reflector is 2,375 m/s; and (3) Top Permian reflector is 2,740 m/s (Fig. 9d). Although simplistic, this method has been found to be one of the most accurate in the Cooper-Eromanga Basin (Rady, 2006; Kulikowski et al., 2016b, 2017c).

4.2.2 Time-Depth Trend Method

The time-depth (T-D) trend method utilises the relationship between the TWT and true depth values for a given reflector, hence is closely related to the average velocity method. The T-D pairs at a given well location for a given seismic reflector are plotted on a two-way graph and a linear ($y = mx + c$), or occasionally exponential ($y = ax^2 + bx + c$), trend is defined, where *y* is depth, *x* is time, *m* is slope, and *a*, *b*, and *c* are constants (Fig. 9b). The T-D trend equation that defines the distribution is used to directly convert the TWT seismic data to depth. The T-D Trend (Fig. 9e) from the 12 3D seismic surveys (Kulikowski et al., 2017a) was found to be approximately;

$$Depth\ (m) = 280.5 * (TWT)^2 + 847.97 * (TWT)$$

Where *TWT* is two-way-time measured in seconds. Not all T-D pairs will plot precisely on this trend, and may create poor well ties. Therefore, when performing a time-to-depth conversion on a gridded reflector, the resultant depth grid must be tied to the well control precisely by firstly gridding the error between the true depth and the time-to-depth converted grid, and secondly subtracting the resultant error correction grid from the time-to-depth converted grid (Kulikowski et al., 2016b, 2017c).

This method of time-to-depth conversion is a commonly used method in the Cooper-Eromanga Basin, with early work utilising check-shot data and continuous velocity logs to calibrate seismic

data. Continuous velocity logs can provide direct input data for velocity models and T-D pairs for key stratigraphic markers. Check-shot data for time-to-depth conversion has somewhat become outdated, with advancements in technology providing more accuracy through vertical seismic profile (VSP) acquisition (Jolly, 1953; Levin & Lynn, 1958; Ganley & Kanasewich, 1980; Hauge, 1981; Balch et al., 1982; Balch & Lee, 1984; Gajewski & Psencik, 1990). Check-shot and VSP data are obtained in a similar fashion to seismic data, where a P-wave travel time is measured from the surface to a receiver (Stainsby & Worthington, 1985). In the case of check-shot and VSP data, the receiver is lowered through the borehole to a key stratigraphic marker. However, the resolution of VSP data is significantly higher, as the number of borehole receivers can be as dense as every 25 m, in contrast to check-shot data that is only collected at key stratigraphic intervals.

4.2.3 Interval (Layer-Cake) Velocity Method

The interval velocity (V_i) method is used to represent the abrupt changes in velocity evident across significant stratigraphic packages. A look at continuous velocity logs and synthetic seismograms shows that velocities are not constant and can abruptly increase or decrease depending on the rock composition (Al Chalabi, 1974). The more basic interval velocity model divides the subsurface into key stratigraphic packages that have unique velocities (V_i), such that the depth can be calculated by;

$$Depth = \sum_{j=1}^{n} V_i(t_{j+1} - t_j)$$

Where *n* is the number of intervals (layers) bound by the j^{th} reflectors, which are measured in the time-domain, *t* (one-way-time), at a given well location.

High velocity cemented calcite zones (CCZ) are present within the Eromanga Basin and can distort the true subsurface image when not incorporated into velocity models (Kulikowski et al., 2016). Precises interval velocity modelling can include these high velocity zones for more accurate seismic depth conversion. Interval velocity models are also used when anomalous velocities are present within a specific stratal-unit, which can be caused by overpressures, cementation, or the presence of faults and fractures.

4.3 Seismic Time-to-Depth Conversion Accuracy

The accuracy of converting post-stack seismic data from the time-domain to the depth-domain has been a significant topic of conversation within the Cooper-Eromanga Basin. Inaccurate seismic depth conversion has significant implications for a number of key processes, which include: (1) drilling low

amplitude Jurassic to Cretaceous pseudo-structures that appear in depth converted seismic data due to velocity anomalies; (2) overlooking low amplitude Jurassic to Cretaceous structural traps that do not appear in depth converted seismic data due to inaccurate velocity modelling; (3) inaccurate economic estimates of new wells that, if depth is underestimated, may require drilling additional 10's of feet that may change the economic feasibility; (4) coring the wrong intervals while drilling; (5) inaccurate reserves calculations that could be under or overestimated; and (6) errors with geomechanical modelling of fault reactivation, as fault geometries will change and could influence the sealing potential of fault bound accumulations (Hillis et al., 1995; Lowe-Young et al., 1997; Kulikowski et al., 2016).

The historical inaccuracy of seismic depth conversions can be attributed to a number of factors ranging from: (1) known high velocity calcite cemented zones (CCZ); (2) the regional system of Cretaceous polygonal faults that can influence the spatial and temporal velocity; (3) velocity characteristics of fluvially deposited channel sands; and (4) the near surface 'statics' attributed to changes in surface conditions (rocky, regolith, etc.) (Hillis et al., 1995; Lowe-Young et al., 1997; Kulikowski et al., 2016b, 2017c). The effect of statics on seismic depth conversion is difficult to constrain, but can be slightly mitigated through up-hole seismic refraction surveys that deliberately drill shallow wells to target the velocity of the near surface (Igboekwe & Ohaegbuchu, 2011). This technique can accurately measure the velocity at the wellbore, but, as with most wellbore derived data, must be extrapolated to the wider and often kilometre-scale field, which is a large assumption that can influence accuracy. To entirely mitigate the large effect of statics in seismic depth conversion accuracy within the Cooper-Eromanga Basin, a method of velocity acquisition targeting the near surface must be investigated.

At this present moment, much of the work on seismic time-to-depth conversion accuracy in the basin appears to be kept behind closed doors by operating companies. Literature provides only two studies in the Cooper-Eromanga Basin that are focused on this topic (Hillis et al., 1995; Kulikowski et al., 2017c), with Hillis et al. (1995) choosing to focus on a small local dataset. The only regional study assessing the depth conversion accuracy in the basin used a statistical approach testing the accuracy of the four most commonly used methods (average (pseudo) velocity, time-depth trend, kriging with external drift using TWT, and kriging with external drift to tie stacking velocities to average well velocities) by employing a cross-validation, or blind-well test, method (Kulikowski et al., 2017c). An automated looping script was developed to manage their large dataset, comprising of 13 3D seismic volumes, 73 interpreted TWT grids, and 657 wells (Kulikowski et al., 2017c). Their results found that although the average (pseudo) velocity method was the most accurate at a high-level (±24.9 ft), the

accuracy of methods changes by 10's of feet depending on the unique dataset and the combination of significant variables (Kulikowski et al., 2017c).

The significant variables to the accuracy of depth conversion were the distance between the well that is being predicted and an existing well control, the spatial location within the basin, the reflector of interest, and the location of the well that is being predicted relative to the existing well data envelope (Kulikowski et al., 2017c). Interestingly the number of well controls had a negligible effect on accuracy, but rather the proximity of well controls to the well that is being predicted (Kulikowski et al., 2017c). The regional study (Kulikowski et al., 2017c) reiterates the argument that depth conversion accuracy in the Cooper-Eromanga Basin is a complicated issue that must be further investigated.

4.4 Seismic Data Analysis

Analysis of seismic data through the use of seismic attributes, amplitude versus offset (AVO) analysis, spectral decomposition, and seismic inversion modelling can unlock hidden details that may not be obvious within the amplitude volume. These techniques have become a common tool for exploration and development programs around the world and would be highly beneficial in the fluvially dominated Cooper-Eromanga Basin (Fig. 10). Incoherency (coherency or similarity) is a seismic attribute that was first introduced by Bahorich and Farmer (1995) and further developed by Gersztenkorn and Marfurt (1999) and is used to visually emphasise the discrepancy (typically faults) between adjacent seismic traces along a horizon or time-slice (Neves et al. 2004; Mai et al. 2009; Backé et al. 2011; Basir et al. 2013). This attribute has been shown to be particularly beneficial when interpreting basement and polygonal faults (Fig. 10b) from the low resolution seismic data typical to the Cooper-Eromanga Basin (Kulikowski et al., 2017a). Curvature is another structural attribute that is defined as the rate of change of the direction of a curve (Roberts, 2001), where significant curvature values are often associated with reflector displacement such as those caused by fractures or faults (Roberts, 2001; Al-Dossary and Marfurt, 2006; Backe et al., 2011; King et al., 2011; Abul Khair et al., 2012; Kulikowski et al., 2017b). This attribute has the potential to constrain the distribution of natural fracture sweet-spots away from the wellbore (Kulikowski et al., 2017b).

Considering that hydrocarbons are predominantly reservoired within fluvial sandstones in the Cooper-Eromanga Basin, displaying the spatial distribution of amplitude along a reflector surface can aid in detecting these strong amplitude reservoirs (Fig. 10a), particularly if associated with characteristic amplitude versus offset (AVO) responses. In some cases, these reservoirs can verge on being at a sub-seismic resolution scale and can be overlooked in seismic data. The application of

spectral decomposition on the seismic volume can assist in detecting these thin fluvial beds (Fig. 10d) and can also provide a more visual representation of small scale faults (Partyka et al., 1999). Another issue facing explorationists is the discrimination between the signature of thin gas reservoirs and coals in stacked seismic data. Owing to the significant difference in Poisson's ratio between sandstone and coal, the application of AVO analysis to Cooper-Eromanga Basin seismic data has provided evidence to suggest that such discrimination is possible and most effective when using a rotated extended elastic impedance attribute in the presence of tuning (Fig. 10c) (Tyiasning and Cooke, 2015).

Insert Fig. 10

5. CONTEMPORARY STRESS TENSOR

Contemporary stress tensors are well constrained in the basin, calculated from borehole breakouts and drilling induced tensile fractures, diagnostic fracture injection tests, and leak off tests (e.g. Hillis et al., 1999; Hillis & Reynolds, 2000, 2003; Reynolds et al., 2002, 2003, 2004, 2005, 2006; Sandiford et al., 2004; Nelson et al., 2006, 2007; Muller et al., 2012; Pokalai et al., 2016, 2017). The far-field origin of in situ stresses has been explained by Reynolds et al. (2003) to originate from the Tonga-Kermadee subduction zone and the New Zealand collisional boundary. These tectonic stresses are transferred through the upper crust of eastern Australia to give an approximately ESE-WNW maximum horizontal stress within the Cooper-Eromanga Basin. The stress regime is dominantly strike-slip, but can transition to a compressional stress regime with increased depth, as the overpressures will decrease the effective vertical stress magnitude more than the effective horizontal stress magnitudes (Reynolds et al., 2006; Cooke et al., 2015). Alternatively, depletion of hydrocarbon reservoirs can reduce pore pressure, which in turn increases the effective vertical stress magnitude (Teufel, 1991). Given that the effective vertical stress magnitude can become larger than both effective horizontal stress magnitudes through reservoir depletion, the in situ stress can transition into an extensional stress regime (Teufel, 1991). This transition between regimes will have implications for late-stage development programs incorporating hydraulic fracturing and infill drilling, as the unexpected stress regime can impact the effectiveness of those programs.

For the majority of the basin a strike-slip stress regime is present, with an ESE-WNW oriented maximum principal stress (Fig. 11a); however, local stress perturbations caused by faults can cause stress rotation (Fig. 11b). The magnitude of maximum horizontal stress has been constrained to approximately 41 MPa/km based on a combination of frictional limit theory (Sibson, 1974), drilling induced tensile fractures, and the use of tensile strength and knowledge of horizontal fabrics at the

wellbore wall (Reynolds et al., 2005; Nelson et al., 2005; 2007). The vertical principal stress magnitude is dependent on the overburden rock thickness and density, as well as the local pore pressure (Fig. 11c). The range of magnitudes present within the basin for the vertical stress is between approximately 17 and 20 MPa/km (Reynolds et al., 2006; Nelson et al., 2007; Pokalai et al., 2016, 2017). As mentioned earlier, a decrease in the pore pressure caused by depletion can increase the effective magnitude of the vertical principal stress. Minimum horizontal stress magnitudes are typically calculated from leak off tests or obtained from the minimum closure pressure during a mini-frac test (Fig. 11c). Within the Cooper-Eromanga Basin, the minimum horizontal stress magnitude can vary significantly between approximately 12 and 27 MPa/km and can depend on the interpretation technique used to read closure pressures (Nelson et al., 2007).

Insert Fig. 11

Equally as important as the principal stress magnitude, the pore pressure gradient can influence the reactivation and development of natural fractures and faults. Increases in pore pressure effectively shift the Mohr's circle to the left, closer to the failure and reactivation envelopes. This effect can be induced by hydraulic fracture stimulation treatments and through gas and water injection wells. Pore pressure within the basin remains at a hydrostatic gradient (0.433 psi/ft) until depths of between 8000 and 8800 ft, where overpressure is first observed and is largely depended on the location (van Ruth & Hillis, 2000; Kulikowski et al., 2016a). A recent study within the basin calculated the effective tectonic strain to be between approximately 400 and 500 microstrains, with strain in the maximum horizontal stress direction being three times greater than that in the minimum horizontal stress direction (Pokalai et al., 2016, 2017).

6. GEOMECHANICAL MODELLING OF FAULT REACTIVATION

6.1 Theory

Reactivation refers to the movement of faults and fractures under present day stress conditions and can be analysed by creating a geomechanical model and measuring the shear or tensile (dilation) reactivation potential. A poor understanding of the local and regional geomechanical conditions has tremendous implications for hydrocarbon migration pathway models, hydraulic fracture stimulation treatments, reservoir development, and seal integrity. Faults that are optimally oriented to undergo tensile reactivation, or dilate, can provide permeable conduits for hydrocarbon migration. An increase in pore pressure, through hydraulic fracture stimulation or water/gas injection wells, can facilitate shear or tensile fracture reactivation/development. Geomechanical models have shown to effectively predict the shear and tensile reactivation potential of faults under

paleo-stress conditions, which becomes most beneficial when incorporated with hydrocarbon migration pathway modelling (Kulikowski & Amrouch, 2017c). To improve such models, the unique rock properties, potential cementation, plane roughness, and pressure variation must be considered; however, these parameters are difficult to constrain and often overlooked for model simplicity. The following measures provide an indication of fault and fracture stability that simplify the in-situ mechanical conditions. These are applied to three groups of structural data common to the Cooper-Eromanga Basin: (1) Basement Faults; (2) Polygonal Faults; and (3) Natural Fractures.

The Dilation Tendency (T_d) measures the likelihood that faults and fractures will tensile reactive and is governed by the orientation and magnitude of the effective normal stress, ${\sigma_n}'$, acting on a fault plane. The T_d is normalised to the differential stress to give values between zero (low likelihood) and one (high likelihood), where ${\sigma_1}'$ is the maximum effective stress and ${\sigma_3}'$ is the minimum effective stress (Ferrill et al., 1999; Jolie et al., 2015);

$$T_d = \frac{{\sigma_1}' - {\sigma_n}'}{{\sigma_1}' - {\sigma_3}'}$$

Fracture Stability is a measure of the pore pressure required to effectively shift the Mohr's circle to the left and intersect the failure or reactivation envelope for a given fault plane. The relationship between an increase in pore pressure (ΔP_p) and the change in horizontal stress magnitude (ΔS_{Hor}) is such that (Hung and Wu, 2012);

$$\Delta S_{Hor} = \alpha\left(\frac{1-2v}{1-v}\right)\Delta P_p$$

Where α is Biot's coefficient that describes the difference between the total and effective stresses, and *v* is the Poisson ratio. This equation shows the direct relationship between increasing pore pressure to an increase in the horizontal stress magnitudes. Therefore, the Fracture Stability results are provided as the pore pressure increase required to induce shear reactivation. The Slip Tendency of faults provides a normalised scale of the Fracture Stability, where zero (0) has a low likelihood, and one (1) has a high likelihood of shear reactivating. The likelihood of faults and fractures to act as conduits can be measured through the Leakage Factor that relates the pore pressure (P_p) with the difference between the normal stress (σ_n) and shear stresses (τ) acting on a given fault plane;

$$Leakage\ Factor = \frac{P_p}{\sigma_n - \tau}$$

6.2 Basement Faults

6.2.1 SUMMARY

The majority of the basement-involved faults developed during the early tectonic development of the Australian-Mawson Block (Fig. 4a), where a Pre-Cambrian (650-575 Ma) SE-NW oriented extensional stress regime event created NE-SW striking normal faults and SE-NW strike-slip faults throughout much of Australia (Kuang, 1985; Haines, 2002; Apak et al., 1997; Gibson et al., 2013; Kulikowski and Amrouch, 2017a). These two dominant fault sets are present throughout the Cooper-Eromanga Basin and form close relationships with anticlinal hydrocarbons traps (Fig. 12) and the NE-SW striking GMI and MN ridges (Fig. 3b). Through time, these pre-existing basement-involved faults were repeatedly reactivated by subsequent compressional and strike-slip stress regime events (Apak et al., 1997; Gravestock & Jensen-Schmidt, 1998; Kulikowski & Amrouch, 2017a, 2017b; Kulikowski et al., 2017a). Repeated reactivation of pre-existing faults is supported by multiple erosional unconformities and the negligible distribution of low angle compressional faults, albeit up to four compressional events (Mid-Permian Event, Hunter-Bowen Event, Late Cretaceous Event, and Paleogene Event) had affected the region (Kulikowski & Amrouch, 2017a). Under Andersonian faulting theory (Anderson, 1951), such compressional events would develop low angle (30º) faults; however, due to the abundance of high angle (60º) normal faults, it would be more stress economic to reactivate existing faults rather than develop new faults (Kulikowski & Amrouch, 2017a).

Insert Fig. 12

The original NE-SW striking normal faults, which are present throughout the basin (Fig. 13a & 13b), are now observed to positively displace reflectors (Apak et al., 1997; Gravestock & Jensen-Schmidt, 1998; Radke, 2009; Kulikowski & Amrouch, 2017a, 2017b; Kulikowski et al., 2017a). Their stratigraphic distribution is often limited to terminating within basement or Middle Permian stratigraphy, and rarely penetrating into younger units (Apak et al., 1997; Gravestock & Jensen-Schmidt, 1998; Radke, 2009; Kulikowski & Amrouch, 2017b). Due to the poor seismic resolution below Permian coal measures, detailed fault growth studies (e.g. Giba et al., 2012; Jackson and Rotevatn, 2013; Robson et al., 2018) have not been possible and their interpretation becomes more difficult with depth. The difficulty is also exaggerated when developing fault models from seismic data that remains in the time-domain, as the true fault angle is not being captured (Fig. 8b & 8c). The difference in basement-fault geometry between the time and depth-domains has proven to be problematic for previous researchers that used sparse 2D seismic data, as their work interpreted purely extensional faults, which were later re-interpreted as compressional faulting, and which are now known to be a combination of inverted normal faults, compressional faults and strike-slip faults

(e.g. Kuang, 1985; Stanmore & Johnstone, 1988; Apak et al., 1997; Sun, 1997; Gravestock & Jensen-Schmidt, 1998; Radke, 2009; Grant-Woolley et al., 2014; Kulikowski & Amrouch, 2017b; Kulikowski et al., 2017a).

Insert Fig. 13

The SE-NW strike-slip faults are present throughout the region and have been attributed to reducing reservoir performance through cataclasis, compartmentalisation of reservoirs, and potentially complicating hydraulic fracture stimulation treatments (Grant-Woolley et al., 2014; Kulikowski et al., 2016c). These strike-slip faults appear predominantly within basement and can extend into the hydrocarbon-rich Patchawarra Formation (Apak et al., 1997; Radke, 2009; Kulikowski & Amrouch, 2017b; Kulikowski et al., 2017a). This fault set can easily be overlooked in cross-section due to the seismic resolution at basement and must be investigated in time-slice (or depth-slice) views to observe lateral displacements or linear features. A series of large basin-scale en echelon NNE-SSW strike-slip faults are present in the Patchawarra Trough (Fig. 3a) and form pop-up or positive flower structures that have been developed into highly economic fields. Their presence elsewhere in the basin may be equally as fruitful; however, are yet to be discovered!

6.2.2 REACTIVATION POTENTIAL UNDER PALEO-STRESSES

A new approach for assessing the reactivation and dilation potential of faults through time was presented by Kulikowski & Amrouch (2017c), using the Cooper-Eromanga Basin as a case study. This approach utilises complete paleo-stress tensors for six events that were obtained through calcite twin stress inversion analysis (Kulikowski & Amrouch, 2017a). Complete paleo-stress tensors were integrated with geomechanical models to simulate the stress conditions present during each of the six key stages of basin evolution. Results found that after the critical moment in the Cooper-Eromanga Basin petroleum system (90 Ma), E-W (Late Cretaceous Event) and N-S (Paleogene Event) striking high angle (50-70°) faults were most likely to be dilated and acting as permeable hydrocarbon conduits (Fig. 13c). The critical moment defines the major period of hydrocarbon generation, migration and entrapment. This provides critical information that improves hydrocarbon migration pathway models that previously considered faults to have static 2D mechanical properties.

The history of basement fault reactivation is often constrained through fault growth analysis using 3D seismic data (e.g. Williams et al., 1989; Childs et al., 1996; Baudon & Cartwright, 2008); however, this cannot be performed in regions that have poor seismic resolution. For such regions, including the Cooper-Eromanga Basin, the Slip Tendency of faults is calculated using paleo-stress tensors and geomechanical modelling to provide insights into the 4D evolution of fault reactivation. Kulikowski &

Amrouch (2017c) measured the Slip Tendency of four major fault sets modelled using the paleo-stress tensors during six tectonic events (Fig. 13d). The results showed that N-S striking high angle (50-70°) faults were most likely to reactivate during the Alice Springs Event, and E-W striking high angle (50-70°) faults likely reactivated during the Mid-Permian Event (Fig. 13d). Since these two events NE-SW striking high angle (50-70°) faults were most likely to shear reactivate under the subsequent Daralingie Event, Hunter-Bowen Event, Late Cretaceous Event and Paleogene Event (Fig. 13d). This is in line with other research suggesting considerable exhumation and erosion along the major NE-SW striking GMI and MN ridges (Kuang, 1985; Apak et al., 1997; Gravestock & Jensen-Schmidt, 1998; Mavromatidis, 2006, 2007; Kulikowski & Amrouch, 2017b).

6.2.3 REACTIVATION POTENTIAL UNDER CONTEMPORARY STRESSES

A case study on the Swan Lake 3D and Dullingari 3D seismic surveys, located adjacent to the GMI and MN ridges, respectively, investigated the reactivation potential of basement-involved faults under contemporary stresses by measuring the Slip Tendency, Dilation Tendency, and Fracture Stability (Kulikowski et al., 2016c). The study analysed four unique fault sets modelled using hydrostatic pressure, in situ stress, and typical rock mechanics parameters from the Cooper Basin.

Results from Kulikowski et al. (2016c) showed that E-W striking faults have the highest Dilation Tendency (0.900) and thus most likely to act as permeable hydrocarbon conduits under the present day stress (Fig. 13c). The study also identified SE-NW strike-slip faults within both 3D seismic surveys and found that they are most likely to shear reactivate (Fig. 13d). A pore pressure increase of between only 0.5 and 5.0 MPa is required for this fault set to intersect the reactivation curve. Shear reactivation can compartmentalise the reservoir, reduce reservoir properties through cataclasis, complicate hydraulic fracture propagation, and facilitate tertiary migration of hydrocarbons. Therefore, precise seismic interpretation, particularly in depth-slice to observe lateral offsets, must focus on the identification of SE-NW striking strike-slip faults in order to incorporate their presence with the development of hydraulic fracture stimulation and drilling programs.

6.3 Cretaceous Polygonal Fault System

6.3.1 SUMMARY

Layer bound polygonal faults are present within Cretaceous Eromanga Basin marine sediments across the entire basin (Heath et al., 1989; Watterson et al., 2000; Kulikowski et al., 2017a; Kulikowski & Amrouch, 2017b). These faults were first identified from 2D seismic data (Rumph, 1982; Moore & Pitt, 1984; Newton, 1986; Gilby & Mortimore, 1989; Scholefield, 1989; Gorter et al., 1989; Young et al., 1989; Longley, 1989), with the 3D distribution and regional extent only recently

discovered in literature (Oldham & Gibbins, 1995; Watterson et al., 2000; Kulikowski et al., 2017a). A detailed analysis of polygonal faults within the Lake Hope 3D seismic survey suggests that their development is linked to a density inversion, where a low density and overpressured stratal unit was buried and de-watered by overlying normally pressured and higher density sediments (Watterson et al., 2000). The planar normal faults are mostly contained within the Mackunda Formation, Coorikiana Sandstone, Bulldog Shale and Wallumbilla Formation; however, larger faults are found to penetrate into the underlying and oil-rich Murta Member (Fig. 7). Maximum throw was found within the Coorikiana Sandstone. The dip angle of faults remains constant along a given fault plane and can range between 44° and 61° (Watterson et al., 2000). This polygonal fault system may present a new hydrocarbon exploration opportunity targeting shallow oil that has migrated from Lower Cretaceous oil-rich reservoirs through permeable polygonal faults (Fig. 7) (Watterson et al., 2000).

The normal displacement across polygonal faults can tilt shallow reservoirs such that low relief structural traps are developed and potentially fault sealing. Low relief structures that are bound by deeply penetrating faults can facilitate the accumulation of oil in shallow reservoirs. This play has yet to be truly tested in this region, but is analogous to the polygonal fault system associated with Tertiary hydrocarbon-rich shales in the North Sea (Cartwright & Lonergan, 1997; Lonergan et al., 1998). The presence of faults within hydrocarbon reservoirs can have tremendous implications for effective production and development, such as compartmentalisation of the reservoir, tertiary hydrocarbon migration, and complications with hydraulic fracture stimulation treatments. Considering that Lower Cretaceous and Jurassic hydrocarbon reservoirs are currently being explored and developed, an understanding of the geometry, intensity and reactivation potential of the Cretaceous polygonal fault system is highly beneficial.

6.3.2 REACTIVATION POTENTIAL UNDER CONTEMPORARY STRESSES

This potential new play type was first suggested by Watterson et al. (2000), who suggested the possibility that these faults may be facilitating the tertiary migration of hydrocarbons from known reservoirs to shallow sedimentary rocks. Little literature has since appeared in relation to this exploration opportunity, with the regional extent of this system only recently discovered (Kulikowski et al., 2017a). The Leakage Factor and Dilation Tendency of this regional polygonal fault system were modelled to determine the optimum fault geometry required for fluid flow (Kulikowski et al., 2017a).

The results show that high dip angle (50-90°) polygonal faults striking 080-260°N and 125-305°N have the largest Leakage Factor, and fault planes with high dip angle (50-90°) striking 105-285°N have the largest Dilation Tendency (Kulikowski et al., 2017a). These fault planes are therefore most

likely to facilitate the tertiary migration of hydrocarbons from Lower Cretaceous hydrocarbon-rich reservoirs into shallow structures, given that they penetrate below the Cadna-owie Formation into the hydrocarbon-rich Murta Member.

6.4 Natural Fractures

6.4.1 SUMMARY

Natural fractures can provide highly permeable pathways for hydrocarbon production if the local and regional fracture set geometries are known. The strike and dip angle of fracture sets are equally as important for optimising hydrocarbon recovery. Six regionally pervasive conjugate natural fracture sets (Fig. 14a) are present in the Cooper-Eromanga Basin (Kulikowski & Amrouch, 2017a). The timing of their development, stratigraphic distribution, and spatial intensity has been well constrained (Kulikowski et al., 2016a; Kulikowski & Amrouch, 2017a). Extrapolation of wellbore derived natural fractures to the wider reservoir has also been investigated by a number of authors (Backe et al., 2011; Abul Khair et al., 2012; King et al., 2011; Kulikowski et al., 2017b), suggesting that upwards of 70% of wellbore fractures are represented in seismic curvature results.

Insert Fig. 14

6.4.2 NATURAL FRACTURES AT THE WELLBORE

Low dip angle (30°) conjugate fracture sets striking E-W and N-S are present throughout the stratigraphic column and associated with the Paleogene Event, and the Upper Cretaceous and Hunter-Bowen events, respectively. A third low dip angle conjugate fracture set is present only within the Patchawarra, Tirrawarra, Merrimelia and Basement formations striking NE-SW and associated with the Mid-Permian Event. A vertical conjugate natural fracture set striking NNE-SSW and SE-NW is present only within Basement and developed during the Alice Springs Event. Two additional conjugate natural fracture sets are present throughout the stratigraphic column, striking NE-SW and SE-NW with high dip angles (50-70°), and most likely associated with periods of post-compressional flexural relaxation, or basin sag (Abul Khair et al., 2016; Kulikowski & Amrouch, 2017a). The majority of interpreted fractures have high dip angles (50-70°) making the true wellbore fracture intensity of vertical wells difficult to constrain. A comparison between the fracture intensity interpreted from vertical, horizontal and inclined wells would provide more meaningful and representative fracture intensities.

A robust natural fracture study was performed for the Warburton Basin (Sun, 1999) using core, borehole image logs, and dip meter logs. The conclusions present a number of fracture sets;

however, their methods relied too heavily on the strike of fractures and did not consider that slight changes in dip angle (20°) can have a different interpretation (Anderson, 1951). For this reason the use of seismic attributes, such as most positive and most negative curvature, can be misleading by only providing the strike of possible fractures and faults. Fracture sets with similar strike direction but different dip angles cannot be distinguished from these seismic trending methods.

Horizontal fractures have also been proposed to exist in the basin, and likely associated with periods of significant exhumation and erosion (Flottmann et al., 2004; Tyiasning & Cooke, 2016; Cooke et al., 2016). Significant erosion can reduce the vertical stress magnitude and create local compressional stress regimes that can develop tensile horizontal fractures. These horizontal fractures can complicate hydraulic fracture stimulation treatments by preferentially reactivating and causing rotation of hydraulic fractures into the horizontal plane, which is a common phenomenon in the Cooper-Eromanga Basin (Cooke et al., 2016; Pokalai et al., 2016, 2017).

6.4.3 NATURAL FRACTURES AWAY FROM THE WELLBORE

A common assumption within the petroleum industry is that wellbore data can be extrapolated to the wider reservoir, which assumes that stress conditions, structural data, pore pressures, reservoir properties and characteristic, and other important criteria remain constant. If incorrect, this assumption can lead to obvious implications for exploration and development programs. As the Cooper-Eromanga Basin contains low permeability reservoirs, the presence of permeable fracture networks can add great economic value to prospects; however, much of the existing work assumes that borehole data is representative of the wider kilometre-scale fields (Kulikowski et al., 2017b). Recent advancements in seismic acquisition and processing have enabled the use of seismic attributes to provide information away from the wellbore that is otherwise overlooked in the original amplitude volumes.

Curvature analysis is a seismic attribute that has been shown to correlate well with wellbore derived fracture and fault data (e.g. Murray, 1968; Lisle, 1995; Stewart & Podolski, 1999; Hakami et al., 2004; Al-Dosary & Marfurt, 2006; Chopra & Marfurt, 2007; King et al., 2011; Abul Khair et al., 2012; Kulikowski et al., 2017b). The value for curvature is defined as the rate of change of the direction of a curve (Roberts, 2001), such that for any point (P) the curvature (K) is defined as the rate of change of the dip angle ($d\omega$) with respect to the arc length (dS) (Roberts, 2001). The arc length (dS) is obtained from the osculating circle that has a common tangent to *P* and makes the greatest possible contact with the curve (Roberts, 2001). The radius of the osculating circle forms the radius of curvature (R); such that in two-dimensions the value for *K* is defined as (Roberts, 2001);

$$K = \frac{d\omega}{dS} = \frac{2\pi}{2\pi R} = \frac{1}{R}$$

Curvature analysis has previously been performed within the Cooper-Eromanga Basin (Backe et al., 2011; King et al., 2011; Abul Khair et al., 2012; Kulikowski et al., 2017b) showing a close relationship with fractures measured at the wellbore (Fig. 14b & 14c). The spatial and temporal distribution of permeable fracture networks away from the wellbore using curvature analysis has shown that high angle E-W and SE-NW striking fractures are highly pervasive and most likely to be permeable under contemporary stresses (Kulikowski et al., 2017b). These E-W and SE-NW striking fracture sets are present in each of the five 3D seismic surveys analysed by Kulikowski et al. (2017b) and were found to increase in intensity along E-W elongate anticlinal structures, which may present an exploration target for future programs. The use of curvature analysis for field development programs that target fracture networks appears invaluable, as it can provide the spatial and temporal distributions of permeable fracture networks in the subsurface away from the wellbore.

6.4.4 REACTIVATION POTENTIAL UNDER CONTEMPORARY STRESSES

Understanding the distribution, geometry, and intensity of permeable fracture networks is an important aspect of development programs in the low permeability Cooper-Eromanga Basin. The likelihood of fractures to reactivate and be open to fluid flow is primarily controlled by the contemporary stress conditions relative to the fracture geometry. The contemporary stress in the Cooper-Eromanga Basin has an approximately E-W oriented maximum horizontal stress and is under a strike-slip stress regime, but the orientation can vary by up to 20° and the regime can alternate between a compressional stress regime (Nelson et al., 2007; Reynolds & Hillis, 2000; Reynolds et al., 2004; King et al., 2008, 2011; Abul Khair et al., 2012; Pokalai et al., 2016, 2017). This variation of in situ stress has a profound influence on the reactivation potential of fractures, and infers that geomechanical modelling performed on the basin-scale may not be representative of the field-scale.

King et al. (2011) and Abul Khair et al. (2012) measured the fracture susceptibility of natural fractures on a basin-scale assuming an E-W oriented maximum horizontal stress that alternates between a strike-slip and compressional stress regime. Their study found that NE-SW and SE-NW striking fractures with moderate dip angles are most prone to reactivation (Fig. 14d & 14e). Understanding the shear reactivation potential is important; however, measuring the likelihood of tensile reactivation is equally as important. Kulikowski et al. (2017b) measured the Dilation Tendency of 454 fractures to show that E-W and SE-NW striking high angle (60°) fractures are optimally oriented to dilate and act as potential hydrocarbon conduits under contemporary stresses

(Fig. 14f). These sets are regionally pervasive away from the wellbore within the Patchawarra Formation and would form ideal fracture sweet-spots given sufficient intensity (Fig. 14b & 14c).

7. HYDRAULIC FRACTURE STIMULATION AND WELL SURVEILLANCE

Hydraulic fracturing has been performed in the Cooper Basin since 1969 (McGowen et al., 2007). The majority of hydraulic fracturing treatments are focus on the predominately Permian sandstone reservoirs, especially in the tight sand Patchawarra Formation. This formation has low (milliDarcy) permeability and requires multistage hydraulic fracturing to optimise production and be economically feasible. There is significant gas potential to explore and develop in this area; however, the stress complexity and high pressure and temperature conditions are challenging to effectively execute hydraulic fracturing programs.

During injection and fracture propagation a considerable pressure loss can be observed near the wellbore. This near-wellbore pressure loss (NWBPL) was first discussed by Chipperfield et al. (2000) and Roberts et al. (2000), who stated that the causes of NWBPL are related to pressure loss within the perforations, and tortuosity within the induced fracture path near the wellbore. Johnson et al. (2002) and Johnson and Greenstreet (2003) discussed pressure dependent leak-off (PDL) and NWBPL in the Cooper Basin and showed the significant impact it can have on production performance. NWBPL is caused by frictional pressure loss at the wellbore and closely related to tortuosity. Four different types of fracture propagation can result from high tortuosity including fracture turning, fracture twisting, multiple fracturing and fracture migration. High NWBPL can therefore complicate the hydraulic fracture process and result in a lower percentage of proppant being placed within the target reservoir (Pokalai et al., 2015a, 2015b).

When pre-existing natural fractures are present within a reservoir the near-wellbore pressure loss is considerably higher due to the complex interactions that create multiple fractures with tortuous paths. This tortuous path will shear and tensile reactivate pre-existing natural fractures to create a large amount of pressure dependent leak-off. Therefore, pressure dependent leak-off can have both positive and negative impacts. It can increase rock permeability by increasing the stimulated rock volume, while at the same time causing a high near-wellbore pressure drop. However, to have better proppant placement and to maximise the flowback of fracturing fluid, near-wellbore pressure needs to be reduced.

The majority of the Patchawarra Formation consists of thick sand intervals that cycle between coal measures and shale, and is currently exposed to high pressure, high stress, and high temperature conditions. Therefore, the fracturing fluid system and proppant need to be selected in order to suit

these conditions. Fracturing fluid is commonly a water-based fluid system within the Cooper-Eromanga Basin comprising of either a Linear Gel or a Borate Crosslink Gel that is injected during the pad stage, slurry stage and the flushing stage. Proppant is typically 100 mesh sand and is pumped into the target zone to reduce NWBPL and to bridge-off the PDL. This is followed by the injection of ceramic proppant to provide high fracture conductivity. The perforations that the hydraulic fracture is pumped into are typically made by lowering expendable hollow carrier (EHC) or link guns down the wellbore to perforate the casing completion at the target location. The style of perforating guns is primarily dependant on well completion, with EHC guns commonly used in monobore completions to mitigate rat-hole loss, and link guns are used in conventional completion designs.

Once perforations and hydraulic fracture stimulations are complete and the well begins producing hydrocarbons, there is a significant need for well surveillance and intervention programs due to the harsh subsurface conditions within the Cooper-Eromanga Basin. These can range from high temperatures, high pressures, and high CO_2 concentrations, to liquid loading (water in the wellbore) issues that can lead to reduced production (Rigby & Smith, 1981; Wycherley et al., 1999; McGowen et al., 2007; Winterfield et al., 2014). Hydrocarbon production can also be inhibited by the development of scale (halite and calcite) within the perforations, where pressure and temperature rapidly decrease causing solutes to precipitate. The CO_2 concentration within the Cooper-Eromanga Basin is significantly higher (10-30 v/v%) than the average sedimentary basin (Rigby & Smith, 1981; Wycherley et al., 1999), contributing to the need to mitigate calcite scale through acid treatments, re-perforation, and regular wireline drift and broach intervention programs (Pitkin et al., 2012). Salts (NaCl) have also been found to precipitate within perforations originating from salty groundwater invading the reservoir.

Other than causing scale build-up, the invasion of groundwater into the wellbore can also increase the production rate required to lift, and unload, the liquids to surface and can cause liquid loading within the wellbore to effectively stop production (Winterfield et al., 2014). Mitigation techniques for this may include artificial lifts (nitrogen injection), compressor installation to reduce back-pressure, plunger lift systems, injection of foaming agents via micro-strings, installation of siphon strings (or recompletion to small diameter tubing) to reduce the minimum rate to lift liquids, well cycling (pressure build-up), and producing the well to atmospheric pressures for a short period of time to unload liquids (McGowen et al., 2007; Winterfield et al., 2014).

8. EXPLORATION AND DEVELOPMENT

8.1 Current Programs

Current exploration programs are somewhat simplistic and have remained inline with the original anticlinal theory; identify and drill an anticlinal closure (Apak et al., 1997; Lowe-young et al., 1997; Morton, 1998; O'Neil, 1998). This approach has generated in excess of 6.5 trillion cubic feet (TCF) of sales gas, with 1.6 TCF remaining to be produced (Mackie, 2015). Oil exploration, now primarily targeting the Jurassic Eromanga Basin reservoirs, has also become highly profitable, generating 520 million barrels (mmbbls) from Jurassic to Cretaceous reservoirs, with 150 mmbbls of recoverable reserves remaining (Mackie, 2015). The largest discovered oil producer is the Early Permian Tirrawarra Formation (braided delta and braided stream sandstone), particularly within the Tirrawarra Field where more than 80% of Cooper-Eromanga Basin oil is reservoired (Gravestock et al., 1998a). Taking into account the number of exploration wells drilled versus new Permian gas field discoveries, the success rate for current exploration programs is approximately 40% (Mackie, 2015). The success of Mesozoic oil exploration wells grew from 12% to 45% after the introduction of 3D seismic data acquisition, illustrating the significance of geophysical advancements in discovering new fields and new play types (Mackie, 2015).

There are currently two major plays in the province; targeting the Jurassic Eromanga Basin oil reservoirs, and persisting with the anticlinal theory in the oil and gas saturated Cooper Basin (Lowe-Young et al., 1997; Radke, 2009; Scott et al., 2013; Mackie, 2015). The central portion of the Eromanga Basin oil play overlies the South Australian portion of the Cooper Basin and forms Australia's most prolific oil province (Lowe-Young et al., 1997). The majority of Jurassic oil is reservoired within the Birkhead Formation, Hutton Sandstone, and Poolowanna Formation given that a structural trap exists (Lowe-Young et al., 1997; Kulikowski et al., 2016b, 2017c). It is important to note, however, that the presence of these typically low-relief structural traps can depend on the seismic time-to-depth conversion method being used, as the conversion errors can be greater than the structural closure (Lowe-Young et al., 1997; Radke, 2009; Kulikowski et al., 2016b, 2017c). The source of Jurassic oil in the central portion of the play has been attributed to Permian source rocks migrating vertically through leaky seals or along fault conduits (Lowe-Young et al., 1997; Radke, 2009). Recently, the Eromanga Basin oil play has been extended to the western flank of the Cooper Basin, where major oil exploration and production is currently taking place (Lowe-Young et al., 1997). The western flank oil play targets low amplitude anticlinal traps within the Jurassic Eromanga Basin reservoirs that are also charged by Permian source rocks (Lowe-Young et al., 1997; Rake, 2009).

The anticlinal closures common to the basin are often associated with reactivated basement-involved faults that develop broad structures in the overlying stratigraphy, but they can also be associated with positive flower (pop-up) features that are common in the Patchawarra Trough, or as fault-bound anticlines where large basement-involved faults have reactivated and penetrated through overlying units (Apak et al., 1997; Lowe-Young et al., 1997; Radke, 2009; Scott et al., 2013; Mackie, 2015; Kulikowski et al., 2017a). The case of fault-bound anticlines is most common along the GMI and MN ridges where the large NE-SW striking high angle (50-70°) faults have shown evidence of relatively more recent reactivation (Apak et al., 1997; Gravestock et al., 1998; Kulikowski and Amrouch, 2017b). These anticlinal traps allow for the accumulation of oil and gas within all reservoir quality sandstones in both the Cooper and Eromanga basins (Kantsler, 1984; Lowe-Young et al., 1997; Alexander et al., 1998; Morton, 1998; Radke, 2009; Scott et al., 2013).

8.2 Future Research and Exploration Programs

As the humble anticline becomes entirely exploited in this province, companies will transition into the next phase of hydrocarbon exploration targeting technically more challenging plays, such as the basin centred gas play, deep coal measure play, stratigraphic plays, polygonal fault play, and potentially fractured basement play that is juxtaposed to Permian source rocks. Each of these relatively unconventional plays will require a more thorough understanding of the basin. Therefore, as exploration within the Cooper-Eromanga Basin becomes more challenging, the collaboration between academic researchers and explorationists will become more integral to exploration success. Much of the regional structural, stratigraphic, and stress framework for the basin has been well constrained in recent times (e.g. Apak et al., 1997; Gravestock & Jensen-Schmidt, 1998; Hillis et al., 1999, 2001, 2008; Reynolds et al., 2002, 2003, 2004, 2005, 2006; Mavromatidis, 2006, 2007; Nelson et al., 2006, 2007a, 2007b; Radke, 2009; Pokalai et al., 2015a, 2015b, 2016, 2017; Kulikowski & Amrouch, 2017a, 2017b, 2017c; Kulikowski et al., 2016a, 2017a); however, there does remain a large volume of research that can directly impact the success of future hydrocarbon exploration and development programs. Additionally, exploration and production companies play an important role in the effective exploitation of Australia's largest onshore hydrocarbon province by testing new concepts and acquiring new data that will promote further research in the basin.

A complete 2D reconstruction of the basin has not yet been completed and would provide valuable information on the fault growth through time. Detailed fault growth analyses are not possible in the basin given the poor seismic resolution at basement; however, with continued improvement in seismic acquisition and processing techniques, a fault growth study may be possible in the future. This may ultimately lead to a complete structural and stratigraphic 3D reconstruction of the basin

and provide a 3D view of the temporal and spatial distribution of the four overlying basins. The spatial extent of major unconformities would also be useful, particularly as oil migration from Permian sources to Eromanga Basin reservoirs relies on the presence of unconformities that have effectively removed regional seals (Lowe-Young et al., 1997). The distribution and magnitude of overpressure has previously been investigated (Hillis et al., 2001; van Ruth et al., 2000, 2003; Kulikowski et al., 2016a); however, the mechanism for overpressure generation in the basin remains questionable and may be investigated by integrating reservoir pressure, vertical stress magnitude, and sonic velocity data (Tingay et al., 2007). The degree of stress perturbation caused by pre-existing faults should also be investigated in more detail, as local stress rotation does exist (Fig. 11b).

To accurately interpret seismic data, the amplitude volume must be converted from the time-domain to the depth-domain using an appropriate depth conversion method (Kulikowski et al., 2016b, 2017c). The errors associated with seismic depth conversion can be attributed to a number of factors, but an understanding of the near surface velocity variation (statics) has not been explored. Mapping the spatial variation of statics in a form that can be incorporated into velocity modelling would provide more accurate results. Considering that the contemporary stress alternates between a strike-slip and compressional stress regime (Fig. 11c), an understanding of the spatial variation in vertical stress magnitudes (calculated from density logs) would be highly beneficial and, if in a gridded map format, could be used to predict stress regimes across the basin.

Rock mechanics data does exist for key parts of the region but is selectively sampled and not representative of heterogeneities, and can contradict with other works (Abul Khair et al., 2013; Nelson et al., 2007; Pokalai et al., 2015). A detailed study focused on constraining the complete and representative rock mechanics data for the Warburton, Cooper and Eromanga basins would provide more certainty on geomechanical and hydraulic fracture stimulation models. Ideally, future hydraulic fracture stimulation models would incorporate the certain interaction between induced fractures and naturally occurring fractures and faults, with particular attention to SE-NW strike-slip faults that are most likely to reactivate under contemporary stresses (Kulikowski et al., 2016c). These SE-NW strike-slip faults are difficult to interpret in low resolution seismic data, but can reduce reservoir properties through cataclasis, can compartmentalise the reservoir, and contribute to tertiary hydrocarbon migration if reactivated (Grant-Woolley et al., 2014; Kulikowski et al., 2016c). A study investigating the possible relationship between well and reservoir performance with distance to these SE-NW strike-slip faults would provide a better understanding on their effect on production.

Finally, although not directly applicable to academic researchers, operating companies may discovery new opportunities and hydrocarbon reserves by testing such concepts as the: (1) fracture

basement play; (2) basin centred gas play; (3) hydraulic fracturing of deep coal; (4) polygonal fault system play; (5) targeting stratigraphic traps; (6) cutting-edge use of seismic data (direct hydrocarbon indicators); and (7) cost effective alternatives to optimise production (pad drilling, deviated wells from existing wellbores, deepening old shallow oil wells to target Permian reservoirs, and perforating thin (1-2 feet) gas saturated and pressurised reservoirs that were initially dismissed).

9. CONCLUSIONS

This review forms a robust synthesis of recent developments within Australia's largest onshore hydrocarbon province, the Cooper-Eromanga Basin. New technologies and software application have armed researchers with cutting edge analysis techniques and applications that have generated a recent increase in information that was previously not available. The purpose of this study is to provide readers with a holistic insight into the province that includes: (1) a detailed tectonic and stratigraphic evolution; (2) a summary of geomechanical modelling results that predict fault and fracture reactivation (tensile and shear) through time to better understand hydrocarbon migration pathways; (3) a synthesis of the petroleum system processes and elements; (4) the spatial and temporal distributions of permeable natural fracture networks through wellbore and seismic data analysis; (5) common hydraulic fracturing and well surveillance programs contrast with a discussion on the common difficulties and risks; (6) a discussion on the seismic time-to-depth conversion methods that are being used and their individual accuracies and limitations; (7) current and future hydrocarbon exploration and development targets; and (8) a discussion on the future research opportunities that can directly impact the effectiveness of exploration and development programs.

Reviewing the province has highlighted opportunities for future exploration and identified possible research topics that will be fundamental to the success of future exploration and development programs. These future programs will begin to target technically more challenging plays as the humble anticline becomes entirely exploited and will require a thorough understanding of the province. The methodologies and approaches summarised within this review forms a research framework that can be applied to other hydrocarbon provinces to better understand the dynamic structural geology, tectonic evolution and application of geophysics.

10. ACKNOWLEDGEMENTS

The authors appreciate the financial contribution made by the GeoFrac Consortium, which includes the sponsoring companies: Santos, Beach Energy, Chevron, Halliburton and BG Group (QGC). DUG Insight software (v.4.0, 2016) was used for seismic visualisation, interpretation and analysis.

11. REFERENCES

Abul Khair, H.A., Cooke, D., King, R., Hand, M., Tingay, M. (2012). Preliminary workflow for subsurface fracture mapping using 3D seismic surveys: A case study from the Cooper Basin, South Australia. In: Geothermal Research Council Conference, Reno, Nevada, 36, 339-350.

Abul Khair H., Cooke D., Hand M. (2013). The effect of present day in situ stresses and paleo-stresses on locating sweet spots in unconventional reservoirs, a case study from Moomba-Big Lake fields, Cooper Basin, South Australia. Journal of Petroleum Exploration and Production Technology, 3, (4), 207-221.

Abul Khair H., Cooke D., Hand M. (2015). Seismic mapping and geomechanical analyses of faults within deep hot granites, a workflow for enhanced geothermal system projects. Geothermics, 53, 46-56.

Al-Chalbi, M. (1974). An analysis of stacking, RMS, average, and interval velocities over a horizontally layered ground. Geophysical Prospecting, 22(3), 458-475.

Alexander, E.M., Gravestock, D.I., Cubitt, C., Chaney, A. (1998). Lithostratigraphy and environments of deposition. In: Gravestock, D.I., Hibburt, J.E., Drexel, J.F., (Eds), The Petroleum Geology of South Australia. Vol. 4: Cooper Basin, South Australia. Department of Primary Industries and Resources. Report Book, 98/9, 69-116.

Anderson, E.M. (1951). The Dynamics of Faulting and Dyke Formation with Applications to Britain, Oliver and Boyd, Edinburgh.

Apak, S.N., Stuart, W.J., Lemon, N.M., Wood, G. (1997). Structural evolution of the Permian-Triassic Cooper Basin, Australia: Relation to hydrocarbon trap styles. AAPG Bulletin, 81, 533-555.

Backe, G., Abul Khair, H., King, R., Holford, S. (2011). Fracture mapping and modelling in shale-gas target in the Cooper basin, South Australia. The APPEA Journal, 51, 397-410.

Balch, A.H., Lee, M.W., Miller, J.J., Ryder, R.T. (1982). The use of vertical seismic profiles in seismic investigations of the earth. Geophysics, 47(6), 906-918.

Balch, A.H., Lee, M.W. (1984). Vertical Seismic Profiling: Techniques, Applications, and Case Histories. International Human Resources Development Corporation, Boston, 488 p.

Baudon, C., Cartwright, J. (2008). The kinematics of reactivation of normal faults using high resolution throw mapping. Journal of Structural Geology, 30(8), 1072–1084.

Borazjani, S., Kulikowski, D., Amrouch, K., McCabe, P., Bedrikovetsky, P. (2017a). Composition changes of hydrocarbons during secondary petroleum migration. The APPEA Journal, extended abstract, accepted.

Borazjani, S., Kulikowski, D., Amrouch, K., McCabe, P., Bedrikovetsky, P. (2017b). Deep bed filtration of hydrocarbons during secondary petroleum migration. Geofluids, under review.

Boreham C. J., Hill A. J. (1998). Source rock distribution and hydrocarbon geochemistry. In: The petroleum geology of South Australia. Vol. 4: Cooper Basin (eds. D.I. Gravestock, J.E. Hibburt and J.F. Drexel), pp 129-142. South Australia. Department of Primary Industries and Resources. Report Book, 98/9.

Bradshaw, M.T., (1993). Australian petroleum systems. PESA Journal 21, 43-53.

Childs, C., Nicol, A., Walsh, J.J., Watterson, J. (1996). Growth of vertically segmented normal faults. Journal of Structural Geology, 18(12), 1389-1397.

Cooke, D., Tyiasning, S., Abul Khair, H. (2016). Unexpected behaviors of stimulated fractures in the high-stress Cooper Basin. The Leading Edge, 35(1), 78-84.

Deighton, I., Hill, A.J., 1998. Thermal and Burial History. In: The petroleum geology of South Australia. Vol. 4: Cooper Basin (eds. D.I. Gravestock, J.E. Hibburt and J.F. Drexel), pp 143-156. South Australia. Department of Primary Industries and Resources. Report Book, 98/9.

Elliott, L.G. (1993). Post-Carboniferous tectonic evolution of eastern Australia. APEA Journal, 33, 215-215.

Evans, P.R. (1988). The formation of petroleum and geological history of Australia. In: Petroleum in Australia: the first century. APEA Journal, Special Publication, 26-47.

Flottmann, T., Campagna, D.J., Hillis, R., Warner, D. (2004). Horizontal microfractures and core discing in sandstone reservoirs, Cooper Basin, Australia. In: Eastern Australasian basins symposium II: Petroleum Exploration Society of Australia Special Publication (pp. 689-694).

Gajewski, D., Pšenčik, I. (1990). Vertical seismic profile synthetics by dynamic ray tracing in laterally varying layered anisotropic structures. Journal of Geophysical Research: Solid Earth, 95(B7), 11301-11315.

Ganley, D.C., Kanasewich, E.R. (1980). Measurement of absorption and dispersion from check shot surveys. Journal of Geophysical Research: Solid Earth, 85(B10), 5219-5226.

Giba, M., Walsh, J.J., Nicol, A. (2012). Segmentation and growth of an obliquely reactivated normal fault. Journal of Structural Geology, 39, 253-267.

Gravestock, D.I., Jensen-Schmidt, B. (1998). Structural setting. In: Gravestock, D.I., Hibburt, J.E., Drexel, J.F., (Eds), The Petroleum Geology of South Australia. Vol. 4: Cooper Basin, South Australia. Department of Primary Industries and Resources. Report Book, 98/9, 47-68.

Gray, M.E, Daniel, R., Kaldi, J., Kulikowski, D. (2017). Determining the Accuracy of Pseudo-Capillary Pressure Curves Generated from Nuclear Magnetic Resonance (NMR) Data: The Cooper Basin, Australia. Australian Journal of Earth Sciences, submitted.

Green, P.M., Brain, T.J., John, B.H. (1989). Possible stratigraphic controls on hydrocarbon distribution within the Jurassic-Early Cretaceous rocks, Eromanga Basin, southern Queensland. In: The Cooper and Eromanga Basins, Australia (ed. B.J. O'Neil), pp. 251-264. Petroleum Exploration Society of Australia, Society of Petroleum Engineers, Australian Society of Exploration Geophysicists (S.A. Branches), Adelaide (Proceedings of Cooper and Eromanga Basins Conference).

Haines, P.W., Hand, M., Sandiford, M. (2001). Palaeozoic synorogenic sedimentation in central and northern Australia: A review of distribution and timing with implications for the evolution of intracontinental orogens. Australian Journal of Earth Sciences, 48, 911-928.

Hardage, B.A. (1985). Vertical seismic profiling. The Leading Edge, 4(11), 59-59.

Hauge, P.S. (1981). Measurements of attenuation from vertical seismic profiles. Geophysics, 46(11), 1548-1558.

Heath, R., McIntyre, S., Gibbins, N. (1989). A Permian origin for Jurassic reservoired oil in the Eromanga Basin. In: The Cooper and Eromanga Basins, Australia (ed. B.J. O'Neil), pp. 405-416.

Petroleum Exploration Society of Australia, Society of Petroleum Engineers, Australian Society of Exploration Geophysicists (S.A. Branches), Adelaide (Proceedings of Cooper and Eromanga Basins Conference).

Hillis, R.R., Macklin, T.A., Siffleet, P. (1995). Regional depth-conversion of mapped seismic two-way-times in the Cooper-Eromanga Basins. Exploration Geophysics, 26(2/3), 412-418.

Hoffmann, K.L. (1989). The influence of pre-Jurassic tectonic regimes on the structural development of the southern Eromanga Basin, Queensland. In: The Cooper and Eromanga Basins, Australia (ed. B.J. O'Neil), pp. 315-328. Petroleum Exploration Society of Australia, Society of Petroleum Engineers, Australian Society of Exploration Geophysicists (S.A. Branches), Adelaide (Proceedings of Cooper and Eromanga Basins Conference).

Igboekwe, M.U., Ohaegbuchu, H.E. (2011). Investigation into the weathering layer using up-hole method of seismic refraction. Journal of Geology and Mining Research, 3(3), 73-86.

Jackson, C.A.L., Rotevatn, A. (2013). 3D seismic analysis of the structure and evolution of a salt-influenced normal fault zone: a test of competing fault growth models. Journal of Structural Geology, 54, 215-234, doi:10.1016/j.jsg.2013.06.012.

Jadoon, Q.K., Roberts, E., Blenkinsop, T., Raphael, A.J., Shah, S.A. (2016). Mineralogical modelling and petrophysical parameters in Permian gas shales from the Roseneath and Murteree formations, Cooper Basin, Australia. Petroleum Exploration and Development, 43(2), 277-284.

Johnson, Jr., R.L., Abul Khair, H., Jeffrey, R.G., Meyer, J.J., Stark, C., Tauchintz, J. (2015). Improving fracture initiation and potential impact on fracture coverage by implementing optimal well planning and drilling methods for typical stress conditions in the Cooper Basin, Central Australia. The APPEA Journal and Conference Proceedings, 55, extended abstract.

Kantsler, A.J., Prudence, T.J.C., Cook, A.C., Zwigulis, M. (1984). Hydrocarbon habitat of the Cooper/Eromanga basin, Australia. In: Petroleum geochemistry and basin evolution (eds. G. Demaison and R. J. Murris), pp 373-390. American Association of Petroleum Geologists Memoir 35.

King, R., Abul Khair, H., Bailey, A., Backe, G., Holford, S., Hand, M. (2011). Integration of In-Situ Stress Analysis and Three-Dimensional Seismic Mapping to Understand Fracture Networks in Australian Basins. In: Proceedings from the Australian Geothermal Energy Conference, 16-18 November, Melbourne, Australia, 129-134.

Kuang, K.S. (1985). History and style of Cooper-Eromanga Basin structures. Exploration Geophysics, 16, 245-248.

Kulikowski, D., Cooke, D., Amrouch, K. (2016a). Constraining the distribution and relationship between overpressure, natural fracture density and temperature in the Cooper Basin. The Australian Petroleum Production and Exploration Association Journal, 56, 11-28, doi:10.1071/AJ15002.

Kulikowski, D., Hochwald, C., Cooke, D., Amrouch, K. (2016b). A Statistical Approach to Assessing Depth Conversion Uncertainty on a Regional Dataset: Cooper-Eromanga Basin, Australia. ASEG-PESA-AIG 2016 Conference, Adelaide. Extended Abstract #200, 484-490, doi:10.1071/aseg2016ab200.

Kulikowski, D., Amrouch, K., Cooke, D. (2016c). Geomechanical Modelling of Fault Reactivation in the Cooper Basin, Australia. Australian Journal of Earth Sciences, 63(3), 295-314, doi:10.1080/08120099.2016.1212925.

Kulikowski, D., Amrouch, K. (2017a). Combining Geophysical Data and Calcite Twin Stress Inversion to Refine the Tectonic History of Subsurface and Offshore Provinces: A Case Study on the Cooper-Eromanga Basin, Australia. Tectonics, 36(3), 515-541, doi:10.1002/2016TC004366.

Kulikowski, D., Amrouch, K. (2017b). 3D Seismic Analysis Investigating the Relationship Between Structural Activity and Stratigraphic Architecture in the Intracratonic Cooper and Eromanga Basins, Australia. Marine and Petroleum Geology, submitted.

Kulikowski, D., Amrouch, K. (2017c). 4D Modelling of Fault Reactivation using Complete Paleo-Stress Tensors from the Cooper-Eromanga Basin, Australia. Australian Journal of Earth Sciences, submitted.

Kulikowski, D., Amrouch, K., Cooke, D., Gray, M.E. (2017a). Basement Structural Architecture and Hydrocarbon Conduit Potential of Polygonal Faults in the Cooper-Eromanga Basin, Australia. Geophysical Prospecting, in press, doi:10.1111/1365-2478.12531.

Kulikowski, D., Amrouch, K., Burgin, H.B. (2017b). Mapping Permeable Subsurface Fracture Networks: A Case Study on the Cooper Basin, Australia. Journal of Structural Geology, Submitted.

Kulikowski, D., Hochwald, C., Amrouch, K. (2017c). An automated cross-validation method to assess seismic time-to-depth conversion accuracy: A case study on the Cooper-Eromanga Basin, Australia. Unsubmitted.

Lowe-Young, B.S., Mackie, S.I., Heath, R.S. (1997). The Cooper-Eromanga petroleum system, Australia: Investigation of essential elements and processes. Indonesian Petroleum Association. Proceedings of the Petroleum Systems of SE Asia and Australasia Conference, Jakarta, 199-211.

Mackie, S. (2015). History of Petroleum Exploration and Development in the Cooper and Eromanga Basins. AAPG/SEG International Conference and Exhibition, Melbourne, Australia, Search and Discovery Article #10814.

Mavromatidis, A. (2006). Burial/exhumation histories for the Cooper-Eromanga Basins and implications for hydrocarbon exploration, Eastern Australia. Basin Research, 18, 351-373.

Muller, R.D., Dyksterhuis, S., Rey, P. (2012). Australian paleo-stress fields and tectonic reactivation over the past 100 Ma. Australian Journal of Earth Sciences, 59, 13-28.

Nelson, E.J., Meyer, J.J., Hillis, R.R., Mildren, S.D. (2005). Transverse drilling-induced tensile fractures in the West Tuna area, Gippsland Basin, Australia: implications for the in situ stress regime. International Journal of Rock Mechanics and Mining Sciences, 42(3), 361-371.

Othman, A.A., Fathy, M., Maher, A. (2016). Use of spectral decomposition technique for delineation of channels at Solar gas discovery, offshore West Nile Delta, Egypt. Egyptian Journal of Petroleum, 25(1), 45-51.

Partyka, G., Gridley, J., Lopez, J. (1999). Interpretational applications of spectral decomposition in reservoir characterization. The Leading Edge, 18(3), 353-360.

Pokalai, K., Fei, Y., Ahmad, M., Haghighi, M., Gonzalez, M. (2015a). Design and optimisation of multi-stage hydraulic fracturing in a horizontal well in a shale gas reservoir in the Cooper Basin, South Australia. The Australian Petroleum Production and Exploration Association Journal, 55, 1–14.

Pokalai K., Haghighi M., Sarkar S., Tyiasning S., Cooke D. (2015b). Investigation of the Effects of Near-Wellbore Pressure Loss and Pressure Dependent Leakoff on Flowback during Hydraulic Fracturing with Pre-Existing Natural Fractures. SPE/IATMI Asia Pacific Oil and Gas Conference and Exhibition, Nusa Dua, Bali, SPE-176440.

Pokalai, K., Kulikowski, D., Johnson, Jr., R.L., Haghighi, M., Cooke, D. (2016). Development of a new approach for hydraulic fracturing in tight sand with pre-existing natural fractures. The Australian Petroleum Production and Exploration Association Journal, 56, 225-238.

Pokalai, K., Kulikowski, D., Amrouch, K., Haghighi, M., Johnson, Jr., R.L. (2017). Integrated 3D modelling of hydraulic fracturing in tight reservoirs with pre-existing natural fractures and complex stress conditions: A case study from the Cooper Basin, Australia. Journal of Petroleum Science and Engineering, submitted.

Radke, B. (2009). Hydrocarbon and Geothermal Prospectivity of Sedimentary Basins in Central Australia; Warburton, Cooper, Pedirka, Galilee, Simpson and Eromanga Basins. Geoscience Australia Record 2009/25.

Reynolds, S.D., Mildren, S.D., Hillis, R.R., Meyer, J.J., Flottmann, T. (2005). Maximum horizontal stress orientations in the Cooper Basin, Australia. implications for plate-scale tectonics and local stress sources. Geophysical Journal International, 160, 332-343.

Reynolds, S.D., Mildren, S.D., Hillis, R.R., Meyer, J.J. (2006). Constraining stress magnitudes using petroleum exploration data in the Cooper-Eromanga Basins, Australia. Tectonophysics, 415, 123-140.

Rezaee, M.R., Sun, X. (2007). Fracture-Filling Cements in the Palaeozoic Warburton Basin, South Australia. Journal of Petroleum Geology, 30(1), 79-90.

Roberts, G.A., Chipperfield, S.T., Miller, W.K. (2000). The evolution of a high near-wellbore pressure loss treatment strategy for the Australian Cooper Basin. In SPE Annual Technical Conference and Exhibition. Society of Petroleum Engineers.

Robson, A.G, Holford, S.P., King, R.C., Kulikowski, D. (2018). Structural evolution of horst and half-graben structures proximal to a transtensional fault system using a 3D seismic dataset from the Shipwreck Trough, offshore Otway Basin, Australia. Marine and Petroleum Geology, 89, 615-634, doi:10.1016/j.marpetgeo.2017.10.028.

Senior, B.R., Galloway, M.C., Ingram, J.A., Senior D. (1968). The geology of the Barrolka, Eromanga, Durham Downs, Thargomindah, Tickalara and Bulloo 1:250,000 Sheet areas, Queensland. Bureau of Mineral Resources.

Stainsby, S.D., Worthington, M.H. (1985). Q estimation from vertical seismic profile data and anomalous variations in the central North Sea. Geophysics, 50(4), 615-626.

Stanmore, P.J. (1989). Case studies of stratigraphic and fault traps in the Cooper Basin, Australia. In The Cooper and Eromanga Basins, Australia. Proceedings of the Cooper and Eromanga Basins Conference, Adelaide (pp. 361-369).

Stuart, W.J. (1976). The genesis of Permian and lower Triassic reservoir sandstones during phases of southern Cooper Basin development. APEA Journal, 16(1), 27-48.

Sun, X. (1997). Structural style of the Warburton Basin and control in the Cooper and Eromanga Basins, South Australia. Exploration Geophysics, 28(3), 333-339.

Tyiasning, S., Cooke, D. (2015). A comparison of competing amplitude variation with offset techniques applied to tight gas sand exploration in the Cooper Basin of Australia. Interpretation, 3(3), SZ15-SZ26.

Tyiasning, S., Cooke, D. (2016). Anisotropy signatures in the Cooper Basin of Australia: Stress versus fractures. Interpretation, 4(2), SE51-SE61.

Veevers, J.J., Jones, J.G., Powell, C.M. (1982). Tectonic framework of Australia's sedimentary basins. APEA Journal, 22(1), 283-300.

Veevers, J.J., Powell, C.M. (1984). Uluru and Adelaidean regimes, in J. J. Veevers, ed., Phanerozoic earth history of Australia: Oxford, Clarendon Press, p. 329–339.

Watterson, J., Walsh, J., Nicol, A., Nell, P.A.R., Bretan, P.G. (2000). Geometry and origin of a polygonal fault system. Journal of the Geological Society, 157(1), 151-162.

Williams, G.D., Powell, C.M., Cooper, M.A. (1989). Geometry and kinematics of inversion tectonics. Geological Society, London, Special Publications, 44(1), 3-15.

12. FIGURES

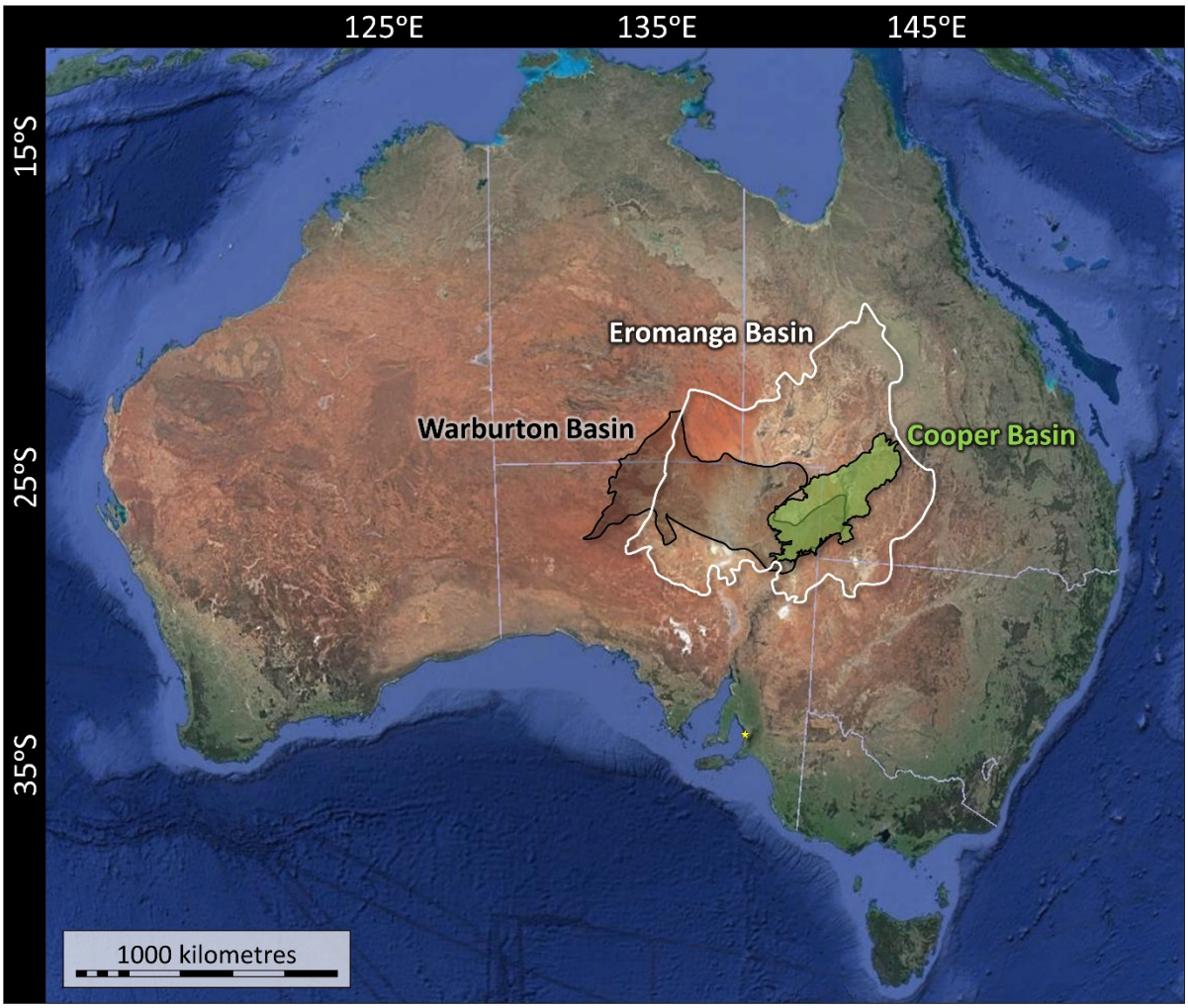


Figure 1. Location of the Warburton, Cooper, and Eromanga basins (after Kulikowski et al., 2016c).

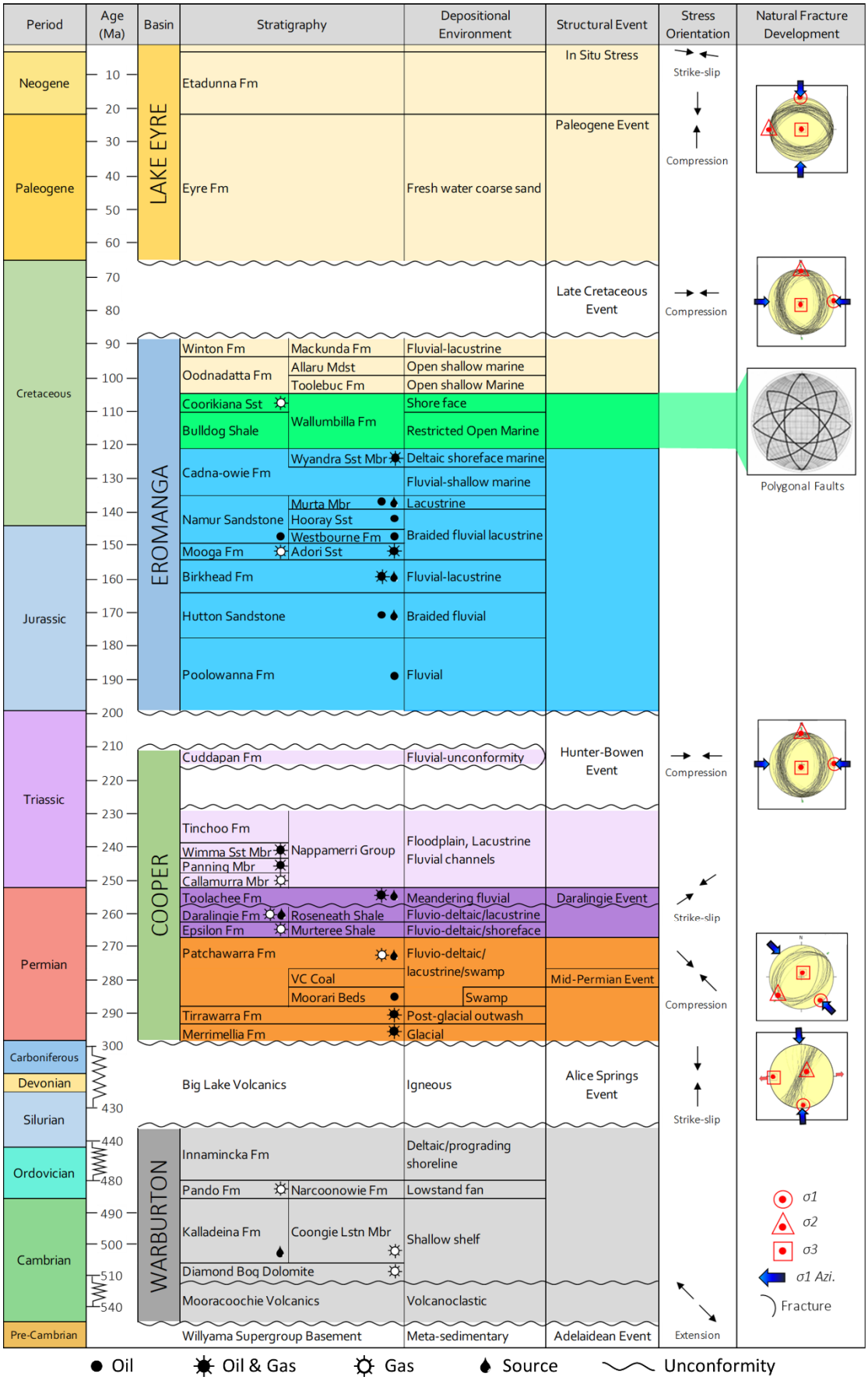


Figure 2. Tectonostratigraphy of the Cooper-Eromanga Basin (after Kulikowski & Amrouch., 2017a).

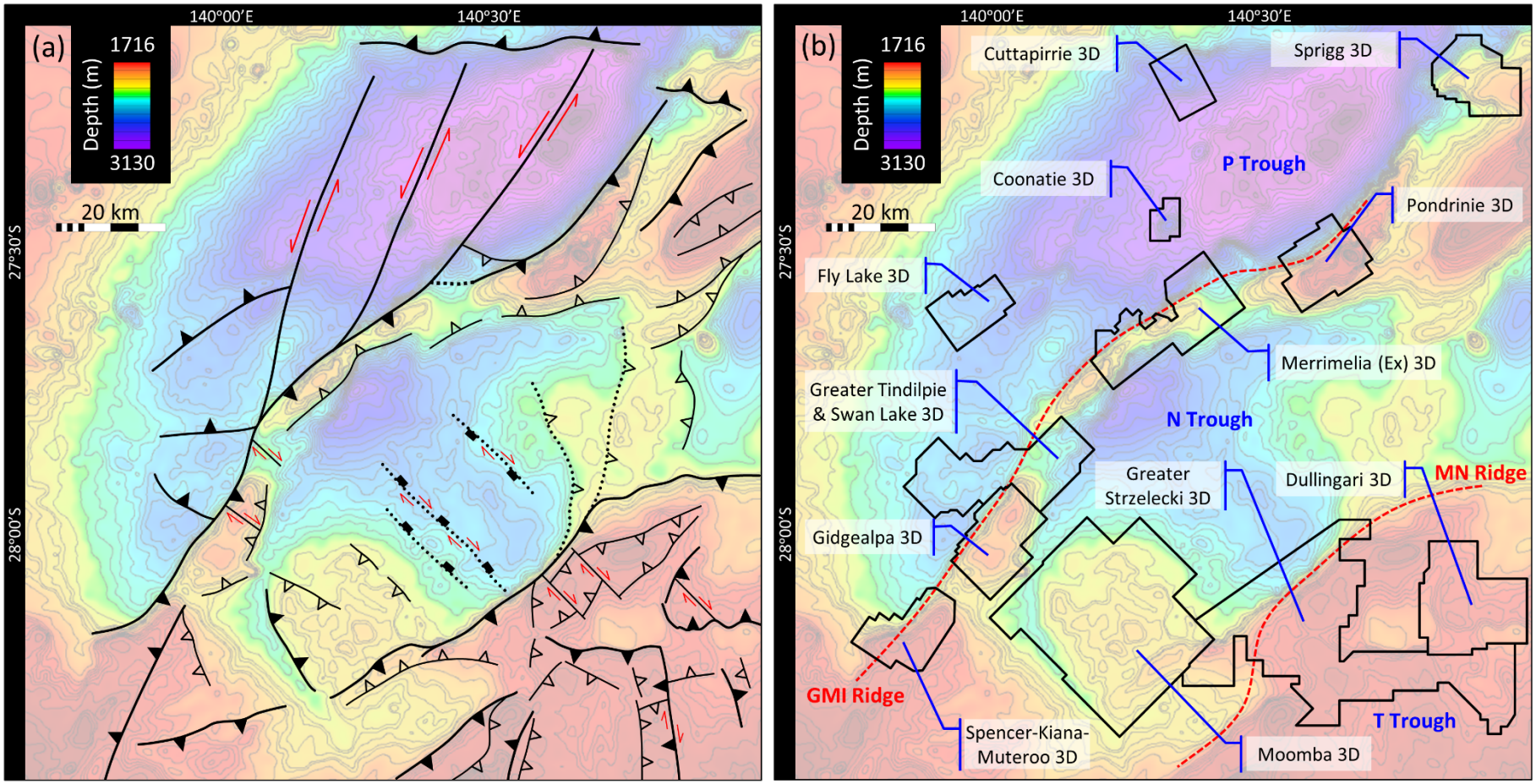


Figure 3. (a) Fault map of the South Australian Cooper-Eromanga Basin (after Kulikowski et al., 2017a). (b) Location of 12 3D seismic surveys commonly used for research. The location of the Gidgealpa-Merrimelia-Innamincka (GMI) and Murteree Nappacoongee (MN) ridges, and the Patchawarra (P Trough), Nappamerri (N Trough), and Tenappera (T Trough) troughs are shown (after Kulikowski et al., 2017a).

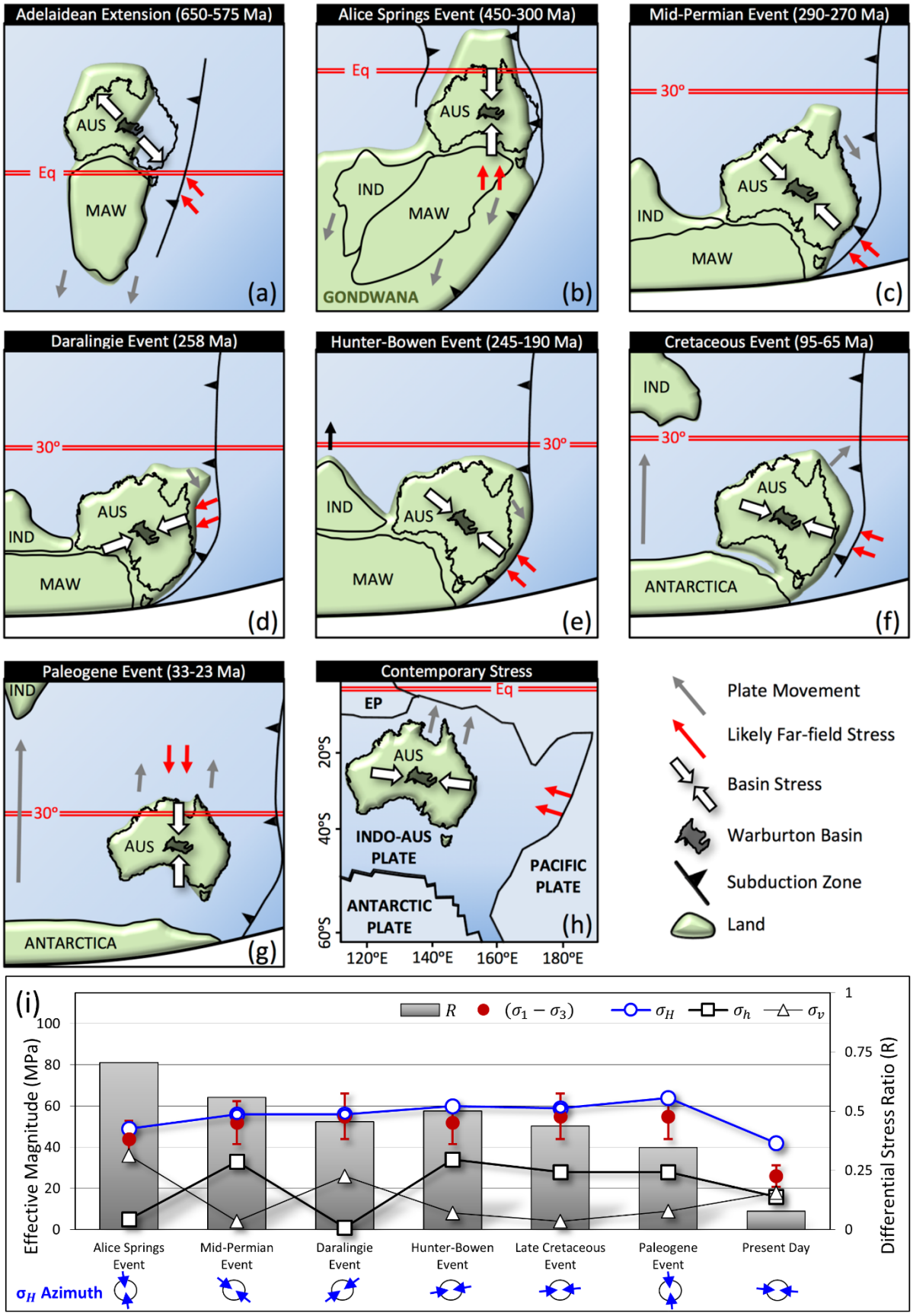


Figure 4. (a)→(h) Geodynamic evolution of Australia with Cooper-Eromanga Basin derived stresses through time. (i) Evolution of principal stresses (after Kulikowski & Amrouch, 2017a, 2017c).

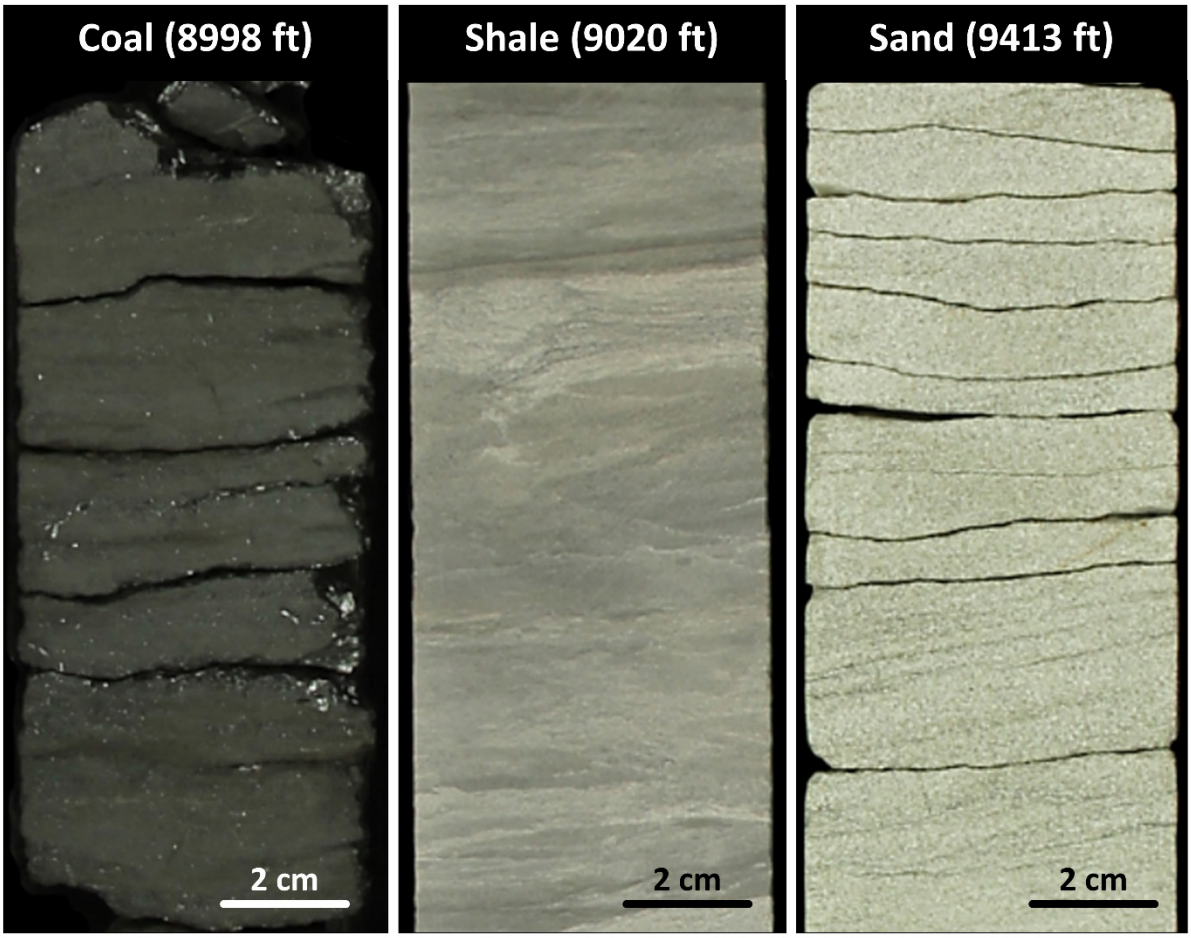


Figure 5. Cyclic lithology variation within the Patchawarra Formation (Core images obtained from Tindilpie 11 well completion report).

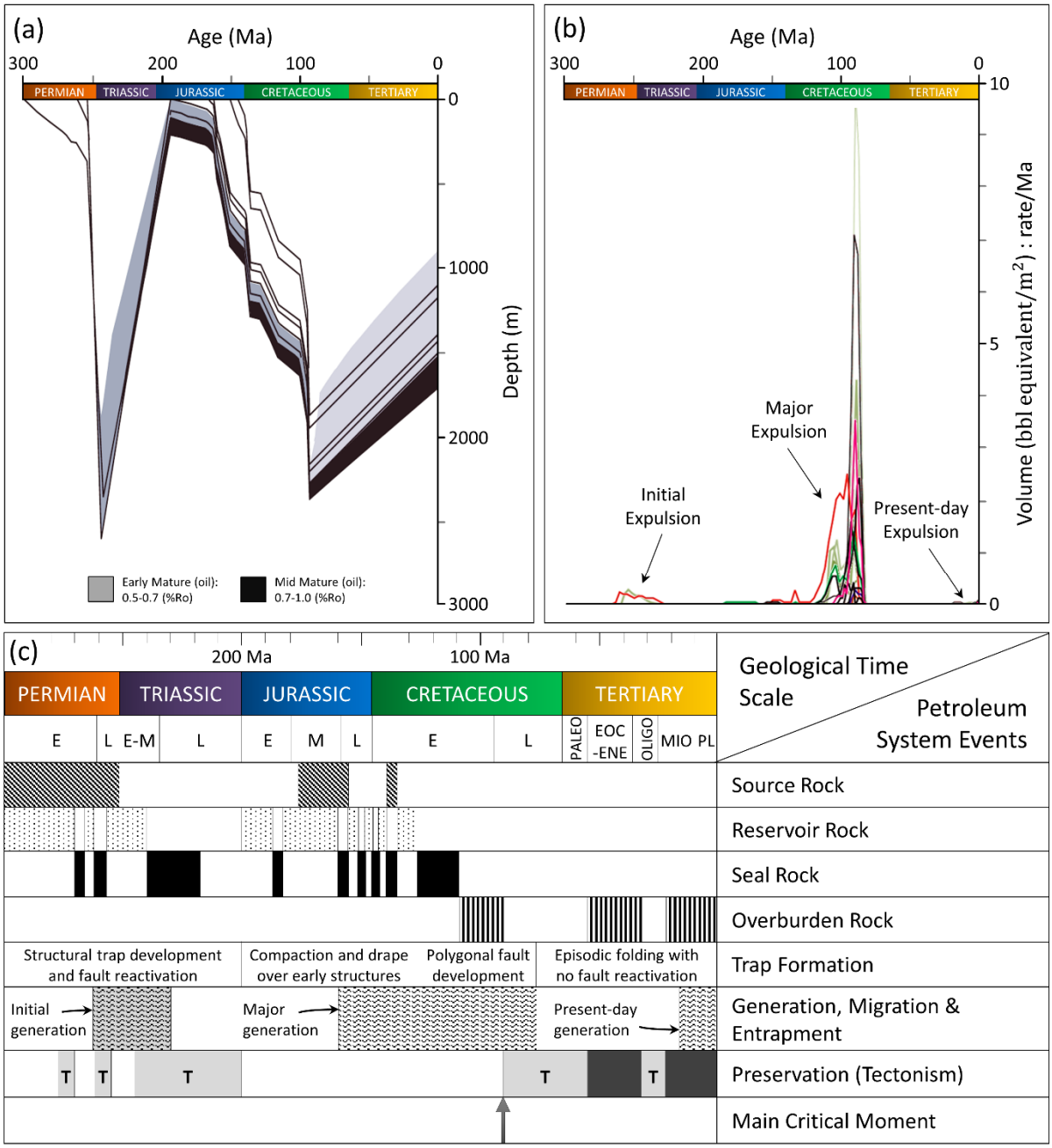


Figure 6. (a) Burial history of Cooper-Eromanga Basin sediments (after Mavromatidis, 2006). (b) Gas (per well) and oil expulsion through time (after Deighton & Hill, 2009). (c) Timing of key petroleum system processes (after Lowe-Young et al., 1997).

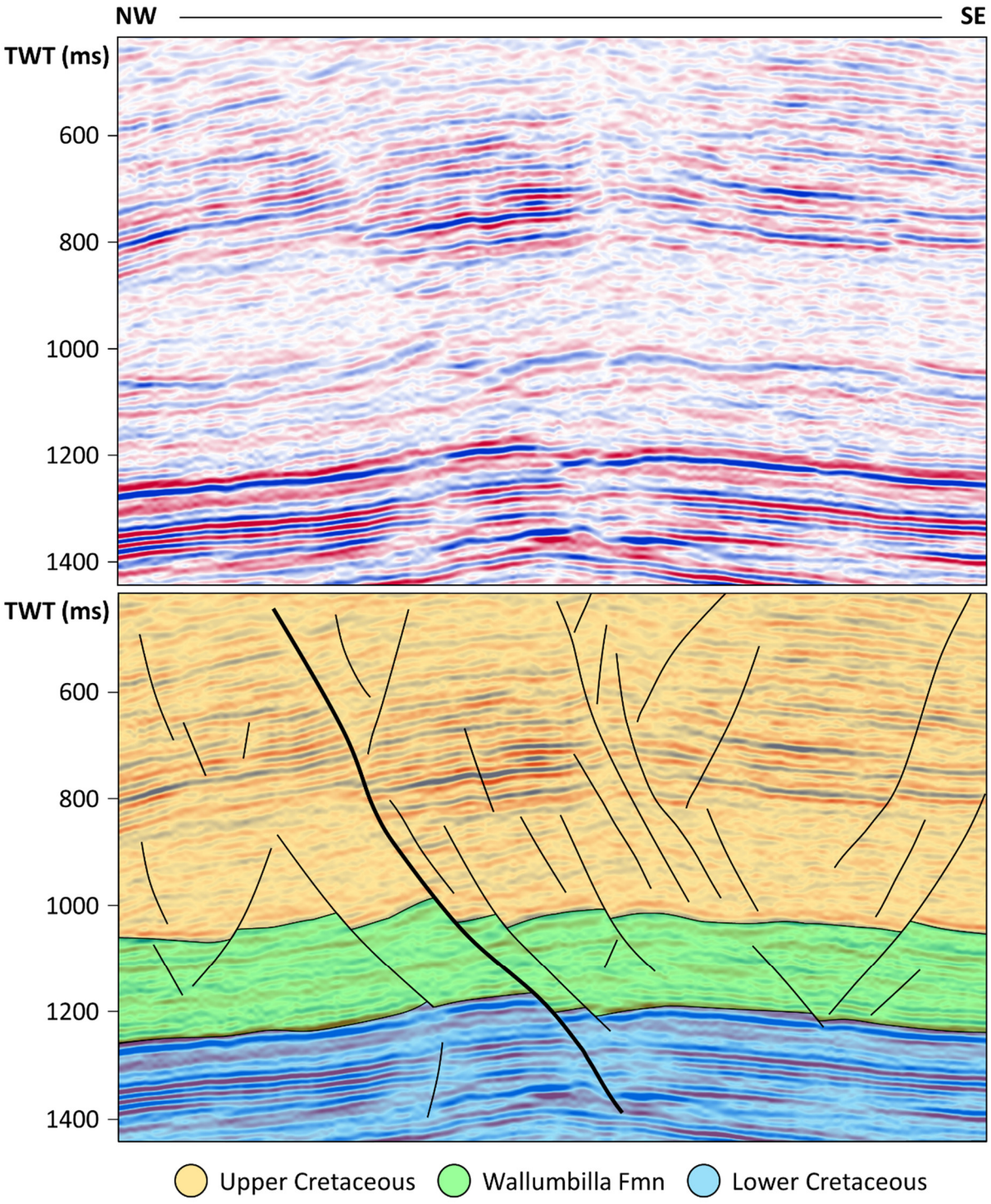


Figure 7. Cross-section from the Spencer-Kiana-Murteree 3D seismic survey (Inline 640) showing the polygonal fault system with large normal faults observed to displace the Cadna-owie Formation reflector and extend into oil-rich Lower Cretaceous reservoirs (Kulikowski et al., 2017a). See Figure 3b for seismic survey location.

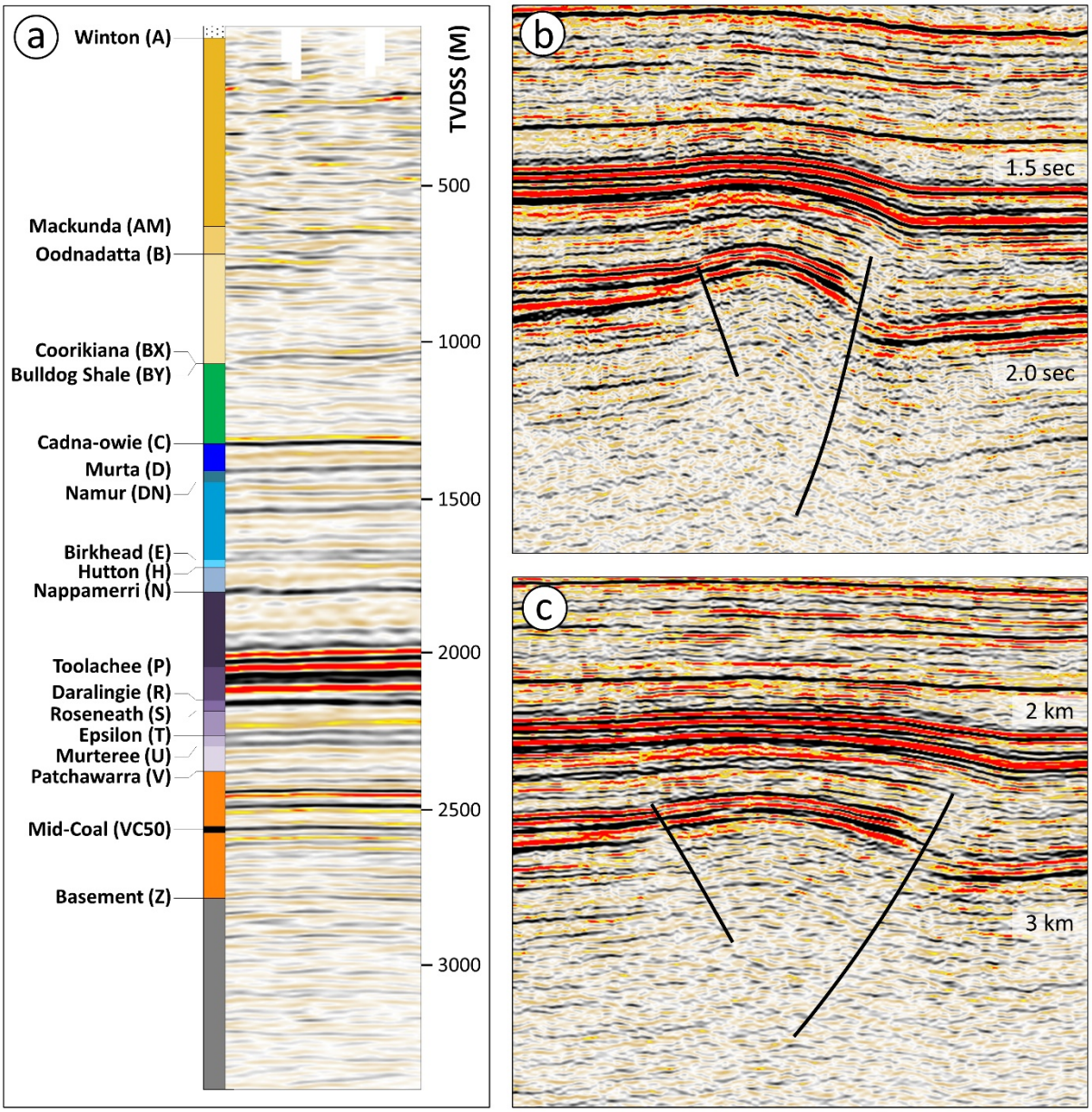


Figure 8. (a) Typical seismic reflection profile showing stratigraphic and seismic markers. `The difference in fault geometry when seismic data is in: (b) the time-domain; and (c) the depth-domain.

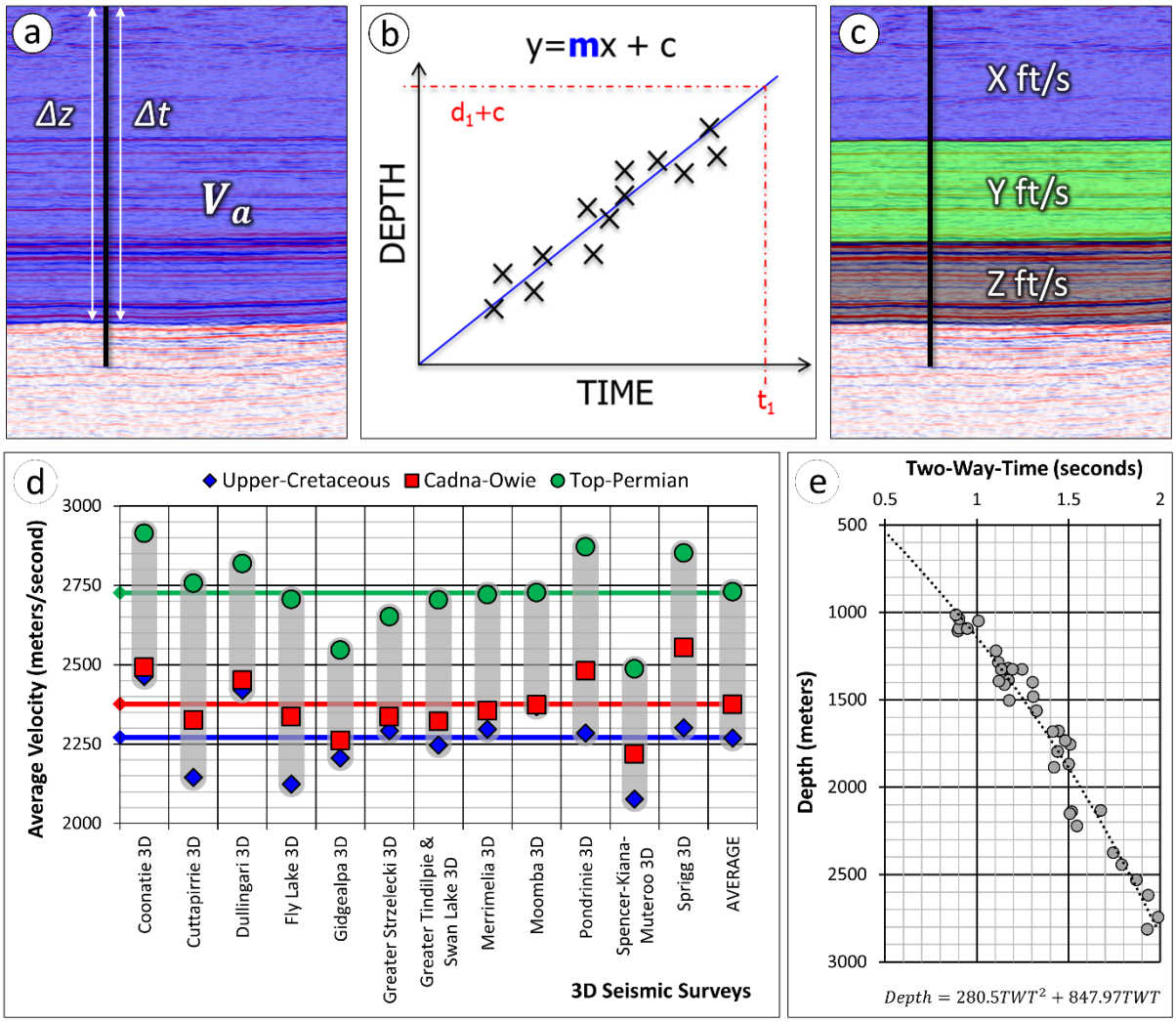


Figure 9. Common seismic time-to-depth conversion methods. (a) Average velocity (V_a) method uses the ratio between depth (from well) and time (from seismic data) for a reflector. (b) Time-depth trend method fits a trend for the time-depth pair data. (c) Interval velocity, or layer-cake, method divides the seismic survey into key stratal units and applies different velocities to those layers. (d) Average Velocities for key seismic reflectors. (e) Time-Depth trend obtained from 12 3D seismic surveys (after Kulikowski et al., 2016b, 2017a). See Figure 3b for seismic survey location.

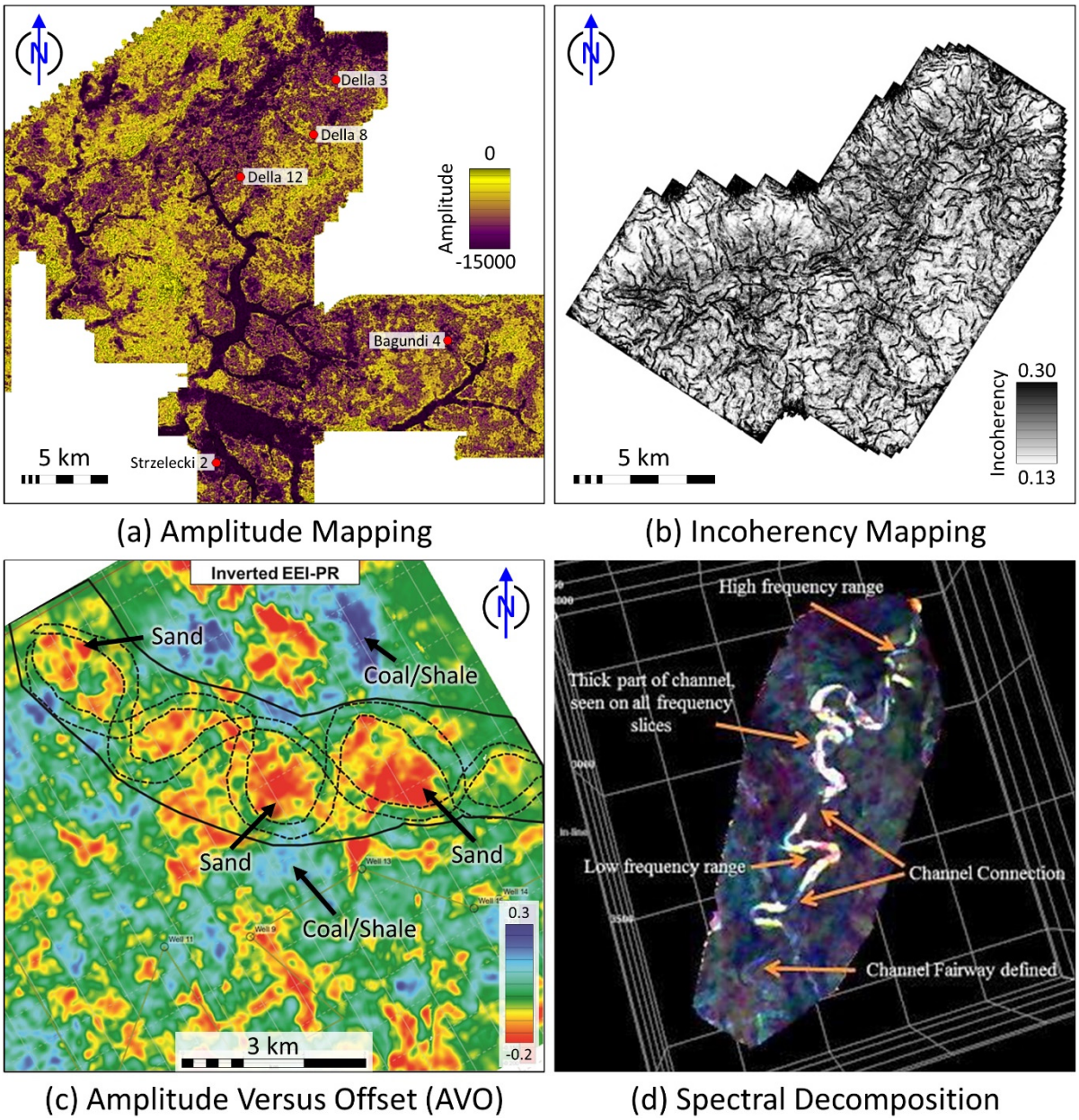


Figure 10. Seismic data analysis techniques beneficial to the fluvial dominated Cooper-Eromanga Basin. (a) Amplitudes extracted along reflector surfaces to locate channel systems. Example from Greater Strzelecki 3D showing a large regional channel system (after Kulikowski and Amrouch, 2017); (b) Incoherency analysis along a reflector to identify subtle faults. Example from Spencer-Kiana-Muteroo 3D showing the distribution of polygonal faults along the Upper Cretaceous reflector (after Kulikowski and Amrouch, 2017b); (c) Application of amplitude versus offset (AVO) to differentiate between sandstone and coal measures. The example shows the distribution of sandstone (red-yellow) and shale/coal (green-blue) in the Cooper Basin (after Tyiasning and Cooke, 2015); and (d) A spectral decomposition analysis used to delineate the geometry of a fluvial channel in the West Nile Delta, Egypt (Othman et al., 2016).

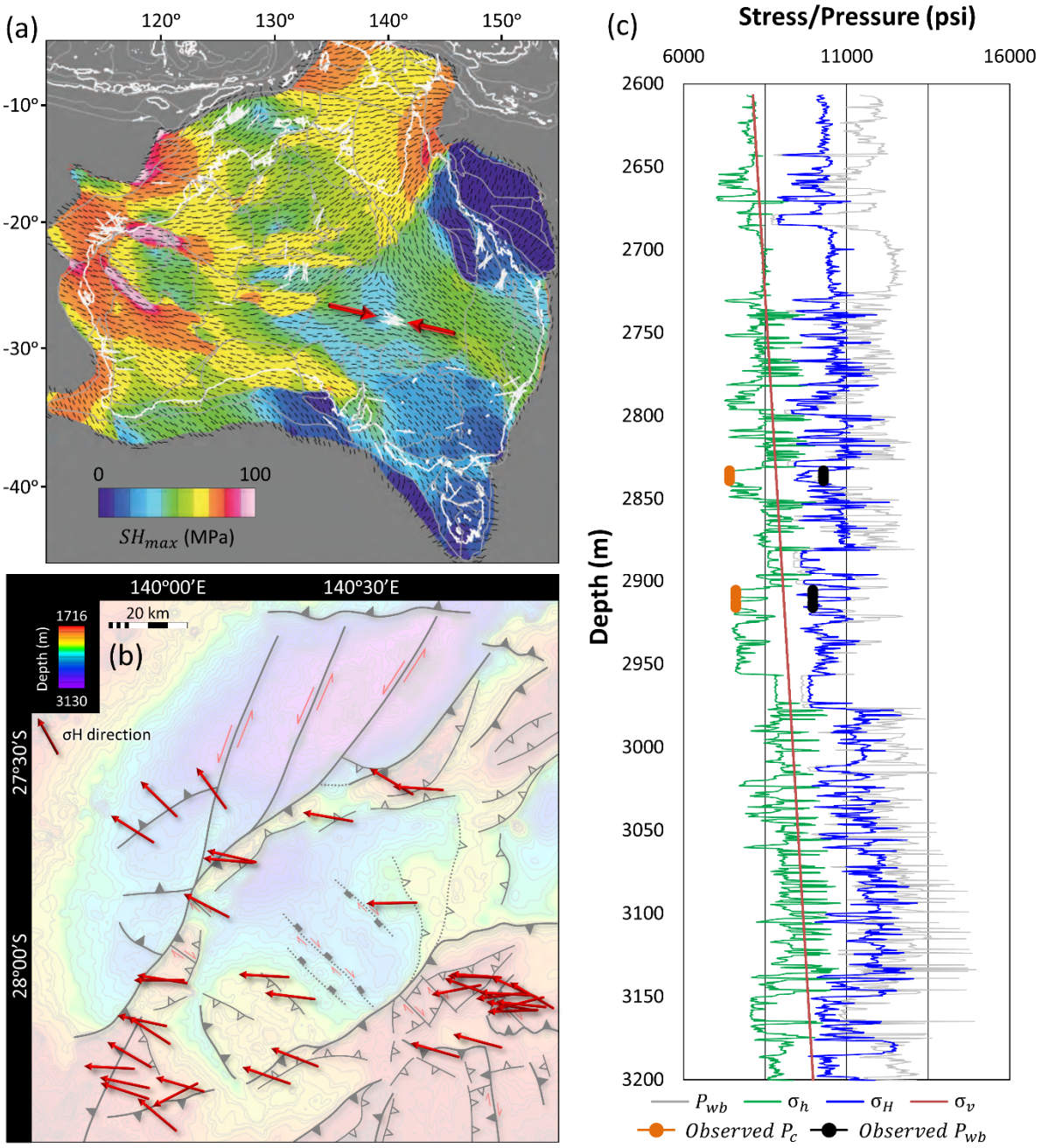


Figure 11. Orientation of the maximum horizontal stress orientation across: (a) Australia (after Muller et al., 2012); and (b) the Cooper-Eromanga Basin (after Kulikowski et al., 2017a). (c) A typical mechanical earth model for the Patchawarra Formation showing the minimum (σ_h) and maximum (σ_H) horizontal stresses, vertical stress (σ_v), breakdown pressure from logs (P_{wb}) and well test data (observed P_{wb}), and closure pressure (observed P_c) (after Pokalai et al., 2017). See Figure 4i for the origin of far-field stresses.

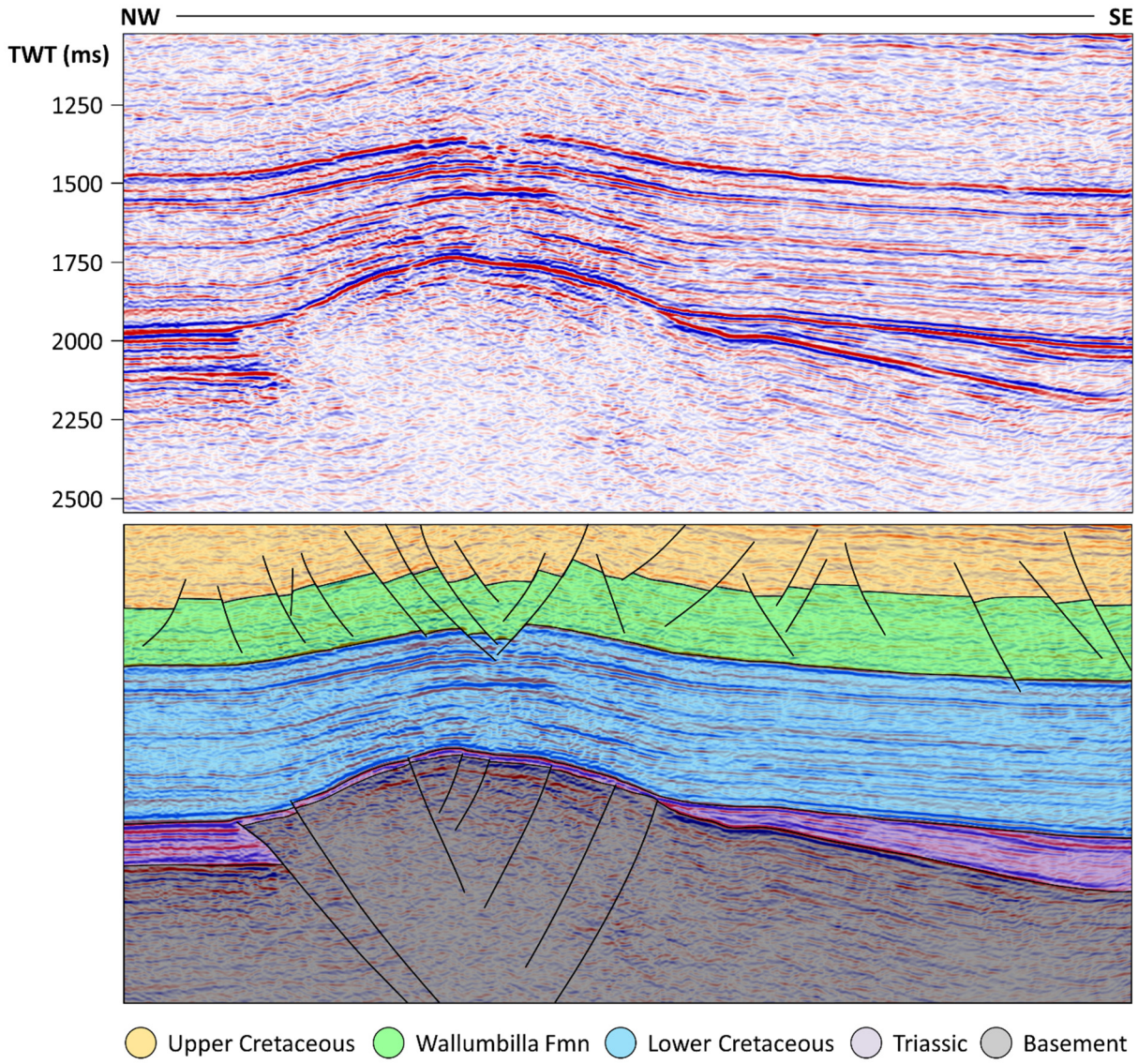


Figure 12. Basement and polygonal faults in the Merrimelia (Extension) 3D seismic survey interpreted along Inline 4295 (Kulikowski et al., 2017a). See Figure 3b for seismic survey location.

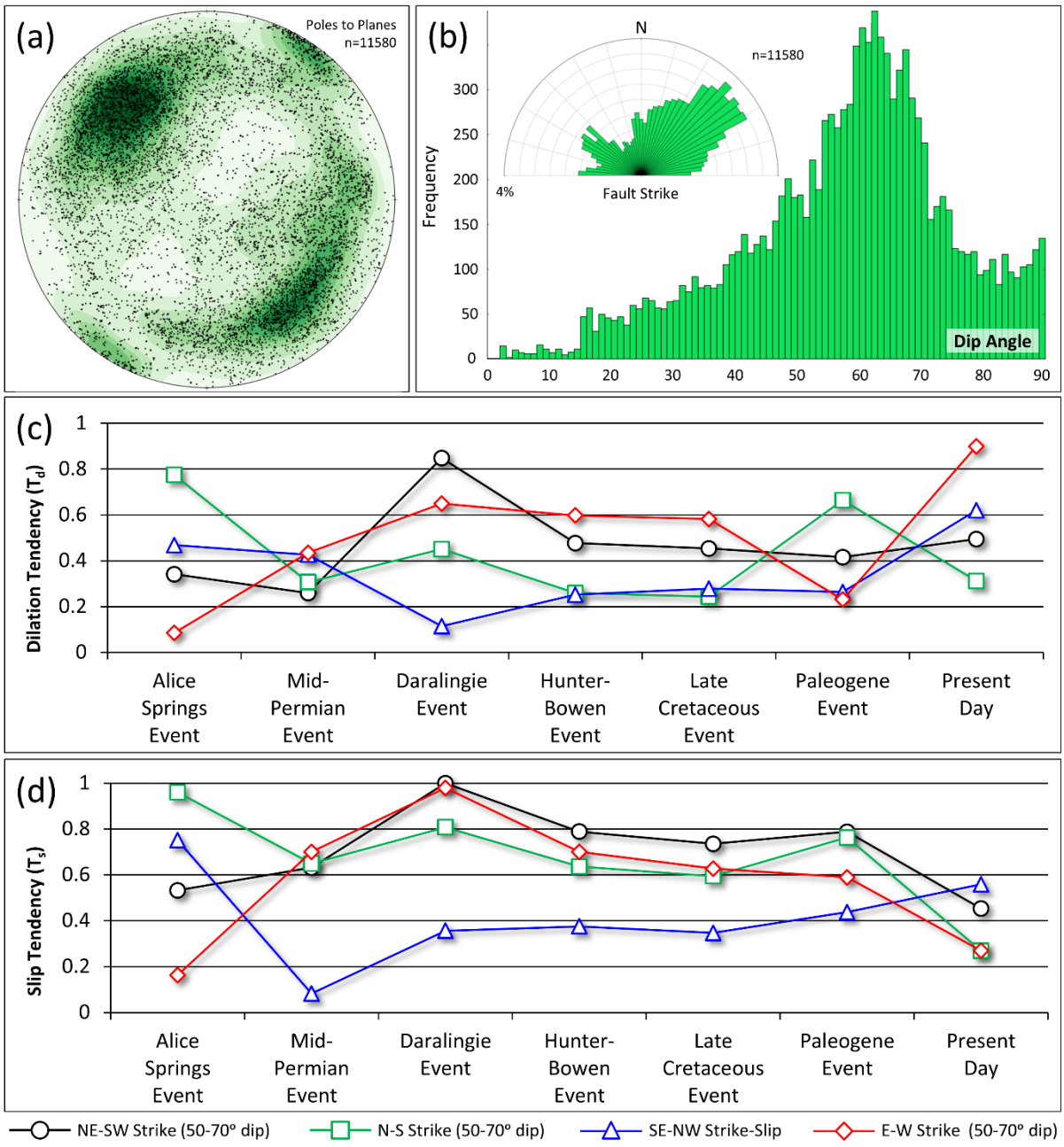


Figure 13. Fault geometry from six 3D seismic surveys (Dullingari 3D, Greater Tindilpie & Swan Lake 3D, Gidgealpa 3D, Greater Strzelecki 3D, Merrimelia (Ext) 3D, and Fly Lake 3D) presented as: (a) poles to planes; and (b) dip and strike (after Kulikowski & Amrouch, 2017a). Reactivation potential of the four most common fault sets measured using the: (c) Dilation Tendency; and (d) Slip Tendency (after Kulikowski & Amrouch, 2017c). See Figure 3 for location of 3D seismic surveys.

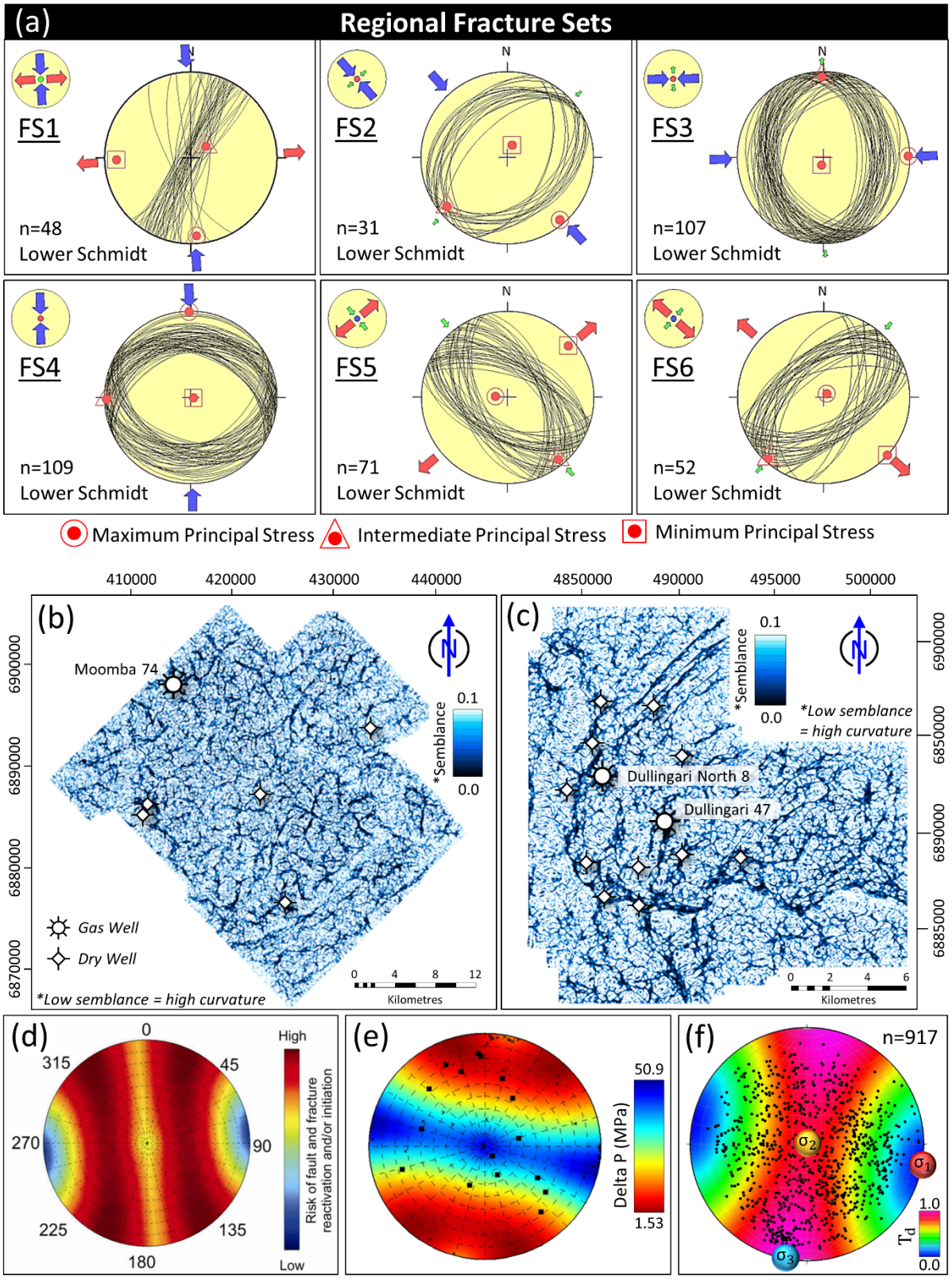


Figure 14. (a) Regional natural fracture sets (Kulikowski & Amrouch, 2017a). Most positive curvature processed into semblance in: (b) Moomba 3D; and (c) Dullingari 3D (Kulikowski et al., 2017b). In situ stress showing: (d) Fracture susceptibility (King et al., 2011); (e) Structural Permeability (Abul Khair et al., 2013); and (f) Dilation Tendency (T_d) (Kulikowski et al., 2017a). See Figure 3b for location.

6. THESIS CONCLUSIONS

This thesis presents a modern approach that can be applied to other subsurface provinces to constrain the structural geology and tectonic evolution by incorporating micro-, meso-, and macro-scale data with cutting-edge methods and analysis techniques. In the Cooper-Eromanga Basin (case study) the structural evolution models have relied solely on sparse and low resolution 2D seismic data, which has led to researchers having contradicting and unclear ideas on the timing, orientation and stress regime of tectonic events. An improved understanding of the basin evolution model, structural geology and geomechanics, and geophysics has tremendous implications for efficient hydrocarbon exploration and development. Each of the manuscripts has investigated an important aspect of this subsurface province using data that was not obtained from outcrop.

The application of Etchecopar's calcite twin stress inversion technique has better defined the orientation and magnitude of tectonic events and has never been applied to an Australian dataset prior to this study. Precise stress orientations and stress regimes were defined for the six tectonic events that were previously poorly constrained:

i. **Carboniferous Alice Springs Event:** N-S strike-slip stress regime;
ii. **Middle Permian Event:** SE-NW compressional stress regime;
iii. **Daralingie Event:** NE-SW strike-slip stress regime;
iv. **Hunter-Bowen Event:** E-W compressional stress regime;
v. **Late Cretaceous Event:** E-W compressional stress regime;
vi. **Paleogene Event:** N-S compressional stress regime.

In addition to this, six regionally extensive conjugate natural fracture sets were defined and integrated with calcite twin results to constrain the timing of their development, such that: (1) SE-NW and NNE-SSW striking vertically dipping fracture set is present in Warburton Basin stratigraphy and developed during the Alice Springs Event; (2) NE-SW striking low angle conjugate set is present between the Patchawarra Formation and Warburton Basin stratigraphy and developed during the Middle Permian Event; (3) N-S striking low angle conjugate set is present within the Eromanga, Cooper, and Warburton basins and developed during the Hunter-Bowen and Late Cretaceous events; and (5) NE-SW and SE-NW striking high angle conjugate sets present throughout the stratigraphic column and developed during intermittent periods of SE-NW and NE-SW extension (flexural relaxation), respectively. The spatial and temporal distribution of natural fractures is also presented and no relationship was found between increased fracture intensity and overpressure; however, increased geothermal gradient was commonly associated with uranium-rich shallow volcanics and did have a relationship to overpressure.

Geomechanical modelling of fault reactivation identified SE-NW strike-slip faults as the most prone to dilate, slip and shear reactivate under the present-day stress regime. A pore pressure increase of 4 MPa was found to be enough to induce shear reactivation. Constraints on paleo-stress magnitude allowed for accurate 4D geomechanical models to be created at six key stages of basin development. These models were used to analyse a fault model and constrain the fault geometries most likely to tensile and shear reactivate through time. NE-SW striking high angled faults, which are present throughout the basin, were found to be optimally oriented to facilitate hydrocarbon migration since the critical moment (90 Ma) in the hydrocarbon system.

Regional structural and stratigraphic interpretation of a large 2D and 3D seismic dataset presented a modern basement fault map, which was previously not available. Large N-S strike-slip faults were identified within the Patchawarra Trough and associated with positive flower structures that now form producing hydrocarbon fields. A regional system of Cretaceous polygonal faults was also presented. Polygonal faults that extend into underlying oil-rich stratigraphy were geomechanically modelled to find that faults striking between 60^{o}N and 140^{o}N with high dip angles are most likely to facilitate hydrocarbon migration into overlying shallow reservoirs. Stratigraphic interpretation of 3D seismic data found extensive on-lapping features and pin-out traps present within Permian stratigraphy associated with uplift during the Middle Permian and Daralingie events. Initial structural traps in the gas-rich Patchawarra Formation were created by the Middle Permian Event. The integration of curvature analysis along the Patchawarra Formation seismic reflector with a geomechanical model and interpreted natural fractures identified structural “sweet-spots” within known hydrocarbon fields. The study found E-W and SE-NW striking high angled fractures as the most likely to dilate and shear reactivate under present-day stress. These permeable natural fracture sets were identified in curvature analysis results and found to increase in intensity along E-W elongate anticlines. The structural "sweet-spots" present areas of improved structural permeability.

As a comprehensive study on time-to-depth conversion accuracy was not available, an automated cross-validation method was created to assess the accuracy of four common methods. The results showed that the average velocity method is the most accurate (~25 feet error); however, the expected error and most accurate method changed by tens of feet depending on the combination and value of the most significant variables. This novel approach to assess depth conversion accuracy highlighted the importance of selecting a depth conversion method based on the dataset, rather than using a single method for the entire basin. This thesis presents research that has improved our understanding of the tectonic evolution, structural geology, and geophysics within Australia's largest and most prospective onshore hydrocarbon provinces; the Cooper-Eromanga Basin.

7. APPENDIX

In addition to the main body of work, contributions were made to several other pieces of work in the form of co-author publications, presentations at conference events, and academic research awards. Only two co-authored publications have been included in the Appendix as these align with the scope of this thesis; however, the contribution was not significant enough to include in the thesis body. Publications that did not meet the scope of this thesis are not included, but are presented in the thesis Publication List.

7.1. CO-AUTHOR MANUSCRIPT A: Optimising hydraulic fracturing

Development of a New Approach for Hydraulic Fracturing in Tight Sand with Pre-Existing Natural Fractures

Understanding the interaction between hydraulic fracture stimulation treatments and pre-existing natural fractures is a critical aspect for effective stimulation, particualrly in the low permeability Patchawarra Formation, Cooper Basin, Australia. Other factors affecting hydraulic fracturing in the Cooper Basin include high entry pressure and tortuosity, which can cause hydraulic fracture plane rotation and complexities that ultimately reduce proppant placement. To combat these issues, we integrate rock mechanical properties, measured natural fractures, the in situ stress tensor, tectonic strain, and a calibrated gemechanical model with 3D hydraulic fracture stimulation simulations to optimise the well design. This new approach for hydraulic fracture stimulation design increases the final stimulated rock volume while minimising complexity and optimising propant placement to ultimately improve the efficiency of hydrocarbon prduction from tight sand reservoirs.

CITATION:

Pokalai, K., Kulikowski, D., Johnson, Jr., R., Haghighi, M., & Cooke, D. (2016). Development of a New Approach for Hydraulic Fracturing in Tight Sand with Pre-Existing Natural Fractures. The Australian Petroleum Production & Exploration Association Journal, 56, 225-238, doi:10.1071/AJ15017.

Statement of Authorship

Title of Paper:	Development of a new approach for hydraulic fracturing in tight sand with pre-existing natural fractures
Publication Status:	**Manuscript Published**
Publication Details:	Pokalai, K., Kulikowski, D., Johnson, Jr., R.L., Haghighi, M., & Cooke, D. (2016). Development of a new approach for hydraulic fracturing in tight sand with pre-existing natural fractures. The APPEA Journal, 56, 225-238, doi:10.1071/AJ15017.

Principal Author

Principal Author (Candidate):	Kunakorn Pokalai		
Contribution to the Paper:	Data collection, interpretation, analysis, and writing.		
Overall percentage (%):	60%		
Certification:	This paper reports on original research I conducted during the period of my Higher Degree by Research candidature and is not subject to any obligations or contractual agreements with a third party that would constrain its inclusion in this thesis. I am the primary author of this paper.		
Signature:		Date:	08 March 2017

Co-Author Contribution

By signing the Statement of Authorship, each author certifies that:

i. the candidate's stated contribution to the publication is accurate (as detailed above);
ii. permission is granted for the candidate to include the publication in the thesis; and
iii. the sum of all co-author contributions is equal to 100% less the candidate's stated contribution.

Name of Co-Author:	David Kulikowski (10%)		
Contribution to the Paper:	Interpreted the image log, wrote geology section, and review of paper		
Signature:		Date:	08 March 2017

Name of Co-Author	Raymond (Ray) L. Johnson, Jr		
Contribution to the Paper	Interpreted 1D MEM and review the paper (10 %)		
Signature		Date	4/6/2017

Name of Co-Author	Manouchehr Haghighi (10%)		
Contribution to the Paper:	Supported with the structure, writing and review of paper.		
Signature:		Date:	09 March 2017

Name of Co-Author:	Dennis Cooke (10%)		
Contribution to the Paper:	Initiated the research and review of paper.		
Signature:		Date:	28 March 2017

Development of a new approach for hydraulic fracturing in tight sand with pre-existing natural fractures



Lead author
Kunakorn Pokalai

K. Pokalai, D. Kulikowski, R.L. Johnson, Jr., M. Haghighi and D. Cooke
Australian School of Petroleum
University of Adelaide
Adelaide, SA 5005
kunakorn.pokalai@adelaide.edu.au

ABSTRACT

Hydraulic fracturing in tight gas reservoirs has been performed in the Cooper Basin for decades in reservoirs containing high stress and pre-existing natural fractures, especially near faults. The hydraulic fracture is affected by factors such as tortuosity, high entry pressures, and the rock fabric including natural fractures. These factors cause fracture plane rotation and complexities, leading to fracture disconnection or reduced proppant placement during the treatment.

In this paper, rock properties are estimated for a targeted formation using well logs to create a geomechanical model. Natural fracture and stress azimuths within the interval were interpreted from borehole image logs. The image log interpretations inferred that fissures are oriented 30–60° relative to the maximum horizontal stress. Next, diagnostic fracture injection test (DFIT) data was used with the poro-elastic stress equations to predict tectonic strains. Finally, the geomechanical model was history-matched with a planar 3D hydraulic fracturing simulator, and gave more insight into fracture propagation in an environment of pre-existing natural fractures.

The natural fracture azimuths and calibrated geomechanical model are input into a framework to evaluate varying scenarios that might result based on a vertical or inclined well design. A well design is proposed based on the natural fracture orientation relative to the hydraulic fracture that minimises complexity to optimise proppant placement. In addition, further models and diagnostics are proposed to aid predicting the hydraulically induced fracture geometry, its impact on gas production, and optimising wellbore trajectory to positively interact with pre-existing natural fractures.

KEYWORDS

Tight gas, Cooper Basin, hydraulic fracturing, pre-existing natural fractures, rock mechanical model.

INTRODUCTION

Hydraulic fracturing is a wellbore stimulation process using injected fluid and proppant to create a flow path in a low-permeability reservoir. Since most tight gas reservoirs often contain natural fractures, the interaction between natural fractures and hydraulically induced fractures is a complex process. Another issue is the existence of a complex stress regime (e.g., the Cooper Basin) where normal, strike-slip and reverse fault regimes exist (Reynolds et al, 2006). This can lead to complexity in fracture propagation, reducing effective proppant placement and leading to lower gas production.

In those areas like the Cooper Basin, highly complex stress regimes and pre-existing natural fractures can manifest near-wellbore pressure loss (NWBPL) and pressure dependent leak-off behavior during fluid injection (Johnson and Greenstreet, 2003). NWBPL is caused by fracture path tortuosity (Roberts et al, 2000) and can be predicted and estimated from the turning radius of the fracture (Johnson et al, 2015). To optimise the hydraulic fracturing treatment in such a complicated system, it was proposed that drilling an inclined well perpendicular to natural fracture orientation might maximise the intersection between open natural fracture networks and induced hydraulic fractures (Murphy and Fehler, 1986). Previous research by Zhou et al (1994) presented that inclined wellbores should consider the shear stress anisotropy that would impact wellbore stability, based on data from stress regimes in Australia. They recommended drilling in strike-slip stress regimes at 55–70° azimuth relative to the maximum horizontal stress. In a case with a similar strike-slip stress regime and anisotropy values similar to the Cooper Basin, Bentley et al (2013) used this drilling approach to reduce hydraulic fracture propagation complexity, based on surface deformation tiltmeter and microseismic monitoring results relative to vertical wells.

This paper attempts to use a multidisciplinary approach to study a tight gas reservoir in the Cooper Basin. First, borehole breakout geometries are interpreted from a wellbore image log and extrapolated to the remainder of the field. Then diagnostic fracture injection test (DFIT) data is used to calibrate a rock mechanical model constrained by the image log data for planar 3D hydraulic fracturing modelling of existing hydraulic fracturing data from the area. Finally, based on this modelling, an optimum well trajectory for drilling an inclined well is proposed.

THEORETICAL BACKGROUND

Deviated wellbore

For an inclined well, the stress distribution around the wellbore can be determined using analytical or numerical models. Kirsch equations (Kirsch, 1898) analytically describe the breakdown behavior around a vertical well (cylindrical geometry) under a linear elastic deformation assumption, where the effective radial stress (σ_r) and tangential stress (or hoop stress), shear stress ($\tau_{r\theta}$) and vertical stress (σ_v) are trigonometric functions of the horizontal stresses and reservoir pressure (Eqs 1–4).

$$\sigma_r = \frac{\sigma_h + \sigma_H}{2}\left(1 - \frac{r_w^2}{r^2}\right) + \frac{\sigma_h - \sigma_H}{2}\left(1 - 4\frac{r_w^2}{r^2} + 3\frac{r_w^4}{r^4}\right)\cos 2\theta + \frac{r_w^2}{r^2}(P_w - \alpha P_0) \quad (1)$$

$$\sigma_t = \frac{\sigma_h + \sigma_H}{2}\left(1 + \frac{r_w^2}{r^2}\right) - \frac{\sigma_h - \sigma_H}{2}\left(1 + 3\frac{r_w^4}{r^4}\right)\cos 2\theta - \frac{r_w^2}{r^2}(P_w - \alpha P_0) \quad (2)$$

$$\tau_{r\theta} = -\frac{\sigma_h + \sigma_H}{2}\left(1 + 2\frac{r_w^2}{r^2} - 3\frac{r_w^4}{r^4}\right)\sin 2\theta - \frac{r_w^2}{r^2}(P_w - \alpha P_0) \quad (3)$$

$$\sigma_v = P_{ob} - \alpha P_0 \quad (4)$$

The Kirsch equations were modified by Barree and Miskimins (2015) for a deviated wellbore with the principle stress tensor on the wellbore inclination, where azimuth (β) is defined relative to the maximum horizontal stress direction and the deviation angle (α) is defined relative to the vertical stress direction (Fig. 1). The transformed stresses can be described in three dimensions using Equations 5–10.

$$S_x = \sigma_H \sin(\beta)^2 + \sigma_h \cos(\beta)^2 \quad (5)$$

$$S_y = \cos(\alpha)^2\left(\sigma_H \cos(\beta)^2 + \sigma_h \sin(\beta)^2\right) + \sigma_v \sin(\alpha)^2 \quad (6)$$

$$S_z = \sin(\alpha)^2\left(\sigma_H \cos(\beta)^2 + \sigma_h \sin(\beta)^2\right) + \sigma_v \cos(\alpha)^2 \quad (7)$$

$$S_{xy} = \cos(\alpha)\sin(\beta)\cos(\beta)(\sigma_H - \sigma_h) \quad (8)$$

$$S_{yz} = \sin(\alpha)\cos(\alpha)\left(\sigma_v - \sigma_H \cos(\beta) - \sigma_h \sin(\beta)^2\right) \quad (9)$$

$$S_{zx} = \sin(\alpha)\sin(\beta)\cos(\beta)(\sigma_h - \sigma_H) \quad (10)$$

After transformation of the stress and shear stress along the wellbore axis, the resulting values can be substituted into Equations 1–4 to describe the radial (σ_r), tangential (σ_t) and axial (σ_z) well stress values. For the case of transverse fractures, if there are existing cracks, the internal pressure must exceed the axial stress and the tensile strength of any infill material. For breakdown criteria in a deviated or horizontal well, in the case of the longitudinal fracture, the internal pressure must exceed the minimum tangential stress plus the rock strength. Considering that the fractures are open, the breakdown pressure based on exceeding the axial stress is perpendicular to the fissure only, and can be estimated for a deviated or horizontal well using Equations 11–13.

$$\sigma_r = P_w - P_0 \quad (11)$$

$$\sigma_t = S_x + S_y - 2(S_x - S_y)\cos(2\lambda) - 4S_{xy}\sin(2\lambda) - \sigma_r \quad (12)$$

$$\sigma_z = S_z - 2\upsilon\left((S_x - S_y)\cos(2\lambda) + 2S_{xy}\sin(2\lambda)\right) \quad (13)$$

The angle for fracture propagation (λ) is given with respect to a vertical well; for example, in a vertical fracture $\lambda = 0$ and for a horizontal fracture $\lambda = 90$.

One-dimensional mechanical earth model

The construction and calibration of a one-dimensional (1D) rock mechanical model (1D MEM) is an important requirement for hydraulic fracturing simulation and fracture containment assessment, and can be obtained using the following workflow. Firstly, the input data is obtained from well logging suites typical for hydraulic fracturing design; gamma ray, full-waveform sonic log and bulk density logs data are used to estimate elastic rock properties such as Poisson's ratio (v) and Young's modulus (E). The DFIT provides observable values for breakdown pressure (P_{wb}) and closure pressure (P_c), a representative value for the minimum horizontal stress ($\sigma_{h\min}$) within an interval (Fig. 2). Formation pseudo radial flow behaviour may be observable in the shut-in data after the closure pressure has been observed using after-closure analysis (ACA) methods based on impulse test analytical solutions (Nolte et al, 1997). ACA can provide necessary data for the model such as pore pressure (p_p) and transmissibility. Then, estimates for the minimum horizontal ($\sigma_{h\min}$) and the maximum horizontal stress ($\sigma_{H\max}$) can be derived by history matching the DFIT data using the isotropic form of the poroelastic stress equations (Thiercelin and Plumb, 1994; Eqs 14 and 15) using the maximum (ε_H) and minimum horizontal (ε_h) strains to calibrate the model.

$$\sigma_{h\min} = \frac{\upsilon}{1-\upsilon}(\sigma_v - \alpha_v p_p) + \frac{E}{1-\upsilon^2}\varepsilon_h + \frac{E\upsilon}{1-\upsilon^2}\varepsilon_h + \alpha_h p_p \quad (14)$$

$$\sigma_{H\max} = \frac{\upsilon}{1-\upsilon}(\sigma_v - \alpha_v p_p) + \frac{E}{1-\upsilon^2}\varepsilon_H + \frac{E\upsilon}{1-\upsilon^2}\varepsilon_h + \alpha_h p_p \quad (15)$$

The parameters of highest uncertainty in matching the observed values to the calculated values are the tectonic strains in the maximum (ε_H) and the minimum horizontal directions (ε_h). Previous research by Teufel (1983) described anelastic strain recovery measurements as a method to determine the strains

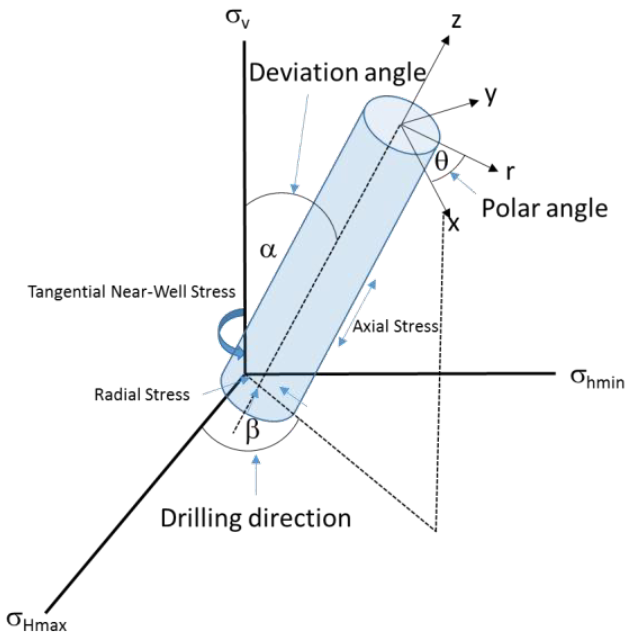


Figure 1. Borehole orientation in an inclined well.

based on the Blanton model (Blanton, 1983). This method, however, is based on core measurements that are obtained on a small scale and may not necessarily represent the reservoir scale.

To better constrain this process, the observed breakdown pressure and natural fissure opening pressures can also be used to constrain calculated values. The breakdown pressure during a DFIT is the pressure that acts on the rock and initiates the fracturing under an assumption that the rock is homogenous and elastic. It is the early and often maximum pressure, and pressure generally drops as more fluid is injected into the rock. The Kirsch equations can be resolved to describe the breakdown pressure for the horizontal stresses (Zoback, 2007) using Equation 16, based on the pore pressure and tensile rock strength (T_0).

$$P_{Breakdown} \text{ or } P_{wb} = 3\sigma_{h\min} - \sigma_{H\max} - P_{Pore} + T_0 \qquad (16)$$

T_0 can be estimated from core testing or observed values from past DFITs. The tensile strength can be neglected and the observed reopening fracture used when a second injection occurs for the same fracture after previous closure.

Another constraint for horizontal stresses can be derived from the fissure opening (closing) pressure (P_{fo}). The magnitude of pressure dependent leakoff (PDL) and P_{fo} can be determined from before-closure analysis (BCA) of a DFIT using the G-function time and semi G-function derivative (Barree et al, 2009) (Fig. 3). A characteristic hump in the semi G-function derivative is indicative of PDL behaviour in the early time shut-in pressure decline data of a DFIT. This effect is caused as fluid passes through pre-existing natural fractures, and can be described as an exponential fluid leak off rate relative to conventional leakoff. A Mohr circle failure criterion can be used to derive the fissure opening angle, or the angle at which a rock would preferentially break between the maximum and minimum horizontal stresses (Jaeger and Cook, 1979). Using this criterion, the angle (θ) of the natural fractures relative to the horizontal stress directions can be determined from P_{fo} using Equation 17 (Fig. 4), and further constraining the values of $\sigma_{H\max}$ and $\sigma_{h\min}$.

$$P_{FissureOpening} \text{ or } P_{fo} = \frac{1}{2}(\sigma_{H\max} + \sigma_{h\min}) + \frac{1}{2}(\sigma_{H\max} - \sigma_{h\min})\cos 2\theta \qquad (17)$$

In this paper, the tectonic strains and horizontal stress values have been determined by matching observed data to calculated data, solving Equations 14–17 simultaneously using a generalised reduced gradient (GRG) nonlinear solving method (Lasdon et al, 1978). This method, which is based on the genetic algorithm, helps to minimise the sum of the error function between the calculated and observed values derived from the logs to the values of closure pressure, breakdown pressure and fissure opening pressure observed from the DFIT data. For each value, Equation 18 describes the process where x represents the observed values and x is the value derived from logs for each parameter.

$$\text{Error function (ErrFn)} = \sum(x - x)^2 \qquad (18)$$

Finally, the values of horizontal stress derived from this history matching process are compared with values predicted from image log analyses of borehole breakout and drilling induced tensile failure criteria (Zoback, 2007) to further constrain the resulting model.

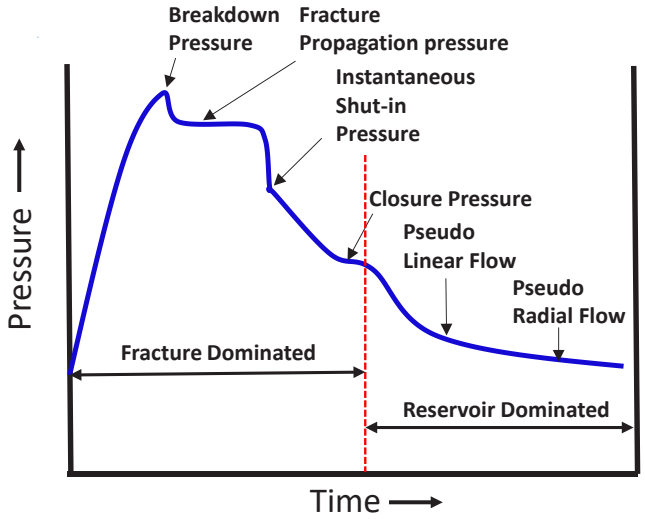


Figure 2. DFIT typical pressure profile.

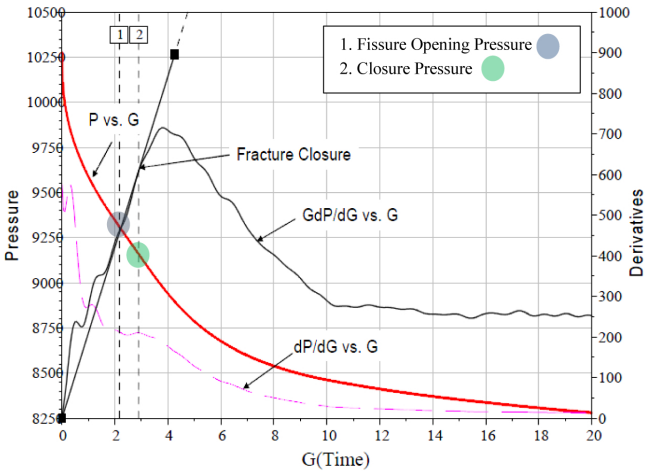


Figure 3. G-function analysis plot with PDL detected (Barree et al, 2009).

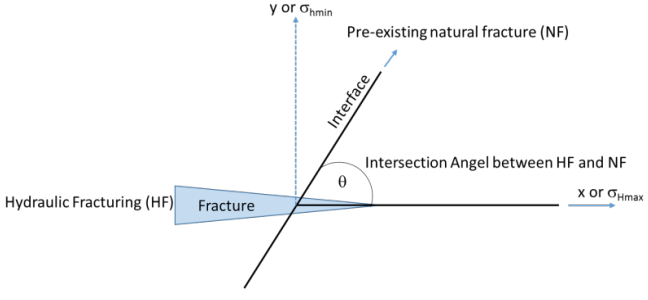


Figure 4. Hydraulic fracture interaction with a natural fracture.

CASE STUDY

The study area (C-Field) is located west of the Gidgealpa-Merrimelia-Innamincka (GMI) Ridge within the Greater Tindilpie (GT) region of the Permian to Triassic aged Cooper Basin (SA). The Cooper Basin is Australia's largest onshore hydrocarbon province, with tremendous unconventional hydrocarbon potential in low permeability fluvial to lacustrine reservoirs. The region contains northeast–southwest striking ridges (GMI and Murteree-Nappacoongee) that separate the northeast–southwest elongate Patchawarra, Nappamerri and Tenappera troughs. Initial accommodation space is believed to have generated through southeast–northwest oriented extension (650 Ma) developing northeast–southwest and southeast–northwest oriented structural lineaments (Kuang et al, 1985; Haines et al, 2001). Successive crustal shortening events during the Sakmarian, late Permian and Upper Triassic periods are believed to have reactivated pre-existing basement-involved faults and controlled the depositional patterns in the Cooper Basin and potentially influence hydrocarbon migration pathways (Apak et al, 1997; Kulikowski et al, 2015). These events likely controlled the development and possible reactivation of natural fractures within the Patchawarra Formation, which hosts the largest volume of known hydrocarbons within the basin.

Within the C-Field, the Early Permian aged Patchawarra Formation comprises of approximately 1,640 ft of gas charged and cyclically deposited very fine to coarse grained sandstone, siltstone, shales and coals under meandering fluvial to lacustrine conditions (Camac et al, 2012). The field is a low to moderate relief structure elongate in a northeast–southwest direction (Fig. 5) and bound from the east and west by northeast–southwest striking reverse faults. The wells used in this analysis (C-13 and C-7) are approximately 4,600 ft apart (Fig. 5). The maximum horizontal stress within the field is oriented approximately 116°N (Camac et al, 2012). Fracture stimulation treatments are becoming increasingly relied upon, with the majority of development wells requiring at least one fracture stimulation treatment, particularly within the relatively lower permeability C-Field (typically <1 mD). The influence of pre-existing natural fractures during fracture stimulation treatments within the Cooper Basin is not well understood in literature, albeit up to six regionally pervasive natural fracture sets may exist throughout the basin (Kulikowski et al, 2015; 2016). The authors' investigation into optimising well trajectory to positively interact with pre-existing natural fractures oriented parallel, 30°, 60° and perpendicular to the hydraulically induced fracture plane, while incorporating the local stress field, will provide a new approach for hydraulic fracturing in tight sand reservoirs to optimise hydrocarbon production.

Natural fracture planes typically exhibit a reduced strength and are favorably reactivated, rather than new fractures developing, and has been observed in prior studies in the Cooper Basin (Nelson et al, 2007). This fundamental rock failure principal is vital to better understanding the complex mechanics taking place during fracture stimulation treatments, and particularly in the stress and rock conditions of the Cooper Basin. The authors use wells C-7 and C-13, which contain an interpretable borehole image log, adequate well tests, and know effectiveness of fracture stimulation treatments, to showcase the effect that natural fractures play in tight sand hydrocarbon production. Natural fractures from the C-13 borehole image log were interpreted using Paradigm Geolog 7.2 software (Fig. 6). Natural fracture geometries ranged from horizontal to near vertical and with a large spread of strike orientations; however, up to three natural fracture sets can be realised. The dominant natural fracture set strikes north-northeast to south-southwest with a dip angle of 60° (Fig. 7). Fracture sets with dip angles of 30° are also present, dipping towards the east, south, west and northeast.

Together with natural fractures, the authors interpret borehole breakout occurrence to calculate the local maximum horizontal stress orientation and magnitude at the depth of interest (9,500 ft). The average strike of borehole breakouts is approximately 18.3°, inferring that the maximum horizontal stress orientation is approximately 108.3° (Fig. 7). The average borehole breakout width was approximately 74.1°, which was used for calculating the stress magnitude. The maximum horizontal stress magnitude—based on borehole breakout data, pore pressure, minimum horizontal stress magnitude (obtained from leak off tests), rock strength and the effect of temperature—was calculated within the C-13 well, and at 9,500 ft depth is approximately 9,900 psi, a value to constrain estimates from the DFIT data.

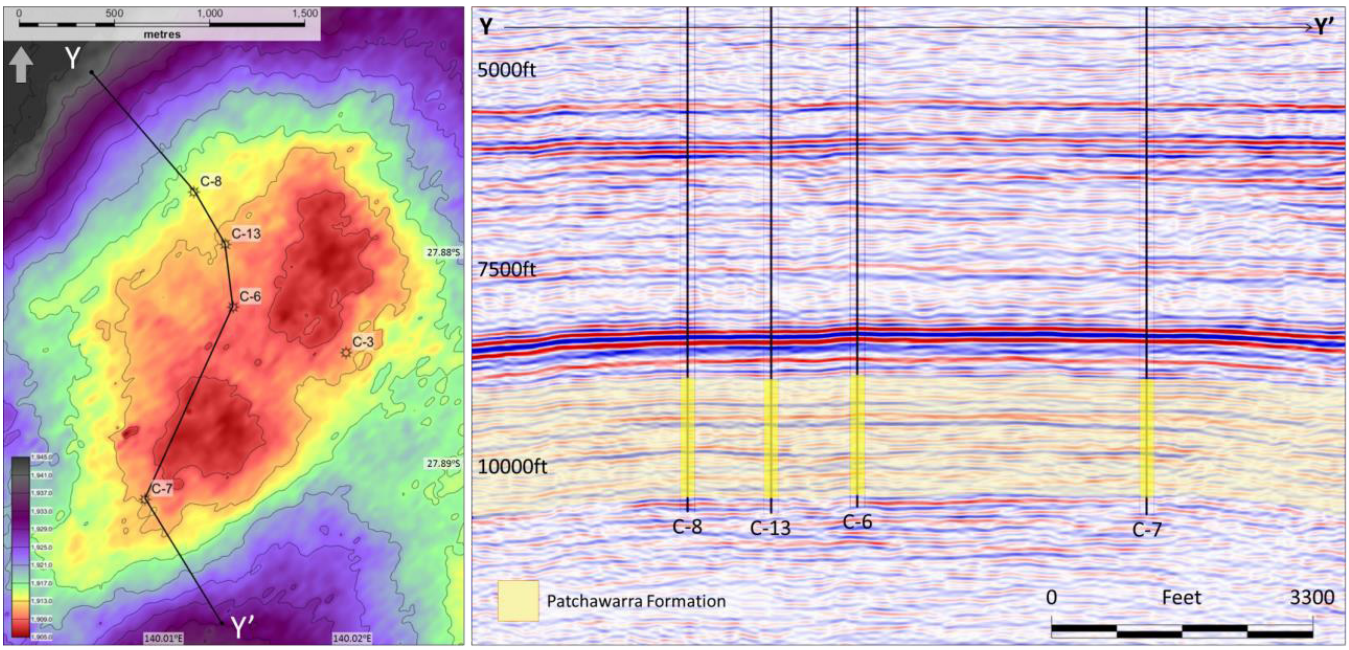


Figure 5. Structural map of the C-Field with a cross-section showing the Patchawarra Formation correlation across wells.

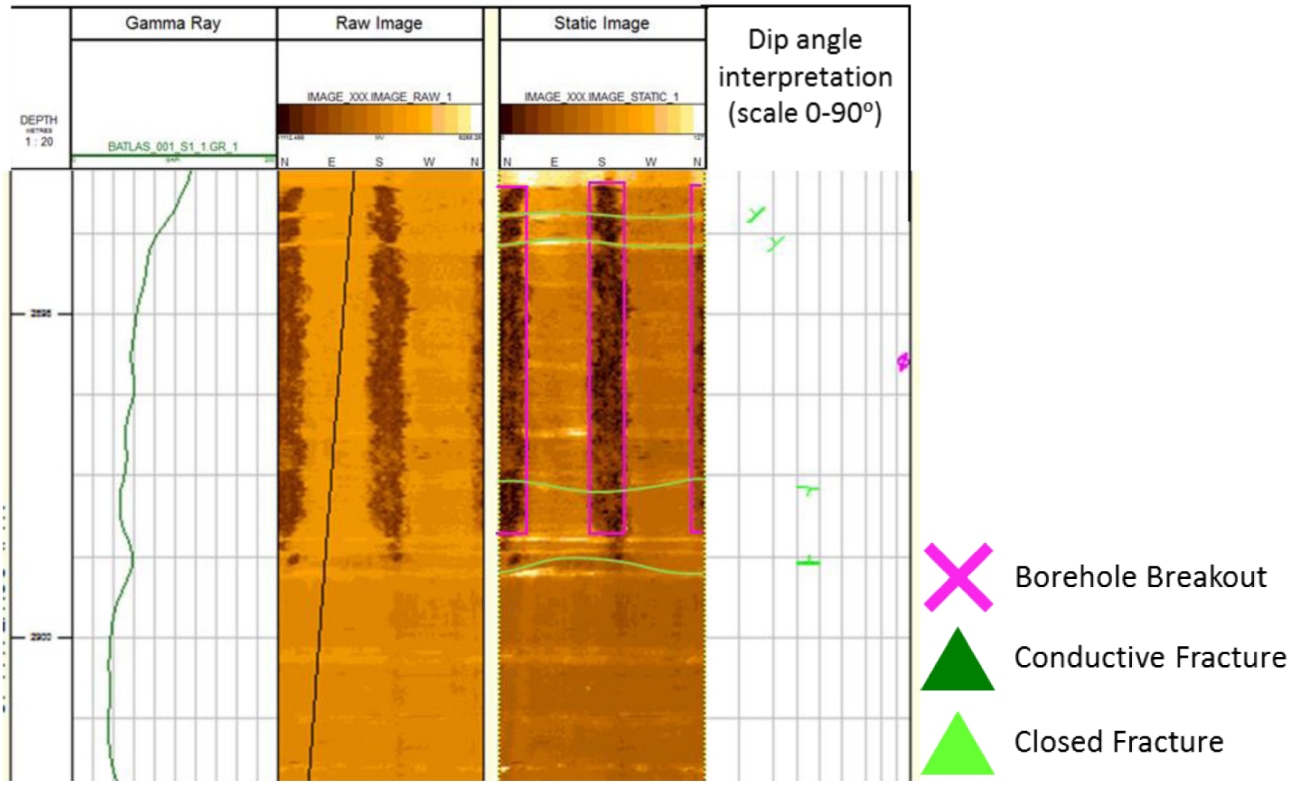


Figure 6. Acoustic image log interpretation.

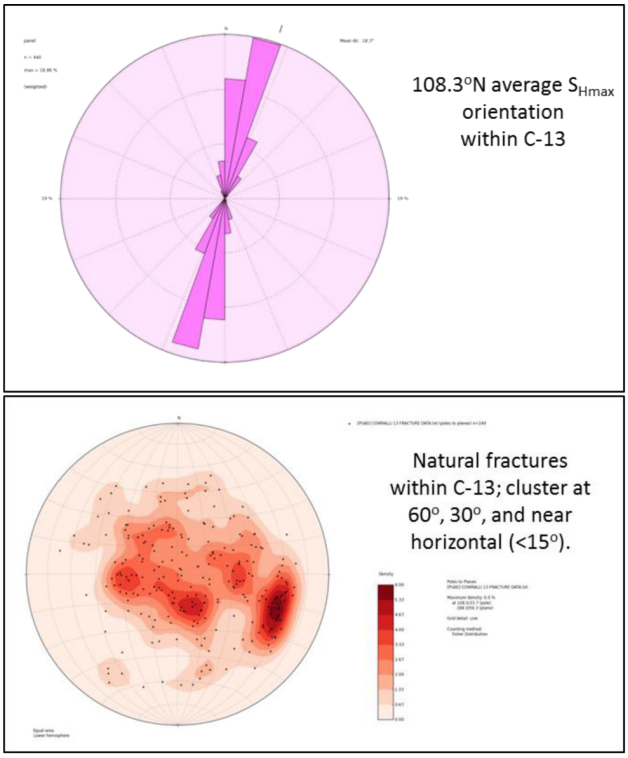


Figure 7. Borehole breakout and natural fracture analysis.

RESULTS AND DISCUSSION

There are two stages of fracture treatment that have been carried out in well C-7 to obtain commercial gas rates in the Patchawarra Formation (Fig. 8). Based on Pokalai et al (2015b), the tight gas target intervals have been analysed from depths between 9,000–10,000 ft with an average low permeability of 0.7 mD and temperatures up to 280°F, as shown in Table 1.

Interpretation of DFIT

STEP DOWN TEST

Well C-7 stage 1 and stage 2 were injected with the delayed borate crosslinked fluid for eight minutes with an average rate of 25 barrels per minute (bpm), with the total injected volume being 8,000 gallons (Fig. 9). The step down test was performed by reducing the injection rate by approximately 7.5 bpm in each step until pumping had been stopped. Stage 1 and stage 2 indicated average NWBPL of 522 psi (Table 2). This average indicates that the pressure's loss is dominated by tortuosity rather than pressure loss through perforations.

The delay borate crosslinked fluid was used for DFIT; the gel may damage the fracture and affect the fracture fluid cleanup during production. Also, because pumping time is held at eight minutes, it would impact the longer observe closure pressure and radial flow behavior.

BEFORE-CLOSURE ANALYSIS

During pumping, the breakdown pressure reached a value of 9,962 psi for stage 1 and 10,291 psi for stage 2. Once the pumping stopped, the stabilised pressure was observed within one hour. Based on the G-function analysis, both stages in well C-7's semi G-function (GdP/dG) versus G-function time (G) plot showed a hump, which means the leakoff type is pressure dependent leakoff (PDL) (Fig. 10). The fissure opening in stage 1 is shown at the G-function time of 1.28 with the fissure opening pressure (P_{fo}) of 7,822 psi. The closure pressure occurs at a G-function time of 1.58 at 7,596 psi, which is higher than stage 2 by 190 psi. In this case, the first derivative of the square root time plot confirmed the closure from the G-function analysis. Finally, the average fluid efficiency for the fracturing fluid injection was determined to be 56% from G-function analysis.

AFTER-CLOSURE ANALYSIS

As mentioned previously, ACA methods are used to identify different flow regimes in the post-closure fall-off data. In the data, a negative slope of 0.5 is observable in the plot of pressure difference and its derivative, an indication of a pseudo-linear formation flow regime, likely natural fracturing. Also, a negative slope of one in the late time data is observable, indicating a formation pseudo-radial flow regime. In Table 2, the pore pressure gradient reported from ACA is 0.443 psi/ft. Also, stage 1 provides the highest reservoir transmissibility of around 325 mD.ft/cP by using the net pay thickness of 36 ft, which gives a permeability of 0.116 mD.

Analysis of the mechanical earth model

A calibrated 1D MEM was developed based on the elastic rock properties from well log derived data (Fig. 11). The pore pressure and stress profiles have been generated for well C-7 encompassing the Patchawarra Formation stimulated for stages 1 and 2. Closure pressure, breakdown pressure and pore pressure have been determined from DFIT data for stages 1 and 2. For stages 1 and 2, the DFIT closure pressures are 7,596 psi and 7,406 psi, and breakdown pressures are 9,962 and 10,291 psi, respectively. These observed values were used to calibrate the log-derived values using the workflow described with Equations 14–16 and 18.

From this calibration process, the maximum horizontal tectonic strain is 504 microstrains and the minimum horizontal tectonic strain is 155 microstrains; this produces an effective tectonic strain of 338 microstrains in the minimum horizontal stress direction, based on the sum of the two tectonic strain components in Equation 14. As aforementioned, the borehole breakout data from the image log in the field was used to constrain the maximum horizontal stress magnitude to approximately 9,900 psi at 9,500 ft. The correlation between the observed closure pressure and calculation from log data generally show a good match. Some stress misalignment could, however, result from high near wellbore pressure losses observed in the breakdown pressures for both stages. In the coal, the stress values determined from full wave form sonic data appear to be unreliable and differ from values estimated from published compressional sonic travel time log models for a coal lithology. This is likely due to washouts affecting the shear wave data, giving inaccurate elastic rock properties and impacting the stress profile.

The stress regime in C-7 changes from the bottom of the Patchawarra Formation to the top of the well. As can be seen in Figure 11, the top part shows a strike-slip stress regime followed by a normal fault and reverse fault stress regime in other lithologies. A stress contrast of 1,200 psi is estimated between sand and coal at the level of the Patchawarra Formation; this stress contrast along with modulus changes could limit fracture initiation out of the sand section. There is, however, a high degree of uncertainty in the coal rock mechanical and stress values based on the sonic log data. Nevertheless, change in the stress regime can affect hydraulic fracturing propagation and potential cause orientation as it encounters strike slip, normal fault and thrust faulting conditions. In this case, hydraulic fracturing stage 1 and stage 2 indicate a normal fault condition, which is likely to propagate less complicated vertical fractures. At the boundaries of the Patchawarra, however, changes to reverse faulting may cause t-shaped fractures or blunting to occur at the boundaries, potentially limiting growth out of the intervals.

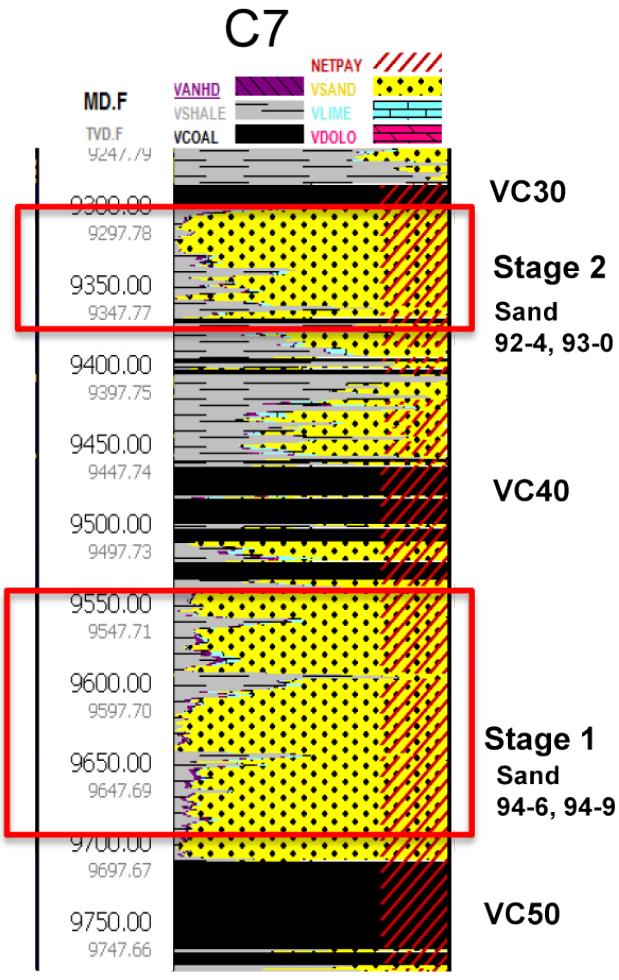


Figure 8. Different stages of hydraulic fracturing in well C-7.

Hydraulic fracture simulation

3D hydraulic fracture models have been constructed for the C-7 well using a planar 3D hydraulic fracturing propagation simulator (GOHFER) (Barree,1983) using the calibrated geomechanical model (1D MEM) as the initial input for the simulator to perform history-matching of observed pressures (Pokalai et al, 2015a). Figure 10a shows the plot of injection fluid rate and treating pressure in C-7 during stage 1. In this stage, 12,000 gal of delayed borate crosslinked fluid was injected as a pad stage, and calculated bottom hole treating pressures up to 9,000 psi were observed. In the next stage, 4,000 lbs of 100 mesh sand followed by slurry stages with increasing concentrations and mesh sizing of high-density ceramic proppant were used; both 20/40 then 16/30 proppant were used, pumped in concentrations from 0.5–8 lbm/gal. Finally, 5,500 gal of linear gel was pumped to displace the proppant stages and complete the job. A good match was obtained by history-matching observed and

Table 1. Petrophysical properties in well C-7.

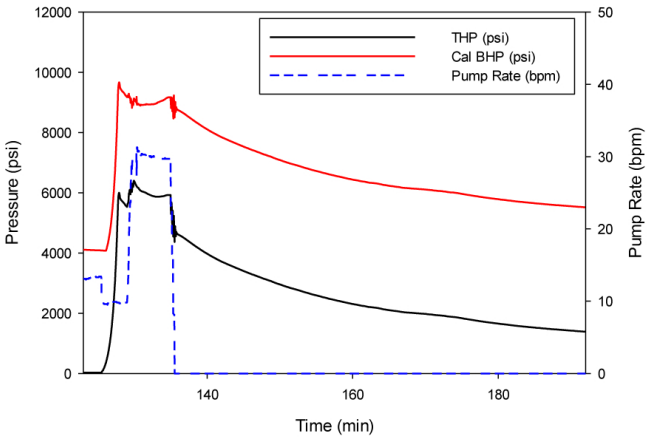
Well/stage	Depth	Net pay	Permeability	Porosity	Water saturation	Temperature
C-7, stage 1	9,533–9,634 ft	70 ft	0.12 mD	11.3%	34%	282°F
C-7, stage 2	9,294–9,351 ft	36 ft	0.06 mD	10.0%	31%	275°F

simulated surface results and calculated bottomhole pressures, and was used to further refine the geomechanical model. The purple dashed line in Figure 12a represents measured surface treating pressure (STP), and the solid purple line model predicted STP data. The pressure matching has been achieved by adjusting variables such as stress, fluid leak off (PDL) and excess pressure derived from the hydraulic fracture tortuosity.

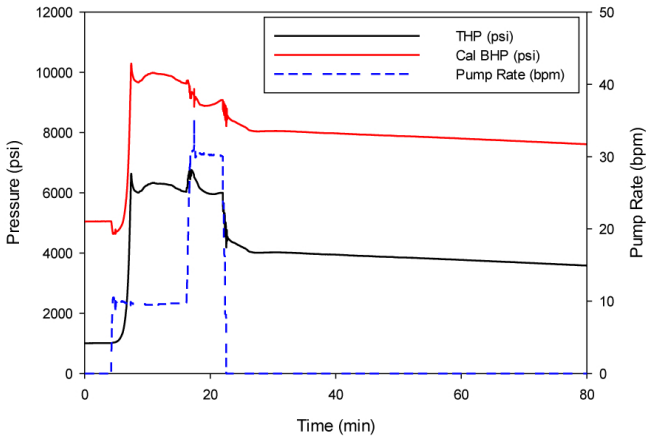
Based on the fracture history matching (Fig. 12b), the fracture propagates with good height containment within the target formation and achieves an average baseline conductivity of 10 md.ft, with results shown in Table 3. This fracture geometry takes into account the geomechanical model and estimated fracturing fluid properties from the field reports, and models the proppant transport in the model based on extensive StimLab modelling and conductivity studies. Furthermore, this modelling includes the impact of pressure independent leakoff and pressure drop from tortuosity. All these factors can impact the treating pressure resulting from the simulator and create a more realistic model; however, it cannot visually show the effects or fracture geometry induced from created versus natural fracture extension, being only a single planar model.

To complete the process of evaluation, the fracture propagation has also been interpreted using net pressure analysis (Nolte and Smith, 1981), which is derived using a log-log plot of net pressure versus time (Fig. 12c). Initially, Mode I behaviour was observed with a small positive slope, indicating the fracture was propagating in a confined height and length growing within the target zone. Next, a period of Mode II behaviour was observed (i.e., constant slope) inferring that a stable growth in fracture height or fissure opening was occurring. Then a period of Mode IV behaviour was observed (i.e., negative slope), which is generally associated with uncontrolled fracture growth. Finally, Mode II behavior was again observable until Mode III, or restricted fracture growth, was noted. Mode III often indicates a high positive slope and is associated with the beginning of proppant fill-up in the fracture, creating high treating pressures until a screen out or pressure out occurs.

Ultimately, the complex interaction between pre-existing natural fractures needs to be investigated more fully when performing hydraulic fracturing in high-stress unconventional reservoirs with natural fracturing. Areas for future investigations could include stochastic processing of multiple realisations



(a) Well C 7 Stage 1



(b) Well C 7 Stage 2

Figure 9. Diagnostic fracture injection test plots in well C-7.

Table 2. DFIT data observed in well C-7.

Rate-pressure step-down test analysis results					
Well/stage	**ΔP tortuosity at 30 bpm**	**ΔP perforation at 30 bpm**	**Tortuosity pressure loss coefficient (K_{tort})**	**Perforation pressure loss coefficient (K_{perf})**	**NWBP**
C-7, stage 1	461 psi	67 psi	85 psi/(stb/d)^2	0.0076 psi/(stb/d)^2	528 psi
C-7, stage 2	368 psi	148 psi	67 psi/(stb/d)^2	0.163 psi/(stb/d)^2	516 psi

BCA results						
Well/stage	**Breakdown pressure (P_{wb})**	**ISIP**	**Closure pressure (P_c)**	**Fissure opening pressure (P_{fo})**	**Leakoff type**	**Pressure dependent leakoff (PDL) coefficient**
C-7, stage 1	9,962 psi	8,812 psi	7,596 psi	7,822 psi	PDL	0.005
C-7, stage 2	10,291 psi	8,528 psi	7,406 psi	8,064 psi	PDL and height recession	0.003

ACA results					
Well/stage	**Reservoir pressure**	**Transmissibility (kH/μ)**	**Flow capacity (kH)**	**Permeability (k)**	**Flow behaviours**
C-7, stage 1	4,520 psi	325 mD.ft/cp	8.12 mD.ft	0.116 mD	Pseudo linear and radial flow
C-7, stage 2	4,262 psi	91 mD.ft/cp	2.27 mD.ft	0.063 mD	Pseudo linear and radial flow

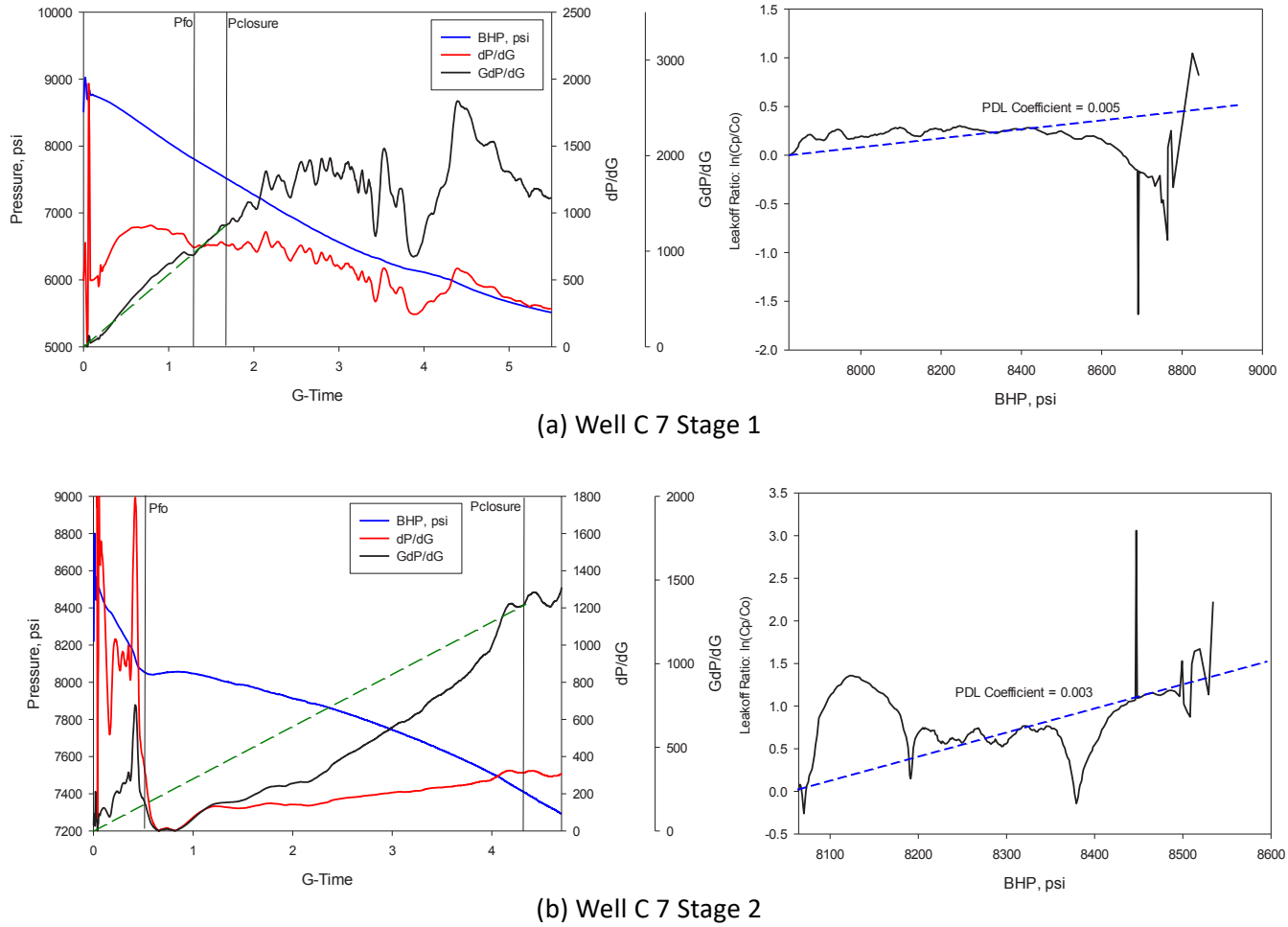


Figure 10. G-function and PDL plots in well C-7.

with discrete fracture networks and finite element methods to correctly account for the fluid flow in fractures. Although a simplistic planar model was used, predicted dimensions, production modelling and history-matching reasonably matched the observed average gas production rate of 300 Mscf/day across five years (Fig. 12d).

Fracture orientation and well design

Ultimately the greatest benefit of creating a calibrated geomechanical model and history matched hydraulic fracture model is to provide insight for future wells to better optimise stimulation treatments. To achieve this, the authors will show how the data can be used in a framework to provide insight on future wellbore deviation and inclination to optimise hydraulic fracture treatments for this environment. The authors will guide readers on their approach to achieve this optimisation.

Firstly, the existing data is summarised. Figure 13 shows the breakdown gradient and the breakdown angle in well C-7 at a depth of 9,500 ft. A Poisson's ratio value of 0.24, an overpressured reservoir gradient of 0.5 psi/ft, and an effective tectonic strain value of 338 microstrains in the $\sigma_{h\min}$ direction creates a stress anisotropy or horizontal stress differential of 2,400 psi. Since this stress regime is considered to be in a strike-slip stress regime, the stress values are represented by a large ellipsoid shape and more anisotropic ratios in the figure.

The Kirsch modification equations (Eqs 5–13) have been applied for the breakdown pressure plot (Fig. 13a) and the breakdown angle (Fig. 13b.). The left-hand side of Figure 13a shows the azimuth starts from 0–360° north around the edge of each circle. The vertical well falls in the centre of the plot, whereas the horizontal well falls on the outer plot. The light blue to grey colour shows the breakdown pressure, which ranges from 0.4–1.2 psi/ft; any pressure gradient greater than 1.2 psi/ft is shown as a grey color. The maximum stress direction shows 108° on the plot with an average breakdown gradient of 0.8 psi/ft. Figure 13b shows the fracture initiation angle from transverse fracture initiation (0° from vertical direction) to longitudinal fracture (90° from vertical direction). In this situation, the average fracture initiated with 20° from the vertical direction is shown in the inclined wellbore design.

Results from both the image log and the fissure opening equation can aid determination of an optimum drilling direction based on the fracture azimuth using Equation 19. In this case, using 60°—obtained from the DFIT data and Equation 17—results in the following natural fracture azimuth.

$$\text{Azimuth of fracture} = \text{Azimuth of maximum horizontal stress} - 60° \quad (19)$$

The azimuth of drilling needs to be drilled perpendicular to the natural fracture system to enhance propagation in the pre-existing fractures, thereby maximising the number of fractures from an optimally inclined well placement. As shown in Equation 20, to perform an optimal hydraulic fracture stimulation within the well, the recommended drilling plan is to drill at an azimuth of 138° and with an inclination of 60° (Fig. 14).

$$\text{Azimuth of drilling} = \text{Azimuth of fracture} + 90° \quad (20)$$

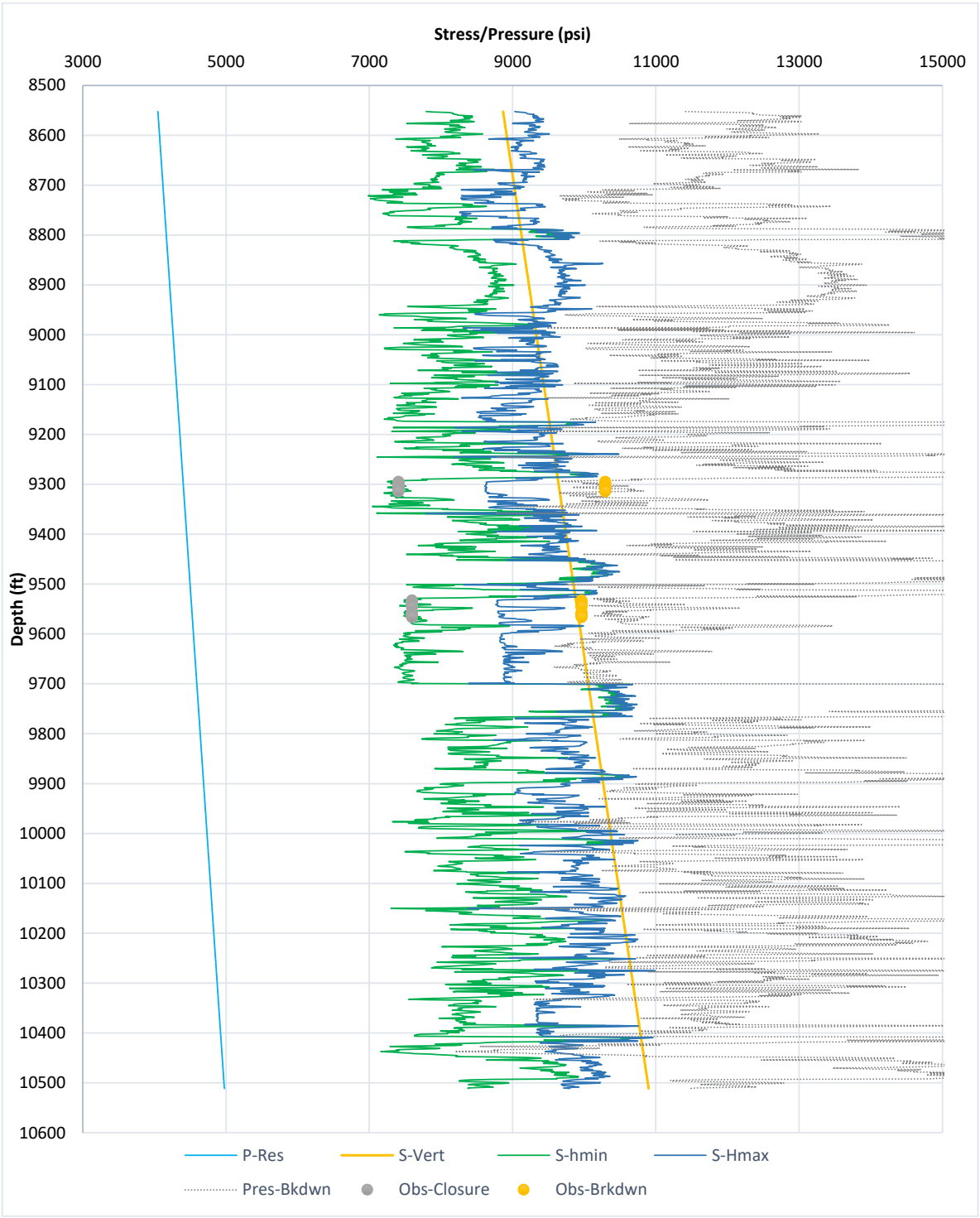
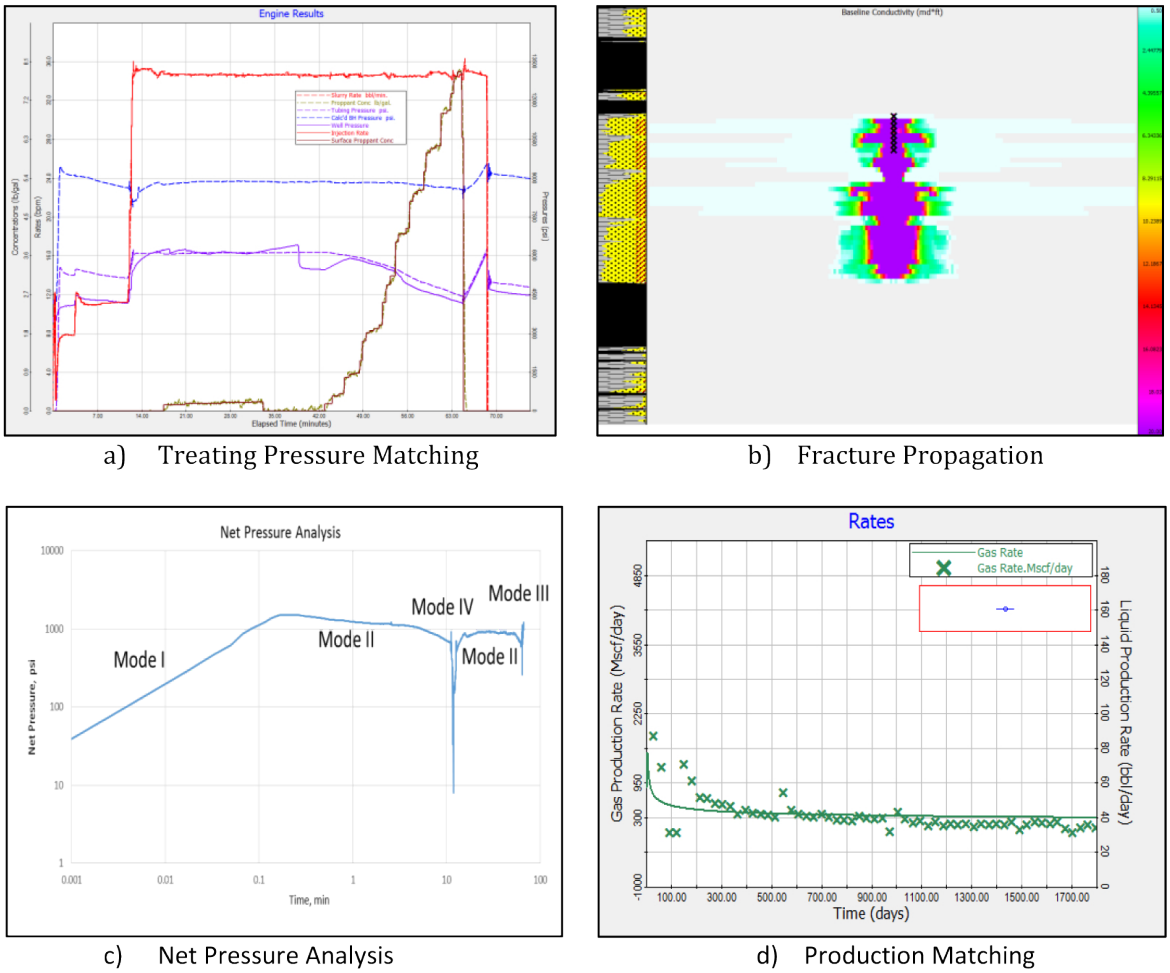


Figure 11. 1D MEM in well C-7.

In Figure 14, the blue color represents the fracture direction and the orange line represents the inclined well direction. In addition, the authors also make the assumption that the natural fractures interpreted from the C-13 image log are all present within well C-7. The distance between these wells is approximately 4,600 ft and covered the target formation. No image log was run within C-7, and an incomplete pressure data set was found in well C-13. As the distance between wells is quite large, the accuracy of the authors' natural fracture set geometries may be affected. This is often the case in fields where analog wells must be rationalised to provide the best go-forward plan.

Therefore, for new areas or areas where a number of wells are combined to generate the optimised plans, a pilot hole is recommended to investigate the likely intersection between the hydraulic fracture and natural fractures. This pilot well can give more confidence in optimising fracture dilation and propagation using all the data from a single wellbore prior to sidetracking the deviated wellbore, reducing the costs relative to two wells. Finally, to fully close the optimisation loop, it is recommended to verify the results using microseismic monitoring and history-matching the geomechanical model using numerical methods. The results of this process can greatly enhance understanding of a complex fracture network and aid an optimal hydraulic fracture design for complex stress regimes as early as possible in the well development planning stage.

Continued from previous page.



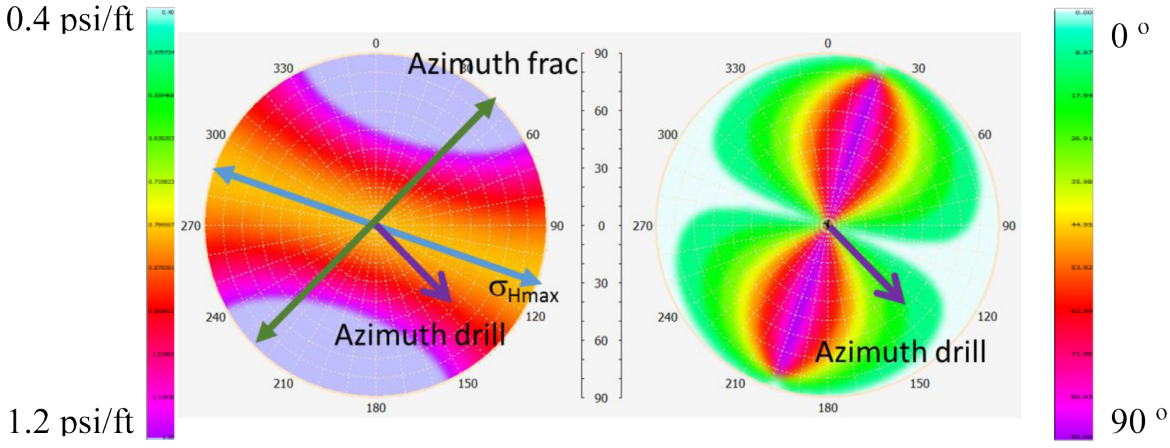
a) Treating Pressure Matching b) Fracture Propagation

c) Net Pressure Analysis d) Production Matching

Figure 12. Results of 3D hydraulic fracturing simulation in well C-7, stage 1.

Table 3. Results of 3D hydraulic fracturing in well C-7.

Well/stage	Fracture half length	Fracture height	Fracture width	Fracture conductivity	Dimensionless fracture conductivity
C-7, stage 1	96 ft	175 ft	0.2 in	154 mD.ft	30
C-7, stage 2	176 ft	35 ft	0.2 in	315 mD.ft	30



a) Breakdown Gradient b) Breakdown Angle

Figure 13. Fracture orientation.

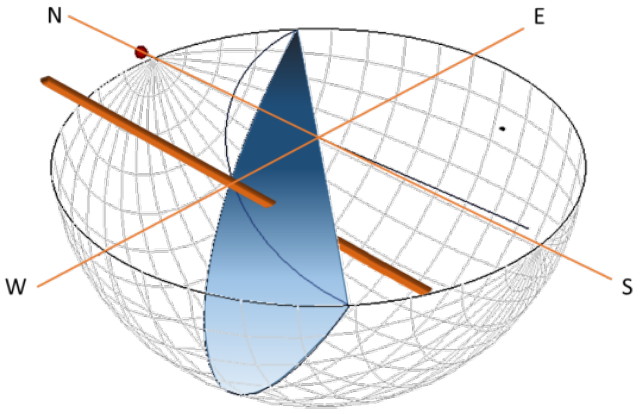


Figure 14. Well inclined drilling (azimuth 138° and inclination 60°).

CONCLUSIONS

New approaches and well-defined workflows for hydraulic fracturing planning have been proposed for tight sands in high stress environments with pre-existing natural fractures based on image log and DFIT data, and are refined using 3D planar hydraulic fracture history-matching. This multidisciplined approach is extended to develop an optimised deviation/inclination for future well drilling to enhance hydraulic fracture stimulation of a natural fracture network. Key elements of this process are as follows.

- A rigourous process of DFIT interpretation has been proposed, incorporating step down, before closure and after closure analysis methods. In the example case, this process identified tortuosity in the fracture path as the dominant mechanism for near wellbore pressure loss. Furthermore, the data indicated a high-level pressure dependent leak off, supporting the theory that dominant fluid leakoff mechanism in this environment is leakoff occurring through natural fractures.
- The process of developing a 1D MEM has been presented for this case study in the Cooper Basin using the DFIT and image log data. The outcome confirms that strike-slip, normal and reverse stress regimes all exist within the wellbore. The minimum horizontal stress and the maximum horizontal stress values were estimated from well logs and calibrated by observed DFIT data using a non-linear, least-square based genetic algorithm. The key finding for this case is that the maximum horizontal tectonic strain is roughly three times higher than the minimum horizontal tectonic strain, creating a highly stressed and anisotropic stress environment.
- A calibrated hydraulic fracture model was developed and validated by pressure history matching. A good match was found between simulated and observed data, and indicated good fracture propagation and vertical coverage with good fracture height containment.
- From this data, a deviated well plan could be developed to maximise hydraulic fracture interaction by striking a well perpendicular to the natural fracture orientation and at an inclination favourable for fracture breakdown. In this case the plan was developed using a vertical wellbore fissure opening pressure and incorporating the natural fracture azimuth from image log data. For future wells in this case study area, the is recommendation is for using a deviated and inclined wellbore with an azimuth of 138° and inclination of 60° to maximise natural fracture interaction. A similar process could be used for other wells in high-stress strike-slip stress regimes using offset or pilot hole image log and DFIT data.

ACKNOWLEDGEMENTS

The authors would like to acknowledge the financial contribution made by Santos. The authors would also like to thank GOHFER, Paradigm (Geolog 7.2), Down Under Geosolutions (DUG Insight 3.1), and Carlos H. Grohmann and Ginaldo A.C. Campanh (OpenStereo 0.1.2) for permissions to use their software.

NOMENCLATURE

α	Inclination from the vertical direction (°)
α_h	Horizontal poroelastic constant (dimensionless)
α_v	Vertical poroelastic constant (dimensionless)
β	Azimuth relative to maximum horizontal stress (°)
θ	Angle from the direction of minimum horizontal stress (°)
υ	Poisson's ratio (dimensionless)
σ	Vertical net stress (psi)
σ_h	Minimum horizontal net stress (psi)
σ_H	Maximum horizontal net stress (psi)
$\sigma_{h\min}$	Minimum horizontal stress (psi)
$\sigma_{H\max}$	Maximum horizontal stress (psi)
σ_r	Radial net stress (psi)
σ_t	Tangential (hoop) net stress (psi)
σ_z	Axial well stress (psi)
$\tau_{r\theta}$	Shear stress in the plane of the borehole stress (psi)
P_0	Far-field pore pressure (psi)
P_{ob}	Overburden pressure (psi)
p_p	Pore pressure (psi)
P_w	Wellbore fluid pressure (psi)
r	Distance from wellbore (in)
r_w	Wellbore radius (in)
S_x	Transformed x-direction stress
S_y	Transformed y-direction stress
S_z	Transformed z-direction stress
S_{xy}	Shear stress in x-y plane
S_{yz}	Shear stress in y-z plane
S_{zx}	Shear stress in z-x plane

REFERENCES

APAK, S.N., STUART, W.J., LEMON, N.M. AND WOOD, G., 1997—Structural evolution of the Permian Triassic Cooper Basin, Australia: relation to hydrocarbon trap styles. AAPG Bulletin, 81 (4), 533–55.

BARREE, R.D., 1983—A Practical Numerical Simulator for Three-Dimensional Fracture Propagation in Heterogeneous Media. SPE Reservoir Simulation Symposium, San Francisco, California, 15–18 November, SPE-12273.

BARREE, R.D., BARREE, V.L. AND CRAIG, D., 2009—Holistic fracture diagnostics: consistent interpretation of prefrac injection tests using multiple analysis methods. SPE Production & Operations, 24 (3), 396–406.

BARREE, R.D. AND MISKIMINS, J.L., 2015—Calculation and Implications of Breakdown Pressures in Directional Wellbore Stimulation. SPE Hydraulic Fracturing Technology Conference, The Woodlands, Texas, 3–5 February, SPE-173356.

BENTLEY, P.J.D., JIANG, H. AND MEGORDEN, M.P., 2013—Improving Hydraulic Fracture Geometry by Directional Drilling in Coal Seam Gas Formation. SPE Unconventional Resources Conference and Exhibition-Asia Pacific, Brisbane, Queensland, 11–13 November, SPE-167053.

BLANTON, T.L., 1983—The Relation Between Recovery Deformation and In-Situ Stress Magnitudes. SPE/DOE Low Permeability Gas Reservoirs Symposium, Denver, Colorado, 14–16 March, SPE-11624.

CAMAC, B.A., WALDRON, A.W., DONLEY, J.A. AND HUNT, S.P., 2012—Microseismic and 3D VSP for Infill Evaluation in Greater Tindilpie, Cooper Basin, Australia. 46th US Rock Mechanics/Geomechanics Symposium, Chicago, Illinois, 24–27 June, ARMA-2012-618.

GROHMAN, C.H AND CAMPANHA G.A.C., 2010—OpenStereo: Open source, Cross-platform Software for Structural Geology Analysis. 2010 AGU Fall Meeting, San Francisco, California, 13–17 December, abstract #IN31C-06.

HAINES, P.W., HAND, M. AND SANDIFORD, M., 2001—Palaeozoic synorogenic sedimentation in central and northern Australia: a review of distribution and timing with implications for the evolution of intracontinental orogens. Australian Journal of Earth Sciences, 48 (6), 911–28.

JAEGER, J.C. AND COOK, N.G.W., 1979—Fundamentals of rock mechanics. London: Chapman and Hall.

JOHNSON, R.L. JR., ABUL KHAIR, H.F., JEFFREY, R.G., MEYER, J.J., STARK, C. AND TAUCHINTZ, J., 2015—Improving fracture initiation and potential impact on fracture coverage by implementing optimal well planning and drilling methods for typical stress conditions in the Cooper Basin, Central Australia. The APPEA Journal and Conference Proceedings, 55, extended abstract.

JOHNSON, R.L., JR. AND GREENSTREET, C.W., 2003—Managing Uncertainty Related to Hydraulic Fracturing Modeling in Complex Stress Environments with Pressure-Dependent Leakoff. The SPE Annual Technical Conference and Exhibition, Denver, Colorado, 5–8 October, SPE-84492.

KIRSCH, E.G., 1898—Die Theorie der Elastizität und die Bedürfnisse der Festigkeitslehre. Zeitschrift des Vereines Deutscher Ingenieure, 42 (28), 797–807. Translation: The theory of elasticity and the requirements of the resistance of materials. Journal of the Association of German Engineers.

KUANG, K.S., 1985—History and style of Cooper–Eromanga Basin structures. Exploration Geophysics, 16 (2/3), 245–8.

KULIKOWSKI, D., AMROUCH, K., AL BARWANI, K.H.M., LIU, W. AND COOKE, D., 2015—Insights into the tectonic stress history and regional 4D natural fracture distribution in the Australian Cooper Basin using Etchecopar's calcite twin stress inversion technique, 2D/3D seismic interpretation and natural fracture data from image logs and core. AAPG International Conference and Exhibition, Melbourne, Victoria, 13–16 September, extended abstract #2224164.

KULIKOWSKI, D., COOKE, D. AND AMROUCH, K., 2016—Constraining the distribution and relationship between overpressure, natural fracture density and temperature in the Cooper Basin. The APPEA Journal, this volume, in press.

LASDON, L.S., WARREN, A.D., JAIN, A. AND RATNER, M., 1978—Design and testing of a generalized reduced gradient code for nonlinear. ACM Transactions on Mathematical Software, 4 (1), 34–50.

MURPHY, H.D. AND FEHLER, M.C., 1986—Hydraulic Fracturing of Jointed Formations. International Meeting on Petroleum Engineering, Beijing, China, 17–20 March, SPE-14088.

NELSON, E.J., CHIPPERFIELD, S.T., HILLIS, R.R., GILBERT, J., MCGOWEN, J. AND MILDREN, S.D., 2007—The relationship between closure pressures from fluid injection tests and the minimum principal stress in strong rocks. International Journal of Rock Mechanics and Mining Sciences, 44 (5), 787–801.

NOLTE, K.G., MANIERE, J.L. AND OWENS, K.A., 1997—After-Closure Analysis of Fracture Calibration Tests. SPE Annual Technical Conference and Exhibition, San Antonio, Texas, 5–8 October, SPE-38676.

NOLTE, K.G. AND SMITH, M.B., 1981—Interpretation of fracturing pressures. Journal of Petroleum Technology, 33 (9), 1,767–75.

POKALAI, K., FEI, Y., AHMAD, M., HAGHIGHI, M. AND GONZALEZ, M., 2015—Design and optimisation of multi-stage hydraulic fracturing in a horizontal well in a shale gas reservoir in the Cooper Basin, South Australia. The APPEA Journal, 55, 1–14.

POKALAI, K., HAGHIGHI, M., SARKAR, S., TYIASNING, S. AND COOKE, D., 2015—Investigation of the Effects of Near-Wellbore Pressure Loss and Pressure Dependent Leakoff on Flowback during Hydraulic Fracturing with Pre-Existing Natural Fractures. SPE/IATMI Asia Pacific Oil and Gas Conference and Exhibition, Nusa Dua, Bali, 20–22 October, SPE-176440.

REYNOLDS, S.D., MILDREN, S.D., HILLIS, R.R. AND MEYER, J.J., 2006—Constraining stress magnitudes using petroleum exploration data in the Cooper–Eromanga Basins, Australia. Tectonophysics, 415 (1–4), 123–40.

ROBERTS, G.A., CHIPPERFILED, S.T. AND MILLER, W.K., II, 2000—The Evolution of a High Near-Wellbore Pressure Loss Treatment Strategy for the Australian Cooper Basin. SPE Annual Technical Conference and Exhibition, Dallas, Texas, 1–4 October, SPE-63029.

TEUFEL, L.W., 1983—Determination of In-Situ Stress From Anelastic Strain Recovery Measurements of Oriented Core. SPE/DOE Low Permeability Gas Reservoirs Symposium, Denver, Colorado, 14–16 March, SPE-11649.

THIERCELIN, M.J. AND PLUMB, R.A., 1994—A core-based prediction of lithologic stress contrasts in east Texas formations. SPE Formation Evaluation, 9 (4), 251–8.

ZHOU, S., HILLIS, R. AND SANDIFORD, M., 1994—A study of the design of inclined wellbores with regard to both mechanical stability and fracture intersection, and its application to the Australian North West Shelf. Journal of Applied Geophysics, 32 (4), 293–304.

ZOBACK, M.D., 2007—Reservoir geomechanics. Cambridge: Cambridge University Press.

Authors' biographies next page.

THE AUTHORS



Kunakorn Pokalai is presently a production engineering PhD candidate at the University of Adelaide. He has a BEng in petrochemical engineering from Silpakorn University (Thailand), and completed a Graduate Certificate in Management, and a master's in petroleum engineering from the University of Adelaide.

Kunakorn's research interests are in the simulation of unconventional reservoirs and hydraulic fracturing. He mainly focuses on the issue of fracturing fluid flowback in the Cooper Basin. He was the recipient of the prestigious AAPG Imperial Barrel Award in the Asia Pacific Region in 2014. Member: SPE and AAPG.

kunakorn.pokalai@adelaide.edu.au



David Kulikowski holds a BSc (Honours) in petroleum geoscience and geophysics, and is now completing a PhD by publication in structural geology at the Australian School of Petroleum, University of Adelaide. David's main research interests are in better understanding the structural and stress history of the Cooper Basin through the integration of micro- (calcite twinning), meso- (natural fractures) and macroscale (faults) structural data.

David is a recipient of the 2015 American Association of Petroleum Geologists (AAPG) Grants-in-Aid Foundation Scholarship. He was also a team member in the first Australian team to win the prestigious Asia-Pacific Region AAPG Imperial Barrel Award (IBA) in 2014. During the early stages of his PhD, David was employed as a part-time technical assistant at Santos in the gas production and optimisation engineering team.

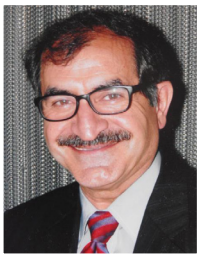
david.kulikowski@adelaide.edu.au



Raymond (Ray) L. Johnson, Jr. is presently Principal at Unconventional Reservoir Solutions, and serves as Adjunct Associate Professor at The University of Adelaide, and Senior Lecturer at The University of Queensland. He has a PhD in mining engineering, a MSc in petroleum engineering, a Graduate Diploma in information technology, and a BA in chemistry. Ray has been active in the Society of Petroleum Engineers (SPE) as past Chair of the SPE Queensland Section, and served as 2013 and 2015 technical co-Chair of the SPE Unconventional Reservoir Conference and Exhibition Asia Pacific.

He has authored, co-authored and presented numerous papers on unconventional reservoir technologies at SPE and APPEA conferences, as well as published in peer-reviewed journals.

ray.johnson@adelaide.edu.au



Manouchehr (Manny) Haghighi is Associate Professor of Petroleum Engineering. His research and teaching focus is on unconventional reservoirs, reservoir simulation, well testing, and formation evaluation. He has supervised more than 40 MSc and 10 PhD students.

Before joining the University of Adelaide in 2009, Manouchehr was Associate Professor of Petroleum Engineering at the University of Tehran (Iran). From 2000–07 he was Head of the petroleum engineering program at the University of Tehran.

In 2000, Manouchehr established Simtech, a consulting company for the integrated reservoir simulation. He has been project director of several full field simulation projects for oil and gas reservoirs.

From 1995 to 2000, Manouchehr was working with the National Iranian Oil Company (NIOC) and was the director of a program for training NIOC staff at several universities in the US, UK, Canada, France, Australia and Norway. Manouchehr was a visiting professor at the University of Calgary from 2007–08.

Manouchehr has published more than 80 articles in peer review journals or presented in international conferences. He has served as a reviewer for different journals such as the Journal of Petroleum Science and Engineering. Member: SPE.

manouchehr.haghighi@adelaide.edu.au



Dennis Cooke has a PhD in geophysics from the Colorado School of Mines, and more than 25 years of experience in oil and gas exploration and development. He is a past-president of the Australian Society of Exploration Geophysicists (ASEG), and a former vice president of the Society of Exploration Geophysicists (SEG).

Dennis owns and operates ZDAC Geophysical Technology, which provides technology and services for seismic inversion and reservoir characterisation. He is an Adjunct Assistant Professor at the University of Adelaide's Australian School of Petroleum.

dennis.cooke@adelaide.edu.au

THIS PAGE LEFT BLANK INTENTIONALLY.

7.2. CO-AUTHOR MANUSCRIPT B: 3D Hydraulic Fracturing with a DFN

Integrated 3D modelling of hydraulic fracturing in tight reservoirs with pre-existing natural fractures and under high stress conditions: A case study from the Cooper Basin, Australia

The aim of this research is to: (1) better understand the complex interaction between hydraulic fracturing and pre-existing natural fractures; (2) quantify the effectiveness of hydraulic fracturing in strike-slip and compressional stress regime conditions; and (3) provide insights into why hydraulic fractures are rotating in the high stress Cooper Basin. To achieve these aims, a discreet fracture network and calibrated mechanical earth model are created and integrated with a hydraulic fracture simulation that is run under a compressional and a strike-slip stress regime to simulate the alternating in situ stress regime conditions present in the Cooper Basin. The results quantify the in situ stress and strain, the stimulated reservoir volumes, the indiced fracture growth, and interaction with pre-existing natural fractures.

CITATION:

Pokalai, K., Kulikowski, D., Amrouch, K., Haghighi, M., & Johnson, Jr., R.L. (2017). Integrated 3D modelling of hydraulic fracturing in tight reservoirs with pre-existing natural fractures and complex stress conditions: A case study from the Cooper Basin, Australia. Journal of Petroleum Science and Engineering, under review.

Statement of Authorship

Title of Paper:	**Integrated 3D modelling of hydraulic fracturing in tight reservoirs with pre-existing natural fractures and complex stress conditions: A case study from the Cooper Basin, Australia**
Publication Status:	**Manuscript Submitted**
Publication Details:	Pokalai, K., Kulikowski, D., Amrouch, K., Haghighi, M., & Johnson, Jr., R.L. (2017). Integrated 3D modelling of hydraulic fracturing in tight reservoirs with pre-existing natural fractures and complex stress conditions: A case study from the Cooper Basin, Australia. Journal of Petroleum Science and Engineering, under review.

Principal Author

Principal Author (Candidate):	Kunakorn Pokalai		
Contribution to the Paper:	Data collection, model building, interpretation, analysis, writing, and review of paper.		
Overall percentage (%):	40%		
Certification:	This paper reports on original research I conducted during the period of my Higher Degree by Research candidature and is not subject to any obligations or contractual agreements with a third party that would constrain its inclusion in this thesis. I am the primary author of this paper.		
Signature:		Date:	11 July 2017

Co-Author Contribution

By signing the Statement of Authorship, each author certifies that:

i. the candidate's stated contribution to the publication is accurate (as detailed above);
ii. permission is granted for the candidate to include the publication in the thesis; and
iii. the sum of all co-author contributions is equal to 100% less the candidate's stated contribution.

Name of Co-Author:	David Kulikowski (40%)		
Contribution to the Paper:	Data collection, model building, interpretation, analysis, writing, and review of paper		
Signature:		Date:	11 July 2017

Name of Co-Author:	Khalid Amrouch (10%)		
Contribution to the Paper:	Supported with the structure, writing and review of paper.		
Signature:		Date:	11 July 2017

Name of Co-Author	Manouchehr Haghighi (5%)		
Contribution to the Paper:	Supported with the structure, writing and review of paper.		
Signature:		Date:	21 September 2017

Name of Co-Author	Raymond Johnson (5%)		
Contribution to the Paper:	Supported with the structure, writing and review of paper.		
Signature:		Date:	21 September 2017

Integrated 3D modelling of hydraulic fracturing in tight reservoirs with pre-existing natural fractures and complex stress conditions: A case study from the Cooper Basin, Australia

*Kunakorn **Pokalai**[a] (kunakorn.pokalai@adelaide.edu.au)

David **Kulikowski**[a] (david.kulikowski@adelaide.edu.au)

Khalid **Amrouch**[a] (khalid.amrouch@adelaide.edu.au)

Manouchehr **Haghighi**[a] (manouchehr.haghighi@adelaide.edu.au)

Raymond L. **Johnson**, Jr. (ray.johnsonjr@adelaide.edu.au)

[a]Australian School of Petroleum, University of Adelaide, North Tce, 5005, South Australia, Australia

***Corresponding Author:** Kunakorn Pokalai (+61 449 044 385)

ABSTRACT

Hydraulic fracturing is an essential element of effective hydrocarbon production in low permeability reservoirs; however, subsurface geological features can be highly anisotropic and can lead to ineffective treatments. To provide a better understanding on the effectiveness of hydraulic fracture interactions with pre-existing natural fractures, we integrate a calibrated mechanical earth model with a discrete fracture network to simulate hydraulic fracture treatments under an alternating (compressional and strike-slip) stress regime in both a vertical and inclined well. The trajectory of the inclined well was optimised to intersect the largest number of pre-existing natural fractures and has been found to increase the stimulated reservoir volume (SRV) by five times compared to the base case (vertical well under a strike-slip stress regime and with no pre-existing natural fractures) and by three times in the vertical wells, irrespective of the stress regime. This presents valuable information on the effectiveness of hydraulic fracturing when the geometry of pre-existing natural fractures is established. A common phenomenon in the case study location (Cooper Basin, Australia) is the rotation of induced hydraulic fractures from a vertical position at the wellbore to horizontal with distance away from the well. This was discussed and found to be most likely related to the preferential migration of fluid through the path of least resistance, which will often be affected by high horizontal permeability intervals within tight sandstones, or alternatively through the reactivation of the interface plane between different lithologies or the reactivation of low dip angle natural fractures.

Key Words: Hydraulic Fracturing; Discrete Fracture Network; Stress; Fracture; Cooper Basin.

1. INTRODUCTION

The use of hydraulic fracturing to enhance the permeability of tight reservoirs can be a crucial aspect of effective hydrocarbon production as it can improve the economic feasibility. However, these treatments can become complicated in some provinces because of the: (1) complex stress conditions; (2) reactivation of pre-existing natural fractures and faults; and (3) intra-formational heterogeneities such as permeability anisotropy and changes in lithology (Hubbert and Willis, 1957; McGowen et al., 2007; Scott et al., 2013; Cooke et al., 2016). This study quantifies the effectiveness of hydraulic fracturing using a discrete fracture network (DFN) model and different scenarios that include: (1) altering the stress regime from strike-slip to compressional; and (2) simulating a hydraulic fracture program within a vertical and inclined well. A case study from the Cooper Basin, Australia, is chosen because of the abundance of publicly available data and extensive use of hydraulic fracturing within the low permeability gas reservoirs.

The Cooper-Eromanga Basin is Australia's largest onshore hydrocarbon province that has been producing hydrocarbons from low permeability reservoirs since the first natural gas discovery in 1963 (Radke, 2009; Mackie, 2015). Attempts have been made to better understand the growth of hydraulic fractures within the complex stress conditions of the Cooper Basin (e.g. Roberts et al., 2000; Johnson et al., 2002, 2015; McGowen et al., 2007; Camac et al., 2012; Cooke et al., 2016; Pokalai et al., 2016; Waldron and Camac, 2016). These studies found that the effect of near wellbore pressure loss (NWBPL) coupled with reactivation of pre-existing natural fractures, and a complex and alternating stress regime are the major contributors to ineffective hydraulic fracturing (Warpinski and Teufel, 1987; Reynolds et al., 2006; Nelson et al., 2007; Scott et al., 2013; Pokalai et al., 2015a, 2015b, 2016; Cooke et al., 2016). A significant concern within the basin is the unknown reason behind hydraulic fractures rotating from a vertical position at the wellbore to a horizontal position with increasing distance away from wellbore (Scott et al., 2013; Cooke et al., 2016).

The aim of this research is to: (1) better understand the complex interaction between hydraulic fracturing and pre-existing natural fractures; (2) quantify the effectiveness of hydraulic fracturing under strike-slip and compressional stress regime conditions in vertical and inclined wells; and (3) provide insights into why hydraulic fractures are rotating in the complex stress Cooper Basin. A DFN model is created for a tight sandstone interval within the prolific Patchawarra Formation using interpreted natural fractures from the C-13 borehole image log (Fig. 1). The DFN model was created by statistically populating these natural fractures within the interval using the Elliptical Fisher Distribution and using reservoir properties obtained from well logs and pressure diagnostic tests.

Well logs are also used to develop a mechanical earth model (MEM) to constrain the tectonic stress and strain conditions, which is calibrated using well test data.

The DFN model is used to simulate a three-dimensional (3D) hydraulic fracture stimulation treatment in vertical and inclined wells and under compressional and strike-slip stress regimes to investigate the change in: (1) hydraulic fracture growth; (2) interaction with pre-existing natural fractures; and (3) stimulated reservoir volume (SRV). Rotation of the hydraulic fracture to the horizontal plane is also discussed. The results provide companies operating in the Cooper Basin with an improved understanding of hydraulic fracturing in the complex stress environment.

2. GEOLOGICAL SETTING

The Cooper Basin is an intracratonic Permian-Triassic aged hydrocarbon-rich province located within central Australia (Fig. 1a). Major hydrocarbon fields are commonly located along the NE-SW striking Gidgealpa-Merrimelia-Innamincka (GMI) and Murteree-Nappacoongee (MN) ridges, and within the NE-SW elongate Patchawarra, Nappamerri, and Tenappera troughs (Fig. 1a) (Apak et al., 1997; Kulikowski et al., 2017). Deposition of the oil and gas-rich Late Carboniferous to Early Permian aged Merrimelia and Tirrawarra formations under glacial and post-glacial outwash environments, respectively, marks the initial period of flexural relaxation that generated accommodation space for Cooper Basin sediment deposition (Apak et al., 1997; Alexander et al., 1997).

Cyclic deposition of reservoir rocks (sands), seal rocks (shale and coal), and source rocks (coal and shale) during the Middle Permian formed the gas-rich Patchawarra Formation (Alexander et al., 1998). This thick, but low permeability, stratigraphic interval is the primary target for exploration companies in the basin; however, it requires hydraulic fracturing or the presence of pre-existing natural fractures to improve the economic significance (Kulikowski et al., 2016b; Pokalai et al., 2016). Within the study area (C-Field region), the top Patchawarra Formation is at a depth of approximately 2700m (Fig. 1b) and can reach a total thickness of 700 m (Fig. 1c). West of the GMI Ridge, significant accommodation space developed during the Middle Permian Event, where major NE-SW striking faults were reactivated and facilitated significant deposition of the middle Patchawarra Formation (VC30-VC50 coal) interval (Fig. 1c) (Kulikowski and Amrouch, 2017). Field scale NE-SW striking inverted normal faults are present throughout the basin and have a strong control on structural trap development, which includes the C-Field (Fig. 1d). This field was selected as a case study because it contains abundant well data and a thick Patchawarra Formation interval.

Insert Fig. 1

The depositional environment transitioned to fluvio-deltaic, shoreface, and lacustrine, which was coincident with an east to west transgression that deposited the Late Permian Murteree Shale, Epsilon Formation, Roseneath Shale, and Daralingie Formation (Alexander et al., 1998). The NE-SW oriented Daralingie Event regionally eroded much of the Daralingie Formation, upon which the fluvial to deltaic Toolachee Formation was deposited (Apak et al., 1997; Kulikowski and Amrouch, 2017). The Toolachee Formation contains cycles of sands, shales, and coals that are comparable to the Patchawarra Formation, but not nearly as thick (Alexander et al., 1998). The Triassic Nappamerri Group was deposited onto the Toolachee Formation under floodplain, lacustrine and fluvial environments, which continued until the Late Triassic E-W Hunter-Bowen Event uplifted and peneplaned the Cooper Basin. This event created a regional unconformity that marks the top of the Cooper Basin (Apak et al., 1997; Alexander et al., 1998; Kulikowski and Amrouch, 2017).

The overlying Jurassic to Cretaceous Eromanga Basin was deposited under fluvial, lacustrine and shallow marine conditions during a prolonged period of tectonic quiescence (Apak et al., 1997; Kulikowski and Amrouch, 2017). The E-W Late Cretaceous Event created a regional unconformity that separates the Eromanga Basin from the overlying Paleogene to Quaternary Lake Eyre Basin (Apak et al., 1997; Alexander et al., 1998; Kulikowski and Amrouch, 2017). The subsequent N-S oriented Paleogene Event followed, and was succeeded by the in situ ESE-WNW oriented strike-slip to compressional stress regime (Müller et al., 2012; Pokalai et al., 2016; Kulikowski and Amrouch, 2017). The alternating stress regime (compressional to strike-slip) conditions present within the Cooper Basin may have a significant influence on the effectiveness of hydraulic fracturing treatments, as the induced fracture geometry, growth, and interaction with pre-existing natural fractures can change from highly effective to ineffective depending on the regime.

3. METHODOLOGY

3.1 Constructing a Mechanical Earth Model

Developing an accurate and calibrated mechanical earth model (MEM) is an important aspect for effective hydraulic fracturing, as it provides constraints on the elastic rock properties, pore pressure, transmissibility, and the in-situ stress and strain conditions present within a target interval (Nolte et al., 1997; Zoback, 2007; Johnson, 2016; Pokalai et al., 2016). The Poisson's ratio (v), Young's modulus (E) and vertical (σ_v) stress magnitude are calculated from a series of wireline logs from the C-7 well (Fig. 1) that include the gamma ray log, full-waveform sonic logs, and bulk density log. The dynamic Young's Modulus obtained from the full-wave sonic log is converted to the static Young's Modulus following the Eissa-Kazi model (Barree et al., 2009a).

The values for E and v are then used to constrain the minimum (σ_h) and maximum (σ_H) horizontal stress magnitudes that are calibrated to the diagnostic fracture injection test (DFIT) data using the isotropic form of the poro-elastic stress equations (Eq. 1 and Eq. 2; Thiercelin and Plumb, 1994). The DFIT data provides measured values for the breakdown (P_{wb}) and closure (P_c) pressures, and for the σ_h magnitude at two separate depths (2840m and 2920 m) within the formation, which are used to calibrated the MEM. The model is further calibrated to existing measurements (Nelson et al., 2007) by constraining the minimum (ε_h) and maximum (ε_H) horizontal tectonic strains (Eq. 1 and Eq. 2).

$$\sigma_h = \frac{v}{v-1}\left(\sigma_v - \alpha_v P_p\right) + \frac{E}{1-v^2}\varepsilon_h + \frac{Ev}{1-v^2}\varepsilon_H + \alpha_h P_p \quad \text{(Eq. 1)}$$

$$\sigma_H = \frac{v}{v-1}\left(\sigma_v - \alpha_v P_p\right) + \frac{E}{1-v^2}\varepsilon_H + \frac{Ev}{1-v^2}\varepsilon_h + \alpha_h P_p \quad \text{(Eq. 2)}$$

Where the Biot's poro-elastic constant (α) refers to transmissibility heterogeneities in the vertical (α_v) and horizontal (α_h) direction. The breakdown pressure, pressure dependent leak-off (PDL) coefficient, and fissure opening pressures (P_{fo}), and closure pressure (P_c) or minimum horizontal stress (σ_h) magnitude, can be obtained directly or observed from the DFIT data during the before closure analysis (BCA) period using the G-function time and the semi derivative of the G-function (Barree et al., 2009b). These values are used to further calibrate the calculated σ_h and σ_H magnitudes by resolving the Kirsch's equations (Kirsch, 1898) to describe the P_{wb} in terms of the horizontal stresses, pore pressure, and tensile rock strength (T_o) (Eq. 3), and the P_{fo} in terms of the horizontal stress (σ_h and σ_H) magnitudes and the fissure opening angle (θ) (Eq. 4). The θ describes the angle at which fractures will preferentially develop with respect to the orientation of principal horizontal stresses and can also be obtained from Mohr's circle construction of in situ stresses (Jaeger et al., 2009).

$$P_{wb} = 3\sigma_h - \sigma_H - P_p + T_o \quad \text{(Eq. 3)}$$

$$P_{fo} = \frac{1}{2}(\sigma_H + \sigma_h) + \frac{1}{2}(\sigma_H - \sigma_h)cos2\theta \quad \text{(Eq. 4)}$$

The tectonic stress and strain magnitudes are determined by integrating several measured and theoretical methods to allow equations 1 to 4 to be solved simultaneously following the generalised reduced gradient (GRG) nonlinear solving method (Lasdon et al., 1978). An error function (ErrFn) is used to minimise the error between the observed (x) and calculated ($\bar{x}$) values (Eq. 5). Once the MEM is calibrated and representative of the interval, it provides valuable information on the

Poisson's ratio, Young's modulus, the magnitude of principal stresses, and highlights differential stress contrasts between the target and surrounding rocks (Pokalai et al., 2016).

$$ErrFn = \sum(x - \bar{x})^2 \quad \text{(Eq. 5)}$$

3.2 Interpretation of Pre-Existing Natural Fractures

Pre-existing natural fractures are interpreted from the C-13 wellbore image log, which covers the entire 434m Patchawarra Formation interval. As the South Australian portion of the Cooper Basin is entirely subsurface, geophysical data and core measurements are the only avenue for obtaining structural data (Kulikowski et al., 2016a; Kulikowski and Amrouch, 2017). Borehole image logs measure the electrical resistivity of the borehole at the centimetre scale by pressing six pads, containing a total of 150 microelectrodes, against the borehole wall. The digital data is converted into an oriented interpretable image of the borehole, highlighting changes in the micro-resistivity. Natural fractures will be imaged as sinuous features that are either resistive (open) or conductive (closed). Both resistive and conductive natural fractures were interpreted from the entire 434m image log interval. The data is used to populate the discrete Fracture Network (DFN) model and to analyse the natural fracture intensity for the entire Patchawarra Formation interval.

3.3 Discrete Fracture Network (DFN) Model

The subsurface distribution of pre-existing natural fractures can be modelled using a discrete fracture network (DFN), which incorporates natural fracture data measured from borehole image logs. Once the DFN model is populated with natural fractures, reservoir properties, stress conditions, and the hydraulic fracturing parameters, the simulation commences. The reactivation of pre-existing natural fractures during hydraulic fracturing is modelled as either tensile (dilation) or shear reactivation. These two interactions could be more stress economic than the development of new fractures (Hubbert and Willis, 1957; Jaeger et al., 2009).

The DFN model was created for the middle (VC30-VC50) Patchawarra Formation (2903-2955m) in the C-13 well using Golder Associates' FracMan 7 software. The C-13 well is vertical and contains 434m of Patchawarra Formation stratigraphy. The DFN model (grid size of 10m × 10m × 10m) represents a 52m sandstone reservoir interval with homogenous reservoir properties. In addition to this vertical well (which is simulated under a strike-slip and a compressional stress regime), a well with an inclination of 60^{o} drilled towards the ESE is simulated within the DFN model using identical hydraulic fracturing properties and a strike-slip stress regime. The geometry of this additional well was suggested by previous works (Pokalai et al., 2016) to intersect the largest number of pre-existing

natural fractures, and therefore would result in the largest stimulated reservoir volume (SRV). The effectiveness of this well geometry is compared to the results from the two vertical wells. Growth of the hydraulic fracture was simulated within a contained volume of $2.08 \times 10^8 m^3$ for each of the three scenarios. Importantly, this well trajectory is neither within the high-risk wellbore stability limits under the present-day stress conditions, nor within the best trajectory for maximum production, which was found using the modified Kirsch equations for breakdown pressure gradient and breakdown angle (Pokalai et al., 2016).

The Poisson's ratio, Young's modulus, and the magnitude of principal stresses for the target depth are obtained from the calibrated MEM. A reservoir porosity of 10%, permeability of 0.115mD, pressure of 27.6MPa, and temperature of 138^{o}C were used. The maximum principal stress direction was taken from previous works and assumed to be 101^{o}N for the entire model (Pokalai et al., 2016). As the in situ stress can alternate between compressional and strike-slip stress regimes, two models were created to interchange the minimum and intermediate principal stress orientations. The distribution of pre-existing natural fractures within these two models remained constant and were controlled by the interpreted natural fractures from the C-13 borehole image log. The Elliptical Fisher Distribution was used to statistically populate the measured natural fractures within the model. This method was used because it captures the anisotropic variation of natural fracture geometries (strike and dip angles), whereas the Fisher Distribution requires a symmetrical variation around the mean pole, which is not observed in the dataset.

3.4 Three-Dimensional Hydraulic Fracture Simulation

Hydraulic fracturing is simulated within a sandstone reservoir at 2903-2955m depth, which belongs to the middle Patchawarra Formation (VC30-VC50) in the C-13 well. The growth of the hydraulic fracture and its interaction with the intersecting natural fractures is based on the orientation of principal stresses, such that opening (dilation) of the induced fracture will occur towards the minimum principal stress direction and its growth will be parallel to the maximum principal stress direction (mode 1 opening). Reactivation of pre-existing natural fractures followed the Mohr-Coulomb model using in situ stress conditions derived from the MEM and a standard friction angle of 30^o (Kulikowski et al., 2016c). Natural fractures intersecting the hydraulic fracture ($1^{st}\ order$) must have an internal pore pressure greater than the normal stress magnitude to tensile reactivate. This continues for $n^{th}\ order$ natural fracture intersections until the n^{th} fracture cannot accommodate the total volume of pumped material, at which point the hydraulic fracture is extended. To incorporate the pore pressure decrease in dilated natural fractures with increasing distance away from the wellbore (P_{pump}), a standard linear slope (s) (the standard value for s was

used due to the lack of published information specific to the Cooper Basin) of 0.5 (Fig. 2a) was used to determine fracture pore pressure (P_{frac}) in Eq. (6) (Golder Associates Inc., 2015).

$$P_{frac} = \left(P_{pump} - \sigma_n\right)\left(1 - s\frac{d}{d_{max}}\right) + \sigma_n + \rho g(\Delta h) \quad \text{(Eq. 6)}$$

Where P_{pump} is the pumping pressure, σ_n is the normal stress magnitude acting on the fracture end element, s is the slope representing fracture pore pressure (Fig. 2a), d is the flow distance from the well to the fracture element, d_{max} is the maximum hydraulic fracture distance, ρ is the slurry density, g is the gravitational acceleration, and Δh is the vertical elevation from the well intersection point to the fracture element (Golder Associates Inc., 2015). After the hydraulic fracture simulation is completed, the model comprises of the hydraulic fracture and the network of dilated natural fractures that act as fluid conduits. The next stage in the simulation is to calculate whether the pressure remaining at the tips of these fractures is sufficient enough to induce shear reactivation of uninflated natural fractures (Fig. 2c). Here the dissipating pressure (P_{dis}) at the fracture tip is calculated using Eq. (7) with a standard slope (s) (the standard value for s was used due to the lack of published information specific to the Cooper Basin) of 3 (Fig. 2b) (Golder Associates Inc., 2015).

$$P_{dis} = P_{tip} - (P_{tip} - P_R)(\frac{d-d_{tip}}{d_R-d_{tip}})^s \quad \text{(Eq. 7)}$$

Where P_{tip} is the pressure at the inflated fracture tip, P_R is the reservoir pressure at d_R, d_R is the path distance from the injection point to the point where the pore pressure is unperturbed by the hydraulic fracturing and equal to the P_R, d is the path distance from the injection point to the local point beyond the fracture tip, and d_{tip} is the path distance from the injection point to the fracture tip (Golder Associates Inc., 2015). Again, as the distance away from the fracture tip increases, the effect of pressure within dilate fractures is reduced (Fig. 2b). Reservoir pressure is 27.6MPa, and d_R is 1000m. A high-temperature, borate cross-linked, modified guar gelled fluid system consisting of $0.10m^3/s$ of clean water and $0.10m^3/s$ of slurry is used with 15 time steps representing the viscosity profile over a period of 1.5 hours. Properties for a general ceramic (20/40) proppant type with a diameter of 0.854cm and a bulk density of $2099.55kg/m^3$ were used in the simulation. The fluid and proppants are consistent with current industry practice in the Cooper Basin. An initial shut-in pressure (ISIP) of 60.8MPa was observed from a DFIT data and matched to the fracture simulation model.

Insert Fig. 2

4. RESULTS

4.1 Calibrated Mechanical Earth Model

The mechanical earth model (MEM) was constructed across the entire Patchawarra Formation from well log derived data (Fig. 3a), and calibrated by DFIT data at two separate depths (Fig. 3b and 3d). Analysis of the DFIT data at 2920m and 2840m using the semi derivative (GdP/dG) of the G-function (dP/dG) found closure pressures (P_c) of approximately 52.4MPa and 51.0MPa, and breakdown pressures (P_{wb}) of approximately 68.6MPa and 71.0MPa, respectively (Fig. 3c and 3e). These values for P_c and P_{wb} were used to calibrate the log derived MEM using Eq. 1-3 and Eq. 5 and adjusting lateral tectonic strains as described in part 3.1. Further analysis of the GdP/dG shows a increase above ideal GdP/dG behaviour in the early G-Time (Fig. 3c), indicating fissure opening of natural fractures in this formation. In Figure 3e the GdP/dG behaviour in the early time illustrates height or transverse recession leak-off of the GdP/dG and suggests that the fracture stimulation has propagated vertically or laterally into less permeable regions. For these reasons, the bottom DFIT interval (2903-2955m) was selected for hydraulic fracture stimulation as it involves interaction with pre-existing natural fractures. The Poisson's ratio and Young's modulus were log derived with mean values of 0.245 and 31826.2MPa, over the target interval and were incorporated into MEM calibration and later DFN modelling.

This MEM calibration process produced tectonic strain values three times greater in the σ_H than in the σ_h directions, or approximately 600 and 200 microstrains, respectively. The resulting magnitude of σ_h and σ_H were approximately 51.7MPa and 72.4MPa at the target depth (2910m), respectively (Fig. 3a). The σ_v magnitude within the Patchawarra Formation followed a gradient of approximately 0.0224MPa/m with a median magnitude of 65.5MPa at the target depth. The key observation from this MEM is that the σ_h and σ_v magnitudes can cross over and cause the MEM to alternate between a compressional ($\sigma_h > \sigma_v$) and strike-slip ($\sigma_h < \sigma_v$) stress regime based on moduli values (Barree et al., 2009a). The breakdown pressure, P_{wb}, rapidly decreases below the σ_H in regions of known coal presence, but is otherwise is greater than σ_H elsewhere in the MEM (Fig. 3a). The σ_h stress contrast between sandstones and coals (7MPa) is relatively low (Fig. 3a). Based on moduli value these low contrasts between σ_h in sandstones and coals would lead to containment issues when stimulating adjoining sandstone and coal sequences and as observed by prior researchers (Johnson and Greenstreet, 2003).

Insert Fig. 3

4.2 Analysis of Pre-Existing Natural Fractures

A total of 249 natural fractures were interpreted from the C-13 borehole image log covering the entire 434m Patchawarra Formation interval (Fig. 4a). The stereographic projection shows a significant cluster of natural fractures dipping towards the WNW at an angle of approximately 60^{o} from horizontal. Low dipping (<40^{o}) natural fractures are also common with no preference to dip direction. These form the main natural fracture clusters; however, a wide range of natural fracture geometries are present that vary from 70^{o} dip angle to horizontal, and striking in all directions.

The cumulative fracture intensity with depth is presented for the upper (2727-2847m), middle (2847-2934m) and lower (2934-3161m) Patchawarra Formation (Fig. 4c). The P10 fracture intensity (fractures per meter) is much greater in the middle Patchawarra Formation (0.977012/m) than the upper (0.558333/m) and lower (0.405859/m) intervals. DFIT analysis within the target interval (2903-2955m) suggested interaction with natural fractures (Fig. 3c), which is expected considering that this interval (middle Patchawarra Formation) contains the highest fracture intensity (Fig. 4c). The rock quality designation (RQD) is a statistic used to describe the expected core quality (number of separate pieces) and is defined as the total length of core pieces with lengths greater than 10cm divided by the total borehole length. High RQD values are found in the middle (RQD=33.6917) and upper (RQD=23.6923) intervals, with the lowest RQD value (RQD=8.51968) found in the lower Patchawarra Formation (Fig. 4c).

The three-dimensional distribution of natural fractures measured from the borehole image log is shown in Fig. 4b together with an example of an interpreted natural fracture. The distribution of natural fractures shows a dominant set dipping towards the WNW at a high dip angle, as well as a significant number of low angle fractures with no directional preference. To match this natural fracture distribution in the DFN model using the Elliptical Fisher Distribution, four natural fracture sets were statistically defined (pole plunge/pole trend): (1) 29/108^{o}N; (2) 66/299^{o}N; (3) 74/110^{o}N; and (4) 32/111^{o}N. The creation of these sets ensured that the software would distribute fractures within the DFN model (Fig. 4d) in a way that would ultimately represent the original interpreted borehole fracture data (Fig. 4a).

Insert Fig. 4

4.3 Three-Dimensional Hydraulic Fracture Simulation with Natural Fractures

4.3.1 VERTICAL WELL (C-13)

4.3.1.1 Strike-Slip Stress Regime

Under a strike-slip stress regime, the hydraulic fracture grew towards the maximum horizontal stress (σ_H) direction while opening towards the minimum horizontal stress (σ_h) direction (Fig. 5a) giving a total stimulated reservoir volume (SRV) of $116.4m^3$ (base case). The interaction between the hydraulically induced fracture and the pre-existing natural fractures displayed a consistent trend that preferentially reactivated high angled (>50^o) natural fractures striking ESE-WNW (Fig. 5b and 5c). A total of 9 pre-existing natural fractures were reactivated along the hydraulically induced fracture giving a total fracture area of $73516.4m^2$ and a SRV of $405.2m^3$.

4.3.1.2 Compressional Stress Regime

The hydraulic fracture growth under a compressional stress regime again grew towards the σ_H direction, but the opening was towards the σ_v direction (Fig. 5d) forming a pancake-like shape. This induced fracture geometry is sub-parallel to the stratigraphy and results in a fracture aspect ratio that is negligible (<1) and strongly dictated by the lack of vertical fracture growth. Inflation of near horizontal pre-existing natural fractures was strongly preferred under these stress conditions (Fig. 5e). The strike of these reactivated natural fractures was largely irrelevant and dominantly controlled by the dip angle; however, a slight preference for ESE-WNW striking fractures can be observed (Fig. 5f). A total of 11 pre-existing natural fractures were reactivated with significantly more second, and multiple, order interactions than under the strike-slip stress regime, with the reactivated natural fracture planes becoming increasingly more sub-horizontal with distance away from the wellbore (Fig. 5e). The hydraulic fracture covered an area of $64050.3m^2$ giving a SRV of $397.9m^3$.

Insert Fig. 5

4.3.2 INCLINED WELL

4.3.2.1 Strike-Slip Stress Regime

The inclined (30^o) well scenario was modelled under a strike-slip stress regime and resulted in the hydraulic fracture growing parallel to the σ_H direction and opening towards σ_h (Fig. 5g). The induced hydraulic fracture reactivated seven pre-existing natural fractures (Fig. 5h). Again, this simulation contained multiple order interactions that covered an area of $60039.3m^2$, giving a SRV of $643.4m^3$.

These reactivated pre-existing natural fractures were consistently high (>50^{o}) angled with a preferred ESE-WNW strike (Fig. 5i).

5. Discussion

The aims of this work were to quantify the effectiveness of hydraulic fracturing under different scenarios and attempt to better understand the complex interactions between the hydraulically induced fracture and pre-existing natural fractures. The calibrated mechanical earth model (MEM) shows high stress and strain conditions with a possible alternating stress regime between compressional and strike-slip (Fig. 3a). Such a complex stress environment can cause significant variations in hydraulic fracture growth and interaction with pre-existing natural fractures, which can ultimately compromise the effectiveness of hydrocarbon production.

Under both the vertical well (C-13) scenarios, the strike-slip stress regime conditions foster high (>50^{o}) angled natural fractures to be preferentially reactivated (Fig. 5c), compared to the preferential reactivation of near horizontal natural fractures under a compressional stress regime (Fig. 5f). This contrast results in a slight increase in the stimulated reservoir volume (SRV) for the strike-slip stress regime scenario. Although this is only slight, a key difference comes from the difficulty of keeping near horizontal natural fractures dilated after reactivation due to the overlying weight of rock. Correct proppant placement is essential in this case and it may be beneficial to implement several stages of proppant, or coarse sand, placement to ensure that these natural fractures remain dilated. Horizontal hydraulic fractures may be preferred in some instances where vertical fracture growth would result in unwanted connection of previously isolated and vertically stacked reservoirs.

The work of Pokalai et al. (2016) suggested that an inclined (30^{o}) well drilled towards the ESE-WNW would intersect a larger number of pre-existing natural fractures and result in a greater SRV. This well trajectory was modelled by Pokalai et al. (2016) without a DFN model, giving a SRV of $116.0m^3$ (base case), which was matched ($116.4m^3$) in our study. In addition to intersecting the largest number of pre-existing natural fractures using this well geometry, inclined wells have a larger wellbore contact in the reservoir compared to vertical wells, which in our case has a negligible effect on the SRV. The G-Function analysis shows a leak off behaviour consistent with the interaction of pre-existing natural fractures during the shut-in time (Fig. 3c & 3e). This suggests that an understanding of natural fracture behaviour during hydraulic fracturing is essential.

To expand on previous work (Pokalai et al., 2016), hydraulic fracturing was simulated using this optimised well trajectory in the DFN model, finding that the SRV increased by five times compared to

the vertical well scenario; albeit the total fracture area was larger in the vertical well. The reason behind this was the more complex multiple order interactions between natural fractures in the inclined well, which created a more intense fracture network compared to the vertical well. This infers that the effectiveness of hydraulic fracturing, and therefore hydrocarbon production, may be improved significantly by optimising the well trajectory to intersect the largest number of pre-existing natural fractures, which fostered greater multiple order natural fracture interactions. However, an inclined well can be subject to increased wellbore instability if the distribution of principal stress magnitudes and the stress regime are not carefully managed.

For each of the three modelled scenarios, the interaction between the hydraulic fracture and pre-existing natural fractures remains consistent within each case, and phenomenon such as hydraulic fracture plane rotation is not observed. Rotation of the hydraulic fracture from vertical at the wellbore to horizontal within the reservoir, as suggested by recent works (Scott et al., 2013; Cooke et al., 2016; Pokalai et al., 2016), would therefore require conditions that were not included in our model. For such a phenomenon to occur there can only be few reasons: (1) the stress regime transitions from strike-slip at the wellbore to compressional within the reservoir; (2) horizontal pre-existing natural fractures are preferentially reactivated; (3) the contact plane (bedding) between stacked lithologies is preferentially reactivated; (4) the hydraulic fracture initiates in the vertical position at the wellbore before the fracture fluid begins to preferentially flow through high permeability layers within the reservoir; or (5) a combination of the above.

It is unlikely that the stress regime consistently transitions from strike-slip at the wellbore to compressional within the reservoir for each of the many wells; however, it may be possible for the hydraulic fracture to grow in height and interact with adjacent lithologies, which have contrasting mechanical properties that may foster a change in stress regime. This may be observed in the MEM where a change in lithology (and therefore a change in Poisson's ratio and Young's modulus) will influence the σ_h (and σ_H) magnitude (Fig. 3a). This is particularly the case between sandstones and coals where the difference in σ_h magnitude is approximately 7MPa and can contain the hydraulic fracture within the sandstone interval (Fig. 3a). Additionally, the significant decrease in the σ_h magnitude within coals can be sufficient enough to cause a transition from compressional to strike-slip stress regimes (Fig. 3a). Given that the σ_h and σ_v magnitudes are similar throughout the basin, the stress regime may alternate between strike-slip ($\sigma_h < \sigma_v$) and compressional ($\sigma_h > \sigma_v$) between adjacent lithologies (Fig. 3a). Vertical initiation of the hydraulic fracture at the wellbore (McGowen et al., 2007) implies a strike-slip stress regime (or extensional, but this is not the case here). To

transition from a strike-slip stress regime at the wellbore to a compressional regime with increasing distance, the principal σ_v magnitude could be reduced, or the principal σ_h magnitude be increased.

As the stress regime must be strike-slip, preferential reactivation of horizontal natural fractures is geomechanically incorrect if high (>50^o) angle ESE-WNW striking natural fractures are present (Anderson, 1905; Zoback, 2007). Based on these studies, historical evidences of high propagation pressures (i.e., ISIP gradients > σ_v) can be explained by a combination of tensile fracture and natural fracture reactivations in an environment of high σ_H magnitude. A more plausible explanation for observed horizontal fracture components from surface deformation tiltmeter experiments (Pitkin et al., 2012; Scott et al., 2013) is the potential for dip-slip or tensile fracture propagations along weak lithological boundaries. This occurs since the contact boundary between two lithologies forms a plane of weakness that may be preferentially reactivated if it is more stress economic than reactivating natural fractures, or initiating new fracture development (Warpinski and Teufel, 1987; Cooke et al., 2016). In this case, the cause of horizontal components would relate to the fracturing fluid seeking the path of least resistance, which is through high horizontal permeability sections in the tight sandstones that cycle to weaker boundaries with shales and coals within the Patchawarra sequence. The fracturing fluid would traverse vertically through these high horizontal permeability sections within the tight sandstones then induce shear along the contact plane with adjacent shales and coals. Future work and additional diagnostics would be required to resolve this observation of horizontal fracture components from surface deformation tiltmeter experiments in the Cooper Basin.

6. Conclusions

Integrating a calibrated mechanical earth model, discrete fracture network model, and three-dimensional (3D) hydraulic fracture simulation has provided vital constraints on the effectiveness of hydraulic fracturing under different stress regimes and with different well trajectories. This 3D hydraulic fracture simulation study has also presented the unique interactions between hydraulic fractures and pre-existing natural fractures and quantified the in situ tectonic stress and strain conditions. Hydraulic fracturing within an optimised well trajectory under a strike-slip stress regime generated a stimulated reservoir volume (SRV) five times greater than the vertical well scenario (base case with no natural fracture interactions) under identical conditions. Compared to this base case the SRV under compressional and strike-slip stress regimes was three times greater if pre-existing natural fractures are present. High angled (>50^o) ESE-WNW striking natural fractures were found to exclusively reactivate under a strike-slip stress regime, and low angled (<40^o) to near horizontal natural fractures were found to reactivate under a compressional stress regime.

Although the simulations were not able to capture the hydraulic fracture plane rotation from vertical at the wellbore to horizontal within the reservoir, four likely reasons are presented, with the most likely reasons being a combination of two effects. The first is that fracturing fluid will preferentially seek the path of least resistance, which will typically be through high permeability fractures within the tight sandstones in either tensile or strike-slip mode generating higher than expected propagation pressures. The second plausible explanation for observed horizontal fracture components is that the contact plane between lithologies forms planes of weakness that may be preferentially reactivated if it is more stress economic to do so than to reactivate the pre-existing natural fractures or induce rock failure. This paper provides the most plausible physical explanations for the complex hydraulic fracturing behaviour and high pressures observed in strike-slip stress regimes, and provides companies operating in the Cooper Basin with constraints on the in situ stress and strain conditions for future design considerations.

7. Acknowledgments

Thanks to DownUnder Geosolutions (DUG Insight 4.2), Paradigm (Geolog 7.2), Barree & Associates (GOHFER) and Golder Associates (FracMan 7) for academic licencing. We thank Carlos H. Grohmann and Ginaldo A.C. Campanha for the development of the 'OpenStereo 0.1.2' software.

8. References

Alexander, E.M., Gravestock, D.I., Cubitt, C., Chaney, A., 1998. Lithostratigraphy and environments of deposition. In: Gravestock, D.I., Hibburt, J.E., Drexel, J.F., (Eds.), The Petroleum Geology of South Australia. Vol. 4: Cooper Basin, South Australia. Department of Primary Industries and Resources. Report Book, 98/9, 69-116.

Anderson, E.M., 1905. The dynamics of faulting. Transactions of the Edinburgh Geological Society. 8(3), 387-402.

Apak, S.N., Stuart, W.J., Lemon, N.M., Wood, G., 1997. Structural evolution of the Permian-Triassic Cooper Basin, Australia: Relation to hydrocarbon trap styles. AAPG Bulletin. 81, 533-555.

Barree, R.D., Gilbert, J.V., Conway, M., 2009a. Stress and rock property profiling for unconventional reservoir stimulation. In: SPE Hydraulic Fracturing Technology Conference. 1-18, SPE 118703.

Barree, R.D., Barree, V.L., Craig, D., 2009b. Holistic fracture diagnostics: consistent interpretation of prefrac injection tests using multiple analysis methods. SPE Production & Operations. 24(3), 396-406.

Camac, B.A., Waldron, A.R., Donley, J.A., Hunt, S.P., 2012. Microseismic and 3D VSP for infill evaluation in Greater Tindilpie, Cooper Basin, Australia. In: 46th U. S. Rock Mechanics/Geomechanics Symposium, American Rock Mechanics Association.

Cooke, D., Tyiasning, S., Abul Khair, H., 2016. Unexpected behaviors of stimulated fractures in the high-stress Cooper Basin. The Leading Edge. 35(1), 78-84.

Golder Associates Inc., 2015. FracMan® Discrete Fracture Network Modelling Software, FracMan 7.5 Workshop, Golder Associates Inc., Redmond.

Grohmann, C.H., Campanha, G.A.C., 2010. OpenStereo: Open source, cross-platform software for structural geology analysis, paper presented at 2010 Fall Meeting, AGU, San Francisco, Calif.

Hubbert, M.K., Willis, D.G., 1957. Mechanics of Hydraulic Fracturing. In: Transactions of SPE of AIME. 210, 153-168.

Jaeger, J.C., Cook, N.G.W., Zimmerman, R., 2009. Fundamentals of rock mechanics, fourth edition. Blackwell Publishing Ltd., Oxford, UK.

Johnson, Jr., R.L., Aw, K.P., Ball, D., Willis, M., 2002. Completion, Perforating and Hydraulic Fracturing Design Changes Yield Success in an Area of Problematic Frac Placement - the Cooper Basin, Australia. Presented at the SPE Asia Pacific Oil & Gas Conference and Exhibition, Melbourne, Australia, 8–10 October. SPE-77906-MS.

Johnson, Jr., R.L., Greenstreet, C.W., 2003. Managing Uncertainty Related to Hydraulic Fracturing Modeling in Complex Stress Environments with Pressure-Dependent Leakoff. The SPE Annual Technical Conference and Exhibition, Denver, Colorado, 5–8 October, SPE-84492.

Johnson, Jr., R.L., Abul Khair, H., Jeffrey, R., Meyer, J., Stark, C., Tauchnitz, J., 2015. Improving fracture initiation and potential impact on fracture coverage by implementing optimal well-planning and drilling methods for typical stress conditions in the Cooper Basin, central Australia. The Australian Petroleum Production and Exploration Association Journal. 55(2), 403-403.

Johnson, Jr., R.L., 2016. Improving diagnostic fracture injection testing for in situ stress profiling, reservoir characterisation and well optimisation in unconventional gas reservoirs. International

Conference on Geomechanics, Geo-Energy and Geo-resources (IC3G 2016), Melbourne, Australia, 28-29 September.

Kirsch, E.G., 1898. Die Theorie der Elastizität und die Bedürfnisse der Festigkeitslehre. Zeitschrift des Vereines Deutscher Ingenieure. 42(28), 797-807.

Kulikowski, D., Hochwald, C., Cooke, D., Amrouch, K., 2016a. A Statistical Approach to Assessing Depth Conversion Uncertainty on a Regional Dataset: Cooper-Eromanga Basin, Australia. ASEG-PESA-AIG 2016 Conference, Adelaide. Extended Abstract #200, 484-490.

Kulikowski, D., Cooke, D., Amrouch, K., 2016b. Constraining the distribution and relationship between overpressure, natural fracture density and temperature in the Cooper Basin. The Australian Petroleum Production and Exploration Association Journal. 56, 11-28, doi:10.1071/AJ15002.

Kulikowski, D., Amrouch, K., Cooke, D., 2016c. Geomechanical Modelling of Fault Reactivation in the Cooper Basin, Australia. Australian Journal of Earth Sciences. 63(3), 295-314, doi:10.1080/08120099.2016.1212925.

Kulikowski, D., Amrouch, K., 2017. Combining Geophysical Data and Calcite Twin Stress Inversion Analysis to Refine the Structural and Stress History of Complex Provinces: A Case Study on the Cooper-Eromanga Basin, Australia. Tectonics. 36(3), 515-541, doi:10.1002/2016TC004366.

Kulikowski, D., Amrouch, K., Cooke, D., Gray, M.E., 2017. Basement Structural Architecture and Hydrocarbon Conduit Potential of Polygonal Faults in the Cooper-Eromanga Basin, Australia. Geophysical Prospecting, in press, doi:10.1111/1365-2478.12531.

Lasdon, L.S., Warren, A.D., Jain, A., Ratner, M., 1978. Design and testing of generalised reduced gradient code for nonlinear programming. ACM Transactions on Mathematical Software. 4(1), 34-50.

Mackie, S., 2015. History of petroleum exploration and development in the Cooper and Eromanga basins. In: AAPG/SEG international conference and exhibition, 13-16 September, Melbourne, Australia. Search and Discovery Article #10814.

McGowen, J.M., Gilbert, J.V., Samari, E., 2007. Hydraulic fracturing down under. SPE Hydraulic Fracturing Technology Conference, Texas, USA, 29-31 January.

Müller, R.D., Dyksterhuis, S., Rey, P., 2012. Australian paleo-stress fields and tectonic reactivation over the past 100 Ma. Australian Journal of Earth Sciences. 59(1), 13-28.

Nelson, E.J., Chipperfield, S.T., Hillis, R.R., Gilbert, J., McGowen, J., Mildren, S.D., 2007. The relationship between closure pressures from fluid injection tests and the minimum principal stress in strong rocks. International Journal of Rock Mechanics and Mining Sciences. 44(5), 787-801.

Nolte, K.G., Smith, M.B., 1981. Interpretation of fracturing pressures. Journal of Petroleum Technology. 33(9), 1-767.

Pitkin, M.C., Wadham, T.H., McGowen, J.M., Thom, W.W., 2012. Taking the First Steps: Stimulating the Nappamerri Trough Resource Play. SPE Asia Pacific Oil and Gas Conference and Exhibition, Perth, Australia, 22-24 October 2012.

Pokalai, K., Fei, Y., Ahmad, M., Haghighi, M., Gonzalez, M., 2015a. Design and optimisation multi-stage hydraulic fracturing in a horizontal well in a shale gas reservoir in the Cooper Basin, South Australia. The Australian Petroleum Production and Exploration Association Journal. 55, 1-14.

Pokalai, K., Haghighi, M., Sarkar, S., Tyiasning, S., Cooke, D., 2015b. Investigation of the Effects of Near Wellbore Pressure Loss and Pressure Dependent Leakoff on Flowback during Hydraulic Fracturing with pre-existing Natural Fractures. SPE/IATMI Asia Pacific Oil and Gas Conference and Exhibition, Nusa Dua, Bali. SPE-176440.

Pokalai, K., Kulikowski, D., Johnson, Jr., R.L., Haghighi, M., Cooke, D., 2016. Development of a new approach for hydraulic fracturing in tight sand with pre-existing natural fractures. The Australian Petroleum Production and Exploration Association Journal. 56, 225-238.

Radke, B., 2009. Hydrocarbon and Geothermal Prospectivity of Sedimentary Basins in Central Australia; Warburton, Cooper, Pedirka, Galilee, Simpson and Eromanga Basins. Geoscience Australia Record 2009/25.

Reynolds, S.D., Mildren, S.D., Hillis, R.R., Meyer, J.J., 2006. Constraining stress magnitudes using petroleum exploration data in the Cooper–Eromanga Basins, Australia. Tectonophysics. 415(1), 123-140.

Roberts, G.A., Chipperfield, S.T., Miller, W.K., 2000. The Evolution of a High Near-Wellbore Pressure Loss Treatment Strategy for the Australian Cooper Basin. Presented at the SPE Annual Technical Conference and Exhibition, Dallas, Texas, 1–4 October. SPE-63029-MS.

Scott, M.P., Stephens, T., Durant, R., McGowen, J., Thom, W., Woodroof, R., 2013. Investigating Hydraulic Fracturing in Tight Gas Sand and Shale Gas Reservoirs in the Cooper Basin. Presented at The SPE Unconventional Resources Conference and Exhibition-Asia Pacific, Brisbane, Australia, 11–13 November. SPE-167073-MS.

Thiercelin, M.J., Plumb, R.A., 1994. A core-based prediction of lithologic stress contrasts in east Texas formations. SPE Formation Evaluation. 9(4), 251-258.

Waldron, A.R., Camac, B.A., 2016. Microseismic monitoring of hydraulic-fracturing programs in the Cooper Basin, Australia. The Leading Edge. 35(1), 72-76.

Warpinski, N.R., Teufel, L.W., 1987. Influence of geologic discontinuities on hydraulic fracture propagation. Journal of Petroleum Technology. 39(2), 209-220.

Zoback, M.D., 2007. Reservoir geomechanics. Cambridge University Press.

9. Figures

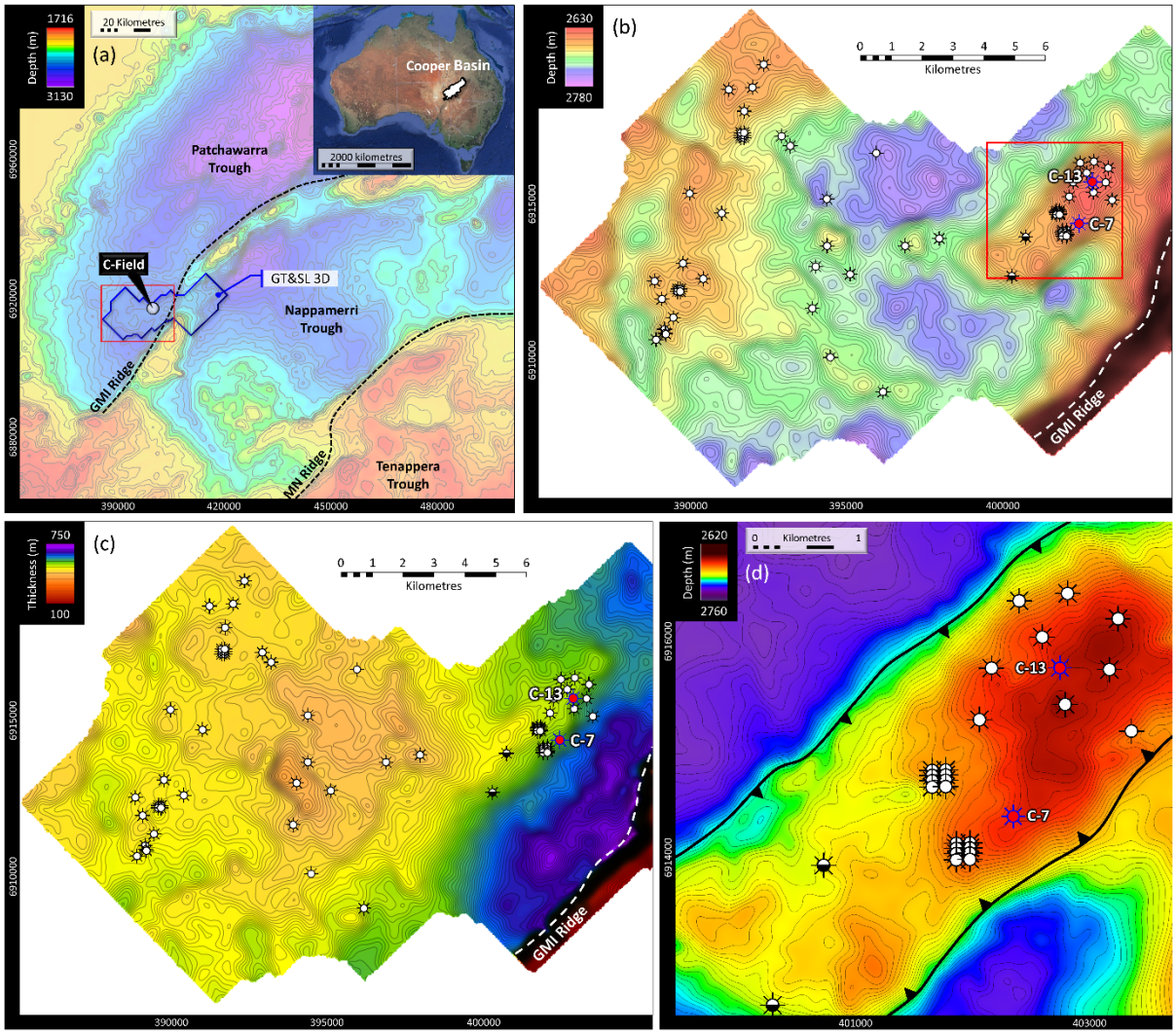


Figure 1. (a) Location of the study area (C-Field) within the GT&SL 3D seismic survey located in the South Australian portion of the Cooper Basin (inset map of Australia). Location of the Gidgealpa-Merrimelia-Innamicnka (GMI) and Murteree-Nappacoongee (MN) ridges and Patchawarra, Nappamerri, and Tenaperra troughs shown. (b) Depth map to the top Patchawarra Formation with the location of C-7 and C-13 wells shown. See Fig. 1a for location. (c) Isopach map of the Patchawarra Formation with location of C-7 and C-13 wells shown. (d) Depth map of the top Patchawarra Formation within the C-Field. See Fig. 1b for location.

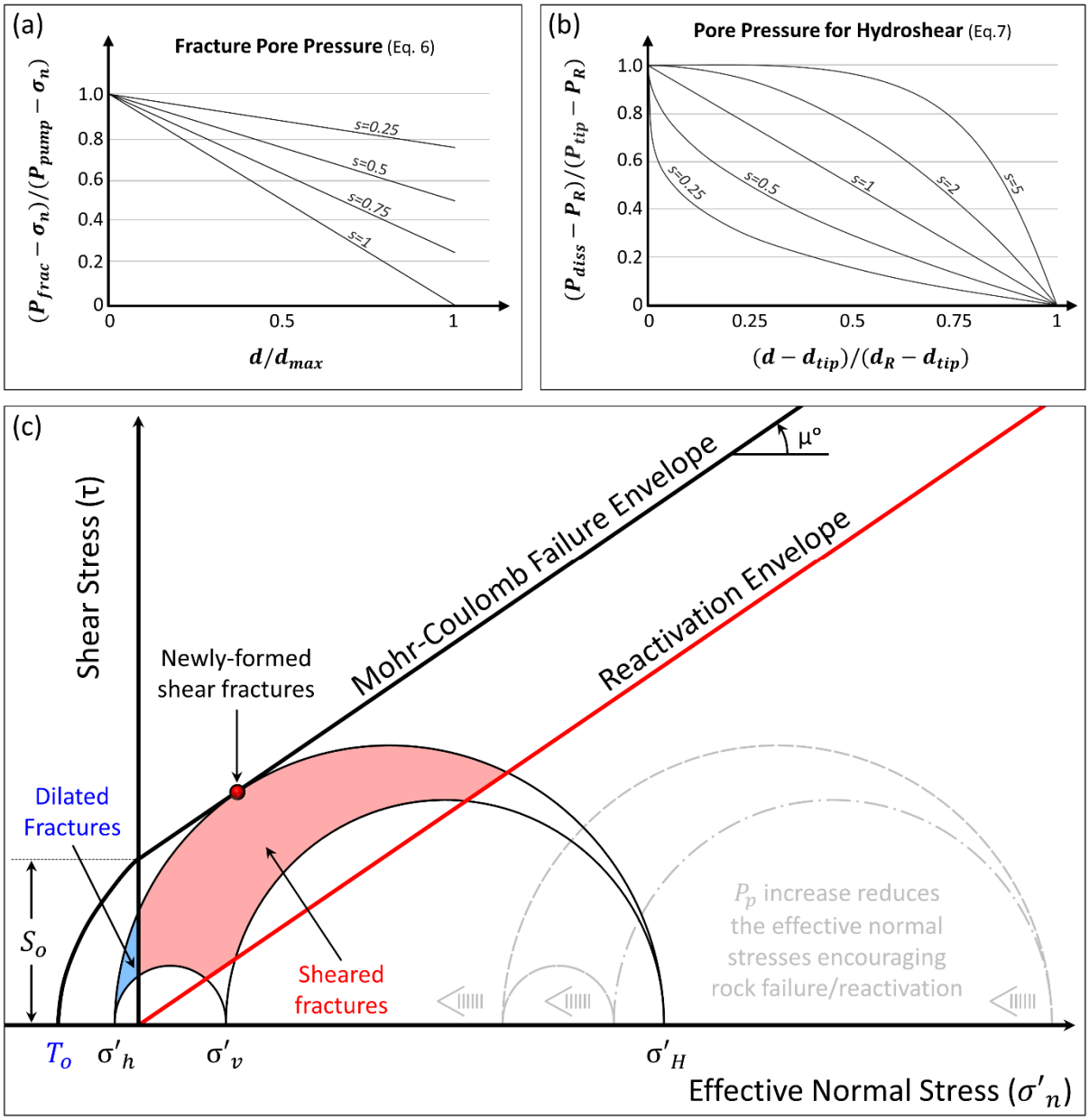


Figure 2. (a) The decrease in fracture pore pressure (P_{frac}) with increasing distance away from the well (d), with respect to the normal stress (σ_n), pumping pressure (P_{pump}) and maximum hydraulic fracture distance away from the well (d_{max}). A standard slope (s) of 0.5 was used for this study as no detailed information was available for the Cooper Basin (after Golder Associates Inc., 2015). (b) The pressure dissipation (P_{diss}) from inflated natural fracture into the reservoir and uninflated natural fractures with respect to the distance away from fracture tip. P_R is initial reservoir pressure, P_{tip} is pressure at inflated natural fracture tip, d is the path distance from injection point to the local point beyond the fracture tip, d_R is the distance from injection point to the point where reservoir pressure is unperturbed by the simulation and equal to P_R. A standard slope (s) of 3 was used for this study as no detailed information was available for the Cooper Basin (after Golder Associates Inc., 2015). (c) A theoretical Mohr-Coulomb circle construction illustrating the stress conditions required for dilation and shear reactivation, and new fracture development. The increase in pore pressure (P_p) during hydraulic fracturing reduces the maximum (σ'_H) minimum (σ'_h), and vertical (σ'_v) effective principal stress magnitudes shifting the Mohr's circle towards the failure and reactivation envelopes. T_o is the tensile rock strength, S_o is the cohesive shear strength, and μ is the angle of internal friction.

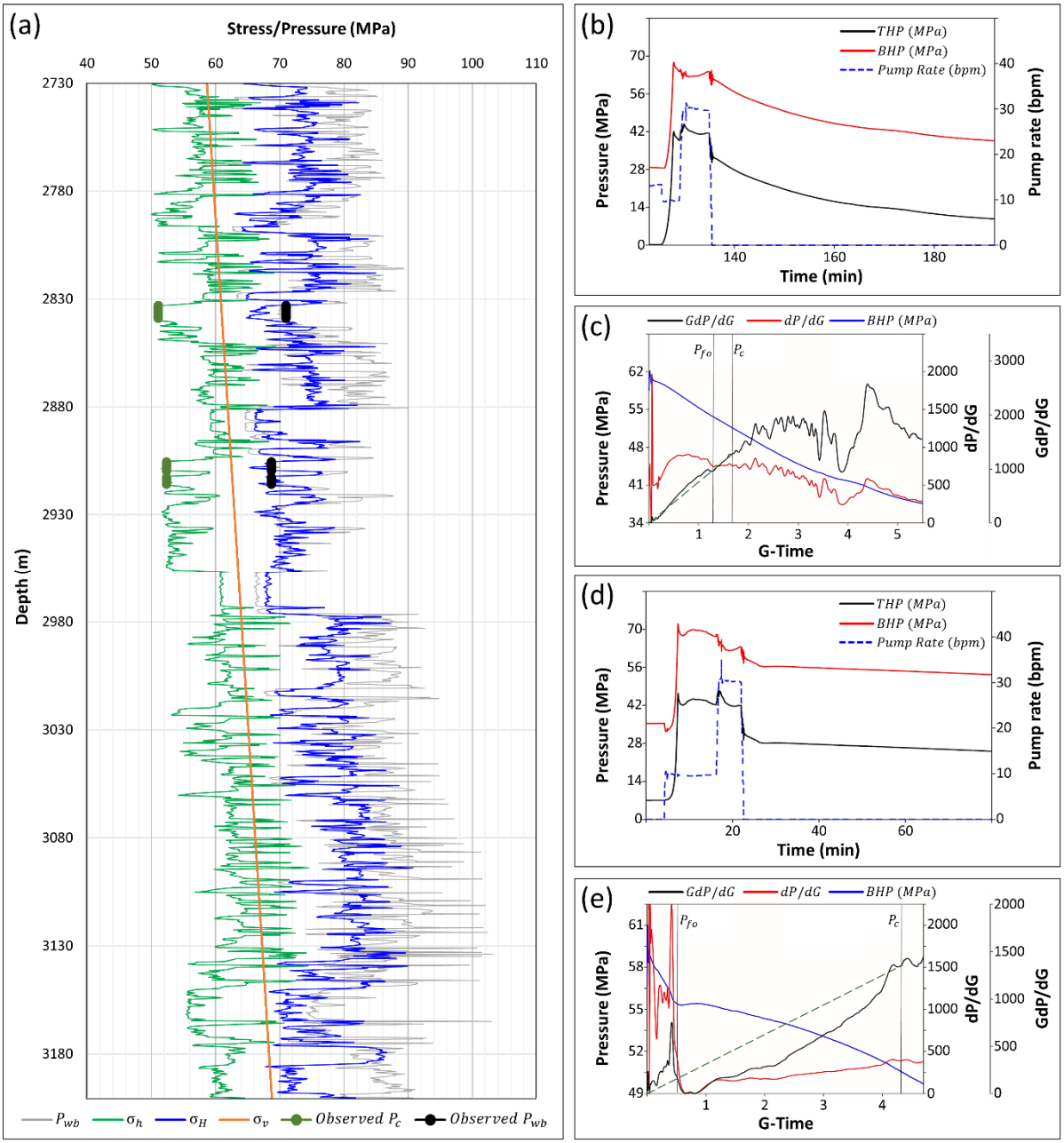
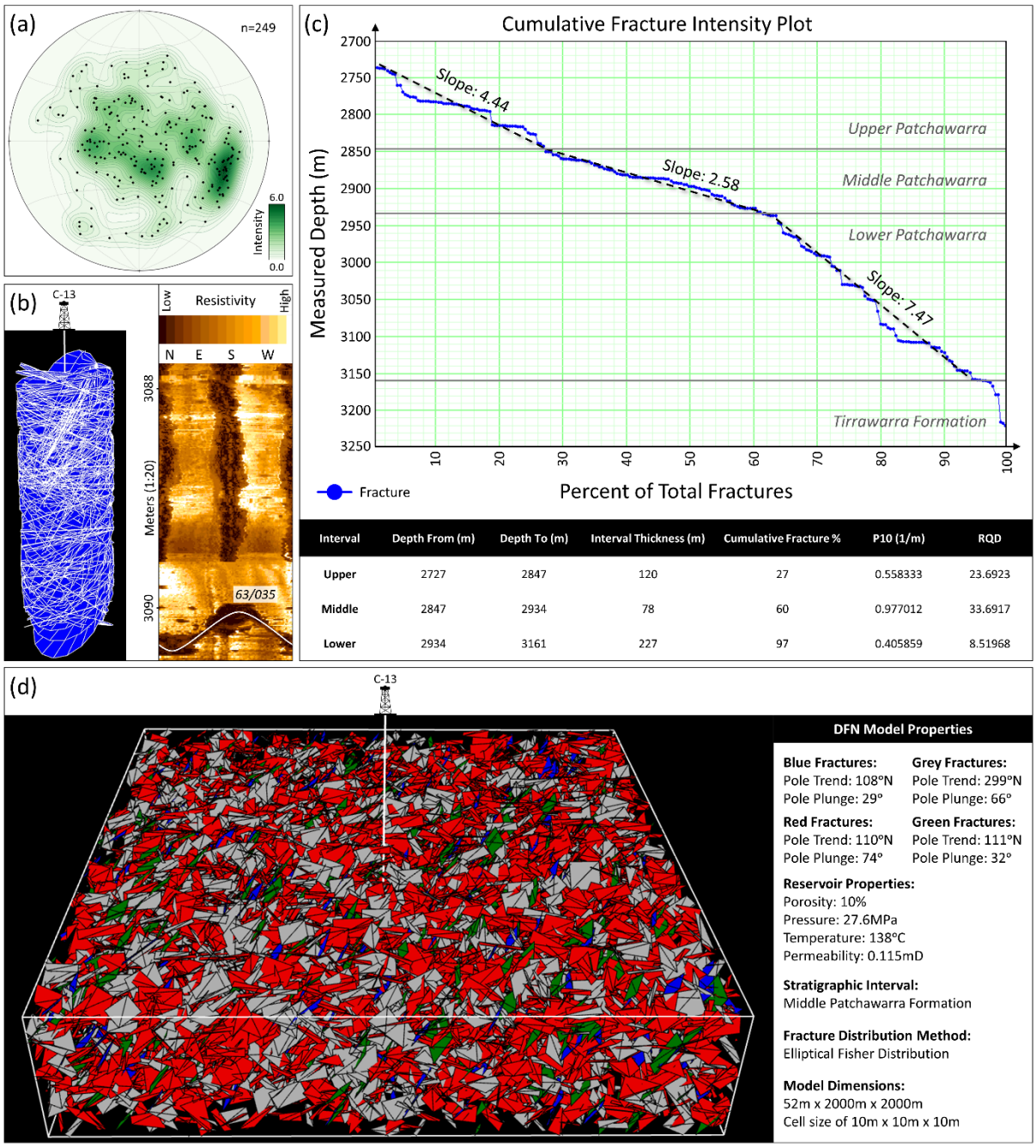


Figure 3. (a) Construction of the mechanical earth model in the C-7 well for the entire Patchawarra Formation interval. The observed closure ($Observed\ P_c$) and breakdown ($Observed\ P_{wb}$) pressures are compared with the calculated breakdown pressure (P_{wb}), maximum horizontal (σ_H), minimum horizontal (σ_h), and vertical stress (σ_v) magnitudes. (b) Diagnostic fracture injection test (DFIT) at 2920m depth. (c) G-function (dP/dG) and semi G-function (GdP/dG) analysis at 2920m depth. (d) DFIT at 2840m depth. (e) G-function (dP/dG) and semi G-function (GdP/dG) analysis at 2840m depth. Where THP is tubing head pressure, and BHP is the bottom hole pressure.



Interval	Depth From (m)	Depth To (m)	Interval Thickness (m)	Cumulative Fracture %	P10 (1/m)	RQD
Upper	2727	2847	120	27	0.558333	23.6923
Middle	2847	2934	78	60	0.977012	33.6917
Lower	2934	3161	227	97	0.405859	8.51968

Figure 4. (a) Pre-existing natural fractures within the Patchawarra Formation interpreted from the C-13 borehole image log and projected onto an equal-area lower hemisphere stereonet (Grohmann and Campanha, 2010). (b) Natural fracture distribution ion the C-13 well and an example of a natural fracturing in the borehole image log. (c) Natural fracture cumulative intensity analysis for the upper, middle, and lower Patchawarra Formation presenting the fracture intensity slope, fracture intensity per meter (P10), and rock quality designation (RQD). (d) The discrete fracture network (DFN) used for this analysis showing four different natural fracture sets within the Patchawarra Formation.

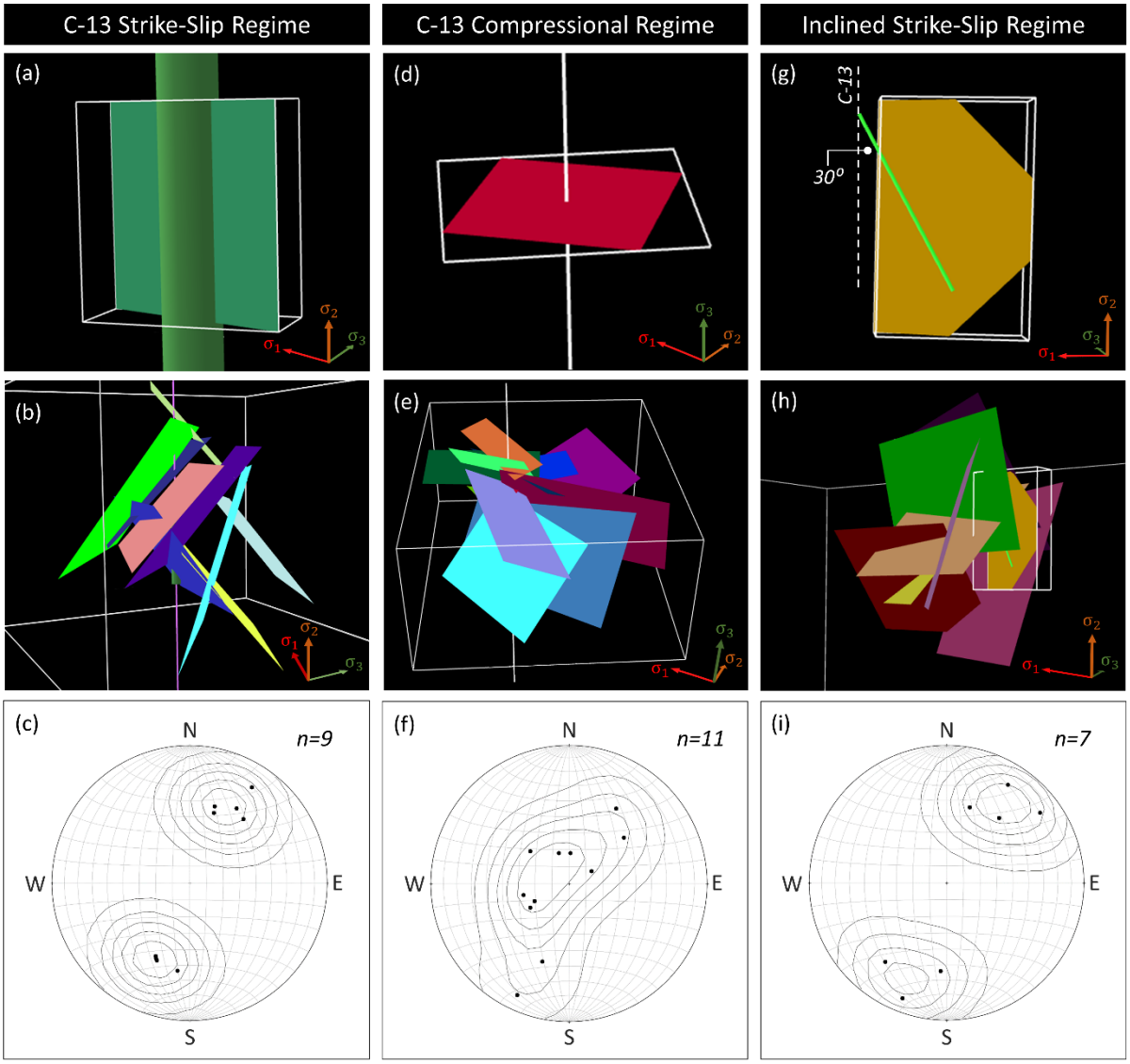


Figure 5. Hydraulic fracture simulation results. Using a strike-slip stress regime, the (a) induced hydraulic fracture, (b) interaction between the induced hydraulic fracture and pre-existing natural fractures, and (c) the pole to inflated pre-existing natural fractures is shown. Using a compressional stress regime, the (d) induced hydraulic fracture, (e) interaction between the induced hydraulic fracture and pre-existing natural fractures, and (f) the pole to inflated pre-existing natural fractures is shown. Using a strike-slip stress regime for the inclined well, the (g) induced hydraulic fracture, (h) interaction between the induced hydraulic fracture and pre-existing natural fractures, and (i) the pole to inflated pre-existing natural fractures is shown. σ_1: maximum principal stress; σ_2: intermediate principal stress; σ_3: minimum principal stress.

7.3. POSTER PRESENTATION A: The APPEA Conference

The Australian Petroleum Production and Exploration Association (APPEA)
2016 Annual Conference and Exhibition, Brisbane, Australia

Constraining the Distribution and Relationship between Overpressure, Natural Fracture Density and Temperature in the Cooper Basin, Australia

G07

Constraining the distribution and relationship between overpressure, natural fracture density and temperature in the Cooper Basin, Australia



David Kulikowski
Australian School of Petroleum,
The University of Adelaide

THE UNIVERSITY of ADELAIDE

1. INTRODUCTION

This research explores the potential relationship between increased temperature, overpressure and natural fracture density within the Cooper Basin, Australia (Fig. 1). The study area is a highly complex intracratonal basin that formed under a SE-NW extensional stress regime (650-575 Ma) with subsequent crustal shortening events developing intra-basin highs through basement fault reactivation (Fig. 2). The basin is Australia's largest onshore hydrocarbon province producing oil and gas from low permeability shales and sandstone reservoirs.

To effectively produce from these low permeability and overpressured reservoirs, a thorough understanding of the regional and field scale distribution of temperature, pore pressure and natural fracture density is essential. This research collates natural fracture data from 28 bore hole image logs (Fig. 3), and temperature and pressure data from 1095 wells to investigate a potential link between high temperature, pressure and fracture density.

PURPOSE

Present the regional pore pressure, temperature and natural fracture density data within the low permeability Cooper Basin to investigate whether a relationship exists between increased present day temperature and high pore pressure, which may lead to patterns in the natural fracture density.

Fig. 1 Location of the study area shown in red.

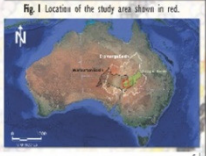
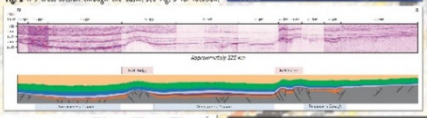


Fig. 2 N-S cross-section through the basin. See Fig. 3 for location.



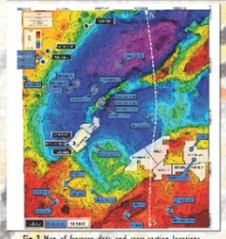


Fig. 3 Map of fracture data and cross-section locations.

2. PORE PRESSURE

Mechanisms for overpressure generation range from:

- Hydrocarbon generation
- Fluid expansion
- Increased geothermal gradient
- Increased mean compressive stress (tectonic loading)
- Disequilibrium compaction
- Vertical and lateral transfer of overpressure.

Rock failure principals show that overpressure can effectively shift the Mohr's circle to the left (Fig. 4), and promote the development and/or reactivation of fractures and faults (Anderson, 1951; Barton et al., 1995).

Previous research on the Cooper Basin has suggested that an increase in the mean compressive stress (50 MPa) may have generated the overpressure observed within the study area. However, considering that the geothermal gradient has recently increased, overpressure may also be related to fluid expansion or hydrocarbon generation mechanisms.

Overpressured tests (exceeding the hydrostatic gradient of approximately 0.45 psi/ft) were recorded in 385 wells with the following key observations:

- High overpressure appears in the Moomba/Big Lake and Coonatie fields, as well as in the deeper portions of the Nappamerri Trough.
- No obvious pattern to overpressure distribution.
- From the 33.3% of overpressured data, 14.3% were found to have pressure gradients above 0.50 psi/ft.
- Overpressure is observed from 7000 ft depth.
- Regional average = 0.46 psi/ft; excluding <0.42 psi/ft.

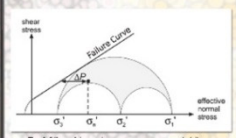


Fig. 4 Effect of increasing pore pressure on rock failure.

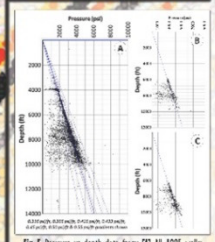


Fig. 5 Pressure vs depth data from: [A] All 1095 wells; [B] Too-Do-REM Group; and [C] Patchawarra Formation.

3. NATURAL FRACTURES

Natural fractures interpreted from borehole image logs are given in Figure 6, displaying data as regional stereographic projection (Fig. 6a), rose diagram (Fig. 6b), and bar graph of strike orientations (Fig. 6c). A high volume of measured data appears to have a strike of north-south, northeast-southwest, or east-west. (Fig. 6b). Normalised natural fracture densities (fracture count/sediment thickness) are illustrated in Figure 6d, with red highlighting relatively high normalised fracture density, orange showing relatively intermediate normalised natural fracture density, and blue indicating relatively low normalised natural fracture density.

- Relatively high normalised natural fracture densities were found along the GMI Ridge and on the basin flanks, as well as in the Moomba and Coonatie fields.
- Relatively low normalised natural fracture densities were found within the Tirrawarra, Dullingari and Bonna fields.
- Fracture frequency increases with depth; however, average fracture density is only ~0.12 f/m.
- Up to six natural fracture groups based on the dip direction (Fig. 6c), and three to four groups based on strike (Fig. 6b). The complete geometry must be assessed to find fracture sets present.

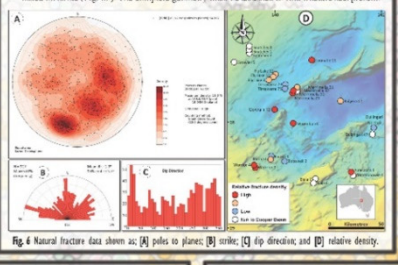


Fig. 6 Natural fracture data shown as: [A] poles to planes; [B] strike; [C] dip direction; and [D] relative density.

4. TEMPERATURE

Drilling wells into high geothermal gradient rocks can present risks associated with completions, logging and commission processes. Increased geothermal gradients can also increase pore pressures through fluid expansion and hydrocarbon generation (including the conversion of gas in CO_2 mechanisms leading to a greater chance of blow outs or fluid kicks occurring. Assuming a surface temperature of 70°F, the maximal geothermal gradient of wells identified some key findings:

- Average geothermal gradient of 2.5 - 3.5°F/100 ft.
- High temperatures within the Nappamerri Trough, Moomba/Big Lake and Dullingari fields, and along the Murteree-Nappacoongee Ridge, mostly associated with uranium-rich Volcanics (Fig. 7).
- Low basin temperatures (2.5°F/100 ft) are still higher than the continent average of 2.3°F/100 ft (Fig. 8).

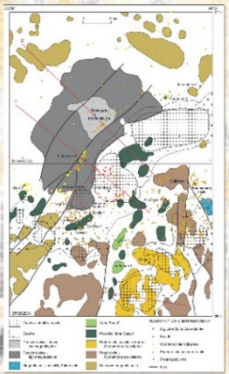


Fig. 7 Basement below the Cooper Basin (Meixner et al, 2000).

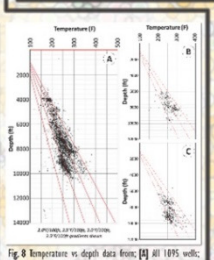


Fig. 8 Temperature vs. depth data from: [A] All 1095 wells; [B] Too-Do-REM Group; and [C] Patchawarra Formation.

Future Work:

- Calculating the orientations and magnitudes of structural events following Etchecopar's calcite twin stress inversion technique.
- Tectonostratigraphic evolution of several depth converted 3D seismic surveys.
- Geomechanical modelling of fault reactivation.
- Modern structural interpretation of old 2D/3D seismic data to define basement fault geometry and improve the structural evolution model.

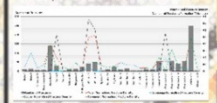


Fig. 9 Normalised natural fracture density per well.

5. CONCLUSIONS

This high level investigation into the spatial and depth distribution of temperature, pressure and natural fracture density identified some key points:

- Natural fractures are dominantly N-S, NE-SW and E-W striking with up to six fracture sets present (Fig. 6c) and a low normalised fracture density (Fig. 9).
- Patchawarra Trough lower geothermal gradient likely due to absence of uranium-rich Big Lake Granites.
- The presence of uranium-rich Big Lake Granites in the Moomba/Big Lake Field and within the deeper portions of the Nappamerri Trough appear to have close association with overpressure (Fig. 10a & 10b).
- No clear relationship between increased temperature and overpressure (Fig. 11).
- No obvious relationship found between increased pore pressure and increased natural fracture density.

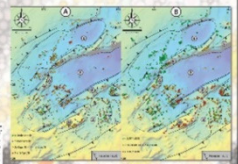


Fig. 10 Spatial distribution of: [A] Pressure; and [B] Temperature.

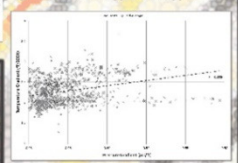


Fig. 11 Plot of pressure vs temperature for individual well tests and field averages where more than 3 data points are available.

ACKNOWLEDGEMENTS

The authors would like to thank the GeoFrac Consortium (Santos, Beach Energy, Chevron, Halliburton & OGC) for their financial contribution. Thank you to Paradigm (Geolog & Petrosys), and Carlos H. Grohmann and Ginaldo A.C. Campanh for software. See conference publication for reference list.

7.4. POSTER PRESENTATION B: The ASP Annual Board Meeting

Australian School of Petroleum
2016 Annual Board Meeting

Better Understanding the Structural Geology and Evolution of the Cooper-Eromanga Basin, Australia

Better Understanding the Structural Geology and Evolution of the Cooper-Eromanga Basin, Australia.

David Kulikowski, Dennis Cooke, & Khalid Amrouch 2016

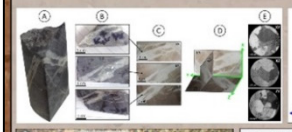
Introduction

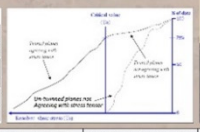
The primary objective of this research is to better understand the structural geology within the Cooper-Eromanga Basin that can be used to develop more accurate basin evolution models and improve and/or clarify common assumptions. Previous research has been limited to poor resolution, sparse and old two-dimensional (2D) seismic data that has led to uncertain conclusions on the paleo-stress orientation and regime. This research integrates micro-, meso-, and macro-scale data and numerous methods to provide a clearer picture of the structural geology within the basin.

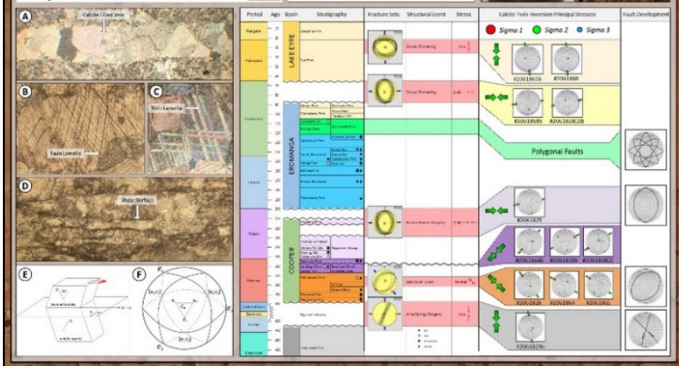
1. Calcite Twin Stress Inversion

Calculated the paleo-stress orientations, shape ratios, differential stress magnitudes, and stress regimes of 6 structural events using the Etchecopar calcite twin stress inversion method on 7 core samples. Results integrated with natural fracture and fault stress inversion. Future work will constrain the absolute magnitude of structural events with results used to predict fault activity through time.



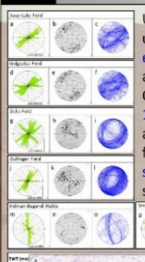


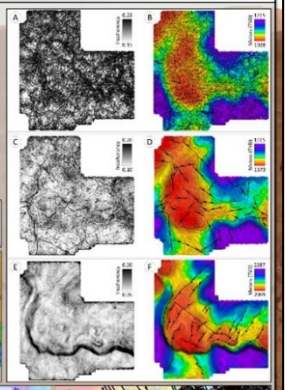


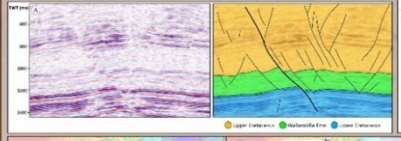


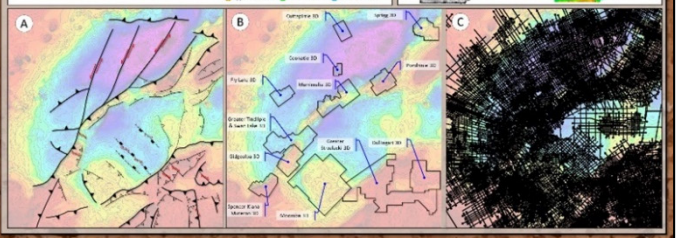
2. Seismic Interpretation

Used 2D/3D seismic data to better understand the tectonostratigraphic evolution of the basin and more accurately interpret basement faults. Complete structural interpretation of 12 3D seismic surveys. Incoherency analysis helpful to interpret basement faults and to map the polygonal fault system. Polygonal faults extend from shallow sediments into oil reservoirs.







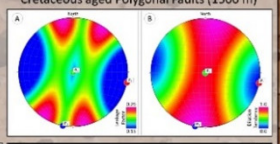


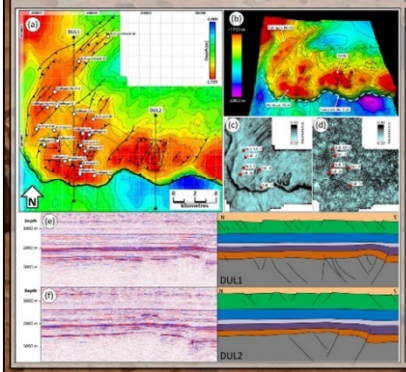
3. Fault Reactivation Potential

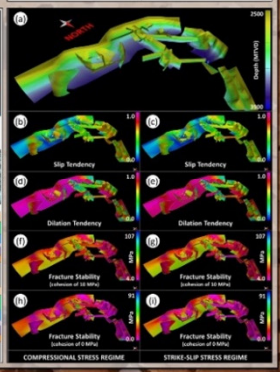
The risk of fault reactivation under the present day stress was modelled for basement faults within the Swan Lake 3D and Dullingari 3D (shown below) seismic surveys. Results showed that the SE-NW striking strike-slip faults are most likely to reactivate/dilate.

Modelled Leakage Factor and Dilation Tendency of the Polygonal Fault System at 1500 m depth (right).

Cretaceous aged Polygonal Faults (1500 m)

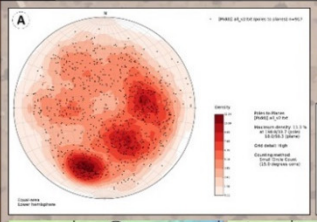


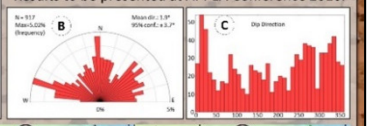


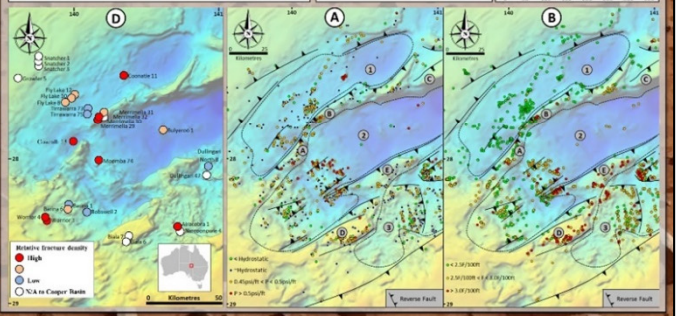


4. Pressure, Temperature & Natural Fractures

Pore pressure and temperature data collated from 1095 wells to test a possible relationship between high temperature, over pressure and increased fracture density. Interpretation of 28 image logs. Results to be presented at APPEA Conference 2016.







Conclusion

The key findings of this study were: (a) calculated the paleo-stress of structural events; (b) predicted the likelihood of basement faults and Cretaceous polygonal faults reactivating under the present day stress; and (c) Developed a regional basement fault interpretation map. We are currently working on predicting fault activity during basin evolution using the paleo-stress results from calcite twin stress inversion.

THE UNIVERSITY of ADELAIDE

ASP Australian School of Petroleum

GeoFrac Consortium

Kulikowski, D., K. Amrouch, K.H. Al Barwani, W. Liu & D. Cooke, 2015, *Insights into the tectonic stress history and regional 4D natural fracture distribution in the Australian Cooper Basin using Etchecopar's calcite twin stress inversion technique, 2D/3D seismic interpretation and natural fracture data from image logs and core*. American Association of Petroleum Geologists International Conference and Exhibition, Melbourne, Victoria, 13–16 September, extended abstract number #2224164.

Kulikowski, D., D. Cooke & K. Amrouch, 2016, *Constraining the distribution and relationship between overpressure, natural fracture density and temperature in the Cooper Basin*. The Australian Petroleum Production and Exploration Association Journal, 56, in press.

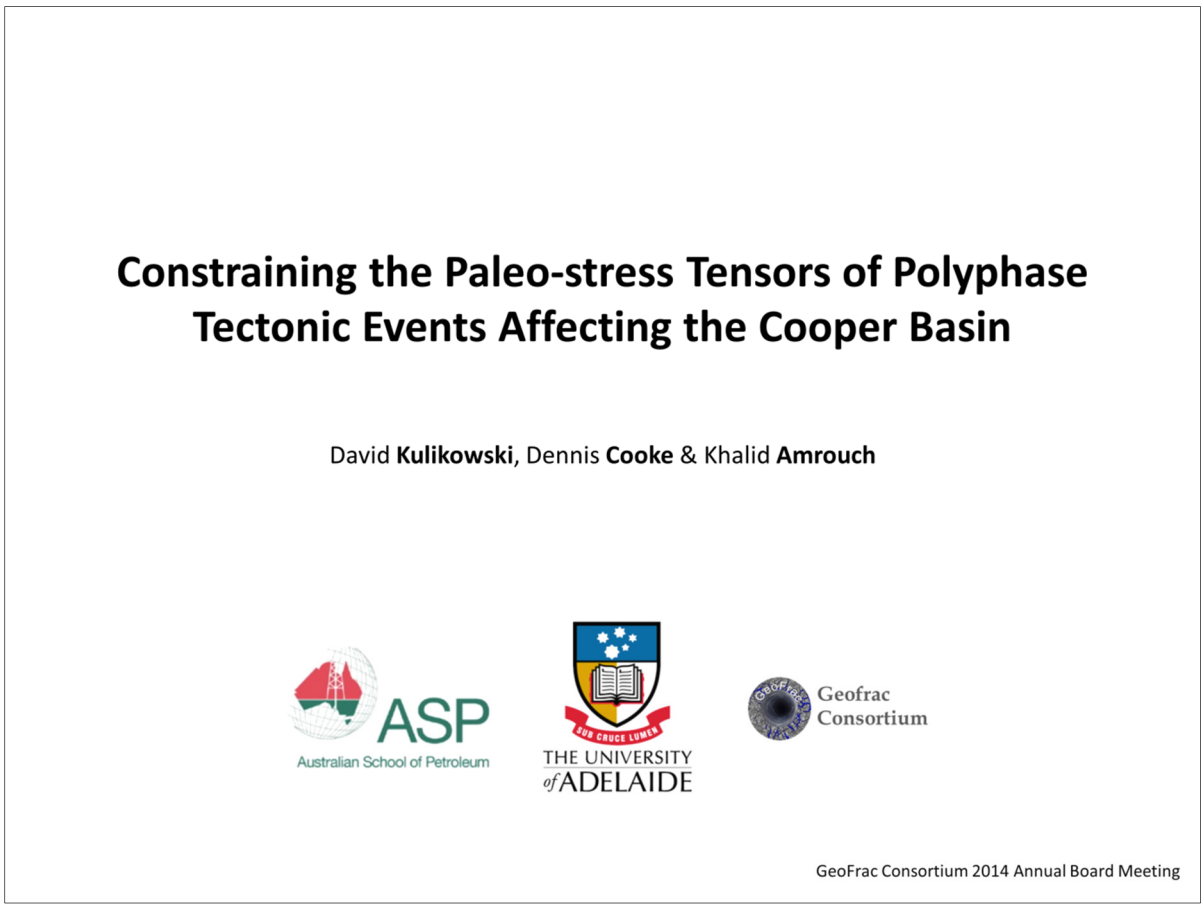
Kulikowski, D., K. Amrouch & D. Cooke, 2016b, Geomechanical Modelling of Fault Reactivation in the Cooper Basin, Australia. Australian Journal of Earth Sciences, 63(3), in press.

Kulikowski, D., C. Hochwald, D. Cooke & K. Amrouch, 2016, *A Statistical Approach to Assessing Depth Conversion Uncertainty on a Regional Dataset: Cooper-Eromanga Basin, Australia*. ASEG-PESA-AIG 2016 Conference, Extended Abstract, in press.

7.5. SPOKEN PRESENTATION A: GeoFrac Consortium Board Meeting

GeoFrac Consortium (Santos, Beach Energy, Chevron, Halliburton, and BG Group)
2014 Annual Board Meeting

Constraining Paleo-stress Tensors of Polyphase Tectonic Events Affecting the Cooper Basin



7.6. SPOKEN PRESENTATION B: The AAPG International Conference

American Association of Petroleum Geologists (AAPG)
2015 International Conference and Exhibition, Melbourne, Australia

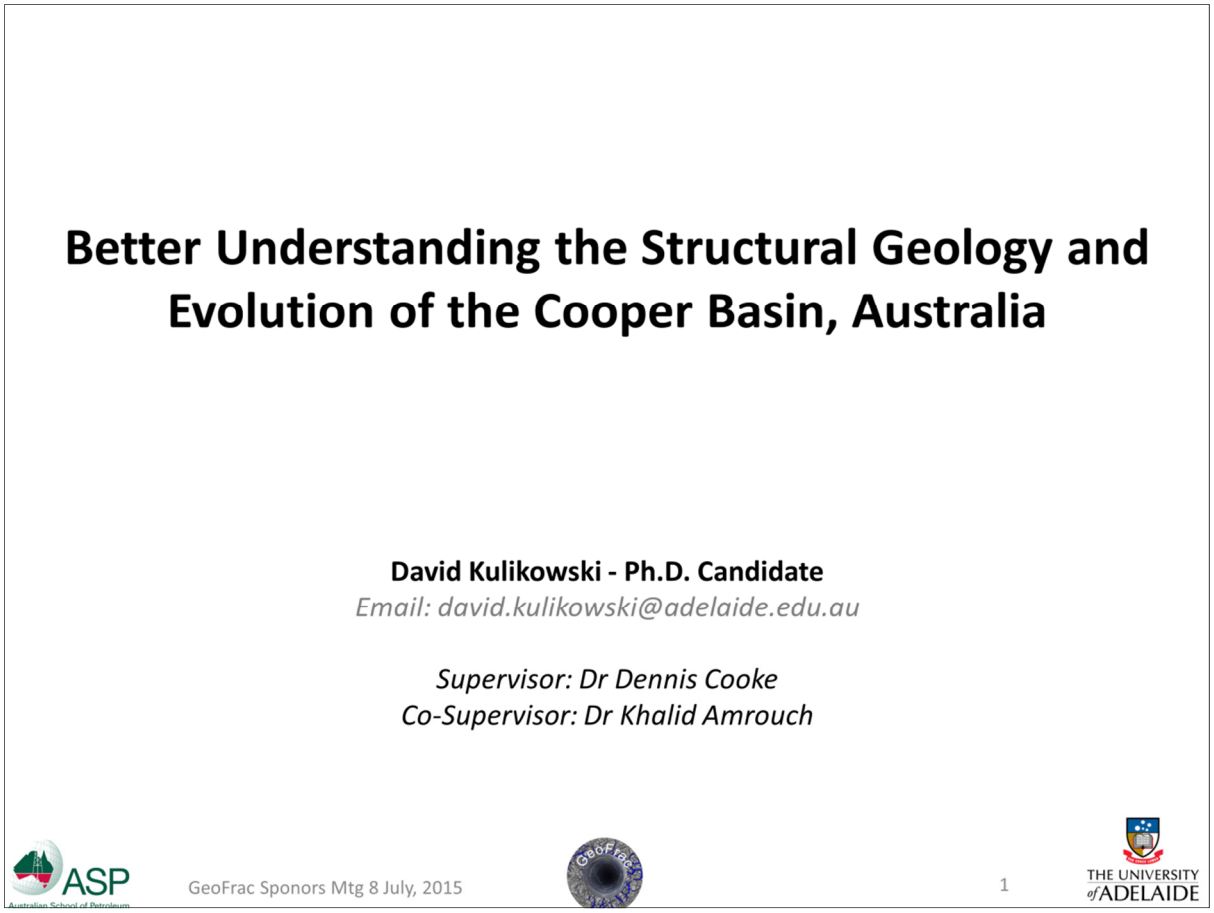
Structural and Stress History: Cooper Basin, Australia



7.7. SPOKEN PRESENTATION C: GeoFrac Consortium Board Meeting

GeoFrac Consortium (Santos, Beach Energy, Chevron, Halliburton, and BG Group)
2015 Annual Board Meeting

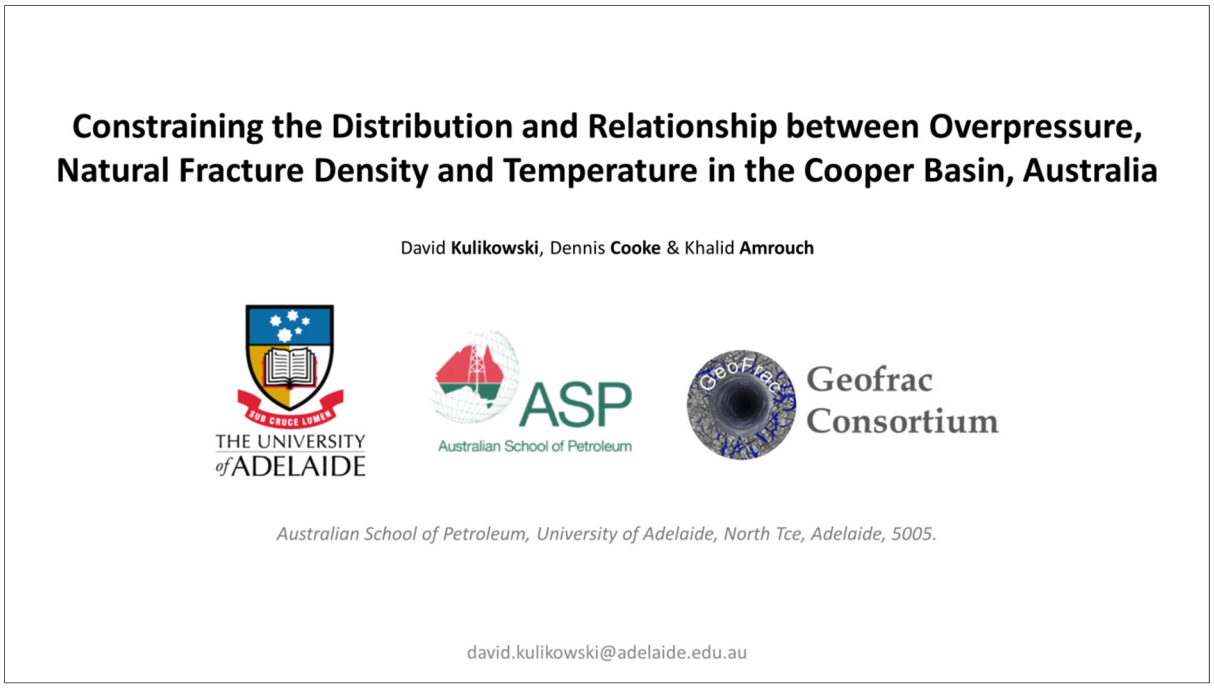
Better Understanding the Structural Geology and Evolution of the Cooper Basin, Australia



7.8. SPOKEN PRESENTATION D: The APPEA Conference

The Australian Petroleum Production and Exploration Association (APPEA)
2016 Annual Conference and Exhibition, Brisbane, Australia

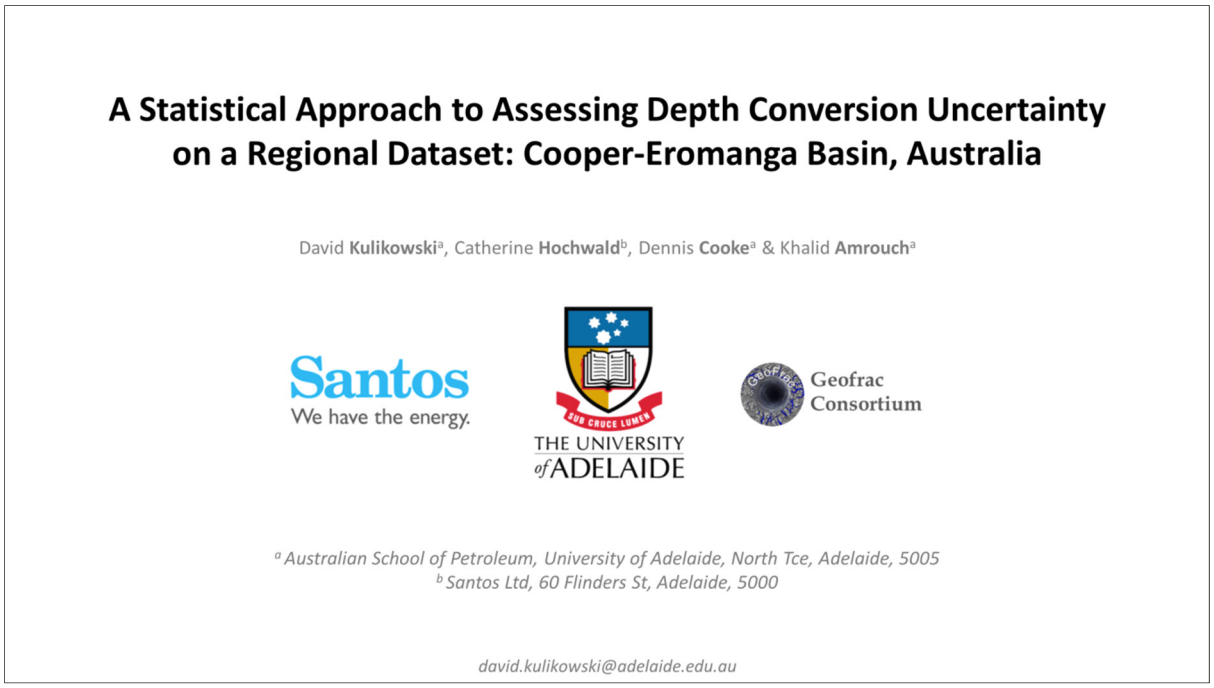
Constraining the Distribution and Relationship between Overpressure, Natural Fracture Density and Temperature in the Cooper Basin, Australia



7.9. SPOKEN PRESENTATION E: The ASEG-PESA-AIG Conference

Australian Society of Exploration Geologists - Petroleum Exploration Society of Australia - Australian Institute of Geoscientists (ASEG-PESA-AIG) 25th Geophysical Conference and Exhibition, Adelaide, Australia

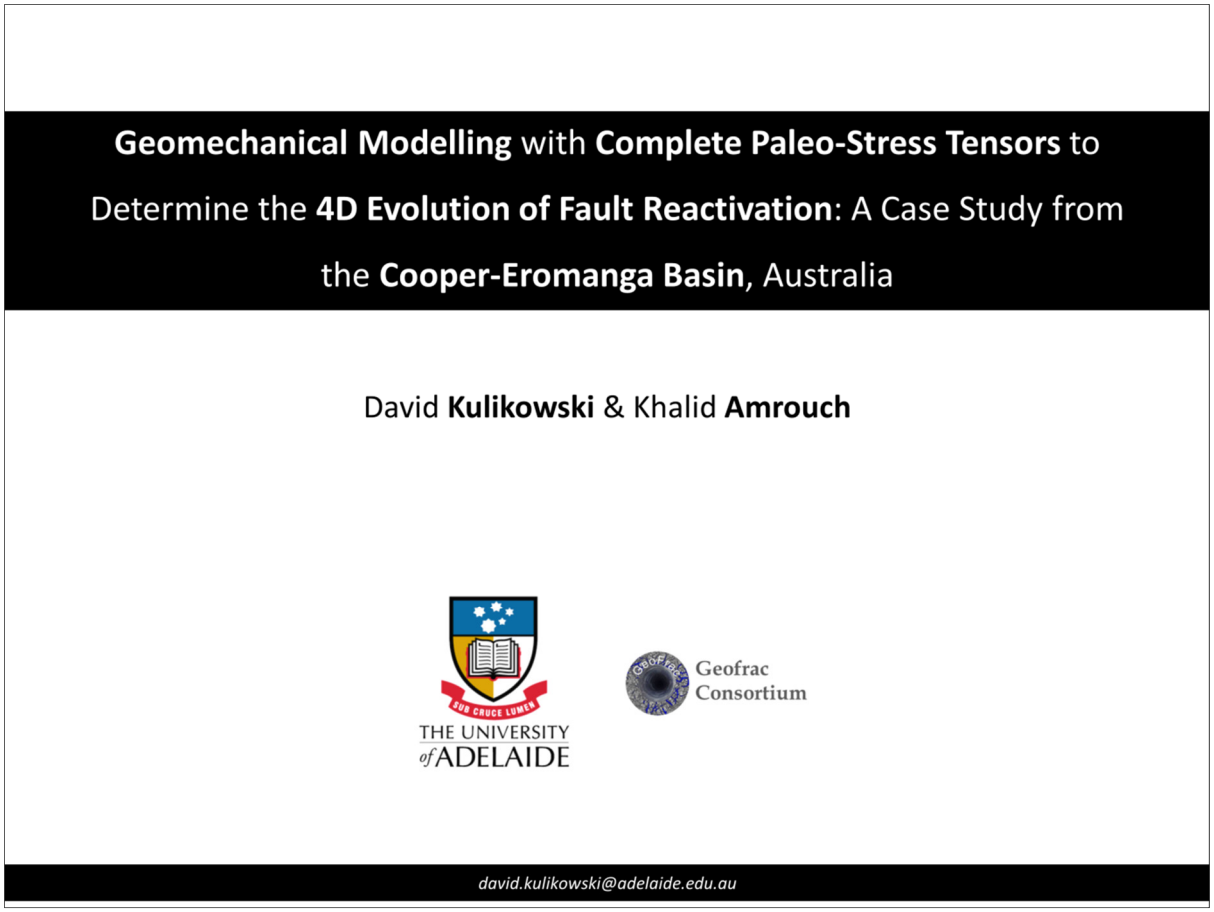
A Statistical Approach to Assessing Depth Conversion Uncertainty on a Regional Dataset: Cooper-Eromanga Basin, Australia



7.10. SPOKEN PRESENTATION F: The ASP research seminar

2016 Australian School of Petroleum (ASP) Seminar Session
Monthly Research Seminar

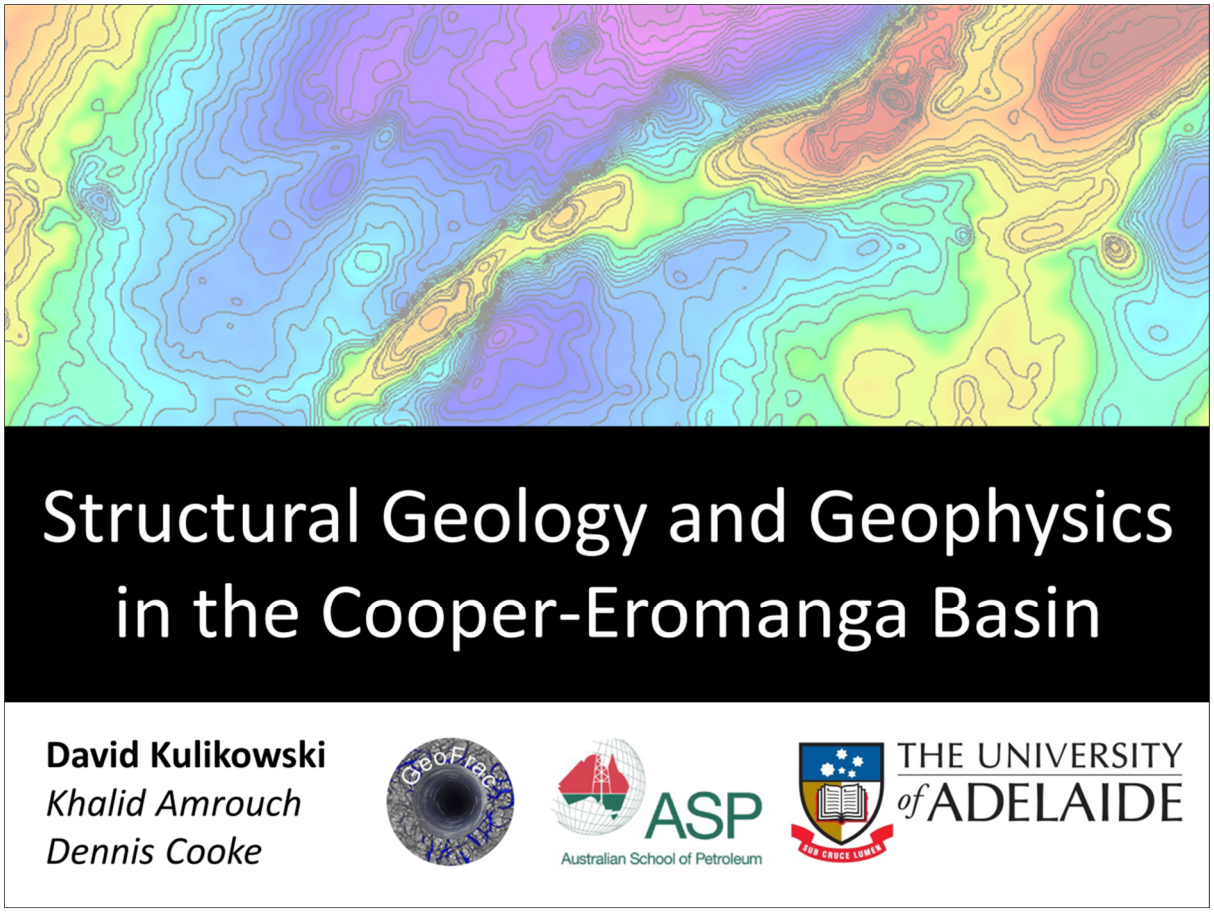
Geomechanical Modelling using Complete Paleo-Stress Tensors to Determine the 4D Evolution of Fault Reactivation in Structurally Complex Provinces: A Case Study from the Cooper-Eromanga Basin, Australia



7.11. SPOKEN PRESENTATION G: The ASP research seminar

2016 Australian School of Petroleum (ASP) Seminar Session
Weekly Research Seminar

Structural Geology and geophysics in the Cooper-Eromanga Basin, Australia
(Final PhD Research Presentation)



7.12. RESEARCH SCHOLARSHIP A: AAPG Grants-in-Aid

American Association of Petroleum Geologists (AAPG)
2015 Grants-in-Aids Foundation Scholarship

Insights into the Tectonic Stress History and Regional 4D Natural Fracture Distribution in the Australian Cooper Basin using Etchecopar's Calcite Twin Stress Inversion Technique, 2D/ 3D Seismic Interpretation and Natural Fracture Data from Image Logs and Core

"The purpose of the AAPG Foundation Grants-in-Aid program is to foster research in the geosciences. Grants are based on merit and are made to provide financial assistance to graduate students (enrolled in Masters or Ph.D.) whose thesis research has application to the search for and development of petroleum and energy-mineral resources, and/or to environmental geology issues"



INSIGHTS INTO THE TECTONIC STRESS HISTORY AND REGIONAL 4D NATURAL FRACTURE DISTRIBUTION IN THE AUSTRALIAN COOPER BASIN USING ETCHECOPAR'S CALCITE TWIN STRESS INVERSION TECHNIQUE, 2D/ 3D SEISMIC INTERPRETATION AND NATURAL FRACTURE DATA FROM IMAGE LOGS AND CORE

David Kulikowski

The Australian School of Petroleum, The University of Adelaide, South Australia, Australia
david.kulikowski@adelaide.edu.au

Abstract

The Cooper Basin is Australia's largest onshore hydrocarbon basin with tremendous value for unconventional resources. Optimization of these resources will benefit from an understanding of the paleo-stress, current stress, natural fracture distribution and orientation, and a modern tectonic history model. The timing and magnitude of polyphase tectonic activity will be the primary focus, with outcomes to include constraining the paleo-stress and natural fracture distribution sustained by rocks with change in time, as well as the potential to extrapolate findings between wells and comment on likely reservoir quality variations. This research will aim to reconstruct the stress history of the Cooper Basin through the integration of current regional tectonic models with two-dimensional and three-dimensional seismic interpretation and Etchecopar's calcite twin stress inversion technique (CSIT). The CSIT, unlike conventional stress analysis, determines not only a current day stress orientation but also paleostress orientations and magnitudes. Calcite that is appropriate for sampling is commonly found within matrix, or as veins in non-carbonate formations. With the successful completion of the CSIT component, a technique that incorporates CSIT results will be explored to estimate the evolution of overpressure. Our results will (1) benefit unconventional drilling programs utilizing fracture stimulation treatments to exploit natural fractures; (2) provide and test models to predict reservoir quality as a function of the structure and stress through time; (3) provide valuable data for future research; and (4) generate a modern structural model for the tectonic evolution of the Cooper Basin.

AAPG Search and Discovery Article #90249 © 2016 AAPG Foundation 2015 Grants-in-Aid Projects

7.13. RESEARCH HONOUR A: Selected as IMNIS Student

Academy of Technological Sciences and Engineering (ATSE)
2016 Industry Mentoring Network in STEM (IMNIS) PhD Student

Description: *Highly motivated and hard working PhD students were nominated by their respective University Faculty, from which only 15 (5 from each University) were selected in South Australia to participate in this pilot program.*

IMNIS (Industry Mentoring Network in STEMS) is a mentoring program aimed at preparing STEM (Science, Technology, Engineering and Math) PhD Students for better careers in the industry and/or government, as well as enhancing research translation skills and networks for careers academics.

Mentors are established industry based professionals, entrepreneurs and/or product developers with personal interest in helping PhD Students gain awareness and knowledge of the skills required for successful commercial, engagement and leadership careers outside of academia.

IMNIS
INDUSTRY MENTORING
NETWORK IN STEM

Principles of IMNIS

- Experienced Industry individuals mentoring PhD students in Science, Technology, Engineering and Mathematics (STEM).
- A strong personal commitment from Industry Leaders in each sector.
- IMNIS in an initiative of the Australian Academy of Technological Sciences and Engineering (ATSE).
- It is not about finding students jobs, it is about preparing them for a career.

7.14. RESEARCH HONOUR B: Featured in PETROSYS Map Book v6

2017 The Big Book of PETROSYS Maps Version 6

An automated cross-validation method to assess seismic time-to-depth conversion accuracy: A case study on the Cooper-Eromanga Basin, Australia



SEND US YOUR PETROSYS MAPS TO WIN $300 (USD)

We're running a competition for Universities using Petrosys software.

All map entries will be judged by our in house Gurus and the winner will receive USD $300 in cash, prizes of $200 and $100 for 2nd & 3rd places will also be awarded.

The best maps entered will be published and credited in our annual publication, "The Big Book of Petrosys Maps", which is circulated globally by Petrosys at industry tradeshows and conferences in which we participate.

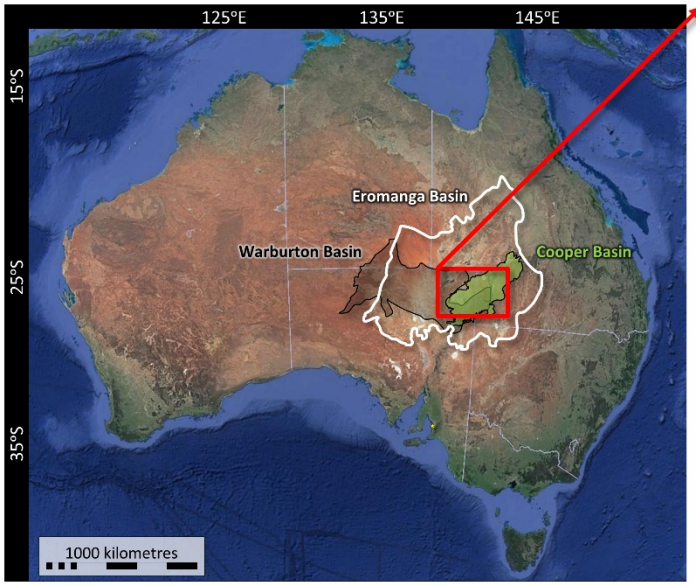
To get your own personal education license go to:

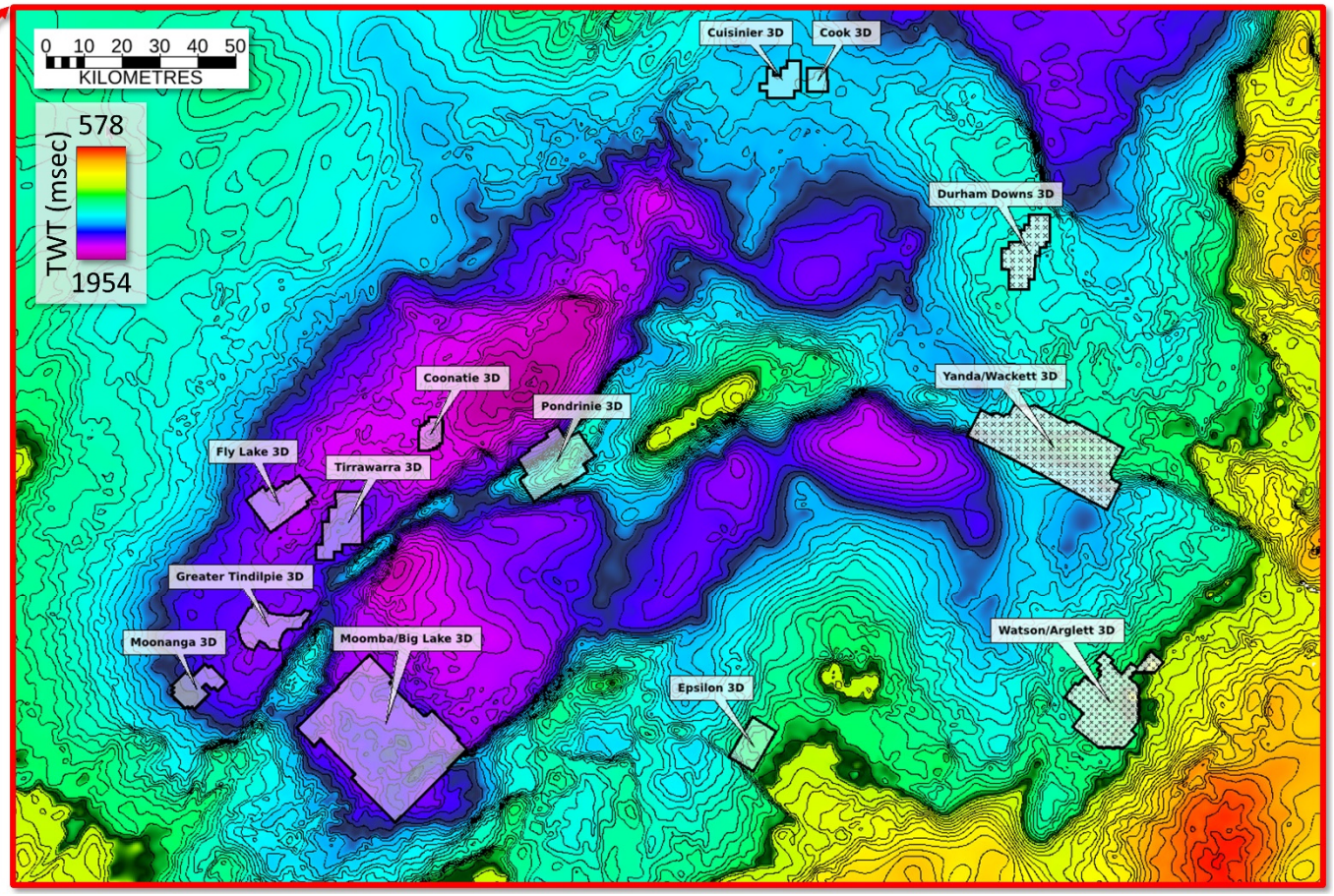
www.petrosys.com.au/about/educational-licenses

Like us on Facebook *facebook.com/PetrosysInfo* or Follow us on Twitter *@PetrosysInfo* to get regular words of wisdom from the Petrosys Mapping Gurus on how to make a winning map!

Closing Date: 31st March 2017

If you think you can make a map in Petrosys worthy of the title "Petrosys Mapping Guru" then send it to us now!





To investigate the seismic depth conversion uncertainty in the Cooper-Eromanga Basin, this research developed a looping script within PETROSYS to automate the depth conversion process while integrating the cross-validation (blind well test) method (use *n* wells to predict the *n*th +1 well). The study utilised 13 3D seismic surveys with 73 interpreted TWT grids and 657 wells to constrain the most accurate depth conversion method from the four most commonly used methods; (1) average (pseudo) velocity; (2) time-depth trend; (3) kriging with external drift using TWT; and (4) kriging with external drift to tie stacking velocities to average well velocities. Statistics (number of wells, closest well distance, inside/outside data envelope, crestal/flank well, etc.) were captured during each of the ~10,000 loops to define the most significant variables for depth conversion accuracy. Further information can be found in the below reference.

Kulikowski, D., Hochwald, C., Cooke, D., & Amrouch, K. (2016). A Statistical Approach to Assessing Depth Conversion Uncertainty on a Regional Dataset: Cooper-Eromanga Basin, Australia, ASEG-PESA-AIG Conference, Adelaide, Extended Abstract 200, 484–490.